

# SSA 2016 Annual Meeting Announcement

Seismological Society of America  
Technical Sessions  
20–22 April 2016  
Reno, Nevada

IMPORTANT DATES	
Meeting Pre-registration Deadline	13 March 2016
Hotel Reservation Cutoff	27 March 2016
Online Registration Cutoff	08 April 2016
Pre-Meeting Workshops	19 April 2016
Opening Reception	19 April 2016
Technical Sessions	20–22 April 2016
Additional Workshops	20–22 April 2016
Field Trips	23 April 2016

## PROGRAM COMMITTEE

The 2016 technical program committee consists of co-chairs Graham Kent and Kenneth Smith (Nevada Seismological Laboratory, University of Nevada Reno), Annie Kell (University of Nevada Reno Seismological Lab), Bill Hammond (University of Nevada Reno, Nevada Bureau of Mines and Geology), Mohammed Moustafa (University of Nevada Reno Civil Engineering) and Neal Driscoll (University of California San Diego Scripps Institution of Oceanography).

### Meeting Contacts

*Technical Program Co-Chairs*  
Graham Kent and Ken Smith  
2016Program@seismosoc.org

### *Abstract Submissions*

Joy Troyer  
Seismological Society of America  
510.559.1784  
joy@seismosoc.org

### *Registration*

Sissy Stone  
Seismological Society of America  
510.559.1780  
registration@seismosoc.org

### *Exhibits*

Nan Broadbent  
Seismological Society of America  
510.559.1782  
nbroadbent@seismosoc.org

### *Press Relations*

Becky Ham  
SSA Press Liaison  
press@seismosoc.org

## TECHNICAL PROGRAM

The SSA technical program comprises oral and poster presentations presented over three days. The session descriptions, detailed program schedule, and all abstracts appear in the following pages. Searchable abstracts are at <http://www.seismosoc.org/meetings/2016/abstracts/>.

## LECTURES

### **President's Address**

The President's Address will be presented by Ruth A. Harris at the Annual Luncheon on Wednesday 20 April 2016.

### **Joyner Lecture**

The Joyner Lecture will be presented by Jonathan P. Stewart, University of California at Los Angeles, at 5:15 PM Thursday, 21 April 2016. The 2016 Joyner Lecture is entitled, "Site Response Uncertainty and its Implications for Seismic Risk Characterization."

## WORKSHOPS

### **Workshop: Communicating Post-Earthquake with the Press and the Public**

*Tuesday, 19 April 2016, 2–5 PM.*

*Registration required; limited to 20 attendees.*

*Fee: \$25.*

Workshop leader: Denise Graveline, a Washington, DC-based communications consultant.

A major earthquake just happened, perhaps nearby or on the other side of the world. When reporters call, how do you answer their questions even if it's not your exact area of expertise?

It's a situation often faced by SSA members—even those who thought they would never, ever talk to a reporter. In this small-group workshop, you'll learn how to field those questions effectively by explaining the science behind earthquakes so that reporters and the public can put the event in context. And these same skills will serve you well in your grant proposals, government testimony, faculty meetings, or anywhere else you need a clear and compelling message.

Denise Graveline, a top trainer based in Washington DC, will lead the workshop, where you will learn how to develop your communications skills; learn an organizing principle for creating a message or outline that boils down your technical information into three key points; learn how to deliver them; and create and rehearse a plan for preparing yourself quickly when the Earth shakes and the phone rings.

### **Workshop: Getting Published—Q&A with Editors**

*Tuesday, 19 April 2016, 2:30–5:30 PM.*

*Registration required.*

*No fee.*

Workshop leaders: Roland Bürgmann, University of California Berkeley, a *BSSA* associate editor emeritus; John Ebel, Boston College, founding editor-in-chief of *SRL*; and Brent Grocholski, who is the editor for seismology papers at *Science*.

Learn what makes an excellent paper, how to handle constructive—and not so constructive—reviews and how to become a reliable reviewer from those who know—editors at *Science*, *SRL* and *BSSA*. This free SSA workshop is geared toward students and early career seismologists but is open to all Annual Meeting attendees.

### **Workshop: How Congress Works & How You Can Work Congress**

*Wednesday, 20 April 2016, 7:30–8:30 PM.*

*Thursday, 21 April 2016, 2:45–3:45 PM.*

*No registration required.*

*No fee.*

Workshop leader: Elizabeth Duffy, president of the Federal Affairs Office, Washington, D.C., and government affairs coordinator for SSA.

Elections provide the potential for change in leadership in the federal government's administration as well as the U.S. House, and the U.S. Senate—and 2016 is no exception! Regardless of the outcome of this year's election, there are bound to be contentious legislative environments, declining budgets, and increased competition for funding. It is crucial that every scientist knows how to make the best case for his or her science. Come for an informative session and learn more about the inner workings of Congress, how laws are made, and how you can become an effective advocate for your science. Workshop leader Elizabeth Duffy brings more than 20 years of business, politics, and advocacy experience to this topic. She will inform you how to speak to representatives to get your message heard, how to establish productive relationships with elected officials and their offices, and how to best impact legislation in Congress, even in today's political environment.

### **Workshop: Congressional Update—What to Expect Heading into the 2016 Election**

*Friday, 22 April 2016, 7:00–7:55 AM.*

*No registration required.*

*No fee.*

Workshop convener: Lisa Grant Ludwig, chairman of the SSA Government Relations Committee.

Workshop speaker: Elizabeth Duffy, president of the Federal Affairs Office, Washington, D.C., and government affairs coordinator for SSA.

As the 2016 election process is heating up, come to a special briefing by Elizabeth Duffy, SSA's Washington, DC-based government affairs coordinator, speak about pending legislation that is important to geoscientists, what's ahead for the remainder of 2016, and what to expect after the elections in November.

## FIELD TRIPS

### **Field Trip: Faulting History of the Lake Tahoe Basin**

*Saturday, 23 April 2016, 8 AM–5 PM.*

*Registration required.*

*Fee: \$85 (includes box lunch).*

Trip leaders: Graham Kent (UNR), Neal Driscoll (UC San Diego), and Gordon Seitz (California Geological Survey)

The field trip will visit the major fault lines in the Tahoe basin and the Polaris fault in the Truckee basin. The field trip will also visit other important geomorphic features such as glacial moraines, wave-cut caves displaced by faulting, etc. Itinerary is weather-dependent. Ideally stops will begin at the Mt. Rose pediment dissected by faults, followed by the Incline Village HWY 431 overlook, Incline Village fault scarp at the closed elementary school, wave-cut Cave Rock, West Tahoe fault at Angora Lakes (or alternative location if it's a heavy snow year), Emerald Bay moraines, Eagle Rock, and Polaris fault (Truckee).

**Field Trip: A Day with the Surface Ruptures of the Ms 7.2 1954 Dixie Valley and Ms 6.8 Fairview Peak Earthquakes of the Central Nevada Seismic Belt**

*Saturday, 23 April 2016, 7 AM–8 PM.*

*Registration required.*

*Fee: \$95 (includes box lunch)*

Trip leader: Steve Wesnousky (UNR)

This trip will take participants to Dixie Valley to see the remnant scarps from the 1954 ruptures as well as discuss the active tectonics in Central Nevada. Scarps associated with the 100-km length of surface ruptures produced by the earthquakes remain well-preserved in the arid environment of the Basin and Range. The trip is offered to provide those who have not seen them an opportunity to do so, simple as that. The trip will leave Reno at 7 AM and return by 8 PM. The ruptures are situated about a two-hour drive east of Reno. The game thereafter will be to get the group on to as many sites as logistics of group size allow. Most sites are off the main highway and up roads best navigated with 4WD. The weather will likely be quite cold, so plan to dress warmly and in rugged shoes. Hiking will consist of touring the fault zones, not long or rugged hikes.

**PRELIMINARY SCHEDULE**

Most conference events will be held at the Peppermill Resort in Reno, Nevada. *This schedule is subject to change.*

**Tuesday, 19 April**

Board of Directors Meeting (9:30 AM–5:00 PM)

Workshop: Communicating Post-Earthquake with the Press and the Public (2–5 PM)

Workshop: Getting Published—Q&A with Editors (2:30–5:30 PM)

Registration (3:00–8:00 PM)

Icebreaker (6:00–8:00 PM)

**Wednesday, 20 April**

Technical Sessions (8:30 AM–6:00 PM)

Annual Luncheon (12:00–2:00 PM)

Student Reception (5:45–7:30 PM)

Workshop: How Congress Works (6:00–7:00 PM)

Early Career Reception (5:45–7:30 PM)

Technical Session on the Iniskin Alaska Earthquake (7:30–9:00 PM)

**Thursday, 21 April**

Workshop: How Congress Works (7:00–7:55 AM)

Technical Sessions (8:30 AM–5:00 PM)

Public Policy Lunch (12:00–1:00 PM)

Joyner Lecture (5:15–6:15 PM)

Reception (6:15–7:30 PM)

**Friday, 22 April**

Workshop: Congressional Update (7:00–7:55 AM)

Technical Sessions (8:30 AM–5:00 PM)

Lunch (12:00–1:00 PM)

**Saturday, 23 April**

Field Trips

**HOTEL AND TRAVEL INFORMATION**

The conference will be held at the **Peppermill Resort** at 2707 S. Virginia Street, Reno, Nevada. SSA has a room block at the Peppermill with a room rate of \$109. The Peppermill has reserved a portion of the SSA block at the government per diem rate for attendees with valid U.S. government employee identification. Please note that the cutoff date for reservations at the SSA rate is **27 March**.

**EXHIBITORS, SPONSORS AND ADVERTISERS**

Information for organizations wishing to register as exhibitors, sponsor events at the meeting, or advertise in the meeting program can be found on the SSA website at <http://www.seismosoc.org/meetings/ssa2016/>. ✉

# Technical Sessions

## Active Tectonics, Faults and Large Earthquakes

Faults generating very large earthquakes may appear as surface ruptures or may remain blind within the crust. This latter case was seen most recently with the Katmandu earthquake in Nepal, 2015. It is important to identify seismogenic faults and to understand their nature and kinematics. There are many faults that have been associated with historical large earthquakes. Whereas several other faults may be identified as having the potential to be reactivated in the recurrence interval of say 500-1000 years. Data generated through local and regional seismicity monitoring have helped in identifying many seismogenic faults. Paleoseismic studies can be used to constrain the amount of displacement on active faults, and in some cases, the recurrence interval between large events. Active faults may have varying geomorphic expressions in different tectonic environments. The mapping of active faults is also an important aspect. Identification of active faults and understanding their kinematic behavior vis-à-vis seismicity has direct societal relevance in earthquake hazard reduction. The session invites all recent findings in active tectonic regions that focus on the studies of active faults through seismicity, GPS, Remote Sensing, GIS, paleoseismology and tectonic geomorphology. Recently, a series of unusual earthquake phenomena is under investigation such as slow earthquakes; these are earthquake-like events that release energy over a period of hours to months, rather than seconds to minutes characteristic of a typical earthquake. This unusual earthquake phenomenon includes deep episodic tremor, low-frequency earthquakes, very-low-frequency earthquakes and slow slip events. Each of these has been demonstrated to arise from shear slip, just as do regular earthquakes, but with longer characteristic durations and radiating much less seismic energy. Slow seismic events may be useful for better understanding of the subduction process and large earthquake generation—especially in those regions where stress is accumulating but no major earthquake has triggered for a long time, and may be considered a ‘seismic gap’. Here, many seismologists speculate the potential of large earthquakes in such regions. In this session, we welcome papers on slow earthquakes.

During more typical rupture events, various information on the kinematics and dynamics of earthquakes are now available. In many recent large earthquakes such information includes slip evolution, frictional properties during faulting, fault system geometry and the structure of fault zones. This provides the fundamental knowledge base with which to build an ‘earthquake mechanism’ capable of simulating the earthquake generation process and cycles of earthquake activity. In this session, we welcome papers earthquake simulation models as well as aiming to provide insight on the kinematics and dynamics of earthquake generation and cycles.

Seismic waves generated by earthquakes have been interpreted to provide us information about the earth’s structure across a variety of scales. Seismic tomography is promising

tool to understand various heterogeneous structures. In this session, we also welcome papers on earth’s evolving crust and upper mantle structure.

*Session Chairs:* Sushil Kumar (sushil\_rohella@yahoo.co.in), Sudhir Rajaure (nscdmg@mos.com.np), and Rama Sushil (ramasushil@yahoo.co.in).

## Advancements in Network Operations and Station Design

To perform the best science, we need high-quality and complete datasets. While there are standards for network operation and station installations, there are improvements, often at the local network scale, happening all the time. This session will focus on sharing these local improvements to the wider audience. We encourage submissions featuring: 1) removing instrument response prior to data analysis; 2) running (and analyzing) regular calibrations network wide; 3) Vault/installation design aimed at reducing long period horizontal (tilt) noise; 4) Improvements or enhancements to station installations that improve data recovery; and 5) Lessons learned in network design and station installation: Case histories from the last few years.

*Session Chairs:* Kristine Pankow (pankow@seis.utah.edu) and David Wilson (dwilson@usgs.gov).

## Advances in Earthquake Science Using Digital Photogrammetry

Recent advances in digital photogrammetry have pushed the bounds of the quality and quantity of surficial data that researchers can collect on a small budget. Using inexpensive or open source software, researchers can now quickly create high-resolution point clouds, surface models, and orthophotos for a given area of interest. This session addresses advances in earthquake science as a result of digital photogrammetric methods. We encourage abstracts focusing on innovative applications of structure-from-motion, pixel tracking, and other image-based techniques across all scales and tectonic settings. We also welcome studies addressing the accuracy and validity of these methods.

*Session Chairs:* Nadine Reitman (nreitman@usgs.gov), Kendra Johnson (kejohnso@mines.edu), and Lia Lajoie (llajoie@mines.edu).

## Advances in Noninvasive Approaches to Characterizing Seismic Site Conditions

Site effects associated with near-surface geological conditions constitute an important part of any seismic hazard assessment. In situ measurements of shear-wave velocity (VS) are commonly used to evaluate the seismic response of sites under investigation. Traditional invasive approaches “directly” measure VS; however, these methods are often costly and (or) envi-



ronmentally prohibitive. In comparison, non-invasive methods (using body- and surface-waves) are generally more cost-effective and by nature, considered environmentally friendly. Thus, the appeal and use of non-invasive methods has significantly increased in recent years. Non-invasive methods, however, do not directly measure VS and have inherent uncertainties. The purpose of this session is to facilitate discussions about the state-of-practice in the application of non-invasive approaches for characterizing seismic site conditions and disseminate recent advances. Topics of interest include, but are not limited to: evaluation of forward algorithms, in particular, for cases of velocity inversions; the effects of lateral velocity variation; non-uniform impedance contrasts (*e.g.*, dipping or undulating bedrock subsurface, etc.); uncertainty analyses including effect(s) of data quality, and, the quantification and (or) propagation of data uncertainty; model parameterization; effective- and multi-mode analyses; non-uniqueness of inversions; advanced inversion methods (joint, 2- and 3-D, nonlinear, Monte Carlo, etc.). Presentations on applying passive seismic interferometry, and, on comparing different techniques on data from the same site and those integrating a variety of datasets are encouraged. The session conveners are members of a facilitation committee supported by the Consortium of Organizations for Strong Motion Observation Systems (COSMOS) to develop international guidelines for applying non-invasive geophysical techniques to characterize seismic site conditions. This Seismological Society of America session was developed by the COSMOS committee in coordination with conveners of the Site Effects special session of 35th General Assembly of the European Seismological Commission to be held from 5–9 September 2016 in Trieste, Italy.

COSMOS Facilitation Committee for Development of the International Guidelines for the Application of Non-invasive Geophysical Techniques to Characterize Seismic Site Conditions: Yong, Alan (Chair); Molnar, Sheri; Askan, Aysegul; Xia, Jianghai; Cassidy, John; Lawrence, Martin; Parolai, Stefano; Bindi, Dino; Wotherspoon, Liam; Mucciarelli, Marco; Albarello, Dario; Steidl, Jamison; Nigbor, Robert; Stephenson, William; Foti, Sebastiano; Socco, Laura; Cornou, Cécile; Bard, Pierre-Yves; Hollender, Fabrice; Asten, Michael; Yilmaz, Öz; Crow, Heather; Matsushima, Shinichi; Yamanaka, Hiroaki.

*Session Chairs:* Alan Yong (yong@usgs.gov), Sheri Molnar (smolnar8@uwo.ca), and Aysegul Askan (aaskan@metu.edu.tr).

### **Behavior of Structures in Subduction Zones under Long Duration Earthquakes**

Over the past few years, several large magnitude earthquakes struck Indonesia, Chile, and Japan as a result of a major subduction activity, which resulted in long duration excitations. Some stations in the 2011 Tohoku earthquake, for instance, recorded seismic activity and ground motions that lasted for almost 4 minutes (~up to 250 seconds). Severe structural damage was observed in the build environment and infrastructures due to such devastating events. The objective of this session is

to present the latest research activities that focused on analyzing the structural damage and causes of failure associated with long duration earthquakes in different sectors of the build environment that include buildings, bridges, pipelines, power transmission and distribution lines...etc. Some topics of particular interest are: case studies and failure analysis of concrete, steel, and masonry structures damage during the recent Chile and Japan earthquakes; analytical and computational studies that utilized the published long duration records from recent subduction earthquakes; comparative structural performance of structures under short and long duration earthquakes. However, relevant work that considered application of long duration recorded or synthetic ground motions to structures performance and seismic behavior is also encouraged.

*Session Chair:* Mohamed Moustafa (mmoustafa@unr.edu).

### **Characterizing the Stress Field and Stress Drop for Earthquake Source Physics and Hazard Assessment**

Accurate estimation of the state of stress and pore fluid pressure within a region is becoming of increased importance due to their role in earthquake nucleation and propagation. The main purpose of this session is to bring together researchers focused on the characterization of the stress field and its relevance to earthquake source physics, seismic hazard and/or reservoir geomechanics. Of particular interest will be to link estimations from seismology of the stress field and pore pressure with state-of-the-art modelling techniques. Studies from both natural and anthropogenic seismicity are encouraged. Contributions may regard (but are not limited to) studies of: 1) New methodologies to improve characterization of stress field orientation, stress magnitudes and pore pressure. 2) Analysis of the main factors perturbing the stress field (*e.g.* large earthquakes, anthropogenic activities, temperature changes), implications of these perturbations and their spatio-temporal extent. 3) How the main regional fault orientation with respect to the local/regional stress field affects the seismic hazard. 4) Stress heterogeneity at different scales and potential relation with earthquake source physics (*e.g.* stress drop, b-value). 5) Characterization of the stress field at global, regional (*e.g.* near large faults or subductions zones) and local scale (*e.g.* in relation to man-made perturbations). 6) The role of the background stress field and pore pressure for earthquake triggering via stress redistribution.

*Session Chairs:* Patricia Martínez-Garzón (patricia@gfz-potsdam.de), Jeanne Hardebeck (jhardebeck@usgs.gov), Marco Bohnhoff (bohnhoff@gfz-potsdam.de), and Karen Luttrell (kluttrell@lsu.edu).

### **Citizen Seismology: Citizens as an Information Source to Advance Earthquake Response and Science**

When earthquakes strike they can instantly focus millions of people's attention on a single, common event. In times like

these people are compelled to share their experiences and help others. Almost since the inception of seismology scientists have used these shared observations to advance earthquake science. The proliferate use of the Internet, social media, and mobile phone based applications has increased the access, speed, and volume of this information opening up new data sources for both rapid assessment of an earthquake's effects and for further in-depth study. Citizens provide information to seismologists directly by hosting seismometers and filling in online forms about first hand experiences, both are used to create derived information products. Also, devices such as inexpensive mems sensors, attached to desktop computers or in mobile devices, hold the possibility of greatly increasing monitoring coverage and public participation. Citizens also help seismologists indirectly when using social media and creating heavy traffic at earthquake websites which seismologists monitor to produce rapid earthquake detections and for gathering early reports of damage and impact. We invite contributors to share how they are tapping into citizen sourced data streams and integrating this information into their science both for real-time response and historical studies. We also encourage contributions on ways to better engage with citizens to improve our science and enable better use of earthquake information products.

*Session Chairs:* Michelle Guy (mguy@usgs.gov) and Remy Bossu (bossu@emsc-csem.org).

## **Complexities in Site Response**

Assessing and mapping seismic shaking hazards requires estimating site response, perhaps including potential soil-structure interaction. Whether there is an abundance or a scarcity of geostatistical and seismological analyses, the effects of deep and shallow structures add complexity to the task. This session pulls together a variety of innovative data sets and approaches that gain some control over the complexity.

*Session Chair:* John Louie (johnlouie@gmail.com).

## **Deep Earthquakes and Surrounding Slab Structures**

About 25% of global seismicity happens below 70km, mostly within subducted slabs. Their rupture mechanisms under the high confining pressures and temperatures are still enigmatic. To make a significant progress, we need to understand both the source properties and the hosting slab environment (*e.g.*, pressure, temperature, mineral phase). For example, what are the variations and controlling factors of deep rupture properties (*e.g.*, rupture speed, stress drop)? Where do deep earthquakes nucleate/rupture with respect to the internal structure of the subducted slab? Does subducted slab provide the required ingredients for the proposed rupture mechanisms (*e.g.*, dehydration embrittlement, transformational faulting, and shear thermal instability)? Seismic images of deep earthquakes and slab structures are continuously improving with new data/methods. In this session, we would like to bring these two

aspects together to shed more light on deep earthquake physics. We welcome contributions about seismic observations, laboratory experiments, and numerical simulations related to deep earthquakes.

*Session Chairs:* Zhongwen Zhan (zwzhan@gps.caltech.edu), Meghan S. Miller (msmiller@usc.edu), and Germán Prieto (gprieto@mit.edu).

## **Earthquake Early Warning: Network Design, Implementation, Production and Outreach**

This session focuses on recent and future efforts to design and implement earthquake early warning systems worldwide. Submissions addressing the variety of earthquake detection algorithms, network design for robust data delivery, and outreach efforts are encouraged. Multi-hazard networks that address early ignition detection for wildfire and other monitoring systems such as extreme weather would also benefit this session.

*Session Chairs:* Graham Kent (gkent@unr.edu) and Ken Smith (ken@unr.edu).

## **Earthquake Source Parameters and Slip from Seismic, Geodetic and Laboratory Data: Theory, Observations and Interpretations**

Understanding origin and spatio-temporal evolution of seismicity and deformation needs a careful quantitative analysis of earthquake source parameters for large sets of earthquakes in studied seismic sequences. Determining focal mechanisms, seismic moment tensors, slip distributions, radiated energy, aseismic deformation and other earthquake source properties and establishing their mutual relations can give an insight into tectonic stress and crustal strength in the area under study, material properties and prevailing fracturing mode (shear/tensile) in the focal zone, and other details of the earthquake source processes. Studying the relationship between static and dynamic parameters with earthquake size is essential to understanding the self-similarity of earthquakes and the scaling laws but also to help improve our ground motion prediction equations. The session aims to focus on methodological and observational aspects of estimating earthquake source parameters of natural or induced earthquakes on various scales from large to small earthquakes including laboratory experiments which can provide an opportunity to analyze seismic sources under partially controlled conditions. Presentations of new approaches to determining focal mechanisms, seismic moment tensors and other source parameters as well as interpretations of the source parameters for sets of earthquakes in case studies are welcome. Equally, contributions about self-similarity of earthquakes down to very small ruptures and about scaling relations for static and dynamic parameters of earthquakes are invited.

*Session Chairs:* Vaclav Vavrycuk (vv@ig.cas.cz), Grzegorz Kwiatek (kwiatek@gfz-potsdam.de), and German Prieto (gprieto@mit.edu).

## Ground Motion Spatial Variability: Models, Methods and Impacts

The spatial correlation structure of earthquake ground-motions is widely recognized as a manifestation of the complexity of the wavefield and as exerting substantial influence on losses to distributed inventories (portfolios) of structures and infrastructure. Different strategies for representing and understanding spatial variability are employed—depending on needs and circumstances—and range from purely-empirical parametric analyses of intensity measures (IMs) to full-waveform numerical simulations. To date, forward calculations of site-to-site IM correlations needed for loss estimation and risk analyses are often (and presumably successfully) represented with empirical spatial correlation functions. As the sophistication of ground motion modeling increases, variability previously considered random becomes attributable to knowable source, path and site effects. In principle then, spatial-correlation of the stochastic component of the wavefield must be adjusted to be commensurate with the sophistication of the ground motion model, which is critically important for seismic hazard analysis. We encourage submissions focusing on empirical and numerical calibration of spatial variability, analyses of the physical factors that control variability, and strategies for including the effects of variability on loss calculations.

*Session Chairs:* David Wald (wald@usgs.gov), Kim Olsen (kbolsen@mail.sdsu.edu), Jack Baker (bakerjw@stanford.edu), and Paolo Bazzurro (paolo.bazzurro@iusspavia.it).

## How Close are We to an Eruption?

This session seeks to explore how seismology can contribute to the question, “How close are we to an eruption?” As geophysical networks on volcanoes expand throughout the world, we are becoming better and better at detecting unrest. While useful in determining that the volcanic hazard has increased, the question of eruption timing still remains, and is most important to impacted populations and government officials. We invite submissions to this session that help shed light on new or repurposed techniques that may lead to a better sense of the “critical” state of a volcanic system and when it might erupt or escalate in activity.

*Session Chairs:* Weston Thelen (wthelen@usgs.gov) and Matthew Haney (mhaney@usgs.gov).

## Induced Seismicity

In the past decades, induced and triggered seismicity associated with anthropogenic activity has attracted considerable interest among citizens and scientists in Europe and North America. Understanding this seismicity is a key challenge for many applications. There is evidence that hydraulic fracturing (HF) is a dominant driver for fluid-induced seismicity in some areas. Although the general, physical mechanisms of injection induced seismicity are known, the specific conditions that

lead to earthquake triggering up to Mw 5.6 in case of waste water injection and ML 4.6 for HF are not as well understood. Seismicity is also observed in connection with geothermal energy production, waste water-injection, geothermal production, and carbon sequestration. Key questions include: - What controls the dynamics of induced earthquakes, the maximum magnitude and the total amount of seismic energy release? - How do they start, and are induced earthquakes different from tectonic slip processes? - What methods can be used to distinguish natural and induced earthquakes? The answers to these questions have implications for seismic hazard assessment and may help guide mitigation approaches. We invite numerical, observational and laboratory contributions from a variety of research areas such as geomechanical modeling, ground motion observations, source characterization studies, and seismic hazard assessment. Papers focusing on industry practices and public outreach are welcome to better inform the research community about recent developments.

*Session Chairs:* Thomas Braun (thomas.braun@ingv.it), Ivan G. Wong (Ivan.Wong@AECOM.com), Justin Rubinstein (jrubinstein@usgs.gov), Thomas Goebel (tgoebel@ucsc.edu), David Eaton (eatond@ucalgary.ca), Gail Atkinson (gmatkinson@aol.com), and Honn Kao (honn.kao@canada.ca).

## Induced Seismicity Monitoring: What is Really Needed?

There is now heightened concern from regulators, and the general public, over the real or perceived impact of unconventional oil and gas production operations on local seismicity. In Alberta and British Columbia, where fracking operations are believed to have caused a significant increase in the number of induced earthquakes, regulations have been introduced that requires Frac Operators to monitor all seismic activity and to report any local magnitude events greater than 2 and stop operations over 4. Many other jurisdictions—including Ohio, Australia and Holland—have either banned fracking or introduced new regulations that often maintain steep fines should oil and gas producers cause damage or fail to report potentially damaging seismic activities. It is important to understand the state of seismic induced monitoring technology to detect and monitor seismic activity vis-à-vis the regulatory requirements to monitor and report.

Topics of interest to address include: (1) the various technologies to monitor induced seismicity; (2) methods to distinguish natural and induced earthquakes; (3) the current regulations to monitor and report seismic activity; (4) the current traffic light reporting system used in many jurisdictions; (5) how to estimate magnitude, distance and resolution.

We invite papers on all forms of induced seismicity monitoring, the advancing technologies and underlying regulatory requirements. Papers from industry and governmental agencies are particularly welcome to develop a better framework for seismic induced monitoring in the Oil and Gas Industry.

*Session Chairs:* Iain Weir-Jones (iainw@weir-jones.com) and Steven Taylor (srt-rmg@comcast.net).



## The M7.1 Iniskin Earthquake, Alaska

The most significant earthquake in half a century in the Cook Inlet region of Alaska occurred on January 24, 2016. The  $M_w$  7.1 earthquake occurred in the subducting Pacific Plate at a depth of 123km beneath the Iniskin Peninsula. The earthquake was felt throughout mainland Alaska and caused isolated damages in towns 100 km away on the Kenai Peninsula. Most damage was caused by slumping soils and a ruptured natural gas line with minor damage attributed directly to the shaking. Moment tensor solutions indicate a minimum stress direction roughly parallel to slab dip. Aftershocks map out a near-vertical fault plane striking northeast. These orientations are consistent with normal faulting in the Pacific Plate, reflecting relative tension in the direction of slab dip. The earthquake occurred in a region of prodigious intermediate-depth seismicity where the slab bends to accommodate flat slab subduction immediately to the northeast. The aftershock region abuts a highly similar M6.4 earthquake that occurred six months prior, strongly suggesting a relationship. Finite fault modeling suggests slip of 2-3 m on a patch 20-30 km in diameter, consistent with the aftershock zone. Because of the depth and orientation, static displacements are largest 100 km east on the Kenai Peninsula. Instrumental and anecdotal reports of ground motion were highly variable and consistent with the directionality of the source. Felt reports are limited in the immediate vicinity of the epicenter, but seem to confirm the instrumental record of relatively modest ground motion directly above the source. The overlying Cook Inlet sedimentary basin profoundly influenced ground motions to the east and north of the epicenter. This is the strongest earthquake recorded to date by the cooperative free field and structural strong motion stations in Anchorage, 250km northeast of the epicenter. Recorded peak ground accelerations in Anchorage varied from 3-15% g across distances of just 1-2 km. In-structure accelerations exceeded 18% g. Several of the seismic stations closest to the source had been installed just a few months prior as part of the EarthScope USArray project. The earthquake provided a sensitivity test for new posthole instrumentation and installation methods.

*Session Chair:* Michael West (mewest@alaska.edu).

## Machine Learning and its Application to Earthquake and Explosion Signal Analysis

This session focuses on the application of machine learning techniques to the analysis of seismic, infrasound, hydro-acoustic, remote sensing, electromagnetic, and other signals. The goals of machine learning applied to these signals include improved signal and event detection, phase identification, event discrimination, signal association, explosive yield estimation, and general signal characterization.

*Session Chair:* Timothy Draelos (tjdrael@sandia.gov).

## Marine Paleoseismology: Assessing Offshore Hazards

New geophysical approaches have provided unprecedented images of seafloor fault systems. These data together will targeted sampling strategies employing AUVs and ROVs as well as more traditional shipboard coring efforts place important constraints on fault history. We encourage submissions that present new geological and geophysical data of marine fault systems, specifically new constraints on slip rates, most recent event (MRE), and recurrence interval. Despite recent efforts offshore, marine seismological hazards [rendriscoll@ucsd.edu](mailto:rendriscoll@ucsd.edu) remain poorly constrained and future efforts need to marshal our resources to understand better these marine fault systems and the attendant hazard.

*Session Chair:* Neal Driscoll ([ndriscoll@ucsd.edu](mailto:ndriscoll@ucsd.edu)).

## Multi-Phenomenology Approaches to Explosion Source Studies

To accurately predict far field observations used in explosion monitoring, it is necessary to first understand signal generation by explosion sources and then effectively relate those generated signals to remote/far-field observations. Incorporating near-field observations, comprehensive material properties, and subsurface imaging into first-principle calculations is critical to that first step. At the same time, testing of models by comparison with both near and far field predictions is necessary to refinement of the models, and validation of hypotheses concerning explosion signal generation. Quantification of uncertainties due to propagation is essential to understanding the constraints that far field observations can place on generation, and quantification of uncertainties due to generation, propagation, and measurement is essential to development of practical monitoring tools. We invite contributions from all research focus areas and technologies that meld efforts described above.

*Session Chairs:* Catherine Snelson ([snelsonc@lanl.gov](mailto:snelsonc@lanl.gov)), Christopher Bradley ([cbradley@lanl.gov](mailto:cbradley@lanl.gov)), and G. Eli Baker ([glenn.baker.3@us.af.mil](mailto:glenn.baker.3@us.af.mil)).

## Multidisciplinary Studies of Earthquakes - Slow, Fast, and In Between: A Broad Range of Fault Behavior in Space and Time

Faults show a variety of motion over a range of spatiotemporal scale and frictional regime. It includes large damaging earthquakes in the seismogenic zone, slow earthquakes at the edges of the seismogenic zone, tsunamigenic earthquakes near the subduction trench and so on. How they influence and interact with each other, however, remain enigmatic. There are indications that slow slip precedes large damaging megathrust earthquakes in some cases. Regular fast earthquake results in changes in behavior of slow earthquakes. Repeated slow earthquakes load the updip seismogenic part that nucleates large destructive earthquakes. While these findings are compelling, the underlying physics is poorly understood. Controls of fault



rheology on different modes of fault slip over a range of pressure and temperature and its effects on the seismic cycles are largely unknown. I invite studies aiming to understand the broad nature of fault slip and their implications on seismic hazard based on theory, observation, modeling, field and/or laboratory experiments. In-depth studies focusing on mechanism of diverse modes of fault slip including but not limited to slow slip, tremor, swarms, repeating earthquakes in all tectonic settings are welcome. I encourage holistic studies involving a wide spectrum of fault slip behavior.

*Session Chair:* Abhijit Ghosh (aghosh.earth@gmail.com).

### **Near Field and Directivity Considerations in Developing Fault Normal and Fault Parallel Spectra and Selecting and Scaling Time Histories for Nonlinear Analysis**

Building codes for new and existing buildings require that for sites within 5 km of a fault (near field), both fault normal (FN) and fault parallel (FP) spectra are developed and time histories should be rotated to FN and FP components. However, besides the permissibility of taking maximum direction spectrum as the FN component and the geometric mean spectrum as the FP spectrum in ASCE 41-13, there are no particular guidelines how to develop the FN and FP spectra. In addition, codes require that for near field conditions, time histories shall be rotated to FN and FP components. However, there are three significant issues related to ground motions in near field situations: 1) Forward directivity; 2) ground motion orientation (FN and FP); and 3) velocity pulse effects. Forward directivity effects have been observed for distances up to 25 to 30 km and both velocity pulse effects and differences in FN and FP motions have been observed for distances greater than 5 km. In addition, it has been observed that FN motions may not represent the larger component as previously thought. In order to obtain true FN and FP motions, time histories should be rotated to major and minor principal axes. This session will entertain presentations and posters describing proposed procedures for developing FN and FP spectra and recent developments in incorporating near field and directivity effects into selecting and then scaling/spectra matching of time histories for nonlinear analysis.

*Session Chair:* Zia Zafir (zzafir@kleinfelder.com).

### **NGA-East: Research Results and Ground-Motion Characterization Products for Central and Eastern North America**

The Next Generation Attenuation project for Central and Eastern North America (NGA-East) is a major multi-disciplinary project coordinated by the Pacific Earthquake Engineering Research Center (PEER). NGA-East was tasked to develop a new ground-motion characterization (GMC) model for the Central and Eastern North-America (CENA) region. The GMC model consists in a set of ground motion models (GMMs, aka GMPEs) for median and standard deviation of ground motions and their associated weights, combined into

logic-trees for use in probabilistic seismic hazard analyses (PSHA). NGA-East tackled the complex task of characterizing ground motions with a limited recording dataset. One key solution strategy was to rely on ground-motion simulations to supplement the available data. Important scientific issues were addressed through targeted research projects on topics such as the regionalization of seismic source, path and attenuation of motions, the treatment of variability and uncertainties and on the evaluation of site effects. Seven working groups were formed to cover the complexity and breadth of topics in the NGA-East project, each focused on a specific technical area. Through its multi-year span, NGA-East developed a comprehensive database of ground-motion records, numerous interim products for the quantification of ground motions in CENA as well as new GMMs. This session aims to cover the recent scientific advances and ground-motion products that emerged from NGA-East.

*Session Chairs:* Christine Goulet (goulet@berkeley.edu) and Yousef Bozorgnia (yousef@berkeley.edu).

### **Numerical Modeling of Earthquake Ground Motion, Rupture Dynamics and Seismic Wave Propagation**

Continuous development of numerical modeling methodology in seismology is not only driven by emerging requirements in observational seismology (*e.g.*, the advent of very dense seismic arrays; demand for near-real-time simulations; the multi-scale, multi-physics modeling of seismic phenomena; etc.), but also by developments in the mathematical sciences, and through the adaptation of methods originating in other scientific fields. Moreover, future methods for very large scale simulations will be increasingly influenced by (and may in turn influence) the evolution of computer architectures and programming models.

This session is a forum for presenting advances in numerical methodology, whether the principal context is observational, mathematical/numerical, or computational.

We invite contributions focused on development, verification and validation of numerical-modeling methods, and methodologically important applications, especially to earthquake ground motion and rupture dynamics (both single-event and event-sequence models). Contributions on the analysis of methods, fast algorithms, high-performance implementations, large-scale simulations, non-linear behavior, multi-scale problems, and confrontation of methods with data are especially encouraged.

*Session Chairs:* Peter Moczo (moczo@fmph.uniba.sk), Steven Day (sday@mail.sdsu.edu), Emmanuel Chaljub (Emmanuel.Chaljub@ujf-grenoble.fr), and Jozef Kristek (kristek@fmph.uniba.sk).

### **Past and Future Seismic Moment Release: Contributions from Statistics and Geodesy**

Reliable estimations of past earthquake moment release and its projection into the future are important from a theoretical perspective as well as for immediate practical use in earthquake

hazard assessments. A long-standing issue is the typically large discrepancy between geodetic moment rate estimations and observed rates of seismic moment release reported in various tectonic environments with high seismic activity. Another question that has received attention is whether the large moment release in the last decade is a statistically significant deviation from a long-term expectation. This session proposes a forum for an inter-disciplinary dialog among experts in geodesy, seismology, and statistics to revisit these issues and address the following questions: How reliable are geodetic moment rate estimates given the unknowns in the strain-to-moment rate conversion? How to construct robust projections of seismic moment release with different time spans (years to hundreds of years) and spatial resolution? How to relate the existing estimations of geodetic and seismic moment release in different regions? We also welcome theoretical and observational studies that address closely related problems: estimating the regional maximal magnitude, testing the hypothesis of clustering of the largest earthquakes, developing approaches to assess seismic coupling, and more.

*Session Chairs:* Corné Kreemer (kreemer@unr.edu) and Ilya Zaliapin (zal@unr.edu).

### **Physical and Statistical Properties of Earthquake Swarms and Clustered Seismicity: Constraining Driving Mechanisms**

Earthquake swarms, seismicity sequences clustered in space and time that lack a clear mainshock, are poorly understood phenomena. Swarms are less well studied than mainshock-aftershock sequences, perhaps due to moderate ( $\sim M5$ ) maximum magnitudes that cause relatively little damage. However, swarms near population centers generate public interest in complex earthquake processes and potentially pose a higher short-term hazard. The recent surge in induced seismicity has ignited research on moderate earthquake swarms, with particular focus on fluid diffusion and migration as the driving mechanism. We invite contributions that characterize physical and statistical properties of earthquake swarms and clustered seismicity and address the following questions: What mechanisms control the size and occurrence of moderate earthquake swarms? What criteria identify fluid diffusion, or distinguish it from other mechanisms? Do the inherent physical and statistical properties of a swarm, and the earthquakes therein, vary with driving mechanism? Submissions from observational seismology, clustering and earthquake statistics, earthquake source physics, and earthquake triggering and interaction studies are welcome.

*Session Chairs:* Christine Ruhl (christineruhl@gmail.com), Ilya Zaliapin (zal@unr.edu), and Rachel Abercrombie (rea@bu.edu).

### **Research Efforts to Improve Regulatory Performance for Induced Seismicity**

In response to the occurrence of relatively large (and felt) earthquakes that are potentially induced by man-made activi-

ties, there is an increasing trend for the industry and government regulators to include a “traffic light” system in their decision-making process. Despite its significant implications to the cost of operations and the protection of public safety, the protocol that defines the different scenarios for different lights (“green”, “yellow”, or “red”) has not been thoroughly validated to truly reflect the associated seismic risk. Most government regulators adopt a traffic light protocol (TLP) that depends on both local community reports and the magnitude of the earthquake, despite significant scatter and uncertainties for local magnitude calculations. Contributions are invited on all topics related to improving regulatory performance for induced seismicity, including hazard analysis, new innovations and mitigation measures.

*Session Chairs:* David Eaton (eatond@ucalgary.ca), Honn Kao (honn.kao@canada.ca), and Gail Atkinson (gmatkinson@aol.com).

### **Risk Management Applications of Earthquake Seismology**

In this session, we invite professionals working around risk management, or the science support teams thereof, to come and present what aspects of earthquake seismology they currently use, or wish they could get access to, or wish they had very quantitative estimates of. The academic community needs to learn from you when a qualitative picture is all you need, vs expected values at a point, vs probability density functions at a point, vs joint probabilities along lifelines or in a region. The properties of interest might be *e.g.*, surface fault displacement during an event of some probability of occurrence, or surface deformation due to same event, or ground motion, or liquefaction, or hypocenter location. It would be helpful to set the context for the use of these properties, whether it is for decision-making procedures, or to assess needs for risk transfer. We welcome all underwriters, actuaries (or science support team thereof), investors (in catastrophe bonds), members of teams of urban resiliency officers, emergency managers, engineers, etc. We encourage the presentation of actual processes or case studies where a currently unmet earthquake science need was identified, or success stories where the need was met and integrated into a strategy or process. What format was used to transfer science information? We also welcome members of the academic community who want to present new datasets formerly not available, which they think could start playing a major role in any one of the many facets of risk management.

*Session Chairs:* Delphine Fitzenz (delphine.fitzenz@rms.com) and Nico Luco (nluco@usgs.gov).

### **The Role of Shallow Slip on Faults**

Resolving the spatial and temporal distribution of shallow fault slip is difficult since only the most near-field data are sensitive to shallow slip. Complicating these analyses is the fact that near-field data are rare: seismic and GPS station spacing is often too sparse, and interferograms tend to decorrelate near the rup-

ture zone. But new datasets (including LiDAR, UAVSAR, new SAR satellites with shorter repeat times, and various types of optical imagery) are providing unprecedented, spatially dense, near-field observations. These new observations are allowing for a new generation of high-resolution shallow slip models which, in turn, are leading to new discoveries in the rheology and evolving deformation of fault zones. We invite presentations that look at innovative data sources and analyses (including methods for integrating near-field data that image the shallow parts of the fault with far-field data that are sensitive to deeper slip), advances in modeling methods, and case studies of shallow slip before, during, and after earthquakes.

*Session Chairs:* Sarah Minson (sminson@usgs.gov), Benjamin Brooks (bbrooks@usgs.gov), and Jessica Murray (jrmurray@usgs.gov).

## Secondary Earthquake Hazards and Losses

Secondary hazards, such as landslides and liquefaction, can result in significant losses but are not often included in hazard and loss assessments. Developing reliable models requires consistent documentation of event inventories and new advances in modeling techniques. General approaches to hazard modeling include physical, statistical, and heuristic models. Losses are typically accounted for through the use of fragility curves. The choice of modeling strategy is often determined by the application. For example, rapid response products may require different strategies than long term hazard assessments. The quality of inventories that are used for model development is highly variable both in terms of the resolution and attributes that are documented. This creates a challenge for developing and assessing models across many events.

We encourage contributions on 1) hazard and loss modeling strategies, including probabilistic and event-specific analyses; 2) datasets, including both inventories and complementary data, such as estimates of seismic loading and geologic/climatic conditions; and 3) issues related to synthesizing inconsistent datasets.

*Session Chairs:* Eric Thompson (emthompson@usgs.gov) and Kate Allstadt (kallstadt@usgs.gov).

## Seismicity and Seismic Hazards of the Walker Lane and Western Great Basin

The region along and within the eastern side of the Sierra Nevada Mountains, from the Mojave Desert to southern Oregon, and extending a couple hundred kilometers into Nevada, is a prominent region of high hazards on the National Seismic Hazard Map. The region is characterized by distributed extensional and strike-slip faults. It experienced earthquakes with magnitudes  $\sim 7$  in 1872, 1915, 1932, and 1954. Geodetic studies find that  $\sim 20$ - $25\%$  of the total deformation between the interiors of the North American and the Pacific plates take place in this region. Much has been learned about the seismic hazards of the region. However, the faults that accommodate the deformation may not all be identified, while slip rates and earthquake

magnitudes on many known faults have large uncertainties. Some strain is partitioned through southern Nevada from the Walker Lane to the Wasatch fault system, but the mechanism and rate of this process, and its implication for hazards in Las Vegas is uncertain. Heterogeneous path effects due to the basin and range geology, together with highly variable site conditions, complicate ground motion prediction. Normal faults dip underneath the urban areas, including the spectacular Genoa - Mt. Rose system that dips beneath Carson City and Reno and the Frenchman Mountain fault that dips beneath Las Vegas, but the fault and basin geometries, expected ground motions, and other urban earthquake-related hazards, require more research. This session invites contributions related to all aspects of the seismic hazard of the region, including paleoseismology, seismicity, geodesy, and ground motions.

*Session Chairs:* John Anderson (jga@unr.edu), John Louie (louie@seismo.unr.edu), Richard Koehler (rkoehler3@gmail.com), Corné Kreemer (kreemer@unr.edu), and Wanda Taylor (wanda.taylor@unlv.edu).

## Seismo-Acoustics and Infrasound

We invite any contribution that addresses the broad topic areas of seismo-acoustics or infrasound. This session intends to capture any research associated with atmospheric infrasound including sensors, signal analysis, propagation studies, and modeling in addition to any seismological research that isn't capped at the free surface.

*Session Chairs:* Stephen Arrowsmith (sjarrow@sandia.gov) and Omar Marcillo (omarcillo@lanl.gov).

## Seismotectonics Beyond the Plate Boundary

In the past decade, the passage of the USArray across the United States and the drastic increase in induced seismicity in the mid-continent have provided unprecedented opportunities to understand the physical and seismotectonic state of the lithosphere. We hope to bring together researchers interested in the state of stress, crustal and upper mantle structure and the interaction between ancient features and modern strain, intra-plate fault properties, and ultimately the geodynamic context of both natural and induced seismicity in continental interiors, both in North America and worldwide.

*Session Chairs:* Will Levandowski (wlevandowski@usgs.gov), Christine Powell (capowell@memphis.edu), and Oliver Boyd (olboyd@usgs.gov).

## Short and Long-Term Deformation on Active Faults: Integrating Geodetic, Geologic and Seismic Constraints on Slip Rates and Off-fault Deformation in the Walker Lane and Beyond

Developing a complete and accurate understanding of the hazards posed by earthquakes increasingly relies on a framework that integrates data from geologic, seismic, and geodetic studies of faults. Each of these datasets has key strengths and weak-



nesses which can be addressed through comparison with the others. A growing body of evidence based on such comparisons suggests that some fraction of the plate boundary zone deformation budget is aseismic or occurs in a manner not recorded in the geologic or seismic record of slip on the trace major faults. Similarly, it is often unclear how geodetically-measured surface strain relates to earthquake potential. Thus these disagreements represent opportunities to gain a better understanding of the processes and strain budgets of earthquakes, and the modes of active crustal deformation. This session will focus on new constraints and analyses on patterns, style and rates of deformation that are the basis for comparison of fault behavior across the earthquake cycle, from strain accumulation to release. We welcome contributions on earthquake geology, paleoseismology, neotectonics, LiDAR, GPS, InSAR or other measurements that improve understanding of the behavior of active faults, especially integrative studies that shed new light on complete deformation budgets.

*Session Chairs:* William Hammond (whammond@unr.edu), Rich Briggs (rbriggs@usgs.gov), Rich Koehler (rkoehler3@gmail.com), and Corné Kreemer (cornelisk@unr.edu).

### **Theoretical and Methodological Innovations for 3D/4D Seismic Imaging of Near-Surface, Crustal, and Global Scales**

This session will focus on recent theoretical and methodological developments of seismic imaging and monitoring (*i.e.*, time-resolved imaging) techniques to better understand the Earth's structure on various scales. In previous years, imaging techniques have developed rapidly thanks to the advent of high-density networks, new modeling techniques, and unprecedented computation capacities. This includes, for example, seismic noise surface wave tomography, precise location of the sources of microseismic events, and full-wave inversion with active sources. However, significant problems, both well-known and lesser-known, remain. These include model resolution, uncertainty, repeatability, nonlinearity, and non-uniqueness.

We invite novel approaches for solving common practical problems for 3D/4D imaging. To this regard, we welcome innovations and advances in physics-based imaging, 3D/4D tomography, waveform tomography, effects of structure outside the modeled region, uneven ray coverage, new migration techniques, advanced signal processing, multi-component seismic noise correlations, monitoring and locating of velocity changes, and joint inversion of multiple geophysical observations. Studies that compare real-Earth results obtained using different methods, and assess repeatability, are particularly encouraged as well as methods of unique seismic data acquisition and instrumental studies.

*Session Chairs:* Marco Pilz (marco.pilz@sed.ethz.ch) and Nori Nakata (nnakata@stanford.edu).

### **Tsunami Resilience Strategies: Application of Tsunami Science and Mitigation Advancements to Protect Communities**

New techniques and technologies are being developed to mitigate the impacts of tsunami hazards. Evaluation of recent tsunamis have led to an influx in both new scientific data and improved community preparedness and planning activities. Availability of detailed geological and geophysical data sets from past and recent events has improved tsunami source characterization, numerical analyses, and hazard mapping. Advanced tsunami engineering, vulnerability, and risk analysis products are being utilized by emergency managers, maritime communities, land-use planners, and design and building code producers. The use of real-time tsunami hazard analysis products and decision making tools, alongside community preparedness, will improve life-safety worldwide. This session will focus on new tsunami hazard assessment information and the application of techniques and technologies into mitigation efforts and their effect on community resilience

*Session Chairs:* Rick Wilson (Rick.Wilson@conservation.ca.gov), Kevin Miller (Kevin.Miller@caloes.ca.gov), and Lori Dengler (Lori.Dengler@humboldt.edu).

### **Upper Crustal Passive Imaging for Hazards and Exploration**

Recent years have seen a proliferation of passive seismic methods for assessing velocities at upper-crustal depths of 0.1 to 10 kilometers. These new methods are starting to find application to the imaging of upper-crustal geologic structures. Two of these applications of passive imaging are becoming popular: 1) obtaining the shear-velocity structure of urban basins for prediction of earthquake shaking; and 2) imaging stratigraphy and structure of sedimentary basins containing fluid energy reserves such as oil, gas, and geothermal brine. In the earthquake-hazard application, SPAC and Deep ReMi surveys are adding to well-established surface-wave dispersion analyses of empirical Green's functions (EGFs) derived from passive data recorded on monitoring networks. In the energy-exploration application, EGFs derived from passive recordings are augmenting the well-established virtual-source techniques that use EGFs derived from active-source records. Some passive exploration efforts are able to derive P-wave reflections from the EGFs, in addition to the standard surface-wave group velocities. For this session, we welcome contributions on passive-imaging theory, recording and data-processing techniques, or imaging results; focusing on upper-crustal depths of 0.1 to 10 kilometers. Case histories showing how passive imaging can improve hazard mapping, or compare to active-source imaging results, are particularly welcome.

*Session Chairs:* John Louie (louie@seismo.unr.edu) and Ileana Tibuleac (imtseismic@yahoo.com).



# Overview of Technical Program

## ORAL SESSIONS

### Wednesday, 20 April

<i>Time</i>	<i>Tuscany 1/2</i>	<i>Tuscany 3/4</i>	<i>Tuscany 5/6</i>	<i>Tuscany 7/8</i>	<i>Tuscany A</i>
8:30–9:45 AM	Advances in Noninvasive Approaches to Characterizing Seismic Site Conditions	Seismotectonics Beyond the Plate Boundary	Past and Future Seismic Moment Release: Contributions from Statistics and Geodesy	Multidisciplinary Studies of Earthquakes— Slow, Fast, and In Between: A Broad Range of Fault Behavior in Space and Time	Induced Seismicity
10:45 AM–noon					
2:15–3:30 PM	Earthquake Early Warning: Network Design, Implementation, Production and Outreach	Ground Motion Spatial Variability: Models, Methods and Impacts	Theoretical and Methodological Innovations for 3D/4D Seismic Imaging of Near-Surface, Crustal, and Global Scales	Near Field and Directivity Considerations in Developing Fault Normal and Fault Parallel Spectra and Selecting and Scaling Time Histories for Nonlinear Analysis	
4:30–5:45 PM				How Close are We to an Eruption?	
7:30–8:30 PM	The M7.1 Iniskin Earthquake, Alaska • Tuscany A				

### Thursday, 21 April

<i>Time</i>	<i>Tuscany 1/2</i>	<i>Tuscany 3/4</i>	<i>Tuscany 5/6</i>	<i>Tuscany 7/8</i>	<i>Tuscany A</i>
8:30–9:45 AM	Induced Seismicity Monitoring: What is Really Needed?	Machine Learning and its Application to Earthquake and Explosion Signal Analysis	The Role of Shallow Slip on Faults	Tsunami Resilience Strategies: Application of Tsunami Science and Mitigation Advancements to Protect Communities	Active Tectonics, Faults and Large Earthquakes
10:45 AM–noon	Marine Paleoseismology: Assessing Offshore Hazards	Seismo-Acoustics and Infrasonics			
1:30–2:45 PM	Multi-Phenomenology Approaches to Explosion Source Studies	Numerical Modeling of Earthquake Ground Motion, Rupture Dynamics and Seismic Wave Propagation	Characterizing the Stress Field and Stress Drop for Earthquake Source Physics and Hazard Assessment	Advancements in Network Operations and Station Design	
3:45–5:00 PM					
5:15 PM	Joyner Lecture • Naples Ballroom				

## Friday, 21 April

<i>Time</i>	<i>Tuscany 1/2</i>	<i>Tuscany 3/4</i>	<i>Tuscany 5/6</i>	<i>Tuscany 7/8</i>	<i>Tuscany A</i>
8:30–9:45 AM	Earthquake Source Parameters and Slip from Seismic, Geodetic and Laboratory	Deep Earthquakes and Surrounding Slab Structures	Secondary Earthquake Hazards and Losses	NGA-East: Research Results and Ground-Motion Characterization Products for Central and Eastern North America	Seismicity and Seismic Hazards of the Walker Lane and Western Great Basin
10:45 AM–noon	Data: Theory, Observations and Interpretations		Advances in Earthquake Science Using Digital Photogrammetry		
1:30–2:45 PM		Upper Crustal Passive Imaging for Hazards and Exploration	Citizen Seismology: Citizens as an Information Source to Advance Earthquake Response and Science	Physical and Statistical Properties of Earthquake Swarms and Clustered Seismicity: Constraining Driving Mechanisms	
3:45–5:00 PM	Research Efforts to Improve Regulatory Performance for Induced Seismicity		Short- and Long-Term Deformation on Active Faults: Integrating Geodetic, Geologic and Seismic Constraints on Slip Rates and Off-fault Deformation in the Walker Lane and Beyond		

## POSTER SESSIONS

### *Tuscany F*

- Wednesday
- Advances in Noninvasive Approaches to Characterizing Seismic Site Conditions
  - Earthquake Early Warning: Network Design, Implementation, Production and Outreach
  - Ground Motion Spatial Variability: Models, Methods and Impacts
  - How Close are We to an Eruption?
  - Induced Seismicity
  - Multidisciplinary Studies of Earthquakes—Slow, Fast, and In Between: A Broad Range of Fault Behavior in Space and Time
  - Past and Future Seismic Moment Release: Contributions from Statistics and Geodesy
  - Seismotectonics Beyond the Plate Boundary
  - Theoretical and Methodological Innovations for 3D/4D Seismic Imaging of Near-Surface, Crustal, and Global Scales
  - Complexities in Site Response

## Poster Sessions (continued)

### *Tuscany F*

---

Thursday

- Active Tectonics, Faults and Large Earthquakes
- Advancements in Network Operations and Station Design
- Characterizing the Stress Field and Stress Drop for Earthquake Source Physics and Hazard Assessment
- Induced Seismicity Monitoring: What is Really Needed?
- Machine Learning and its Application to Earthquake and Explosion Signal Analysis
- Marine Paleoseismology: Assessing Offshore Hazards
- Multi-Phenomenology Approaches to Explosion Source
- Numerical Modeling of Earthquake Ground Motion, Rupture Dynamics and Seismic Wave Propagation
- Seismo-Acoustics and Infrasonic
- The Role of Shallow Slip on Faults
- Tsunami Resilience Strategies: Application of Tsunami Science and Mitigation Advancements to Protect Communities
- The M7.1 Iniskin Earthquake, Alaska

Friday

- Active Tectonics, Faults and Large Earthquakes
- Advances in Earthquake Science Using Digital Photogrammetry
- Behavior of Structures in Subduction Zones under Long Duration Earthquakes
- Citizen Seismology: Citizens as an Information Source to Advance Earthquake Response and Science
- Deep Earthquakes and Surrounding Slab Structures
- Earthquake Source Parameters and Slip from Seismic, Geodetic and Laboratory Data: Theory, Observations and Interpretations
- NGA-East: Research Results and Ground-Motion Characterization Products for Central and Eastern North America
- Physical and Statistical Properties of Earthquake Swarms and Clustered Seismicity: Constraining Driving Mechanisms
- Research Efforts to Improve Regulatory Performance for Induced Seismicity
- Risk Management Applications of Earthquake Seismology
- Secondary Earthquake Hazards and Losses
- Seismicity and Seismic Hazards of the Walker Lane and Western Great Basin
- Short- and Long-Term Deformation on Active Faults: Integrating Geodetic, Geologic and Seismic Constraints on Slip Rates and Off-fault Deformation in the Walker Lane and Beyond
- Upper Crustal Passive Imaging for Hazards and Exploration

# Program for 2016 SSA Annual Meeting

Presenting author is indicated in bold.

## Wednesday, 20 April—Oral Sessions

<i>Time</i>	<i>Tuscany 1/2</i>	<i>Tuscany 3/4</i>	<i>Tuscany 5/6</i>	<i>Tuscany 7/8</i>	<i>Tuscany A</i>
	<b>Advances in Noninvasive Approaches to Characterizing Seismic Site Conditions</b> Session Chairs: Alan Yong, Sheri Molnar, and Aysegul Askan (see page 449)	<b>Seismotectonics Beyond the Plate Boundary</b> Session Chairs: Conveners: Will Levandowski, Christine Powell, and Oliver Boyd (see page 449)	<b>Past and Future Seismic Moment Release: Contributions from Statistics and Geodesy</b> Session Chairs: Corné Kreemer and Ilya Zaliapin (see page 458)	<b>Multidisciplinary Studies of Earthquakes—Slow, Fast, and In Between: A Broad Range of Fault Behavior in Space and Time</b> Session Chair: Abhijit Ghosh (see page 462)	<b>Induced Seismicity</b> Session Chairs: Thomas Braun, Ivan G. Wong, Justin Rubinstein, Thomas Goebel, David Eaton, Gail Atkinson, and Honn Kao (see page 466)
8:30 AM	Site Response Implications Associated with Common Methods used to Account for Vs Profile Uncertainty. <b>Cox, B. R.</b> , Teague, D. P.	Damaged Crust and Concentrations of North American Intraplate Seismic Zones. Thomas, W. A., <b>Powell, C. A.</b>	INVITED: Assessing the Sensitivity of Statistical Tests on Earthquake Catalogs. <b>Daub, E. G.</b> , Trugman, D. T., Johnson, P. A.	INVITED: Universality of Slow Earthquakes in the Very Low Frequency Band: Summary of Regional Studies. <b>Ide, S.</b>	INVITED: Observations of Numerous Hydraulic Fracturing Induced Earthquake Sequences in Harrison County Ohio since 2013. <b>Friberg, P. A.</b> , Brudzinski, M. R., Skoumal, R. J., Currie, B. S.
8:45 AM	Blind-Test Case Studies to Validate Non-Invasive Shear-Wave Velocity Profiling in Diverse Geologic Settings in Canada and Chile. <b>Molnar, S.</b> , Ventura, C. E., Boroschek, R., Crow, H.	Roaming Midcontinental Earthquakes: Occurrence, Causes, and Hazards. <b>Liu, M.</b> , Stein, S.	INVITED: Earthquake Forecasts based on Seismological, Geological, and Geodetic Information. <b>Jackson, D. D.</b>	Very Low Frequency Earthquakes (VLFs) in Cascadia NOT Coincident with Strong Tremor. <b>Ghosh, A.</b> , Hutchison, A.	INVITED: Linking Fossil Reefs with Earthquakes: Geologic Insight to Where Induced Seismicity occurs in Alberta. <b>Schultz, R.</b> , Corlett, H., Haug, K., Kocon, K., MacCormack, K., Stern, V., Shipman, T.



Wednesday, 20 April (continued)

<i>Time</i>	<i>Tuscany 1/2</i>	<i>Tuscany 3/4</i>	<i>Tuscany 5/6</i>	<i>Tuscany 7/8</i>	<i>Tuscany A</i>
	<b>Noninvasive Approaches...</b>	<b>Seismotectonics Beyond the Plate Boundary</b>	<b>Past and Future Seismic Moment Release...</b>	<b>Slow, Fast, and In Between...</b>	<b>Induced Seismicity</b>
9:00 AM	STUDENT: Bayesian Trans-Dimensional Inversion of Surface-Wave Dispersion for Earthquake Site Response Estimation in Northern British Columbia, Canada. <b>Gosselin, J. M.</b> , Cassidy, J. F., Dosso, S. E., Brillon, C.	North America's Midcontinent Rift: when Rift met LIP. <b>Stein, S.</b> , Stein, C., Kley, J., Keller, G. R., Wiens, D., Wysession, M., Aleqabi, G., Shen, W., Merino, M., Fredricksen, A., Darbyshire, F., Jurdy, D., Waite, G., Rose, W., Rooney, T., Moucha, R., Brown E.	On the Uncertainty of the Seismic to Geodetic Moment Rate Ratio. <b>Kreemer, C.</b> , Zaliapin, I.	Slow Active Intra-plate Faults: the Paleoseismology of the Rurrand Fault, Germany. <b>Reicherter, K. R.</b> , Grützner, C., Fischer, P.	Natural Versus Anthropogenic Trigger of the Emilia 2012 Earthquakes. Pezzo, G., <b>Chiarabba, C.</b> , De Gori, P., Lucente, F. P.
9:15 AM	Vs IMASW and Vp-Depth Profiling, NEHRP Site Classifications, and Linear Shallow Amplification Functions: Geophysical Site Characterization of Bay Area Seismic Monitoring Stations Following the M6.0 South Napa Earthquake. <b>Turner, J. P.</b> , Brossy, C. C., O'Connell, D. R. H., Roughley, C.	INVITED: Moho Temperature and Compositional Controls on Lithospheric Bending Strength in the Western United States. <b>Schutt, D. L.</b> , Lowry, A. R., Buehler, J. S.	INVITED: Complete Seismic Release of Tectonic Strain and Earthquake Recurrence in the Apennines (Italy). <b>D'Agostino, N.</b>	STUDENT: Cascadia Seismogenic Zone Earthquake Detection and Location. <b>Morton, E. A.</b> , Bilek, S. L., Rowe, C. A.	Wastewater Disposal, Hydraulic Fracturing, and Seismicity in Southern Kansas. <b>Rubinstein, J. L.</b> , Ellsworth, W. L.
9:30 AM	INVITED: Applications of Refraction Microtremor Done Right, and Pitfalls of Microtremor Arrays Done Wrong. <b>Louie, J. N.</b> , Pullammanappallil, S.	INVITED: Joint Inversion of Rayleigh Wave Ellipticity and Phase Velocity across USArray. <b>Lin, F.</b> , Schmandt, B.	A Discussion of the Earthquake Risk at The Geysers Geothermal Area, California, Based on Strain Rates and Seismic Moment Rates. <b>Turcotte, D. L.</b> , Hawkins, A., Yikilmaz, M. B., Kellogg, L. H., Rundle, J. B.	Fortnightly Tidal Triggering of Low-frequency Earthquakes Constrains the Stress Budget of the Deep San Andreas Fault. <b>van der Elst, N. J.</b> , Delorey, A. A., Shelly, D. R., Johnson, P. A.	Stress Variations Across Oklahoma and Kansas, Natural Earthquakes, Induced Seismicity, and Their Links with Crustal and Upper Mantle Structure. <b>Levandowski, W.</b> , McNamara, D. E.
9:45–10:45 AM	BREAK				

Wednesday, 20 April (continued)

<i>Time</i>	<i>Tuscany 1/2</i>	<i>Tuscany 3/4</i>	<i>Tuscany 5/6</i>	<i>Tuscany 7/8</i>	<i>Tuscany A</i>
	<b>Noninvasive Approaches...</b>	<b>Seismotectonics Beyond the Plate Boundary</b>	<b>Past and Future Seismic Moment Release...</b>	<b>Slow, Fast, and In Between...</b>	<b>Induced Seismicity</b>
10:45 AM	Inversion of Velocity Structures Based on the Empirical Relationship of Earthquake and Microtremor Horizontal-to-Vertical Ratios. Mori, Y., <b>Kawase, H.</b> , Matsushima, S., Nagashima, F.	INVITED: GPS Imaging of the North American Intracontinental Strain Rate Field. <b>Kreemer, C.</b> , Hammond, W. C., Blewitt, G.	Comparison of Geodetic and Geological/ Seismological Moment Rates for the Wasatch Front Region, Utah. <b>Pechmann, J. C.</b> , Zeng, Y., Thomas, P. A., Petersen, M. D.	INVITED: Prospecting for Stress Changes Driven by SSEs with the HOBITSS Ocean-bottom Array, Offshore New Zealand. <b>Fry, B.</b> , Henrys, S., Wallace, L., Mochizuki, K., Lebedev, S., Sheehan, A., Schwartz, S., Webb, S.	Wastewater Disposal and Earthquake Swarm Activity at the Southern End of the Central Valley, California. <b>Goebel, T. H. W.</b> , Hosseini, S. M., Cappa, F., Hauksson, E., Ampuero, J. P., Aminzadeh, F., Saleeby, J. B.
11:00 AM	Directional Dependent H/V Spectral Ratio of Microtremors at Onahama, Japan. <b>Matsushima, S.</b> , Kosaka, H., Kobayashi, T., Kawase, H.	Crustal Model of the St. Lawrence Corridor from Charlevoix to Montreal. <b>Bent, A. L.</b> , Kao, H.	Long-Term and Short-Term Seismicity Rates in Cascadia: Gutenberg-Richter instead of Characteristic. <b>Brocher, T. M.</b>	STUDENT: Understanding the Size and Impact of Non-Volcanic Tremors in Parkfield: Deriving Tremor Energy Magnitudes and Exploring their Statistics. <b>Staudenmaier, N.</b> , Edwards, B., Tormann, T., Wiemer, S.	STUDENT: Mechanism of Intraplate Earthquakes and Anthropogenic Causes in USA. <b>Hagen, M. H.</b>
11:15 AM	Source and Stability of Ambient Noise in the Mississippi Embayment, Central United States. <b>Langston, C. A.</b> , Shahjouei, A.	A Map of Faults and Lineaments of the St. Lawrence Rift System. <b>Lamontagne, M.</b> , Nadeau, L., Brouillette, P., Bédard, M. P.	Earthquakes in the Clockwork Earth. <b>Rundle, J. B.</b> , Donnellan, A., Grant Ludwig, L., Turcotte, D. L.	UAVSAR Observation of Multi-Temporal Multi-Fault Behavior Associated with the 2010 M7.2 El Mayor—Cucapah Earthquake. <b>Donnellan, A.</b> , Parker, J. W.	Seismic Hazard Assessment for Gas Extraction Induced Seismicity in the Context of Building Codes. <b>Kraaijpoel, D. A.</b> , Steenbergen, R. D. J. M.
11:30 AM	INVITED: Shallow 3D Velocity Imaging based on Seismic Noise. <b>Pilz, M.</b>	Location of CEUS vs. Gulf Coast Q Boundary from USArray Data. <b>Cramer, C. H.</b> , Al Noman, M. N.	STUDENT: Supercycles and Synchronization Signatures in Synthetic Seismic Sequences. <b>Milner, K. R.</b> , Jordan, T. H.	STUDENT: Detailed Spatio-Temporal Evolution of Aftershocks and Repeating Earthquakes Following the 2012 Mw7.6 Nicoya Earthquake. <b>Yao, D.</b> , Meng, X., Peng, Z., Newman, A. V., Walter, J. I., Schwartz, S. Y., Protti, M.	A Ground Motion Prediction Equation for Induced Earthquakes in Oklahoma. <b>Yenier, E.</b> , Atkinson, G. M., Sumy, D. F.

Wednesday, 20 April (continued)

<i>Time</i>	<i>Tuscany 1/2</i>	<i>Tuscany 3/4</i>	<i>Tuscany 5/6</i>	<i>Tuscany 7/8</i>	<i>Tuscany A</i>
	<b>Noninvasive Approaches...</b>	<b>Seismotectonics Beyond the Plate Boundary</b>	<b>Past and Future Seismic Moment Release...</b>	<b>Slow, Fast, and In Between...</b>	<b>Induced Seismicity</b>
11:45 AM	Non-Linear Seismic Site Characterization Using Noninvasive Geophysics and Strong-Motion Recordings. <b>Wang, Z.</b> , Woolery, E. W., Rong, M.	An Issue with the National Seismic Hazard Maps: Where Is the Boundary That Separates the Use of the Western U.S. and CEUS Ground Motion Prediction Models? <b>Wong, I. G.</b>	STUDENT: How Detailed Should Earthquake Hazard Maps Be: Comparing the Performance of Japan's Maps to Uniform, Randomized, and Smoothed Maps. Brooks, E. M., <b>Stein, S.</b> , Spencer, B. D., Liu, M.	STUDENT: Detection and Location of Earthquakes Along the West Coast of Chile: Examining Seismicity in the 2010 M 8.8 Maule Rupture Zone. <b>Diniakos, R. S.</b> , Bilek, S. L., Rowe, C., Dragonov, D.	INVITED: Geomechanical Analysis of Fluid Injection and Seismic Fault Slip for the M4.8 Timpson, Texas, Earthquake. Fan, Z., <b>Eichhubl, P.</b> , Gale, J. F. W.
12:00 -2:15 PM	ANNUAL LUNCHEON				
	<b>Earthquake Early Warning: Network Design, Implementation, Production and Outreach</b> Session Chairs: Graham Kent and Ken Smith (see page 451)	<b>Ground Motion Spatial Variability: Models, Methods and Impacts</b> Session Chairs: David Wald, Kim Olsen, Jack Baker, and Paolo Bazzurro (see page 455)	<b>Theoretical and Methodological Innovations for 3D/4D Seismic Imaging of Near-Surface, Crustal, and Global Scales</b> Session Chairs: Marco Pilz and Nori Nakata (see page 460)	<b>Near Field and Directivity Considerations in Developing Fault Normal and Fault Parallel Spectra and Selecting and Scaling Time Histories for Nonlinear Analysis</b> Session Chair: Zia Zafr (see page 464)	<b>Induced Seismicity</b> (continued)
2:15 PM	Rapid Finite Faults with Real-Time GPS: the Geodetic Alarm System. <b>Grapenthin, R.</b> , Aranha, M., Melgar, D., Allen, R. M.	INVITED STUDENT: Ground Motion Variability from 3-D Deterministic Broadband (0-8 Hz) Ensemble Simulations of Mw 7.1 Strike-slip and Mw 6.7 Blind Thrust Events Incorporating Rough Fault Topography, Frequency-Dependent Viscoelasticity, Small-Scale Media Heterogeneity, and Plasticity. <b>Withers, K. B.</b> , Olsen, K. B., Shi, Z., Day, S.	Direct Methods and High Performance Computing for Seismic Tomography. <b>Bogiatzis, P.</b> , Ishii, M., Davis, T. A.	INVITED: Building Codes' Requirements for Near Field and Directivity Considerations in Ground Motions. <b>Zafir, Z.</b>	Are ENA Potentially Induced Earthquakes Different From Natural Earthquakes? <b>Cramer, C. H.</b>

Wednesday, 20 April (continued)

<i>Time</i>	<i>Tuscany 1/2</i>	<i>Tuscany 3/4</i>	<i>Tuscany 5/6</i>	<i>Tuscany 7/8</i>	<i>Tuscany A</i>
	<b>Earthquake Early Warning...</b>	<b>Ground Motion Spatial Variability...</b>	<b>3D/4D Seismic Imaging...</b>	<b>Near Field and Directivity...</b>	<b>Induced Seismicity (continued)</b>
2:30 PM	Testing the G-FAST Earthquake Early Warning System for Megathrust Earthquakes. <b>Crowell, B. W.</b> , Schmidt, D. A., Bodin, P., Vidale, J. E.	INVITED STUDENT: Computing Spatial Correlation of Ground Motion Intensities for ShakeMap. <b>Verros, S.</b> , Wald, D. J., Ganesh, M., Worden, C. B., Hearne, M., Horspool, N.	Moho Depth and Structure of the Crust and Upper Mantle Beneath Southern Alaska from Dix Inversion of Rayleigh-Wave Phase Velocity Maps. <b>Haney, M. M.</b> , Tsai, V. C., Ward, K. M.	Near-field and Regional Ground Motions During the 2015 Gorkha, Nepal, Earthquake. <b>Hough, S. E.</b> , Ampuero, J. P., Martin, S. S., Meng, L., Thompson, E. M., Zhang, A., Asimaki, D.	Evaluating the Damage Potential of Injection-Induced Earthquakes in the Central and Eastern U.S. and Western Canada. <b>Wong, I.</b> , Bott, J., Dober, M., Thomas, P.
2:45 PM	A-21st-century-approach to Firefighting in the Western US: How Microwave-based Seismic Networks Can Change Fire Suppression from Reactive to Proactive. <b>Kent, G. M.</b> , Smith, K. D., Slater, D., Plank, G., Williams, M., Vernon, F., Driscoll, N. W.	STUDENT: Spatial Distribution Model of Earthquake Strong-motion Amplitude and Frequency Variation on the Icelandic Strong-motion Array (ICEARRAY I) in South Iceland. <b>Rahpeyma, S.</b> , Halldorsson, B., Hrafnkelsson, B.	Towards Full Waveform Inversion at the Fault Zone Scale: Moment Tensor Inversion, Waveform Modeling, and Initial Velocity Model Selection. <b>Allam, A. A.</b> , Tape, C., Ben-Zion, Y.	Mean Spectral Modification in the Near Field for use in Nonlinear Analysis. <b>Mazzoni, S.</b> , <b>Wright, A.</b> , Lew, M., Wells, D., Hachem, M.	Near-distance Ground-Motion Saturation Effects for Small-to-Moderate Induced Earthquakes. <b>Atkinson, G. M.</b> , Yenier, E., Sharma, N., Convertito, V.
3:00 PM	Update on the Next Generation Earthquake Early Warning in SeisComP3. <b>Behr, Y.</b> , Böse, M., Smith, D., Clinton, J. F., Meier, M. A.	STUDENT: Spatial Incoherency Analysis of Seismic Ground Motions from 2014-Argostoli Earthquake Dense Array. <b>Svay, A.</b> , Clouteau, D., Cottreau, R., Zentner, I.	STUDENT: Evaluations of the effects of the basin edge in H/V spectral ratios of microtremors based on diffuse field interpretation. <b>Fukuoka, Y.</b> , Matsushima, S., Kawase, H., Anderson, J. G., Loyd, T. W.	STUDENT: Implications of Forward Directivity Effects on Design Ground Motions. <b>Moghimi, S.</b> , Akkar, D. S.	A Causal Link between Overpressured Hydrocarbon Source Rocks and Seismicity Induced by Hydraulic Fracturing. <b>Eaton, D. W.</b> , Cheadle, B., Fox, A.
3:15 PM	Improving the Seismic Network for Earthquake Early Warning in Hawai'i. <b>Hotovec-Ellis, A. J.</b> , Bodin, P., Thelen, W. A., Okubo, P., Vidale, J. E.	STUDENT: Magnitude, Region and Site-specific Spectral Value Correlations and Conditional Mean Spectra. <b>Kotha, S. R.</b> , Bindi, D., Cotton, F.	Shallow Crustal Discontinuities Inferred from Waveforms of Microearthquakes: Method and Application to KTB Drill Site and West Bohemia Swarm Area. <b>Hrubcova, P.</b> , Vavrycuk, V., Bouskova, A., Bohnhoff, M.	STUDENT: Simulation of 13 March 1992 Erzincan (Turkey) Earthquake including a Near-field Forward Directivity Pulse Model: Implications for Earthquake Engineering. Azari Sisi, A., <b>Askan, A.</b> , Erberik, M. A.	Normal Stress Drops for Induced Earthquakes in the Central U.S. <b>Huang, Y. H.</b> , Beroza, G. C. B., Ellsworth, W. L. E.
3:30-4:30 PM	BREAK				



Wednesday, 20 April (continued)

<i>Time</i>	<i>Tuscany 1/2</i>	<i>Tuscany 3/4</i>	<i>Tuscany 5/6</i>	<i>Tuscany 7/8</i>	<i>Tuscany A</i>
	<b>Earthquake Early Warning: Network Design, Implementation, Production and Outreach</b> (continued)	<b>Ground Motion Spatial Variability: Models, Methods and Impacts</b> (continued)	<b>Theoretical and Methodological Innovations for 3D/4D Seismic Imaging...</b> (continued)	<b>How Close are We to an Eruption?</b> Session Chairs: Weston Thelen and Matthew Haney (see page 465)	<b>Induced Seismicity</b> (continued)
4:30 PM	Numerical Shake Prediction for Earthquake Early Warning: Precise and Rapid Prediction even for Heterogeneous Distribution of Ground Shaking. <b>Hoshiaba, M.</b> , Ogiso, M.	Sensitivity of Annualized Earthquake Loss Estimates in California to Site Amplification. <b>Chen, R.</b> , Jaiswal, K. S., Bausch, D., Seligson, H., Wills, C. J.	Using Microquakes to Illuminate the Subsurface. <b>Matzel, E. M.</b> , Morency, C. E., Rhode, A., Pyle, M. L., Templeton, D. C.	INVITED: Forecasting of Eruptions at Stratovolcanoes. <b>White, R. A.</b> , McCausland, W. A.	STUDENT: Implications of Faulting Regimes on Required Pore-pressure Change for Induced Seismicity in the Central and Eastern U.S. <b>Hosseini, S. M.</b> , Aminzadeh, F., HajNasser, Y.
4:45 PM	S- and P-Wave Spectral Ratios for On-site Earthquake Early Warning. <b>Zhao, J. X.</b>	Implementation of Monte-Carlo Simulations for Probabilistic Loss Assessment of Geographically Distributed Portfolio Using Multi-Scale Random Fields: A Case Study for Istanbul. <b>Akkar, S.</b> , Cheng, Y., Erdik, M.	Improvements in Earthquake Location from Joint Inversion of Seismic and Gravity Observations—Application to the Iran Region. <b>Maceira, M.</b> , Syracuse, E. M., Bergman, E., Phillips, W. S., Begnaud, M., Nippres, S., Zhang, H.	Arc-wide Application of the Distal VT Model for Eruption Forecasting in Alaska. <b>Pesicek, J. D.</b> , Wellik, J., Prejean, S., White, R., Cameron, C., McCausland, W., Buurman, H.	INVITED: Influence of Industrial and Tectonic Factors on Fluid-Injection Induced Earthquakes. <b>McGarr, A.</b>
5:00 PM	ElarmS 2015 Performance and New Filterbank Teleseismic Filter. <b>Chung, A. I.</b> , Allen, R. M., Henson, I., Hellweg, M., Neuhauser, D.	How Much Can the Total Aleatory Variability of Empirical Ground Motion Prediction Equations Be Reduced Using Physics-Based Earthquake Simulations? <b>Jordan, T. H.</b> , Wang, F., Graves, R. W., Callaghan, S., Olsen, K. B., Cui, Y., Milner, K., Juve, G., Vahi, K., Yu, J., Deelman, E., Gill, D., Maechling, P.J.	Active Source Joint Inversion of Travel Time with Gravity for 3D Vp and Density Tomography and Seismic Reflection Imaging of the Irish Hills, California, Using Active Seismic, Gravity, and Magnetic Data. <b>O'Connell, D. R. H.</b> , Turner, J. P., Nishenko, S., Stankovic, G.	INVITED: Fluid-faulting Interactions: Fracture-mesh and Fault-valve Behavior in the February 2014 Mammoth Mountain, California, Earthquake Swarm. <b>Shelly, D. R.</b> , Taira, T., Prejean, S. G., Hill, D. P., Dreger, D. S.	Induced Earthquakes in the 20th Century: Connecting the Dots. <b>Hough, S. E.</b> , Page, M. T.

Wednesday, 20 April (continued)

Time	<i>Tuscany 1/2</i>	<i>Tuscany 3/4</i>	<i>Tuscany 5/6</i>	<i>Tuscany 7/8</i>	<i>Tuscany A</i>
	<b>Earthquake Early Warning...</b>	<b>Ground Motion Spatial Variability...</b>	<b>3D/4D Seismic Imaging...</b>	<b>How Close are We to an Eruption?</b>	<b>Induced Seismicity</b>
5:15 PM	Implementing ElarmS for the Israeli Seismic Network—New Tools and Approaches. <b>Nof, R. N.</b> , Allen, R. M.	A Non-Ergodic Ground-Motion Model for California with Spatially Correlated Coefficients. Landwehr, N., <b>Kuehn, N. M.</b>	STUDENT: Rayleigh Wave Attenuation Along Linear Arrays Across the San Jacinto Fault Zone from Statistical Analysis of Noise Cross-correlations. <b>Liu, X.</b> , Ben-Zion, Y., Zigone, D.	INVITED: Near Real-time Detection, Clustering, and Analysis of Repeating Earthquakes: Application to Mount St. Helens and Redoubt Volcanoes. <b>Hotovec-Ellis, A. J.</b> , Jeffries, C.	STUDENT: Moment Tensor Inversion for the Induced Earthquakes in the Western Canadian Sedimentary Basin. <b>Zhang, H.</b> , Eaton, D. W.
5:30 PM	Characteristics of Initial P wave Observed from Moderate to Large Earthquakes. <b>Noda, S.</b> , Ellsworth, W. L.	Conditional Simulation of Spatially Variable Ground Motions and its Application to an Input Wave Field from the San Andreas Fault ShakeOut Scenario. <b>Ancheta, T. D.</b> , Stewart, J. P.	STUDENT: High Attenuation Zones beneath Sierra Negra Volcano: Evidence for a Shallow Sill and Feeder System. <b>Rodd, R. L.</b> , Lees, J. M.	The Yellowstone Magmatic System from the Mantle Plume to the Upper Crust. <b>Huang, H. H.</b> , Lin, F. C., Schmandt, B., Farrell, J., Smith, R. B., Tsai, V. C.	Trying to Discriminate Between Natural and Anthropogenic Earthquakes Recorded at Mt. Amiata Volcano (Italy). <b>Braun, T.</b> , Spinelli, R.
5:45–7:30 AM	DINNER				
	<i>Tuscany 3/4</i>				
	<b>The M7.1 Iniskin Earthquake, Alaska</b> Session Chair: Mike West (see page 470)				
7:30 PM	Perspectives on the Mw7.1 Iniskin Earthquake. <b>West, M.</b> , Gardine, M., Ruppert, N., Tape, F., Holtkamp, S., Freymueller, J., Abers, G.				
7:45 PM	Does the M7.1 Iniskin Earthquake Change Alaska Seismic Hazard Maps? <b>Cramer, C. H.</b>				
8:00 PM	M7.1 Iniskin Earthquake Site Response of a Downhole Array Site in Anchorage, Alaska. <b>Thornley, J.</b> , Dutta, U., Yang, J.				
8:15 PM	The 2016 Mw7.1 Iniskin, Alaska, Earthquake as seen by High-rate GPS and Early Warning Potential. <b>Grapenthin, R.</b> , Freymueller, J. T.				

### Wednesday 20 April—Poster Sessions

#### Advances in Noninvasive Approaches to Characterizing Seismic Site Conditions (see page 471)

1. Applicability of Exploration Geophones to Large Scale Passive Surface Wave Methods. **Hayashi, K.**
2. STUDENT: Mapping the Geometry of the San Leandro Block, Hayward Fault Zone Using Geologic and Geophysical methods; California State University, East Bay Campus. **McEvelly, A. T.**, Strayer, L. M., Abimbola, A., Chan, J. H.
3. Advanced Concepts for Microtremor Measurements in Order to Characterize Site Conditions in the Course of

4. Seismic Hazard Analyses and Microzonation. **Spies, T. S.**, Schlittenhardt, J. S., Ibs-von Seht, M. I., Horstmann, T. H., Marjiyono, M., Sohami, A. S., Brüstle, A. B., Schmidt, B. S.
5. Spatial Variability of VS in Quaternary Alluvium. **Wagstaffe, D.**, Moss, R. E. S.
6. Effects of Poisson Ratio and Density Values on Vs Profiles and Vs30 at ARRA-funded Sites. **Yong, A.**, Boatwright, J., Martin, A.
7. Insights from the New Zealand Strong Motion Site Meta-Data: Update for the 2015 Strong Motion Database. **Kaiser, A. E.**, Van Houtte, C., Perrin, N., Wotherspoon, L., McVerry, G., Cousins, J.

Wednesday, 20 April (*continued*)

7. Estimation of Site Amplifications at the K-Net Ocean Bottom Seismograph Stations in the Sagami Bay Area based on Spectral Inversion Method. **Dhakal, Y. P.**, Suzuki, W., Kunugi, T., Aoi, S.
8. Site Effects Assessment in Almaty (Kazakhstan) in Light of Destructive Past Earthquakes. **Parolai, S.**, Pilz, M., Abakanov, T., Silacheva, N., Kulbayeva, U., Kravchenko, N., Rayimbek, B., Orunbaev, S., Moldobekov, B.
9. Characteristics of Microtremor Observed near Quay Walls—Example of Observed Records at Yaizu Fishing Port, Japan. **Suzuki, H. S.**, Manabe, S. M., Nagata, S. N., Yamada, T. Y., Nagasaka, Y. N., Nozu, A. N.
10. Site Characterization at Napa Strong Motion Sites Using Tomography, MASW, and MALW. **Chan, J. H.**, Catchings, R. D., Goldman, M. R., Criley, C. J.
11. Near Surface Shear Wave Velocity Measurements in the Sacramento-San Joaquin Delta. **Craig, M. S.**, Hayashi, K., Shuler, S. E.
12. STUDENT: Implementation of the Spectral Ratio Method on Data from a High-Density Seismic Experiment in the Los Angeles Basin. **Ng, R.**, Polet, J.
13. STUDENT: Interpreting Site Amplifications from Surface Wave Tomography. **Bowden, D. C.**, Tsai, V. C., Lin, F. C.
14. STUDENT: Spatial and Temporal Variation in Ambient Seismic Noise Site Response in Charleston, South Carolina. **Cobb, S. E.**, Jaume, S. C., Odum, J., Stephenson, W.
15. Observation and Modeling of HVSR in Charleston, South Carolina: Implications for Earthquake Hazard on a Deep Coastal Plain. **Jaume, S. C.**, Levine, N. S., Braud, A.

**Earthquake Early Warning: Network Design, Implementation, Production and Outreach** (see page 474)

16. Ground Motion Forecasting Using a Reference Station and Complex Site Response Functions Accounting for the Shallow Geology. **Pilz, M.**, Parolai, S.
17. STUDENT: An Envelope Based Earthquake Early Warning Algorithm—Ground Motion Envelope Predictor (GMEP). **Karakus, G.**, Heaton, T. H.
18. MEMS Accelerometers Mini Array (MAMA)—a Low Cost Solution for Array-based Earthquake Early Warning System. **Nof, R. N.**, Chung, A. I., Meng, L., Kong, Q., Allen, R. M.
19. HPWREN - Building a Sustainable Resilient Infrastructure for Realtime Observations. **Vernon, F.**
20. ElarmS Performance in Hawai'i. **Thelen, W. A.**, Hotovec-Ellis, A., Hartog, R., Bodin, P., Vidale, J., Okubo, P.
21. Monitoring Data Quality from the PBO, TLALOCNet and COCONet Real-Time GNSS Networks for Earthquake Early Warning. **Hodgkinson, K. M.**

Mencin, D., Fox, O., Walls, C., Mann, D., Austin, K., Blume, F., Berglund, H., Phillips, D. A., Meertens, C. M., Mattioli, G. S.

**Ground Motion Spatial Variability: Models, Methods and Impacts** (see page 475)

22. Estimating Spatial Correlations between Earthquake Source, Path, And Site Effects for Non-Ergodic Seismic Hazard Analysis. **Kuehn, N. M.**, Abrahamson, N., Baltay, A.
23. Characterization of Spatial Variability of Ground Motion Using a Very Dense Array at Long Beach, California. **Nori Nakata, N.**, Gregory C. Beroza, G. C.
24. STUDENT: Estimation of VS30 from Geology-Based Proxy Developed for the Pacific Northwest. **Ahdi, S. K.**, Stewart, J. P., Ancheta, T. D., Kishida, T., Bozorgnia, Y.
25. STUDENT: A Vs30-dependent Velocity Model for High-frequency Simulated Ground Motions in the Los Angeles Basin. **Shi, J.**, Asimaki, D., Yong, A. K.
26. Impact of Spatial Correlation of Peak Ground Motion Intensity in Catastrophe Modeling. **Lee, Y.**, William, G.

**How Close are We to an Eruption?** (see page 476)

27. Intermediate-Depth Long Period Seismicity Prior to a Shallow Earthquake Swarm at Little Sitkin Volcano, Alaska. **Haney, M. M.**, Buurman, H., McNutt, S. R.

**Induced Seismicity** (see page 476)

28. Characterizing Microseismicity at the Newberry Volcano Geothermal Site using PageRank. **Aguiar, A. C.**, Myers, S. C.
29. The Seismic Response at the Aquistore CO2 Injection Project, Saskatchewan, Canada. **Stork, A. L.**, Nixon, C., Schmitt, D. R., White, D. J., Kendall, J. M., Worth, K.
30. STUDENT: Long-term Decay and Possible Reactivation of Induced Seismicity at the Basel EGS Site. **Herrmann, M.**, Kraft, T., Wiemer, S.
31. Effects of Long-term Fluid Injection on Induced Seismicity Parameters and Maximum Magnitude at Northwestern The Geysers Geothermal Field. **Kwiattek, G.**, Martínez-Garzón, P., Dresen, G., Bohnhoff, M., Sone, H., Hartline, C.
32. Detailed Analysis of an Earthquake Cluster Potentially Driven by Fluid Flow in Central Oklahoma. **Chen, X.**, Peng, Z., Meng, X., Chen, C., Haffener, J., Chang, J.
33. Spatiotemporal Analysis of the 2010-2011 Guy-Greenbrier Sequence and the Associated Pore-pressure Beyond Fluid Disposal Period. **Ogwari, P. O.**, Horton, S. P.
34. Explaining the 24 January 2013  $M_L 4.4$  Induced Earthquake in Paradox Valley, Colorado. Denlinger, R. P., **Roeloffs, E. A.**

Wednesday, 20 April (*continued*)

35. The August 17, 2015 Mw 4.6 Hydraulic Fracturing-Induced Earthquake in Northern Montney Play, British Columbia, Canada. **Babaie Mahani, A.**, Schultz, R., Kao, H., Walker, D., Johnson, J., Salas, C.
36. Matched Filtering Analysis of Induced Seismicity in the Crooked Lake region, Alberta: Correlation with Hydraulic-fracturing Operations. **Bao, X.**, Eaton, D. W., Caffagni, E.
37. STUDENT: Induced Seismicity due to Wastewater Injection Near Peace River, Alberta. **Anderson, Z.**, Eaton, D. W.
38. STUDENT: Triggered Seismicity Source Mechanisms: Modelling Fault Complexity in Critically Stressed Crust. **MacKay, M.**, Eaton, D.
39. Simulating Hydraulic Fracturing using Finite-Discrete Element Method (FDEM): Effects of Pre-existing Joints and Lateral Stress Gradient. **Abuaisha, M.**, Eaton, D. W., Priest, J., Wong, R.
40. STUDENT: An Investigation on the Effects of Different Stress Regimes on the Magnitude of Induced Seismic Events. **Amini, A.**, Eberhardt, E.
41. A Coda Based Method for Precise Focal Depth Determination in Sedimentary Basins. **Daniels, R.**
42. STUDENT: Dynamic Stress Considerations for Induced and Triggered Events. **Walker, R. L.**
43. On the Importance of Inter-Event Triggering in Microseismicity Induced by Hydraulic Fracturing. **Maghsoudi, S.**, Eaton, D., Baro, J., Davidsen, J.
44. STUDENT: Finite Element Modelling of Fault Reactivation: Stress Drop and Slip. **Sattari, A.**, Eaton, D. W.
45. Earthquake Stress-drop Tensors and Critical States during Fluid Injection. **Eaton, D. W.**, Krebes, E.
46. West Texas Seismicity and Distinguishing Natural from Anthropogenic Causes. **Walter, J. I.**, Frohlich, C., Gale, J. F. W., Borgfeldt, T., Bilek, S., Gerzina, J., Dotray, P. J.
47. Frequency-magnitude Distribution for Natural and Mining-induced Seismicity in UK. **Segou, M.**, Baptie, B.
48. Effects of Hydraulic Diffusivity and Rate- and State-dependent Friction in Simulations of Injection Induced Seismicity. **Kroll, K. A.**, Richards-Dinger, K. B., Dieterich, J. H.
49. Prediction of Earthquake Ground Motions in Western Alberta. **Yenier, E.**, Baturan, D., Law, A., Atkinson, G. M.
50. Shallow Microearthquakes Near Chongqing, China Triggered by the Rayleigh Waves of the 2015 M7.8 Gorkha, Nepal Earthquake. **Han, L. B.**, Peng, Z. G., Li, L., Wang, B. S., Wu, J., Li, Q.

---

**Multidisciplinary Studies of Earthquakes - Slow, Fast, and In Between: A Broad Range of Fault Behavior in Space and Time** (see page 481)

---

51. Transient Creep Events Detected by PBO Strainmeters in the Parkfield Region of the San Andreas Fault. Gottlieb, M., Mencin, D. J., **Hodgkinson, K. M.**, Bilham, , Mattioli, G. S., Johnson, W., Van Boskirk, E., Henderson, D., Meertens, C.M.
52. Foreshock and Aftershock Detection around the 2014 Mw6.1 Kangding Earthquake. **Han, L. B.**, Peng, Z. G., Yao, D. D., Su, J. R., Long, F.
53. STUDENT: Ambient Tremor Detection in the Geysers Region, CA. **Damiao, L. G.**, Nadeau, R. M., Luna, B., Taira, T., Dreger, D. S., Guilhem, A., Zhang, H.
54. STUDENT: Modeling Pore Pressure Changes due to Slow Earthquakes: Implications for Tectonic Tremor Generation in Guerrero, Mexico. **Villafuerte, C. D.**, Cruz-Atienza, V. M., Bhat, H. S.

---

**Past and Future Seismic Moment Release: Contributions from Statistics and Geodesy** (see page 482)

---

55. STUDENT: Seismic Hazard Estimation of Northern Iran Using Smoothed Seismicity. **Khoshnevis, N.**, Azizzadeh-Roodpish, S., Taborda, R., Cramer, C. H.
56. Statistically Significant Global Variations of Seismic Moment. **Zaliapin, I.**, Kreemer, C.
57. Scaling of Maximum Earthquake Magnitudes with Geometrical and Stress Properties of Strike-Slip Faults. **Martinez-Garzón, P.**, Bohnhoff, M., Ben-Zion, Y., Dresen, G.
58. A Global Mmax for Stable Continental Regions? Vanneste, K., **Vleminckx, B.**, Stein, S., Camelbeeck, T.
59. Estimation of the Frequency-Magnitude Gutenberg-Richter *b*-Value Without Making Assumptions on Levels of Completeness. **Kijko, A.**, Smit, A.
60. Assessing the Hazard of Large Aftershocks in Alaska. **Kilb, D. L.**
61. Improved Omori Parameters for Global Aftershock Forecasts. **Page, M. T.**, Hardebeck, J. L., van der Elst, N. J., Felzer, K. R., Michael, A. J.
62. Recent Achievements of the Collaboratory for the Study of Earthquake Predictability. **Jackson, D.**, Werner, M., Liukis, M., Schorlemmer, D., Yu, J., Maechling, P., Rhoades, D., Zechar, J., Marzocchi, W., Jordan, T.
63. STUDENT: The Virtual Quake Earthquake Simulator. **Schultz, K. W.**, Wilson, J. M., Sachs, M. K., Heien, E. M., Rundle, J. B., Turcotte, D. L.
64. Time-dependent Models of Interseismic Deformation in the Northwestern United States. **Pollitz, F. F.**, Evans, E. L.



**Seismotectonics Beyond the Plate Boundary** (see page 484)

65. INVITED: Seismic Imaging of a Continental Intraplate: Long-Term Persistence of Fossil Rifts and Hot Spots in the Central and Eastern United States. **Pollitz, F. F.**, Mooney, W. D.
66. Using the Locations of  $M \geq 4$  Earthquakes to Delineate the Extents of the Ruptures of Past Major Earthquakes. **Ebel, J. E.**, Chambers, D. W.
67. A Hybrid-Empirical Ground-Motion Relation for Central and Eastern North America. **Shahjoui, A.**, Pezeshk, S.
68. Using Geophysics and Geochemistry to Trace Quaternary Faults in the El Paso, Texas—Ciudad Juárez, Chihuahua Region. **Doser, D. I.**, Avila, V. M., Dena-Ornelas, O. S., Hiebing, M., Ma, L.
69. STUDENT: Crustal and Upper Mantle Structure Beneath Eastern Flank of the Rio Grande Rift Revealed by Receiver Function Velocity Analysis. **Agrawal, J.**, Pulliam, J., Sen, J., Grand, S.
70. STUDENT: Seismicity Associated with Northwest Trending Basement Faults, Southwest Montana, USA. **Szkody, J. A.**, Stickney, M. C., Schmidt, C. J.
71. STUDENT: The 6 November 2011 M5.6 Prague, Oklahoma Aftershock Sequence Studied Using Subspace Detection. **McMahon, N. D.**, Benz, H. M., Johnson, C. E., Aster, R. C., McNamara, D. E.
72. Recent Slip History and Surface Deformation Along the Southern Arm of the New Madrid Seismic Zone, Central United States from High Resolution Seismic Reflection Data and River Sediments. **Magnani, M. B.**, Holbrook, J. M.
73. Velocity Structure and Seismic Anisotropy beneath the Mississippi Embayment and New Madrid Seismic Zone. **Nyamwandha, C. A.**, Powell, C. A.
74. 3d Averaged and Gradient P- and S- Wave Velocity Models for the Unconsolidated Mississippi Embayment Sediments. **Mostafanejad, A.**, Langston, C. A., Chai, C., Ammon, C. J., Herrmann, R. B.
75. Re-Evaluation of Interpreted Paleoseismic Sites in the Eastern Tennessee Seismic Zone: Evaluating Origin and Uncertainty of Potential Paleoseismic Data for Seismic Source Characterizations (SSC) in the Central and Eastern US (CEUS). **Clahan, K. B.**, Lindvall, S. C., Dee, S., Sowers, J., Lewandowski, N., Toro, G.
76. Recent Fault Activity in the 1886 Charleston, South Carolina Earthquake Epicentral Area and its Relation to Buried Structures. **Pratt, T. L.**, Shah, A. K., Horton, J. W., Chapman, M. C., Beale, J. N.
77. New Measurements of Shear-wave Splitting in Saudi Arabia. **Chen, S. W.**, **Mooney, W. D.**, Klemperer, S. L., Suzuki, J., Zahran, H. M., El-Hadidy, S. Y.

78. Pn Wave Geometric Spreading and Attenuation Models in and around the Tibetan Plateau. **Zhao, L. F.**, Xie, X. B., Yao, Z. X.
79. Western US and Tibetan Crust in 3-D: A Preliminary Report. **Chen, W. P.**, Yu, C. Q., Jiang, Y.
80. Joint Inversion for Lithospheric Density Variations Beneath the Tarim Block, Western China, and their Geodynamic Implications. **Deng, Y.**, **Levandowski, W.**
81. Repeated Event Detection in Eastern Asia using Historical Archives. **Slinkard, M.**, Sundermier, A., Heck, S., Young, C., Schaff, D., Richards, P.
82. Seismic Hazard Assessment for Kwajalein. **Mueller, C. S.**, Milburn, T. W.

**Theoretical and Methodological Innovations for 3D/4D Seismic Imaging of Near-Surface, Crustal, and Global Scales** (see page 488)

83. STUDENT: Monte Carlo Inversion for a 3D Local Earthquake Tomography. **Lanza, F.**, Waite, G. P.
84. Ambient Noise Tomography in Shanxi Rift. **Song, M. Q.**, Wang, X., Li, H. W., Wu, H. Y., Liang, X. J., Jin, Y. Z.
85. STUDENT: Seismic Structure Beneath the Northern Mississippi Embayment: Inverting Receiver Functions, Surface-Wave Dispersion, and Gravity Observations. **Chai, C.**, Ammon, C. J., Herrmann, R. B., Mostafanejad, A., Langston, C. A.
86. Connecting the Dots: Location and Continuity of Shallow Structures within the Seattle Fault Zone Interpreted from Land Based High-Resolution Seismic-Reflection Profiles. **Odum, J. K.**, Stephenson, W. J., Pratt, T. L., Blakely, R. J.
87. Shallow Structure and Location of the Piedmont Thrust Splay of the Hayward Fault, Oakland, California. **Goldman, M. R.**, Catchings, R. D., Trench, D., Buga, M., Chan, J. H., Criley, C.
88. Seismic Evidence of a Widely Distributed West Napa Fault Zone, Hendry Winery, Napa, California. **Catchings, R. D.**, Goldman, M. R., Chan, J. H., Criley, C. J.
89. STUDENT: Three Dimensional  $V_p$  and  $V_p/V_s$  Structural Models for The Geysers, California. **Tyagi, A.**, Lin, G., Wu, B.
90. STUDENT: Internal Structure of the San Jacinto Fault Zone in the Trifurcation Area Southeast of Anza, California, from Data of Spatially-Dense Linear Arrays. **Qin, L.**, Ben-Zion, Y., Qiu, H., Share, P., Ross, Z. E., Vernon, F.
91. STUDENT: Retrieval of the Empirical Green's Tensor using Ambient Noise Cross-Correlation at The Geysers Geothermal Field. **Nayak, A.**, Taira, T., Dreger, D. S., Gritto, R.
92. Imaging the 3D Structure at the Source Physics Experiment using Seismic Interferometry. **Matzel, E. M.**, Mellors, R. J., Pitarka, A.

Wednesday, 20 April (*continued*)

93. Seismic Imaging of Open Subsurface Fractures. **Myers, S. C.**, Pitarka, A., Matzel, E., Aguiar, A. C.
94. Ambient Noise Correlations on a Floating Ice Shelf: Wave Guiding, Temporal Monitoring, and Structural Inversion for the Ross Ice Shelf, Antarctica. **Chaput, J. A.**, Aster, R., Cheney, M., Baker, M., Brenguier, F., Moreau, L., Nyblade, A., Wiens, D., Hernandez, S.; Gerstoft, P.; Diez, A.; Anthony, R.
95. Velocity Change in the Zone of a Moderate Mw = 5.0 Earthquake Revealed by Autocorrelations of Ambient Noise and by Event Spectra. **Von Seggern, D. H.**, Anderson, J. G.
96. STUDENT: 3D Passive Source Reverse Time Migration: A New Imaging Method using Converted Wave. **Li, J.**, Shen, Y., Zhang, W.
97. STUDENT: Application of Effective Medium Theory to the Three-Dimensional Heterogeneity of Mantle Anisotropy. **Song, X.**, Jordan, T. H.
98. Joint Inversion of Seismic and Gravity Data Beneath the Iberian Peninsula for Crustal and Upper Mantle Structure. **Syracuse, E. M.**, Maceira, M., Villasenor, A., Zhang, H.
99. STUDENT: Eikonal Tomography of the Southern California Plate Boundary Region. **Qiu, H.**, Ben-Zion, Y., Zigone, D., Lin, F. C.
100. STUDENT: 3D Full Waveform Tomography in Central Mexico. **Juarez, A.**, Ramirez-Guzman, L., Rabade-Garcia, S.
101. STUDENT: The Lithospheric Structure of the Central Anatolian Plateau. **Cloud, J.**, Russell, J., Ku, W., Kaviani, A., Beck, S., Sandvol, E.
102. Rayleigh wave phase velocity structure of South China block and its neighboring regions. **Lü, J.**, Xie, Z. J., Zheng, Y., Zhou, L. Q., Zhang, Z. W., Hu, R., Zeng, X. F., Zha, X. H.
103. STUDENT: Teleseismic Earthquake Signals Observed on an Ice Shelf: Prospects for Earth Imaging Employing Floating-Platform Seismographs. **Baker, M. G.**, Aster, R., Chaput, J., Anthony, R., Wiens, D., Nyblade, A., Bromirski, P., Gerstoft, P., Stephen, R., Woods Hole Oceanographic Institute; Diez, A., Scripps Institution of Oceanography
- 
- Complexities in Site Response** (see page 493)
104. Magnitude Dependent Site Proxies for Soft Sites. Leyton, F., **Montalva, G. A.**
105. Mapping of VS30 Assimilating Uncertain Velocity Profile and Measurement Errors. **Ancheta, T. D.**, Lee, S. J., Mitra, D., Rangaswamy, A.
106. STUDENT: Methodology of Adjoint-tomography Inversion of the Small-scale Shallow Sedimentary Basins. Kubina, F., **Moczo, P.**, Kristek, J., Michlik, F.
107. STUDENT: Removing the Effect of an Ice Layer on the P-wave Response: An Application to Antarctic Studies. **Graw, J. H.**, Hansen, S. E., Langston, C. A., Young, B. A., Mostafanejad, A.
108. STUDENT: Evaluation of Ground Motions Recorded During the 2014 South Napa Earthquake at the Crocket-Carquinez Downhole Arrays. Li, G. L., **Motamed, R. M.**, Dickenson, S. D.
109. Revisiting Earthquake Site Response in Vancouver, Canada. **Molnar, S.**, Cassidy, J. F., Jackson, F., Brillon, C.
110. STUDENT: Sensitivity Tests of Effects of Detailed Shear-Wave Velocity Profiles to 100 m Depth on Response Spectra, Clark County, Nevada. **West, L. T.**, Louie, J., Pullammanappallil, S.
111. Improving Our Understanding of 1D Site Response Model Behavior: Physical Insights for Statistical Deviations from 114 KiK-net Sites. **Kaklamanos, J.**, Bradley, B. A.
112. Estimation of K0 Implied by the High-Frequency Shape of the NGA-West2 Ground Motion Prediction Equations. **Zandieh, A.**, Campbell, K. W., Pezeshk, S.
113. Improved Estimation of Site Response using Random Vibration Theory. **Seifried, A. E.**, Toro, G. R.
114. Joint Deconvolution of Borehole and Building Strong Motion Recordings: an Application to Three Different Test Cases. **Petrovic, B.**, Parolai, S., Dikmen, S. U., Safak, E., Pianese, G., Paolucci, R., Orunbaev, S., Moldobekov, B.
115. Improved Risk Management through a Novel Semi-empirical SSI Model Calibration for Vertical Ground Motions. **Di Alessandro, C.**, Dinsick, A.

Wednesday, 20 April (continued)

**Thursday, 21 April—Oral Sessions**

<i>Time</i>	<i>Tuscany 1/2</i>	<i>Tuscany 3/4</i>	<i>Tuscany 5/6</i>	<i>Tuscany 7/8</i>	<i>Tuscany A</i>
	<p><b>Induced Seismicity Monitoring: What is Really Needed?</b> Session Chairs: Iain Weir-Jones and Steven Taylor (see page 466)</p>	<p><b>Machine Learning and its Application to Earthquake and Explosion Signal Analysis</b> Session Chair: Timothy Draelos (see page 500)</p>	<p><b>The Role of Shallow Slip on Faults</b> Session Chairs: Sarah Minson, Benjamin Brooks, and Jessica Murray (see page 504)</p>	<p><b>Tsunami Resilience Strategies: Application of Tsunami Science and Mitigation Advancements to Protect Communities</b> Session Chairs: Rick Wilson, Kevin Miller, and Lori Dengler (see page 508)</p>	<p><b>Active Tectonics, Faults and Large Earthquakes</b> Session Chairs: Sushil Kumar, Sudhir Rajaure, and Rama Sushil (see page 512)</p>
8:30 AM	<p>Challenges and Strategies for Monitoring Induced Seismicity. Baturan, D., <b>Karimi, S.</b>, Yenier, E.</p>	<p>Adaptive Self-Tuning of Seismic Sensors. <b>Draelos, T. J.</b>, Knox, H. A., Peterson, M. G., Lawry, B. J., Chael, E. P., Young, C. J.</p>	<p>INVITED: Can We Predict Surface Deformation Patterns in Future Earthquakes with any Degree of Certainty? The Importance of Documenting Patterns of On- versus-off-fault Deformation in Large Earthquakes. <b>Dolan, J. F.</b></p>	<p>INVITED: Evidence for Frequent Large Tsunamis in the Eastern Aleutians that Bridge the Boundary Between a Locked and Creeping Megathrust. <b>Witter, R. C.</b>, Briggs, R., Gelfenbaum, G., Engelhart, S. E., Koehler, R. D., Nelson, A. R., La Selle, S., Corbett, R.</p>	<p>INVITED: Geological Results and Archival Information on the Central Himalayan Earthquakes and Their Implications for Seismic Source Zones. <b>Rajendran, C. P.</b>, Rajendran, K., John, B., Sanwal, J., Parameswaran, R.</p>
8:45 AM	<p>TexNet: A New, Integrated Seismic Monitoring Program in Texas. <b>Savvaids, A.</b>, Young, M., Tinker, S., Rathje, E. M., Frohlich, C. A., Walter, J., De Shon, H., Gale, J. F., Hennings, P., Eichhubl, P., Olson, J., Olson, H. C., Markman, A., Kahlor, L. A.</p>	<p>Empirical Seismic Phase Separation from Polarization Analysis. <b>Jones, J. P.</b>, Eaton, D., Caffagni, E.</p>	<p>INVITED: Influence of Compliant Sediments on Shallow Slip and Rupture Dynamics. <b>Dunham, E. M.</b>, Lotto, G. C., Erickson, B. A., Allison, K., Jeppson, T. N., Tobin, H. J.</p>	<p>INVITED: Earthquakes, Tsunamis, and Storms Recorded at Crescent City, California, USA. <b>Hemphill-Haley, E.</b>, Kelsey, H. M., Loofbourrow, C., Caldwell, D., Graehl, N., Robinson, M.</p>	<p>Macroseismic Intensity Assignments in Kathmandu Valley for the 2015 M7.8 Gorkha, Nepal Earthquake Based on Structural Damage Statistics. <b>McGowan, S. M.</b>, Jaiswal, K. S., Wald, D. J.</p>
9:00 AM	<p>Induced Seismicity Monitoring and the Traffic Light Protocol. <b>Taylor, S. R.</b>, Jarpe, S. P., Harben, P. E., Weir-Jones, I.</p>	<p>INVITED: SpectRobot: Automated Time/Frequency Pattern Recognition in the Gabor Spectrogram. <b>Lees, J. M.</b>, Bowman, D. C.</p>	<p>INVITED: Large Shallow Slip on the Central Imperial Fault in the 1940 Earthquake: Evidence for a Shallow Asperity. <b>Rockwell, T. K.</b>, Klinger, Y.</p>	<p>Predicting Sediment Instability during Tsunami Loading: Hypothetical, Laboratory, and Field Case Studies. <b>Mason, H. B.</b>, Fischer, R. M., Abdollahi, A., Adams, R. K., Exton, M. C.</p>	<p>INVITED: Seismic Structure Beneath the Great Valley, Central California: Implications for the Tectonic Origin of the Isabella Anomaly. <b>Dougherty, S. L.</b>, Hoots, C. R., Hansen, S., Schmandt, B., Clayton, R. W.</p>

<i>Time</i>	<i>Tuscany 1/2</i>	<i>Tuscany 3/4</i>	<i>Tuscany 5/6</i>	<i>Tuscany 7/8</i>	<i>Tuscany A</i>
	<b>Induced Seismicity Monitoring...</b>	<b>Machine Learning...</b>	<b>The Role of Shallow Slip on Faults</b>	<b>Tsunami Resilience Strategies...</b>	<b>Active Tectonics, Faults...</b>
9:15 AM	STUDENT: The Eastern Kentucky Microseismic Monitoring Project: A Public-Private Collaborative Project at the Onset of Unconventional Oil and Gas Production in the Rome Trough, Eastern Kentucky. <b>Carpenter, N. S., Wang, Z., Moores, A. O., Roche, S. L., Woolery, E. W.</b>	STUDENT: Data Mining for Earthquake Detection using Computationally Efficient Search for Similar Seismic Signals. <b>Bergen, K. J., Yoon, C. E., Beroza, G. C.</b>	Shallow Fault Slip and 'Off-Fault' Deformation From Some Recent Strike-Slip Earthquakes. <b>Brooks, B. A., Barnhart, W., Minson, S. E., Glennie, C. L., Murray, J., Hudnut, K., Ericksen, T. L.</b>	The Global Tsunami Model (GTM) Network. <b>Thio, H. K., Løvholt, F., Lorito, S.</b>	INVITED: UCERF3-ETAS: Including Spatiotemporal Clustering for a California Operational Earthquake Forecast. <b>Field, E. H.</b>
9:30 AM	STUDENT: Hybrid Seismic Denoising Using Higher Order Statistics and Improved Wavelet Block Thresholding. <b>Mousavi, S. M., Langston, C. A.</b>	STUDENT: Automatic Detection and Classification of Seismic Events. <b>Li, Z., Peng, Z.</b>	Shallow Slip Deficit and Low-angle Detachment Faulting in the 2010 El Mayor-Cucapah (Mexico) Earthquake Revealed with Differential Lidar. <b>Nissen, E., Lajoie, L., Arrowsmith, J. R., Glennie, C., Hinojosa Corona, A., Oskin, M. E.</b>	Local Tsunami Warnings: Perspectives from Recent Large Events. <b>Melgar, D., Allen, R. M.</b>	INVITED: Understanding of Active Tectonics of Himalayan Frontal Fault System in Northern India using Micro and Paleo Seismic Studies. <b>Kumar, S.</b>
9:45–10:45 AM	BREAK				
	<b>Marine Paleoseismology: Assessing Offshore Hazards</b> Session Chair: Neal Driscoll (see page 496)	<b>Seismo-Acoustics and Infrasond</b> Session Chairs: Stephen Arrowsmith and Omar Marcillo (see page 501)	<b>The Role of Shallow Slip on Faults</b> (continued)	<b>Tsunami Resilience Strategies: Application of Tsunami Science and Mitigation Advancements to Protect Communities</b> (continued)	<b>Active Tectonics, Faults and Large Earthquakes</b> (continued)
10:45 AM	Central and Northern Cascadia Revised Segment Boundaries and Probabilities from Onshore and Offshore Core Data. <b>Goldfinger, C., Galer, S., Black, B., Hausmann, R., Mason, B., Patton, J.</b>	INVITED: Assessment of Infrasond Signals Recorded on Seismic Stations and Infrasond Arrays in the Western US Using Ground Truth Sources. <b>Park, J., Hayward, C. T., Stump, B. W.</b>	Characterization of Shallow Slip Variability in California UAVSAR Repeat-Pass Interferograms. <b>Parker, J. W., Donnellan, A., Glasscoe, M. T., Pierce, M., Wang, J.</b>	Drone Based Visual Tsunami Warning System. <b>Hayashi, H., Schirling, P.</b>	Comprehensive Comparison of the Campbell-Bozorgnia NGA-West2 and Three Pan-European Ground Motion Models. <b>Campbell, K. W.</b>



Thursday, 21 April (continued)

<i>Time</i>	<i>Tuscany 1/2</i>	<i>Tuscany 3/4</i>	<i>Tuscany 5/6</i>	<i>Tuscany 7/8</i>	<i>Tuscany A</i>
	<b>Marine Paleoseismology...</b>	<b>Seismo-Acoustics and Infrasond</b>	<b>The Role of Shallow Slip on Faults</b>	<b>Tsunami Resilience Strategies...</b>	<b>Active Tectonics, Faults...</b>
11:00 AM	Determining Slip Along the Queen Charlotte-Fairweather Fault Zone. Greene, H. G., Barrie, J. V., <b>Nishenko, S.</b> , Conway, K., Enkin, R., Conrad, J., Maier, K. L., Stacey, C.	INVITED: Explosive Yield Estimation from Acoustic Waveform Inversion Including Three-Dimensional Propagation Effects. <b>Kim, K.</b> , Rodgers, A. J.	Constraining Models of Shallow Fault Slip with Remote Sensing Data. <b>Glasscoe, M.</b> , Donnellan, A., Lyzenga, G., Parker, J., Milliner, C.	Investigation of Tsunami Generation due to Asteroid Water Impacts or Air Bursts and their Consequences on Coastline Cities. <b>Ezzedine, S. M.</b> , Dearborn, D. S. P., Miller, P. L.	Fragility of Precariously-Balanced Rocks at Double Rock Site, Diablo Canyon Power Plant. <b>Stirling, M. W.</b> , Della Pasqua, F. N., Madugo, C. M., Abrahamson, N. A.
11:15 AM	Segmentation along the Newport-Inglewood Rose Canyon Fault Zone: Mapping and Implications for Rupture Propagation. <b>Sahakian, V. J.</b> , Bormann, J. M., Driscoll, N. W., Harding, A. J., Kent, G. M., Wesnousky, S. G.	STUDENT: Seismo-Acoustic Monitoring of Snowmelt Runoff in the Northern Colorado Rocky Mountains. <b>Anthony, R. E.</b> , Aster, R. C., Ryan, S. E., Rathburn, S. L.	Numerical Modeling of Surface Fault Rupture in Reverse Events. <b>Buelna, M.</b> , Moss, R. E. S.	Tsunami Debris Boat Forges Japan—California Connections and Promotes Tsunami Education Efforts. <b>Dengler, L. A.</b>	Sensitivity of Rupture Propagation to Nucleation Location and Slip Partitioning on the Imperial and Southern San Andreas Faults. <b>Kyriakopoulos, C.</b> , Meltzner, A. J., Rockwell, T. K., Oglesby, D. D.
11:30 AM	STUDENT: New High-Resolution 3D Imagery of Fault Deformation and Segmentation of the Newport-Inglewood Rose Canyon Fault and San Onofre Trend. <b>Holmes, J. J.</b> , Driscoll, N. W., Kent, G. M.	Seismic Equivalents of Acoustic Multipoles and Volcanic Jet Scaling Laws. <b>Haney, M. M.</b> , Matoza, R., Fee, D., Aldridge, D. F.	On Co- and Post-Seismic Slip of the 2014 South Napa Earthquake. <b>Minson, S. E.</b> , Murray, J. R., Brooks, B. A., Beck, J. L., Glennie, C. L., Ericksen, T. L., Hudnut, K. W.		Imaging 2015 Mw 7.8 Gorkha Earthquake and Its Aftershocks using Multiple Global Seismic Arrays. <b>Ghosh, A.</b> , Li, B.
11:45 AM	Modeling 3D Earthquake Scenarios on the Newport-Inglewood/Rose Canyon Fault. <b>Boudjema, M.</b> , Louie, J., Kent, G., Sahakian, V., Driscoll, N.	STUDENT: The Design of Free Flying Acoustic Stations. <b>Bowman, D. C.</b> , Lees, J. M., Jones, K. R.	Bayesian Inversion for Fault Frictional Parameters and Afterslip Following the South Napa Earthquake. <b>Murray, J. R.</b> , Minson, S. E.		INVITED: Imaging Coseismic Deformation from Large Thrust Earthquakes on the Edges of the Tibetan Plateau with Geodetic and Seismic Data. <b>Fielding, E. J.</b> , Liang, C. R., Huang, M. H., Sangha, S., Yue, H., Agram, P. S., Yun, S. H., Samsonov, S. V., Simons, M., Peltzer, G., Owen, S., Moore, A.

Thursday, 21 April (continued)

Time	Tuscany 1/2	Tuscany 3/4	Tuscany 5/6	Tuscany 7/8	Tuscany A
12:00 –1:30 PM	LUNCH				
	<b>Multi-Phenomenology Approaches to Explosion Source Studies</b> Session Chairs: Catherine Snelson, Christopher Bradley, and G. Eli Baker (see page 498)	<b>Numerical Modeling of Earthquake Ground Motion, Rupture Dynamics and Seismic Wave Propagation</b> Session Chairs: Peter Moczo, Steven Day, Emmanuel Chaljub, and Jozef Kristek (see page 502)	<b>Characterizing the Stress Field and Stress Drop for Earthquake Source Physics and Hazard Assessment</b> Session Chairs: Patricia Martínez-Garzón, Jeanne Hardebeck, Marco Bohnhoff, and Karen Luttrell (see page 506)	<b>Advancements in Network Operations and Station Design</b> Session Chairs: Kristine Pankow and David Wilson (see page 510)	<b>Active Tectonics, Faults and Large Earthquakes</b> (continued)
1:30 PM	Evaluation of a Seismic Event, 12 May 2010, in North Korea. Kim, W. Y., <b>Richards, P. G.</b> , Schaff, D. P., Koch, K.	Earthquake Ground Motion Simulations: SCEC Community Code Development and Validation Efforts. <b>Goulet, C. A.</b> , Maechling, P. J., Jordan, T. H., Luco, N., Rezaeian, S.	INVITED: Weak Fault Mechanisms Imply Creeping Faults. <b>Scholz, C. H.</b>	Theoretical Limits on Detectability of Small Earthquakes. <b>Kwiatek, G.</b> , Ben-Zion, Y.	STUDENT: Neotectonics of Java, Indonesia: Crustal Deformation in the Overriding Plate of an Orthogonal Subduction System. <b>Marliyani, G. I.</b> , Arrowsmith, J. R., Haq, S. S. B.
1:45 PM	Three-Component High Frequency Amplitude Models for Discrimination and Yield Estimation. <b>Phillips, W. S.</b> , Fisk, M. D., Stead, R. J., Begnaud, M. L., Yang, X., Ballard, S.	Taylor-expansion, Dispersion-relation Preserving, and Combined-approximation Finite-difference Schemes on the Staggered and Collocated Grids. Etemadsaeed, L., <b>Moczo, P.</b> , Kristek, J., Ansari, A., Kristekova, M.	Stress Variations across the Central and Eastern United States and a 3-D Model of Stress in the New Madrid Seismic Zone. <b>Levandowski, W.</b> , Boyd, O. S., Ramirez-Guzmán, L.	Detecting and Locating Seismic Events Without Phase Picks or Velocity Models. <b>Arrowsmith, S. J.</b> , Young, C., Ballard, S., Slinkard, M.	Crustal Response to Spatiotemporal Variations of Coseismic Slip along the Combined 1999 Izmit-Düzce Rupture. <b>Bohnhoff, M.</b> , Ickrath, M., Dresen, G.
2:00 PM	On Multi-Phenomenological Explosion Screening: Combining Waveform Signatures to Screen Above-Ground from Buried-Ejection Explosions. <b>Carmichael, J. D.</b> , Sentz, K., Arrowsmith, S. J., Nemzek, R.	STUDENT: Modeling Nucleation and Propagation of Shear Rupture on Rough Faults with a Large Range in Wavelengths. <b>Tal, Y.</b> , Hager, B. H.	Inference of Stress from Faulting and Topographic Loading of Faults. <b>Hetland, E. A.</b> , Medina Luna, L., Styron, R. H., Hines, T. T.	STUDENT: Semi-Auto Picking Using Array Seismogram Volume. <b>Shimoda, N.</b> , Reshetnikov, A., Shapiro, S. A.	Seismic Risk Management: From Earthquake Science, Seismic Risk Assessment, and Communication to Decision Making. <b>Wang, Z.</b>

Thursday, 21 April (continued)

Time	Tuscany 1/2	Tuscany 3/4	Tuscany 5/6	Tuscany 7/8	Tuscany A
2:15 PM	<b>Multi-Phenomenology...</b> A New Spectrogram-based Method for Automated Rg Detection. <b>O'Rourke, C. T.</b> , Baker, G. E.	<b>Numerical Modeling...</b> Fault Zone Plasticity Effects Quantified by Spontaneous Rupture Simulations. <b>Roten, D.</b> , Olsen, K. B., Day, S. M., Cui, Y.	<b>Stress Field and Stress Drop...</b> Stress Orientations along Megathrusts in Subduction Zones: Fault Strength and Seismic Coupling. <b>Hardebeck, J. L.</b>	<b>Network Operations and Station Design</b> Near Real-time Discrimination of Quarry and Mining Related Seismicity in the Central and Eastern United States. <b>Yeck, W. L.</b> , Benz, H. M., Earle, P. S.	<b>Active Tectonics, Faults...</b> An Open-Source Tool for Probabilistic Seismic Hazard Assessment Based on Monte Carlo and Random Fields Techniques. <b>Cheng, Y.</b> , Akkar, S.
2:30 PM	Cavity Radius Scaling and Seismic Radiation from Explosions. <b>Stroujkova, A.</b> , Vorobiev, O., Carnevale, M.	A New Viscoelastic 3D 4th-order Staggered-grid Finite-difference Scheme for Media with Material Discontinuities. <b>Kristek, J.</b> , Moczo, P., Kristekova, M., Chaljub, E.	Revisiting Apparent Stress Drop as a Possible Tool for Distinguishing Swarm and Mainshock/Aftershock Sequences. <b>Fischer, T.</b> , Hainzi, S.	Small-aperture Seismic Array Data Processing using the Representation of Seismograms at Zero-amplitude Points. <b>Brokešová, J.</b> , Malek, J.	Progress Toward a Uniform Magnitude Scale for Earthquake Hazard Assessment in Canada. <b>Bent, A. L.</b>
2:45–3:45 PM	BREAK				
3:45 PM	<b>Multi-Phenomenology Approaches to Explosion Source Studies</b> (continued)	<b>Numerical Modeling of Earthquake Ground Motion, Rupture Dynamics and Seismic Wave Propagation</b> (continued)	<b>Characterizing the Stress Field and Stress Drop for Earthquake Source Physics and Hazard Assessment</b> (continued)	<b>Advancements in Network Operations and Station Design</b> (continued)	<b>Active Tectonics, Faults...</b> (continued)
3:45 PM	The Challenges of Discriminating Explosions from Earthquakes at Local Distances with P/S Methods. <b>Walter, W. R.</b> , Pyle, M., Ford, S. R.	Ground Motion Simulation of Basin and Site Effects and the Resulting Structural Response of Representative Buildings. <b>Rodgers, A. J.</b> , Pitarka, A., McCallen, D. B.	Heat Flow Constraints on Fault-normal Stresses near the San Andreas Fault and Application to the Rupture Tip of Large Strike-slip Events and to Near-fault Deformation. <b>Sleep, N. H.</b>	New Research and Monitoring Opportunities with the Central and Eastern United States Seismic Network. <b>Sumy, D. F.</b> , Busby, R. W., Woodward, R. L., Brudzinski, M.	The High Frequency Seismic Wave Field Generated from Breaking Ocean Waves and the Link to Time-variable Sea States. <b>Poppeliers, C.</b>
4:00 PM	Source Characterization and Prediction of SPE5 from Full Waveform Inversions of SPE2, SPE3, and SPE4prime. Phillips-Alonge, K., <b>Knox, H.</b> , Ober, C., Abbott, R. E.	Dynamic Modeling of Potential Earthquake Rupture Paths through Cajon Pass, Southern California. <b>Lozos, J. C.</b> , Dolan, J. F., Oglesby, D. D.	INVITED: Regional Tectonic Stress Field and Earthquake Stress Drops in Southern California: Understanding Distributed Continental Plate Boundary Tectonics. <b>Hauksson, E.</b>	Field Studies of Non-double-couple and Mixed-source Proximal Earthquakes at The Geysers and Long Valley, California: Arrays and Experiments. <b>Evans, J. R.</b> , Brokešová, J. P., Málek, J., Hartline, C., Wilkinson, S. K.	Rapid Late-Quaternary Slip in the Tersky Range, Central Kyrgyz Tien Shan. <b>Campbell, G. E.</b> , Walker, R. T., Abdrakhmatov, K., Mackenzie, D., Jackson, J. A., Rizza, M., Elliott, J. R., Rhodes, A.

Thursday, 21 April (continued)

Time	Tuscany 1/2	Tuscany 3/4	Tuscany 5/6	Tuscany 7/8	Tuscany A
	<b>Multi-Phenomenology...</b>	<b>Numerical Modeling...</b>	<b>Stress Field and Stress Drop...</b>	<b>Network Operations and Station Design</b>	<b>Active Tectonics, Faults...</b>
4:15 PM	Near-Field Modeling of SPE Experiments using an Upscaled Model based on Geophysical Characterization. <b>Vorobiev, O. Y.</b> , Ezzedine, S., Hurley, R., Antoun, T., Glenn, L.	Simulation of Strong Ground Motions for the 2011 Tohoku Earthquake with Considerations of Multiple Nonlinear Effects. <b>Nozu, A.</b>	Fluid Injection Impact on Fracture Reactivation Potential at The Geysers Geothermal Field. <b>Martínez-Garzón, P.</b> , Kwiatek, G., Bohnhoff, M., Dresen, G.	Remote Determination of the In Situ Sensitivity of Galperin-Oriented Broadband Seismometers. <b>Hellweg, M.</b> , Uhrhammer, R. A. U., Taira, T.	A Note on the Scatter of Strong-motion Data in the Context of the Specific Barrier Model. <b>Halldorsson, B.</b> , Papageorgiou, A. S., Sonnemann, T.
4:30 PM	Near-Field to Far-Field Uncertainty Propagation and Quantification of Ground Motions Generated by the Source Physics Experiments (SPE). <b>Ezzedine, S. M.</b> , Vorobiev, O. Y., Hurley, R. C., Pitarka, A., Antoun, T. H., Walter, W., Glenn, L. A.	STUDENT: Scenario Earthquake and Ground Motion Simulations in the North China Basin: Effects of Heterogeneous Stress and 3D Basin Structure. <b>Liu, D.</b> , Duan, B.	Regional-scale Models of Crustal Stress in Southern California, with Implications for Heterogeneous Tectonic Loading and In Situ Stress Magnitude. <b>Luttrell, K.</b> , Smith-Konter, B.	Detection and Characterization of Pulses in Broadband Seismometers. <b>Wilson, D. C.</b> , Ringler, A. T., Hutt, C. R.	Tectonic Geomorphology and Paleoseismology of the Gatún Fault in Central Panamá. <b>Gath, E. M.</b> , Gonzalez, T., Rockwell, T. K., Franceschi, P.
4:45 PM	Yield and Depth Dependence of Joint Response to Explosive Loading. <b>Steedman, D. W.</b> , Bradley, C. R.	Soil-Topography Coupling Effects at Strong Motion Stations in California. of South China block and its neighboring regions, <b>Mohammadi, K.</b> , Asimaki, D.	Remote Triggering Inside Versus Outside Geothermal Fields in California. <b>Lin, G.</b> , Zhang, Q.	STUDENT: The Internet of Things: Geoscience-related Applications of Embedded Systems. <b>Sepulveda, F.</b> , Pulliam, J.	Complicated Kinematics of the Southern Cascadia Subduction Zone Near the Mendocino Triple Junction. <b>McPherson, B. C.</b>
<b>Joyner Lecture • Naples Ballroom</b>					
5:15 PM	Joyner Lecture: Site Response Uncertainty and its Implications for Seismic Risk Characterization. <b>Stewart, J. P.</b>				

**Active Tectonics, Faults and Large Earthquakes** (see page 516)

1. INVITED: Improved Comparison of PBRs With Hazard Maps for Rocks Near the San Andreas Fault in the Mojave Desert. **Brune, J. N.**, Brune, R. J., Anderson, J. G., Biasi, G. P.
2. INVITED: The Location of Indian Lithosphere Beneath Tibet: Insights from Group and Shear Wave Velocity Structure. Gilligan, A., **Priestley, K.**
3. Empirical Observations of the Influence of Steps on Rupture Propagation. **Biasi, G. P.**, Wesnousky, S. G.
4. Magnitude Thresholds Associated with Instruments of the Seismographic Network Used by the U.S. Coast and Geodetic Survey from 1930-1960. **Dewey, J. W.**
5. Compilation and Analysis of a Database of Local Tsunami Bulletins issued by the Pacific Tsunami Warning Center (PTWC) to the Hawaii Emergency Management Agency (HI-EMA) between October 2002 and July, 2015. **Sardina, V.**, Becker, N., Koyanagi, K., Walsh, D., McCreery, C.
6. STUDENT: Multi-Component C3 to Improve Amplitude Reliability for Hazard Analysis Using the Ambient Seismic Field. **Sheng, Y.**, Beroza, G. C., Denolle, M.



Thursday, 21 April (continued)

7. Earthquake-Protective Desks for Vulnerable Bhutanese Schools. Tschering, K. E., Bruno, I., O'Donnell, A., Kianirad, E., Sonam, K., **Tucker, B. E.**
8. INVITED: Advancing the Presentation of Earthquake Hazard: The USGS NSHMP Unified Hazard Tool. **Powers, P. M.**, Martinez, E. M., Fee, J. M.
9. Improved Estimation of Temporal Variation in Earthquake Detectability with Time-dependent Smoothness Constraint. **Iwata, T.**
10. Additional Period and Site Class Maps for the 2014 USGS National Seismic Hazard Model. **Shumway, A. M.**, Petersen, M. D., Powers, P. M., Rezaeian, S.
11. The Effect of Uncertainty in Predictor Variables on the Estimation of Ground-Motion Prediction Equations. **Kuehn, N. M.**, Abrahamson, N.
12. Unusual Characteristics of Seismicity Preceding and Following The 2010 Simeulue, Sumatra Earthquake Mw 7.8. **Sianipar, D. S.**, Subakti, H.
13. Seismic Activity Characteristic of the 2015 Nepal Ms8.1 and Ms7.5 Earthquake. **Xue, Y.**, Ren, X., Liu, S. Q., Liu, J., Wang, Y. X.
14. Extending Seismological Database through the Digitization of Analog Seismograms with DigitSeis: An Example from the Harvard - Adam Dziewonski Observatory Collection. **Bogiatzis, P.**, Altoé, I. L., Karamitrou, A., Ishii, M., Ishii, H.
15. STUDENT: Development of Ground Motion Data Catalog for Iran and Regions with Similar Tectonic Activities. **Farajpour, Z.**, Zare, M., Pezeshk, S.
16. STUDENT: Ground-Truth on the CSUEB Campus: Results from Integrating Geophysical, Geological and Geospatial Methods and Fault Trench Studies. **Abimbola, A. O.**, Strayer, L. M., McEvelly, A. T., Chan, J. H.
17. Compatibility of a Greek Within-Slab Earthquake Dataset with Published Ground-Motion Prediction Models. **Skarlatoudis, A. A.**
18. STUDENT: A Note on the Probabilistic Seismic Hazard Assessments of Húsavík, North Iceland. **Kowsari, M.**, Halldorsson, B.
19. STUDENT: A Comprehensive Study on a Site-Specific Hazard Analysis for a Liquid Natural Gas Tank Station. **Haji-Soltani, A.**, Pezeshk, S.
20. Spatial Relation Between Source Properties and Aftershock Distribution of the 2015 Nepal Earthquake. **Liu, B. Y.**, Shi, B. P.
21. Ground-Motion Prediction Equation for Vertical Component Derived from Subduction Slab Earthquake Records. **Zhao, J.**
22. STUDENT: Activation of Dead Thrust Faults and Formation of Stable Back Thrusts due to Back Limb Rotation after Thrust-front Propagation: An Example from the Western Transverse Ranges, Southern California. **Levy, Y.**, Rockwell, T.
23. The Short-term and Impending Trace of Frequency and P Wave Dispersion in Datong Seismic Sensitive Window. **Zhou, L.**, Zhang, Y., Song, M., Wang, X.
24. STUDENT: A Two-tiered Approach to Event Calibration across the Zagros Mountains of Iran. **Karasozen, E.**, Nissen, E., Bergman, E., Ghods, A.
25. Development of Ground Motion Prediction Equation for East Malaysia Considering Shallow Crustal Earthquakes. **Adnan, A. B.**, Harith, N., Shoushtari, A. V.
26. Seismic Waveform Spectrum Shift of Foreshocks in North Tibetan Plateau. **Yang, L. M.**, Mei, X. P., Jiang, J. J.
27. STUDENT: Bimaterial Interfaces at the Karadere Segment of the North Anatolian Fault, Northwestern Turkey. **Najdahmadi, B.**, Bohnhoff, M., Ben-Zion, Y.
28. STUDENT: Variations in the Crustal Shear Wave Velocity Structure above the Peruvian Flat Slab. **Knezevic Antonijevic, S.**, Wagner, L. S., Beck, S. L., Zandt, G., Long, M. D., Tavera, H.
29. Lithospheric Structure of an Incipient Rift Basin: Results from Receiver Function Analysis of Bransfield Rift Basin, NW Antarctic Peninsula. **Biryol, C. B.**, Lee, S. J., Lees, J. M., Shore, M. J.

---

#### Advancements in Network Operations and Station Design (see page 523)

---

30. The Design and Data Translation of the Rotaphone, with an Example of the Instrument. Málek, J., Brokešová, J. P., **Evans, J. R.**
31. Feasibility of Tilt Measurement Using Seismometer Mass Position Data. Bainbridge, G., **Karimi, S.**, Yenier, E., Moores, A.
32. Short-Period Sensors with Extended Frequency Response for Earthquake Monitoring. **Besedina, A. N.**
33. Seismic Observations of Surface-Hole Installation Techniques. Sweet, J., Beaudoin, B., **Barstow, N.**, Pfeifer, C., Reusch, M., Anderson, K.
34. Review of Recent Improvements in Design and Performance of the Alaska Regional Seismic Network. **Merz, D. K.**, Bruton, C. P., Buurman, H., Dalton, S. M., Ruppert, N. A., West, M. E.
35. Waveform Recovery Enhancements in the Utah Network. **Rusho, J.**, Hatch, C., Drobeck, D., Pankow, K.
36. Microseismic Network Design in 3D Velocity Models. **Wuestefeld, A.**, Naesholm, S. P., Lang, D.
37. A Procedure for CISN Ground Motion Packet Association. **Hagos, L.**, Haddadi, H., Shakal, T.
38. Seismic Data Quality Control using DQA, Data Quality Analyzer. **Holland, A. A.**, Baker, A. M., Falco, N., Holland, J., Ringler, A. T., Wilson, D.
39. The EarthScope USArray Array Network Facility (ANF): Metadata, Network and Data Monitoring for

Thursday, 21 April (continued)

- the Transportable Array in Alaska. **Eakins, J.**, Vernon, F., Cox, T., Martynov, V., Tytell, J., Reyes, J., Davis, G., Meyer, J., Busby, R.
40. Array Network Facility Operations for the Central and Eastern United States Seismic Network. Cox, T., **Vernon, F.**, Eakins, J., Davis, G., Meyer, J., Reyes, J., Tytell, J., Busby, R.
41. Data Sets and Data Delivery Services from the Northern California Earthquake Data Center. **Neuhauser, D. S.**, Zuzlewski, S., Allen, R. M.

#### Characterizing the Stress Field and Stress Drop for Earthquake Source Physics and Hazard Assessment (see page 525)

42. STUDENT: Using Finite Fault Inversions and Near-Field Data to Determine the Uncertainty Range of Co-Seismic Stress Drop of Large Earthquakes. **Adams, M. N.**, Ji, C., Twardzik, C., Archuleta, R.
43. STUDENT: Structural Context of the 2015 Pair of Nepal Earthquakes (Mw 7.8 And Mw 7.3): An Analysis Based on Slip Distribution, Aftershock Growth and Static Stress Changes. **Parameswaran, R. M.**, Rajendran, K., Rajendran, C. P.
44. Probabilistic Seismic Hazard Assessment for East Anatolian Fault Zone Using Planar Source Models. **Gulerce, Z.**, Menekse, A., Ozacar, A. A., Cetin, K. O., Kaymakci, N.
45. Study on Focal Mechanism Solutions and Stress Field of Lushan M7.0 Earthquake Sequence. **Zhang, Z. W.**, Zhou, L. Q.

#### Induced Seismicity Monitoring: What is Really Needed? (see page 526)

46. Performance Evaluation of the Regional Seismograph Network in Northeast British Columbia, Canada, for Monitoring of Induced Seismicity. **Babaic Mahani, A.**, Kao, H., Walker, D., Johnson, J., Salas, C.
47. Real-time Ground-motion Mapping based on an Automatic Response System (ARS), with Applications to Induced-seismicity Traffic Light Protocols. **Assatourians, K.**, Atkinson, G.
48. STUDENT: Detecting Induced Micro-Seismic Events during Hydraulic Fracturing to build more Complete Event Catalogs. **Smith, T.**, Arce, A., Ji, C.
49. Design and Realization of a Seismic Monitoring System for the Geothermal Production Site of Torre Alfina (Italy). **Braun, T.**, Carapezza, M. L., Pagliuca, N., Famiani, D., Frepoli, A., Gattuso, A., Lisi, A., Marchetti, A., Badiali, L., Mele, G.
50. Using a Large-N Array to Probe Injection-induced Seismicity in Oklahoma. **Dougherty, S. L.**, Cochran, E. S., Harrington, R. M.
51. STUDENT: Template Hunting For Small Events Using Frequency Domain Array Processing in Regions of

Induced Seismicity. **Linville, L. M.**, Pankow, K. L., Kilb, D. L., Garrett, N.

52. Hydraulic Fracturing Operation Monitoring with Sparse Surface Networks; Duvernay Case Study. Baturan, D., **Karimi, S.**, Law, A., Yenier, E.

#### Machine Learning and its Application to Earthquake and Explosion Signal Analysis (see page 528)

53. Unsupervised Classification of Microseismic Events. **Langet, N.**, Wuestefeld, A., Oye, V.
54. Improved Bulletin Generation using an Iterative Processing Framework. Ballard, S., **Slinkard, M.**, Encarnacao, A., Draelos, T., Young, C., Brogan, R.
55. STUDENT: Explore Social Network Analysis using Seismic Array. **Kong, Q.**, Allen, R.
56. Comparing Time and Frequency Domain ANN Methods for Rapidly Searching Large Seismic Signal Archives. **Young, C.**, Gonzales, A., Kwok, J.
57. Challenges for Adaptive Self-Tuning of Seismic Sensors: Detailed Case Study at Erebus Volcano, Antarctica. **Knox, H. A.**, Draelos, T. J., Young, C. J., Chael, E. P., Peterson, M. G., Lawry, B. J.

#### Marine Paleoseismology: Assessing Offshore Hazards (see page 529)

58. Constraining the Paleoseismic History and Maximum Event Magnitude for the San Diego Trough Fault Zone, Offshore Southern California. **Bormann, J. M.**, Kent, G. M., Driscoll, N. W., Harding, A. J.
59. Bradley Lake Revisited: Sedimentary Evidence for Shorter Return Periods. **Patton, J. R.**, Goldfinger, C.
60. STUDENT: Upper Plate Structure and Forearc Deformation above the Kodiak Segment of the Alaska-Aleutian Megathrust. **Ramos, M. D.**, Liberty, L. M., Haeussler, P. J.
61. Buenas no(t)ches: Geometry of Holocene Tidal Notches in Paleoseismic Studies, an Example from Perachora Peninsula, Greece. Schneiderwind, S., Kazmer, M., Boulton, S. J., Papanikolaou, I. D., Stewart, I. S., **Reicherter, K.**
62. STUDENT: The Footprints of Typhoons on Seismic Records and their Implications on Small-scale Coupling Mechanisms in South China Sea. **Xiao, H.**, Xue, M., Yang, T., Liu, C. G., Hua, Q. F., Xia, S. H., Huang, H. B., Le, B. M., Huo, D., Tongji University; Pan, M.H., Tongji University; Li, L., Tongji University

#### Multi-Phenomenology Approaches to Explosion Source Studies (see page 530)

63. Reflection Seismic Images from a Novel Seismic Source: Seeking Buried Targets at the Nevada National Security Site. **Rowe, C. A.**, Snelson-Gerlicher, C. M., Ralston, M. D.

Thursday, 21 April (continued)

64. Improved Seismic Characterization Using Joint Inversion of Disparate Data Types. **Preston, L.**, Watson-Ross, C.
65. High Resolution Regional Attenuation Modeling for the Source Physics Experiment. **Pyle, M. L.**, Walter, W. R., Pasyanos, M. E.
66. Observations of Explosion Seismic Energy Partitioning: Insights from the Source Physics Experiment. **Ford, S. R.**, Pitarka, A., Ezzedine, S. M., Walter, W. R., Chiang, A., Mellors, R. J.
67. Shear Motion Energy Budget for the SPE-4Prime Underground Explosion. **Pitarka, A.**, Ezzedine, S., Vorobiev, O., Ford, S., Walter, W., Antoun, T.
68. Performance of High Frequency P/S Seismic Source Discriminant at Local Distances. **Pitarka, A.**, Walter, W., Chiang, A., Wagoner, J., Pyle, M., Ford, S.
69. Source Analysis of Underground Chemical Explosions from the Source Physics Experiment. **Chiang, A.**, Ford, S. R., Pitarka, A.
70. Study of the Near-Source Effects on Local Seismic Signals: Case of SPE4prime. **Larmat, C. S.**, Delorey, A. A., Steedman, D. W., Rougier, E., Knight, E. E., Bradley, C. R.
71. Modeling Wave Propagation in Jointed Rock Masses at Variable Spatial Resolutions: Theory and Simulations for the Source Physics Experiments (SPE). **Hurley, R. C.**, Vorobiev, O. Y., Ezzedine, S. M., Antoun, T. H., Walter, W., Glenn, L. A.
72. Multi-Phenomenology Yield Estimation of Near-Surface Chemical and Nuclear Explosions. **Rodgers, A. J.**, Ford, S. R., Ramirez, A. R., Kim, K., Dodge, D. A., Knapp, D. R., Pitarka, A., Bulaevskaya, V.
73. The 12 August 2015 Tianjin, China Chemical Explosions. **Zhao, L. F.**, Xie, X. B., Wang, W. M., Hao, J. L., Yao, Z. X.
74. STUDENT: Preliminary Numerical Validation of the Fault Mechanism of the 2007 Mw6.6 Niigata-Chuetsu-Oki Strong Ground Motion Earthquake by Spectral Element Method. **Gatti, F.**, Paolucci, R., Lopez-Caballero, F., Clouteau, D.
75. The SCEC Broadband Platform: Open-Source Software for Strong Ground Motion Simulation and Validation. Silva, F., **Goulet, C.**, Maechling, P., Callaghan, S., Jordan, T.
76. STUDENT: Source Depth and Azimuth Dependent Synthetic Lg Attenuation. **Hui, H.**, Sandvol, E.
77. STUDENT: High Frequency Regional Phase Modeling in Crustal Pinch and Bulge Structures Simulated with Radiative Transport. **Sanborn, C. J.**, Walsh, S., Cormier, V. F.
78. STUDENT: Source Geometry and Free Surface Influence on Earthquake Rupture Characteristics in the Subduction Zone of Mexico's Pacific Coast. **Carrillo Lucia, M. A.**, Ramirez-Guzmán, L.
79. Pointwise Functions for Flexible Implementation of Crustal Deformation Physics in PyLith. **Aagaard, B. T.**, Knepley, M. G., Williams, C. A.
80. Initiation of Dynamic Ruptures in Numerical Simulations and its Effects on Rupture Propagation and Ground Motion. Galis, M., Ampuero, J. P., Mai, P. M., Kristek, J., **Moczo, P.**
81. Effects of the Wasatch Front, Utah, Sedimentary Basins on Earthquake Ground Motions from Observed and Simulated Waveforms. **Moschetti, M. P.**, Hartzell, S., Ramirez-Guzman, L., Rennolet, S.
82. STUDENT: Ground Motion Simulations for Scenario Earthquakes in the Xianshuihe Seismic Zone of Southwestern China. **Zhang, L. F.**, Wang, Z. M.
83. STUDENT: Supershear Transition Analysis in 3D Rough Fault Dynamic Simulations. **Yao, Q. Y.**, Day, S. D., Shi, S. Z. Q.
84. STUDENT: Extracting the Statistics of 3D Rough Fault Dynamic Rupture Simulations for Pseudo-Dynamic Source Generation. **Savran, W. H.**, Olsen, K. B.
85. Modeling Topographic Effects and Site Response on a Mesa near Los Alamos, New Mexico. **Larmat, C. S.**, Lee, R. C.

---

#### Seismo-Acoustics and Infrasond (see page 535)

---

86. Seismic and Ionospheric Signatures for the Study of Underwater Earthquakes: Modeling Developments. Rolland, L. M., **Larmat, C.**, Rémillieux, M., Khelifi, K., Lognonné, P.
87. Infrasond Scaling Characteristics from Small Earthquakes in the Utah Region. **Hale, J. M.**, Pankow, K. L., Arrowsmith, S. J., Stump, B., Hayward, C.
88. Detection and Association of Seismoacoustic Data from a Series of Chemical Explosions in New Mexico. **Euler, G. G.**, Blom, P. S., Anderson, D. N.
89. Amplitude and Frequency Calibration on Infrasond Sensors. Zeiler, C. P., **Allison, F.**, Wuertley, R.
90. A Global Infrasond Event Catalog. **Arrowsmith, S. J.**
91. STUDENT: Infrasond Waves in the Stratosphere: Sources and Implications for Atmospheric Dynamics. **Bowman, D. C.**, Lees, J. M.
92. STUDENT: Improving Infrasond Detection and Location Catalogs in the Western US Using Atmospheric Modeling. **Dannemann, F. K.**, Park, J., Marcillo, O., Blom, P., Hayward, C., Stump, B. W.

---

#### The Role of Shallow Slip on Faults (see page 536)

---

93. Paleoseismic Results from Two Sites on the Principal Strand of the August 24, 2014 South Napa Earthquake Rupture. **Dawson, T. E.**, Rubin, R. S., Mareschal, M.

Thursday, 21 April (continued)

94. STUDENT: Lidar Investigation of Scarp Degradation along the 1959 Hebgen Lake Earthquake Surface Rupture. **Johnson, K. L.**, Nissen, E. K., Lajoie, L. J.

**Tsunami Resilience Strategies: Application of Tsunami Science and Mitigation Advancements to Protect Communities** (see page 537)

95. USGS-National Tsunami Hazard Mitigation Program Workshop and Collaborations. **Ross, S. L.**, Wilson, R. I., Wood, N. J., Gately, K., Geist, E. L., Nicolsky, D. J.
96. NOAA National Tsunami Warning Center Operations during the 2015 Chile Earthquake and Tsunami. Huang, P. Y., Bahng, B., Gately, K., Hale, D. A., Kim, Y. Y., **Nyland, D.**, Popham, C., Waddell, J., Whitmore, P. M.
97. Compilation and Analysis of a Database of Observatory Messages and Tsunami Bulletins issued by the Pacific Tsunami Warning Center (PTWC) for the Southwest Pacific Region between 2000 and 2015. **Sardina, V.**, Weinstein, S., Becker, N.
98. "Beat the Wave" Cascadia Tsunami Evacuation Maps for Oregon Coastal Communities. **Madin, I.**, Gabel, L. L., Allan, J. C., Watzig, R. J.

99. The September 17, 2015, Chilean Tsunami in California: Response Activities and Field Observations. **Wilson, R.**, Lynett, P., Synolakis, C., Miller, K.

**The M7.1 Iniskin Earthquake, Alaska** (see page 538)

100. M7.1 Iniskin, Alaska Earthquake of January 24, 2016: A Preliminary Review of Responses of Three Instrumented Buildings in Anchorage, Alaska. **Çelebi, M. K.**
101. Earthquake Ground Motions from the 2016 M7.1 Iniskin Earthquake in Anchorage, Alaska Related to Distribution of Sedimentary Deposits. **Cannon, E. C.**, Dutta, U., Thornley, J. D.
102. Seismic Response of a Highway Bridge during the Iniskin Earthquake. **Yang, Z.**, Still, B., Dutta, U., Thornley, J.
103. Estimation of Site Response and its Correlation with Vs30 at Strong Motion Station Sites in Anchorage Basin from M7.1 Iniskin Earthquake, Alaska. **Dutta, U.**, Thornley, J., Cannon, E. C., Yang, Z. J.
104. USArray Transportable Array Observations of the 7.1 Mw Iniskin Earthquake in Cook Inlet, Alaska. **Eakins, J.**, Busby, R. W., Vernon, F., Ruppert, N.
105. Aftershock Sequence of the 24 January, 2016 M7.1 Iniskin Earthquake, Southern Alaska. Ruppert, N. A., Holtkamp, S., **West, M.**



Thursday, 21 April (continued)

Friday, 22 April—Oral Sessions

Time	Tuscany 1/2	Tuscany 3/4	Tuscany 5/6	Tuscany 7/8	Tuscany A
	<b>Earthquake Source Parameters and Slip from Seismic, Geodetic and Laboratory Data: Theory, Observations and Interpretations</b> Session Chairs: Vaclav Vavryčuk, Grzegorz Kwiatek, and German Prieto (see page 539)	<b>Deep Earthquakes and Surrounding Slab Structures</b> Session Chairs: Zhongwen Zhan, Meghan S. Miller, and Germán Prieto (see page 543)	<b>Secondary Earthquake Hazards and Losses</b> Session Chairs: Eric Thompson and Kate Allstadt (see page 548)	<b>NGA-East: Research Results and Ground-Motion Characterization Products for Central and Eastern North America</b> Session Chairs: Christine Goulet and Yousef Bozorgnia (see page 553)	<b>Seismicity and Seismic Hazards of the Walker Lane and Western Great Basin</b> Session Chairs: John Anderson, John Louie, Richard Koehler, Corné Kreemer, and Wanda Taylor (see page 557)
8:30 AM	INVITED: Accounting for 3D Earth Structure in Seismic Moment Tensor Inversion. <b>Dreger, D. S.</b> , Nayak, A., Chiang, A.	Rupture Mechanism of the May 24, 2013 Mw8.3 Sea of Okhotsk Deep-Focus Earthquake. <b>Zhang, H.</b> , van der Lee, S., Bina, C., Ge, Z.	INVITED: Searching for Correlations: Landslide Distribution from the 2015 <i>M</i> 7.8 Gorkha, Nepal Earthquake. <b>Collins, B. D.</b> , Jibson, R. W., Kargel, J. S., Shugar, D. H., Haritashya, U. K.	PEER NGA-East Overview: Development of a Ground Motion Characterization Model and Ground Motion Prediction Equations for Central and Eastern North America. <b>Goulet, C. A.</b> , Bozorgnia, Y., Abrahamson, N. A.	Fault Reactivation, Network Connectivity, and Strike-slip Deformation in the Transtensional Walker Lane. <b>Briggs, R. W.</b> , Stephenson, W. J., McBride, J. H., Gold, R. D., McNamara, D. E.
8:45 AM	STUDENT: Seismic Moment Tensors of Acoustic Emissions Recorded During Laboratory Rock Deformation Experiments: Sensitivity to Attenuation and Velocity Anisotropy. <b>Stierle, E.</b> , Vavryčuk, V., Kwiatek, G., Charalampidou, E. M., Bohnhoff, M.	INVITED: Investigating the Effects of Plate Age and Tectonic Regime on the Rupture Dynamics of Intermediate-Depth Earthquakes using Dynamic Inversion. <b>Twardzik, C.</b> , Ji, C.	INVITED: A New Method for Assessing Coseismic Landslide Hazard in Regions Without Historical Landslide Inventories. <b>Robinson, T. R.</b> , Kritikos, T., Davies, T. R. H., Rosser, N. J.	INVITED: NGA-East Database. <b>Kishida, T.</b> , Goulet, C. A., Ancheta, T. D., Cramer, C. H., Darragh, R. B., Silva, W. J., Hashash, Y. M., Harmon, J., Stewart, J.P., Wooddell, K. E., Youngs, R.R., Mazzoni, S.	INVITED: Neotectonics Brings Interesting Challenges to the Assessment of Seismic Hazard in the Northern Walker Lane. <b>Wesnousky, S. G.</b> , Pierce, I. K., Milawsky, E., Louie, J., Kreemer, C., Hammond, W., Faulds, J., Carlson, C., Brune, J.N., Borman, J.
9:00 AM	INVITED: Scaling of Finite-Source Parameters at Parkfield California. <b>Wooddell, K. E.</b> , Dreger, D. S., Taira, T., Nadeau, R., Malagnini, L.	Static and Dynamic Parameters of Intermediate-depth and Deep Earthquakes from Spectral Analysis and Source Inversions. <b>Prieto, G. A.</b> , Poli, P., Herrera, C., Ruiz, S., Cruz-Atienza, V.	INVITED: Rapid Assessment of Liquefaction Movements for Use in Earthquake Loss Estimates. van Ballegooy, S., Martin, J. G., Deterling, O., Secara, S., Hu, J. (Presenter: <b>Ellen Rathje.</b> )	INVITED: A Review of Seed Ground-Motion Models used in NGA-East. <b>Graves, R. W.</b> , The NGA-East Ground-Motion Model Developer Working Group	INVITED: Tectonic Evolution and Structural Framework of the Walker Lane: Implications for Seismic Hazards. <b>Faulds, J. E.</b> , Carlson, C. W., Henry, C. D., Wesnousky, S. G.

<i>Time</i>	<i>Tuscany 1/2</i>	<i>Tuscany 3/4</i>	<i>Tuscany 5/6</i>	<i>Tuscany 7/8</i>	<i>Tuscany A</i>
	<b>Earthquake Source Parameters...</b>	<b>Deep Earthquakes...</b>	<b>Secondary Earthquake Hazards...</b>	<b>NGA-East: Research Results...</b>	<b>Walker Lane and W. Great Basin...</b>
9:15 AM	Evidence for and Implications of Rupture Velocity Acceleration During Earthquake Rupture Onsets. <b>Meier, M. A.</b> , Heaton, T. H., Clinton, J. F.	Rupture Processes of M>7 Hindu Kush Intermediate-depth Earthquakes. <b>Zhan, Z.</b> , Ye, L., Lay, T., Kanamori, H.	INVITED: Estimation of Liquefaction-Induced Land, Building and Infrastructure Damage from Measured Ground Surface Movements. <b>van Ballegooy, S.</b> , Rathje, E. M., O'Rourke, T. D.	INVITED: Treatment of Epistemic Uncertainties in Median Predictions for NGA East. <b>Kuehn, N. M.</b> , Goulet, C., Al-Atik, L., Abrahamson, N. A., Atkinson, G., Graves, R. W., Youngs, R. R., Bozorgnia, Y.	Strong Ground Motions in Normal Faulting Earthquakes: Nevada, Japan, and Worldwide. <b>Anderson, J. G.</b> , Kawase, H., Biasi, G. P.
9:30 AM	Inversion for the Composite Moment Tensor. <b>Vavrycuk, V.</b>	INVITED: Source Models for Intermediate and Deep Focus Earthquakes: Parameterization and Non-uniqueness. <b>Lay, T.</b>	INVITED: Overview and Recent Progress on the Next-Generation of Liquefaction Assessment Project. <b>Stewart, J. P.</b> , Kramer, S. L., Kwak, D. Y., Greenfield, M. W., Kayen, R. E., Tokimatsu, K., Bray, J. D., Beyzaei, C. Z., Cubrinovski, M., Sekiguchi, T., Nakai, S., Bozorgnia, Y.	INVITED: Aleatory Variability Model for NGA-East. <b>Al Atik, L.</b> , Goulet, C., Abrahamson, N., Youngs, R., Graves, R., Atkinson, G.	Review of the Seismotectonics, Historical and Instrumental Seismicity of Nevada and Eastern California. <b>Smith, K. D.</b> , Ruhl, C. J., Kent, G. M.
9:45–10:45 AM	BREAK				

Friday, 22 April (continued)

<i>Time</i>	<i>Tuscany 1/2</i>	<i>Tuscany 3/4</i>	<i>Tuscany 5/6</i>	<i>Tuscany 7/8</i>	<i>Tuscany A</i>
	<b>Earthquake Source Parameters and Slip from Seismic, Geodetic and Laboratory Data: Theory, Observations and Interpretations</b> (continued)	<b>Deep Earthquakes and Surrounding Slab Structures</b> (continued)	<b>Advances in Earthquake Science Using Digital Photogrammetry</b> Session Chairs: Nadine Reitman, Kendra Johnson, and Lia Lajoie (see page 549)	<b>NGA-East: Research Results and Ground-Motion Characterization Products for Central and Eastern North America</b> (continued)	<b>Risk Management Applications of Earthquake Seismology</b> Session Chairs: Delphine Fitzenz and Nico Luco (see page 558)
10:45 AM	INVITED: Scaling and Uncertainty of PGA and PGV with Respect to Moment Magnitude 3.3–7.7: Implications for Stress Drop and the Moment Rate Function. <b>Archuleta, R. J.</b> , Ji, C.	INVITED: Deformation of the Nazca Slab in the Deep Upper Mantle and Mantle Transition Zone beneath South America. <b>Long, M. D.</b> , Eakin, C. M., Scire, A., Beck, S. L., Wagner, L. S., Zandt, G., Tavera, H.	Ultra-high Resolution Topographic Data for Earthquake Science: Laser Scanning Versus Photogrammetry. <b>DeLong, S. B.</b> , Crosby, C. J., Pickering, A. J., Prentice, C. S., Lienkaemper, J. J., Rubin, R. S., Dawson, T. E., Scharer, K. M., Hecker, S. Clahan, K. B., Sickler, R. R., Schwartz, D. P.	INVITED: Use of Seismic Hazard Calculations in the NGA East SSHAC Process. <b>Youngs, R. R.</b> , Goulet, C. A., Abrahamson, N. A., Al-Atik, L., Atkinson, G. M., Graves, R. W., Kuehn, N. M., Bozorgnia, Y.	INVITED: Feedback from the 2015 ATC/USGS Seismic Hazard User-needs Workshop. <b>Olsen, A. H.</b> , Luco, N., Rojahn, C., Powers, P. M.
11:00 AM	M <sub>w</sub> (ML)—using ML to estimate M <sub>w</sub> —a continental approach. <b>Herrmann, R. B.</b> , Benz, H.	Detecting Slab Structure Beneath the Banda Arc from Waveform Analysis of Deep Focus Earthquakes. <b>Miller, M. S.</b> , Holt, A. F., Sun, D.	STUDENT: The Landers Rupture Revisited: A Test Case in Computing Topography and Deformation From Legacy Aerial Photographs. <b>Lajoie, L. J.</b> , Johnson, K. E., Nissen, E., Scharer, K. M., Hudnut, K. W.	Prediction Equation for Central and Eastern North America based on a Regionally-Adjustable Generic Ground Motion Model. <b>Yenier, E.</b> , Atkinson, G. M.	INVITED: Project '17: Balancing Precision in Ground Motion Mapping with Uncertainty. <b>Hamburger, R. O.</b> , Luco, N.
11:15 AM	A Near-Field, Near-Instantaneous Earthquake Doublet ( $M_w$ 6.9, 6.7): Implications for Dynamic Triggering and Rupture Forecasting. <b>Nissen, E.</b> , Elliott, J. R., Sloan, R. A., Craig, T. J., Funning, G. J., Hutko, A., Parsons, B. E., Wright, T. J.	INVITED: The Role of Homologous Temperature in Global Earthquake Locations. <b>Davis, P. M.</b>	STUDENT: Quantifying Near-Field Deformation Patterns of Large Magnitude Strike-Slip Earthquakes Using High-Resolution Air Photos. <b>Milliner, C.</b> , Dolan, J., Hollingsworth, J., Sammis, C., Allam, A., Leprince, S., Ayoub, F.	Ground Motion Prediction Equations for the Central and Eastern United States. <b>Graizer, V.</b>	STUDENT: Effects of Epistemic Uncertainty in Seismic Hazard Estimates on Building Portfolio Losses. <b>Kotha, S. R.</b> , Bazzurro, P., Pagani, M.

Friday, 22 April (continued)

<i>Time</i>	<i>Tuscany 1/2</i>	<i>Tuscany 3/4</i>	<i>Tuscany 5/6</i>	<i>Tuscany 7/8</i>	<i>Tuscany A</i>
	<b>Earthquake Source Parameters...</b>	<b>Deep Earthquakes...</b>	<b>Digital Photogrammetry</b>	<b>NGA-East: Research Results...</b>	<b>Risk Management Applications...</b>
11:30 AM	Observations and Physical Interpretations of Double-corner Frequency Source Spectra. <b>Denolle, M. A.</b> , Shearer, P. M.	Seismic Evidences for Dynamic Activity of the Japan Subduction Zone beneath Northeast China. <b>Chen, Q. F.</b> , Li, T. J.	Analysing Three-dimensional Surface Displacements from Pleiades Stereo Imagery for the 2013 Balochistan and 2010 El-Major Cucupah Earthquakes. <b>Parsons, B.</b> , Zhou, Y., Elliott, J. R., Barisin, I., Walker,	STUDENT: A Simulation-Based Ground Response Model to Guide Development of a Generalized Site Amplification Model for Central and Eastern North America. Harmon, J. A., <b>Hashash, Y. M. A.</b> , Stewart, J. P., Rathje, E. M., Campbell, K. W., Silva, W. J., Parker, G., Xu, B.	Seismic Site Characterizations and Earthquake Loss Estimation Analyses for 25 Schools in Thurston County, Washington State. <b>Cakir, R.</b> , Walsh, T. J., Hayashi, K., Norman, D. K.
11:45 AM	Seismicity Statistics and Stress in Regions with High Tectonic Complexity: A Comparative Study of the Greater San Gorgonio and Ventura Regions in Southern California. <b>Goebel, T. H. W.</b> , Hauksson, E., Plesch, A., Shaw, J. H.	Early Aftershock Sequences of the 2015 Mw7.5 Hindu Kush Intermediate-Deep Earthquake by Waveform Matching Detection. Li, C., <b>Peng, Z.</b> , Yao, D.	Determining Source Characteristics of Historic and Prehistoric Earthquake Ruptures in Central Asia Using Multi-scale, Multi-platform Photogrammetry. <b>Elliott, A. J.</b> , Walker, R., Parsons, B., Gruetzner, C., Mackenzie, D., Ainscoe, E., Abdrakhmatov, K.	STUDENT: Empirical Seismic Site Amplification in Central and Eastern North America from NGA-East Ground Motion Database. <b>Parker, G. A.</b> , Stewart, J. P., Hashash, Y. M. A., Rathje, E. M., Campbell, K. W., Silva, W. J., Harmon, J. A., Xu, B.	Quantifying the Location, Width, and Style of Coseismic Surface-Fault Displacement at Gas Transmission Pipeline Fault Crossings in Northern California. <b>Givler, R.</b> , Hull, A., Madugo, C., Lifton, Z., Lewandowski, N., Thomsson, S., Lowry, D.
12:00 -1:30 PM	LUNCH				



Friday, 22 April (continued)

<i>Time</i>	<i>Tuscany 1/2</i>	<i>Tuscany 3/4</i>	<i>Tuscany 5/6</i>	<i>Tuscany 7/8</i>	<i>Tuscany A</i>
	<b>Earthquake Source Parameters and Slip from Seismic, Geodetic and Laboratory Data: Theory, Observations and Interpretations</b> (continued)	<b>Upper Crustal Passive Imaging for Hazards and Exploration</b> Session Chairs: John Louie and Ileana Tibuleac (see page 546)	<b>Citizen Seismology: Citizens as an Information Source to Advance Earthquake Response and Science</b> Session Chairs: Michelle Guy and Remy Bossu (see page 550)	<b>Physical and Statistical Properties of Earthquake Swarms and Clustered Seismicity: Constraining Driving Mechanisms</b> Session Chairs: Christine Ruhl, Ilya Zaliapin, and Rachel Abercrombie (see page 555)	<b>Risk Management Applications of Earthquake Seismology</b> (continued)
1:30 PM	Source Parameters in the Middle East Estimated by Accounting for Lateral Variations in Coda Amplitudes. <b>Pasyanos, M. E.</b> , Gok, R., Walter, W. R.	Mapping Love/Rayleigh Phase/Group Velocity Dispersion Between 2–100 Seconds in North America using Ambient Noise Cross-correlations and Earthquake Observations. <b>Herrmann, R. B.</b> , Benz, H., Ammon, C. J.	INVITED: Development of the Citizen Seismometer Network System Utilizing Smartphones and Applicability of these Data Estimating Seismic Damages. <b>Naito, S.</b> , Nakamura, H., Ikuo Takahashi, , Azuma, H., Fujiwara, H.	INVITED: Identification and Characterization of Earthquake Swarms in Southern California. <b>Shearer, P. M.</b> , Zhang, Q.	Risk Model for a System-Wide Dam Risk Reduction Program in Northern California. <b>Wooddell, K.</b> , Donahue, J., Watson-Lamprey, J., Abrahamson, N., AbramsonWard, H., Lewandowski, N., Madugo, C., Thompson, S.
1:45 PM	Coseismic Slip Model of the Nov 17, 2015 M=6.5 South Lefkada Earthquake, Ionian Sea, Greece from Inversion of Geodetic Data. Ganas, A., <b>Melgar, D.</b> , Briole, P., Papathanassiou, G., Geng, J., Bozionelos, G., Argyrakis, P., Valkaniotis, S., Mendonidis, E., Moshou, A., Elias, P.	Joint Surface Wave and Earthquake Travel-Time Inversion for Western North Island, New Zealand, 3-D Velocity Model. <b>Eberhart-Phillips, D.</b> , Fry, B.	INVITED STUDENT: Validation and Calibration of Predictive Relationships between Earthquake Intensity and Tweets Rate for Improving Real-Time Estimation Intensity. <b>Kropivnitskaya, Y. Y.</b> , Tiampo, K. F., Qin, J., Bauer, M. A.	Earthquake Declustering via a Nearest-Neighbor Approach in Space-Time-Magnitude Domain. <b>Zaliapin, I.</b> , Ben-Zion, Y.	INVITED: Modeling Community Disaster Resilience for Optimal Investment Strategies. <b>van de Lindt, J. W.</b> , Ellingwood, B. R.
2:00 PM	Nucleation and Growth Process of the Mw 6.2 Northern Nagano Prefecture, Japan, Earthquake of November 22, 2014. <b>Noda, S.</b> , Ellsworth, W. L.	Shear-wave Velocity model from Ambient Noise Tomography near the Sacramento/San Joaquin Delta, California. <b>Fletcher, J. B.</b> , Erdem, J. E.	INVITED STUDENT: MyShake: Smartphone based Seismic Network. <b>Kong, Q.</b> , Allen, R., Schreier, L., Kwon, Y. W.	INVITED: Earthquake Swarms and Mainshock-aftershock Sequences Hosted by a Single Fault: The 2000-2014 Activity in West Bohemia/Vogtland. <b>Fischer, T.</b> , Hainzl, S., Cermakova, H., Bachura, M., Vlcek, J.	Case Studies of Financial Decision-Making using Near-Real-time Post-Earthquake Information. <b>Wald, D. J.</b> , Worden, C. B., Thompson, E. M., Franco, G.

Friday, 22 April (continued)

<i>Time</i>	<i>Tuscany 1/2</i>	<i>Tuscany 3/4</i>	<i>Tuscany 5/6</i>	<i>Tuscany 7/8</i>	<i>Tuscany A</i>
	<b>Earthquake Source Parameters...</b>	<b>Upper Crustal Passive Imaging...</b>	<b>Citizen Seismology...</b>	<b>Earthquake Swarms</b>	<b>Risk Management Applications...</b>
2:15 PM	STUDENT: Stress Drop and Source Scaling of the 2011 Mineral, Virginia Mainshock and Aftershock Sequence. <b>Wu, Q.</b> , Chapman, M. C.	Microtremor Array Measurements for Estimating S-wave Velocity Profiles in Sedimentary Basins in Pacific Northwest of The United States. <b>Hayashi, K.</b> , Cakir, R., Walsh, T. J.	LastQuake: A Smartphone App for Rapid Public Information, Rapid Crowdsourcing and Seismic Risk Reduction. <b>Bossu, R.</b> , Roussel, F., Mazet-Roux, G., Steed, R.	INVITED: Fluid-Faulting Evolution in High Definition: Connecting Fault Structure and Frequency-Magnitude Variations During the 2014 Long Valley Caldera, California Earthquake Swarm. <b>Shelly, D. R.</b> , Ellsworth, W. L., Hill, D. P.	INVITED: Use of Seismic Data and Information in Validation of Natural Catastrophe Models and Other Applications in the Insurance Industry. <b>Karaca, E.</b> , Aslani, H.
2:30 PM	Earthquake Source Parameters for Earthquake Swarms Adjacent to Slow Slip, Tremor, and Large Earthquakes in the Oaxaca, Mexico Region. <b>Bilek, S. L.</b> , Phillips, W. S., Brudzinski, M., Cabral Cano, E., Arciniega-Ceballos, A.	INVITED: Deep ReMi Imaging—Mapping Shear-Wave Velocities to 1 km Depth and Greater Using Refraction Microtremor. <b>Pullammanappallil, S.</b> , Pancha, A., Louie, J.	AcceleROB: Low-cost Accelerometric Stations in Belgium. Lecocq, T., Rapagnani, G., <b>Vleminckx, B.</b> , Camelbeeck, T.	A Slow Rupture Episode inferred from Seismic and Geodetic Data during the 2000 Miyakejima Dike Intrusion. <b>Cattania, C.</b> , Rivalta, E., Hainzl, S., Passarelli, L., Aoki, Y.	Building an Earthquake Source Model for Hazard and Risk. <b>Porto, N. M.</b>
2:45–3:45 PM	BREAK				

Friday, 22 April (continued)

<i>Time</i>	<i>Tuscany 1/2</i>	<i>Tuscany 3/4</i>	<i>Tuscany 5/6</i>	<i>Tuscany 7/8</i>	<i>Tuscany A</i>
	<p><b>Research Efforts to Improve Regulatory Performance for Induced Seismicity</b> Session Chairs: David Eaton, Honn Kao, and Gail Atkinson (see page 542)</p>	<p><b>Upper Crustal Passive Imaging for Hazards and Exploration</b> (continued)</p>	<p><b>Short- and Long-Term Deformation on Active Faults: Integrating Geodetic, Geologic and Seismic Constraints on Slip Rates and Off-fault Deformation in the Walker Lane and Beyond</b> Session Chairs: William Hammond, Rich Briggs, Rich Koehler, and Corné Kreemer (see page 551)</p>	<p><b>Physical and Statistical Properties of Earthquake Swarms and Clustered Seismicity: Constraining Driving Mechanisms</b> (continued)</p>	<p><b>Risk Management Applications of Earthquake Seismology</b> (continued)</p>
3:45 PM	<p>2016 USGS Seismic Hazard Model for Induced Seismicity. <b>Petersen, M.</b>, Mueller, C., Moschetti, M., Hoover, S., Rubinstein, J., Ellsworth, W., Llenos, A., Michael, A., McGarr, A.</p>	<p>INVITED: Shear-wave Velocities to Depths Greater than 1 km Using the krSPAC Microtremor Array Method: Examples from Seattle, Washington and Charleston, South Carolina. <b>Stephenson, W. J.</b>, Odum, J. K., Asten, M. W.</p>	<p>INVITED: Geodetic Slip Rates and Uncertainties in the Eastern California Shear Zone and Walker Lane. <b>Evans, E. L.</b></p>	<p>STUDENT: Variability of Source Parameter Estimates for the 2008 Mogul Earthquake Swarm near Reno, NV using EGF-derived Spectral Ratios. <b>Ruhl, C. J.</b>, Abercrombie, R. E., Smith, K. D.</p>	<p>A New Seismic Hazard Model for Loss Estimation in the Conterminous United States: Beyond the National Seismic Hazard Map. <b>Thenhaus, P. C.</b>, Campbell, K. W., Gupta, N., Smith, D. F., Khater, M. M.</p>
4:00 PM	<p>A Predictive Statistical Model of Wastewater Injection-Induced Earthquakes in Oklahoma: Application of the Seismogenic Index. <b>Langenbruch, C.</b>, Zoback, M. D.</p>	<p>INVITED: Understanding the Behavior of Microtremor H/V Spectral Ratio using the Energy Partitions within a Diffuse Field Regime. <b>Sánchez-Sesma, F. J.</b>, Piña-Flores, J., Perton, M., García-Jerez, A., Luzùn, F., Kawase, H., Matsushima, S., Campillo, M.</p>	<p>Seasonally Varying Strain Rate and Its Relationship with Seismicity in the California-Nevada Area. <b>Zeng, Y.</b></p>	<p>Exploring Statistical and Physical Properties of the 2015 San Ramon Earthquake Swarm, California. <b>Taira, T.</b>, Xue, L., Burgmann, R.</p>	<p>Understanding Science and Its Limitation in Catastrophe Modeling Through Robust Simulation. <b>Lee, Y.</b>, William, G.</p>

Friday, 22 April (continued)

Time	Tuscany 1/2	Tuscany 3/4	Tuscany 5/6	Tuscany 7/8	Tuscany A
	<b>Regulatory Performance for Induced Seismicity</b>	<b>Upper Crustal Passive Imaging...</b>	<b>Short- and Long-Term Deformation on Active Faults</b>	<b>Earthquake Swarms</b>	<b>Risk Management Applications...</b>
4:15 PM	INVITED: Geomechanical Modeling of Induced Seismicity from Multi-Stage Hydraulic Fracturing. <b>Maxwell, S. C.</b> , Grob, M.	Use of Ambient Noise Surface Wave Tomography for Weathering Corrections in Controlled-Source Seismic Reflection Exploration. <b>Hollis, D. D.</b> , Clayton, R. W., Lin, F. C., Barklage, M. E.	Can Paleoseismic and Slip Rate Data be Replicated? Insights from the San Andreas Fault in the Carrizo Plain. <b>Grant Ludwig, L.</b>	Tidal Triggering of Earthquakes Near Parkfield, California. <b>Delorey, A. A.</b> , Johnson, P. A.	Pinpointing the Cost of Natural Disasters: Local Devastation and Global Impact. <b>Bolton, M. K.</b> , Larsen, T., David, K. M.
4:30 PM	INVITED: STUDENT: Magnitudes Scale Discrepancies for Near-Event Receivers. <b>Butcher, A. C.</b> , Luckett, R., Kendall, J. M., Baptie, B., Verdon, J. P., Wookey, J.	INVITED: Shallow Crustal Imaging using Dense Geophone Arrays. <b>Lin, F.</b> , Bowden, D. C., AlTheyab, A., Tsai, V. C., Schuster, G. T., Clayton, R. W., Hollis, D.	Stringing Pearls Along the Wasatch Fault Zone: An Objective Look At Earthquake Rupture Length and Fault Segmentation. <b>Biasi, G. P.</b> , DuRoss, C. B., Bennett, S. E. K.	The McAdam, New Brunswick Earthquake Swarm: Extremely Shallow, Natural Events. <b>Bent, A. L.</b> , Adams, J., Butler, K., Burke, K. B. S., Brown, J., Halchuk, S., Peci, V., Hayek, S.	Systematic Generation of USGS Earthquake Scenarios. <b>Thompson, E. M.</b> , Field, N., Luco, N., Petersen, M. D., Powers, P. M., Wald, D. J., Worden, C. B.
4:45 PM	Discriminating Seismic Sources (Mining-induced Seismicity, Fluid Injection Induced Seismicity, and Tectonic Earthquakes) in Central Utah, USA. Stein, J. R., <b>Pankow, K. L.</b> , Koper, K. D., Chambers, D.	STUDENT: Seismic Interferometry with Distributed Acoustic Sensing for Near-surface Monitoring of Critical Infrastructure. <b>Lindsey, N. J.</b> , Ajo-Franklin, J. B., Dou, S., Dreger, D., Martin, E. R., Wagner, A., Freifeld, B., Daley, T.	STUDENT: Towards a Geodesy-based Picture of Strain Accumulation in the Los Angeles Basin. <b>Rollins, J. C.</b> , Argus, D. F., Landry, W., Barbot, S. D., Avouac, J. P.	Communication Challenges Faced by Seismologists during Earthquake Swarm Periods. <b>Lamontagne, M.</b> , Flynn, B. W., Goulet, C. A.	Potential Impacts of the Wasatch Fault on Salt Lake City, Utah: A Risk Analysis. <b>Williams, C. R.</b> , Fitzenz, D. D.

**Active Tectonics, Faults and Large Earthquakes** (see page 562)

1. INVITED: Site Amplification Model Dependent on Site Natural Frequency and Sharpness of H/V peak using Ground Motions from Japanese NIED Network. **Kwak, D. Y.**, Park, D., Stewart, J. P.
2. STUDENT: Three Dimensional Earthquake Ground Motion Simulation for the Bengal Basin Region. **Huda, M. M.**, Taborda, R.
3. Design and Efficacy of a Theory-based Intervention Intended to Motivate Seismic Risk Reduction in Nepal. **Sanquini, A. M.**, Thapaliya, S. M., Wood, M. M.
4. Geodetically-constrained Interseismic Deformation and Fault Activities in Southwestern Taiwan. **Huang, M.**, Evans, E., Burgmann, R.
5. Updating the Hawaii Source Model for Hazard and Risk. **Porto, N. M.**, Apel, E. V., Seyhan, E.
6. The Effect of True and Auxiliary Plane Solutions on Distance Definitions for Generating GMPEs. **Sandikkaya, M. A.**
7. Sources of Latency and Associated Design Trade-offs in Earthquake Early Warning Systems. Cordahi, C., **Easton, D.**, Hayman, T., MacCharles, R.
8. STUDENT: The New Zealand Strong Motion Database and Performance of Response Spectral Models against New Zealand Data. **Van Houtte, C.**
9. STUDENT: PG and LG Attenuation in Northeast China. **Ranasinghe, N. R.**, Gallegos, A. C., Hearn, T. M., Ni, J., Sandvol, E. A., Phillips, S.
10. Source Parameters, Aftershocks, and the Abnormal Character of PmP Phases of the 11 May 2012 Mw4.8 Sunan Earthquake, Gansu, China. **Chen, J.**, Carpenter, N. S., Wang, Z., Yang, L.



Friday, 22 April (*continued*)

11. Basin Edge and Depth Effects on Ground Motion Amplifications in the Kanto Basin, Japan. **Seyhan, E.**, Kim, B.
12. Ground-Motion Attenuation for the South Napa Earthquake in the Sacramento-San Joaquin Delta, California. **Erdem, J. E.**, Boatwright, J., Fletcher, J. B.
13. Study of Ground Motion Nonlinear Effects at CGS Geotechnical Arrays using Wave Propagation Analysis of Strong-Motion Data. **Haddadi, H.**, Shakal, A., Huang, M.
14. Increased Access to Observed Data and Synthetic Data using IRIS DMC Web Services. Trabant, C., **Hutko, A.**, Van Fossen, M., Weekly, R. T., Bahavar, M., Ahern, T.
15. STUDENT: Coseismic Deformation During the December 2015 Sarez Lake Earthquake Measured from Sentinel-1A, Alos-2, and Landsat-8 Data, with Insights into the Coseismic Fault Geometry. **Sangha, S. S.**, Peltzer, G., Fielding, E., Huang, M. H., Liang, C.
16. STUDENT: Establishing the Rupture Extent of A.D. 1255 Giant Medieval Earthquake through Paleoseismological Investigations and Bayesian Statistical Modeling. **Mishra, R. L.**, Singh, I., Rao, P. S., Pandey, A., Sahoo, H. K., Jayangondaperumal, R.

#### Advances in Earthquake Science Using Digital Photogrammetry (see page 565)

17. Spatial Distribution of Displacement along the Northern Part of the 1983 M 6.9 Borah Peak Earthquake Rupture. **DuRoss, C. B.**, Gold, R. D., Personius, S. F., Briggs, R. W., Reitman, N. G., Bunds, M. P., Toké, N. A., Johnson, K., Lajoie, L., Schwartz, D.P.
18. STUDENT: Repeat Surface Analysis of the Phelan Creeks Reach of the San Andreas Fault, Carrizo Plain, CA. **Salisbury, J. B.**, Arrowsmith, J. R.
19. Paleoseismology from Paleotopography: Combining Legacy and Modern Topographic Data for Earthquake Geology Studies. **Reitman, N. G.**, Briggs, R. W., Gold, R. D., DuRoss, C. B.
20. STUDENT: Lidar and Luminescence Dating Analysis of Latest Pleistocene-Holocene Slip Rates on the Awatere Fault: Recent Updates to Fluvial Terrace Dating at Saxton River, South Island, New Zealand. **Zinke, R.**, Dolan, J. F., Van Dissen, R., McGuire, C. P., Rhodes, E. J., Hatem, A. E., Grenader, J. R., Langridge, R. M.
21. STUDENT: Incremental Holocene Slip Rates from the Hope Fault at Hossack Station, Marlborough Fault Zone, South Island, New Zealand. **Hatem, A. E.**, Dolan, J. F., Langridge, R. M., Zinke, R. W., McGuire, C. M., Rhodes, E. J., Van Dissen, R. J.

#### Behavior of Structures in Subduction Zones under Long Duration Earthquakes (see page 566)

22. STUDENT: Quantifying Ground Motion Intensity to Estimate Collapse Vulnerability of Buildings and

Application to 6-Story Steel Moment Frame Buildings in Los Angeles. **Buyco, J. K.**, Heaton, T. H.

23. STUDENT: Quantifying the Effect of Ground Motion Duration on Structural Collapse Risk. **Chandramohan, R.**, Baker, J. W., Deierlein, G. G.
24. STUDENT: Effect of Long Duration Ground Motions on Bridge Columns. **Mohammed, M. S.**, Sanders, D. H., Buckle, I. G.

#### Citizen Seismology: Citizens as an Information Source to Advance Earthquake Response and Science (see page 567)

25. INVITED: Use of U. S. Geological Survey's "Did You Feel It?" Responses for Near Real-Time Earthquake Location. **Quitoriano, V.**, Wald, D. J.
26. INVITED: Crowd-Sourcing Seismic Data for Research and Education Opportunities with the Quake-Catcher Network. Cochran, E. S., **Sumy, D. F.**, de Groot, R. M.
27. A Web Interface for QCN Volunteers to Visualize Seismological Data. Frobert, L., **Bossu, R.**, Mazet-Roux, G.
28. Rapid Crowd-Sourced Earthquake Detections Integrated Into Traditional Seismic Processing. **Guy, M.**, Earle, P., Turner, J.

#### Deep Earthquakes and Surrounding Slab Structures (see page 568)

29. Diverse Rupture Processes in the 2015 Peru Deep Earthquake Doublet. Ye, L., **Lay, T.**, Kanamori, H., Zhan, Z., Duputel, Z., Tavera, H.
30. Slab2—Updated Subduction Zone Geometries and Modeling Tools. **Hayes, G. P.**, Moore, G., Flamme, H., Portner, D. E., Hearne, M.
31. STUDENT: Focal Mechanisms of Intermediate-Depth Earthquakes Beneath the Northeast Caribbean. **Mejia, H. P.**, Pulliam, R. J., Polanco, E., Pujols, R., Huerfano, V.

#### Earthquake Source Parameters and Slip from Seismic, Geodetic and Laboratory Data: Theory, Observations and Interpretations (see page 568)

32. What Stress Drop Is Determined by the Far-field Spectrum When Stress on the Fault Is Heterogeneous? Crempien, J. G. F., **Archuleta, R. J.**, Ji, C.
33. STUDENT: Determination of Moment Tensors for the Earthquakes in the Central and Eastern US for Earthquakes below M4.0. **Dahal, N. R.**, Ebel, J. E.
34. Implementation of Uncertainty of Green Functions in the Earthquake Source Inversion. **Hallo, M.**, Galovic, F.
35. Source Functions and Path Effects from Earthquakes in the Farallon Transform Fault Region, Gulf of California, Mexico that occurred during October 2013. **Castro, R. R.**, Stock, J., Hauksson, E., Clayton, R.

Friday, 22 April (*continued*)

36. hybridMT—A MATLAB Software Package for Seismic Moment Tensor Inversion and Refinement. **Kwiatek, G.**, Martínez-Garzón, P., Bohnhoff, B.
37. Triggering Processes in Fracture and Compaction Experiments: On the Importance of Large-scale Heterogeneities. Davidsen, J., **Kwiatek, G.**, Goebel, T., Stanchits, S., Dresen, G., Charalampidou, E. M., Rueck, M.
38. STUDENT: Estimating Directivity and Related Source Properties of Moderate Earthquakes in Southern California with Second Seismic Moments Utilizing Stacked Empirical Green's Functions. **Meng, H.**, Ben-Zion, Y., McGuire, J.
39. STUDENT: Estimating Rupture Directivity of moderate San Jacinto Fault Zone Earthquakes with Spectral Analysis. **Abolfathian, N.**, Ben-Zion, Y., Ross, Z. E.
40. STUDENT: Enhancing Ground-motion Prediction with Near Real-time Rupture Directivity Assessment. **Lui, S. K. Y.**, Helmberger, D. V.
41. STUDENT: Magnitude Scaling Relations for Small to Moderate Southern California Earthquakes from Body Wave Spectra of Over 13,000 Events. **Ross, Z. E.**, Ben-Zion, Y., Vernon, F. L., White, M. C.
42. Source Parameters of the 25th April 2015 Nepal Earthquake and Its Aftershocks. Mitra, S., Paul, H., Manna, S., **Priestley, K.**, Dayal, S.
43. Attenuation and Source Characteristics of the December 30, 2015 **M**4.7 Vancouver Island In-Slab Earthquake. **Ghofrani, H. G.**, Atkinson, G. M. A., Assatourians, K. A.
44. STUDENT: Impact of Uncertainty in Magnitude-Area Scaling Relations on SCEC Broadband Platform Simulations. **Bayless, J. R.**, Skarlatoudis, A. A., Somerville, P. G.

#### NGA-East: Research Results and Ground-Motion Characterization Products for Central and Eastern North America (see page 571)

45. STUDENT: Improved CENA Regression Relationships between Modified Mercalli Intensities and Ground Motion Parameters. **Ogwen, L. P.**, Cramer, C. H.
46. STUDENT: Hybrid Empirical Ground-Motion Prediction Equations for the Gulf Coast Region. **Haji Soltani, A.**, Pezeshk, S., Zandieh, A.
47. STUDENT: Empirical Ground Motion Prediction Equations for Eastern North America with the Addition of Intensity Observations. **Al Noman, M. N.**, Cramer, C. H.
48. Improving Attenuation Models in the Central United States by Considering Source Radiation Pattern Effects. **Hosseini, M.**, Somerville, P. G., Thio, H.
49. Comparison of Random Vibration Theory Peak Factor Formulations for the NGA-East Project. **Kottke, A. R.**

50. STUDENT: Investigation of the Path Effect Term in the New Madrid Seismic Zone. **Sedaghati, F.**, Pezeshk, S.
51. STUDENT: Applicability of Site Fundamental Frequency as a Descriptive Variable for Site Response in Central and Eastern North America. **Hassani, B.**, Atkinson, G. M.
52. Hard-rock Amplification for NGA-East Sites. **Ktenidou, O. J.**, Abrahamson, N. A.

#### Physical and Statistical Properties of Earthquake Swarms and Clustered Seismicity: Constraining Driving Mechanisms (see page 573)

53. The 2015 San Ramon, CA Swarm: Operational Earthquake Forecasting and Background Rate Changes. **Llenos, A. L.**, Michael, A. J.
54. Optimized Physics-based Earthquake Forecasts for Inland Japan. **Segou, M.**, Zhuang, J.
55. STUDENT: Capturing Fractal Fault Structure in Virtual Quake Simulations. **Wilson, J. M.**, Rundle, J. B., Schultz, K. W., Turcotte, D. L., Yikilmaz, M. B.
56. STUDENT: A Look at Slip and Dilation Tendencies on Preexisting Faults in Areas of Recent Earthquake Swarms in Western Nevada. **Molisee, D. D.**, Ruhl, C. J.
57. STUDENT: Moderate-to-Small Magnitude Seismicity Clusters Persist in Northwest Nevada for over 19 Months. **Ruhl, C. J.**, Smith, K. D.
58. STUDENT: Application of Template-Based Seismic Detection Methods to Recent Seismicity Near the **M**6.9 1983 Borah Peak, Idaho Earthquake. **Pang, G. N.**, Koper, K. D., Burlacu, R.
59. STUDENT: Waveform Correlation Detection Methods as Applied to Utah Seismic Swarms. **Batchelor, C. E.**, Koper, K. D., Pankow, K. L., Burlacu, R.

#### Research Efforts to Improve Regulatory Performance for Induced Seismicity (see page 574)

60. STUDENT: Characterization of Earthquake Site Amplification In Alberta, Canada for Induced-Seismicity ShakeMap Applications. **Farrugia, J. J.**, Atkinson, G. M., Molnar, S.
61. Optimal Fault Orientations Determined from Focal Mechanisms for Oklahoma Earthquakes: 2010 to 2015. **Darold, A. P.**, Holland, A. A.
62. Monitoring Background Level of Seismicity in Regions with Shale Oil and Gas Potential in Eastern Canada. **Lamontagne, M.**, Lavoie, D., Kao, H.
63. Sensitivity Study for the 2016 USGS Seismic Hazard Model for Induced Seismicity. **Hoover, S. M.**, Moschetti, M. P., Petersen, M. D., Mueller, C. S.
64. Seismic Real-time Monitoring of Induced Earthquakes at the Landau and Insheim Geothermal Reservoirs (SW Germany). Brüstle, A., Vasterling, M., **Schmidt, B.**, Wegler, U.

Friday, 22 April (*continued*)

65. Determining the Impact of Induced Seismicity—A Fully Integrated Modeling Approach. **Bachmann, C. E.**, Foxall, W., Jeanne, P.
66. STUDENT: Science-based Decision Making in a High-risk Energy Production Environment. **Weiser, D. A.**, Jackson, D. D.
67. Detecting and Relocating Potentially Induced Earthquakes in Southern Kansas. **Dougherty, S. L.**, Cochran, E. S., Harrington, R. M., Rubinstein, J. L.
68. The First Step Toward an Effective Traffic Light Protocol for Induced Seismicity: A Data-Sharing Framework for Earthquake Monitoring in Northeast British Columbia, Canada. **Kao, H.**, Mahani, A. B., Walker, D., Atkinson, G. M., Eaton, D. E.

#### **Risk Management Applications of Earthquake Seismology** (see page 576)

69. Seismic Source Model for a System-Wide Dam Risk Reduction Program in Northern California. **Madugo, C.**, Abramson, H., Hitchcock, C., Lewandowski, N., Page, W., Sawyer, T., Thompson, S., Wooddell, K., Donahue, J.
70. Background Seismic Source Model Uncertainty Impacts on Hazard and Risk. **Apel, E.**
71. A Methodology for Quantifying the Hazard of Surface-Fault Displacement to Gas Pipelines in Northern California. **Thompson, S.**, Madugo, C., Lewandowski, N., Givler, R., Ingemansson, B.
72. The Regularity of Very Large Complex Events, and its Impact on Risk. **Fitzenz, D. D.**, Nyst, M.
73. Using MMI Shaking Probabilities to Assess the Exposure to Damaging Earthquakes in Canada. **Allen, T.**, Onur, T., Seemann, M., Journeay, M., Halchuk, S.

#### **Secondary Earthquake Hazards and Losses** (see page 577)

74. Towards Rapid Likelihood Estimation of Earthquake-Triggered Gravitational Mass Movements in Switzerland Based on Ground-Shaking Scenarios, Geomorphology and Geotechnical Information. **Cauzzi, C.**, Fäh, D., Wiemer, S., Wald, D. J., Clinton, J.
75. STUDENT: Use of an Expanded Global Earthquake Data Set to Develop a Near Real-time Model for Predicting Seismically Induced Landslides. **Jessee (Nowicki), M. A.**, Hamburger, M. W., Wald, D. J., Hearne, M., Robeson, S. M., Thompson, E. M., Tanyas, H., Allstadt, K.
76. STUDENT: Updated Geospatial Liquefaction Model for Global Use. **Zhu, J.**, Baise, L. G.
77. Combining Case History Observations with Different Completeness Levels in Empirical Ground-Failure Models. **Thompson, E. M.**, Wald, D. J., Allstadt, K., Hearne, M.

78. Spatiotemporal Modeling of Groundwater Elevation for Liquefaction Hazard and Loss Estimation. **Lee, S. J.**, Akita, Y., Ancheta, T. D.
79. Comparison of Liquefaction Triggering Methods on Borehole Data from Four Quadrangles in the Santa Clara Valley, California. **Branum, D. M.**, Moskovitz, B., Real, C.

#### **Seismicity and Seismic Hazards of the Walker Lane and Western Great Basin** (see page 579)

80. Geologic Model of the Development of Las Vegas Basin, Nevada. **Taylor, W. J.**, Wagoner, J., Abdelhaleem, S. A., Luke, B.
81. STUDENT: Surface Slip during Large Owens Valley Earthquakes. **Haddon, E. K.**, Amos, C. B., Zielke, O., Jayko, A. S., Burgmann, R.
82. Holocene-Age Earthquakes and Surface Rupture Zoning of the West Tahoe Fault. **Seitz, G.**, Mareschal, M.
83. Quaternary Faulting in the Pyramid Lake Basin, Northern Walker Lane, Nevada. **Dee, S.**, Kell, A., Angster, S. J., Kent, G. M., Driscoll, N., Faulds, J. E., Anderson, R. P.
84. Seismicity of the Southern Mina Deflection and the 2004-2005 Adobe Hill Earthquake Sequence, Nevada-California. **Baca, A.**, Ruhl, C., Hatch, R., Smith, K., Kent, G., Louie, J.
85. The 2008 Wells, Nevada Earthquake Sequence: Application of Subspace Detection and Multiple Event Relocation Techniques. **Nealy, J. L.**, Hayes, G. P., Benz, H. M.
86. The Mw 4.3 December 22, 2015 Thomas Creek Earthquake, South Reno, Nevada. **Hatch, R.**, Baca, A., Ruhl, C., Brailo, C., Smith, K. D., Louie, J., Kent, G., Rodgers, A.
87. Ground Motion Simulations of the December 22, 2015 Thomas Creek Earthquake, South Reno, Including 3D Basin Structure. **Rodgers, A. J.**, Hatch, R., Louie, J., Smith, K., Ruhl, C., Brailo, C., Kent, G., Pullammanappallil, S.

#### **Short- and Long-Term Deformation on Active Faults: Integrating Geodetic, Geologic and Seismic Constraints on Slip Rates and Off-fault Deformation in the Walker Lane and Beyond** (see page 581)

88. STUDENT: New Slip Rates and Characterization of Active Faults in Mason and Smith Valleys of the Northern Walker Lane using <sup>10</sup>Be Terrestrial Cosmogenic Nuclide (TCN) Surface Exposure Dating and Newly Acquired Lidar. **Pierce, I. K.**, Wesnousky, S. G., Owen, L. A.
89. Characterizing the Quaternary Expression of Active Faulting along the Olinghouse, Carson and Wabuska Lineaments of the Northern Walker Lane using Lidar. **Li, X.**, Pierce, I. K. D., Wesnousky, S. G.



Friday, 22 April (*continued*)

90. STUDENT: Application of UAV Photography to Refining the Slip Rate on the Pyramid Lake Fault Zone, Nevada. **Angster, S.**, Wesnousky, S. G., Huang, W., Kent, G., Nakata, T., Goto, H.
  91. High-resolution Seismic Profiling Reveals Subsurface Faulting Associated with the 1934 M 6.6 Hansel Valley, Utah, Earthquake. Bruno, P. P., **DuRoss, C. B.**, Kokkalas, S.
  92. STUDENT: A LiDAR and GPS Study of the Greater Truckee Meadows: Evidence for a Distinct Transition from Primarily East-west Dominated Extension to NW-trending Right-lateral Slip Centered in Reno, Nevada. **Brailo, C. M.**, Kent, G. M., Wesnousky, S. G., Hammond, W. C., Kell, A. M., Pierce, I. K., Ruhl, C. J., Smith, K. D.
  93. Preliminary Tectonic Geomorphic Observations Along the East Reno Fault Zone, Nevada. **Koehler, R.**
  94. Paleearthquake Chronology from the Echo Playa Site on the Central Garlock Fault, California. **Kemp, C. D.**, Hartleb, R. D., Lutz, A. T., Frost, E. K., Lindvall, S. C., Alm, S., Walker, J. D.
  95. New Lidar Topography Reveals Tectonic Geomorphology Along the 1958 Southern Fairweather Fault Surface Rupture, Southeast Alaska. **Witter, R. C.**, Bender, A., LeWinter, A., Haeussler, P., Brothers, D., DuRoss, C., Glennie, C., Koehler, R. E., Scharer, K., Plafker, G.
  96. The 1990 Lee Vining, California, Earthquake and Implications for the Kinematics of the Central Walker Lane. **Humphrey, J. R.**
  97. STUDENT: Postseismic Deformation Following the 2010 M=7.2 El Mayor-Cucapah Earthquake: New Methods, Interpretations and Implications. **Rollins, J. C.**, Barbot, S. D., Avouac, J. P.
  98. A Reconnaissance Fault Activity and Fault Slip-Rate Analysis of Quaternary Faults in Central Nevada. **dePolo, C. M.**
- 
- Upper Crustal Passive Imaging for Hazards and Exploration** (see page 583)
99. On the Relationship between Near-surface Attenuation and Scattering. **Pilz, M.**, Faeh, D.
  100. Progress on the USGS National Crustal Model for Seismic Hazard Studies. **Boyd, O. S.**, Shah, A. K.
  101. STUDENT: Passive Seismic Body-Wave Interferometry using Noise Auto-correlations for Crustal and Upper Mantle Structure. **Oren, C.**, Nowack, R. L.
  102. INVITED: STUDENT: Retrieval of Green's functions in the Valley of Mexico using Historical Accelerations as Generalized Diffuse Fields. **Baena-Rivera, M.**, Piña-Flores, J., Pertou, M., Pérez-Rocha, L. E., Sánchez-Sesma, F. J.
  103. STUDENT: Very Dense Ambient Noise Arrays for Subsurface Imaging. **Rabade, S.**, Ramirez-Guzman, L., Juarez, A., Aguirre, J., Avila Carrera, R., Sanchez, J.



# SSA 2016

## Abstracts of the Annual Meeting

Late changes at [www.seismosoc.org/meetings/2016/abstracts/](http://www.seismosoc.org/meetings/2016/abstracts/).

### Advances in Noninvasive Approaches to Characterizing Seismic Site Conditions

Oral Session · Wednesday · 8:30 AM · 20 April · Tuscany 1/2  
Session Chairs: Alan Yong, Sheri Molnar, and Aysegul Askan

#### Site Response Implications Associated with Common Methods used to Account for Vs Profile Uncertainty

COX, B. R., University of Texas, Austin, TX, USA, [brcox@utexas.edu](mailto:brcox@utexas.edu);  
TEAGUE, D. P., University of Texas, Austin, TX, USA

A number of strategies exist to account for the epistemic uncertainty and aleatory variability in shear wave velocity ( $V_s$ ) profiles used for site response analyses. Often, epistemic uncertainty is accounted for using median and bounding-type  $V_s$  profiles (e.g.,  $\pm 20\%$ ), while aleatory variability is accounted for using  $V_s$  randomization procedures (e.g., Toro 1995). This research investigates a surface wave dispersion misfit approach for evaluating statistical models meant to account for  $V_s$  uncertainty in site response. Specifically, many unique surface wave inversions were performed on a common synthetic dispersion dataset using variable numbers of layers, and all  $V_s$  profiles with reasonable dispersion misfit values were selected for site response. Additionally, bounding-type and statistically-based, randomly generated Toro (1995)  $V_s$  profiles were developed for site response. Equivalent linear site response analyses were then performed on all candidate  $V_s$  profiles, including the true synthetic  $V_s$  profile. Despite significant visual differences in the  $V_s$  profiles derived from different surface wave inversions, the computed spectral accelerations (SA) matched those of the true profile very well. In contrast, the bounding-type  $V_s$  profiles commonly used to account for epistemic uncertainty significantly under- and over-predicted SA. Furthermore, these bounding-type profiles also yielded theoretical dispersion curves that did not match the synthetic dispersion data and had high dispersion misfit values. The randomly generated Toro  $V_s$  profiles exhibited high variability in SA, and their theoretical dispersion curves only fit the synthetic dispersion data in a few cases. Thus, whenever possible, the authors recommend comparing theoretical dispersion curves for candidate statistical  $V_s$  profiles/layered earth models with measured dispersion data at a site prior to using statistical profiles to account for  $V_s$  uncertainty in site response analyses.

#### Blind-Test Case Studies to Validate Non-Invasive Shear-Wave Velocity Profiling in Diverse Geologic Settings in Canada and Chile

MOLNAR, S., University of Western Ontario, London, ON, Canada, [smolnar8@uwo.ca](mailto:smolnar8@uwo.ca); VENTURA, C. E., University of British Columbia, Vancouver, BC, Canada, [ventura@civil.ubc.ca](mailto:ventura@civil.ubc.ca); BOROSCHEK, R., University of Chile, Santiago, Chile, [rborosch@ing.uchile.cl](mailto:rborosch@ing.uchile.cl); CROW, H., Natural Resources Canada, Ottawa, ON, Canada, [heather.crow@canada.ca](mailto:heather.crow@canada.ca)

A variety of invasive and non-invasive field methodologies have been developed to provide reliable  $v_s$ -depth profiles for earthquake site classification purposes. Blind-test case studies of non-invasive surface wave methods (performed by the first author) with respect to invasive methods (performed by a second party) are presented here for diverse geologic settings in Canada and Chile.

In Canada, blind-test comparisons of invasive and non-invasive  $v_s$  profiling is accomplished in two end-member geologic environments: soft sites on the Fraser River delta, south of Vancouver, British Columbia, comprised of up to ~300 metres of Holocene silt with channel sands; and stiff sites on Pleistocene glaciated sands and till in mid-eastern Vancouver Island (Parksville). For the delta sites, the non-invasive surface wave testing provides average  $v_s$  in agreement with invasive  $v_s$  measurements to ~150-m depth. For the stiff glaciated sites, excellent agreement is obtained between non-invasive and invasive  $v_s$  profiling, with an average relative difference in  $v_s$  of ~20 m/s (4%) at 2-65 m depth and ~45 m/s (5%) between 90-115 m depth.

In Chile, blind-test comparisons of invasive and non-invasive  $v_s$  profiling methods is accomplished at 11 strong-motion stations that recorded the 2010 M8.8 Maule earthquake. The geologic material at these 11 sites is highly variable: generally fine-grained silt and clay sites over marine sedimentary terraced bedrock along the western coast transitioning eastward to coarser-grained gravel sites

over igneous bedrock as well as the presence of volcanic ash deposits. Excellent to good agreement is obtained between non-invasive and invasive  $v_s$  profiling at five stations over the entire borehole length and in the uppermost layer at three other stations. For the majority of stations,  $v_{s30}$  site classification is consistent irrespective of methodology.

#### Bayesian Trans-Dimensional Inversion of Surface-Wave Dispersion for Earthquake Site Response Estimation in Northern British Columbia, Canada

GOSSSELIN, J. M., University of Victoria, Victoria, BC, Canada, [jeremyg@uvic.ca](mailto:jeremyg@uvic.ca); CASSIDY, J. F., Pacific Geoscience Centre, Natural Resources Canada, Sidney, BC, Canada, [john.cassidy@canada.ca](mailto:john.cassidy@canada.ca); DOSSO, S. E., University of Victoria, Victoria, BC, Canada, [sdosso@uvic.ca](mailto:sdosso@uvic.ca); BRILLON, C., Pacific Geoscience Centre, Natural Resources Canada, Sidney, BC, Canada, [camille.brillon@canada.ca](mailto:camille.brillon@canada.ca)

Knowledge of the shear-wave velocity ( $V_s$ ) profile over the upper 10s of metres of the soil column is important for characterizing the expected ground response to earthquake shaking at a specific site. Non-invasive and passive methods based on recording ambient seismic noise are increasingly popular for estimating  $V_s$  structure with minimal cost and site disruption. This study applies an advanced Bayesian inversion methodology to estimate  $V_s$  structure from surface-wave dispersion measurements processed from passive seismic array recordings using frequency-wavenumber analysis. A fully non-linear trans-dimensional (trans-D) Bayesian inversion based on parallel tempering is used to estimate  $V_s$  models and associated model uncertainties. In trans-D inversion, the model parameterization (e.g., number of layers of the  $V_s$  profile) is included as an unknown which is sampled probabilistically, accounting for the uncertainty of the model parameterization in the uncertainty of the model parameter estimates. Shear-wave velocity profiles and uncertainties are obtained from the velocity-depth marginal distribution of the trans-D posterior probability density. These probabilistic results for the  $V_s$  profile allow for probabilistic estimates of site response factors such as peak ground velocity/acceleration and amplification/resonance spectra, which ultimately quantify the confidence in the site characterization. This methodology is applied to passive seismic array recordings collected at five sites in Kitimat, British Columbia, Canada. Inversion results from several sites are compared to active-source (vibro-seis) reflection data collected nearby.

#### Vs IMASW and Vp-Depth Profiling, NEHRP Site Classifications, and Linear Shallow Amplification Functions: Geophysical Site Characterization of Bay Area Seismic Monitoring Stations Following the M6.0 South Napa Earthquake

TURNER, J. P., Fugro Consultants, Inc., Denver, CO, USA, [j.turner@fugro.com](mailto:j.turner@fugro.com); BROSSY, C. C., Fugro Consultants, Inc., Walnut Creek, CA, USA, [c.brossy@fugro.com](mailto:c.brossy@fugro.com); O'CONNELL, D. R. H., Fugro Consultants, Inc., Denver, CO, USA, [d.oconnell@fugro.com](mailto:d.oconnell@fugro.com); ROUGHLEY, C., Napa Valley College, Napa, CA, USA, [Croughley@napavalley.edu](mailto:Croughley@napavalley.edu)

The 2014 South Napa earthquake was recorded by more than 400 strong-motion stations within 100 km of the epicenter, including CSMIP strong motion recordings at 40+ sites within 40 km. The maximum horizontal peak accelerations observed at many of these sites generally follow the ground-motion attenuation relation of Boore and Atkinson (2008) (comparison of results with updated NGA-WEST 2 is forthcoming), but several ground-motion values depart from this trend, indicating significantly greater spectral values that may reflect local strong amplification. In response, seismic monitoring stations with no site-specific velocity measurements are targeted for geophysical surveys, with priority to sites with anomalous PGA and PGV measurements at varying distances from the 2014 M6.0 South Napa earthquake and in areas of denser population or critical infrastructure. As part of a 2016 NEHRP grant, active-source seismic ( $V_s$  and  $V_p$ ) are measured at targeted seismic monitoring station locations to measure site-specific ground motion amplification effects, soil depth, depth to rock ( $Z_{1.0}$   $V_s=1$  km/s), calculate site specific  $V_s$ -depth and  $V_{s30}$ , and develop NEHRP site classes for each site. Results provide inputs for updating GMPEs and delineate shallow ground motion amplification site effects. Bedrock reference sites nearby to anomalous site-response sites are also targeted to provide site-specific data for the use of generalized site amplification inversion of Hartzell and Mendoza. GIS-based mapping compares  $V_s$ -depth data to surficial lithology for development of characteristic  $V_s$ -lithologic relationships to update the statewide California  $V_s$ -geologic unit database. P-wave tomographic data are processed at slow- $V_s$  sites (NEHRP Site Class D-E) to map depth to 100% water saturation to identify sites

with high liquefaction susceptibility. Students of Napa Valley College supported data collection and developed interpretations from processed data as part of their coursework.

### **Applications of Refraction Microtremor Done Right, and Pitfalls of Microtremor Arrays Done Wrong**

LOUIE, J. N., Nevada Seismological Lab., Univ. of Nevada, Reno, NV, USA, louie@seismo.unr.edu; PULLAMMANAPPALLIL, S., Optim, Reno, NV, USA, satish@optimsoftware.com

Since Louie's original paper on the refraction microtremor shear-wave velocity measurement technique in 2001, the method has been widely adopted by the geotechnical industry, and is accepted by building authorities around the world. After successful initial commercialization, the developers have further adapted the method to new applications. Clark County and the City of Henderson, Nevada populated their Earthquake Parcel Map with over 10,000 site measurements for building code enforcement, made over a three-year period. A new 2D refraction microtremor analysis now allows engineers to image lateral shear-wave velocity variations and do passive subsurface imaging. The developers have extended the range of 2-D refraction microtremor analysis to kilometer depths, completing several deep-basin shear-wave velocity measurement programs for the USGS.

Unfortunately, any useful and popular measurement technique can be abused. Practitioners must carefully follow correct data collection, analysis, interpretation, and modeling procedures, or the results cannot be labeled "refraction microtremor" or "ReMi™" results. Inexperienced or ill-informed practitioners have at times failed to produce correct shear-wave velocities, due to either improper data acquisition or faulty analysis techniques. We will present some of the common mistakes, and provide solutions with the objective of establishing a best practices template for getting consistent, reliable models from refraction microtremor measurements.

We will also present an uncertainty analysis that incorporates uncertainties in picking of the dispersion curves together with trade-offs in the modeled shear-wave velocities. The uncertainty analyses extend to 2-D refraction microtremor sections. The goal is to provide users with confidence limits on the results when using them for site classification, geological interpretation, or community velocity models for scenario-shaking computations.

### **Inversion of Velocity Structures Based on the Empirical Relationship of Earthquake and Microtremor Horizontal-to-Vertical Ratios**

MORI, Y., J-POWER, Tokyo, Japan, yuta\_mori@jpower.co.jp; KAWASE, H., DPRI, Kyoto University, Kyoto, Japan, kawase@zeisei.dpri.kyoto-u.ac.jp; MATSUSHIMA, S., DPRI, Kyoto University, Kyoto, Japan, matsushima@zeisei.dpri.kyoto-u.ac.jp; NAGASHIMA, F., Grad. School of Engineering, Kyoto University, Kyoto, Japan, nagashima@zeisei.dpri.kyoto-u.ac.jp

In order to establish a method to estimate velocity structures using single-station microtremor records, we need a simple yet accurate theory to reproduce observed spectral characteristics. There have been long-lasting discussions on the validity of the Horizontal-to-Vertical ratio (HVR) as a substitute of the S-wave amplification characteristics. After the advent of the diffuse field theory, however, now we can calculate theoretical HVRS for not only microtremors but also earthquakes.

In this study we first compared horizontal-to-vertical spectral ratio of earthquakes (EHVR) with that of microtremors (MHVR) at 100 K-NET and KiK-net sites in Japan. We found that they share similarities but have some differences in their shapes, especially after the first peak in HVRS. This is because MHVR mainly consists of surface waves so that peaks associated with higher modes would not be so prominent.

Based on this observation, we calculated EHVR-to-MHVR ratios (here we called them as EMRs) to investigate if there are statistical difference to find that there are systematic difference in the observed EMRs. Using EMRs averaged over different peak-frequency categories, we converted MHVRs to pseudo EHVRs by multiplying the EMRs to MHVRs, which are found to have higher correlation with EHVRs than MHVRs.

Finally, we identified velocity structures by using EHVRs, MHVRs and pseudo EHVRs, and found that velocity structures obtained from pseudo EHVRs are closer to those obtained from EHVRs than MHVRs. When we use MHVRs directly as a simple substitute of EHVRs, we can obtain velocity structures that can reproduce MHVRs quite well but the structures obtained from MHVRs are not necessarily reflecting the true structures.

### **Directional Dependent H/V Spectral Ratio of Microtremors at Onahama, Japan**

MATSUSHIMA, S., DPRI, Kyoto University, Uji, Japan, matsushima@zeisei.dpri.kyoto-u.ac.jp; KOSAKA, H., Institute of Construction Technology, Toda

Corporation, Tsukuba, Japan, hiroyuki.kosaka@toda.co.jp; KOBAYASHI, T., School of Engineering, Kyoto University, Kyoto, Japan, toga.kobayashi@zeisei.dpri.kyoto-u.ac.jp; KAWASE, H., DPRI, Kyoto University, Uji, Japan, kawase@zeisei.dpri.kyoto-u.ac.jp

As observational evidence of 3-D microtremor H/V spectral ratios, we have shown that significant directional dependency is observed in and around Uji campus, Kyoto University, Japan, where the bedrock depth varies from east to west about 400m in depth within the distance of 1 km. The observed microtremor at Uji campus showed that the NS/UD has higher peak amplitude and EW/UD has higher peak frequency. This directional dependence is considered to be the result of 2-D surface geology.

In this study, we observed H/V spectral ratios of microtremors at a strong motion observation site of Port and Harbor Research Institute in Onahama, Japan and found that directional dependence exists in some parts of the area surrounding the site. The directional dependence is more apparent and has a higher dominant frequency, at around 5 Hz, compared to those observed in Uji. The observed H/V spectral ratios with directional dependence lie in two straight lines, forming a T-like shape. We also conducted exploration using Multichannel Analysis of Surface Wave method in order to get information about the very shallow subsurface structure at the area where the directional dependence of H/V spectral ratio exists.

Based on the diffuse field theory, microtremor H/V spectral ratio corresponds to the square root of the ratio of the imaginary part of horizontal displacement for a horizontally applied unit harmonic load,  $\text{Im}[G_{11}]$  or  $\text{Im}[G_{22}]$ , and the imaginary part of vertical displacement for a vertically applied unit load,  $\text{Im}[G_{33}]$ .

For a laterally heterogeneous subsurface structure, we use a numerical approach, particularly the Spectral Element Method, in order to calculate the Green's functions using a 2-D basin model of Onahama constructed from results of MASW in 3-D media and simulate the observed directional dependent H/V spectral ratios.

### **Source and Stability of Ambient Noise in the Mississippi Embayment, Central United States**

LANGSTON, C. A., CERL, University of Memphis, Memphis, TN, USA, clangstn@memphis.edu; SHAHJOUËI, A., Cat Management and Analytics Center of Excellence at AIG, Philadelphia, PA, USA, alireza.shahjouei@aig.com

A two-year record of continuous data recorded by a three-component, 19 element, 600 m aperture seismic array within the New Madrid Seismic Zone has been analyzed to investigate the stability and seismic wave source of ambient ground motions associated with the fundamental and first higher mode H/V frequency peaks due to the unconsolidated sediments in the Mississippi embayment. One hour intervals of data recorded between 1:00-2:00 AM and 2:00-3:00 PM local time between Julian Day 320, 2009, and Julian Day 263, 2011, were subset for each operational day of the array to examine any effects of seasonal and local cultural sources. The H/V power spectral ratio was calculated to examine the time stability of the fundamental spectral peak near 0.26 Hz and the first higher mode at 0.65 Hz. Although the array is much too small to use with frequency-wave-number methods for estimating azimuth and slowness to determine wave provenance, we use a novel statistical approach of estimating the largest plane wave contribution to the wavefield based on wave gradiometry. Results show that both H/V peaks do not vary in frequency, within measurement errors, over the two-year time period, nor do they vary between night and day, suggesting that noise sources are stationary. Preliminary gradiometry azimuth and slowness estimates indicate that ambient noise for the fundamental frequency peak is dominated by surface waves induced by wave action on the continental shelves of North America in the North Atlantic although our search is not complete yet. These results support the use of ambient noise in determining average characteristics of sediment velocity models important for evaluating earthquake hazards and geological structure in the region.

### **Shallow 3D Velocity Imaging based on Seismic Noise**

PILZ, M., Swiss Seismological Service—ETH Zurich, Zurich, Switzerland, marco.pilz@sed.ethz.ch

The desire for an imaging technique applicable to areas where conventional active seismic methods are difficult or impossible to implement, has given rise to the development of methods based on seismic noise, found in abundance anywhere on the Earth's surface. Since the beginning of this century, seismic interferometry has rapidly become popular in a variety of applications. One of the most intriguing applications of the method, shown both theoretically and experimentally, is that a random wavefield has correlations, which, on average, take the form of the Green's function of the media. Between pairs of receivers, the Green's function

can be extracted from cross-correlations of ambient noise, in turn allowing an estimate of the propagation delay between the stations. Such traveltime measurements of surface waves reconstructed from seismic noise have been used at lower frequencies to produce high-resolution images on continental and regional scales but only limited attention has been paid to applications on much smaller and shallow scales.

Here we will provide an overview on local scale tomography methods, as well as to highlight recent theoretical and experimental advances that spearheaded these developments. Special attention will be given to innovative techniques based on Rayleigh and Love waves, which allow a direct calculation of 3D shear-wave velocity structures even in complex environments, as well as techniques based on body waves extracted from seismic noise. Such innovative approaches, in many ways, revolutionize seismic imaging of heterogeneous local structures with strong lateral velocity variations. We will further discuss details of the implementation, resolution and potential challenges. Moreover, since reliable velocity estimates for the frequency range investigated can be obtained rather fast due to increasing computing power, such methods might further open the way to temporarily high-resolved imaging and monitoring of critical environments.

### **Non-Linear Seismic Site Characterization Using Noninvasive Geophysics and Strong-Motion Recordings**

WANG, Z., University of Kentucky, Lexington, KY, USA, zmwang@uky.edu; WOOLERY, E. W., University of Kentucky, Lexington, KY, USA, woolery@uky.edu; RONG, M., Institute of Crustal Dynamics, Beijing, China, rongmianshui@gmail.com

There are several noninvasive approaches, including surface refraction/reflection, spectral analysis surface waves (SASW), ambient noise spectral ratio, and random micro-tremor (REMI), for characterizing site conditions (*i.e.*, shear-wave velocity structure) as part of seismic hazard and other geotechnical assessments. Although these approaches have many advantages, such as cost-effectiveness and being environmentally friendly, they also have some disadvantages, such as non-uniqueness and other physical limitations (*e.g.* blind zones, etc.). Moreover, all the noninvasive approaches are based on small-strain soil conditions (*i.e.*, linear-elastic). However, soil nonlinear response is more important for seismic hazard assessment, as well as for other engineering applications. We demonstrate more reliable shear-wave velocity structures from the noninvasive approaches for nonlinear site response analyses using strong-motion recordings, and vertical strong-motion arrays in particular.

---

## **Earthquake Early Warning: Network Design, Implementation, Production and Outreach**

Oral Session · Wednesday · 2:15 PM · 20 April · Tuscany 1/2

Session Chairs: Graham Kent and Ken Smith

---

### **Rapid Finite Faults with Real-Time GPS: the Geodetic Alarm System**

GRAPENTHIN, R., New Mexico Institute of Mining and Technology, Socorro, NM, USA, rg@nmt.edu; ARANHA, M., University of California, Berkeley, CA, USA, maranha@berkeley.edu; MELGAR, D., University of California, Berkeley, CA, USA, dmelgar@berkeley.edu; ALLEN, R. M., University of California, Berkeley, CA, USA, rallen@berkeley.edu

The Geodetic Alarm System (G-larmS) is a software system developed in collaboration between the Berkeley Seismological Laboratory (BSL) and New Mexico Tech (NMT) for real-time Earthquake Early Warning (EEW). It currently uses high rate (1Hz), low latency (< ~5 seconds), accurate positioning (cm level) time series data from a regional GPS network and P-wave event triggers from the ShakeAlert EEW system. G-larmS extracts static offsets from real-time GPS time series upon S-wave arrival and performs a least squares inversion on these offsets to determine slip on a finite fault. These computations are repeated every second for the duration of the event. G-larmS has been in continuous operation at the BSL since 2014 using event triggers from the California Integrated Seismic Network (CISN) ShakeAlert system and real-time position time series from a fully triangulated network consisting of BARD, PBO and USGS stations across northern California. Pairs of stations are processed as baselines using trackRT (MIT software package). G-larmS produced good results in real-time during the South Napa (M 6.0, August 2014) earthquake as well as on several replayed and simulated test cases. We evaluate the performance of G-larmS for EEW by analyzing the results using a set of well defined test cases to investigate the following: (1) using multiple fault regimes and concurrent processing with the ultimate goal of achieving model generation (slip and magnitude computations) within each 1 second GPS epoch on very large magnitude earthquakes (up to M 9.0) and

(2) the use of Precise Point Positioning (PPP) real-time data streams of various operators, accuracies, latencies and formats along with baseline data streams. We will also discuss the recent expansion and performance of the G-larmS algorithm along the U.S. West Coast on a regional network basis for Northern California, Southern California and Cascadia.

### **Testing the G-FAST Earthquake Early Warning System for Megathrust Earthquakes**

CROWELL, B. W., University of Washington, Seattle, WA, USA, crowellb@uw.edu; SCHMIDT, D. A., University of Washington, Seattle, WA, USA, dasc@uw.edu; BODIN, P., University of Washington, Seattle, WA, USA, bodin@uw.edu; VIDALE, J. E., University of Washington, Seattle, WA, USA, vidale@uw.edu

The G-FAST earthquake early warning module is part of a joint seismic and geodetic earthquake early warning system running alongside ElarmS independently for ~9 months at the Pacific Northwest Seismic Network (PNSN). Our two-stage approach to earthquake early warning includes: (1) initial detection and characterization from PNSN strong-motion and broadband data with the ElarmS algorithm within ShakeAlert, and then (2) modeling of real-time high-rate GPS data from the Pacific Northwest Geodetic Array (PANGA). Our geodetic module, G-FAST, consists of two geodetic modeling modules: (1) a fast peak-ground-displacement magnitude and depth estimate and (2) a CMT-based finite fault inversion that utilizes coseismic offsets to compute earthquake extent, slip and magnitude. In addition to the operational system, we have developed a test system that permits us to: (1) replay segments of actual seismic waveform data recorded from the PNSN and neighboring networks to investigate both earthquakes and noise conditions, and (2) broadcast synthetic data into the system to simulate signals we anticipate from earthquakes for which we have no actual ground motion recordings. The test system lets us also simulate various error conditions (latent and/or out-of-sequence data, telemetry drop-outs, etc.) in order to explore how best to mitigate them. Here we report on the replay performance of G-FAST for several large earthquakes in Japan and Chile, as well as hypothetical megathrust events in Cascadia. Each modeling module has different limitations imposed by latency, network architecture, noise, drop-outs, and earthquake size/location. We finish by discussing how to best improve the robustness and timing of the warnings from G-FAST and challenges associated with integration into the ShakeAlert system.

### **A-21st-century-approach to Firefighting in the Western US: How Microwave-based Seismic Networks Can Change Fire Suppression from Reactive to Proactive**

KENT, G. M., Nevada Seismological Laboratory, UNR, Reno, NV, USA, gkent@unr.edu; SMITH, K. D., Nevada Seismological Laboratory, UNR, Reno, NV, USA, ken@unr.edu; SLATER, D., Nevada Seismological Laboratory, UNR, Reno, NV, USA, davideslater@gmail.com; PLANK, G., Nevada Seismological Laboratory, UNR, Reno, NV, USA, gabep plank@gmail.com; WILLIAMS, M., Nevada Seismological Laboratory, UNR, Reno, NV, USA, mark.c.will@gmail.com; VERNON, F., Scripps Institution of Oceanography, UCSD, San Diego, CA, USA, flvernon@ucsd.edu; DRISCOLL, N. W., Scripps Institution of Oceanography, UCSD, San Diego, CA, USA, ndriscoll@ucsd.edu

The Nevada Seismological Laboratory at UNR has recently embarked on a bold technical initiative, installing a high-speed (up to 190 Mb/sec) mountaintop-based Internet Protocol microwave network, enabling a myriad of sensor systems for Multi-Hazard Early Warning detection and response. In the Tahoe Basin, this system is known as AlertTahoe; a similar network has been deployed in north-central Nevada as part of a 5-year-long grant with BLM. The UNR network mirrors the successful HPWREN multi-hazard network run through UCSD; the UNR "Alert" program (Access to Leverage Emergency information in Real Time) has expanded on the original concept by providing a framework for early fire detection and discovery. Both systems do not rely on open-access public Internet services such as those provided by cellular service providers. Instead, they utilize private wireless communication networks to collect data 24/7 in real-time from multiple sensors throughout the system. Utilizing this restricted-access private communication platform enhances system reliability, capability, capacity and versatility for staff and its community of certified users. Both UNR/UCSD fire camera systems are presently being confederated under a common framework to provide end users (*e.g.*, BLM) a unified interface.

Earthquake response has been both organizations' primary mission for decades; high-speed IP microwave fundamentally changes the playing field allowing for rapid early detection of wildfires, earthquakes and other natural disasters, greatly improving local and regional disaster response/recovery. For example, networked cameras can be optimally placed for wildfire detection and are significantly less vulnerable due infrastructure hardening and the ability to avoid



extreme demands by the public on cellular and other public networks during a crisis. These systems also provide a backup for emergency responders to use when public access communications become overwhelmed or fail during an event.

#### **Update on the Next Generation Earthquake Early Warning in SeisComP3**

**BEHR, Y.**, Swiss Seismological Service, ETH Zurich, Zurich, Switzerland, behr@sed.ethz.ch; **BÖSE, M.**, Institute of Geophysics, ETH Zurich, Zurich, Switzerland, maren.boese@googlemail.com; **SMITH, D.**, U.S. Geological Survey, Menlo Park, CA, USA, deborahsmith@usgs.gov; **CLINTON, J. F.**, Swiss Seismological Service, ETH Zurich, Zurich, Switzerland, jclinton@sed.ethz.ch; **MEIER, M. A.**, California Institute of Technology, Pasadena, CA, USA, mmeier@caltech.edu

An effective Earthquake Early Warning (EEW) system has to be evolutionary, updating its alerts as new data becomes available progressively in real-time. Typically, this involves combining different algorithms tailored towards providing alerts for either moderate or large sized earthquakes using seismic and/or geodetic data. An approach common to most algorithms is to rapidly estimate rupture parameters and then use ground motion prediction equations to compute the expected peak ground motion at a target site. For moderate size earthquakes (<M6.5) the potential damage zone is small requiring very fast alerts. EEW algorithms that model the fault rupture as a point source and estimate the hypocenter and magnitude starting with the first available seismic P-wave recordings are effective in this case. For larger earthquakes, an appropriate EEW approach should allow source parameter estimates to evolve from fast point source estimates, providing the hypocenter and lower bounds on magnitude, to slower but more accurate estimates of the finite rupture kinematics from seismic and geodetic measurements. As it also becomes common to operate several similar algorithms for robustness, effective EEW systems are becoming increasingly complex and difficult to operate and maintain unless implemented within a common real-time processing framework. We show first results of such an evolutionary EEW system implemented within the earthquake monitoring platform SeisComP3, combining point-source algorithms (Gutenberg algorithm; Virtual Seismologist) with a finite rupture algorithm (FinDer2). Relying on a widely used real-time monitoring platform, such as SeisComP3, facilitates testing and operating new algorithms in real-time in different seismic networks and thus different tectonic regimes. Special focus has also been given to modularity of the new system, facilitating the inclusion of additional algorithms, and the compatibility with different real-time monitoring platforms.

#### **Improving the Seismic Network for Earthquake Early Warning in Hawai'i**

**HOTOVEC-ELLIS, A. J.**, University of Washington, Seattle, WA, USA, ahotovec@uw.edu; **BODIN, P.**, University of Washington, Seattle, WA, USA, bodin@uw.edu; **THELEN, W. A.**, U.S. Geological Survey Cascades Volcano Observatory, Vancouver, WA, USA, wthelen@usgs.gov; **OKUBO, P.**, U.S. Geological Survey Hawaiian Volcano Observatory, Volcano, HI, USA, pokubo@usgs.gov; **VIDALE, J. E.**, University of Washington, Seattle, WA, USA, vidale@uw.edu

In earthquake early warning a few extra seconds of warning can provide significant impact, particularly where tens of kilometers separate earthquake sources and assets. Warning times can be increased by reducing data latencies, improving processing times, or tuning seismic station distributions. We have focused our first efforts on seismic network layout, as this aspect currently offers the greatest increases in warning time for the Hawaiian early warning effort. However, while network density and layout can affect warning times by several seconds, there are diminishing returns as more stations are added.

We suggest that the choice of locations for new sites be informed not only by improvements in warning time, but also by seismic hazard. That is, preference should be given to sites that improve warning time from earthquakes that are most likely to elicit significant ground motions. We have designed a method to objectively identify the most efficient sites for improving an existing seismic network, taking both seismic station distribution and probabilistic seismic hazard into account. This technique can be applied to any seismically monitored region and target infrastructure, so long as seismic hazard is defined. We demonstrate its use on the Hawaiian network run by the Hawaii Volcano Observatory (HVO), with focus on seismic hazards to island population centers Hilo and Kailua-Kona, and the astronomical observatories on Mauna Kea. We have identified seven candidate sites for new sensors, telemetry, or complete installations in order of descending impact. The addition of these stations should provide an additional 2–4 seconds of warning for earthquakes in the southern Ka'u and northern offshore regions where ~18 and 6–12 seconds of warning are currently estimated, respectively.

#### **Numerical Shake Prediction for Earthquake Early Warning: Precise and Rapid Prediction even for Heterogeneous Distribution of Ground Shaking**

**HOSHIBA, M.**, Meteorological Res. Inst., JMA, Tsukuba, Japan, mhoshiba@mri-jma.go.jp; **OGISO, M.**, Meteorological Res. Inst., JMA, Tsukuba, Japan, mogiso@mri-jma.go.jp

In many methods of the present EEW systems, hypocenter and magnitude are determined quickly, and then the strengths of ground motions (PGA, PGV, seismic intensity) are predicted using the hypocentral distance and magnitude based on a ground motion prediction equation (GMPE), which usually leads the prediction of concentric distribution. However, actual ground shaking is not always concentric, even when site amplification is corrected. At a common site, the strengths of shaking may be much different among earthquakes even when their hypocentral distances and magnitudes are almost the same. For some cases, PGA differs more than 10 times, which leads to imprecise prediction in EEW.

Recently, Numerical Shake Prediction method was proposed (Hoshiba and Aoki, 2015), in which the present ongoing wavefield of ground shaking is estimated using data assimilation technique, and then future wavefield is predicted based on physics of wave propagation. Information of hypocentral location and magnitude is not required. Because future is predicted from the present condition, it is possible to address the issue of the non-concentric distribution. Once the heterogeneous distribution is actually observed in ongoing wavefield, future distribution is predicted accordingly to be non-concentric. We will indicate examples of M6 crustal earthquakes occurred at central Japan, in which strengths of shaking were observed to non-concentrically distribute. We will show their predictions using Numerical Shake Prediction method.

The heterogeneous distribution may be explained by inhomogeneous distribution of attenuation/velocity. If attenuation/velocity structure is introduced, we can predict the future shaking more rapidly. The information of attenuation/velocity structure leads to more precise and rapid prediction in Numerical Shake Prediction method for EEW.

#### **S- and P-Wave Spectral Ratios for On-site Earthquake Early Warning**

**ZHAO, J. X.**, Southwest Jiaotong University, Chengdu, Sichuan, China, j.zhao@gns.cri.nz

Various earthquake early warning (EEW) systems have been used widely. For an on-site EEW system, S-wave parameters, such as peak ground velocity, are usually estimated in the following three steps: 1) estimate magnitude with a predominant period calculated from the first 3s of P-wave; 2) estimate hypocentral distance using a P-wave amplitude parameter from first 3s of P-wave; 3) estimate the S-wave parameters at the site of concern using an empirical mode such as a ground-motion prediction equation. Each step of the calculation brings in prediction errors.

To predict a ground-motion parameter from a large or moderately large earthquake using hypocentral distance for EEW is deeply flawed because the strong-motion generation area for a given station can be a lot of shorter than the hypocentral distance. If 3s of S-wave is used, the energy release area would be the same for both P- and S-waves.

This study proposes to use the S-wave/P-wave (S/P) response spectral ratio as an EEW parameter. The purpose of EEW is to activate a safety measure for facilities in a building or a high-speed train, for example, on a railway bridge. To estimate response spectrum at a period close to these natural periods of the structure is clearly preferred.

A model for response spectral ratio of the first 3s of S/P-waves was derived as a function of magnitude, source distance, site parameter and spectral period. For an event with a magnitude up to 6.6 and a hypocentral distance within about 80km, S/P ratio does not depend on either magnitude or source distance, leading to an extremely simple EEW model with a constant plus a site effect term. For  $M_w$  over 6.6, S/P spectral ratio increases with increasing magnitude. The spectral ratio of the full record of S-wave and the first 3s of P-wave increases moderately with increasing magnitude and this effect can be accounted for if magnitude can be estimated by other means.

#### **ElarmS 2015 Performance and New Filterbank Teleseismic Filter**

**CHUNG, A. I.**, Berkeley Seismological Laboratory, Berkeley, CA, USA, achung@seismo.berkeley.edu; **ALLEN, R. M.**, Berkeley Seismological Laboratory, Berkeley, CA, USA, rallen@berkeley.edu; **HENSON, I.**, Berkeley Seismological Laboratory, Berkeley, CA, USA, henson@seismo.berkeley.edu; **HELLWEG, M.**, Berkeley Seismological Laboratory, Berkeley, CA, USA, peggy@seismo.berkeley.edu; **NEUHAUSER, D.**, Berkeley Seismological Laboratory, Berkeley, CA, USA, doug@seismo.berkeley.edu

ElarmS is a fully operational earthquake early warning (EEW) system developed by UC Berkeley that has been detecting earthquakes throughout California since



2007. It is one of the algorithms contributing to the West Coast ShakeAlert, a prototype EEW system for the US West Coast. Though ElarmS was originally developed for California, it is now also in use in the Pacific Northwest, Israel, Turkey, Chile, and South Korea. Over the past year, ElarmS has continued to perform well, successfully alerting on all significant ( $M \geq 4.5$ ) earthquakes that occurred in California during 2015.

Despite having a teleseismic filter in place to prevent false alerts due to the arrival of P-waves from distant earthquakes, during 2015 9 false events with  $M \geq 2.5$  were generated by ElarmS due to two large and unusually deep teleseismic earthquakes. The problem of teleseismic earthquakes generating false alerts despite the existing teleseismic filter was identified by the ElarmS research team following the May 30, 2015 Japan earthquake, which caused 7 false alerts. We have added a telestif window, so that when a distant earthquake is detected, ElarmS suppresses all alerts during the time window around the P-wave arrival of the teleseism. We also developed a more sophisticated filterbank teleseismic filter, which distinguishes teleseisms from local earthquakes by rapidly analyzing the frequency content of the first 0.5-1 sec of waveform data sent by a station. This new filter is currently being tested in a parallel ElarmS test system. Though it was not running in the main ElarmS system during the November 24, 2015 teleseism, test results show that it would have prevented both false alerts from being created. We are working to implement the new teleseismic filter in the online ElarmS system as soon as possible.

### Implementing ElarmS for the Israeli Seismic Network—New Tools and Approaches

NOE, R. N., University of California, Berkeley, CA, USA, ran.nof@gmail.com; ALLEN, R. M., University of California, Berkeley, CA, USA, rallen@berkeley.edu

Israel proximity to the Dead Sea Transform (DST) have led the Israeli government to initiate the building of an Earthquake Early Warning System (EEWS). The prime objective of this research is to implement, adjust and validate the ElarmS EEWS for the Israeli Seismological Network (ISN). Our approach for analyzing ElarmS performances with the non-EEW optimized ISN is threefold: (1) We analyze the system in real-time between April 2015 and July 2015; (2) analyze the results of replaying historical data from 39 events ( $M_d > 3.0$ ) between January 2012 and May 2015; (3) analyze 4 simulated earthquake records for magnitudes  $5.1 < M < 7.8$ . We develop new tools for replaying historical and simulated data and to visually monitor and analyze ElarmS performance.

Historical playback results show near complete detection of all events. We adjusted magnitude estimation equation with a previously developed equation for Israel. Using the adjusted magnitude, the performance of the system shows a good agreement with catalog magnitudes.

The real-time implementation of ElarmS in Israel is performing well. It issued a warning for the widely felt June 27, 2015  $M 5.5$  Nueba and for the July 30, 2015  $M 4.4$  Dead Sea earthquakes. However, the alert time is very short due to the significant latencies (2-4 sec) and long data packets (up to 10 sec) that exist for the ISN which has still to be optimized for EEWS.

The earthquake simulations results show a very good agreement with data, demonstrating the potential of using earthquake simulated scenarios for developing and testing EEWS. Further work is needed for creating more realistic simulations using more complex 3D velocity models, broader bandwidth and scenarios including foreshock/aftershock or simultaneous events.

The methods and tools developed during this work may be useful for implementing ElarmS in other regions and similar efforts are being made in the US Pacific Northwest, Turkey, Chile and South Korea.

### Characteristics of Initial P wave Observed from Moderate to Large Earthquakes

NODA, S., USGS, Menlo Park, CA, USA, snoda@usgs.gov; ELLSWORTH, W. L., Stanford University, Stanford, CA, USA, wellsworth@stanford.edu

To estimate earthquake magnitude rapidly, it is essential to understand the characteristics of initial P wave. In this study, we investigate the initial P wave observed at the NIED K-NET stations for 99  $M_w$  4.5–9 earthquakes which occurred in Japan. We analyze the seismograms by computing the absolute value of the displacement (high pass filtered by 0.075 Hz), velocity and acceleration averaged over the stations located in a similar hypocentral distance range (e.g. 150 km  $\pm$  10%). Our results demonstrate that; 1) the average displacement rises with bigger amplitude systematically for the larger events, which cannot be explained by the self-similar scaling in terms of the rupture growth. This characteristic is clearer in displacement than in acceleration; 2) the displacement reaches a plateau whose height depends on magnitude, in addition the time to reach the plateau also scales with magnitude; 3) the 2011 Tohoku earthquake ( $M_w$  9) is exceptional, that is, the event nucleates with much smaller amplitude compared to the

other  $M_w \geq 7$  events and then gradually grows up to the level of the  $M_w \geq 7$  events about 10 seconds after the initiation.

Our finding (1) is consistent with that of Meier *et al.* (2015) who used the data within 25 km, whereas we used the greater distance data. This characteristic is opposite to the conclusion of Colombelli *et al.* (2014). Our result (2) agrees with Colombelli *et al.* Although Chu *et al.* (2011) proposed that the Tohoku earthquake initiated as a  $M_w$  4.9 event, the result (3) suggests that the displacement amplitude of the Tohoku event grew more slowly than the other  $M_w \geq 7$  events even after accounting for an initial delay.

---

## Seismotectonics Beyond the Plate Boundary

Oral Session · Wednesday · 8:30 AM · 20 April · Tuscany 3/4  
Session Chairs: Will Levandowski, Christine Powell, and Oliver Boyd

---

### Damaged Crust and Concentrations of North American Intraplate Seismic Zones

THOMAS, W. A., Alabama Geological Survey, Tuscaloosa, AL, USA, geowat@uky.edu; POWELL, C. A., University of Memphis, Memphis, TN, USA, capowell@memphis.edu

Understanding the cause of concentrations of intraplate earthquakes into seismic zones is a key to seismic-hazard analysis. Most intraplate earthquakes are concentrated along or adjacent to large-scale basement structural fabric elements (e.g., rifts); however, the major seismic zones are limited to specific segments and are not distributed uniformly along the lengths of the ancient structures. Our new hypothesis is that major intraplate seismic zones are located where pervasive damage to the crust is overprinted on large-scale basement structural fabrics. Pervasively damaged crust uniquely characterizes the most active intraplate seismic zones in central and eastern North America (Charlevoix, Eastern Tennessee, and New Madrid). A variety of geologic processes may imprint fine fabric elements, locally damaging the crust to the extent that material properties are changed and the rocks are weakened. Local damaged crust can influence the stability of specific parts of large-scale structures in response to regional stress. In this context, the locations of major intraplate seismic zones are not expected to migrate to other places that do not have the critical combination of pervasively damaged crust and large-scale basement structural elements. This hypothesis has important implications for seismic-hazard analyses that consider the possible temporal migration of intraplate seismic zones.

### Roaming Midcontinental Earthquakes: Occurrence, Causes, and Hazards

LIU, M., University of Missouri, Columbia, MO, USA, lium@missouri.edu; STEIN, S., Northwestern University, Evanston, IL, USA

In contrast to interplate earthquakes whose occurrence, causes, and hazards can be studied in the framework of plate tectonics, intraplate earthquakes, especially those in midcontinents, remain enigmatic. Large midcontinental earthquakes often occur in unexpected places; they are episodic and clustered, and apparently roam randomly among distant fault zones over time, as illustrated by large earthquakes in North China, Northern Europe, Australia, and the central and eastern United States. We suggest that the approach used at plate boundaries, which focuses on the loading rates and rupture history of individual faults, is inadequate for studying midcontinental earthquakes. We argue, instead, that we should treat the widespread fault systems in midcontinents as complex dynamic systems, and try to understand fault interactions within the complex system. This paradigm shift means that we should modify how we assess earthquake hazards in midcontinents. The locations of previous large earthquakes, which heavily influence hazard assessment, may not be good indicators of the locations of future earthquakes. Detailed geodetic and paleoseismic studies need to be expanded beyond fault zones with recent large earthquakes; such effort can benefit from comparison of the seismic record of a region, which is incomplete in most places, with the long-term spatial patterns of tectonic strain energy predicted from numerical models.

### North America's Midcontinent Rift: when Rift met LIP

STEIN, S., Northwestern University, Evanston, IL, USA, seth@earth.northwestern.edu; STEIN, C., University of Illinois at Chicago, Chicago, IL, USA, cstein@uic.edu; KLEY, J., Georg-August-Universität Göttingen, Göttingen, Germany, jkley@gwdg.de; KELLER, G. R., University of Oklahoma, Norman, OK, USA, grkeller@ou.edu; WIENS, D., Washington University, St. Louis, MO, USA, doug@wustl.edu; WYSESSION, M., Washington University, St. Louis, MO, USA, michael@wucore.wustl.edu; ALEQABI, G., Washington University, St. Louis, MO, USA, ghassan@seismo.wustl.edu;

SHEN, W., Washington University, St Louis, MO, USA, cv90134@gmail.com; MERINO, M., Chevron Corporation, Houston, TX, USA, merinomi@gmail.com; FREDRICKSEN, A., University of Manitoba, Winnipeg, ON, Canada, Andrew.Fredriksen@umanitoba.ca; DARBYSHIRE, F., Université du Québec à Montréal, Montreal, Canada, f.darbyshire@gmail.com; JURDY, D., Northwestern University, Evanston, IL, USA, donna@earth.northwestern.edu; WAITE, G., Michigan Technological University, Houghton, MI, USA, gpwaite@mtu.edu; ROSE, W., Michigan Technological University, Houghton, MI, raman@mtu.edu; ROONEY, T., Michigan State University, East Lansing, MI, USA, rooneyt@msu.edu; MOUCHA, R., Syracuse University, Syracuse, NY, USA, rmoucha@syr.edu; BROWN, E., Aarhus University, Aarhus, Denmark, basalt78@yahoo.com.

Rifts are segmented linear depressions, filled with sedimentary and igneous rocks, which form by extension and often evolve into plate boundaries. Flood basalts, a class of Large Igneous Provinces (LIPs), are broad regions of extensive volcanism due to sublithospheric processes. Typical rifts are not filled with flood basalts, and typical flood basalts are not associated with significant crustal extension and faulting. The Midcontinent Rift (MCR) is an unusual combination. Its 3000-km length formed as part of the 1.1 Ga rifting of Amazonia (Precambrian NE South America) from Laurentia (Precambrian North America) and became inactive once seafloor spreading was established, but it contains an enormous volume of igneous rocks. MCR volcanics are significantly thicker than other flood basalts, due to deposition in a narrow rift rather than a broad region, resulting in a rift geometry with a LIP's magma volume. Structural modeling of seismic reflection data shows an initial rift phase where flood basalts filled a fault-controlled extending basin, and a postrift phase where volcanics and sediments were deposited in a thermally subsiding basin without associated faulting. The crust thinned during rifting and rethickened during the postrift phase and later compression, yielding the present thicker crust. EarthScope data show two surprising results. Although the MCR's dense volcanic rocks appear clearly on gravity, seismic reflection, and receiver function data, which are sensitive to variations in density, surface wave tomography "sees" primarily low-velocity sediments, with no strong anomaly below. Presumably compared to the surrounding crust, the basalt rift fill is denser but has similar or slightly lower S-wave velocity. Another surprise is that mantle below the MCR shows no significant velocity anomaly or anisotropy, suggesting melt depletion had little effect on seismic velocities and likely reflecting the fact that much of the volcanism occurred after extension ended.

#### **Moho Temperature and Compositional Controls on Lithospheric Bending Strength in the Western United States**

SCHUTT, D. L., Colorado State University, Fort Collins, CO, USA, derek.schutt@colostate.edu; LOWRY, A. R., Utah State University, Logan, UT, USA, tony.lowry@usu.edu; BUEHLER, J. S., Scripps Institution of Oceanography, La Jolla, CA, USA, buehleja@gmail.com

We use measurements of mantle P-wave velocity from the Moho refracted phase, Pn [Buehler and Shearer, 2010, 2012], and mineral physics [Schutt and Lesher, 2006, 2010] to estimate temperature in the uppermost few km of the western U.S. mantle. Relative to other approaches to modeling the deep geotherm, or mapping surface wave velocities to temperatures, Pn requires fewer assumptions and provides a less uncertain temperature within a tightly-constrained depth. Moho temperatures are lowest in the high-plains region of Wyoming and western Kansas/Nebraska, while highest temperatures are observed under recent (<10 Ma) volcanic provinces where they generally exceed 850°C. Moho temperatures east of the Laramide deformation front are also quite hot, ~850°C, but crustal thicknesses here are 10-20 km thicker than in the Basin and Range, so these temperatures are not surprising.

Using a range of estimates of crustal heat production values, surface heat-flow measurements are extrapolated to depth under the assumption of steady-state conduction, and with the constraint that Pn velocity observations are fit. Preliminary results are very encouraging, and also provide an indication of where Pn velocities are modulated by composition rather than temperature or where the assumption of steady-state heat flow is invalid.

These geotherms are used to predict lithospheric bending strength parameterized as effective elastic thickness,  $T_e$ , for various assumed rheologies. The model predictions are compared to measurements [Lowry & Pérez-Gussinyé, 2011], to show that a weak, hydrous rheology is required to fit observations in the westernmost U.S. The hydrous rheology zone significantly overlaps with the part of North America formed from accreted terranes over the last 300 M.y. To the east of this region, a dryer and stronger rheology is needed to fit the  $T_e$  observations.

#### **Joint Inversion of Rayleigh Wave Ellipticity and Phase Velocity across USArray**

LIN, F., University of Utah, Salt Lake City, UT, USA, fanchi.lin@utah.edu; SCHMANDT, B., University of New Mexico, Albuquerque, NM, USA

The development of ambient noise and surface wave tomography has now allowed detailed crustal structure to be studied across broadband arrays. In this presentation, I will summarize our recent work on jointly inverting Rayleigh wave phase velocity and ellipticity measurements between 8 and 100 sec period observed across USArray to construct a high-resolution 3D crust and uppermost mantle  $V_s$  model for the contiguous US. Because of the complementary sensitivity of the two measurement types, the upper crustal structure in particular can be well resolved. Clear correlations are observed between the resolved velocity anomalies and known geological features at all depths. Besides the isotropic  $V_s$  model, I will also discuss two new directions of research. First, I will show how directionally dependent Rayleigh wave ellipticity measurements can be used to study azimuthal anisotropy in the upper crust and infer local stress orientation and structural fabric. Second, I will discuss the potential of studying density structure using the joint inversion method.

#### **GPS Imaging of the North American Intracontinental Strain Rate Field**

KREEMER, C., University of Nevada, Reno, NV, USA, kreemer@unr.edu; HAMMOND, W. C., University of Nevada, Reno, NV, USA, whammond@unr.edu; BLEWITT, G., University of Nevada, Reno, NV, USA, gblewitt@unr.edu

Strain rate fields derived from GPS velocity data have proven powerful indicators of the underlying lithospheric forces and the expected earthquake activity rate. However, strain rate estimates for intraplate areas have been hard to determine, leaving many questions in regard to intraplate seismicity unanswered; e.g., for North America what is 1) the significance of induced seismicity, 2) the explanation for relatively high seismicity rates in places such as New Madrid, and 3) the role of Glacial Isostatic Adjustment (GIA)? Estimating intraplate strain rates from GPS velocities needs to be done with care, given that the signal is likely at the level of the data uncertainty, and outlier GPS velocities will dominate the results. To remedy this problem, we deploy a new scheme that takes advantage of the recent increase in the number of freely accessible GPS stations and new techniques for processing data from tens of thousands of stations automatically. We use these new algorithms to obtain continental-scale long-wavelength images of horizontal displacement field. In this approach we apply a weighted median spatial filter to the observed velocities, which effectively despeckles the data and leaves the long-wavelength signal. Here, we will focus on the North American intracontinental area. The signal derived from >2,000 stations consists of three parts: 1) a plate rotation (when the data are in a geodetic reference frame), 2) a long-wavelength GIA displacement field, and 3) a strain rate field associated with the derivatives of the GIA field and any other coherent deformation. We then use the despeckled velocities (or the densely interpolated gridded values thereof) to estimate the strain rate tensor field. We will present the sensitivity of different variants to our imaging technique to the found results, and discuss the implications of the strain rate field in terms of the observed and expected intraplate seismicity distribution.

#### **Crustal Model of the St. Lawrence Corridor from Charlevoix to Montreal**

BENT, A. L., Geological Survey of Canada, Ottawa ON Canada, allison.bent@canada.ca; KAO, H., Geological Survey of Canada, Sidney, BC, Canada, honn.kao@canada.ca

Three of the most active seismic zones in eastern Canada (Charlevoix, West Quebec and the Lower St. Lawrence) are located along the St. Lawrence River but separated by regions of very low seismicity. While seismicity along the St. Lawrence is believed to be associated with a reactivated rift structure, the reasons for the variations in seismicity level are not well understood. This is a heavily populated region and a better understanding of the hazard is important for risk reduction. To evaluate whether there could be structural differences along the St. Lawrence, we have modeled the crustal structure beneath broadband seismograph stations using a teleseismic receiver functions and a Neighborhood Algorithm inversion. Data from a series of temporary broadband stations deployed to fill in gaps in the coverage by the Canadian National Seismograph Network (CNSN) as well as some USTA and CNSN stations were modeled. Work in the region between the Charlevoix Seismic Zone and Montreal has been completed and we are now beginning to focus our attention on the region from Charlevoix to the Lower St. Lawrence. Regional scale features including a crustal discontinuity at about 20 km depth and Moho at 35-40 km can be correlated from one station to another allowing for a pseudo-3D model to be developed. These features are also seen in models developed via other methods. Modeling this region is somewhat complicated by the fact that the stations sit on or near the boundary of three



geological provinces and signals from some azimuths travel primarily through a different geological province than the one in which the station is located. The structural models do not indicate any significant difference in velocity structure between the seismic and aseismic regions although we cannot rule out smaller scale structural differences.

#### **A Map of Faults and Lineaments of the St. Lawrence Rift System**

LAMONTAGNE, M., Geological Survey of Canada, Ottawa, ON, Canada, malamont@nrcan.gc.ca; NADEAU, L., Volunteer, Geological Survey of Canada, Quebec City, QC, Canada, lnadeau@nrcan.gc.ca; BROUILLETTE, P., Geological Survey of Canada, Quebec City, QC, Canada, pierre.brouillette@canada.ca; BÉDARD, M. P., Contractor, Quebec City, QC, Canada

This project aims at producing a digital map of the faults and lineaments of the St. Lawrence Rift System (SLRS), including those of the Ottawa-Bonnechere (OBG) and the Saguenay (SG) grabens. Although the SLRS is central to the seismic zoning in eastern Canada, the position of the rift faults are seldom available in a digital format or at a scale usable in seismic hazard studies. The digital map will help defining the relationships between earthquakes and faults, including when new sizeable earthquakes occur within the SLRS. Seismic hazard studies will also benefit from this knowledge. Since most Quebec earthquakes occur in the Precambrian Shield rocks, only the lineaments and faults of the Grenville Province are considered.

The project integrates the results of the existing structural geology mapping along the SLRS, most notably along the OBG on the Ontario side and along the SG. Additional lineaments were interpreted mostly from the Digital Elevation Model (DEM) of the Canadian National Topographic Data Base (NTDB) at a scale of 1:250,000. The DEMs illuminated from two directions were used to visually interpret lineaments and georeferenced their surface traces in a Geographic Information System. Since the final goal is to better map the SLRS faults, only the brittle structures were considered; the ductile structures of the Grenvillian orogeny were not mapped. Brittle structures are generally linear whereas ductile structures are curved or present a distinct pattern. Also, only the lineaments with a length greater than 5 km were considered. From this first detection pass, regional scale lineaments were drawn by interpolating between segment of lineaments where the topography was subdued and did not create a conspicuous trace. Where possible, other sources of data such as magnetics, gravity, bathymetry and Lidar (for Charlevoix) will be included in an upcoming Open File publication.

#### **Location of CEUS vs. Gulf Coast Q Boundary from USArray Data**

CRAMER, C. H., CERl, Univ. of Memphis, Memphis, TN, USA, ccramer@memphis.edu; AL NOMAN, M. N., CERl, Univ. of Memphis, Memphis, TN, USA

We have determined the location of the Q boundary between the more attenuating Gulf Coast and the less attenuating CEUS mid-continent. Our approach is to use observations from profiles of USArray TA stations radiating from selected ~M4 earthquakes to locate slope changes with distance due to differing crustal Qs. The Q transition boundary seems fairly sharp within the resolution of the ~70 km spacing of the TA array. For earthquake sources outside the Gulf Coast region, the location of the transition appears significantly different for high frequencies (5 Hz and PGA) than for lower frequencies (1 Hz). For 1 Hz, the transition boundary is near the coast of the Gulf of Mexico in Texas, Louisiana, and Mississippi, and offshore further east. This confirms the 1 Hz Q tomography results of Gallegos, *et al.*, 2014. For 5 Hz (and PGA), the transition is further north in Oklahoma (35°N), Arkansas (34-35°N), Mississippi (32-33°N), and the panhandle of Florida (30°N). In Texas west of 97°W the Gulf Coast boundary is below 30°N. For earthquakes within the Gulf Coast region, the 1 Hz boundary agrees with the 5 Hz boundary above and crustal Q is similar to WUS (low). The Q in the Florida Peninsula is similar to CEUS Q, as is the Q in most of Alabama and Georgia, and along the Atlantic coastal margin of the Carolinas. These results are significantly different from the Q boundary estimates of EPRI (1993) and the NGA East project (Dreiling *et al.*, 2014), and seem to follow the Alabama-Oklahoma transform of Thomas (2010). Our observations are important for earthquake hazard analyses, suggesting higher hazard along much of the Gulf Coast, particularly for large regional earthquakes. Additionally, maps of amplitude residuals relative to a profile totally in CEUS mid-continental crust reveal ground motion amplitudes strongly influenced by radiation pattern and possibly propagation and site effects, which may bias amplitude residuals and possibly tomography results.

#### **An Issue with the National Seismic Hazard Maps: Where Is the Boundary That Separates the Use of the Western U.S. and CEUS Ground Motion Prediction Models?**

WONG, I. G., AECOM, Oakland, CA USA, ivan.wong@aecom.com

In developing the National Seismic Hazard Maps since 1996, the USGS has divided the continental U.S. into a western region where ground motion prediction models for tectonically active regions (NGAWest-2) are used in calculating probabilistic hazard and a central and eastern U.S. (CEUS) region where CEUS ground motion models are implemented. Seismological studies since the early 1980's suggest that the USGS boundary should be further to the east than currently defined. The USGS boundary puts most of Wyoming and Colorado, the Colorado Plateau in eastern Utah, northeastern Arizona and northwestern New Mexico, and eastern New Mexico in the CEUS region. The resulting hazard in these five states as characterized by the USGS is higher than it should be due to the use of the CEUS ground motion models. The criteria used in delineating the boundary is uncertain, but considering available information on both seismic source characteristics and crustal structure and attenuation (Q), a boundary that separates the tectonically active western U.S. from the stable CEUS craton should be on the eastern front of the Rocky Mountains. Also, it is likely that the ground motion boundary should not be a sharp boundary but transitional in nature. To address the appropriateness of ground motion models in a transitional zone, a weighted combination of NGA-West and CEUS models might be used. In addition to the issue that the probabilistic hazard depicted on the National Seismic Hazard Maps for the areas in the five states is too high, the USGS portrayal that the above areas should be in the CEUS ground motion domain can lead to overly conservative design or safety evaluation ground motions for critical and important facilities. The results of site-specific seismic hazard analyses in the areas covered by the five states will be presented to illustrate the overconservatism of the National Hazard Maps.

---

#### **Ground Motion Spatial Variability: Models, Methods and Impacts**

Oral Session · Wednesday · 2:15 PM · 20 April · Tuscany 3/4

Session Chairs: David Wald, Kim Olsen, Jack Baker, and Paolo Bazzurro

---

#### **Ground Motion Variability from 3-D Deterministic Broadband (0-8 Hz) Ensemble Simulations of Mw 7.1 Strike-slip and Mw 6.7 Blind Thrust Events Incorporating Rough Fault Topography, Frequency-Dependent Viscoelasticity, Small-Scale Media Heterogeneity, and Plasticity**

WITHERS, K. B., San Diego State University/University of California San Diego, San Diego, CA, USA, quantumkylew@aol.com; OLSEN, K. B., San Diego State University, San Diego, CA, USA, kbolsen@mail.sdsu.edu; SHI, Z., San Diego State University, San Diego, CA, USA, zshi@mail.sdsu.edu; DAY, S., San Diego State University, San Diego, CA, USA, sday@mail.sdsu.edu

We model ground motion variability for large strike-slip and blind thrust earthquakes including frequencies up to 8 Hz. The earthquake source is obtained through dynamic rupture propagation using SORD along several realizations of rough fault topographies. An ensemble of sources is modeled by varying the hypocenter location that results in similar moment magnitudes. The slip-rate data from the rupture modeling is converted to a kinematic source and input into the wave propagation code AWP-ODC, which incorporates frequency-dependent attenuation (Q(f)) as well as Drucker-Prager plasticity. We also include small-scale medium complexity in both a 1D-layered model and a 3D medium extracted from SCEC CVM-S4 including a surface geotechnical layer. The ground motion is analyzed spatially by binning the ground motion as a function of distance and comparing with leading GMPEs. The median ground motion follows a similar decay as compared to GMPEs when using a Q(f) power-law exponent in the range 0.6-0.8. Nonlinear effects are needed to reduce near-field ground motion to observable levels in regions of near-surface low velocity layers. Small-scale media complexity is observed to decrease the polarization ratio to that of similar to observations. The intra-event variability for the layered model simulations is near observed values of single-station standard deviation. Small-scale heterogeneity can significantly affect the intra-event variability at frequencies greater than ~1 Hz, becoming increasingly important at larger distances from the source. The intra-event variability of our simulations in the CVM is typically larger than that for the observations at frequencies > 1 Hz. However, this discrepancy tends to decrease when small-scale heterogeneities are included, suggesting the need for a highly complex velocity model to fit ground motion variability. Plastic effects in the medium also reduce the variability, particularly at distances close to the source.

### Computing Spatial Correlation of Ground Motion Intensities for ShakeMap

YERROS, S., Colorado School of Mines; U.S. Geological Survey, Golden, CO, USA, sverros@usgs.gov; WALD, D. J., U.S. Geological Survey, Colorado School of Mines, Golden, CO, USA, wald@usgs.gov; GANESH, M., Colorado School of Mines, Golden, CO, USA, mganesh@mines.edu; WORDEN, C. B., U.S. Geological Survey, Golden, CO, USA, cworden@usgs.gov; HEARNE, M., U.S. Geological Survey, Golden, CO, USA, mhearne@usgs.gov; HORSPOOL, N., GNS Science, Lower Hutt, New Zealand, n.horspool@gns.cri.nz

Modeling the spatial correlation of ground motion intensity measures (IMs) caused by coherent contributions from earthquake source, path, and site, can provide valuable loss and hazard information, as well as a more realistic depiction of ground motions. Previous studies have developed for spatial correlation IM models as a function of site-to-site separation distance. Using ShakeMap grid distances, we simulate spatially-correlated random fields conditioned on seismic observations, where the random field converges to zero; they can then be added to a ShakeMap grid to obtain realizations of spatially correlated ground motions. Simulating the correlated fields is computationally expensive in terms of both time and memory. We explore two efficient algorithms to compute the correlated field: successive conditional simulation (SCS) and the Karhunen-Loeve Transformation (KLT). Our ShakeMap-grid dependent SCS algorithm alleviates memory requires, enables parallelization and brings the computations closer to real-time. The ShakeMap-grid independent stochastic KLT algorithm utilizes the distance-dependent correlation function. Setting up the KLT is an offline/pre-computation process. The decay of the angular power spectrum in the KLT facilitates reduction in stochastic dimensions for efficient online evaluation of the random field. To understand the impacts on potential losses, we apply the USGS PAGER system to estimate the fatalities and economic losses for realizations of the spatially correlated ground motions for several damaging earthquakes. Adding spatial correlation to the ground motion field constrained with observations does not significantly alter the distribution of loss estimates; however, for scenarios (or real-time events with few stations), the loss distribution noticeably changes with an increased mean and standard deviation. Further, we investigate the combined effects of directivity and spatial variability on the losses for a series of earthquake scenarios.

### Spatial Distribution Model of Earthquake Strong-motion Amplitude and Frequency Variation on the Icelandic Strong-motion Array (ICEARRAY I) in South Iceland

RAHPEYMA, S., Earthquake Engineering Research Centre, University of Iceland, Reykjavik, Iceland, sahar@hi.is; HALLDORSSON, B., Earthquake Engineering Research Centre, University of Iceland, Reykjavik, Iceland, skykkur@hi.is; HRAFNKELSSON, B., University of Iceland, Reykjavik, Iceland, Birgirhr@hi.is

Iceland, the largest subaerial part of the Mid-Atlantic Ridge, is the most seismically region in northern Europe. The South Iceland Fracture Zone (SIFZ) is one of two major fracture zones where earthquake hazard is the highest. For the earthquake resistant design of structures in Iceland residential buildings are assumed to have relatively uniform form-factors for which site effects are typically assumed to be negligible. However, recent recordings data during and after the  $M_w$  6.3 Ölfus earthquake on May 2008 collected on twelve strong-motion stations of the ICEARRAY I in the town of Hveragerði provides the opportunity to quantify the spatial distribution of ground motion amplitudes and their frequency variation on lava rock. The data shows 100% difference in peak ground acceleration (PGA) during the mainshock and more than 1700 aftershocks. The local site conditions account for the strong spatial variation of ground motion peak parameters such as PGA and Spectral Acceleration (SA) as a function of oscillator period. The key peak-parameters are calculated for each record and their spatial variation in terms of amplitudes and frequency is quantified across the array. Furthermore, the data on PGA are modeled and analyzed using the Bayesian hierarchical framework to model physical phenomena and quantify uncertainty of the latent physical process. The spatial model includes event effects (moment magnitude, distance, source location, etc.) and site effects which are imposed on all of the parameters of the data density, to model the spatial variation of the underlying process. The new maps showing the spatial variation of PGA, SA, and Predominant frequency, HVSR-amplification obtained from Horizontal to Vertical Spectral Ratio (HVSR) approach have been produced. A new hazard estimate will enable a more optimal earthquake resistant design of structures as well as urban planning. The results are expected to apply in other urban areas in Iceland with similar geology.

### Spatial Incoherency Analysis of Seismic Ground Motions from 2014-Argostoli Earthquake Dense Array

SVAY, A., CentraleSupélec, Chantenay-Malabry, France, angkeara.svay@ecp.fr; CLOUTEAU, D., CentraleSupélec, Chantenay-Malabry, France, didier.clouteau@ecp.fr; COTTEREAU, R., CentraleSupélec, Chantenay-Malabry, France, regis.cottreau@ecp.fr; ZENTNER, I., EDF R&D, Clamart, France, irmela.zentner@edf.fr

In seismic soil-structure interaction studies, the common practice in Civil Engineering is to consider a uniform movement of free field at any point on the ground surface. However, that assumption is not completely realistic since the seismic ground motions can vary spatially due to wave passage effects, dispersions and reflections of wave propagating in the random heterogeneous media and site effects. Therefore, in order to increase the security of buildings and equipment, it is necessary to do the analyses of seismic soil-structure interactions in the most realistic way. This can be achieved by taking into account the spatial variability of seismic ground motions.

The spatial incoherence of seismic ground motions due to dispersions and reflections of waves can generally be modelled in such analysis by a coherency function in frequency domain. Several models of coherency function (empirical and semi-empirical) are presented and widely used in the literature. However, those coherency models cannot be applied to all different types of soil because they strongly depend on the properties of the sites where the seismic signals were recorded.

The work presented in this paper is the result of the statistical analysis of spatial variability of seismic ground motions from experimental data measured at Argostoli dense array (Kefalonia island, Greece) for the earthquakes in February 2014 (few days after a main shock of  $M_w=6.0$ ). For such analysis, one hundred earthquake events were selected from several thousands of events recorded. The spatial coherencies for small separations (from 10m to 100m) were estimated from the strong motion window of earthquake signals and then compared to the existing coherency models in the literature to discuss their limitations in soil-structure interaction applications.

### Magnitude, Region and Site-specific Spectral Value Correlations and Conditional Mean Spectra

KOTHA, S. R., GeoForschungsZentrum, Potsdam, Germany, sreeram@gfz-potsdam.de; BINDI, D., GeoForschungsZentrum, Potsdam, Germany, bindi@gfz-potsdam.de; COTTON, F., GeoForschungsZentrum, Potsdam, Germany, fcotton@gfz-potsdam.de

The observed correlation of total-residuals of horizontal peak spectral acceleration across spectral time periods is empirically modeled and used in estimating a conditional mean spectrum, in vector-valued PSHA, and in time history selection for dynamic analysis of structures. Although the total-residuals are known to be GMPE, dataset, region, distance and magnitude dependent, the total-residual correlation models were assumed not to be due to insufficient strong motion data to explore such dependencies. Using the RESORCE and NGA-West2 strong-motion datasets we review this ergodic assumption. Initially the between-event correlations are found to be magnitude dependent, which can be partially ascribed to differences between  $M < 5.5$  and  $M \geq 5.5$  events in terms of corner-frequency and role of high frequency attenuation. However the total-residual correlation model is controlled by the within-event correlations primarily because the within-event variance is much larger than the between-event variance, thus making it magnitude independent. To overcome this limitation we separate the between-station variance from the aleatory within-event variance and reduce it to an event-station corrected variance which is comparable in size to between-event variance. The resulting event-site corrected residuals and their correlations across spectral accelerations by construction are only path dependent, and are found to be region dependent possibly due to the regional differences in distance-decay of strong motion. As an example, the total-residual correlation models now estimated using the magnitude dependent between-event, region dependent event-station corrected correlations are used along with between-station residuals to derive a magnitude, region, and site-specific conditional mean spectra for 4 stations in Italy and Turkey.

### Sensitivity of Annualized Earthquake Loss Estimates in California to Site Amplification

CHEN, R., California Geological Survey, Sacramento, CA, USA, rui.chen@conservation.ca.gov; JAISWAL, K. S., U.S. Geological Survey, Golden, CO, USA, kjaiswal@usgs.gov; BAUSCH, D., Pacific Disaster Center, Kihai, HI, USA, dbausch@pdc.org; SELIGSON, H., MMI Engineering, Huntington



Beach, CA, USA, HSetigson@mengineering.com; WILLS, C. J., California Geological Survey, Sacramento, CA, USA, Chris.Wills@conservation.ca.gov

Input datasets for annualized earthquake loss (AEL) estimation in California were updated recently by the scientific community, including the National Seismic Hazard Models (NSHM), site response models, and estimates of shear wave velocity. Furthermore, Federal Emergency Management Agency's loss estimation tool, Hazus, was updated to include the most recent census and economic exposure. We use Hazus and new hazard data to update AEL estimates for California and to study the effect of alternate inputs related to site amplification. Estimated AELs are presented at the state level and for counties, metropolitan areas, and selected cities.

Site amplification is considered in three ways: (1) use of a Hazus formatted soil map and amplification parameters; (2) ground motions scaled by amplification factors based on National Earthquake Hazards Reduction Program (NEHRP) site classes; and (3) ground motions scaled using the Seyhan and Stewart amplification model. In the first two cases, ground motions are calculated by multiplying ground motion parameters (from 2014 NSHM ground motions on a 5-km grid for a uniform VS30 = 760 m/s site condition) by corresponding NEHRP site amplification factors. In the first case, site amplification is calculated within Hazus and site classes are based on a geologic Vs30 map. In the second case, site amplification is calculated outside Hazus using a hybrid geology and topo-based Vs30 map. Ground motions are amplified directly (using site response model and Vs30 values) in the third case without conversion to site classes. Estimated AELs at the state level (\$3.6–3.7 billion) are relatively insensitive to alternate site amplifications. However, differences are seen for smaller geographic units. The state level estimates are 8% higher than recent estimates by Jaiswal *et al.* (2015) due to increased economic exposure associated with the recent inventory data update within Hazus.

#### Implementation of Monte-Carlo Simulations for Probabilistic Loss Assessment of Geographically Distributed Portfolio Using Multi-Scale Random Fields: A Case Study for Istanbul

AKKAR, S., Bogazici University, Istanbul, Turkey, sinan.akkar@boun.edu.tr; CHENG, Y., Bogazici University, Istanbul, Turkey, yin.cheng1983@gmail.com; ERDIK, M., Bogazici University, Istanbul, Turkey, erdikm@gmail.com

The conventional integral approach is very well established in probabilistic seismic hazard and risk assessment. However, Monte Carlo (MC) simulation technique can become an efficient and flexible alternative against the conventional integral approach whenever more complicated factors (*e.g.*, spatial correlation of ground shaking) are involved in seismic hazard or loss studies. This paper aims at showing the implementation of MC simulation techniques for probabilistic loss assessment of geographically distributed portfolio. We use multi-scale random fields (MSRFs) methodology to incorporate spatial correlation and near-fault directivity while generating MC simulations to assess not only the probabilistic seismic hazard but also the direct probabilistic loss estimation on top of hazard. We discretize the random field to produce more reasonable expected ground motions for an area covered by the grid. This approach is alternative to the conventional grid-based ground-motion fields where the ground motion is taken from a single point at the centroid of the cell. To illustrate the potential use of this alternative approach in hazard and risk assessment of geographically distributed structural systems, we present an example for the probabilistic seismic loss assessment of one of the densely populated districts in Istanbul.

#### How Much Can the Total Aleatory Variability of Empirical Ground Motion Prediction Equations Be Reduced Using Physics-Based Earthquake Simulations?

JORDAN, T. H., USC/SCEC, Los Angeles, CA, USA, tjordan@usc.edu; WANG, F., AIR-Worldwide Corp., Boston, MA, USA, fengo.win@gmail.com; GRAVES, R. W., U.S. Geological Survey, Pasadena, CA, USA, rwgraves@usgs.gov; CALLAGHAN, S., USC/SCEC, Los Angeles, CA, USA, scottcal@usc.edu; OLSEN, K. B., San Diego State University, San Diego, CA, USA, kbolsen@mail.sdsu.edu; CUI, Y., San Diego Supercomputer Center, La Jolla, CA, USA, yfcui@sdsc.edu; MILNER, K., USC/SCEC, kmilner@usc.edu; JUVE, G., USC/ISI, Los Angeles, CA, USA, gideon@isi.edu; VAHI, K., USC/ISI; YU, J., USC/SCEC; DEELMAN, E., USC/ISI; GILL, D., USC/SCEC; MAECHLING, P. J., USC/SCEC

Ground motion prediction equations (GMPEs) in common use predict the logarithmic intensity of ground shaking as a deterministic value conditioned on a set of explanatory variables plus a normally distributed random variable with a standard deviation  $\sigma_T$ . The latter accounts for the unexplained variability in the ground motion data used to calibrate the GMPE and is typically 0.5–0.7 in natural log units. Reducing this residual or “aleatory” variability is a high priority

for seismic hazard analysis, because the probabilities of exceedance at high hazard values go up rapidly with  $\sigma_T$ , adding costs to the seismic design of critical facilities to account for the prediction uncertainty. However, attempts to decrease  $\sigma_T$  by incorporating more explanatory variables to the GMPEs have been largely unsuccessful. An alternative is to employ physics-based earthquake simulations that properly account for source directivity, basin effects, directivity-basin coupling, and other 3D complexities. We have explored the theoretical limits of this approach through an analysis of large ensembles of simulations generated for the Los Angeles region by SCEC's CyberShake project using the new tool of averaging-based factorization (ABF, Wang & Jordan, BSSA, 2014). The residual variance obtained by applying GMPEs to the CyberShake dataset matches the frequency-dependence of  $\sigma_T$  obtained for the GMPE calibration dataset. The ABF analysis allows us to partition this variance into uncorrelated components representing source, path, and site effects. We show that carefully validated simulations can potentially reduce  $\sigma_T$  by about one-third, which could lower the exceedance probabilities at high hazard levels by orders of magnitude. Realizing this gain in forecasting probability would have a broad impact on risk-reduction strategies, especially for critical facilities such as large dams, nuclear power plants, and energy transportation networks.

#### A Non-Ergodic Ground-Motion Model for California with Spatially Correlated Coefficients

LANDWEHR, N., Institute of Computer Science, University of Potsdam, Potsdam, Germany, landwehr@cs.uni-potsdam.de; KUEHN, N. M., PEER Center, University of California, Berkeley, Berkeley, CA, USA, kuehn@berkeley.edu

Traditional probabilistic seismic hazard analysis (PSHA), as well as the estimation of ground-motion models (GMMs), is based on the ergodic assumption, which means that the distribution of ground motions over time at given site is the same as their spatial distribution over all sites for the same magnitude, distance, and site condition. With a large increase in the number of recorded ground-motion data, there are now repeated observations at given sites and from multiple earthquakes in small regions, and this assumption can be relaxed. We use a novel approach to develop a non-ergodic GMM, which is cast as a varying coefficients model (VCM). In this model, the coefficients are allowed to vary by geographical location, which makes it possible to incorporate effects of spatially varying source, path and site conditions. Therefore, a separate set of coefficients are estimated for each source and site coordinate in the data set. The coefficients are constrained to be similar for spatially nearby locations. This is achieved by placing a Gaussian process prior on the coefficients. The amount of correlation is determined by the data. The spatial correlation structure of the model allows one to extrapolate the varying coefficients to a new location and trace the corresponding uncertainties. The approach is illustrated on the NGA West2 data set, using only Californian records. The VCM outperforms a traditionally estimated GMM in terms of generalization error, and leads to a reduction in the aleatory standard deviation by about 40%, which has important implications for seismic hazard calculations. The scaling of the model with respect to its predictor variables such as magnitude and distance is physically plausible. The epistemic uncertainty associated with the predicted ground motions is small in places where events or stations are close and large where data is sparse.

#### Conditional Simulation of Spatially Variable Ground Motions and its Application to an Input Wave Field from the San Andreas Fault ShakeOut Scenario.

ANCHETA, T. D., Risk Management Solutions, Newark, CA, USA, tim.ancheta@rms.com; STEWART, J. P., University of California, Los Angeles, Los Angeles, CA, USA, jstewart@seas.ucla.edu

Spatial variability of ground motions has been shown in previous work to be an important element of demand specification for extended lifelines structures such as pipelines or bridges. Additional applications where such procedures may soon find fruitful application include relatively routine, smaller-scale structures for which kinematic soil-structure interaction effects such as base-slab averaging can be important (NIST 2012). We describe a novel procedure for producing a spatially variable ground motion field from a seed record and guidelines for decisions on the assumed correlation structure. The new simulation methodology produces 2D fields of simulated ground motions that are consistent with a seed record and user-specified models for wave passage, incoherence, and amplitude variability. The incorporation of Fourier amplitude variability is a component of this work that is particularly novel.

The simulation methodology, presented by Ancheta and Stewart (2015), extends and replaces the methodology proposed by Abrahamson (1993). The proposed methodology incorporates a normally distributed random phase as proposed by Ancheta *et al.* (2011). Additionally, using newly proposed Constant

OverLap Addition (COLA) windows attempts to preserve both a Nyquist condition (zero weighting of neighboring frequencies) in the frequency domain and a unity weighting in the time domain during recombination of short time windows. This step is critical for reducing severe leakage (over utilization) of high frequency random components when including Fourier amplitude variations. Finally, use of the Fourier Integral Method in generating correlated random fields reduces computation time for large/dense 2D grids over the Cholesky decomposition methodology.

The approach is applied to a subset of locations from the San Andreas ShakeOut scenario event. The simulations are first tested for adherence to the spatial variability target functions and if deficient are modified by the routine.

---

## Past and Future Seismic Moment Release: Contributions from Statistics and Geodesy

Oral Session · Wednesday · 8:30 AM · 20 April · Tuscany 5/6

Session Chairs: Corné Kreemer and Ilya Zaliapin

---

### Assessing the Sensitivity of Statistical Tests on Earthquake Catalogs

DAUB, E. G., University of Memphis, Memphis, TN, USA, [egdaub@memphis.edu](mailto:egdaub@memphis.edu); TRUGMAN, D. T., Scripps Institution of Oceanography, La Jolla, CA, USA; JOHNSON, P. A., Los Alamos National Laboratory, Los Alamos, NM, USA

We study the ability of statistical tests to identify nonrandom features of earthquake catalogs. We construct synthetic datasets containing varying strengths of clustering, with each dataset containing on average 10000 events over 100 years with magnitudes above  $M=6$ . We apply a suite of statistical tests to each synthetic realization in order to evaluate the ability of each test to identify the sequences of events as nonrandom. Our results show that detection ability is dependent on the quantity of data, the nature of the type of clustering, and the specific signal used in the statistical test. Datasets that exhibit a stronger variation in the seismicity rate are generally easier to identify as nonrandom for a given background rate. We also show that we can address this problem in a Bayesian framework, with the clustered datasets as prior distributions. Using this new Bayesian approach, we can quantitatively bound the range of possible clustering strengths that are consistent with a given earthquake catalog. We show how this approach can be applied to the global earthquake catalog since 1900, as well as a regional catalog by examining seismicity in the New Madrid Seismic Zone.

### Earthquake Forecasts based on Seismological, Geological, and Geodetic Information

JACKSON, D. D., UCLA, Los Angeles, CA, USA, [djackson@ucla.edu](mailto:djackson@ucla.edu)

Most earthquake forecasts employ some combination of the three information sources, nearly always relying on the principle of moment rate balance. Seismic moment rate for a specified region is the integral of the magnitude-frequency relationship times the seismic moment as a function of magnitude. The moment-magnitude relationship is well known, and in principle the magnitude-frequency distribution can be observed directly, but the observation period is always too short and may be abnormal. Thus inferring the seismic moment rate from some combination of the geologic and geodetic moment rates could provide valuable independent information. Geologic moment rate for a fault is approximately product of the slip rate times the fault surface area, the effective coupling over that area, and the rigidity of the rock surrounding the fault. The geodetic moment rate over an area is approximately the integrated strain rate over the area times an effective locking depth, proportion of elastic to total stress accumulation, and average rigidity. Assuming that accumulating tectonic moment (geologic or geodetic) is released over the long term by earthquakes, then all three moment rates should be equal over that long term. But serious questions remain. How long is "long term"? If the present seismic observation period is abnormal, should the forecast period be assumed normal? How can we infer the magnitude-frequency distribution, especially for really large earthquakes? Do all three moment rates depend on the same average of rigidity of the relevant rocks? Are the data precise enough to equate the three moment rates, even if all the other questions are answered? In this presentation I discuss the implications of the open questions and address the uncertainties in the moment-rate calculations. The ultimate question remains: how can we best estimate the future earthquake rate from available data?

### On the Uncertainty of the Seismic to Geodetic Moment Rate Ratio

KREEMER, C., University of Nevada, Reno, NV, USA, [kreemer@unr.edu](mailto:kreemer@unr.edu); ZALIAPIN, I., University of Nevada, Reno, NV, USA, [zal@unr.edu](mailto:zal@unr.edu)

Geodetic measurements of crustal deformation are often used to investigate how much of the deformation is expected to be released seismically by quantifying the ratio of observed seismic moment to geodetic moment rate:  $M_s/M_g=R$ . This ratio is typically interpreted as a measure of the physical coupling on fault(s) and/or as aseismic volumetric deformation, but could also indicate that faults are not oriented at 45 degrees from the principal strain axes; an implicit assumption in the strain-to- $M_g$  conversion. Here, we focus on two, typically ignored, error sources in the observed  $M_g$ , and thus  $R$ : 1) the natural variability of a heavy-tailed statistical distribution of  $M_s$ , and 2) the fluctuating number  $N$  of events in a given space-time volume. Our key modeling tool is the distribution of total moment  $M(N)$  released by a given number  $N$  of events with a common moment distribution. Over infinite time, and thus for infinitely large  $N$ , the observed and expected  $M_s$  converge as required by the Central Limit Theorem. For actual observation spans, the observed moment is typically much smaller than the expected moment for small  $N$ , and the observed moment fluctuates widely around the expected value for intermediate values of  $N$ . So one is typically expected to find a large discrepancy between  $M_s$  and  $M_g$ , with the observed  $R$  often (much) smaller than its limiting value for large  $N$  is. We use the latest geodetic Global Strain Rate Model to present a comprehensive analysis of moment release in space-time volumes of varying size, taking into account the randomness of the observed number  $N$  of events. We show that the discrepancies between  $M_s$  and  $M_g$  are well described by the tapered heavy-tailed modeling approach and suggest specific formulas for the uncertainty in the observed  $M_s$  for given space-time-intensity parameters. We emphasize that the uncertainty is mainly affected by the fluctuations of random moment.

### Complete Seismic Release of Tectonic Strain and Earthquake Recurrence in the Apennines (Italy)

D'AGOSTINO, N., Centro Nazionale Terremoti—Ist. Naz. Geof. Vulc., Roma, Italy

Here I compare estimates of tectonic strain rates from dense Global Positioning System measurements with the seismicity released in the last ~500 years in the Apennines (Italy). The rates of seismic moment accumulation from geodesy and of historical seismic release by earthquakes agree within the uncertainties, ruling out significant aseismic deformation. Within the considered 400 km long section of the Apennines, this balance yields an average recurrence interval of 30–75 years for  $M_w \geq 6.5$  events without requiring a future earthquake larger than those observed historically ( $M_w \sim 7$ ). A minimum estimate of unreleased strain allows  $M_w \geq 6.5$  and  $M_w \geq 6.9$  events to be released in ~35% and ~10% of the central-southern Apennines, respectively. The definition of the seismic potential for smaller events is more uncertain, and their occurrence remains a significant threat throughout the Apennines.

### A Discussion of the Earthquake Risk at The Geysers Geothermal Area, California, Based on Strain Rates and Seismic Moment Rates

TURCOTTE, D. L., University of California, Davis, Davis, CA USA, [dturcotte@ucdavis.edu](mailto:dturcotte@ucdavis.edu); HAWKINS, A., University of California, Davis, Davis, CA USA, [akhawkins@ucdavis.edu](mailto:akhawkins@ucdavis.edu); YIKILMAZ, M. B., University of California, Davis, Davis, CA USA, [mbyikilmaz@ucdavis.edu](mailto:mbyikilmaz@ucdavis.edu); KELLOGG, L. H., University of California, Davis, Davis, CA USA, [kelllogg@ucdavis.edu](mailto:kelllogg@ucdavis.edu); RUNDLE, J. B., University of California, Davis, Davis, CA USA, [rundle@ucdavis.edu](mailto:rundle@ucdavis.edu)

Large quantities of water are injected to enhance production at The Geysers geothermal area, California. This injection has resulted in a high level of induced seismicity with a well defined  $b$ -value and an annual rate that is nearly constant over the last 10 years. High quality GPS data show that the broad region in which the Geysers is located has suffered a near uniform shear strain over this period. This region extends from the rigid Pacific plate to the rigid Sierra Nevada plate. We balance this strain accumulation against the strain drop in the seismicity at The Geysers and find a maximum required earthquake with a magnitude of 4.75. This is consistent with the occurrence of earthquakes in the region and the absence of large faults in the region. In the broader zone the strain drop is dominated by large magnitude 6 to 8 earthquakes on the four major fault systems: San Andreas, Maacama-Rodgers Creek, West Napa, and Bartlett Springs-Green Valley. As a result the background seismicity is much lower than in The Geysers region. It should be noted, however, that the Maacama fault is only about 10 km from the Geysers geothermal area.



### Comparison of Geodetic and Geological/Seismological Moment Rates for the Wasatch Front Region, Utah

PECHMANN, J. C., University of Utah, Salt Lake City, UT, pechmann@seis.utah.edu; ZENG, Y., U.S. Geological Survey, Golden, CO, USA, zeng@usgs.gov; THOMAS, P. A., AECOM, Oakland, CA, USA, patricia.thomas@aecom.com; PETERSEN, M. D., U.S. Geological Survey, Golden, CO, USA, mpetersen@usgs.gov

As a test of the Working Group on Utah Earthquake Probabilities (WGUEP) source model for the Wasatch Front (WF) region of Utah, we compared geological/seismological moment rates calculated from this model with “geodetic moment rates” calculated from crustal deformation measurements. The geodetic moment rates were calculated from Kostrov’s (1974) equation using two reasonable simplifying assumptions: (1) the strain rate field is dominantly uniaxial extension and (2) seismic moment release occurs primarily in normal-faulting earthquakes on faults that dip  $50^\circ \pm 15^\circ$  in the direction of extension, which is ~E-W. This approach essentially assumes a two-dimensional strain accumulation model in which the seismogenic layer is extended at a rate equal to the long-term and large-scale permanent rate of extension caused by earthquakes.

The results show that the geodetic moment rates agree with geological/seismological moment rates calculated from the WGUEP model, within the uncertainty limits, for the WF region as a whole and for three of four subregions that we defined. In the fourth and southernmost subregion, which includes the Levan and Fayette segments of the Wasatch fault, the geodetic moment rate is five times larger than the geological/seismological moment rate with no overlap in the 90% confidence limits. This discrepancy exists because the strain rate in this subregion is similar to the strain rate in the three subregions to the north but the geological moment rate predicted for known faults in the subregion area is much lower. The unexplained geodetic moment rate is so large that it is unlikely that all of it can be explained by missing faults and/or underestimated earthquake rates on known faults in the WGUEP source model. If such factors are responsible for part of the unexplained geodetic moment rate, then the WGUEP forecast would underestimate earthquake probabilities in the southernmost WF region and, to a much smaller extent, in the WF region as a whole.

### Long-Term and Short-Term Seismicity Rates in Cascadia: Gutenberg-Richter instead of Characteristic

BROCHER, T. M., U.S. Geological Survey, Menlo Park, CA, USA, brocher@usgs.gov

Both longer- and shorter-term seismicity rates suggest that earthquakes in the Cascadia subduction system follow a Gutenberg-Richter distribution, in which M8.5 to M9 earthquakes occur at a rate predicted by smaller earthquakes, rather than a characteristic distribution. Cumulative plots of felt earthquakes in the fore-arc, arc, and back-arc of Oregon, Washington, and SW British Columbia, having maximum Modified Mercalli Intensities (MMI) ranging from IV to VIII, define constant seismicity rates going back to 1902. Seismicity rates of felt earthquakes having MMI between I and III were estimated from Did You Feel It? reports going back to 2008. I used 935 felt earthquakes having instrumentally determined magnitudes and depths to estimate the magnitudes of older felt earthquakes lacking instrumental magnitudes and depths. For these felt earthquakes the conversion to magnitude using this empirical relationship reveals a log-linear frequency-magnitude distribution for earthquake magnitudes between 2.3 and 6.8. A similar log-linear distribution is determined for declustered instrumentally recorded seismicity since 1970. These empirical log-linear relationships predict a M8.5 earthquake every 247 to 329 years, matching the 245-year average recurrence interval inferred from turbidite paleoseismology at the southern end of the Cascadia subduction zone, as well as a M9 earthquake every 505 to 700 years, bracketing the observed average recurrence interval of 500 to 600 years inferred from paleoseismology for great Cascadia subduction zone earthquakes. The agreement of these predictions with observed recurrence rates implies that in Cascadia earthquakes along the megathrust as well as in the overriding crust and the descending slab follow a single Gutenberg-Richter distribution rather than a characteristic distribution. The low b-value of the log-linear relationship, 0.62 to 0.65, is consistent with that observed at other locked subduction zones.

### Earthquakes in the Clockwork Earth

RUNDLE, J. B., University of California, Davis, CA USA, jbrundle@ucdavis.edu; DONNELLAN, A., Jet Propulsion Laboratory, Pasadena, CA USA, andrea.donnellan@jpl.nasa.gov; GRANT LUDWIG, L., University of California, Irvine, CA, USA, lgrant@uci.edu; TURCOTTE, D. L., University of California, Davis, CA, USA, dltruncotte@ucdavis.edu

The idea of an earthquake cycle has been discussed for many years. The cycle consists of the occurrence of a large earthquake, followed by aftershocks, then

a period of relative quiescence, followed by the next large earthquake. When this idea is applied to an individual fault, the model is generally called the “characteristic earthquake” model. In recent years, following the zenith of this idea just before the 2004 Parkfield earthquake, the concept seems to have fallen into relative disfavor. The opposing idea has been the Gutenberg-Richter magnitude frequency relation, that an individual fault might exhibit a scaling distribution of earthquakes, with no clear earthquake cycle evident. At the moment, it is not so clear which idea is preferred. In this talk, we discuss a hybrid of these ideas, in which we focus not on defined faults, but on defined seismically active areas for defined large earthquake magnitudes. The areas and magnitudes considered are selected so that there are several tens of large earthquakes during the time period considered. Thus there are several tens of earthquake cycles in the geographic region. Examining instrumental catalog data, we observe that a time-dependent Gutenberg-Richter distribution can be defined for the smaller earthquakes. These time-dependent characteristics suggest that we can define an “earthquake clock” for the defined region and defined large earthquake magnitude. The “clock” provides information as to the state of the region within the current large earthquake regional cycle. With additional assumptions, this “clock” can be used to project the probable calendar time of the next large earthquake in the region.

### Supercycles and Synchronization Signatures in Synthetic Seismic Sequences

MILNER, K. R., University of Southern California, Los Angeles, CA, USA, kmilner@usc.edu; JORDAN, T. H., University of Southern California, Los Angeles, CA, USA, tjordan@usc.edu

Synchronization is a key concept in nonlinear dynamics. Owing to the paucity and uncertainty of paleoseismic data, we can’t say much about the synchronization of large earthquakes in complex fault systems such as the San Andreas, but we know that substantial elastic strain has accumulated in the southern part of this system since its last major earthquake in 1857. One question is whether the distribution of long open intervals is consistent with the recently published Third Uniform California Earthquake Rupture Forecast (UCERF3, Field *et al.*, 2015), which assumes that time-dependent event probabilities can be modeled by Reid renewal processes correlated across faults only by co-rupture. In a UCERF3 world, the probability of observing an open-interval distribution as extreme as the present day would be low, less than 1% according to one estimate (Jackson, 2015). An alternate hypothesis is that we are in a period of low overall energy release; *i.e.*, near the minimum of a “seismic supercycle.” UCERF3 does not explicitly model supercycles, but they emerge from long runs of physics-based rupture simulators, such as the RSQSim model of Dieterich & Richards-Dinger (2010) and the ALLCAL model of Ward (2008). In these models, the synchronization of large events on different fault sections leads to variations in seismic energy release of  $\pm 50\%$  on time scales of about 200 years. Spectral analysis of a million-year RSQSim catalog shows synchronization harmonics with a fundamental period of 200 years and a corresponding depletion at longer event periods. This synchronization signature is absent in UCERF3 and randomized versions of the RSQSim catalog. We further investigate synchronization and its time dependence using two-dimensional “recurrence plots” (Eckmann *et al.*, 1987) to map the temporal recurrence of proximate RSQSim states. We use the results to speculate on the hazard implications of the supercycle hypothesis.

### How Detailed Should Earthquake Hazard Maps Be: Comparing the Performance of Japan’s Maps to Uniform, Randomized, and Smoothed Maps

BROOKS, E. M., Northwestern University, Evanston, IL, USA, eddie@earth.northwestern.edu; STEIN, S., Northwestern University, Evanston, IL, USA, seth@earth.northwestern.edu; SPENCER, B. D., Northwestern University, Evanston, IL, USA, bspencer@northwestern.edu; LIU, M., University of Missouri, Columbia, MO, USA, lium@missouri.edu

Earthquake hazard maps forecast future shaking via assumptions about where, when, and how large future earthquakes will be. These assumptions involve the known earthquake history, models of fault geometry and motion, and geodetic data. Maps are made more detailed as additional data and more complicated models become available. However, the extent to which this process produces better forecasts of shaking is unknown. We explore this issue by comparing how well a 510-year-long record of earthquake shaking in Japan is described by the Japanese national hazard (JNH) maps, uniform maps, and randomized maps. Surprisingly, as measured by the metric implicit in the JNH maps, *i.e.* that during the chosen time interval the predicted shaking should be exceeded only at a specific fraction of the sites, both uniform and randomized maps do better than the actual maps. However, using as a metric the squared misfit between maximum observed shaking and that predicted, the JNH maps do better than uniform or randomized maps. Similarly, by the squared misfit metric, map performance improves up to a ~75-150 km smoothing window, and then decreases with further smoothing. Because the maps were made by using other data and models to try to predict

future earthquake shaking, rather than by fitting past shaking data, these results are probably not an artifact of hindcasting rather than forecasting. They suggest that hazard models and the resulting maps can be over-parameterized, in that including too high a level of detail to describe past earthquakes may lower the maps' ability to forecast what will occur in the future. For example in Nepal, where GPS data show no significant variation in coupling between areas that have had recent large earthquakes and those that have not, past earthquakes likely do not show which parts are more at risk, and the entire area can be regarded as equally hazardous.

---

## Theoretical and Methodological Innovations for 3D/4D Seismic Imaging of Near-Surface, Crustal, and Global Scales

Oral Session · Wednesday · 2:15 PM · 20 April · Tuscany 5/6  
Session Chairs: Marco Pilz and Nori Nakata

---

### Direct Methods and High Performance Computing for Seismic Tomography

**BOGIATZIS, P.**, Dept. of Earth and Planetary Sciences, Harvard University, Cambridge, MA, USA, petrosbogatizis@fas.harvard.edu; **ISHII, M.**, Dept. of Earth and Planetary Sciences, Harvard University, Cambridge, MA, USA, ishii@eps.harvard.edu; **DAVIS, T. A.**, Texas A&M University, College Station, TX, USA, davis@tamu.edu

The deployments of dense seismic networks in recent years provide sufficient data to substantially increase the spatial resolution of the tomographic models. This higher resolving power is achieved by refining the discretization of the model space that consists typically of  $10^5$ - $10^6$  unknown parameters. Combined with comparable numbers of observations, direct computational methods, such as the singular value decomposition, become prohibitively expensive in terms of memory and computational time. Iterative solvers, such as LSQR method, provide a fast and computationally cheap alternative for solving such massive inverse problems. Among the disadvantages of the iterative algorithms is that the inverse of the matrix that defines the system is not explicitly formed. As a consequence, the posterior model resolution and covariance matrices, which provide quantitative assessment of the uncertainty of the tomographic models, cannot be computed. Despite efforts in finding computationally affordable approximations of these matrices, challenges remain, and unreliable approaches such as the checkerboard resolution tests continue to be used. In this presentation, we show that graph partitioning methods and recent developments in sparse algorithms are beginning to make the direct methods feasible for large seismic tomography problems. We demonstrate our approach in a regional tomography problem. Furthermore, we show that structural analysis of the tomographic forward operators, based upon graph theory methods, can provide insights into the inverse problem and be used to increase the efficiency of the solution.

### Moho Depth and Structure of the Crust and Upper Mantle Beneath Southern Alaska from Dix Inversion of Rayleigh-Wave Phase Velocity Maps

**HANEY, M. M.**, Alaska Volcano Observatory/USGS, Anchorage, AK, USA, mhaney@usgs.gov; **TSAI, V. C.**, California Institute of Technology, Seismological Laboratory, Pasadena, CA, USA, tsai@caltech.edu; **WARD, K. M.**, University of Arizona, Department of Geoscience, Tucson, AZ, USA, wardk@email.arizona.edu

The inversion of surface-wave dispersion curves for a shear-wave velocity depth profile is a classic geophysical inverse problem. Recently, Haney and Tsai (2015; Geophysics) developed a new approach to this problem based on assumptions that are similar to those used in the formulation of the Dix equation in reflection seismology. In contrast to conventional surface-wave inversion, the Dix-type relation for surface waves does not require an initial model and solves directly for shear-wave velocity, not a perturbation in shear-wave velocity. Haney and Tsai (2015) demonstrated the method for both under- and over-parameterized cases and used under-parameterization to solve for Moho depth and crustal and mantle shear-wave velocity across the Western US from only three phase velocity maps.

Here we extend the under-parameterized method presented in Haney and Tsai (2015) to the over-determined case when more than three phase velocity maps are available. We apply the technique to phase velocity maps of Southern Alaska measured at 13 periods between 8 and 50 s and use the result as an initial model for subsequent nonlinear inversion. This is the first widespread Moho map beneath Southern Alaska derived from seismic waves. We find that Moho depth is generally correlated with topography, with thicker crust beneath mountain ranges (Alaska Range, Talkeetna, Kenai, and Wrangell Mountains). North of the Denali Fault, the Moho is smoother and located at typical depths of 30-35 km.

The crust thickens to the north of Hayes Volcano, the portion of the Aleutian Arc known as the Denali Volcanic Gap. There are also indications that the "Moho" or waveguide surface we solve for beneath Prince William Sound is actually the subducting slab. The slab structure extends further east than the Pacific slab represented in the Slab1.0 model.

### Towards Full Waveform Inversion at the Fault Zone Scale: Moment Tensor Inversion, Waveform Modeling, and Initial Velocity Model Selection

**ALLAM, A. A.**, University of Utah, Salt Lake City, UT, USA, amir.allam@utah.edu; **TAPE, C.**, University of Alaska Fairbanks, Fairbanks, AK, USA, ctape@alaska.edu; **BEN-ZION, Y.**, University of Southern California, Los Angeles, CA, USA, benzion@usc.edu

Fault zones are complicated structures featuring vertical and semi-vertical interfaces, fault-parallel zones of low seismic velocity which narrow with depth, and lateral heterogeneity at all observable scales. The goal of the present work is to develop and implement a framework for full waveform tomographic inversion which accounts for this strong multi-scale 3D heterogeneity. We examine the San Jacinto Fault Zone, a right-lateral plate boundary fault system which contains multiple segments with vastly different structural properties. We first produce moment tensor solutions by applying the CAP method (Zhu & Helmberger, 1996) to 26 events from a catalog of relocated seismicity (Hauksson *et al.*, 2012). We then simulate these events in several different seismic velocity models using SPECFEM3D (Komatitsch & Tromp, 1999). To quantify model performance, we measure the frequency-dependent misfit between synthetic and data seismograms in terms of phase and amplitude by measuring cross-correlation delay time and correlation coefficient of the time-shifted traces. The compared models were created with a variety of methods, including double-difference tomography (Allam *et al.*, 2014), ambient noise (Zigone *et al.*, 2014), the SCEC community velocity model CVMH (Shaw *et al.*, 2015), regional adjoint tomography, and joint inversion of body waves and ambient noise (Fang *et al.*, 2016). The jointly-inverted model performs best, with agreement between synthetic and data at about 1Hz frequency across the Southern California plate boundary region, and up to 3Hz in specific near-fault regions. The wavelengths of these data can be less than 1km, and thus contain information about fault zone structure at scales relevant to earthquake mechanics. With highly accurate moment tensors, an effective starting model, and frequency-dependent measurements of misfit between data and synthetic now in hand, the next step is to perform the first inversion iteration to produce an updated velocity model.

### Evaluations of the effects of the basin edge in H/V spectral ratios of microtremors based on diffuse field interpretation

**FUKUOKA, Y.**, Kyoto University, Kyoto/Japan, myris.6.y@gmail.com; **MATSUSHIMA, S.**, Kyoto University, Kyoto/Japan, matsushima@zeisei.dpri.kyoto-u.ac.jp; **KAWASE, H.**, Kyoto University, Kyoto/Japan, kawase@zeisei.dpri.kyoto-u.ac.jp; **ANDERSON, J. G.**, University of Nevada, Reno, Reno/NV/USA, jga@unr.edu; **LOYD, T. W.**, University of Nevada, Reno, travisw@optimds.com

Based on diffuse field theory, the Horizontal-to-Vertical (H/V) spectral ratios of microtremors (MHVR) should equal the Green's functions response at the point of harmonic loading for flat layers and for 2-D and 3-D basin structures. Green's functions calculated with a 3-D spectral element method on the surface of a 2-D basin structure qualitatively predict the observed directional dependency in MHVR (Matsushima *et al.*, BSSA, 2014) for the two horizontal components at the Uji campus of Kyoto University, where the NS/UD has higher peak amplitude while the EW/UD has higher peak frequency. Also, the shapes of the MHVR are distorted at sites very close to the basin edge. This indicates that it might also be possible to identify the conditions of the lateral heterogeneity close to the basin edge in detail if we observe microtremors at several sites close to the assumed basin edge.

In this study, we observed microtremors in Uji, Kyoto, Japan and Reno, Nevada, USA. In Uji, the basin is on the footwall of a reverse fault, while in Reno it is on the hanging wall of a normal fault. In both locations, NS is the fault-parallel and EW is the fault normal direction. We focus on the relationship between the basin edge shape and the difference between NS/UD and EW/UD in the observed MHVR. At Uji, as noted, the condition of the lateral heterogeneity close to the basin edge changes the characteristics of the MHVRs. Peaks in HVSR change to higher frequency and the amplitude of the peaks decreases as the site gets closer to the basin edge. This can be modeled with a flat-layered velocity structure, with decreasing layer thicknesses, but the amplitudes and directional dependence of theoretical MHVRs do not match the observations. We are comparing the MHVRs of observed microtremors in Reno to the results in Uji, and will try to identify directional effects and the basin edge shape based on MHVRs there.



## Shallow Crustal Discontinuities Inferred from Waveforms of Microearthquakes: Method and Application to KTB Drill Site and West Bohemia Swarm Area

HRUBCOVA, P., Institute of Geophysics, Prague, Czech Republic, pavla@ig.cas.cz; VAVRYCUK, V., Institute of Geophysics, Prague, Czech Republic, vv@ig.cas.cz; BOUSKOVA, A., Institute of Geophysics, Prague, Czech Republic, ab@ig.cas.cz; BOHNHOFF, M., GeoForschungsZentrum Potsdam, Potsdam, Germany, bohnhoff@gfz-potsdam.de

The waveforms of microearthquakes are of high frequency and complicated. They contain many phases secondarily generated at crustal interfaces and at small-scale inhomogeneities. They are highly sensitive to focal mechanisms and thus very different for each station of local networks. However, with a large number of microearthquakes, the scattered waves present in the waveforms can serve for identifying the prominent crustal discontinuities and for determining their depth.

We develop a new approach for extracting information on crustal structure from such waveforms and apply it for determining depth and lateral variations of crustal discontinuities. We show that strong dependence of microseismic waveforms on radiation pattern requires good station coverage and knowledge of focal mechanisms of the microearthquakes. Analysis of real observations is supported by waveform modeling and by analysis of radiation patterns of scattered waves. The robustness of the inversion for depth of crustal interfaces is achieved by stacking of a large number of waveforms and by applying a grid search algorithm. The method is demonstrated on two microseismic datasets of different origin: microseismicity induced during the KTB 2000 fluid injection experiment and natural seismicity in the West Bohemia swarm region. High-frequency conversions at the KTB site indicate a prominent interface at depths of 2.3–4.1 km consistent with previous interpretations. Geologically, it may represent the contact of granitoids with much faster metabasites underneath. Seismicity in West Bohemia indicates a strong-contrast interface at depths of 3.5–6.0 km. This interface is in agreement with previous profiling and might be related to trapping of fluid emanations ascending from the mantle.

## Using Microquakes to Illuminate the Subsurface

MATZEL, E. M., Lawrence Livermore National Laboratory, Livermore, CA, USA, matzel1@llnl.gov; MORENCY, C. E., Lawrence Livermore National Laboratory, Livermore, CA, USA, morency1@llnl.gov; RHODE, A., University of Texas at Dallas, Dallas, TX, USA, axr116630@utdallas.edu; PYLE, M. L., Lawrence Livermore National Laboratory, Livermore, CA, USA, pyle4@llnl.gov; TEMPLETON, D. C., Lawrence Livermore National Laboratory, Livermore, CA, USA, templeton4@llnl.gov

Microseismicity provides a direct means of measuring the physical characteristics of active tectonic features such as fault zones. Thousands of microquakes are often associated with an active site. This cloud of microseismicity helps define the tectonically active region. When processed using novel geophysical techniques, we can isolate the energy sensitive to the faulting region, itself.

The virtual seismometer method (VSM) is a technique of seismic interferometry that provides precise estimates of the GF between earthquakes. In many ways the converse of ambient noise correlation, it is very sensitive to the source parameters (location, mechanism and magnitude) and to the Earth structure in the source region. In a region with 1000 microseisms, we can calculate roughly 500,000 waveforms sampling the active zone. At the same time, VSM collapses the computation domain down to the size of the cloud of microseismicity, often by 2–3 orders of magnitude.

Using data from the Salton Sea geothermal region, we demonstrate the power of the technique, illustrating our ability to scale the technique from the far-field, where sources are well separated, to the near field where their locations fall within each other's uncertainty ellipse. VSM provides better illumination of the complex subsurface by generating precise, high frequency estimates of the GF and resolution of seismic properties between every pair of events.

## Improvements in Earthquake Location from Joint Inversion of Seismic and Gravity Observations—Application to the Iran Region

MACEIRA, M., Los Alamos National Laboratory, Los Alamos, NM, USA, mmaceira@lanl.gov; SYRACUSE, E. M., Los Alamos National Laboratory, Los Alamos, NM, USA, syracuse@lanl.gov; BERGMAN, E., Global Seismological Services, Golden, CO, USA, bergman@seismo.com; PHILLIPS, W. S., Los Alamos National Laboratory, Los Alamos, NM, USA, wsp@lanl.gov; BEGNAUD, M., Los Alamos National Laboratory, Los Alamos, NM, USA, mbegnaud@lanl.gov; NIPPRESS, S., AWE Blacknest, Reading, UK, stuart@blacknest.gov.uk; ZHANG, H., USTC, Hefei, China, zhang11@ustc.edu.cn

We present a 3D  $V_p$  and  $V_s$  model of Iran generated using a simultaneous joint inversion of body wave travel times, Rayleigh wave dispersion curves, and high-

wavenumber filtered Bouguer gravity observations. The body wave dataset is mainly derived from previous work on location calibration and includes the first-arrival P and S phases of almost 3500 earthquakes whose initial locations qualify as GT50 or better. The surface wave dataset consists of Rayleigh wave group velocity measurements for regional earthquakes, which are inverted for a suite of period-dependent Rayleigh wave velocity maps prior to inclusion in the joint inversion for body wave velocities. We use gravity anomalies derived from the global gravity model EGM2008. To avoid mapping broad, possibly dynamic features in the gravity field into variations in density and body wave velocity, we apply a high-pass wavenumber filter to the gravity measurements. We use a simple, approximate relationship between density and velocity so that the three datasets may be combined in a single inversion.

The final optimized 3D  $V_p$  and  $V_s$  model allows us to explore how multi-parameter tomography addresses crustal heterogeneities in areas of limited coverage and improves travel time predictions. We compare earthquake locations from our models to independent locations obtained from InSAR analysis to assess the improvement in locations derived in a joint-inversion model in comparison to those derived in a more traditional body-wave-only velocity model.

## Active Source Joint Inversion of Travel Time with Gravity for 3D $V_p$ and Density Tomography and Seismic Reflection Imaging of the Irish Hills, California, Using Active Seismic, Gravity, and Magnetic Data

O'CONNELL, D. R. H., Fugro Consultants, Inc., Denver, CO, USA, d.oconnell@fugro.com; TURNER, J. P., Fugro Consultants, Inc., Denver, CO, USA, j.turner@fugro.com; NISHENKO, S., Pacific Gas & Electric Company, San Francisco, CA, USA, SPN3@pge.com; STANKOVIC, G., Agile Seismic, Houston, TX, USA, goran.stankovic@agileseismic.com

Four 64,000 lb. Vibroseis sources were deployed with >5,000 receivers across the Irish Hills and two 17,000 lb. EnviroVibes with 2,500 receivers in and near the Diablo Canyon Power Plant (DCPP) and southeast of DCPP for 2.5 km along a marine terrace to image possible onshore splays of the San Luis Bay fault. The USGS acquired new densely-spaced gravity measurements along transects across the Irish Hills. Travel time data were jointly inverted with gravity to build 60-m cells of 3D P-wave velocity ( $V_p$ ) and density ( $\rho$ ) to ~3 km depth. True amplitude 3D prestack depth migration tomography shows that the Pismo syncline is centered above steeply-dipping faults bounding a deeper asymmetric narrow graben that is 1–1.5 km wide at 3 km depth. Above the inner graben below the Pismo syncline and extending north below Franciscan rocks is a high-velocity layer and underlying low-velocity zone that persists over 5 km in the dip direction and extends 7.5 km along strike. Strong reflectivity is confined to Tertiary sediments and portions of the Franciscan assemblage above this persistent low-velocity zone at 1.5–2 km depth. The shortest wavelength folding occurs above the high-velocity layer within the Pismo Syncline and in an area extending north into shallow sections of Franciscan assemblage containing the surface exposures of the Los Osos fault. 3D traveltimes tomography with >18,000,000 first arrivals and 0.61 m vertical and 3.28 m horizontal cell dimensions combined with 3D prestack depth migration reflectivity were used to delineate the buried bedrock surface below the marine terrace southeast of DCPP. A splay of the San Luis Bay fault system cutting obliquely across the marine terrace was imaged in 3D depth. The fault splays were imaged as lineaments in the buried bedrock surface, as a near-vertical set of closely spaced generally right-stepping faults in the subsurface 3D depth seismic images, and as a tilt-angle magnetic anomaly.

## Rayleigh Wave Attenuation Along Linear Arrays Across the San Jacinto Fault Zone from Statistical Analysis of Noise Cross-correlations

LIU, X., University of Southern California, Los Angeles, CA, USA, liu409@usc.edu; BEN-ZION, Y., University of Southern California, Los Angeles, CA, USA, benzion@usc.edu; ZIGONE, D., Université de Strasbourg, EOST, CNRS, Strasbourg, France, zigone@usc.edu

We estimate frequency-dependent attenuation coefficients of Rayleigh waves ( $Q_R$ ) from cross-correlations of ambient seismic noise recorded by dense linear arrays across the San Jacinto fault in southern California. Based on the error of stacked cross-spectrum from finite amount of data (Liu *et al.*, 2016), the confidence interval of the cross-spectrum can be converted to phase and amplitude errors. These can be used to study the phase velocities and attenuation coefficients, which provide important structural information. We extend previous theoretical results (Liu *et al.*, 2015) on deriving attenuation based on data recorded by linear array of three stations (triplet) by computing frequency-dependent  $Q_R$  values over multiple frequency bands with sufficient Signal-Noise Ratio (SNR). The method assumes similar site conditions for the used triplet of stations within the narrow frequency band centered at each frequency. Phase velocity dispersion is a prerequisite for estimating attenuation  $Q_R$  values and is computed from the real part (time-symmetric component) of the stacked cross-spectra. The phase error associ-

ated with the stacked cross-spectrum is used for selecting phase velocity values with small confidence intervals. The confidence interval for attenuation  $Q_R$  value is estimated through error propagation based on amplitude error and validated using bootstrap resampling technique. Derived  $Q_R$  and velocity values at various locations will be presented in the meeting.

### High Attenuation Zones beneath Sierra Negra Volcano: Evidence for a Shallow Sill and Feeder System

RODD, R. L., University of North Carolina, Chapel Hill, NC, USA, rlrodd@live.unc.edu; LEES, J. M., University of North Carolina, Chapel Hill, NC, USA

Attenuation tomography of Sierra Negra Volcano suggests a sill-like body less than 3 km beneath the caldera and a larger magma storage zone at 3 to 10.5 km depth. This supports previous geodetic models that indicate a sill at 2 km depth responsible for the observed deformation, faulting, and eruptive behavior of Sierra Negra. The  $V_p$  model indicates a large low velocity body beneath Isabella Island, but the resolution is too coarse to image the sill-like body [Tepp *et al.*, JGR 2014]. To resolve such smaller-scale structures, the scope was limited to a 30 x 30 km grid around the caldera. The dataset consists of 309 earthquakes recorded on the SIGNET seismic array from July 2009 to June 2011.  $\tau^*$  spectral decay method for P-wave phases was used to highlight regions of low Q which suggest the presence of magma melt. Low Q extends from 0.5 to 10 km depth which makes distinguishing between the transition from the proposed sill body to a deeper magma storage difficult. The lowest Q is observed from 0.5 to 3 km concentrated directly beneath the caldera. Comparison of attenuation structure with the  $V_p$  model suggests the presence of a high temperature melt from 0.5 to 3 km interpreted as the sill. The attenuation observed from 3 to 10.5 km is lower than at shallower depths. We speculate that this low Q region is a magma accumulation that feeds the sill.

## Multidisciplinary Studies of Earthquakes—Slow, Fast, and In Between: A Broad Range of Fault Behavior in Space and Time

Oral Session · Wednesday · 8:30 AM · 20 April · Tuscany 7/8

Session Chair: Abhijit Ghosh

### Universality of Slow Earthquakes in the Very Low Frequency Band: Summary of Regional Studies

IDE, S., Dept. EPS, Univ. Tokyo, Tokyo, Japan, ide@eps.s.u-tokyo.ac.jp

We often find seismic signals in very low frequency (VLF) band (0.02-0.05 Hz), together with signals of tectonic tremors and slow slip events. These signals are useful to determine moment tensor (MT) solutions corresponding to underground deformation observed in this frequency range. After the development of the VLF-MT inversion method and first application in Nankai subduction zone (Ide and Yabe, 2014), we have applied the same method to tremor records in Taiwan (Ide *et al.*, 2015), Cascadia (Ide, 2016), and Guerrero (Maury *et al.*, 2016). In each region, we successfully determined moment tensor solutions reflecting local plate geometry and relative motions. Average seismic moment in each region increases with accompanying tremor energy and the recurrence interval of episodic activity. These results support the idea that VLF signals are not radiated from an isolated band-limited event, but a part of broadband signal from a slow earthquake, ranging from several Hz to hours or days. If there were no microseism and tidal oscillation, the real spectrum of broadband slow earthquake would be observable, and it would be similar to signals from Brownian slow earthquake model (Ide, 2008).

### Very Low Frequency Earthquakes (VLFs) in Cascadia NOT Coincident with Strong Tremor

GHOSH, A., University of California, Riverside, CA, USA, aghosh.earth@gmail.com; HUTCHISON, A., University of California, Riverside, CA, USA, ahut002@ucr.edu

Deep Very Low Frequency Earthquakes (VLFs) are typically found to be associated with slow earthquakes, and coincide with strong tremor activity in space and time [Ghosh *et al.*, 2015; Ito *et al.*, 2007]. They release majority of the seismic moment during an episodic tremor and slip (ETS) event [Ghosh *et al.*, 2015]. We detect and locate VLFs in Cascadia during 2014 ETS event under Washington and southern Vancouver Island using a grid-search moment tensor inversion method. We found that the VLFs generally migrate south to north roughly mimicking the tremor activity. But interestingly, majority of them occur

when tremor in VLF source locations are weak to non-existent as cataloged by the Pacific Northwest Seismic Network. In fact, the largest cluster of VLFs occurs after the major tremor swarm has ended. Moreover, most of the VLFs are located in and around an area that marks a tremor gap during this ETS. These observations provide important constraints on the interplay between different modes of seismic radiation during slow earthquakes and/or ETS events. These findings are inconsistent with the notion that tremor and VLFs may essentially be the same phenomenon reflected in different frequency band. It suggests that tremor and VLFs may have distinct sources, both associated with slow slip along the plate interface.

### Slow Active Intra-plate Faults: the Paleoseismology of the Rurrand Fault, Germany

REICHERTER, K. R., Inst. of Neotectonics and NatHaz, RWTH Aachen Univ., Aachen, Germany, k.reicherter@nug.rwth-aachen.de; GRÜTZNER, C., Department of Earth Sciences, University of Cambridge, Cambridge, UK, chg39@cam.ac.uk; FISCHER, P., Dept. of Geography, Univ. of Mainz, Mainz, Germany, P.Fischer@geo.uni-mainz.de

The European plate interiors are known to host earthquakes with magnitudes up to M7 or larger, especially in the formerly glaciated areas or close to the Alpine convergence zone. Their recurrence periods are long, because the slip rates of faults are usually less than 1 mm/yr and faults in stable continental interiors tend to break with large stress drops. The Lower Rhine Graben in Central Europe hosts a rift system that has very low deformation rates. The faults in Germany, Belgium and the Netherlands have slip rates of less than 0.1 mm/yr. Destructive earthquakes in this region are rare, but did occur in historic times. In 1755/56, a series of strong earthquakes caused significant destruction in the cities of Düren and Aachen (Germany). Paleoseismologic trenching has been carried to constrain slip rates and to reveal the earthquake history of the Rurrand Fault that has been suspected to be a candidate for the 1756 MW5.8 quake. Tectonic morphological analyses based on 1 m airborne LiDAR data and geophysical studies (GPR and ERT) were applied to trace the fault zone and to image the fault zone at depth, respectively. Our study shows that the Rurrand Fault currently accommodates deformation in earthquakes rather than by creeping. We found evidence for a surface rupturing earthquake in the Holocene, and we identified at least one more surface rupturing event. The coseismic offsets were less than 0.5 m per event. We assign maximum possible magnitudes of MW6.3 ± 0.4 for the Rurrand Fault and a slip rate of at least 0.03 ± 0.01 mm/yr for the last ~130 kyr. The surface ruptures did not occur at the main fault trace that has a clear morphological expression due to older tectonic motions, but on a younger fault strand in the hanging wall of the main fault. Our results indicate that the Düren 1755/56 earthquakes did not produce surface ruptures at the Rurrand Fault, either because they did not rupture the surface at all, or because they occurred at another, neighboring fault.

### Cascadia Seismogenic Zone Earthquake Detection and Location

MORTON, E. A., New Mexico Tech, Socorro, NM, USA, emorton@nmt.edu; BILEK, S. L., New Mexico Tech, Socorro, NM, USA, sbilek@nmt.edu; ROWE, C. A., Los Alamos National Laboratory, Los Alamos, NM, USA, char@lanl.gov

The Cascadia Subduction Zone (CSZ) produces regularly observed episodic tremor and slip (ETS) behavior and geologic evidence indicates past great earthquakes have occurred along the margin. With the absence of a historically observed great earthquake, small and moderate magnitude earthquakes are needed to infer fault zone conditions, but the CSZ is notable for its dearth of such events. The seismogenic zone appears to reside primarily offshore; therefore the paucity of observed small, interplate earthquakes may arise partly from the use of only on-land seismometers, far from the earthquake sources. The Cascadia Initiative (CI) community seismic experiment includes ocean bottom seismometers (OBS) deployed directly above the presumed locked seismogenic zone, in addition to land seismometers. We use the CI dataset to search for small magnitude interplate earthquakes previously undetected by the on-land sensors.

Within the first year of CI waveforms, we select a subset of M0.1-3.7 earthquakes from existing earthquake catalogs, whose preliminary locations and depths suggest that they occurred on the plate interface. We create templates to build a subspace detector by windowing waveforms around the arrival times for these events on CI OBS and land seismometers. Our initial efforts targeted a known cluster of repeating events off the coast of central Oregon, yielding 293 unique detections. Eighty-six are well located, most of which occur in the vicinity of the targeted cluster. Here we present detections and locations for the first year of CI deployment. Ongoing efforts will include continuing detection and location along the margin during CI deployment. Future plans include source parameter analysis of events along the margin for fault zone characterization.



### **Fortnightly Tidal Triggering of Low-frequency Earthquakes Constrains the Stress Budget of the Deep San Andreas Fault**

VAN DER ELST, N. J., USGS Earthquake Science Center, Pasadena, CA, USA, [nvanderelst@usgs.gov](mailto:nvanderelst@usgs.gov); DELOREY, A. A., Los Alamos National Lab, Los Alamos, NM, USA, [andrew.delorey@lanl.gov](mailto:andrew.delorey@lanl.gov); SHELLY, D. R., USGS Volcano Science Center, Menlo Park, CA, USA, [dshelly@usgs.gov](mailto:dshelly@usgs.gov); JOHNSON, P. A., Los Alamos National Lab, Los Alamos, NM, USA, [paj@lanl.gov](mailto:paj@lanl.gov)

Earth tides modulate tremor and low-frequency earthquakes (LFEs) on faults in the vicinity of the brittle-ductile transition. The response to the tidal stress carries otherwise inaccessible information about fault strength and rheology. Here we analyze the LFE response to the fortnightly tide, which modulates the amplitude of both shear and normal stress components of the daily tidal stress over a 14-day cycle. Analyzing the fault-tide interactions at a period that is long with respect to the duration of triggered LFEs provides a clearer picture of the triggering process than can be obtained by examining the daily tides alone. We find that LFE rate is highest during the rising fortnightly tide ( $-90^\circ$  tidal phase), when the daily stress exceeds the previous day's peak by the widest margin. Tidal triggering of LFEs is therefore at least partly a threshold-triggering phenomenon, and not exclusively a modulation of creep rate, which would predict a LFE-tide phase lag of  $0^\circ$ . Applying a simple threshold failure model, the fortnightly modulation constrains the stress drop per LFE (3-30 kPa) and the tectonic loading rate at depth (100-3500 Pa/day). Variations in loading rate are spatially coherent between LFE families, with smaller loading rate for LFE families located within the interiors of tremor-producing regions, and higher loading rate at the margins. This suggests either stress-shielding of the interior LFEs, or variations in the rate of truly aseismic creep in the bulk fault zone.

### **Prospecting for Stress Changes Driven by SSEs with the HOBITSS Ocean-bottom Array, Offshore New Zealand**

FRY, B., Institute of Geologic and Nuclear Sciences, Lower Hutt, New Zealand, [b.fry@gns.cri.nz](mailto:b.fry@gns.cri.nz); HENRYS, S., Institute of Geologic and Nuclear Sciences, Lower Hutt, New Zealand, [s.henrys@gns.cri.nz](mailto:s.henrys@gns.cri.nz); WALLACE, L., University of Texas, Austin, Texas, USA, [lwallace@utexas.edu](mailto:lwallace@utexas.edu); MOCHIZUKI, K., Earthquake Research Institute, University of Tokyo, Tokyo, Japan, [kimi@eri.u-tokyo.ac.jp](mailto:kimi@eri.u-tokyo.ac.jp); LEBEDEV, S., Dublin Institute for Advanced Studies, Dublin, Ireland, [sergei@cp.dias.ie](mailto:sergei@cp.dias.ie); SHEEHAN, A., University of Colorado, Boulder, CO, USA, [Anne.Sheehan@colorado.edu](mailto:Anne.Sheehan@colorado.edu); SCHWARTZ, S., University of California, Santa Cruz, Santa Cruz, CA, USA, [susan@es.ucsc.edu](mailto:susan@es.ucsc.edu); WEBB, S., LDEO, Columbia University, Palisades, NY, USA, [scw@ldeo.columbia.edu](mailto:scw@ldeo.columbia.edu)

The recent discovery of the shallowest, well-documented, slow-slip events (SSEs) on Earth prompted the HOBITSS offshore deployment of 15 ocean-bottom seismometers (OBS) near the northern Hikurangi subduction margin, offshore New Zealand's North Island. This OBS array was retrieved in June 2015, after capturing the second largest SSE ever observed in the area. The SSE potentially extends to the trench and its recordings by the HOBITSS OBS array represent one of the best seismic datasets of an SSE ever recorded. The SSE also occurs in a region that is known to host slow-rupture tsunami earthquakes. As such, the HOBITSS array is well-suited to test existing physical models of both tsunami earthquakes and SSEs. We exploit the relative proximity of the recorders to the subduction megathrust by examining the directional dependence of the ambient noise surface wave field with time-lapse techniques.

Shallow surface wave anisotropy is particularly sensitive to small-scale perturbations in stresses and represents a promising tool for monitoring changes in stress, including possible changes resulting from pore fluid pressurization driven by the SSE. We will present results of 1) inversion of ambient noise cross correlations for anisotropic structure, with critical examination of its time-dependence. We will also present 2) results of recent method advancement in analyzing energy in the off-diagonal elements of the  $3 \times 3$  correlation matrix (given by the 3 components of the seismograms at each of a pair of stations). We adapt the 'phase tensor' approach that is commonly used in analysis of magnetotelluric data to assess the amount of energy in the off-diagonals of the seismic correlation matrix. We do this on a day-by-day recording basis. This is a robust data-driven observable that we suggest is a proxy for rapidly monitoring stress changes during shallow SSEs.

### **Understanding the Size and Impact of Non-Volcanic Tremors in Parkfield: Deriving Tremor Energy Magnitudes and Exploring their Statistics**

STAUDENMAIER, N., SED ETH Zurich, Zurich, Switzerland, [nadine.staudenmaier@sed.ethz.ch](mailto:nadine.staudenmaier@sed.ethz.ch); EDWARDS, B., Liverpool University, Liverpool, Great Britain, [Ben.Edwards@liverpool.ac.uk](mailto:Ben.Edwards@liverpool.ac.uk); TORMANN, T., SED ETH

Zurich, Zurich, Switzerland, [thessa@sed.ethz.ch](mailto:thessa@sed.ethz.ch); WIEMER, S., SED ETH Zurich, Zurich, Switzerland, [stefan.wiemer@sed.ethz.ch](mailto:stefan.wiemer@sed.ethz.ch)

Non-volcanic tremors (NVTs) are observed in transition zones between freely slipping and locked sections of crustal faults and subduction zones, at depths below the seismogenic zone. Based on NVT recordings in the Parkfield region of the San Andreas Fault (SAF), Central California, we provide a novel approach to assess the energy release of these events and assign magnitudes ( $M_e$ ) that compare well with size estimates of small earthquakes in the same region and therefore provide new insights to energy release and physical behaviour of the lower crust south of Parkfield. The energy magnitude assessment of a detected tremor consists of a refined duration estimate and a subsequent spectral analysis, taking into account local attenuation parameters.

For the 218 NVTs that passed high record-quality requirements, we resolve  $M_e$  values in the range of  $-0.67$  to  $0.84$  and study their frequency-magnitude-distribution. We furthermore provide seismic moment and moment magnitude estimates and calculate stress drops in a range of 3-10kPa. To gain a better understanding of parameters influencing the derived energy magnitude, we investigate different relationships between  $M_e$  and other NVT parameters, showing that  $M_e$  seems to be strongly driven by stress drop. Both,  $M_e$  values and stress drops increase with depth and towards the southern end of the tremor cloud, which stretches beneath the locked section of the SAF.

### **UAVSAR Observation of Multi-Temporal Multi-Fault Behavior Associated with the 2010 M7.2 El Mayor-Cucapah Earthquake**

DONNELLAN, A., Jet Propulsion Laboratory, California Institute of Technology, Pasadena, CA, USA; PARKER, J. W., Jet Propulsion Laboratory, California Institute of Technology, Pasadena, CA, USA

The northern end of 2010 M7.2 El Mayor-Cucapah earthquake rupture and continued postseismic deformation was observed using NASA's Uninhabited Aerial Vehicle Synthetic Aperture Radar (UAVSAR) platform. The coseismic interferogram from a pair of images collected 6 months before and one week following the earthquake shows an overprint of broad deformation in the Salton Trough, just north of the US-Mexico border that is consistent with the mainshock rupture. Additional slip was observed on a network of right- and left-lateral conjugate faults branching toward the Elsinore, Superstition Hills, and San Andreas faults. The major faults showing shallow triggered slip from the earthquake were the Yuba, Imperial, Superstition Hills, and East Elmore Ranch faults. A M5.7 aftershock occurred on 15 June 2010 in the gap connecting the El Mayor-Cucapah rupture and the Elsinore fault. The aftershock produced discernable deformation in a UAVSAR pair spanning the event with images collected 13 April 2010 and 1 July 2010. Inversions of the data are consistent with coseismic slip from the aftershock. Left-lateral conjugate slip is observed on two structures about 2 km long and about 900 m apart at the southern end of the aftershock rupture zone. The UAVSAR observations are consistent with afterslip on the main El Mayor-Cucapah rupture plane that continues for at least several months after the earthquake. Continued slip occurs on a conjugate set of faults located between the mainshock rupture and the Elsinore fault. The Imperial, Superstition, and East Elmore Ranch faults do not show continuing slip following the main El Mayor-Cucapah earthquake rupture on 4 April 2010.

### **Detailed Spatio-Temporal Evolution of Aftershocks and Repeating Earthquakes Following the 2012 Mw7.6 Nicoya Earthquake**

YAO, D., Georgia Tech, Atlanta, GA, USA, [dyao30@gatech.edu](mailto:dyao30@gatech.edu); MENG, X., Georgia Tech, Atlanta, GA, USA, [xmeng7@gatech.edu](mailto:xmeng7@gatech.edu); PENG, Z., Georgia Tech, Atlanta, GA, USA, [zpeng@gatech.edu](mailto:zpeng@gatech.edu); NEWMAN, A. V., Georgia Tech, Atlanta, GA, USA, [anewman@gatech.edu](mailto:anewman@gatech.edu); WALTER, J. L., University of Texas at Austin, Austin, TX, USA, [jwalter@utig.utexas.edu](mailto:jwalter@utig.utexas.edu); SCHWARTZ, S. Y., University of California-Santa Cruz, Santa Cruz, CA, USA, [syschwar@ucsc.edu](mailto:syschwar@ucsc.edu); PROTTI, M., Observatorio Vulcanológico Sismológico de Costa Rica, Heredia, Costa Rica, [marino.protti.quesada@una.cr](mailto:marino.protti.quesada@una.cr)

We apply a recently developed waveform matching technique to obtain a more complete earthquake catalog around the 2012  $M_w$  7.6 Nicoya earthquake. Starting with the preliminary catalog from SimulPS incorporating a regionally-defined 3D seismic velocity model, we relocate these data with new phases in HypoDD to better identify spatially clustered behavior. We find that aftershocks are mostly clustered in two regions: one is immediately updip of the dominant mainshock slip patch, overlapping with a zone of shallow afterslip; and a second one is 50 km SE from the mainshock nucleation, which exhibited modest coseismic rupture, and little afterslip.

Using  $\sim 5300$  relocated events as templates, we scan the continuous recording from 07/01/2012 to the end of 2012. So far we have detected 20 times more events using 12 times the median absolute deviation (MAD) as thresholds for

the mean cross-correlation values. The early aftershocks appear to expand along both trench parallel and normal directions for both clusters with logarithmic rates following the mainshock, similar to recent observations following other large earthquakes. In addition, we search for repeating earthquakes with CC values larger than 0.9, followed by additional relocation to ensure that their source patches have significant overlaps. Currently we have identified approximately 50 repeating clusters with at least 4 events per cluster. Most repeating clusters occurred immediately updip of the mainshock slip region where significant afterslip occurred, suggesting that they were driven by afterslip on the plate interface. In contrast, very few repeating clusters were found in the southern edge of the peninsula, a zone with little afterslip. Likewise, many of the observed aftershocks here occurred within the downgoing slab. Our observations suggest that both mainshock slip and afterslip play significant roles in controlling spatio-temporal evolution of aftershocks in this region.

#### **Detection and Location of Earthquakes Along the West Coast of Chile: Examining Seismicity in the 2010 M 8.8 Maule Rupture Zone.**

DINIAKOS, R. S., New Mexico Tech, Socorro, NM, USA, rdiniakos@gmail.com; BILEK, S. L., New Mexico Tech, Socorro, NM, USA, sbilek@nmt.edu; ROWE, C., Los Alamos National Labs, Los Alamos, NM, USA, char@lanl.gov; DRAGONOV, D., Delft University of Technology, Delft, Netherlands, D.S.Dragonov@tudelft.nl

The subduction of the Nazca Plate beneath the South American Plate along Chile has produced some of the largest earthquakes recorded on modern seismic instrumentation. These include the 1960 M 9.5 Valdivia, 2010 M 8.8 Maule, 2014 M 8.1 Iquique, and more recently the 2015 M 8.3 Illapel earthquakes. Slip heterogeneity in the 2010 Maule earthquake has been noted in various studies. It has been suggested that the slip heterogeneity at small scales can provide insight to future seismic potential of the region. In order to explore possible spatial variations in the continued aftershocks of the 2010 event, we are expanding the catalog of weak earthquakes using a template-matching algorithm to find other small earthquakes in this region. We use a starting earthquake catalog developed from regional and local array data; these events form the templates we use to search through seismic waveforms recorded during 2012 by a temporary seismic array in Malargüe, Argentina, that operated in 2012 and located ~300 km east of the Maule region. Our template events were first identified on the array stations, and we used a 10-s window around the P-wave arrival to extract the template seismogram. We then employed a waveform cross-correlation algorithm to correlate the template seismogram to day-long seismograms from stations in the Malargüe array. The newly detected events were then located using the HYPOINVERSE2000 program and a velocity model from Haberland (2009), developed for the south-central Chilean region. Initial results include 1203 new detections. Preliminary locations of a subset of these new events place them within the Maule rupture region. Here, we will present a full set of locations and a comparison of these new events to patterns of high slip along the 2010 Maule earthquake.

---

#### **Near Field and Directivity Considerations in Developing Fault Normal and Fault Parallel Spectra and Selecting and Scaling Time Histories for Nonlinear Analysis**

Oral Session · Wednesday · 2:15 PM · 20 April · Tuscany 7/8  
Session Chair: Zia Zafir

---

#### **Building Codes' Requirements for Near Field and Directivity Considerations in Ground Motions**

ZAFIR, Z., Kleinfelder, Rancho Cordova, CA, USA, zzafir@kleinfelder.com

Building codes for new and existing buildings require that for sites within 5 km of a fault (near field), both fault normal (FN) and fault parallel (FP) spectra are developed and time histories should be rotated to FN and FP components. However, besides the permissibility of taking maximum direction spectrum as the FN component and the geometric spectrum as the FP spectrum in ASCE 41-13, there are no particular guidelines how to develop the FN and FP spectra. In addition, codes require that for near field conditions, time histories shall be rotated to FN and FP components. This presentation will focus on different requirements by ASCE 7-10 and ASCE 41-13. In addition, upcoming code requirements in ASCE 7-16 which are based on NEHRP 2015 provisions, will be presented. The presentation will highlight the issues of 1) Forward directivity; 2) ground motion orientation (FN and FP); and 3) velocity pulse effects. Forward directivity effects have been observed for distances up to 25 to 30 km and both velocity pulse effects and differences in FN and FP motions have been observed for distances greater than 5 km. In addition, it has been observed that FN motions may not represent

the larger component as previously thought. In order to obtain true FN and FP motions, time histories should be rotated to major and minor principal axes. This presentation will explain all the different issues related near field and directivity considerations in ground motions.

#### **Near-field and Regional Ground Motions During the 2015 Gorkha, Nepal, Earthquake**

HOUGH, S. E., US Geological Survey, Pasadena, CA, USA, hough@usgs.gov; AMPUERO, J. P., Caltech, Pasadena, CA, USA, ampuero@gps.caltech.edu; MARTIN, S. S., Earth Observatory of Singapore, Singapore, 7point1@gmail.com; MENG, L., UCLA, Los Angeles, CA, USA, meng@ess.ucla.edu; THOMPSON, E. M., US Geological Survey, Golden, CO, USA, emthompson@usgs.gov; ZHANG, A., UCLA, Los Angeles, CA, USA, aileen808@ucla.edu; ASIMAKI, D., Caltech, Pasadena, CA, USA, domniki@caltech.edu

The 25 April 2015  $M_w$  7.8 Gorkha, Nepal, earthquake occurred along a segment of the Main Himalayan Thrust directly beneath central Nepal and Kathmandu valley. In spite of the magnitude and proximity to the rupture, shaking throughout the near-field region only in rare instances caused damage commensurate with European Macroseismic Intensity (EMS) 8. We conclude that the distribution of ground motions was controlled by several factors, including the distribution of high frequency (HF) radiation along the rupture, and non-linear response of the Kathmandu valley. To better characterize the distribution of ground motions, we convert EMS intensities from Martin *et al.* (2015) into estimated peak acceleration, PGAI, using available instrumental data for calibration. We show that ground motions in central Kathmandu were systematically de-amplified relative to two reference ground motion prediction equations, consistent with the suggestion of Dixit *et al.* (2015) that sediments in the valley experienced a pervasively non-linear response during the mainshock. Across the near-field region, the distribution of ground motions suggests that the distance to sources of HF radiation, as imaged by back-projection using multiple teleseismic arrays with an innovative calibration method, had a first-order effect on shaking intensities throughout Nepal. Since recent studies suggest that deep HF radiation appears to be a common feature of subduction zone earthquakes, it is possible that hazard assessments, a critical first step for building code development, can be improved by considering the expected distribution of HF sources within megathrust ruptures. A comparison of observations from the Gorkha earthquake and Dolakha aftershock with published ground motion prediction equations reveals, however, how near-field and regional ground motions during large earthquakes can be controlled by a complex combination of source, path, and site effects.

#### **Mean Spectral Modification in the Near Field for use in Nonlinear Analysis**

MAZZONI, S., Consultant, Walnut Creek, CA, USA, silviamazzoni@yahoo.com; WRIGHT, A., Amec Foster Wheeler, Rancho Cordova, CA, USA, alexander.wright@amecfw.com; LEW, M., Amec Foster Wheeler, Los Angeles, CA, USA, marshall.lew@amecfw.com; WELLS, D., Amec Foster Wheeler, Oakland, CA, USA, donald.wells@amecfw.com; HACHEM, M., Degenkolb Engineers, Oakland, CA, USA, mhachem@degenkolb.com

Traditional methods of modifying ground motions in the near field for use in nonlinear analysis using spectral matching are limited in application due to their inability to preserve the ground motion variability and their lack of conservatism when used to predict building response. Recently, Mazzoni *et al.* (2012) proposed an alternative approach called mean spectral modification which overcomes many of the limitations of the more traditional approaches, including capturing the expected variability in ground motion. However, little or no guidance exists regarding implementation of this method in the near field. Use of separate targets for the fault normal and fault parallel directions, as is often done in more traditional applications of spectral matching, can destroy the relationship between the fault normal and fault parallel ground motion components. We present a framework for implementation of the mean spectral modification approach in the near field using a single target response spectrum. The proposed framework applies consistent modifications to both horizontal components of motion, while preserving the variability and other characteristics of the ground motions. The implementation of the proposed methodology under various codes is discussed and the advantages and application of the proposed methodology are illustrated for a near field site.

#### **Implications of Forward Directivity Effects on Design Ground Motions**

MOGHIMI, S., Middle East Technical University, Ankara, Turkey, moghimi.saed@metu.edu.tr; AKKAR, D. S., Bogazici Uni. Kandilli Observatory and Earthquake Research Inst, Istanbul, Turkey, sinan.akkar@boun.edu.tr

When rupture and slip direction relative to a site coincide and a significant portion of fault ruptures towards the site, the ground motion can exhibit the effects



of forward directivity (short duration ground motion that consists of one or more pulses). Ground-motion records exhibiting forward directivity effects have large demands on structures in the vicinity of pulse period. We implemented the Shahi and Baker (2011) forward directivity model in PSHA to observe the changes in ground-motion amplitudes due to forward directivity under different circumstances. In essence we looked into the importance of geometric configurations between the ruptured fault segment and the site together with some source parameters that mark the seismic activity of the fault (e.g., slip rate, maximum magnitude, etc). We used the observations from these case studies to set some simple rules for the implications of forward directivity effects on the design spectral ordinates.

We also implemented the directivity model of Chiou and Spudich (2014) that uses the directivity predictor parameter, DPP. We ran our PSHA using the same scenarios as in the case of Shahi and Baker (2011) model to compare and discuss the differences between these two forward directivity models. The points that should be considered here is that these two models predict different components of motion for forward directivity effects. While Shahi and Baker (2011) predicts the ground motion for arbitrary orientations relative to fault strike, the Chiou and Spudich modifies RotD50 (Boore, 2010) component for forward directivity. Besides Shahi and Baker (2011) use pulse period concept in its narrow-band model whereas the other model does not include such a parameter. We discuss these issues in this study by providing some results using different earthquake scenarios.

Reference

Shahi S and Baker JW (2011)

Chiou and Youngs (2014)

Boore (2010)

### **Simulation of 13 March 1992 Erzincan (Turkey) Earthquake including a Near-field Forward Directivity Pulse Model: Implications for Earthquake Engineering**

AZARI SISI, A., Middle East Technical University, Ankara, Turkey, aida.sisi@metu.edu.tr; ASKAN, A., Middle East Technical University, Ankara, Turkey, aaskan@metu.edu.tr; ERBERIK, M. A., Middle East Technical University, Ankara, Turkey, altug@metu.edu.tr

In this study, 13 March 1992 Erzincan ( $M_w=6.6$ , Turkey) earthquake is simulated including the analytical long-period pulse model proposed by Mavroeidis and Papageorgiou (2003). The ERC station recording displays pulsive behavior mostly in the North-South component according to Askan *et al.* (2013) hence it is used for the calibration of parameters herein. The analytical pulse formulation is applied in stochastic finite-fault ground motion simulation based on dynamic corner frequency proposed by Motazedian and Atkinson (2005). The input pulse parameters are derived according to historical pulse-like ground motion recordings in the study region. Pulse amplitude,  $A$ , is determined in order to make the peak ground velocity (PGV) and peak pseudo-velocity spectrum (PSv) values of analytical pulse consistent with the corresponding values of recorded ground motion. Pulse period,  $T_p = 1/f_p$ , is calibrated such that the peak of PSv from synthetic and recorded ground motions occur at the same frequency. Finally, velocity and displacement time histories are attempted to be fitted in order to estimate the oscillatory character and phase angle. The optimized pulse parameters are then used for simulating the 13 March 1992 Erzincan earthquake. The simulated ground motions with and without analytical pulse are compared with each other. These motions are then implemented into nonlinear time history analyses of single degree of freedom systems (SDOF). These SDOF models represent the typical residential buildings in Erzincan region. OPENSEES platform is employed to perform the time history analyses. The effect of calibrated analytical forward directivity pulse is also investigated on seismic demands of the SDOFs.

---

### **How Close are We to an Eruption?**

Oral Session · Wednesday · 4:30 PM · 20 April · Tuscany 7/8

Session Chairs: Weston Thelen and Matthew Haney

---

### **Forecasting of Eruptions at Stratovolcanoes**

WHITE, R. A., US Geological Survey, Menlo Park, CA, USA, rwhite@usgs.gov; MCCAUSLAND, W. A., US Geological Survey, Vancouver, WA, USA, wmccausland@usgs.gov

Seismic monitoring provides important constraints on magmatic ascent and eruption. From experience with 25+ eruptions and review of 10+ additional eruptions at 24 dormant (>20 years) volcanoes, we see a progression of at least three but sometimes four phases of precursory seismicity. 1) Distal volcano-tectonic (DVT) earthquakes occur on local faults from <2 to 30+ km distance from

(not beneath) the eventual eruption site as magma intrudes into and rises out of upper crustal reservoirs to depths of 2-3 km. We show that >90% of eruptions at dormant volcanoes were preceded by significant DVT seismicity, usually reaching felt magnitudes ( $M>3$ ). Most importantly, the cumulative energy of this DVT energy correlates to the intruding magma volume. 2) Low frequency (LF) earthquakes, LF tremor and contained explosions occur as magma interacts with the shallow hydrothermal system (< 2 km depth), while the DVT seismicity usually dies off. 3) Finally, repetitive LF seismicity generally occurs and may dominate records as magma rises to the surface. At least sometimes, these three phases are preceded by an initial phase of deep (>20 km) LF earthquakes that occur near the base of the crust as magma rises toward crustal reservoirs. This seismicity is the most difficult to observe, owing to generally small magnitudes ( $M<2.0$ ) and the significant depth. It is not yet clear how common this phase is. At more open, frequently active systems, phases 1-3 often precede eruptive activity also. However, the more open the system, the more muted is the level of precursory seismicity, and phases 1 and sometimes 2 may be skipped altogether. We present some examples of this seismic progression at both dormant and frequently active systems.

### **Arc-wide Application of the Distal VT Model for Eruption Forecasting in Alaska**

PESICEK, J. D., USGS Volcano Disaster Assistance Program, Vancouver, WA, USA, jpesicek@usgs.gov; WELLIK, J., USGS Volcano Disaster Assistance Program, Vancouver, WA, USA, jwellik@usgs.gov; PREJEAN, S., USGS Volcano Disaster Assistance Program, Anchorage, AK, USA, sprejean@usgs.gov; WHITE, R., USGS Volcano Disaster Assistance Program, Menlo Park, CA, USA, rwhite@usgs.gov; CAMERON, C., Alaska DNR, Fairbanks, AK, USA, cheryl.cameron@alaska.gov; MCCAUSLAND, W., USGS Volcano Disaster Assistance Program, Vancouver, WA, USA, wmccausland@usgs.gov; BUURMAN, H., University of Alaska Fairbanks, Fairbanks, AK, USA, helena@gi.alaska.edu

The Alaska Volcano Observatory (AVO) has responded to 28 eruptions from 10 volcanoes since 2005 and has successfully forecast the most significant of these eruptions. However, eruptions of some volcanoes remain stubbornly difficult to forecast effectively using seismic data alone, including those of frequently active volcanoes with basaltic-andesite magmas, such as Pavlof, Veniaminof, and Okmok volcanoes. In this study, we re-examine earthquake catalogs from eruptions and known intrusive episodes in Alaska to test the effectiveness of the distal VT model (White and McCausland, 2016) commonly employed by the USGS-USAID Volcano Disaster Assistance Program (VDAP). In the distal VT model, volcano-tectonic (VT) earthquake swarms occur as a secondary response to crustal strain induced by magma intrusion in the shallow crust surrounding closed system volcanoes. However, in regions with significant background seismicity, it can be difficult to distinguish distal VT earthquake swarms from crustal tectonic seismicity unrelated to volcanic processes, posing challenges for eruption forecasting. In this study, we use a modified beta-statistic to identify pre-eruptive distal VT swarms and establish their statistical significance with respect to long-term background seismicity. We search for precursory patterns to all eruptive and intrusive episodes, at the arc-wide scale but also amongst subgroups of similar volcanoes. Preliminary results suggest that closed-system stratovolcanoes with longer repose times generally fit the distal VT model well, while caldera systems and frequently active basaltic volcanoes may not. Intrusive episodes are more challenging to analyze. These results allow us to explore the general applicability of the distal VT model and quantify the likelihood of success in eruption forecasting using this model alone.

### **Fluid-faulting Interactions: Fracture-mesh and Fault-valve Behavior in the February 2014 Mammoth Mountain, California, Earthquake Swarm**

SHELLY, D. R., Volcano Science Center, US Geological Survey, Menlo Park, CA, USA, dshelly@usgs.gov; TAIRA, T., Berkeley Seismological Laboratory, University of California, Berkeley, CA, USA, taira@seismo.berkeley.edu; PREJEAN, S. G., Volcano Science Center, US Geological Survey, Anchorage, AK, USA, sprejean@usgs.gov; HILL, D. P., Volcano Science Center, US Geological Survey, Menlo Park, CA, USA, hill@usgs.gov; DREGER, D. S., Berkeley Seismological Laboratory, University of California, Berkeley, CA, USA, douglas.dreger@gmail.com

Faulting and fluid transport in the subsurface are highly coupled processes, which may manifest seismically as earthquake swarms. A swarm in February 2014 beneath densely monitored Mammoth Mountain, California, provides an opportunity to witness these interactions in high resolution. Toward this goal, we employ massive waveform-correlation-based event detection and relative relocation, which quadruples the swarm catalog to more than 6000 earthquakes and produces high-precision locations even for very small events. The swarm's main seismic zone forms a distributed fracture mesh, with individual faults activated

in short earthquake bursts. The largest event of the sequence, M 3.1, apparently acted as a fault valve and was followed by a distinct wave of earthquakes propagating ~1 km westward from the updip edge of rupture, 1–2 h later. Late in the swarm, multiple small, shallower subsidiary faults activated with pronounced hypocenter migration, suggesting that a broader fluid pressure pulse propagated through the subsurface.

#### **Near Real-time Detection, Clustering, and Analysis of Repeating Earthquakes: Application to Mount St. Helens and Redoubt Volcanoes**

HOTOVEC-ELLIS, A. J., University of Washington, Seattle, WA, USA, [ahotovec@uw.edu](mailto:ahotovec@uw.edu); JEFFRIES, C., University of Washington, Seattle, WA, USA, [jeffrc@uw.edu](mailto:jeffrc@uw.edu)

Repeating earthquakes are a nearly ubiquitous feature of the seismicity at active volcanoes, especially leading up to and during eruptions. They present an obvious target for research into their use as an indicator of imminent eruptive activity; however, swarms of repeating earthquakes commonly occur without leading to eruptions as well. Determining whether a swarm will lead to an eruption as it is happening is one of the great challenges in volcano monitoring. This effort would be greatly facilitated by rapid detection and clustering of repeating earthquakes in near real-time, and to this end REDPy (Repeating Earthquake Detector in Python) is being developed as an open-source tool.

While information about the number and size of new earthquake clusters can provide first-order information about whether it is likely indicative of an impending eruption, further analysis of these earthquakes with coda-wave interferometry can reveal whether the source or medium is changing with time. We used coda-wave interferometry of repeating earthquakes to determine changes in seismic velocity leading up to the 2004 eruption of Mount St. Helens, and found remarkable similarity between velocity change and seismicity rate in the days leading up to the appearance of lava at the surface. We are currently investigating whether this similarity is a reproducible feature prior to other eruptions, starting with the 2009 eruption of Redoubt Volcano.

#### **The Yellowstone Magmatic System from the Mantle Plume to the Upper Crust**

HUANG, H. H., California Institute of Technology / University of Utah, Pasadena, CA, USA, [hhuang@caltech.edu](mailto:hhuang@caltech.edu); LIN, F. C., University of Utah, Salt Lake City, UT, USA, [FanChi.Lin@utah.edu](mailto:FanChi.Lin@utah.edu); SCHMANDT, B., University of New Mexico, Albuquerque, NM, USA, [bschmandt@unm.edu](mailto:bschmandt@unm.edu); FARRELL, J., University of Utah, Salt Lake City, UT, USA, [jamie.farrell@utah.edu](mailto:jamie.farrell@utah.edu); SMITH, R. B., University of Utah, Salt Lake City, UT, USA, [robert.b.smith@utah.edu](mailto:robert.b.smith@utah.edu); TSAI, V. C., California Institute of Technology, Pasadena, CA, USA, [tsai@caltech.edu](mailto:tsai@caltech.edu)

The Yellowstone supervolcano is one of the largest active continental silicic volcanic fields in the world. An understanding of its properties is key to enhancing our knowledge of volcanic mechanisms and corresponding risk. Using a joint local and teleseismic earthquake P-wave seismic inversion, we revealed a basaltic lower-crustal magma body that provides a magmatic link between the Yellowstone mantle plume and the previously imaged upper-crustal magma reservoir. This lower-crustal magma body has a volume of 46,000 cubic kilometers, ~4.5 times that of the upper-crustal magma reservoir, and contains a melt fraction of ~2%. These estimates are critical to understanding the evolution of bimodal basaltic-rhyolitic volcanism, explaining the magnitude of CO<sub>2</sub> discharge, and constraining dynamic models of the magmatic system for volcanic hazard assessment.

---

## **Induced Seismicity**

Oral Session · Wednesday · 8:30 AM · 20 April · Tuscany A  
Session Chairs: Thomas Braun, Ivan G. Wong, Justin Rubinstein, Thomas Goebel, David Eaton, Gail Atkinson, and Honn Kao

---

#### **Observations of Numerous Hydraulic Fracturing Induced Earthquake Sequences in Harrison County Ohio since 2013**

FRIBERG, P. A., ISTI, New Paltz, NY, USA, [p.friberg@isti.com](mailto:p.friberg@isti.com); BRUDZINSKI, M. R., Miami University, Oxford, OH, USA, [brudzimr@miamioh.edu](mailto:brudzimr@miamioh.edu); SKOUMAL, R. J., Miami University, Oxford, OH, USA, [skoumarj@miamioh.edu](mailto:skoumarj@miamioh.edu); CURRIE, B. S., Miami University, Oxford, OH, USA, [curriebs@miamioh.edu](mailto:curriebs@miamioh.edu)

We observe numerous sequences of microearthquakes in Harrison county Ohio since the installation of an EarthScope station (TA.O53A) in 2013. These sequences are each linked to hydraulic fracturing (HF) operations by coincidence

in time and in location, suggesting that seismicity induced by HF may be more prevalent than previously thought. The sequences present as a series of repeating earthquakes, some with magnitudes as large as ML 2.8, with a magnitude of completeness below -1.0. The repeating nature of the HF linked sequences enabled us to utilize template matching and a repeating signal detection algorithm to observe over 5000 events on station O53A. Of the many events detected, over 100 were large enough to be recorded on 2-4 additional temporary stations deployed nearby (< 10km distance) and thus be located. We compute the earthquake locations using both traditional and double-difference approaches and examine the uncertainty depending on the number of stations used. All of the HF operations stimulated the Utica/Point Pleasant formation, which is ~500 m above basement rocks where the majority of events locate. Some events do appear to occur above the basement in or near the stimulated formation, and the high b-values in these cases are consistent with operationally induced microseismicity. In general, the located earthquakes tend to form east-west linear clusters oriented ~30 degrees from the maximum stress orientation, consistent with reactivation of critically stressed pre-existing faults. The distribution is indicative of a single fault or possible splays on a series of faults, the size of which is critically dependent on earthquake locations. We will present results of numerous relocation strategies for the earthquakes along with implications for seismic hazard in the region.

#### **Linking Fossil Reefs with Earthquakes: Geologic Insight to Where Induced Seismicity occurs in Alberta**

SCHULTZ, R., Alberta Geological Survey, Edmonton, AB, Canada, [Ryan.Schultz@aer.ca](mailto:Ryan.Schultz@aer.ca); CORLETT, H., Alberta Geological Survey; HAUG, K., Alberta Geological Survey; KOCON, K., Alberta Geological Survey; MACCORMACK, K., Alberta Geological Survey; STERN, V., Alberta Geological Survey; SHIPMAN, T., Alberta Geological Survey,

Recently, a significant increase in North American, mid-continent earthquakes have been associated with contemporaneous development of petroleum resources. Despite the proliferation of drilling throughout sedimentary basins worldwide, earthquakes are only induced at a small fraction of wells. In this study, we focus on cases of induced seismicity where high-resolution data are available in the central Western Canada Sedimentary Basin. Our regional comparison of induced earthquake depths suggests basement controlled tectonics. Complementary to these findings, hypocentres of induced seismicity clusters coincide with the margins of Devonian carbonate reefs. We interpret this spatial correspondence as the result of geographically biased activation potential, possibly as a consequence of reef nucleation preference to paleobathymetric highs associated with Precambrian-basement tectonics. This finding demonstrates the importance of geologic/tectonic factors to earthquake induction, in addition to industrial operational parameters. In fact, the observation of induced seismicity silhouetting deep fossil reef systems may be a useful tool to identify future regions with increased seismogenic potential.

#### **Natural Versus Anthropogenic Trigger of the Emilia 2012 Earthquakes**

PEZZO, G., INGV, Rome, Italy, [giuseppe.pezzo@ingv.it](mailto:giuseppe.pezzo@ingv.it); CHIARABBA, C., INGV, Rome, Italy, [claudio.chiarabba@ingv.it](mailto:claudio.chiarabba@ingv.it); DE GORI, P., INGV, Rome, Italy, [pasquale.degori@ingv.it](mailto:pasquale.degori@ingv.it); LUCENTE, F. P., INGV, Rome, Italy, [pio.lucente@ingv.it](mailto:pio.lucente@ingv.it)

The 2012 Emilia earthquakes is the first debated case in Italy of destructive event supposed to be triggered by anthropic activity. The seismic sequence occurred in the central Po plain, characterized by arcuate blind thrust systems and related growth folds, below the Plio-Quaternary sedimentary cover. The sequence occurred in a low deforming region with scarce records of historical earthquakes since at least the year 1000 A.D. The 2012 sequence was characterized by a  $M_w$  6.0 and a second 9-days-delayed shock of  $M_w$  5.8 (dated 2012 May 20, and 29, respectively) whose focal solutions indicate reverse mechanisms on two adjacent broadly parallel fault segments. Co-seismic surface deformation from InSAR and GPS data analysis shows two main lobes spatially and temporally corresponding to slip over the two adjacent faults. A small transient ground deformation has been observed in the period between the two events, associated to an aseismic pre-slip occurred along the second mainshock fault plane.

Alteration of local stress at the mainshock hypocenters generated by decennial exploitation of a nearby oil field has been firstly not excluded and subsequently quantified as having negligible effects, by two scientific commissions engaged by national and regional governmental agencies. In this study, we present new evidence spanning from seismicity migration, seismic tomography and geodetic modeling that reveal a fluid pressure perturbation after the May 20  $M_w$  6.0 first shock which diffused within a densely cracked volume around the nucleation zone of the May 29  $M_w$  5.8 second shock. Interaction between faults, aseismic slip and pore pressure changes suggest that fluid diffusion along the fault system acted as a natural trigger of the May 2012 seismicity.

## **Wastewater Disposal, Hydraulic Fracturing, and Seismicity in Southern Kansas**

RUBINSTEIN, J. L., U. S. Geological Survey, Menlo Park, CA, USA, jrubinstein@usgs.gov; ELLSWORTH, W. L., Stanford University, Stanford, CA, USA, wellsworth@stanford.edu

The historically aseismic counties of Harper and Sumner in southern Kansas have experienced a remarkable surge of seismic activity since 2014, including the  $M_w$  4.8 Conway Springs earthquake of November 12, 2014. The concurrent appearance of seismicity with increased oil and gas production activities in southern Kansas since September 2012 suggests that industrial operations are inducing earthquakes. These earthquakes occur in a portion of the Mississippian Lime Play, an oil and gas field stretching from central Oklahoma to northwestern Kansas. As has been seen in neighboring parts of Oklahoma, the seismicity appears to be driven by the disposal of produced water by injection into the Arbuckle formation near the base of the sedimentary section. In May 2014 a 14-station teleseismic network was deployed by the USGS to monitor ongoing seismicity. Earthquake locations and magnitudes for  $M \geq 1.5$  earthquakes are included in the USGS Comprehensive Catalog (ComCat). Hypocenters principally occur in the crystalline basement, with some forming lineations extending up to 10 km in length. Focal mechanisms indicate primarily normal faulting, consistent with the regional NW-SE orientation of the least horizontal minimum stress. While some of the clusters of seismicity are located close to high-rate injection wells, other clusters are over 10 km from the nearest high-volume and rate injection wells. Additionally, high-rate wells do not always appear to be associated with seismicity. In response to the increased seismicity, on March 29, 2015 the Kansas Corporation Commission placed limits on the rate of wastewater disposal in 5 areas in southern Kansas centered on the most prominent earthquake clusters at that time. During the first 6 months following the order, earthquake activity has decreased by 40-50% within the zones specified in the order. We report here on the current status of the seismicity and compare it to nearby areas not directly affected by the order.

## **Stress Variations Across Oklahoma and Kansas, Natural Earthquakes, Induced Seismicity, and Their Links with Crustal and Upper Mantle Structure**

LEVANDOWSKI, W., USGS, Golden, CO, USA, wlevandowski@usgs.gov; MCNAMARA, D. E., USGS, Golden, CO, USA, mcnamara@usgs.gov

Regional moment tensors and relocated seismicity reflect a broadly uniform  $\sim N80E$  maximum horizontal stress direction across Oklahoma and southern Kansas. Yet a transition from mixed normal and strike-slip mechanisms in southern Kansas to pure strike-slip in central Oklahoma to oblique-reverse motion recorded on the scarp of the Meers fault in southwestern Oklahoma requires that vertical stress shift from roughly minimally compressive to roughly maximally compressive. To understand the origin of this transition and to explore the connection between lithospheric structures and natural and induced seismicity, we jointly invert hundreds of seismic velocity models derived from Transportable Array data, gravity, and topography for a 3-D model of crustal and upper mantle density. We find that most natural seismicity occurs where the margins of sedimentary basins collocate with anomalously dense lower crust. Furthermore, the shift in focal mechanisms coincides with the transition from dense material associated with the Oklahoma aulacogen to unaltered, buoyant lower crust similar to the rest of the western Great Plains. Finite-element models of the stress created by the modeled density variations reveal that the latent flexural stress supporting this dense material elevates deviatoric stress and produces the change in principal stress state manifest in the shift from normal-oblique to reverse-oblique focal mechanisms. By contrast, induced seismicity generally clusters in the vicinity of isolated, dense bodies in the crystalline upper crust (5-10 km depth) and overlying sediment. Nevertheless, our models at this depth are largely controlled by the seismic velocity models, which lack sufficient resolution for robust interpretations of the link between these anomalies and anthropogenic seismicity. Ongoing work to incorporate the more than 100,000 existing Pg, Pn, Sg, and Sn arrivals from local earthquakes into the inversion will produce more robust images of crustal structure.

## **Wastewater Disposal and Earthquake Swarm Activity at the Southern End of the Central Valley, California**

GOEBEL, T. H. W., UCSC, tgoebel@ucsc.edu; HOSSEINI, S. M., USC; CAPPA, F., Geozur, University of Nice; HAUKSSON, E., Caltech; AMPUERO, J. P., Caltech; AMINZADEH, F., USC; SALEEBY, J. B., Caltech,

Fracture and fault zones can channel fluid-flow and transmit injection-induced pore pressure changes over large distances (>km), at which seismicity is rarely suspected to be human-induced. We use seismicity analysis and hydrogeological models to examine the role of seismically active faults in inducing earthquakes.

We analyze a potentially injection-induced earthquake swarm with three events above  $M4$  in direct proximity to the White-Wolf fault (WWF). The swarm deviated from classic main-aftershock behavior, exhibiting uncharacteristically low Gutenberg-Richter  $b$  of 0.6 and systematic migration patterns. Some smaller events occurred south-east of the WWF in an area of several disposal wells, one of which became active just five months before the main swarm activity. Hydrogeological modeling suggests that wastewater disposal likely contributed to seismicity via localized pressure-increase along a seismically active fault. Our results highlight that induced seismicity may remain undetected in CA without detailed analysis of local geologic setting, seismicity and fluid diffusion.

## **Mechanism of Intraplate Earthquakes and Anthropogenic Causes in USA**

HAGEN, M. H., Indiana University, Bloomington, IN, USA, marhagen@indiana.edu

We carried out an investigation on the possible causes of earthquakes increase in USA the last seven years. Statistical and physical models indicated the evolution of events in the country depends from the human actions. For further analysis we divided the country into three main seismological regions: western, central and, eastern. We roughly classified the areas by their thickness of Earth's crust in a variation 25-45-25 km. The thickest area is in the mid-continent and most of this region is part of the Great Plains. This study investigated the reason for the Mississippi Lime in Oklahoma a very thick area, had unusual seismological activity since 2009, most at Oklahoma/ Kansas border. Anthropogenic disturbance in this area is very high with more than 4000 waste water wells are active in the state. Wastewater disposal wells typically operate for longer duration and inject much more fluid than hydraulic fracturing, making them more likely to induce earthquakes. Enhanced oil recovery injects fluid into rock layers where oil and gas have already been extracted, while wastewater injection often occurs in never-before-touched rocks. A combination of many factors is necessary for injection to induce felt earthquakes. These include the injection rate and total volume injected; the presence of faults or unknown fractures that are large enough to produce felt earthquakes; stresses that are large enough to produce earthquakes; and the presence of pathways for the fluid pressure to travel from the injection point to faults. Other causes of human action triggering earthquakes, fluid injection, hydraulic fracturing, enhanced oil recovery, mining, nuclear explosions, some of them will be mentioned and investigated in this paper. We also intend to explain why not all the waste wells are triggering earthquakes and how it would be strongly attached to the unevenness of the Earth's crust.

## **Seismic Hazard Assessment for Gas Extraction Induced Seismicity in the Context of Building Codes**

KRAAIJPOEL, D. A., TNO, Utrecht, The Netherlands, dirk.kraaijpoel@tno.nl; STEENBERGEN, R. D. J. M., TNO, Delft, The Netherlands

The Groningen Field in the north-east of The Netherlands is one of the largest natural gas fields in the world. It has been in production since 1963. Ever since, its revenues have formed a substantial contribution to the national budget. In the early nineties, the first earthquakes were detected and felt in the previously aseismic region. These seismic events are now recognized to be induced by gas extraction. The depletion of the gas reservoir leads to reduced pore pressures and compaction of the sandstone reservoir rock at around 3 km depth. Stress accumulations at pre-existing fault structures subsequently lead to the occurrence of earthquakes.

Since a bit more than a decade, the seismicity rate has been increasing steadily. Although the magnitudes seen so far have been moderate (currently  $M=3.6$  maximum), several events have caused substantial damage to mainly buildings. As a result, public acceptance in the region has dropped considerably, and public safety has become a political issue at the national level. Risk mitigation measures currently proceed along two complementary tracks. First, a series of increasingly sharp production cuts have been enforced by ministerial decision and court order. Second, a massive strengthening program for the building stock has been initiated. In addition, infrastructure and industrial facilities need to be prepared.

The efficiency of risk mitigation measures depends to a great extent on the rigor and efficacy of the seismic hazard assessment that forms the basis of the risk assessment. We present recent developments in probabilistic seismic hazard assessment in the Groningen area with emphasis on the application in seismic building codes, which are currently under development in The Netherlands. Topics to be discussed include non-stationarity, treatment of maximum magnitude and non-linear site effects.

## **A Ground Motion Prediction Equation for Induced Earthquakes in Oklahoma**

YENIER, E., Western University, London, ON, Canada, emrah.yenier@gmail.com; ATKINSON, G. M., Western University, London, ON, Canada,



gmatkinson@aol.com; SUMY, D. F., Incorporated Research Institutions for Seismology, Washington DC, USA, danielle.sumy@gmail.com

Seismic activity in Oklahoma has substantially increased within the last decade. Deep injection of wastewater from hydrocarbon production is believed to be responsible for the evolving seismicity in the region. The growing seismicity in Oklahoma has raised concerns regarding the hazard associated with induced seismicity. Estimation of ground motions that can be produced by induced earthquakes is key to determining hazard contributions from induced seismicity.

In this study, we aim to develop a ground motion prediction equation (GMPE) for induced earthquakes in Oklahoma. Available ground motion data from induced seismicity are insufficient to develop a robust empirical GMPE for moderate-to-large magnitudes ( $M > 5$ ). In order to obtain a predictive model applicable for a wide range of magnitudes, we adopt a regionally-adjustable generic GMPE whose parameters have been calibrated to the rich empirical data in California. We investigate the region-specific source and attenuation attributes of induced events, using ground motions obtained from the 2011 Prague, Oklahoma earthquake sequence. We examine the spatial and temporal variation of stress parameters determined from ground motions of induced events, and compare their values to those obtained from naturally occurring earthquakes, to gain insights into the source characteristics of induced events in the region. We adjust the generic GMPE using the regional model parameters and calibration factor calculated from empirical data. The adjusted GMPE provides predictions for average horizontal-component response spectra and peak motions that may be produced by induced earthquakes in Oklahoma.

### Geomechanical Analysis of Fluid Injection and Seismic Fault Slip for the M4.8 Timpson, Texas, Earthquake

FAN, Z., Bureau of Economic Geology, The University of Texas, Austin, TX, USA, zhiqiang.fan@beg.utexas.edu; EICHHUBL, P., Bureau of Economic Geology, The University of Texas, Austin, TX, USA, peter.eichhubl@beg.utexas.edu; GALE, J. F. W., Bureau of Economic Geology, The University of Texas, Austin, TX, USA, julia.gale@beg.utexas.edu

An earthquake sequence that culminated in a MW4.8 strike-slip event near Timpson, east Texas, the largest documented earthquake to date in that region, had previously been attributed to wastewater injection starting 17 months prior to the onset of recorded seismic activity. To test if this earthquake sequence can be attributed to wastewater injection, we conducted coupled poroelastic finite element simulations to assess the spatial and temporal evolution of pore pressure and stress field in the vicinity of the injection wells and of the Coulomb failure stress on the seismogenic fault as a function of the permeability of the injection layer, fault orientation, fault permeability, and orientation and magnitude of the in situ stress. We find that injection-induced fault slip is plausible within the range of selected model input parameters, with slip favored by low reservoir permeability, low fault permeability, and a favorable orientation of the fault relative to the in situ stress state, while less favorable but equally plausible input parameters predict no slip within 96 months of simulated injection. Under most favorable boundary conditions for fault slip, fault slip occurs 7 months after the start of injection. Our results highlight the importance of detailed geomechanical site characterization for robust fault stability assessment prior to wastewater injection.

### Are ENA Potentially Induced Earthquakes Different From Natural Earthquakes?

CRAMER, C. H., CERi, Univ. of Memphis, Memphis, TN, USA, ccramer@memphis.edu

The question of whether induced earthquakes have significantly different source characteristics than naturally occurring earthquakes (NOE) is important if such a difference exists. I update my review of the Brune stress parameter (stress drop) estimates from some recent potentially induced earthquakes (PIE). Transverse velocity Fourier spectra are examined for a corner-frequency peak, taking into account the possible presence of a neighboring spectral peak due to the strong surface waves from shallow events. Brune stress parameter for an assumed geometrical spreading of  $R^{-1}$  is estimated from observed magnitude and corner-frequency for each event. (An assumed geometrical spreading of  $R^{-1.3}$  would yield a proportionally higher stress parameter as stated by Boore *et al.*, 2010.) Atkinson and Boore (2006) found that the average ENA Brune stress parameter of this type to be 14 MPa. PIEs in Arkansas, Oklahoma, Texas, Kansas, and Ohio have Brune stress parameters ranging from 5 to 10 MPa. Shallow NOEs (depth less than 5 km) appear to have a similar range of Brune stress parameters. Stress parameter seems to be regionalized between eastern North America and the central and southern US. Ground motions for a given earthquake can be influenced by stress parameter and by crustal attenuation ( $Q$ ). PIEs in Arkansas, Oklahoma, Texas, and Kansas are near a  $Q$  boundary at about 35N latitude between ENA mid-

continental and Gulf Coast  $Q$ , which influences ground motions (and intensities) observed to the north differently than to the south. Justin Hollenback for the NGA East project at the PEER Center also shows that event terms from a mixed effects analysis for the NGA East database are similar for PIEs and shallow NOEs and lower than deeper NOEs. Thus both a Brune stress parameter analysis and an event term analysis (allowing for regional  $Q$ ) show that ENA PIEs are similar to shallow NOEs and different for deeper NOEs and hence may not be distinct from shallow NOEs.

### Evaluating the Damage Potential of Injection-Induced Earthquakes in the Central and Eastern U.S. and Western Canada

WONG, I., AECOM, Oakland, CA USA, ivan.wong@aecom.com; BOTT, J., AECOM, Oakland, CA USA, jacqueline.bott@aecom.com; DOBER, M., AECOM, Oakland, CA USA, mark.dober@aecom.com; THOMAS, P., AECOM, Oakland, CA USA, patricia.thomas@aecom.com

Evaluation of the ground shaking hazard from injection-induced earthquakes resulting from oil and gas-related wastewater disposal or hydraulic fracturing using probabilistic seismic hazard analysis (PSHA) requires determination of the minimum magnitude ( $M_{min}$ ) for the analysis.  $M_{min}$  is especially significant for this application of PSHA in both site-specific applications and the USGS National Seismic Hazard Maps.

The generally accepted  $M_{min}$  has been moment magnitude ( $M$ ) 5.0 based on the lack of observed damage to modern engineered structures at smaller magnitudes. However, arguments have been recently put forth that  $M_{min}$  should be lower because the ground motions from induced earthquakes will be stronger than tectonic earthquakes due to their shallow nature. An additional significant factor is that in areas of low natural seismicity where induced seismicity has occurred and seismic design has not been common practice, there may exist a large inventory of vulnerable buildings and structures which could be subject to damage at magnitudes smaller than  $M$  5.0.

In contrast to the arguments of higher ground motions for shallow induced earthquakes, several researchers suggest that induced earthquakes may have lower stress drops resulting in lower ground motions particularly at high frequencies. Empirical ground motion prediction models for injection-induced earthquakes to address these issues are just now being developed as strong motion data becomes available due to the expansion of seismic networks in the central and eastern U.S. (CEUS). We have evaluated the growing database of observed damage and non-damage in the CEUS and western Canada to develop relationships that attempt to correlate magnitude, PGA, PGV, duration and Arias intensity to both structural and non-structural damage. We are assessing which are the critical parameters that impact damage to address the issue of  $M_{min}$  for induced seismicity.

### Near-distance Ground-Motion Saturation Effects for Small-to-Moderate Induced Earthquakes

ATKINSON, G. M., Western University, London, ON, Canada, gmatkinson@aol.com; YENIER, E., Western University, London, ON, Canada, emrah.yenier@gmail.com; SHARMA, N., Indian Inst. of Geomagnetism, Mumbai, India; CONVERTITO, V., Natl. Inst. Geophys. and Volcanology, Rome, Italy, vincenzo.convertito@ingv.it

A key issue in the development of ground-motion prediction equations (GMPEs) for induced earthquakes concerns the maximum amplitudes attained at short hypocentral distances. As shown by Yenier and Atkinson (2014, 2015 BSSA) the saturation of ground-motion amplitudes near the source can be modeled by a magnitude-dependent effective depth parameter, which causes the ground-motion curves to approach a constant median amplitude for distances less than the effective depth. This saturation parameter has been well-constrained by empirical studies for moderate-to-large events. However, there is significant uncertainty in the value of the effective depth for small-to-moderate events, and this maps into large and consequential uncertainty in the near-source amplitude of motions for induced-earthquake GMPEs (*e.g.* Atkinson, 2015 BSSA).

We use a rich database of ground-motion amplitudes from shallow induced earthquakes of moment magnitude ( $M$ ) 1.5 to 3.5 recorded at close distances in the Geysers region of California (the GEISER project database) to constrain the effective depth parameter for small events. We show that the effective depth parameter attains a value near 2 km for shallow events, at  $M = 3$ ; it reduces to smaller values for  $M < 3$  and gradually increases to larger values for  $M > 3$ . We explore the implications of the new constraints on effective depth for induced seismicity GMPEs. We compare a ground-motion model that considers appropriate near-distance scaling to recorded ground motions from induced events in different environments, including Oklahoma and California. We find that ground motions from induced events in California are in good agreement with the GMPE of Atkinson (2015), while those in Oklahoma, for the larger events,



are in good agreement with the GMPE of Yenier and Atkinson (2015) for central and eastern North America.

### **A Causal Link between Overpressured Hydrocarbon Source Rocks and Seismicity Induced by Hydraulic Fracturing**

EATON, D. W., University of Calgary, Calgary, AB, Canada, eatond@ucalgary.ca; CHEADLE, B., Western University, London, ON, Canada, bcheadle@uwo.ca; FOX, A., Enlighten Geoscience Ltd., Calgary, AB, Canada, amy.fox@enlightengeoscience.com

Fluid injection processes such as large-scale disposal of salt water or hydraulic fracturing of hydrocarbon source rocks can induce earthquake activity, largely by increasing pore pressure on nearby faults. In sedimentary basins, various natural processes, including transformation of organic material (kerogen) into hydrocarbon, can similarly result in fluid overpressure. Depending upon factors such as ambient stress conditions and permeability of the constituent formations, overpressure may cause hydraulic fracturing or slip on pre-existing faults to occur spontaneously. Here we show that earthquakes induced by hydraulic fracturing in western Canada are strongly clustered within regions where formation overpressure is highest. By contrast, earthquakes by hydraulic fracturing are virtually absent in areas of normal pore fluid pressure, despite intensive hydraulic fracturing activity associated with resource development. Monte Carlo simulations confirm that there is negligible probability that the observed distribution could have developed by chance. This spatial correlation implies that formation overpressure may provide an effective predictor of the likelihood of inducing earthquakes by hydraulic fracturing. It also suggests that natural cycles of fault slip over geologic time regulate pore pressure, such that the maximum sustainable overpressure due to hydrocarbon generation is effectively limited by the existing architecture of faults and fractures.

### **Normal Stress Drops for Induced Earthquakes in the Central U.S.**

HUANG, Y. H., Stanford University, Stanford, CA, USA, yihe@stanford.edu; BEROZA, G. C. B., Stanford University, Stanford, CA, USA, beroza@stanford.edu; ELLSWORTH, W. L. E., Stanford University, Stanford, CA, USA, wellsworth@stanford.edu

Stress drop, *i.e.*, the difference of fault shear stresses before and after an earthquake, is a fundamental parameter to characterize the earthquake source process. It provides valuable information about strong ground motions: Higher stress drops usually lead to more high-frequency ground motions. Hough [2014 and 2015] observe low intensities for potentially induced earthquakes using “Did You Feel It?” data and interpret them to be a result of low stress drops. However, instrumental intensities recorded for several  $M_w$  4.0-4.5 potentially induced earthquakes in Oklahoma, Kansas and Texas are not low at distances less than 10km. Shallow depths of induced earthquakes may cause low intensities at far distances [Atkinson *et al.*, 2015]. Hence, it is hard to distinguish these effects if the stress drops of induced earthquakes are not estimated using other independent and accurate approaches.

Here we estimate the stress drops of potentially induced earthquakes using the spectral ratio approach. The multiple highly-similar earthquakes enable us to separate the source effect from the propagation and site effects. We apply this approach to the Guy-Greenbrier sequence in central Arkansas and another induced seismicity sequence near Azle, Texas. We use two source models and the bootstrapping approach for a better understanding of the uncertainties in stress drops. Compared to the Brune’s source model, the Boatwright’s source model usually leads to smaller uncertainties and lower stress drop estimates. Nevertheless, we find that both induced seismicity sequences have comparable stress drops with the stress drops of tectonic earthquakes estimated by the spectral ratio approach. Our results do not support low stress drops for predicting ground motions from potentially induced earthquakes in the central United States.

### **Implications of Faulting Regimes on Required Pore-pressure Change for Induced Seismicity in the Central and Eastern U.S.**

HOSSEINI, S. M., University of Southern California, Los Angeles, CA, USA, seyedmeh@usc.edu; AMINZADEH, F., University of Southern California, Los Angeles, CA, USA, faminzad@usc.edu; HAJNASSER, Y., University of Southern California, Los Angeles, CA, USA, hajnasse@usc.edu

We utilize Mohr-Coulomb failure criteria to provide a regional and spatial characterization of the required pore-pressure change for shear failure along faults at different depths and faulting regimes. Based on the developed formulation, we observe that by assuming a consistent initial pore-pressure regime through depth, *i.e.* hydrostatic pore-pressure gradient, with an increase in depth, the required pore-pressure change for shear failure increases. In this study, we show that as the faulting regime changes from normal faulting to strike-slip faulting and thrust

faulting, the required pore-pressure change for shear failure increases. We use the well-known  $A\phi$  parameter to examine the faulting regime and to assess the regional change in pore-pressure required for shear failure in the Central and Eastern U.S. and South-Eastern Canada. The  $A\phi$  parameter ranges from 0 for uniform horizontal extension, to 1.5 for strike-slip faulting and to 3 for uniform compression. We find that from the South-Central U.S. (primarily strike-slip focal mechanisms;  $A\phi$  between 1 and 2) to the North-Eastern U.S. and South-Eastern Canada (mostly thrust faulting,  $A\phi$  between 2 and 3), the required pore-pressure change for shear failure increases. We conclude that at the regional scale from the Central U.S. to North-Eastern U.S. and South-Eastern Canada the required pore-pressure change for shear failure increases. Similarly, the required pore-pressure change for shear failure increases with depth. Furthermore, this study shows that for a given amount of injected volume, the value as well as the areal extent of the critical pore-pressure increase are highly dependent on the faulting regime and injection depth. We observed that by going from normal faulting regime to thrust faulting regime, the value of critical pore-pressure change increases while its areal extent decreases. These findings can be used towards a comprehensive workflow for induced seismicity risk assessment.

### **Influence of Industrial and Tectonic Factors on Fluid-Injection Induced Earthquakes**

McGARR, A., US Geological Survey, Menlo Park, CA, USA, mcgarr@usgs.gov

The contribution to seismic hazard from fluid-injection induced earthquakes has become significant in recent years. In contrast to hazard from natural seismicity, which cannot be changed, the hazard from induced earthquakes can be reduced. Mitigating the hazard of induced seismicity, however, requires an understanding of the roles played by industrial and tectonic factors. It is clear that the recent increase in seismicity in the central U.S. is the result of industrial activities, primarily the disposal of wastewater associated with modern methods of producing oil and gas from unconventional reservoirs. Whereas the rate of occurrence of fluid-injection induced earthquakes appears to be controlled by the rate of injection down wells that are prone to inducing earthquakes, the question of maximum magnitude is still not settled. Although it has been argued that the total volume of injected fluid imposes an upper bound on the maximum magnitude or seismic moment, it has also been proposed that tectonic factors are what limit magnitudes. The proposed scenario is that an injection operation triggers a large tectonic earthquake. This scenario, however, can be discounted because crustal strength increases with depth and earthquake rupture has a tendency to extend from stronger to weaker regions, but not vice versa (Das and Scholz, Nature, 1983). Injection depth intervals and nearly all induced earthquakes are in the top 5 or 6 km whereas large tectonic earthquakes have hypocenters in the range 10 to 15 km. Thus, triggering a large tectonic earthquake by fluid injection is highly unlikely. This leaves injected volume as the most likely factor limiting the maximum magnitude of fluid-injection induced earthquakes. In contrast, a number of source processes of fluid-injection induced earthquakes are controlled primarily by the crustal state of stress and strength, including focal mechanism and stress drop, both of which influence ground motion.

### **Induced Earthquakes in the 20th Century: Connecting the Dots**

HOUGH, S. E., US Geological Survey, Pasadena, CA, USA, hough@usgs.gov; PAGE, M. T., US Geological Survey, Pasadena, CA, USA, mpage@usgs.gov

Several lines of evidence suggest that most of the  $M_w \geq 3.5$  earthquakes in Oklahoma during the twentieth century, including the  $M_w$  5.7 El Reno earthquake of 9 April 1952, were likely induced by wastewater injection and possibly secondary oil recovery operations, as they exhibit statistically significant temporal and spatial correspondence with permitted disposal wells. An archival search for accounts of the El Reno event unearthed a newspaper article published immediately following the earthquake regarding a prominent Oklahoma City petroleum geologist, W.H. Atkinson, who took out a rare earthquake insurance policy less than 60 days before the earthquake struck. We describe the historical context for this intriguing coincidence. We present a retrospective of oil industry practices in the early- to mid-twentieth century, gleaned from court records and other industry reports, that potentially bear on the interplay between oil exploration activities and earthquakes in the Oklahoma City region. Additionally, an archival search reveals newspaper articles reprinted widely throughout the United States in the five years prior to 1952 about both moderate earthquakes and dramatic ground subsidence in a number of oil and gas-producing regions, including the Po Valley in Italy, the Wilmington oil field in southern California, and the Texas panhandle. By the late 1950s, at least a few researchers, including Charles Richter, suggested or hinted at the possibility of earthquakes induced by oil/gas production. We suggest that earthquakes in the late 1940s through 1951 could plausibly have alerted geologists such as Atkinson to the possibility of induced earthquakes by the time of the El Reno earthquake, although we find no

evidence that the potential for induced earthquakes was recognized by industry at that time.

### **Moment Tensor Inversion for the Induced Earthquakes in the Western Canadian Sedimentary Basin**

ZHANG, H., University of Calgary, Calgary, Canada, hongliang.zhang@ucalgary.ca; EATON, D. W., University of Calgary, Calgary, Canada, eatond@ucalgary.ca

Earthquake source mechanisms can provide important clues to discriminating between natural and induced events. In this study, we calculate moment tensors of one M 5.3 natural event and eight recent induced earthquakes with magnitudes ranging between M 3.2 and M 4.4 in the Western Canadian Sedimentary Basin to investigate physical differences between natural and induced earthquakes. Full moment tensor solutions are obtained by adopting a waveform-fitting procedure based on a 1-D transversely isotropic velocity model. According to the inversion results, nearly all the induced events exhibit a shallower focal depth ranging from 2 to 8 km, which is close to or a slightly deeper than the injection depth during hydraulic fracturing or wastewater disposal. In addition to a dominant double-couple component, most induced events show significant non-double-couple components (> 25%) within the inverted moment tensor. Elastic moduli changes due to the brittle damage production at the source, presence of multiple intersecting fractures, dilatant jogs created at the overlapping areas of multiple fractures, or non-planar pre-existing faults may explain the non-DC components for induced events. To test the effects of the accuracy of velocity model and noise level on the moment-tensor inversion results, a set of sensitivity tests based on synthetic data are performed, which suggests that spurious non-double-couple components are negligible if the signal to noise ratio exceeds 10 and if the 1-D model differs from the true velocity structure by less than 5%.

### **Trying to Discriminate Between Natural and Anthropogenic Earthquakes Recorded at Mt. Amiata Volcano (Italy)**

BRAUN, T., Istituto Nazionale di Geofisica e Vulcanologia, Arezzo (AR) Italy, thomas.braun@ingv.it; SPINELLI, R., Enel Green Power, Pisa (PI) Italy, rebecca.spinelli@enel.com

The increasing population and the society's increasing energy demand implicates that production plants move noticeably closer to the inhabited areas. Dense seismic networks and arrays reveal that anthropogenic activities—as *e.g.* extraction and reinjection of fluids—can induce or trigger seismic activity. This becomes significant in geothermal areas where the hypocenters of the natural seismicity are often at a similar shallow depth level as the human operations.

In Italy the geothermal area of Mt. Amiata volcano is characterized by a high geothermal gradient, extensive fracturing and high porosity values, and can therefore be classified as a Hydrothermal System (HS). Geothermal exploitation at Mt. Amiata started in 1959 by drilling relatively shallow wells (<1000m) for the extraction of vapor and reinjection of cold water, using the natural fracture system of the rock volume for the circulation of the fluids. Due to a general pressure decrease inside the reservoirs during the 80s' the exploitation depths was deepened into a second geothermal reservoir down to a level of 2500–3500 m.

Compared to the “normal” seismicity rate in the Apennines, the number of earthquakes observed in the Tuscan geothermal fields is very low. For the last 30 years less than 300 seismic events have been reported at Mt. Amiata inside an area with a radius of 20 km around the power plant. The high heat flow and the consequential ductile behavior of the upper crust may be the reasons for this low seismic activity.

The strongest earthquake ever recorded at a geothermal field in Italy was the M3.9 event of Apr 01, 2000, located at 4 km depth beneath the small village of Piancastagnaio. The shallow hypocenter, close to the geothermal production depth, and the WNW-ESE normal fault mechanism are coherent with the seismotectonics of the area. It becomes therefore a big challenge to discriminate in the Tuscan geothermal areas between natural and anthropically triggered seismicity.

---

## **The M7.1 Iniskin Earthquake, Alaska**

Oral Session · Wednesday · 7:30 PM · 20 April · Tuscany A  
Session Chair: Mike West

---

### **Perspectives on the Mw7.1 Iniskin Earthquake**

WEST, M., University of Alaska, Fairbanks, AK USA, mewest@alaska.edu; GARDINE, M., University of Alaska, Fairbanks, AK USA, mgardine2@alaska.edu; RUPPERT, N., University of Alaska, Fairbanks, AK USA, naruppert@alaska.edu; TAPE, C., University of Alaska, Fairbanks, AK USA, ctape@alaska.edu; HOLTkamp, S., University of Alaska, Fairbanks, AK USA, sgholtkamp@alaska.edu; FREYMUELLER, J., University of Alaska, Fairbanks, AK USA, jfreymueller@alaska.edu; ABERS, G., Cornell University, Ithaca, NY USA, abers@cornell.edu

edu; HOLTkamp, S., University of Alaska, Fairbanks, AK USA, sgholtkamp@alaska.edu; FREYMUELLER, J., University of Alaska, Fairbanks, AK USA, jfreymueller@alaska.edu; ABERS, G., Cornell University, Ithaca, NY USA, abers@cornell.edu

The  $M_w$  7.1 earthquake on January 24, 2016 was the largest intermediate-depth earthquake ever recorded in mainland Alaska and produced the most significant shaking in the Cook Inlet region in half a century. The earthquake occurred in the subducting Pacific Plate at a depth of 125km. The earthquake ruptured a natural gas line resulting in an explosion and fire that consumed four homes. Additional structural damage was primarily the result of slumping soils. It occurred at the edge of a long-recognized cluster of intermediate-depth earthquakes, with a similar down-dip minimum stress direction observed in prior earthquakes. It was larger however than any previously identified earthquake in this region. From 2001 to 2014 there were no intermediate-depth M6+ earthquakes in Alaska east of the Fox Islands. Since July 2014, there have been four including this one. The Iniskin earthquake aftershock zone extends ~60km northeast and abuts the hypocenter of M6.4 earthquake six months prior, suggesting some relationship. Static displacements are largest 100 km east on the Kenai Peninsula. Ground motion were highly variable and consistent with the directionality of the source. Strong motion records corroborate felt reports of moderate shaking above the hypocenter and significant influences from regional structures including the Cook Inlet sedimentary basin. Significant population centers, and the limited damage, were all at least 100 km or more from the epicenter. This presents two significant public policy challenges. The first is the gross misperception that individuals experienced, and infrastructure survived, the near-field forces of a M7+ earthquake. Instrumental records and felt reports demonstrate clearly that this is not the case. Second, a M7.1 earthquake at intermediate depth, combined with comparable M6+ earthquakes in the past few years necessitate a re-evaluation of the maximum magnitude and frequency of intermediate depth earthquakes across southern Alaska.

### **Does the M7.1 Iniskin Earthquake Change Alaska Seismic Hazard Maps?**

CRAMER, C. H., CERi, Univ. of Memphis, Memphis, TN USA, ccramer@memphis.edu

Earthquake ground motions expected from future earthquakes depend on ground motion models (GMMs—attenuation relations). Earthquake ground motion observations have been limited in Alaska due to the low number of recording stations. The coming of USArray to Alaska potentially changes this by significantly increasing the number of observations and spatial coverage. The January 24, 2016 M7.1 Iniskin earthquake is an example of this. The Iniskin earthquake is an in-slab event at the southwest end of Cook Inlet that ruptured unilaterally to the NE toward Anchorage. The observed ground motions from the Iniskin earthquake are high at PGA, 0.2s, and 1.0s compared to the in-slab GMMs of Youngs *et al.* (1997) and Atkinson and Boore (2003) used in the U.S. Geological Survey's 2007 Alaska seismic hazard maps. Stations with azimuths between 30° and 80° from the earthquake show consistently higher values out to 800 km than other azimuths due to rupture directivity. The remaining observations tend to fall closer to the higher predictions of the Youngs *et al.* GMM, except within 300 km where instrument clipping has eliminated the higher observations in the direction of rupture. The estimate of Brune stress drop from event corner frequency and magnitude is  $15 \pm 5$  MPa for the mainshock and about 10 MPa for the Mb 4.8 and 4.7 aftershocks, which are high for the typically 5 or less MPa for subduction and in-slab earthquakes worldwide (Seno, 2014). Stachnik *et al.* (2004) also show higher mantle wedge Q beneath Cook Inlet near Anchorage. Higher than average earthquake stress drops and mantle wedge Q beneath Cook Inlet can help explain the high ground motion observations from the Iniskin earthquake. If these ground motion observations are typical for the Alaska subduction zone, they suggest that subduction zone GMMs for Alaska should be higher than worldwide subduction zone GMMs and the 2007 Alaska seismic hazard maps should be revised upwards in these hazard estimates.

### **M7.1 Iniskin Earthquake Site Response of a Downhole Array Site in Anchorage, Alaska**

THORNLEY, J., Golder Associates, Inc, Anchorage, AK USA, john\_thornley@golder.com; DUTTA, U., University of Alaska Anchorage, Anchorage, AK USA, udutta2@uaa.alaska.edu; YANG, J., University of Alaska Anchorage, Anchorage, AK USA, zyang2@uaa.alaska.edu

Alaska's largest city, Anchorage, is located within a seismically active region including the Pacific Megathrust subduction zone and crustal faults on the North American Plate. A complex geology of glacial till, Bootlegger Cove Clays, and alluvium exists within the Anchorage area. A downhole array, with three component accelerometers placed at seven depths from the surface to 61 meters

below ground, has been recording strong ground motions since 2004. On January 24, 2016 the  $M_w$  7.1 Iniskin earthquake shook the Cook Inlet region and provided a unique opportunity to evaluate the response of different geologic units within the Downhole array. The recorded ground motions at the Downhole array from the Iniskin earthquake have been analyzed as part of a systematic approach to evaluate the attenuation relationships and impedance characteristics of the soil column of the Anchorage basin. A one-dimensional equivalent linear model has been developed and calibrated using measured ground motions. Recent site-specific shear wave velocity profiling to 61 meters depth and evaluation of shear wave velocity correlations from historic CPT data provide additional improvements and validation to the model. Previously developed models lacked the data support and measured ground motions have not allowed as detailed an analysis to be performed. With the new shear wave velocity profiling, coupled with the ground motions measured at the Downhole array, a significantly improved model has been validated for use as a tool to assist in the evaluation of the response of the Anchorage Basin soils. In addition to the model improvement for the Downhole array, a comparison is performed between the measured ground motions at a depth of 61 meters, located within dense glacial till and the ground motions measured at the hard rock site K216. The results of this comparison provide guidance for the use of the ground motions recorded at 61 meter depth as input ground motions.

#### **The 2016 Mw7.1 Iniskin, Alaska, Earthquake as seen by High-rate GPS and Early Warning Potential**

GRAPENTHIN, R., New Mexico Tech, Socorro, NM USA, rg@nmt.edu; FREYMUELLER, J. T., University of Alaska, Fairbanks, AK USA, jfreymueller@alaska.edu

The January 24, 2016,  $M_w$  7.1 Iniskin Earthquake in Cook Inlet, Alaska, occurred within a dense network of high-rate (1Hz, 5Hz) GPS stations operated by UNAVCO as part of the Plate Boundary Observatory. The normal faulting, intra-plate event was located at a depth of 123 km within the subducting Pacific Plate. The location of the event, just underneath the western shore of Cook Inlet, results in excellent azimuthal coverage with GPS stations on Kodiak Island, the Kenai Peninsula, and, of course, on the Western side of Cook Inlet.

Here, we present static and kinematic slip models for the event derived from GPS observations. As we expect to resolve the reflected seismic energy due to the Cook Inlet Basin and will investigate its impact on kinematic slip models and resulting magnitude estimates. We put the geodetic model in context of moment tensor solutions and aftershock distribution. So far (Feb/03/2016), the aftershocks did not exceed  $M_w$  5.0. We explore the possibility of excess strain release due to episodic slow slip on the subduction zone interface.

This event is a first, albeit deep, earthquake of sufficient size with outstanding geodetic high-rate coverage to create a signal large enough to be resolved in real-time. Hence, we will replay the position waveforms through the Geodetic Alarm System (G-larmS), a Python module that estimates slip on a finite fault and derives earthquake magnitude in real-time within earthquake early warning applications. The Iniskin earthquake provides an end member test to the feasibility of the current geodetic network to characterize events of  $M_w$  7.0 and larger that might be caused by shallower strain release on the subduction interface.

---

## **Advances in Noninvasive Approaches to Characterizing Seismic Site Conditions**

Poster Session · Wednesday · 20 April · Tuscany F

---

### **Applicability of Exploration Geophones to Large Scale Passive Surface Wave Methods**

HAYASHI, K., Geometrics, San Jose, CA, USA, khayashi@geometrics.com

S-wave velocity ( $V_s$ ) to a depth of several hundred meters to several kilometers have large effect on surface ground motion and the methods estimating  $V_s$  at such depths draw a lot of attention. Passive surface wave method, such as microtremor array measurements and seismic interferometry, are getting popular in the  $V_s$  investigation. Penetration depth of the passive surface wave methods depends on the wave length or frequency of surface waves used in the investigations. Generally speaking, investigations to the depths of 10, 100m, 1, and 10 km require frequencies down to approximately 5, 2, 0.5, and 0.1 Hz respectively. Velocity sensors used in exploration geophysics, so called geophones, are inexpensive and easy to use but have been only applied to shallow (< 100 m) investigations since their natural frequency is higher than 1 Hz. Much expensive, fragile, and difficult to use accelerometers or velocity meters, so called broadband sensors, have been used in deeper investigations. The passive surface wave methods will be performed easily and inexpensively if the geophones could be applied to lower frequency range

than the natural frequency. We carried out comparative tests between the broadband sensors and the geophones in South San Francisco Bay Area. The geophones with the natural frequency of 2 and 10 Hz are compared against a broadband sensor. Three pairs of sensors (2 geophones and one broadband sensor) recorded vertical component of ambient noise with several different sensor separations from several meters to several kilometers. Approximately one hour of ambient noise was recorded and coherences were calculated and compared. In conclusions, the 2 and 10 Hz geophones yielded almost identical coherences to the frequencies of 0.2 and 2 Hz respectively compared with broadband sensors. It indicates that the applicability of exploration geophones to large scale passive surface wave methods and enable us to investigate deep  $V_s$  structures much easily and inexpensively.

### **Mapping the Geometry of the San Leandro Block, Hayward Fault Zone Using Geologic and Geophysical methods; California State University, East Bay Campus**

McEVILLY, A. T., California State University, East Bay, Hayward, CA, USA, adrian.mcevilly@csueastbay.edu; STRAYER, L. M., California State University, East Bay, Hayward, CA, USA, luther.strayer@csueastbay.edu; ABIMBOLA, A., California State University, East Bay, Hayward, CA, USA, ayoola.abimbola@csueastbay.edu; CHAN, J. H., California State University, East Bay, Hayward, CA, USA, joanne.chanhoyi@gmail.com

California State University, East Bay (CSUEB), located in Hayward, California, lies atop the San Leandro block (SLB) in the Hayward fault zone. The SLB is a J-K aged lithotectonic assemblage dominated by gabbro and intercalated with minor volcanics and sediments. It is bound by the subparallel northwest-trending western Hayward and eastern Chabot (CF) faults and pervasively cut by anastomosing secondary faults. The block itself is ~30 km along strike and 2-3 km wide. Previous studies suggest the block dips steeply to the northeast and extends to a depth of at least 7 km. In May of 2015, as part of an ongoing collaborative effort led by the USGS to create a 3D velocity model of the San Francisco Bay Area, researchers from CSUEB and the USGS conducted a seismic survey on the CSUEB campus. The primary goal of this pilot study was to locate the trace of the CF on the CSUEB campus and to determine bedrock depth. We deployed a 60-channel, 300m profile using 4.5Hz sensors spaced at 5m intervals. Active seismic sources were used at each geophone location. A 226kg accelerated weight-drop was used to generate P and Rayleigh waves for P-wave tomography and multichannel analysis of surface waves (MASW), and a 3.5kg sledgehammer and block were used to generate S and Love waves for S-wave tomography and multichannel analysis of Love waves (MALW). Preliminary P-wave tomography,  $V_s/V_p$ , Poisson's Ratio, MASW, and MALW results from this pilot study suggest the location of an eastward-dipping CF as well as the presence of a high-velocity unit at about 20m depth, presumably an unmapped sliver of bedrock from the San Leandro block. Further studies planned for the spring of 2016 include additional seismic lines and surface mapping along the Chabot fault on and near the CSUEB campus. These new data will be integrated with LiDAR imagery and existing geological and geophysical data to create a 3-dimensional model of the portion of the SLB underlying the CSUEB campus in Hayward, California.

### **Advanced Concepts for Microtremor Measurements in Order to Characterize Site Conditions in the Course of Seismic Hazard Analyses and Microzonation**

SPIES, T. S., BGR, Hannover, Germany, thomas.spies@bgr.de; SCHLITTENHARDT, J. S., BGR, Hannover, Germany; IBS-VON SEHT, M. I., BGR, Hannover, Germany; HORSTMANN, T. H., BGR, Hannover, Germany; MARJIYONO, M., Badan Geologi, Bandung, Indonesia; SOEHAMI, A. S., Badan Geologi, Bandung, Indonesia; BRÜSTLE, A. B., LRP, Mainz, Germany; SCHMIDT, B. S., LRP, Mainz, Germany

Passive seismic methods, *i.e.* microtremor observations, are widely used in geo-technical practice but limitations and extensions are still the focus of scientific discussion. The present work outlines the refinement of two effective procedures: 1) derivation of detailed depth profiles of S wave velocity mainly based on array measurements at selected sites and 2) characterization of lateral changes between the array sites based on single station measurements (H/V spectra).

As a reference used in practice, triangular arrays with 4 uniaxial vertical sensors are used in combination with single 3 component sensors. For further development of equipment and evaluation procedures larger arrays of up to 10 sensors of 3 components are used. The use of additional seismic data from active seismic experiments and the use of geological data from geological mapping and borehole investigation is tested.

Results obtained with the 4 sensor arrays show that beyond an array aperture of about 60 m correlation between signals vanished due to technical specifications indicating that the investigation is limited roughly to this depth. As most current building codes demand values of shear wave velocity only down to 30 m depth, the seismic soil classes of building codes can be determined. Arrays



consisting of 10 sensors are able to deliver structures down to some 100 meters. The benefit of the integration of additional data is clearly elaborated. Especially the dispersion curves of surface waves are determined with higher reliability: mode mixing is avoided, the frequency range extended and the non-uniqueness of solutions reduced. Because conventional geological borehole data seldom contain elastic properties, they are of limited value as constraint for inversion or for calibration of S wave velocities. Thus vertical seismic profiling is strongly recommended as an extension to conventional geological description of boreholes.

#### **Spatial Variability of VS in Quaternary Alluvium**

WAGSTAFFE, D., Langan Treadwell Rollo, San Francisco, CA, USA, wagstaffe@langan.com; MOSS, R. E. S., Cal Poly, San Luis Obispo, CA, USA, rmoss@calpoly.edu

When designing lifelines (e.g., highways, pipelines, aqueducts) knowing the spatial continuity of the soil properties is important for planning subsurface investigations, siting foundation elements, designing against seismic loads, and performing system-level risk analysis. In this research testing was carried out to assess the spatial variability of a Quaternary Alluvium site using passive surface wave methods. Ten meter diameter circular arrays were marched across at 310 m long profile. Ambient surface waves were measured at 59 locations along the profile and analyzed using SPAC (spatial autocorrelation) to develop Rayleigh wave (VR) dispersion curves. The dispersion curves were inverted to estimate the Shear wave (VS) velocity profile. The data at each location was then depth averaged and the spatial continuity was assessed using geostatistical tools. Semi-variograms gave the clearest results, showing the range (the distance at which the maximum covariance is reached) to be on the order of 100 m for 15 m and 30 m depth averaged VS in Quaternary Alluvium along the Central Coast of CA. This is compared to European and Russian code recommendations for similar lifeline applications herein.

#### **Effects of Poisson Ratio and Density Values on Vs Profiles and Vs30 at ARRA-funded Sites**

YONG, A., U.S. Geological Survey, Pasadena, CA, USA, yong@usgs.gov; BOATWRIGHT, J., U.S. Geological Survey, Menlo Park, CA, USA; MARTIN, A., GEOvision, Inc., Corona, CA, USA, amartin@geovision.com

The 2009 American Recovery and Reinvestment Act (ARRA) funded geophysical site characterizations at 191 seismographic stations in California and in the central and eastern United States. The principal methods applied were non-invasive, passive- and active-source, and body- and surface-wave techniques, including: Array Microtremor (AM), Multi-channel Analysis of Surface Waves (MASW; Rayleigh and Love waves), Spectral Analysis of Surface Waves (SASW), Refraction Microtremor (ReMi), and P- and S-wave refraction tomography. Depending on the apparent geologic or seismic complexity of the site, field crews applied one or a combination of these methods to estimate the shear-wave velocity (Vs) profile and calculate Vs30, the time-averaged Vs to a depth of 30 meters. We study the inter- and intra-method variability of Vs and Vs30 at each seismographic station where more than one technique was applied. For each site, we find both inter- and intra-method variability in Vs30 remain insignificant (5–10% difference) despite substantial variability observed in the Vs profiles. We also find that reliable Vs profiles are best developed using a combination of techniques, e.g., surface-wave Vs profiles correlated against P-wave tomography to constrain variables [Poisson's ratio ( $\nu$ ) and density ( $\rho$ )] that are typical depth-dependent parameters used in modeling Vs profiles. Initial tests on synthetic data indicate Vs30 can vary by as much as 20% when we vary  $\nu$  assignments between 0.1 and 0.495 (dry soil to saturated cohesive soil), demonstrating that it is important to constrain the depth of high  $\nu$  for saturated soils. When we vary  $\nu$  to within the realistic range of 0.25–0.35 (dry soil), we find Vs30 vary by only 6%. We find  $\rho$  assignments affect Vs30 values only by a few percent. We continue our study with the ARRA-funded measurements and report our findings.

#### **Insights from the New Zealand Strong Motion Site Meta-Data: Update for the 2015 Strong Motion Database**

KAISER, A. E., GNS Science, Lower Hutt, New Zealand, a.kaiser@gns.cri.nz; VAN HOUTTE, C., GNS Science, Lower Hutt, New Zealand, c.vanhoutte@gns.cri.nz; PERRIN, N., GNS Science, Lower Hutt, New Zealand, n.perrin@gns.cri.nz; WOTHERSPOON, L., University of Auckland, Auckland, New Zealand, l.wotherspoon@auckland.ac.nz; MCVERRY, G., GNS Science, Lower Hutt, New Zealand, g.mcverry@gns.cri.nz; COUSINS, J., GNS Science, Lower Hutt, New Zealand, j.cousins@gns.cri.nz

The 2015 New Zealand strong-motion database provides a wealth of new strong motion data for engineering applications. An important component of this

database is the compilation of new site meta-data, describing the soil response at GeoNet strong motion stations. This data is intended to guide efforts to develop and test new and existing ground motion prediction models in New Zealand, in particular allowing re-examination of the most important site parameters that control site response in a New Zealand setting.

Current New Zealand GMPEs (McVerry *et al.* 2006; Bradley 2012) use either site classification according to New Zealand design standards (NZS1170.5) or a combination of Vs30 and Z1.0, typically based on rough estimates only. We have compiled these three key site parameters as well as the fundamental site period (Tsite) for the 460 GeoNet stations that recorded significant historical ground motions. Tsite has previously been shown to be a potentially useful parameter for ground motion prediction based on a small local database. In addition, we have assigned a quality estimate (Quality 1–3) to these parameters to provide a qualitative estimate of the uncertainty. New good-quality Tsite estimates have largely been obtained from newly available HVSR amplification curves and spectral ratios from inversion of regional strong motion data and have been reconciled with available geological information. Good quality Vs30 estimates, typically in urban centres, have also been incorporated following recent studies using passive seismic methods (MASW, ReMi etc.). Where site-specific measurements of Vs30 are not available, Vs30 is estimated based on surface geology following the national Vs30 maps of Perrin *et al.* (2014).

We discuss preliminary insights from the database so far, comparing the new strong motion dataset with current GMPEs, as well as investigating the relationship between key site parameters in New Zealand conditions compared to global relationships.

#### **Estimation of Site Amplifications at the K-Net Ocean Bottom Seismograph Stations in the Sagami Bay Area based on Spectral Inversion Method**

DHAKAL, Y. P., NIED, Tsukuba, Japan, ydhakal@bosai.go.jp; SUZUKI, W., NIED, Tsukuba, Japan, wsuzuki@bosai.go.jp; KUNUGI, T., NIED, Tsukuba, Japan, kunugi@bosai.go.jp; AOI, S., NIED, Tsukuba, Japan, aoi@bosai.go.jp

Previous studies in the Nankai Trough area in Japan found that the amplitudes of the ground motions at the ocean bottom seismographs (OBS) are significantly larger than those recorded at the land stations at equal distances. The studies elucidated that the main reason for the large amplitude motions at the OBS is the large amplification effects of low velocity layers beneath the stations. The studies have, therefore, recommended corrections for the estimation of magnitudes using the OBS to be consistent with those based on the land stations. A large scale installation of cable linked network of OBS and pressure gauges (S-net) is undergoing in the Japan Trench area for more accurate and rapid early warning of earthquake and tsunami. It is important to devise a methodology for accurate magnitude estimation applicable to the S-net seismic data. In this paper, we obtain site amplifications by spectral inversion method at the K-NET OBS in the Sagami Bay area. There are six such stations, namely KNG201 through KNG206, in the Sagami Bay area. In the inversion, we also included land stations in the Kanto area. Theoretical amplification factors based on PS-logging data at the KNGH21 KiK-net site are used as constraints to minimize the tradeoff between the various parameters. We used recordings from moderate events ( $M_w$  4 ~ 6) and epicentral distances between 30 to 300 km. The PGAs are mostly < 100 gal for the recordings. The obtained results show that the sites at the Sagami Bay area experience amplifications by five to ten folds compared to the reference KiK-net site in wide frequency ranges. These results are similar to those reported for the Tonankai sea floor areas in Japan. We also estimated the magnitude of the events based on the inverted source spectra and Qs values to check the reliability of the obtained results. We found that the estimated magnitudes agree well with the F-net  $M_w$  and the Qs values are in the range of previous studies.

#### **Site Effects Assessment in Almaty (Kazakhstan) in Light of Destructive Past Earthquakes**

PAROLAI, S., Helmholtz Center Potsdam–GFZ German Research Center for Geosci, Potsdam, Germany, parolai@gfz-potsdam.de; PILZ, M., Swiss Seismological Services, Swiss Federal Institute of Tec, Zurich, Switzerland, pilz@gfz-potsdam.de; ABAKANOV, T., Institute of Seismology of the Republic of Kazakhstan, Almaty, Kazakhstan, seismology@seismology.kz; SILACHEVA, N., Institute of Seismology of the Republic of Kazakhstan, Almaty, Kazakhstan, silacheva\_nat@mail.ru; KULBAYEVA, U., Institute of Seismology of the Republic of Kazakhstan, Almaty, Kazakhstan; KRAVCHENKO, N., Institute of Seismology of the Republic of Kazakhstan, Almaty, Kazakhstan; RAYIMBEK, B., Institute of Seismology of the Republic of Kazakhstan, Almaty, Kazakhstan; ORUNBAEV, S., CAIAG Central Asia Institute for Applied Geosciences, Bishkek, Kyrgyzstan, s.orunbaev@caiag.kg; MOLDOBEKOV, B.,



CAIAG Central Asia Institute for Applied Geosciences, Bishkek, Kyrgyzstan, b.moldobekov@caiag.kg

During the past two centuries, the city of Almaty in Kazakhstan has suffered significant damages caused by several large earthquakes. A crucial step towards preparedness for future events, the mitigation of earthquake risks and the definition of the optimal engineering designs for civil structures involves the accomplishment of site response studies. During this project, a temporary seismological network of 16 stations was installed in the city of Almaty to accurately identify local variations of the site response at different locations. Moreover, single-station noise recordings were collected at more than 220 sites within the city, which can be used for estimating the resonance frequencies and for evaluating the expected level of ground motion at each site. This information is complemented by three array measurements of ambient seismic noise in order to estimate local attenuation and shear-wave velocity profiles, an essential parameter for evaluating the dynamic properties of soil, and to characterize the corresponding sediment layers at each site. The results indicate that thick layers of soft clay deposits give rise to high amplification values at low frequencies particularly in areas which have been destructed already by previous strong events.

#### Characteristics of Microtremor Observed near Quay Walls—Example of Observed Records at Yaizu Fishing Port, Japan

SUZUKI, H. S., OYO Corp., Tsukuba, Ibaraki, Japan, suzuki-haruhiho@oyonet.oyo.co.jp; MANABE, S. M., OYO Corp., Tsukuba, Ibaraki, Japan, manabe-syunpei@oyonet.oyo.co.jp; NAGATA, S. N., Shizuoka Pref. Gov., Shizuoka, Shizuoka, Japan, shinya1\_nagata@pref.shizuoka.lg.jp; YAMADA, T. Y., Shizuoka Pref. Gov., Shizuoka, Shizuoka, Japan, takahiro1\_yamada@pref.shizuoka.lg.jp; NAGASAKA, Y. N., PARI, Yokosuka, Kanagawa, Japan, nagasaka-y@pari.go.jp; NOZU, A. N., PARI, Yokosuka, Kanagawa, Japan, nozu@pari.go.jp

Earthquake ground motions may vary significantly due to the variation of site amplification characteristics even within small regions. The observation of earthquake ground motions is a useful tool for the evaluation of site amplification in a seismically active regions, but it is difficult to perform a very dense observation practically. On the other hand, a lot of studies have been carried out on the issue of site amplification evaluation using microtremor measurements. In the port areas in Japan, microtremor measurements have been performed in order to evaluate seismic performance of coastal structures.

Although it is desirable that the measurement positions should be as close as possible to the target structure in order to estimate of the site amplification characteristics accurately, the data obtained very close to a structure such as a quay wall may be influenced by the structure itself. The effects of coastal structure on microtremor has not been studied sufficiently.

In this study, measurements of microtremor were conducted at Yaizu fishing port, Japan, at a distance ranging from 0.5 to 30 meters from the face line of the coastal structures and the basic characteristic of microtremor observed near quay walls was examined. In addition to the peak frequency at 0.7 Hz which is presumably related to the site characteristics, the H/V spectra included peaks at lower frequencies, which can be attributed to the effects of quay walls, because the predominant direction was perpendicular to the quay walls. To detect peak frequencies related to the site characteristics, the observation should be conducted 30 m away from the face line and quay-wall-parallel components should be used.

#### Site Characterization at Napa Strong Motion Sites Using Tomography, MASW, and MALW

CHAN, J. H., USGS Earthquake Science Center, Menlo Park, CA, USA, jchan@usgs.gov; CATCHINGS, R. D., USGS Earthquake Science Center, Menlo Park, CA, USA, catching@usgs.gov; GOLDMAN, M. R., USGS Earthquake Science Center, Menlo Park, CA, USA, goldman@usgs.gov; CRILEY, C. J., USGS Earthquake Science Center, Menlo Park, CA, USA, ccriley@usgs.gov

The 24 August 2014  $M_w$  6.0 South Napa earthquake caused \$300 million in damage to private and commercial properties. Previous site response studies indicate that areas that experienced extensive structural damage are underlain by deposits with low  $V_{s30}$  values. The goal of our study was to evaluate shear-wave velocity to 30 m depth ( $V_{s30}$ ), which is considered a predictor of strong shaking from earthquakes, at six broadband seismometer sites. We used active-source seismic sources, up to 120 channels, and 4.5-Hz sensors to measure  $V_{s30}$  near broadband seismometers in the City and County of Napa and in the City of Vallejo. To increase the resolution of our data in the upper 30 m, we used 3-m geophone and shot spacing along each profile, which ranged in length from 85 to 260 m. We used a 226-kg accelerated weight-drop and a seisgun to generate P- and Rayleigh-wave sources and a 3.5-kg sledgehammer and block to generate S-wave sources. One of the six broadband sites is housed inside Napa Fire Station #3, where the

local surface geology consists of late Pleistocene to Holocene alluvium and alluvial fan deposits. Our study shows the average  $V_{s30}$  determined from multichannel analysis of surface waves (MASW) using Rayleigh waves method is 312 m/s, and the average  $V_{s30}$  from the multichannel analysis of Love waves (MALW) method is 340 m/s. Rayleigh wave velocities travel at approximately 92% of S-wave velocity, thus these average MASW and MALW  $V_{s30}$  values (312–340 m/s) are similar to those determined from S-wave tomography (375 m/s), which suggests the three methods are complimentary and can be highly useful in accurately evaluating site response.

#### Near Surface Shear Wave Velocity Measurements in the Sacramento-San Joaquin Delta

CRAIG, M. S., California State University, East Bay, Hayward, CA, USA, mitchell.craig@csueastbay.edu; HAYASHI, K., Geometrics, Inc, San Jose, CA, USA, khayashi@geometrics.com; SHULER, S. E., California State University, East Bay, Hayward, CA, USA, sshuler2@horizon.csueastbay.edu

Seismic surface wave surveys were performed at twelve sites in the Sacramento-San Joaquin Delta region, providing improved shear wave velocity ( $V_s$ ) models of the near surface and  $V_{s30}$  measurements. A method combining the MASW (Multichannel Analysis of Surface Waves) and MAM (Microtremor Array Measurement) methods provided depth penetration of 20 m to 40 m, depending on the site. The method was able to detect velocity reversals and surficial layers as thin as 1 m. Velocity models derived from surface wave surveys were in good agreement with lithologic sequences from soil borehole logs. Measured peak velocities were extremely low, ranging from 42 m/s to 150 m/s. Velocities of a deeper sand unit ranged from 220 m/s to 370 m/s. Measured average  $V_s$  from the surface to a depth of 30 m ( $V_{s30}$ ) ranged from 98 m/s to 257 m/s. Sites were assigned to NEHRP site classes D, E, and F, with assignments to class F based on the presence of a near-surface peat layer. All sites have soft near-surface soils and are liable to experience large ground accelerations in the event of a strong earthquake. At four of the sites, additional surveys were performed using the two-station spatial autocorrelation (SPAC) method, extending penetration depth to approximately 2000 m. Velocity was determined to frequencies as low as 5 Hz, 1 Hz, and 0.3 Hz using MASW, MAM, and 2ST-SPAC, respectively. Field tests at several of the sites indicate that near-surface seismic reflection data quality is good and that reflection profiling may be successfully conducted in the area using a relatively modest recording system.

#### Implementation of the Spectral Ratio Method on Data from a High-Density Seismic Experiment in the Los Angeles Basin

NG, R., California State Polytechnic University, Pomona, Pomona, CA, USA, raymondn@cpp.edu; POLET, J., California State Polytechnic University, Pomona, Pomona, CA, USA, jpolet@cpp.edu

We will present results of our investigation of site response and resonance within the Los Angeles Basin through the application of the Horizontal-to-Vertical (H/V) spectral ratio method. This method was applied to 3-component broadband waveforms from the Los Angeles Syncline Seismic Interferometry Experiment (LASSIE). LASSIE is a collaborative, temporary, and dense array of 73 broadband seismometers that were active for a two-month period from October until November 2014, transecting the Los Angeles basin from Long Beach to La Puente. We use the Geopsy software to measure lateral variations in the fundamental frequency and amplitude of the H/V spectral ratio. Data analysis and interpretation were conducted in accordance with the Site Effects Assessment Using Ambient Excitations (SESAME) guidelines. Results from our data analysis indicate an average fundamental period at the basin center of 6–9.5 s and additional peaks in the spectral ratio curves at much shorter periods for sites at the basin edge. Long period H/V ratio peak amplitudes range from 2–5.5, with the highest values measured for the greater Long Beach area. We will show profiles of the long period H/V amplitudes and fundamental frequencies across the LA Basin based on our spectral ratio analysis of the LASSIE data and interpret our results in the context of velocity profiles and site response results from other studies, as well as other models of shallow and deeper basin structure.

#### Interpreting Site Amplifications from Surface Wave Tomography

BOWDEN, D. C., Caltech, Pasadena, CA, USA, dbowden@caltech.edu; TSAI, V. C., Caltech, Pasadena, CA, USA, tsai@caltech.edu; LIN, F. C., Caltech, Salt Lake City, UT, USA, u0919412@utah.edu

Tracking the wavefronts of Rayleigh waves through ambient noise has been demonstrated to reasonably recover site amplification terms across the USArray (12–32 sec periods), as well as a very dense array in Long Beach, CA (0.5–1.5 sec periods). The maps provide empirical observations of the relative strengths of Rayleigh waves, for a given period, laterally across both city and country scales.

The methodology accounts for 2D propagation effects including attenuation, focusing and defocusing of the energy, and requires no assumptions about the structure at depth. Results correlate well with velocity models, and this provides an opportunity to test and understand shortcomings of both the models and method. We particularly focus on the tectonic and geologic structures that give rise to the observations, and the extent to which further 3D complexities such as topography and basin shape are represented in the amplifications. These measurements of surface waves are, however, fundamentally different from the site response terms traditionally estimated by vertically propagating waves in a 1D layered medium, and the relation between the two types of measurements is explored through comparisons of various datasets and simulations.

#### **Spatial and Temporal Variation in Ambient Seismic Noise Site Response in Charleston, South Carolina**

COBB, S. E., College of Charleston, Charleston, SC, USA, cobbse@g.cofc.edu; JAUME, S. C., College of Charleston, Charleston, SC, USA, jaumes@cofc.edu; ODUM, J., US Geological Survey, Golden, CO, USA, odum@usgs.gov; STEPHENSON, W., US Geological Survey, Golden, CO, USA, wstephens@usgs.gov

Previous ambient noise site response studies have revealed a prominent 1-2 Hz peak in horizontal-to-vertical spectral ratios (HVSR) on the Charleston peninsula. These studies have found that the amplitude of this response varies with surface geology and, at a few locations where sufficient long seismic recordings were collected, with time of day. The objective of this study is to use recently acquired (Summer 2015) array ambient seismic noise data to study the spatial and temporal variation of HVSR site response in Charleston. Ten arrays of up to ten seismometers (Nanometrics Trillium Compacts) placed throughout the greater Charleston area recorded up to 7+ hours of daytime ambient seismic noise. For each array, we computed HVSRs using 1 hour-long time segments when all of the seismometers in an array were recording. We then compared the stability of the 1-2 Hz HVSR peak both between instruments in each array and between 1 hour HVSRs for each instrument. Initial results suggest greater spatial variation in the amplitude of the 1-2 Hz HVSR peak within an array than temporal variation for an individual instrument. These results further suggest the observed spatial variation in the 1-2 Hz HVSR is a robust observation.

#### **Observation and Modeling of HVSR in Charleston, South Carolina: Implications for Earthquake Hazard on a Deep Coastal Plain**

JAUME, S. C., College of Charleston, Charleston, SC, USA, jaumes@cofc.edu; LEVINE, N. S., College of Charleston, Charleston, SC, USA, levinen@cofc.edu; BRAUD, A., College of Charleston, Charleston, SC, USA, braudas@g.cofc.edu

Horizontal to vertical spectral ratios (HVSR) of ambient noise collected in the greater Charleston, South Carolina area show consistent amplification at frequencies of 0.2 and 1-2 Hz. Here we examine the 1-2 Hz amplification in detail, both in its relation to damage in the 1886 earthquake and in reference to the expected response of coastal plain sediments beneath Charleston. First, those sites with lower amplification ( $<8$ ) cluster in the middle of the Charleston Peninsula on Quaternary surfaces and show little variation with time of day. Sites with higher ( $>8$ ) 1-2 Hz amplification occur at the edges of the Charleston Peninsula, primarily at locations on artificial fill, and can change by a factor 2 depending on time of day. We find the majority of high amplification sites were unoccupied during the 1886 earthquake, both explaining the apparent lack of site effects on URM structures and implying greater hazard in these "new" sections of Charleston in future events. We also compared this amplification with a newly compiled map of Quaternary and younger sediment thickness, but found no consistent relationship between Quaternary thickness and amplification. Finally, we also attempt to model this amplification by looking at the response of simple velocity models of the coastal plain sediments to point sources on the surface. We find the 1-2 Hz amplification (and its variation) has 3 sources: a) the  $f_2$  mode of the resonance of the entire  $\sim 800$  meter sediment column, b) an impedance contrast within the Tertiary near 75 meters depth, and c) both the thickness and average velocity of the Quaternary section. Our modeling results suggest that the greatest 1-2 Hz amplifications occur when all of these sources of amplification reinforce each other. This implies that simulations of the strong motion response in the Charleston region (and other similar locations?) need to consider the entire coastal plain sediment column, and not just the top 30-100 meters.

---

## **Earthquake Early Warning: Network Design, Implementation, Production and Outreach**

Poster Session · Wednesday · 20 April · Tuscany F

---

#### **Ground Motion Forecasting Using a Reference Station and Complex Site Response Functions Accounting for the Shallow Geology**

PILZ, M., Swiss Seismological Services, Zurich, Switzerland, pilz@gfz-potsdam.de; PAROLAI, S., GFZ German Research Center for Geosciences, Potsdam, Germany, parolai@gfz-potsdam.de

The distribution of damages due to recent earthquakes has shown that the effects of shallow geological structures on the level of ground shaking represent an important factor in engineering seismology. Whereas many previous studies have estimated local site amplification factors in the frequency domain, their application to the real-time modeling and forecasting of ground motion, of particular importance for regional early warning systems, is not yet fully established. Here we present a method for the real-time correction of frequency-dependent site response factors. The method does not only account for the modulus, but also for the changes in the signal phase related to local site conditions. The transformation of the complex standard spectral ratios to a causal recursive filter in the time domain allows for the forecasting of the waveforms for soft soil sites almost in real time when the signal is recorded at a reference site. When considering travel time differences of the various seismic phases between the hypocenter and the studied sites, the level of ground motion at soft soil sites with respect to arrival time, energy, duration and frequency content can be well constrained, even in cases of a high spatial variability of the amplification patterns.

#### **An Envelope Based Earthquake Early Warning Algorithm—Ground Motion Envelope Predictor (GMEP)**

KARAKUS, G., California Institute of Technology, Pasadena, CA, USA, gokcan@caltech.edu; HEATON, T. H., California Institute of Technology, Pasadena, CA, USA, heaton@caltech.edu

Conventional paradigm of earthquake early warning algorithms is based on pick times and amplitudes of ground motions. We propose an earthquake early warning algorithm, which is based on continuous monitoring of waveform envelopes, *i.e.*, envelopes of acceleration, velocity, and displacement. Our algorithm, which is named Ground Motion Envelope Predictor (GMEP), uses Bayesian grid search method to locate an earthquake, and Virtual Seismologist (VS) (Cua&Heaton) ground motion prediction equations to calculate magnitude. Then, GMEP assesses the accuracy of predictions using Bayesian classification. Input features to Bayesian classification are higher order statistics, *i.e.*, kurtosis and skewness, of residuals of ground motion envelopes after a prediction is made by GMEP. Kurtosis and skewness are robust ways of detecting the timing of wrong predictions. In order to assess the accuracy of amplitude predictions, we developed a novel method called Karakus-Heaton Moment for Signal Data (KHM) where we assume residuals of ground motions to be point loads on a weightless beam in 2-D statics. Large magnitudes of these values identify missed and false events.

#### **MEMS Accelerometers Mini Array (MAMA)—a Low Cost Solution for Array-based Earthquake Early Warning System**

NOF, R. N., UC Berkeley, Berkeley, CA, USA, ran.nof@gmail.com; CHUNG, A. I., UC Berkeley, Berkeley, CA, USA, aichung@berkeley.edu; MENG, L., UCLA, LA, CA, USA, meng.caltech@gmail.com; KONG, Q., UC Berkeley, Berkeley, CA, USA, qing kai.kong@gmail.com; ALLEN, R. M., UC Berkeley, Berkeley, CA, USA, rallen@berkeley.edu

Most of the current EEWs utilize conventional seismic stations, housing high quality accelerometers and/or velocity-meters, and consider an earthquake as a point source. For large events, this point-source assumption leads to an underestimation of magnitudes. Recently, Meng *et al.* (BSSA, 2014, doi: 10.1785/0120130277) showed that it was possible to back-trace array waveforms in order to characterize the rupture dimensions of earthquakes in real-time using small-aperture seismic arrays. This approach was demonstrated for earthquakes with  $M > 6$  in a simulated real-time environment. Using small-aperture arrays makes it possible to account for finite-source effects, to better estimate large magnitudes, and to obtain better locations for events located outside of the seismic network. A drawback of the array approach when using traditional seismometers is the high cost of instrumentation.

Low cost MEMS accelerometers are increasingly being used for seismological research. Some applications use a dense network of MEMS devices. Recently, low-cost MEMS have been used to optimize GPS measurements. Most applications use MEMS with resolutions of up to 16-bits, theoretically enabling the recording of  $M > 3.5$  earthquakes at 10 km.

Here, we propose a new low-cost (<\$150) low-noise (50ug/sqrt(Hz)) MEMS accelerometer based device, that includes a 24-bit digitizer and WiFi- or Ethernet-based telemetry using a seedlink data transfer protocol. These higher sensitivity, low-cost accelerometers are deployed as a mini-array around a conventional seismic station, enhancing the network's ability to determine earthquake parameters such as magnitude and location in real-time. This improvement leads to better estimations of the expected shaking at places of interest. We present the device details, benchmarks, and some simulated results of the expected benefit of such an array when using the back-tracing approach implemented in real-time.

### **HPWREN—Building a Sustainable Resilient Infrastructure for Realtime Observations**

VERNON, F., UCSD, La Jolla, CA, USA, [flvernon@ucsd.edu](mailto:flvernon@ucsd.edu)

Starting in 2001 HPWREN created a large-scale wireless high-performance data network that is being used for interdisciplinary research and education applications, as well as a research test bed for wireless technology systems in general. HPWREN provides wide area wireless internet access throughout southernmost California including San Diego, Riverside, Imperial, and Orange counties and the offshore regions. Under UCSD's HPWREN program, real-time observations monitoring is conducted by providing "last kilometer" wireless links and developing networking infrastructure to capture real-time data from multiple types of sensors from seismic networks, hydrological sensors, oceanographic sensors, wildfire cameras, meteorological sensors, as well as data from coastal radar and GPS. HPWREN provides internet connectivity to remote areas that are inaccessible by cell phone technology while allowing seismic stations to be placed next to active faults to facilitate earthquake early warning and earthquake research, allowing wildfire cameras to be placed on remote mountaintops of provide coverage of our wild land areas, and allowing meteorological sensors to be placed at remote sites where coverage did not exist before.

### **ElarmS Performance in Hawai'i**

THELEN, W. A., USGS Cascade Volcano Observatory, Vancouver, WA, USA, [wthelen@usgs.gov](mailto:wthelen@usgs.gov); HOTOVEC-ELLIS, A., Pacific Northwest Seismic Network, Seattle, WA, USA, [ahotovec@u.washington.edu](mailto:ahotovec@u.washington.edu); HARTOG, R., Pacific Northwest Seismic Network, Seattle, WA, USA, [jrhartog@uw.edu](mailto:jrhartog@uw.edu); BODIN, P., Pacific Northwest Seismic Network, Seattle, WA, USA, [bodin@uw.edu](mailto:bodin@uw.edu); VIDALE, J., Pacific Northwest Seismic Network, Seattle, WA, USA, [vidale@uw.edu](mailto:vidale@uw.edu); OKUBO, P., Hawaiian Volcano Observatory, Hawaii Volcanoes Nat'l Park, HI, USA, [pokubo@usgs.gov](mailto:pokubo@usgs.gov)

The Hawaiian Volcano Observatory (HVO) is collaborating with the Pacific Northwest Seismic Network (PNSN) to evaluate the utility of Earthquake Early Warning (EEW) in Hawaii. Since August 11, 2015, HVO has operated ElarmS with configurations that closely resemble those in place in the Pacific Northwest EEW system operated by the PNSN. ElarmS is one of the three algorithms currently used in the ShakeAlert demonstration system being developed for EEW along the west coast of the US, and quickly estimates a location and magnitude from first motions detected at the nearest four stations to an earthquake. In the first three months of testing, ElarmS successfully detected 9 magnitude 3+ earthquakes. There were also several ElarmS detections with no match in the seismic catalog, labeled as teleseisms, that located well offshore. Latencies of the alarms depend on the density of stations around the epicenter, processing time and data latencies. The EEW system in Hawaii has alarm latencies that range between 2 and 10 seconds. Data latencies within the HVO network are large compared to the ShakeAlert system because many digitizers are unable to send 1-second packets. Future work will review ElarmS performance over a longer time period and identify areas where the network and EEW software performance can be optimized. Results will be published in a feasibility study that would serve as a catalyst for implementing EEW in Hawaii.

### **Monitoring Data Quality from the PBO, TLALOCNet and COCONet Real-Time GNSS Networks for Earthquake Early Warning**

HODGKINSON, K. M., UNAVCO, Boulder, CO, USA, [hodgkinson@unavco.org](mailto:hodgkinson@unavco.org); MENCIN, D., UNAVCO, Boulder, CO, USA; FOX, O., UNAVCO, Boulder, CO, USA; WALLS, C., UNAVCO, Boulder, CO, USA; MANN, D., UNAVCO, Boulder, CO, USA; AUSTIN, K., UNAVCO, Boulder, CO, USA; BLUME, F., UNAVCO, Boulder, CO, USA; BERGLUND, H., UNAVCO, Boulder, CO, USA; PHILLIPS, D. A., UNAVCO, Boulder, CO, USA; MEERTENS, C. M., UNAVCO, Boulder, CO, USA; MATTIOLI, G. S., UNAVCO, Boulder, CO, USA;

The GAGE facility, managed by UNAVCO, currently operates a network of ~470, real-time, high-rate GNSS stations (RT-GNSS). The majority of these real-time stations are part of the Earthscope PBO network, which spans the western

US Pacific North-American plate boundary. Approximately 50 are distributed throughout the Mexico and Caribbean region funded by the TLALOCNet and COCONet projects. User demand for both raw and processed data streams has grown almost exponentially since 2010. While usage is multidisciplinary, including tectonic and volcanic deformation studies, meteorological applications and atmospheric research, the growing need for the development of Earthquake Early Warning (EEW) systems worldwide has brought into focus the importance of not only managing a robust data delivery system but monitoring data quality in a near real-time fashion.

EEW systems being developed in the western US rely heavily on access to the PBO real-time data streams. Low-latency, low-noise levels and completeness of the data streams are critical for the success of EEW systems. To assess and meet these requirements, UNAVCO tracks the latency and completeness of the incoming raw observations and is currently developing tools to monitor the quality of the real-time PPP processed data. In this presentation we will share our experiences of the challenges involved associated with the data operations of a continental-scale, real-time GNSS network, summarize the network's performance in terms of latency and completeness and present routines we are developing that will allow UNAVCO to monitor noise levels across the network in near real-time.

---

## **Ground Motion Spatial Variability: Models, Methods and Impacts**

Poster Session · Wednesday · 20 April · Tuscany F

---

### **Estimating Spatial Correlations between Earthquake Source, Path, and Site Effects for Non-Ergodic Seismic Hazard Analysis**

KUEHN, N. M., PEER Center, University of California, Berkeley, CA, USA, [kuehn@berkeley.edu](mailto:kuehn@berkeley.edu); ABRAHAMSON, N., University of California, Berkeley, CA, USA, [kuehn@berkeley.edu](mailto:kuehn@berkeley.edu); BALTAY, A., Earthquake Science Center, USGS, Menlo Park, CA, USA, [abaltay@usgs.gov](mailto:abaltay@usgs.gov)

Traditional probabilistic seismic hazard analysis (PSHA) uses ground-motion models that are based on the ergodic assumption, which implies that the distribution of ground motions over time at a given site is the same as their spatial distribution over different sites. However, evaluations of ground-motion data sets with multiple measurements at a given site and multiple earthquakes in a given region have shown that the ergodic assumption is not appropriate as there are strong systematic, region-specific source terms, site-specific path terms, and site terms which are spatially correlated. We model these correlations using a spatial Gaussian process model, and compare results from both stationary and non-stationary correlation. Non-stationary correlation functions make it possible to model more general, region-specific spatial variations, but are harder to constrain computationally. We investigate spatial correlations on three different data sets: a Taiwanese strong-motion data set, ground motions collected at the ANZA, CA array, and CyberShake simulations. We find that about 40-50% of aleatory variability is explained by accounting for spatial variability. This has important implications for probabilistic seismic hazard analysis. The reduced aleatory variability leads to steeper hazard curves, that is, lower ground motions at a given probability of exceedance, but also leads to increased epistemic uncertainty due to the uncertainty in the source, path, and site terms for a given site, and hence larger uncertainties of the resulting hazard curve distribution. By exploiting the spatial correlation of ground motions, we show how the inclusion of known source and path effects can reduce these uncertainties.

### **Characterization of Spatial Variability of Ground Motion Using a Very Dense Array at Long Beach, California**

NAKATA, N., Stanford University, Stanford, CA, USA, [nnakata@stanford.edu](mailto:nnakata@stanford.edu); BEROZA, G. C., Stanford University, Stanford, CA, USA, [beroza@stanford.edu](mailto:beroza@stanford.edu)

Ground-motion prediction is a key component for seismic hazard analysis, which is typically carried out with ground-motion prediction equations. The standard deviation of the best-fit model characterizes the residual ground motion variability. These residuals are an admixture of random variability (aleatory uncertainty) and modeling error (epistemic uncertainty). When we calculate site-specific ground motion prediction, the residuals become smaller since different sources, paths, and sites are not mixed. Recent development of dense, capable, and long-term seismometer networks allows us to estimate the site-, path-, and source-specific variability. In this study, we use a very dense array at Long Beach, California, and demonstrate the potential to characterize the spatial variability. Because of the density of the array (2500 receivers with 100-m spacing), we can estimate very dense site information (*i.e.*, VS30) from the ambient seismic field. Although the



recording time is only a couple of months, we observed more than 10 earthquakes, and hence we can estimate site-, path-, and source-specific variability of ground motion. Since we do not have multiple events occurring in close proximity to one another, we cannot separate the source-location and source-parameter effects.

#### Estimation of VS30 from Geology-Based Proxy Developed for the Pacific Northwest

AHDI, S. K., University of California, Los Angeles (UCLA), Los Angeles, CA, USA, sahdi@ucla.edu; STEWART, J. P., University of California, Los Angeles (UCLA), Los Angeles, CA, USA, jstewart@seas.ucla.edu; ANCHETA, T. D., Risk Management Solutions, Inc., Newark, CA, USA, Tim.Ancheta@rms.com; KISHIDA, T., Pacific Earthquake Engineering Research (PEER) Center, Berkeley, CA, USA, tkishida@berkeley.edu; BOZORGNIA, Y., Pacific Earthquake Engineering Research (PEER) Center, Berkeley, CA, USA, yousef@berkeley.edu

The time-averaged shear wave velocity in the uppermost 30 meters of the crust (VS30) is commonly used in development of ground motion prediction equations (GMPEs). While it is preferred to obtain VS30 from measured shear wave velocity (VS) profiles, such data is not always available. In these cases other information can be used as a proxy to estimate VS30. As part of a related effort to create an open-access VS profile database in the Pacific Northwest (PNW) region of North America, which encompasses the Cascadia Subduction Zone, we compute VS30 values from 349 measured VS profiles collected from sites throughout Oregon and Washington (USA). These measured VS30 values are used to evaluate the performance of existing VS30 proxies developed for other regions globally, including those based on topographic gradient and terrain categories. We then present a new VS30 proxy for sites in the PNW based on local surface geology and glaciation history. The local proxy should produce reduced dispersion in estimating VS30 compared to proxies developed for other regions that are considered in this study. The new proxy will be used to develop GMPEs within the framework of the Next Generation Attenuation Subduction project to estimate VS30 at strong motion recording station sites in the PNW.

#### A Vs30-dependent Velocity Model for High-frequency Simulated Ground Motions in the Los Angeles Basin

SHI, J., California Institute of Technology, Pasadena, CA, USA, jian.shi@caltech.edu; ASIMAKI, D., California Institute of Technology, Pasadena, CA, USA, domniki@caltech.edu; YONG, A. K., U.S. Geological Survey, Pasadena, CA, USA, yong@usgs.gov

The soft sediments in the top few hundred meters of sedimentary basins can alter the amplitude, frequency and duration of earthquake ground shaking. These phenomena, referred to as site effects, play a very important role in ground-motion simulations, in the development of ground motion prediction equations (GMPEs), and in turn in earthquake hazard and risk predictions on a regional scale. To enable the simulation of these effects, we translate Vs30, the only proxy available to describe the stiffness of the near surface sediments in Southern California, into a generic velocity profile suitable for use in wave propagation-based ground motion models. We specifically develop a Vs30-dependent shear wave velocity model based on the statistics of a few hundred measured Vs profiles, whose Vs30 value ranges from 220 m/s to 600 m/s. We validate the model by comparing the site response amplitude of the true velocity profile to that of the presented Vs30- and depth-dependent velocity model. The long-term goal of the proposed research is to integrate the model into the SCEC Community Velocity Model (CVM) for use in the physics-based ground motion simulations.

#### Impact of Spatial Correlation of Peak Ground Motion Intensity in Catastrophe Modeling

LEE, Y., ImageCat, Inc., Long Beach, CA, USA, yjl@imagecatinc.com; WILLIAM, G., ImageCat, Inc., Long Beach, CA, USA, wpg@imagecatinc.com

In urban environment, previous studies have shown the importance of taking into account the spatial correlation of intensity measure (IM) such as peak ground acceleration (PGA) or spectra acceleration (SA) in modeling portfolio losses (Parker et al., 2007; Yoshikawa and Goda, 2014; Liu and Hong, 2015). Spatial correlation of ground shaking is typically attributable to two sources: 1) the event-wide correlation of shaking intensity through the between-event variability, that is, a systematic lower or higher ground motion of an event, for instance, due to a higher or lower stress drop than an “average” event and 2) the tendency of local lower or higher ground motions than the predicted median due to location proximity through the within-event variability, for instance, due to common source rupture effect and wave propagation paths. For the latter, the larger the distance between the sites, the smaller the correlation of the peak shaking intensity would be. Spatial correlation of IMs is also dependent on frequency

content in seismic waves (Goda and Hong, 2008; Baker and Jayaram, 2008), which poses challenges to implementation in catastrophe modeling. In this study, using Robust Simulation technology, we implement a spatial correlation model based on Hong et al. (2009) for portfolio loss assessments with the USGS 2014 hazards, in which distance- and period-dependent correlation was derived from California events, with the following equation:  $\rho(\Delta, T) = \exp(-\alpha\Delta^\beta)$ , where  $\rho$  is the correlation coefficient,  $\Delta$  is the distance between the two sites,  $T$  is the building response period, and  $\alpha$  and  $\beta$  are the model parameters. Spatial correlation effects were adopted in shaking intensity fields with a stochastic event simulation technique. Our results show that the estimated probabilistic losses for longer return intervals increase when spatial correlation is considered. Conversely, the losses at shorter return intervals are overestimated when spatial correlation is not considered.

---

#### How Close are We to an Eruption?

Poster Session · Wednesday · 20 April · Tuscany F

---

#### Intermediate-Depth Long Period Seismicity Prior to a Shallow Earthquake Swarm at Little Sitkin Volcano, Alaska

HANEY, M. M., Alaska Volcano Observatory/USGS, Anchorage, AK, USA, mhaney@usgs.gov; BUURMAN, H., University of Alaska Fairbanks, Geophysical Institute, Fairbanks, AK, USA, hmbuurman@alaska.edu; MCNUTT, S. R., University of South Florida, School of Geosciences, Tampa, FL, USA, smcnutt@usf.edu

Little Sitkin Volcano in the Western Aleutians has no confirmed historical eruptions; however, evidence from vegetation regrowth on the most recent flows suggests that eruptive activity occurred during the early 1900s. Geothermal springs and fumaroles provide further evidence of an active magma system at Little Sitkin. On August 29, 2012, a swarm of earthquakes began beneath the island between 5–10 km depth that persisted for over 3 months before waning without any eruptive activity.

The swarm was preceded by a remarkable sequence of five low frequency (or long period) earthquakes dominated by nearly monochromatic 0.6 Hz signals. The first two earthquakes occurred on August 23 and August 24. These were followed by a series of three closely spaced low frequency earthquakes on August 25. After the final low frequency earthquake, the most significant seismicity before the onset of the swarm was a 20 km deep volcano-tectonic earthquake on August 27. The low frequency earthquakes were clearly observed on stations on the nearby islands of Semisopochnoi and Amchitka, at distances of up to 100 km; local magnitudes were estimated to be on the order of ML=1.5. On the broadband seismometer at Amchitka, the 0.6 Hz signal had unusual impulsive P- and S-wave onsets. A secondary spectral peak existed at approximately 2 Hz and the S-wave at this higher frequency arrived 1 s later than the 0.6 Hz onset. Based on coherence between the three stations on Little Sitkin Island and S-P times, the earthquakes appear to have originated at approximately 15 km depth beneath the western portion of the island. We interpret the low frequency earthquakes as a type of deep long period seismicity that resulted from magma flowing between 2 reservoirs with characteristic resonance frequencies of 0.6 and 2 Hz. These observations motivate the development of automated algorithms tuned to detect signals in the 0.5-1 Hz frequency band originating deep beneath active volcanoes.

---

#### Induced Seismicity

Poster Session · Wednesday · 20 April · Tuscany F

---

#### Characterizing Microseismicity at the Newberry Volcano Geothermal Site using PageRank

AGUIAR, A. C., Lawrence Livermore National Laboratory, Livermore, CA, USA, aguiar@llnl.gov; MYERS, S. C., Lawrence Livermore National Laboratory, Livermore, CA, USA, myers30@llnl.gov

The Newberry Volcano, within the Deschutes National Forest, has been designated as a candidate site for the Department of Energy's Frontier Observatory for Research in Geothermal Energy (FORGE) program. This site was stimulated using high-pressure fluid injection during the fall of 2012, which generated several hundred microseismic events. Exploring the spatial and temporal development of microseismicity is key to understanding how subsurface stimulation modifies stress, fractures rock, and increases permeability. We evaluate Newberry microseismicity by adapting PageRank, Google's initial search algorithm, during the 2012 stimulation. PageRank is a measure of connectivity, where higher ranking represents highly connected signal windows. In seismic applications connectivity is measured by the cross correlation of 2 time windows recorded on a

common station/channel. We expand on Aguiar and Beroza (2014) PageRank application by using it to define signal-correlation topology for micro-earthquakes, including the identification of signals that are connected to the largest number of other signals. We use this information to create signal families and compare these to the spatial proximity of associated earthquakes; where signals with high cross correlation are referred to as directly linked, and signals linked by the PageRank procedure as indirectly linked. We show that events are in close proximity to one another only when their signals are linked directly and indirectly at many stations; and more close-proximity events are linked when indirect signal links are included. Signal PageRank will potentially allow us to efficiently group earthquakes with similar physical characteristics, such as focal mechanisms and stress drop. Our ultimate goal is to determine whether changes in the state of stress and/or changes in the generation of subsurface fracture networks can be detected using PageRank topology. Prepared by LLNL under Contract DE-AC52-07NA27344. LLNL-ABS-680633.

### The Seismic Response at the Aquistore CO<sub>2</sub> Injection Project, Saskatchewan, Canada

STORK, A. L., University of Bristol, Bristol, UK, [anna.stork@bristol.ac.uk](mailto:anna.stork@bristol.ac.uk); NIXON, C., University of Alberta, Edmonton, AB, Canada, [cnixon@ualberta.ca](mailto:cnixon@ualberta.ca); SCHMITT, D. R., University of Alberta, Edmonton, AB, Canada; WHITE, D. J., Geological Survey of Canada, Ottawa, ON, Canada, [don.white@canada.ca](mailto:don.white@canada.ca); KENDALL, J. M., University of Bristol, Bristol, UK, [gljmk@bristol.ac.uk](mailto:gljmk@bristol.ac.uk); WORTH, K., Petroleum Technology Research Centre, Regina, SK, Canada

The Aquistore Project in Saskatchewan, Canada, managed by the Petroleum Technology Research Centre, is a demonstration CO<sub>2</sub> injection project which receives CO<sub>2</sub> from the Boundary Dam coal-fired power plant, the site of the world's first commercial power plant carbon capture and storage (CCS) project. Since April 2015 over 20kT of CO<sub>2</sub> has been injected into a deep saline aquifer at 3100–3300m below the surface.

Extensive passive seismic monitoring experiments have been deployed to study the seismic response of the site to injection, including a near-surface deployment of 65 1-component and 3-component (3C) geophones covering 2.5km<sup>2</sup>, 3 broadband stations and an array of 5 3C borehole geophones deployed over the depth range of 2850–2910m. A suite of seismic event detection techniques, including manual analysis, short-term average/long-term average (STA/LTA) analysis and stacking techniques, is tested on this data. However, no significant injection-related seismicity ( $M_w > -1$ ) has been detected during the first 8 months of CO<sub>2</sub> injection. Further analysis of the downhole and surface passive data is on-going to detect smaller magnitude microseismicity.

This result has significant implications for fluid injection projects, particularly CO<sub>2</sub> injection projects. It has been suggested that a hydraulic connection between a zone of fluid injection and faults in the basement increases the likelihood of inducing seismicity. The CO<sub>2</sub> injection interval at Aquistore is directly above the Precambrian basement rocks and a fracture pressure of ~48MPa (or a gradient of 14.9 kPa/m) has been estimated from detailed downhole pressure and flow rate information. However, no on-site seismicity has been observed.

### Long-term Decay and Possible Reactivation of Induced Seismicity at the Basel EGS Site

HERRMANN, M., Swiss Seismological Service, ETH Zürich, Zürich, Switzerland, [marcus.herrmann@sed.ethz.ch](mailto:marcus.herrmann@sed.ethz.ch); KRAFT, T., Swiss Seismological Service, ETH Zürich, Zürich, Switzerland, [toni.kraft@sed.ethz.ch](mailto:toni.kraft@sed.ethz.ch); WIEMER, S., Swiss Seismological Service, ETH Zürich, Zürich, Switzerland, [stefan.wiemer@sed.ethz.ch](mailto:stefan.wiemer@sed.ethz.ch)

In December 2006, an extensive fluid injection was carried out below the city of Basel, Switzerland, to stimulate a reservoir for an Enhanced Geothermal System (EGS). After six days of gradual increase of flow rate, wellhead pressure, and seismicity, a strongly felt ML3.4 earthquake led to the immediate termination of the project. The well was opened subsequently and seismicity declined rapidly.

The Basel EGS project might be an unsuccessful attempt in terms of energy supply, but a chance to advance the physical understanding of EGSs. The well-monitored and well-studied induced sequence allowed many new insights in terms of reservoir creation. A special observation in the nine years of monitoring is the revive of seismic activity six years after prolonged seismic decay. This reactivation might relate to a gradual pressure increase due to the ultimate shut-in (closure) of the borehole about one year before. Until now, a detailed analysis of the long-term behavior remained unexplored since a consistent catalog did not exist.

In the current study, we took advantage of the high waveform similarity within a seismic sequence and applied multi-trace template-matching (*i.e.* cross-correlation) to detect seismic events about one order of magnitude below the detection threshold. We detected about 100,000 events within the six-day long stimulation alone; previously, only 13,000 microearthquakes were detected. We

only scanned the recordings of the deepest borehole station (2.7km). This station is very close to the 5km-deep reservoir and has the highest signal-to-noise ratio among all (borehole-)stations.

Our newly obtained catalog spans over more than nine years and features a uniform (and low) detection threshold and a uniform magnitude determination. The improved resolution of the long-term behavior and the later seismicity increase will help to understand involved mechanisms better. More induced or natural sequences can be investigated with our procedure.

### Effects of Long-term Fluid Injection on Induced Seismicity Parameters and Maximum Magnitude at Northwestern The Geysers Geothermal Field

KWIATEK, G., GFZ German Research Centre for Geosciences, Potsdam, Germany, [kwiatek@gfz-potsdam.de](mailto:kwiatek@gfz-potsdam.de); MARTÍNEZ-GARZÓN, P., GFZ German Research Centre for Geosciences, Potsdam, Germany, [patricia@gfz-potsdam.de](mailto:patricia@gfz-potsdam.de); DRESEN, G., GFZ German Research Centre for Geosciences, Potsdam, Germany, [bohnhoff@gfz-potsdam.de](mailto:bohnhoff@gfz-potsdam.de); BOHNHOFF, M., GFZ German Research Centre for Geosciences, Potsdam, Germany; SONE, H., University of Wisconsin-Madison, Madison, WI, USA; HARTLINE, C., Calpine Corporation, Middletown, CA, USA

The long-term temporal and spatial changes in statistical, source and stress characteristics of one cluster of induced seismicity recorded at The Geysers geothermal field (US) are analyzed in relation to the field operations, fluid migration and constraints on the maximum likely magnitude. Two injection wells, Prati-9 and Prati-29, located in the northwestern part of the field and their associated seismicity composed of 1,776 events recorded throughout a seven-year period were analyzed. The seismicity catalog was relocated and the source characteristics including focal mechanisms and static source parameters were refined using first-motion polarity, spectral fitting and mesh spectral ratio analysis techniques. The source characteristics together with statistical parameters (*b* value) and cluster dynamics were used to investigate and understand the details of fluid migration scheme in the vicinity of injection wells. The observed temporal, spatial and source characteristics were clearly attributed to fluid injection and fluid migration towards greater depths, involving increasing pore pressure in the reservoir. The seasonal changes of injection rates were found to directly impact the shape and spatial extent of the seismic cloud. A tendency of larger seismic events to occur closer to injection wells and a correlation between the spatial extent of the seismic cloud and source sizes of the largest events was observed. We found maximum likely magnitude is geometrically constrained and correlated to the volume of formation weakened by fluid injection (=volume of seismicity cloud) which is on the other hand related to the average injection rate at for Prati-9/Prati-29 wells.

### Detailed Analysis of an Earthquake Cluster Potentially Driven by Fluid Flow in Central Oklahoma

CHEN, X., University of Oklahoma, Norman, OK, USA, [xiaowei.chen@ou.edu](mailto:xiaowei.chen@ou.edu); PENG, Z., Georgia Institute of Technology, Atlanta, GA, USA, [zpeng.seismo@gmail.com](mailto:zpeng.seismo@gmail.com); MENG, X., University of Washington, Seattle, WA, USA, [xiaofeng.meng@eas.gatech.edu](mailto:xiaofeng.meng@eas.gatech.edu); CHEN, C., University of Oklahoma, Norman, OK, USA, [c.chen@ou.edu](mailto:c.chen@ou.edu); HAFENER, J., University of Oklahoma, Norman, OK, USA, [jhaffener@gmail.com](mailto:jhaffener@gmail.com); CHANG, J., University of Oklahoma, Norman, OK, USA, [jeffersonchang@ou.edu](mailto:jeffersonchang@ou.edu)

In May 2014, an earthquake cluster started in central Oklahoma near Guthrie. This cluster continues to present with about 200 M2.5+ earthquakes, and one M4 earthquake. High-precision relocation reveals two conjugate fault planes within this cluster. The seismicity initiated at the shallow part along the NW-SE trending fault plane, with gradual expansion of seismicity both horizontally and along depth. The SW-NE trending fault was activated later in the sequence. The migration pattern suggests a likely activation of seismicity by a disposal well 3 km away that started injection about two months ago. Subsequent temporal seismicity rate variation suggests possible correlation with the shut-in and re-inject period of the disposal well. In addition to the seismicity patterns, we analyzed detailed source parameter variations using empirical Green's function method, and find that the stress drops are much lower at shallow depth and the beginning stage of the two major episodes in the sequence, which is consistent with the scenario that fluid flow is involved in the earthquake triggering process.

We are currently applying matched-filter detection, differential time derived from waveform cross-correlation and a 3D velocity model to improve locations and catalog completeness for this cluster. We plan to resolve detailed spatial temporal evolution of this sequence, and examine the relationship with other nearby disposal wells within an expanded radius to identify possible links between earthquakes and injection parameters. In particular, we will focus on the spatial-temporal migration of the seismicity. We will also apply spectral analysis to obtain spectral moment magnitude, and high-quality source parameters cor-

rected by 3D velocity model in order to understand in-situ fault strength variations, and potential correlation with fluid flow propagation.

### **Spatiotemporal Analysis of the 2010-2011 Guy-Greenbrier Sequence and the Associated Pore-pressure Beyond Fluid Disposal Period**

OGWARI, P. O., CERl-University of Memphis, Memphis, TN, USA, opogwari@memphis.edu; HORTON, S. P., CERl-University of Memphis, Memphis, TN, USA, shorton@memphis.edu

Analysis of the initiation of the 2010-2011 Guy-Greenbrier swarm indicates there were thousands more earthquakes during the swarm period than reported in the CERl catalog (~1,000 event of  $m_{blg} > 2$ ). Ogwari *et al.* (2016) used an STA/LTA method to detect ~17,000 events of  $m_l > 0$  and determined their locations using Antelope for the start-up period between 07/01/2010 and 10/21/2010. Approximately, 750 earthquakes in the ~17,000 event catalog (O1-cat) were found to be triggered during hydraulic fracturing stimulation about 2 km west of the Guy-Greenbrier fault. In this study, we apply the single-station template-matching method using 1,300 relocated earthquakes from the CERl catalog (C-cat) as templates on continuous waveforms from two nearby (distance <10 km) seismic stations to determine relative earthquake locations (O2-cat) for the period between 06/01/2010 and 12/30/2012. We then compare the relative earthquake locations of O2-cat with the locations in O1-cat catalog to test the accuracy of the relative location of the detected earthquakes and the significance of the correlation coefficient. Analysis of the relation between the cross-correlation coefficient (CC) and the inter-event separation distance indicates a minimum threshold of  $CC = 0.667$  and a time delay less than 0.31 sec are sufficient to distinguish induced earthquakes on the Guy-Greenbrier fault from earthquakes triggered during hydraulic fracturing process in the surrounding area. We locate over 187,000 recognizable earthquakes that migrate from north to south. Seismicity starts after injection begins at the SRE and Edgmon wells, and the seismicity rate reduces to pre-injection levels ~5 months after the stop of injection at the two wells. A good correlation between the seismicity rate on the Guy-Greenbrier fault and well pressure changes shows interaction of pore pressure from the SRE and Edgmon wells and a possible pressure influence from the Trammel well.

### **Explaining the 24 January 2013 $M_L$ 4.4 Induced Earthquake in Paradox Valley, Colorado**

DENLINGER, R. P., U.S. Geological Survey, Vancouver, WA, USA, roger@usgs.gov; ROELOFFS, E. A., U.S. Geological Survey, Vancouver, WA, USA, evelynr@usgs.gov

On 24 January 2013, a  $M_L$  4.4 earthquake occurred 8.2 km northwest of an injection well in western Colorado where approximately 6.5 million  $m^3$  of brine had been injected since 1995. The Paradox Valley Seismic Network, deployed by the U.S. Bureau of Reclamation in 1985, recorded thousands of microearthquakes spreading from the wellhead after injection began. There is little doubt that the 24 January 2013 earthquake was induced, because seismicity extends throughout a zone from the injection site to its epicenter. We identify two features of this earthquake favoring its occurrence at this location so far from the injection well.

First, volumetric strain imposed by dextral slip on this event's ENE-striking fault plane (as determined by Block *et al.*, 2013) shows that the January 2013 earthquake expanded the injection horizon between its epicenter and the injection well, increasing pore space available for injectate and reducing pore pressure. This is true for a range of assumed rupture depths, whether flow is being channeled into a northwest-striking zone beneath the epicenters, or is radially symmetric about the well.

Next, we simulated numerically the coupled pore pressure and poroelastic stresses caused by injection. Even if injectate flow is radially symmetric, the shear and normal stress changes on steeply dipping, ENE-striking faults favor right-lateral slip only in quadrants northwest and southeast of the well. Moreover, a model that utilizes a realistic configuration of the injected rock units predicts concentrated stresses at the hypocenter of the 24 January 2013  $M_L$  4.4 event, which occurred where the injection horizons pinch out.

This earthquake occurred where poroelastic stresses enhanced the fault's tendency to fail, and its coseismic strain increased the formation's capacity to accept injectate. Such features may help diagnose situations prone to induced earthquakes relatively far from injection wells.

### **The August 17, 2015 $M_w$ 4.6 Hydraulic Fracturing-Induced Earthquake in Northern Montney Play, British Columbia, Canada**

BABAIE MAHANI, A., Geoscience BC, Vancouver, BC, Canada, ali.mahani@mahangeo.com; SCHULTZ, R., Alberta Energy Regulator, Edmonton, AB, Canada, ryan.schultz@aer.ca; KAO, H., Pacific Geoscience Center, Sidney, BC, Canada, honnkao@gmail.com; WALKER, D., BC Oil and Gas commission,

Victoria, BC, Canada, dan.walker@bcogc.ca; JOHNSON, J., BC Oil and Gas Commission, Victoria, BC, Canada, jeff.johnson@bcogc.ca; SALAS, C., Geoscience BC, Vancouver, BC, Canada, salas@geosciencebc.com

We studied a cluster of seismic events in the northern Montney Play, British Columbia, in an area where ongoing hydraulic fracturing and wastewater injection are taking place. The cluster includes the  $M_w$  4.6 earthquake of August 17, 2015 (the largest potentially induced event in Canada from hydraulic fracturing) along with other events with local magnitude ( $M_L$ ) in the range 1.4-3.5. We used broadband waveforms from the regional seismographic stations in western Canada complemented with two dense arrays of seismic stations in northeast British Columbia. This configuration of seismic stations provided data in an epicentral distance range of 7-500 km. Double-difference relocation of these events revealed a hypocentral depth of ~2-3 km consistent with injection depth of hydraulic fracturing in the area. Broadband ground-velocity waveforms of the  $M_w$  4.6, Aug 17, 2015, event recorded in the immediate vicinity of the epicenter (up to ~20 km) were clipped, probably due to the combined effect of a shallow source and the relatively large magnitude. The strong shaking is also evident by felt reports of the  $M_w$  4.6 event at places up to ~100 km away from the epicenter. All these observations suggest that seismic risk from injection-induced earthquakes in this area cannot and should not be ignored.

### **Matched Filtering Analysis of Induced Seismicity in the Crooked Lake region, Alberta: Correlation with Hydraulic-fracturing Operations**

BAO, X., University of Calgary, Calgary, AB, Canada, xubao@ucalgary.ca; EATON, D. W., University of Calgary, Calgary, AB, Canada, eatond@ucalgary.ca; CAFFAGNI, E., University of Vienna, Vienna, Austria, enrico.caffagni@univie.ac.at

Continuous data recorded using a broadband seismograph array for the time period November 17 2014 to March 31, 2015 were analyzed using a matched-filtering algorithm, yielding over 900 small and moderate earthquakes ( $-0.2 \leq M_L \leq 4.2$ ) in 6 distinct clusters. Most of the seismicity exhibits a high degree of spatial and temporal correlation with hydraulic fracturing stimulations in the Duvernay shale. Taken together, the catalog of events has a b-value that is close to unity, in contrast to higher b values of ~2 that are typical of operationally induced microseismicity from hydraulic fracturing. Double-difference relocation of the events reveals a roughly NE-SW linear alignment for the best-resolved cluster at an orientation that is close to optimal for reactivation of a near-vertical fault in the current stress state. A progressive migration of seismicity is observed for several clusters, which is interpreted to reflect fault- or fracture-controlled diffusion of elevated pore-pressure.

### **Induced Seismicity due to Wastewater Injection Near Peace River, Alberta**

ANDERSON, Z., University of Calgary, Calgary, AB, Canada, zanderso@ucalgary.ca; EATON, D. W., University of Calgary, Calgary, AB, Canada, eatond@ucalgary.ca

A cluster of 8 small earthquakes commenced in 1997 near the Town of Peace River, Alberta. The level of seismicity has recently increased sharply, with three events in both 2014 and 2015 (through October). Understanding the potential cause of this small cluster is important to improve hazard assessment. This study explores a possible link between these earthquakes and wastewater injection. On the basis of spatial and temporal correlation with injected volumes, it is interpreted that all eight earthquakes were mainly triggered by a single disposal well. The earthquakes seem to have propagated farther away from the well over time, to a maximum distance of about 27km from the inferred injection point.

### **Triggered Seismicity Source Mechanisms: Modelling Fault Complexity in Critically Stressed Crust**

MACKAY, M., University of Calgary, Calgary, AB, Canada, mason.mackay2@ucalgary.ca; EATON, D., University of Calgary, Calgary, AB, Canada, eatond@ucalgary.ca

This study uses a distinct element modelling approach in order to investigate the slip vectors and resultant moment tensors along a fault with a step over geometry. Fault dimensions are chosen to create moment magnitudes that are in the realm of an observed triggered seismic event. A fault depth of 3000 meters is chosen in order to simulate triggered seismicity conditions associated with oil and gas operations. The main fault segments are critically oriented towards the far field stress. This drives slip on the non-critically oriented step over region. Various cases are modelled with different fault link geometries and fluid pressures.

The first set of models discussed is a case where both the main fault and the linking segments are critically stressed. It is found that in a dilatational step over case, a crack opening and double couple mechanism along the fault link



is observed. Conversely, in a compressional step over, crack closure and double couple slip is the dominant mode in the fault link. In the case where the linking fault normal is parallel to the least compressive principle stress, fluid pressure within the fault controls the amount of opening component. If fluid pressure is equal to the minimum principal stress, the shear displacement along the main fault is communicated across the step over region, and a mixed opening and slip mechanism is produced. Finally, the orientation of the fault link segment controls the slip direction, magnitude and stress drop when perturbed by a uniform fluid pressure change.

Results of this modelling indicate that a complex fault geometry such as in the case of a dilatational or compressional jog, produces various moment tensors that deviate from a pure double couple solution. In triggered seismicity cases, elevated pressures in the fault step over region occurring from industrial operations may enhance the opening mode component of fault slip.

#### **Simulating Hydraulic Fracturing using Finite-Discrete Element Method (FDEM): Effects of Pre-existing Joints and Lateral Stress Gradient**

ABUAISHA, M., University of Calgary, Calgary, AB, Canada, [abuasha@ucalgary.ca](mailto:abuasha@ucalgary.ca); EATON, D. W., University of Calgary, Calgary, AB, Canada, [eatond@ucalgary.ca](mailto:eatond@ucalgary.ca); PRIEST, J., University of Calgary, Calgary, AB, Canada, [japriest@ucalgary.ca](mailto:japriest@ucalgary.ca); WONG, R., University of Calgary, Calgary, AB, Canada, [rckwong@ucalgary.ca](mailto:rckwong@ucalgary.ca)

This numerical study investigates near-wellbore behaviour of Hydraulic Fracture (HF) growth using a Finite-Discrete Element Modeling (FDEM) approach. Our results rarely exhibit a simple bi-wing fracture geometry, but are consistent with analytical solutions and exhibit many features that have been documented in the field. In the case of a homogeneous medium, our simulations show that isotropic far-field stresses ( $Sh_{max} = Sh_{min}$ ) promote the development of complex fractures, whereas anisotropic far-field stresses ( $Sh_{max} \gg Sh_{min}$ ) promote branching and curving fracture growth in the general direction of  $Sh_{max}$ . A set of pre-existing randomly space distributed joints around the wellbore indicates that fractures tend to initiate at the joint tips once intersected by a fluid-driven fracture. Our results also reveal that possible seismic events due to formation deformation may be induced by shear slippage of critically stressed joints. The presence of multiple joints around the wellbore also increases the extent to which fluid-driven fractures can grow for the same injection energy. Single isolated joints that do not intersect the wellbore create a lateral stress gradient. The presence of such a gradient leads to asymmetric fracture initiation, generally away from the pre-existing joint. Such asymmetric fracture growth may explain certain field observations that imply asymmetric distribution of microseismicity around a wellbore.

#### **An Investigation on the Effects of Different Stress Regimes on the Magnitude of Induced Seismic Events**

AMINI, A., University of British Columbia, Vancouver, BC, Canada, [aamini@eos.ubc.ca](mailto:aamini@eos.ubc.ca); EBERHARDT, E., University of British Columbia, Vancouver, BC, Canada, [eeberhar@eos.ubc.ca](mailto:eeberhar@eos.ubc.ca)

Producing oil and gas from shale reservoirs requires permeability enhancement treatments. This is achieved by injecting fluid under pressure to either propagate cracks through the rock (hydraulic fracture) or to stimulate slip across pre-existing faults (hydroshear) which allows gas or oil to flow more readily into the well bore. These permeability-enhancing treatments induce earthquakes, and there have been many reports on events with high magnitudes that were felt on surface. This paper will investigate the possible differences of induced seismicity in a thrust regime to a strike slip regime with respect to maximum magnitude and their distribution. To address this question, we will first study case histories of induced earthquakes in different stress regimes in Canada and USA. By studying the source mechanism of these earthquakes, the magnitude distribution in different stress regimes will be investigated. Next, the two scenarios will be further investigated by numerical modelling. A distinct element code (UDEC) is used to simulate a fault in two stress regimes. The only difference in two scenarios is the stress regime which creates a unique opportunity to study the effect of stress regime on the magnitude of induced seismic event. This study can help governments in setting regulations on oil and gas industry activities and will also be useful for oil and gas industry for location planning of hydraulic fracturing injection and waste water disposal wells.

#### **A Coda Based Method for Precise Focal Depth Determination in Sedimentary Basins**

DANIELS, R., University of Calgary, Calgary, AB, Canada, [rdaniels@repsol.com](mailto:rdaniels@repsol.com)

The occurrence of seismicity induced by hydraulic fracturing in western Canada has been on the rise since 2011, when seismicity associated with the large scale development of the Montney shale was first recorded in British Columbia. The hypocenters of these induced events tend to be shallower than most naturally occurring earthquakes resulting in higher than normal intensities and an increased potential for damage. Identifying the depth of the hypocenter allows an event to be tied back to the triggering activity, which is key for hazard prediction and risk mitigation. This paper proposes a coda-based waveform correlation method for accurate hypocenter location that does not depend on P and S wave arrival times, which have notoriously poor depth resolution. In this method finite-difference modeling is used to generate synthetic templates representing a range of possible hypocenter source depths. This series of templates is then cross correlated with a dataset containing three medium magnitude earthquake sequences recorded on a 3C local network. The synthetic source depth that is most highly correlated to the earthquake waveforms is proposed as the best estimate of hypocenter depth.

#### **Dynamic Stress Considerations for Induced and Triggered Events**

WALKER, R. L., University of Southern California, Los Angeles, CA, USA, [rlwalker@usc.edu](mailto:rlwalker@usc.edu)

The recent, elevated interest in induced seismicity that has brought the topic into the spotlight has largely focused hazards directly related to fluid injection. While drawing needed attention to an important topic, such focus may lead to a simplistic treatment of the otherwise, complex processes associated with such seismic events, yet to be fully understood. It is true some operational errors can be attributed to a clear link between injection and seismicity. Nevertheless, one cannot automatically assume that a problem such as induced seismicity can be described with only one variable. Likewise, the local geological setting must be considered in the consideration of induced seismic hazard. In considering a facet of this variability we consider the impact that dynamic stresses, such as those imparted by passing seismic waves, on a fault at risk for failure. Theoretical and observational findings on stress triggering of earthquakes from previous literature are reviewed with the intention of determining the parameters that, when "optimized," seem to provide the greatest likelihood for failure, as well as maximum subsequent seismic moment release, both immediately, and resulting from a cascading process culminating soon after the initial trigger is felt at the receiving fault. Also considered are geological contrasts that might promote dynamic stress amplification, such as bi-material interfaces, as well as optimal fault orientation with respect to the incoming stress. In addition to the review of prior literature, advanced seismic waveform modeling is performed using a finite difference approach, with the aim of gaining a better picture of the dynamic loading imparted upon a critically stressed fault, particularly in conjunction with the conditions suggested by the literature to provide the greatest hazard.

#### **On the Importance of Inter-Event Triggering in Microseismicity Induced by Hydraulic Fracturing**

MAGHSOUDI, S., Department of Geoscience, University of Calgary, Calgary, AB, Canada, [samira.maghsoodi@ucalgary.ca](mailto:samira.maghsoodi@ucalgary.ca); EATON, D., Department of Geoscience, University of Calgary, Calgary, AB, Canada, [eatond@ucalgary.ca](mailto:eatond@ucalgary.ca); BARO, J., Department of Physics and Astronomy, University of Calgary, Calgary, AB, Canada, [jordi.barourbea@ucalgary.ca](mailto:jordi.barourbea@ucalgary.ca); DAVIDSEN, J., Department of Physics and Astronomy, University of Calgary, Calgary, AB, Canada, [jdavidse@ucalgary.ca](mailto:jdavidse@ucalgary.ca)

Permeability-enhancing treatments such as hydraulic fracturing induce microseismic events with reported magnitudes in the range of -3.0 to -0.5, although significantly larger induced earthquakes up to ML 4.4 have been reported. The primary controlling mechanism is thought to be diffusion of pore pressure away from the hydraulic fracture system, which leads to activation of fractures that are close to optimal orientation a critical state of stress. Understanding the specific primary and secondary triggering mechanisms during hydraulic fracturing is expected to furnish new insights regarding stress, strength of faults and rupture initiation and propagation. Here, we present evidence for the existence of earthquake-earthquake triggering cascades in microseismicity induced by hydraulic fracturing using novel methods from statistical seismology. While background seismicity dominates, we find that these triggering cascades exhibit features that also characterize tectonic aftershock sequences such as the empirical Omori-Utsu law and the productivity law. While this suggests that the underlying physical triggering mechanisms are similar in both cases, there are also pronounced differ-

ences. Specifically, we find that the magnitudes of earthquakes in microseismicity induced by hydraulic fracturing are not random but tend to cluster—independent of whether one considers background events or triggered events. We attribute this to the specific geometry associated with tight shale gas and oil reservoirs, which may lead to the occurrence of fracture arrest at bedding boundaries and gives rise to stratabound fracture networks. This has important implications for seismic hazard assessment and forecasting related to hydraulic fracturing.

#### **Finite Element Modelling of Fault Reactivation: Stress Drop and Slip**

SATTARI, A., University of Calgary, Calgary, AB, Canada, asattari@ucalgary.ca; EATON, D. W., University of Calgary, Calgary, AB, Canada, eatond@ucalgary.ca

A finite-element approach is used to investigate the scaling of fault slip activation, based on a simple model for strain weakening that makes use of a dynamic values of cohesion and friction that are less than the static values. A critically stressed fault is subject to failure in response to a small perturbation in stress, such as a pressure increase due to fluid injection. During a simulated slip event, typical rate-and-state models imply a reduction from static to dynamic coefficients of friction of approximately 10% to 15%. We assume that the stress drop due to slip results in a post-seismic stress state in which the Mohr circle is tangent to a failure line that reflects dynamic friction. This simple model implies that stress drop on the fault plane generally increases with depth, due to the increase in normal stresses acting on the fault. Our modelling results imply that scaling parameters, including average slip and stress drop, vary with friction coefficients in a manner that is consistent with previous experimental and theoretical models. Faults that have experienced a prolonged period of quiescence, such as most faults triggered by fluid injection, are most likely characterized by higher cohesion than is typical of tectonically active faults. As expected, our models indicate that stress drop and slip are increased if a higher cohesion is assigned to the model.

#### **Earthquake Stress-drop Tensors and Critical States during Fluid Injection**

EATON, D. W., University of Calgary, Calgary, AB, Canada, eatond@ucalgary.ca; KREBES, E., University of Calgary, Calgary, AB, Canada, krebes@ucalgary.ca

A tensor expression for earthquake stress drop is derived that is analogous to seismic moment tensors, providing new insight into co-seismic stress changes and earthquake cycles. For both shear slip and tensile mechanisms, co-seismic stress drop can be represented as a shift away from a critical state of stress, accompanied by a reduction in the difference between maximum and minimum principal stresses. For earthquake cycles driven by continuous tectonic loading of a fault, this leads to oscillation between critical and residual stress states. For seismicity caused by increasing pore pressure during fluid injection, our model implies a progressive reduction in radius of the Mohr (stress) circle. As pore pressure increases, the stress field ultimately converges toward an isotropic state that is determined by the tensile strength of the medium.

#### **West Texas Seismicity and Distinguishing Natural from Anthropogenic Causes**

WALTER, J. I., Institute for Geophysics, University of Texas, Austin, TX, USA, jwalter@ig.utexas.edu; FROHLICH, C., Institute for Geophysics, University of Texas, Austin, TX, USA; GALE, J. F. W., Bureau of Economic Geology, University of Texas, Austin, TX, USA; BORGFELDT, T., Institute for Geophysics, University of Texas, Austin, TX, USA; BILEK, S., New Mexico Tech, Socorro, NM, USA; GERZINA, J., University of Texas, Austin, TX, USA; DOTRAY, P. J., University of Texas, Austin, TX, USA

We utilize Transportable Array data to survey regional seismicity in West Texas, including the Permian Basin and Texas Panhandle. Through analyst review and a waveform-matching technique, we identify earthquakes occurring in early 2008 through 2011. Significant seismicity occurred near the North Texas border with New Mexico and may have a natural tectonic origin. In addition to this diffuse clustering, a number of events and clusters appear to be adjacent to areas of active hydrocarbon recovery efforts throughout the Permian Basin and West Texas. Work is underway to deduce possible causes of those seismic events by comparing event catalogs with regulatory filings, including investigating the possibility that the seismicity is natural. The results of this study highlight the continued need for more extensive seismic monitoring in the central and eastern US. In addition, this work provides a baseline seismicity assessment for future monitoring efforts by the State of Texas.

#### **Frequency-magnitude Distribution for Natural and Mining-induced Seismicity in UK**

SEGOU, M., British Geological Survey, Edinburgh, United Kingdom, msego@bgs.ac.uk; BAPTIE, B., British Geological Survey, Edinburgh, United Kingdom, bbap@bgs.ac.uk

Over the last 30 years mining-induced seismicity in United Kingdom has been monitored by the British Geological Survey. About 4000 events with local magnitudes between -0.7 and 3.0 have been reported in coal mining reporting areas. The magnitude-frequency distribution follows a Gutenberg-Richter relation with a higher b-value of about 1.35 and 1.1 in Scotland and England, respectively. The above indicates the absence of large magnitude events for this type of induced seismicity. Within the instrumental seismicity period about 45% of seismicity corresponds to coal mining events. Reliable baseline for natural seismicity is essential to both discriminating from induced seismicity, such as hydraulic fracturing, and providing stake-holders/ decision makers real-time earthquake probabilities during operational phase. The magnitude-frequency distribution suggests a b-value of 0.85 with standard deviation of 0.12 for the entire catalog of naturally triggered events with some variability met at different regions. Analytically b-values of about 0.95, 0.70 and 0.9 are reported in Scotland, Wales and England with standard deviations of 0.1, 0.07 and 0.14, respectively. The 1984 M<sub>L</sub>=5.4 Llyn Peninsula remains the larger earthquake reported the last half-century and it is characterized by a low p-value indicating a slow aftershock decay rate. In the UK a moderate sized event with magnitude larger than 5, occurs on average every 15 years followed by few (<10) felt aftershocks. In this low-seismicity environment only local population at the vicinity of mining fields has experienced light (EMS 5/6) ground shaking in the past.

#### **Effects of Hydraulic Diffusivity and Rate- and State-dependent Friction in Simulations of Injection Induced Seismicity**

KROLL, K. A., UC Riverside, Riverside, CA, USA, kkrol001@ucr.edu; RICHARDS-DINGER, K. B., UC Riverside, Riverside, CA, USA, keithrd@ucr.edu; DIETERICH, J. H., UC Riverside, Riverside, CA, USA, dieterichj@ucr.edu

We couple the 3D, physics-based earthquake simulator, RSQSim, to a reservoir model that calculates pressure changes that reduce effective stress and drive the occurrence of earthquakes. RSQSim is a computer code that generates long catalogs of seismicity based on stress changes due to fault interaction. The rate-state constitutive laws that govern the deterministic fault behavior in RSQSim have been shown to reproduce the spatio-temporal clustering of seismicity that is observed in induced sequences. The computational efficiency of RSQSim allows for multiple simulations to systematically explore the parameters that control induced seismicity. The simulations can contribute to the formalization of optimal injection parameters designed to minimize seismic hazard, provide physics-based statistical data from which stop-light procedures can be developed, and aid in hazard assessments of a given site under specified injection locations, rates, and volumes.

Simulations presented here incorporate optimally oriented, single isolated faults with fractally distributed initial shear stress conditions. Several scenarios are modeled which include variable von Karman fractal parameters, rate-and state-dependent frictional parameters, and values of hydraulic diffusivity. We determine the effect of the initial stress distribution and rate-state parameters on the spatial pattern of injection induced seismicity, the Gutenberg-Richter b-values, changes in post shut-in seismicity rate. We also investigate the spatial and temporal distribution of seismicity after injection ceases to determine the seismicity decay rate and the likelihood of a larger earthquake occurring, as has been observed at some industrial injection localities. Results demonstrate that induced earthquake sequences are sensitive to the constitutive parameters, a and b, of the rate-state formulation. Finally, we find the rate of induced earthquakes decreases for increasing values of hydraulic diffusivity.

#### **Prediction of Earthquake Ground Motions in Western Alberta**

YENIER, E., Nanometrics Inc., Kanata, ON, Canada, emrahyenier@nanometrics.ca; BATURAN, D., Nanometrics Inc., Kanata, ON, Canada, dariobaturan@nanometrics.ca; LAW, A., Nanometrics Inc., Kanata, ON, Canada, andrewlaw@nanometrics.ca; ATKINSON, G. M., Western University, London, ON, Canada, gmatkinson@aol.com

We develop a ground-motion prediction equation (GMPE) for earthquakes in western Alberta, where hazard contributions from induced seismicity is of particular interest. We investigate the regional source and attenuation attributes using peak ground motions and response spectra from recorded seismic events. We supplement the seismic data with ground motions obtained from mining/quarry blasts in the region, to gain insights into the regional attenuation over a

wide distance range. The available empirical data is limited for deriving a robust predictive model in the magnitude range of engineering interest ( $M > 4$ ). We therefore adopt a regionally-adjustable generic GMPE (Yenier and Atkinson, 2015 BSSA), with parameters that have been calibrated to the rich empirical data in California, to ensure seismologically robust predictions for moderate-to-large magnitudes. We modify the model parameters of generic GMPE based on the source and attenuation attributes observed in western Alberta, and determine an empirical calibration factor that accounts for the overall differences between the generic model and the empirical data in the region. This provides a hybrid GMPE that is fully-adjusted for observed motions in western Alberta and is applicable for wide ranges of magnitude and distance.

### Shallow Microearthquakes Near Chongqing, China Triggered by the Rayleigh Waves of the 2015 M7.8 Gorkha, Nepal Earthquake

HAN, L. B., Institute of Geophysics, China Earthquake Administration, Beijing, China, chinakmm@gmail.com; PENG, Z. G., School of Earth and Atmospheric Sciences, Georgia Tech, Atlanta, GA, USA, zpeng.seismo@gmail.com; LI, L., Institute of Geophysics, China Earthquake Administration, Beijing, China, sophia\_lilu@163.com; WANG, B. S., Institute of Geophysics, China Earthquake Administration, Beijing, China, wangbs@cea-igp.ac.cn; WU, J., Institute of Geology and Geophysics, Chinese Academy of Sciences, Beijing, China, xianhua123@yahoo.com; LI, Q., Earthquake Administration of Chongqing Municipality, Chongqing, China

Earthquakes could be triggered dynamic stresses from large earthquakes at long-range distances. In intraplate regions, remotely triggered seismicity is mostly identified near active faults or regions with high background seismicity. These include aftershock zones of previous large earthquakes, or regions with anthropogenic activities such as active mining or reservoirs.

Here we report another case of remotely triggered seismicity in Southwest China by the 2015/04/25 M7.8 Gorkha, Nepal earthquake. The Nepal earthquake is the largest event occurring along the Himalaya frontal thrusts since the 1950 M8.6 Assam-Tibet earthquake, and triggered many aftershocks in Nepal and normal-faulting events in Southern Tibet. We identify a local magnitude ML3.8 ( $M_s 3.1$ ) event listed in the China Earthquake National Center (CENC) catalog, which occurred near Qijiang district south of Chongqing city, about 12 minutes after the Nepal earthquake. This event was recorded by many stations with the distance of  $\sim 400$  km. We also identify a new local event with an estimate magnitude ML1.8 about tens of seconds before the ML3.8 event. Both events occurred during the first two cycles of the Rayleigh waves from the Nepal earthquake, indicating a triggering relationship. We use the two events as templates to scan through the continuous waveform, but find no more events with mean cross-correlation (CC) values larger than 9 times the median absolute deviation values. This suggests that the two events occurred during the Rayleigh waves were indeed triggered, rather than background seismicity.

Because the location of ML3.8 event is close to regions with underground anthropogenic activities (active mining and shale gas development), we speculate that these activities may perturb the subsurface stress conditions, making this region more susceptible for dynamic triggering. Our next step is to accurately determine their focal depths and exact relationship with dynamic stresses of Rayleigh waves.

## Multidisciplinary Studies of Earthquakes—Slow, Fast, and In Between: A Broad Range of Fault Behavior in Space and Time

Poster Session · Wednesday · 20 April · Tuscany F

### Transient Creep Events Detected by PBO Strainmeters in the Parkfield Region of the San Andreas Fault

GOTTLIEB, M., UNAVCO, Boulder, CO, USA, gottlieb@unavco.org; MENCIN, D. J., UNAVCO, Boulder, CO, USA; HODGKINSON, K. M., UNAVCO, Boulder, CO, USA, hodgkinson@unavco.org; BILHAM, CIRES, University of Colorado, Boulder, CO, USA; MATTIOLI, G. S., UNAVCO, Boulder, CO, USA; JOHNSON, W., UNAVCO, Boulder, CO, USA; VAN BOSKIRK, E., UNAVCO, Boulder, CO, USA; HENDERSON, D., UNAVCO, Boulder, CO, USA; MEERTENS, C. M., UNAVCO, Boulder, CO, USA

Strainmeters and creepmeters have been operated along the San Andreas Fault, observing creep events for decades. In particular, the EarthScope Plate Boundary Observatory (PBO) has added a significant number of borehole strainmeters along the San Andreas Fault (SAF) over the last decade. The geodetic data cover a significant temporal portion of the inferred earthquake cycle along this portion

of the SAF. While creepmeters have a resolution of 5  $\mu\text{m}$  over a range of 10 mm and a dynamic sensor with a resolution 25  $\mu\text{m}$  over a range 2.2 m borehole strainmeters measure local deformation some distance from the fault with a broader aperture. Borehole tensor strainmeters principally deployed as part of the PBO, measure the horizontal strain tensor at a depth of 100-200 m with a resolution of 10-11 strain and are located 4–10 km from the fault with the ability to image a 1 mm creep event acting on an area of  $\sim 500$  m<sup>2</sup> from over 4 km away (fault perpendicular). A single borehole tensor strainmeter is capable of providing broad constraints on the creep event asperity size, location, direction and depth of a single creep event.

Since the installation of the first PBO strainmeter in Parkfield in 2006 multiple discrete hour-long creep events have been detected in northern Parkfield, the southern end of the creeping section of the SAF. These events have been confirmed in the creepmeter measurements. By contrast, only a few events,  $\sim 1$  per year, have been detected in southern Parkfield, the northern terminus of the 1857, M7.9 Ft Tejon rupture zone. The synthesis of these unique high-rate strain and creep recordings presents a unique opportunity to constrain the partitioning between aseismic and seismic slip on the central SAF. We show that simple elastic half-space models allow us to loosely constrain the location and depth of any individual creep event on the fault, even with a single instrument, and to image the accumulation of creep with time.

### Foreshock and Aftershock Detection around the 2014 Mw6.1 Kangding Earthquake

HAN, L. B., Institute of Geophysics, China Earthquake Administration, Beijing, China, chinakmm@gmail.com; PENG, Z. G., School of Earth and Atmospheric Sciences, Georgia Tech, Atlanta, GA, USA, zpeng.seismo@gmail.com; YAO, D. D., School of Earth and Atmospheric Sciences, Georgia Tech, Atlanta, GA, USA, yaodong1990@gmail.com; SU, J. R., Earthquake Administration of Sichuan Province, Chengdu, China, sujr0816@163.com; LONG, F., Earthquake Administration of Sichuan Province, Chengdu, China, longfeng1981@gmail.com

Foreshock activity was considered as one of the most important precursors before large earthquakes. However, it is still not clear why foreshocks only occurred before some earthquakes, and so far there is no way to distinguish them from background seismicity before the mainshock happens. Because many small-magnitude events are not listed in standard catalogs around the mainshock time, a systematic detection of missing foreshocks and aftershocks could shed new light on their physical mechanisms and necessary conditions for foreshock generation.

On Nov 22nd 2014, the  $M_w 6.1$  Kangding earthquake occurred along the large left-lateral strike-slip Xiashuihe fault in Southwest China. Three days later, another  $M_w 5.7$  earthquake occurred about 10km to the southeast of the mainshock. Both events were followed by numerous aftershocks (Fang *et al.*, 2015). In addition, the  $M_w 6.1$  mainshock were preceded by two foreshocks in the last day as listed in the regional earthquake catalog. Here we employ the extensive waveform dataset recorded by six permanent broad-band stations and two portable short-period stations deployed about two days after the mainshock. We use waveforms of relocated earthquakes as templates and scan through continuous recordings to detect additional earthquakes that are missing from the catalog. Only events with mean cross-correlation (CC) values larger than 9 times the median absolute deviation values are kept. So far we have detected 95 events within 8 hours after the mainshock. In comparison, only 72 events were listed in the catalog. We plan to systematically relocate those newly detected events to better understand spatio-temporal evolutions of foreshocks and aftershocks in this sequence. In addition, we are about to search for potential repeating earthquakes with mean CC values larger than 0.9, and use them to better constrain aseismic slip before and after the mainshock.

### Ambient Tremor Detection in the Geysers Region, CA

DAMIAO, L. G., UC Berkeley, Berkeley, CA, USA, ldamiaio@berkeley.edu; NADEAU, R. M., UC Berkeley, Berkeley, CA, USA, nadeau@berkeley.edu; LUNA, B., UC Berkeley, Berkeley, CA, USA, bluna@berkeley.edu; TAIRA, T., UC Berkeley, Berkeley, CA, USA, taira@seismo.berkeley.edu; DREGER, D. S., UC Berkeley, Berkeley, CA, USA, ddreger@berkeley.edu; GUILHEM, A., CEA/DAM/DIF Commissariat à l'Energie Atomique, Arpajon, France, aurelie.guilhem@cea.fr; ZHANG, H., University of Science and Technology of China, Hefei, Anhui, China, zhang11@ustc.edu.cn

Ambient tremor in California has been extensively studied in the Parkfield-Cholame, CA region where recordings from numerous cemented-in borehole stations are available. However, the identification and study of ambient tremor is faced with more challenges in other regions of California, due in part to less optimal instrument coverage. We present a new methodology for automated detection of tremor applied to the Geysers region of California. Through an itera-



tive process, the methodology uses a combination of envelope-normalization and quantile-stacking of velocity seismograms from spatially distributed stations to extract an empirically derived time-series 'template' that represents the seismic energy release history for each day. Cross-correlation sweeps of the template with envelopes from distributed stations are then performed for each day. This is done to identify periods of elevated energy release that are coherent among multiple stations and of extended duration (indicative of tremor activity). Initial tests in the Parkfield area of California indicate that an ~ 10-fold increase in detection sensitivity over a previous amplitude-based detection scheme can be achieved using this method. False detections from overlapping local and regional events and complications from anthropogenic, instrumental, and telemetry issues are also reduced using this method. We will report on application of the method to the less optimally instrumented Geysers region in California where it has resulted in the identification of previously unrecognized tremor activity.

### Modeling Pore Pressure Changes due to Slow Earthquakes: Implications for Tectonic Tremor Generation in Guerrero, Mexico

VILLAFUERTE, C. D., Instituto de Geofísica, Universidad Nacional Autónoma de México, México City, México, villafuerte.cd@gmail.com; CRUZ-ATTENZA, V. M., Instituto de Geofísica, Universidad Nacional Autónoma de México, México City, México, cruz@geofisica.unam.mx; BHAT, H. S., Institut de Physique du Globe de Paris, Paris, France, bhat@ipgp.fr

Several studies claim that the origin of tectonic tremors (TT) and slow slip events (SSE) is strongly related to the presence of overpressure fluids. However, in order to determine the role of fluids in the generation of slow phenomena, quantitative models should explain the observations. The complex behavior of TT and SSE exhibited in Guerrero makes it an interesting region to study and prove new hypothesis about the origin of these phenomena. In Guerrero, TTs occur along the horizontal segment of the slab over two regions denominated the Transient zone and Sweet Spot. These regions are located where near-lithostatic pore pressure (Pp) has been inferred by different studies in the upper oceanic crust. By computing the stress field induced by slow slip transients, we calculate the normal and shear stresses acting on the TT regions and solve the poroelastic diffusion equation considering both the permeability as a function of the effective pressure (Pe) and a sealed plate interface. Such a nonlinear problem is solved in 2D by means of a finite volume approach. Our modeling results show that the evolution of the Coulomb Failure Stress (CFS) within the slab, and at the plate interface, mimics the long-term occurrence-rate of the LFEs in the Sweet Spot. In addition, local gradients and Gaussian-like Pp distributions, that may be due to local dehydration processes and lateral temperature changes along the slab, yield solitary pore pressure waves exhibiting two main characteristics: 1) a fast Pp perturbation front at speeds of some km/h (10-25 km/h) and 2) a slower Pp pulse with velocities on the order of km/day (0.5-10 km/day). Both propagation velocities are comparable with the rapid and slow migration of the TT sources recently observed in Guerrero. Further analysis is necessary to compare the lower speed with the slip front propagation of long term SSE and to assess if such a slow pulse may act as an external source leading to the initiation of slow rupture fronts.

## Past and Future Seismic Moment Release: Contributions from Statistics and Geodesy

Poster Session · Wednesday · 20 April · Tuscany F

### Seismic Hazard Estimation of Northern Iran Using Smoothed Seismicity

KHOSHNEVIS, N., University of Memphis, Memphis, TN, USA, nkshnvs@memphis.edu; AZIZZADEH-ROODPISH, S., University of Memphis, Memphis, TN, USA, szzzdrd@memphis.edu; TABORDA, R., University of Memphis, Memphis, TN, USA, rtbrdros@memphis.edu; CRAMER, C. H., University of Memphis, Memphis, TN, USA, ccramer@memphis.edu

In this study we conduct a probabilistic seismic hazard assessment for northern Iran, using recently confirmed ground motion prediction equations and updated seismic catalogs. We evaluate seismic hazard over three complete tectonic seismic zones (Alborz Mountain Range, Azerbaijan, and Kopch-Dagh), as well as parts of two neighboring tectonic zones (Zagros and Central-East Iran). The assessment is done using smoothed seismicity. In our model, events are not assigned to specific fault systems but are instead assumed to be potential seismogenic sources by themselves, and are spatially gridded into area cells. We decluster historical and instrumental seismicity to compute earthquake rates in each grid cell, and smooth these rates to account for uncertainty in the spatial distribution of future earthquakes. Grid cells are regularly spaced at 0.1 degree in both latitude and longitude, and we use a Gaussian filter to smooth the fraction of earthquakes in incremental intervals of magnitude. In order to determine the seismicity rate, we

consider all historical and instrumental earthquakes with magnitude greater than 3. To calculate the seismic hazard, we defined two models based on structural damage threshold magnitude, including  $M_w$  4.5 and  $M_w$  5. Seismicity parameters are calculated for each seismic region, and we obtain final smoothed seismicity results for each region as well. In addition, we also considered the combination of all regions as a uniform study area. We add the probability of exceedance of all regions and then present smoothed seismicity hazard outcomes, for which horizontal peak ground acceleration is selected as the ground motion parameter. Final results are assessed in terms of the expected peak ground acceleration with 10 and 2 percent probability of exceedance in 50 years for rock site conditions.

### Statistically Significant Global Variations of Seismic Moment

ZALIAPIN, I., University of Nevada, Reno, NV, USA, zal@unr.edu; KREEMER, C., University of Nevada, Reno, NV, USA, kreemer@unr.edu

The significance of a clear increase in the number of Great earthquakes since 2004 has been debated extensively. We argue that to truly reveal if the observed change is a significant deviation from a long-term expectation it is important to (i) analyze moment release, not merely the number of events, (ii) consider large enough range of examined moments—say, all events above  $10^{18}$  Nm, and (iii) consider sequential moment release, not the statistical distribution of earthquake moments collected during a given time interval. Here we analyze moment release from 1950-2014 and explicitly include the above aspects in our analysis. We show that the observed global cumulative moment release since 1950 cannot be satisfactorily explained by a tapered Pareto distribution of moments with a time-independent corner magnitude. Furthermore, we show that the observations are consistent with a model that assumes a decreased corner moment (which leads to decreased moment release) during the approximate time interval 1970-2000. Thus the post-2004 period may have appeared anomalous because the previous three decades had a statistically significant low moment release. Our results remain valid for alternative choices of moment distribution such as doubly truncated Pareto, using alternative taper functions, etc. The results are independent of a particular model for the time occurrence of events. The fact that the period of significantly lower moment release followed immediately after the decade with the highest moment release (*i.e.*, the 1960s) may suggest that the global variation in seismic moment release has some physical underpinning. Our findings also have bearings on heavy-tail statistical modeling aimed at explaining the typically large discrepancy between geodetic moment rate estimations and observed rates of seismic moment release reported in various tectonic environments.

### Scaling of Maximum Earthquake Magnitudes with Geometrical and Stress Properties of Strike-Slip Faults

MARTINEZ-GARZON, P., GFZ German Research Centre for Geosciences, Potsdam, Germany, patricia@gfz-potsdam.de; BOHNHOFF, M., GFZ German Research Centre for Geosciences, Potsdam, Germany, bohnhoff@gfz-potsdam.de; BEN-ZION, Y., University of Southern California, Potsdam, Germany, benzion@usc.edu; DRESEN, G., GFZ German Research Centre for Geosciences, Potsdam, Germany, dre@gfz-potsdam.de

Providing constraints for maximum magnitude earthquake on major continental strike-slip faults is important for seismic hazard estimates of populated areas near these faults. We compiled a catalog of major earthquakes on continental strike-slip faults worldwide to investigate the relation between their maximum observed earthquake magnitudes (from instrumental recordings or historical catalogs and trenching studies), with various geometrical properties including cumulative displacement, mapped fault length, seismogenic thickness and angle between fault strike and maximum horizontal stress. Additional compiled data are slip rates and coseismic slip of selected earthquakes (when available).

For 75–80% of the data set, the observed maximum scalar moment scales with the product of seismogenic thickness and either cumulative displacement or mapped fault length. Most faults from this population have slip rates  $>5$ mm/yr (mostly representing interplate faults), cumulative displacement  $>10$  km, and relatively high angles to the maximum horizontal stress orientation. The remaining 20–25% population involves events at some distance from a plate boundary with slip rate  $<5$ mm/yr, cumulative displacements  $<10$ km, and forming  $\approx 45^\circ$  to the maximum horizontal stress. These faults ruptured in significantly larger earthquakes than the previous population. By examining the coseismic slip and earthquake rupture length of these earthquakes we observe that they likely ruptured with larger stress drops. Some of the faults from the second population are the onshore strike-slip faults from Japan (Tanna, Atera and Neodani Fault Zones) as well as the Eastern California Shear Zone.

The most likely interpretation of the results is that the maximum earthquake rupture length, and hence earthquake magnitude correlates with the cumulative displacement and the fault surface length. The results also suggest that progressive fault smoothing may lead to decreasing coseismic stress drops.

### A Global Mmax for Stable Continental Regions?

VANNESTE, K., Royal Observatory of Belgium, Brussels, Belgium, kris.vanneste@oma.be; VLEMINCKX, B., Royal Observatory of Belgium, Brussels, Belgium, bart.vleminckx@oma.be; STEIN, S., Northwestern University, Evanston, IL, USA, s-stein@northwestern.edu; CAMELBECK, T., Royal Observatory of Belgium, Brussels, Belgium, thierry.camelbeck@oma.be

One can ask if the largest observed earthquake magnitude in a region ( $M_{\text{maxobs}}$ ) is the largest that can occur in that region ( $M_{\text{max}}$ ). This question is difficult to answer for seismically active regions and even more so for stable continental regions (SCR). Such regions are often characterized by low seismicity with large recurrence periods for larger earthquake magnitudes and no or little information on active faults. Traditionally it has been argued that  $M_{\text{max}}$  should be similar in tectonically similar SCR around the world. Such a tectonic division of SCR was first proposed by Johnston *et al.* (1994) and later updated by U.S. NRC *et al.* (2012), resulting in 255 SCR domains, which were further grouped into superdomains, each characterized by an  $M_{\text{maxobs}}$ .

We consider whether  $M_{\text{maxobs}}$  of the superdomains reflect a different  $M_{\text{max}}$  for each or if a global  $M_{\text{max}}$  could exist for all SCR. In the latter case the difference in  $M_{\text{maxobs}}$  between superdomains would just be due to a limited period of observation. To explore this question, we simulate earthquake catalogs assuming a global  $M_{\text{max}}$  of 7.9, the largest earthquake magnitude observed in SCR to date. Using published average recurrence parameters per continent, a Poisson temporal occurrence model, catalog completeness thresholds for different regions within each continent and catalog lengths similar to what we presently have, 10,000 random catalogs were simulated for each SCR domain and combined into superdomain catalogs.

The resulting superdomain  $M_{\text{maxobs}}$  distributions appear very similar to the one observed in reality, suggesting that a single global  $M_{\text{max}}$  could exist for SCR and that this possibility should be considered in seismic hazard assessments. If done carefully this would not necessarily increase the predicted hazard because earthquakes with magnitude  $M_{\text{max}}$  are very rare. We also investigate the effect of a larger global  $M_{\text{max}}$  and longer catalog, and find that catalog length is the limiting factor in our knowledge of  $M_{\text{max}}$ .

### Estimation of the Frequency-Magnitude Gutenberg-Richter $b$ -Value Without Making Assumptions on Levels of Completeness

KIJKO, A., University of Pretoria, Pretoria, South Africa, andrzej.kijko@up.ac.za; SMIT, A., University of Pretoria, Pretoria, South Africa, ansie.smit@up.ac.za

A pronounced weakness of the classic Aki-Utsu  $b$ -value estimator is its heavy dependence on the level of magnitude completeness  $m_c$  whose assessment is in itself not a trivial task and reliant on human opinion. New estimators for frequency-magnitude Gutenberg-Richter  $b$ -value which are not dependent on the level of completeness  $m_c$  are proposed in the place of the Aki (1965) maximum likelihood and Utsu (1965) moment estimators. The Monte-Carlo simulations show that these newly derived estimators are especially effective when the incomplete frequency-magnitude distribution is gradually curved and has only one maximum *i.e.* it belongs to the distributions of category IV according to classification by Mignan (2012). The most striking feature of the newly derived moment estimator is its simplicity as it can be expressed by the first three sample central magnitude moments—the mean, standard deviation and skewness. The simulations also show that the proposed maximum likelihood estimator of the  $b$ -value can be considerably less accurate than its moment counterpart. In cases where the applied sample of earthquake magnitudes is complete, the equations describing the newly derived moment and maximum likelihood  $b$ -value estimators take the form of the classic Aki (1965) and Utsu (1965)  $b$ -value solutions. Since the newly proposed  $b$ -value estimators also incorporate weak seismic events, they can generate more reliable earthquake hazard, forecasting and prediction assessments.

### Assessing the Hazard of Large Aftershocks in Alaska

KILB, D. L., Scripps Institution of Oceanography, La Jolla, CA, USA, dkilb@ucsd.edu

The seismological community does not yet have an operational plan in place to issue aftershock probability forecasts following a large damaging earthquake in subduction zone regions such as Alaska or Cascadia. Because the bulk of statistical aftershock analyses have been conducted using earthquakes on California crustal strike-slip faults, exporting probability forecast algorithms from California to subduction zones environments might not be appropriate. Here, we generate mainshock/aftershock statistics with the aim to assist future earthquake forecasting efforts in subduction zones. To begin, using 20 years (1995-2015) of ANSS Alaska data we identify 50 mainshocks ( $M \geq 6.5$ ) and use K-means clustering to identify aftershocks. For each sequence we determine the magnitude differential between the mainshock and largest aftershock ( $a \sim 1.2$  value is

expected based on Bath's law) and use a maximum likelihood method to estimate the  $b$ -value (a magnitude frequency distribution measurement). We investigate if the magnitude differentials correlate with the  $b$ -values and to what extent there is a space/time pattern in these parameters. Alaska data are optimal for this task because there are far more data from the Alaska region than the entire lower-48 combined. Also, Alaska has deep subduction zones and shallow strike-slip zones, allowing us to test if faulting regime plays a role in these parameter characteristics. We find the magnitude differentials span a wide range (0.1 to 2.6 units), albeit, the larger differentials could result from large aftershocks missing from the catalog. Our initial results show the two deepest events (135km on 28 July 2001; 109km on 23 June 2014) have some of the largest differentials and smallest  $b$ -values and that the two most northern events along the strike-slip Denali Fault in 2002 have relatively high  $b$ -values and large differentials. This spatial partitioning suggests it is worthwhile to tune aftershock probability forecasts for subduction zones.

### Improved Omori Parameters for Global Aftershock Forecasts

PAGE, M. T., USGS, Pasadena, CA, USA, pagem@caltech.edu; HARDEBECK, J. L., USGS, Menlo Park, CA, USA, jhardebeck@usgs.gov; VAN DER ELST, N. J., USGS, Pasadena, CA, USA, nvanderelst@usgs.gov; FELZER, K. R., USGS, Pasadena, CA, USA, kfelzer@usgs.gov; MICHAEL, A. J., USGS, Menlo Park, CA, USA, michael@usgs.gov

Following a large earthquake, seismic hazard can be orders of magnitude higher than the long-term average as a result of aftershock triggering. Due to this heightened hazard, there is a demand from emergency managers and the public for rapid, authoritative, and reliable aftershock forecasts.

In the past, USGS aftershock forecasts following large, global earthquakes have been released on an ad-hoc basis with inconsistent methods, and in some cases, aftershock parameters adapted from California. To remedy this, we are currently developing an automated aftershock product that will generate more accurate forecasts based on the Reasenberg and Jones (Science, 1989) method. To better capture spatial variations in aftershock productivity and decay, we estimate regional aftershock parameters for sequences within the Garcia *et al.* (BSSA, 2012) tectonic regions. We find regional variations in mean aftershock productivity of almost a factor of 10.

The Reasenberg and Jones method combines modified-Omori aftershock decay, Utsu productivity scaling, and the Gutenberg-Richter magnitude distribution. We additionally account for a time-dependent magnitude of completeness following large events in the catalog.

In addition to estimating average parameters, we develop an inversion method to solve for the inter-sequence productivity variability. This allows for a more complete quantification of the forecast uncertainties and Bayesian updating of the forecast as sequence-specific information becomes available. We find that aftershock productivity is more variable for lower mainshock magnitudes and in regions where the mean stress drop is high.

### Recent Achievements of the Collaboratory for the Study of Earthquake Predictability

JACKSON, D., UCLA, Los Angeles, CA, USA, djackson@g.ucla.edu; WERNER, M., University of Bristol, Bristol, UK, max.werner@bristol.ac.uk; LIUKIS, M., SCEC, USC, Los Angeles, CA, USA, liukis@usc.edu; SCHORLEMMER, D., GFZ, Potsdam, Germany, ds@gfz-potsdam.de; YU, J., SCEC, USC, Los Angeles, CA, USA, johnyu@usc.edu; MAECHLING, P., SCEC, USC, Los Angeles, CA, USA, maechlin@usc.edu; RHOADES, D., GNS Science, Lower Hutt, New Zealand, D.Rhoades@gns.cri.nz; ZECHAR, J., Swiss Seismological Service, ETH, Zurich, Switzerland, jeremy.zechar@sed.ethz.ch; MARZOCCHI, W., INGV, Rome, Italy, warner.marzocchi@ingv.it; JORDAN, T., SCEC/USC, Los Angeles, USA, tjordan@usc.edu

The Collaboratory for the Study of Earthquake Predictability (CSEP) supports a global program to conduct prospective earthquake forecasting experiments. CSEP testing centers are now operational in California, New Zealand, Japan, China, and Europe with 436 models under evaluation. The California testing center, started by SCEC, Sept 1, 2007, currently hosts 30-minute, 1-day, 3-month, 1-year and 5-year forecasts, both alarm-based and probabilistic, for California, the Western Pacific, and worldwide. Our tests are now based on the hypocentral locations and magnitudes of cataloged earthquakes, but we plan to test focal mechanisms, seismic hazard models, ground motion forecasts, and finite rupture forecasts as well. We have reduced testing latency, implemented prototype evaluation of M8 forecasts, and are currently developing formats and procedures to evaluate externally hosted forecasts and predictions. CSEP supports the USGS program in operational earthquake forecasting and a DHS project to register and test external forecast procedures from experts outside seismology. We found that earthquakes as small as magnitude 2.5 provide important information on subse-

quent earthquakes larger than magnitude 5. A retrospective experiment for the 2010-2012 Canterbury earthquake sequence showed that some physics-based and hybrid models outperform purely statistical (*e.g.*, ETAS) models. This experiment also demonstrates the ability of the CSEP infrastructure to support retrospective forecast testing. Current CSEP development activities include implementation of evaluation strategies that increase computational efficiency for high-resolution global experiments, such as the evaluation of the Global Earthquake Activity Rate (GEAR) model. We describe the open-source CSEP software that is available to researchers as they develop their forecast models. We also discuss how CSEP procedures are being adapted to intensity and ground motion prediction experiments as well as hazard model testing.

#### The Virtual Quake Earthquake Simulator

SCHULTZ, K. W., University of California, Davis, Davis, CA, USA, kwschultz@ucdavis.edu; WILSON, J. M., University of California, Davis, CA, USA; SACHS, M. K., University of California, Davis, CA, USA; HEIEN, E. M., University of California, Davis, CA, USA; RUNDLE, J. B., University of California, Davis, CA, USA; TURCOTTE, D. L., University of California, Davis, CA, USA

Virtual Quake is a boundary element code designed to explore the seismicity of today's fault systems. Virtual Quake (VQ) simulates any input fault network to produce seismic histories of 100,000 years or more. Virtual Quake has had numerous improvements and additional features added in the past year. Here we present revised conditional probabilities for large California earthquake scenarios in addition to summarizing other VQ projects currently underway.

Virtual Quake is hosted by the Computational Infrastructure for Geodynamics, free to use, and comes with a user's manual. Virtual Quake has been downloaded by researchers around the world, and we are currently collaborating with researchers who are using Virtual Quake to assess seismic hazard in their regions.

<http://geodynamics.org/software/vq/>

#### Time-dependent Models of Interseismic Deformation in the Northwestern United States

POLLITZ, F. E., USGS, Menlo Park, CA, USA; EVANS, E. L., USGS, Menlo Park, CA, USA

GPS velocity fields in the Western US have been traditionally interpreted with time-independent block models driven by backslip at the 'locking rate' on model faults that divide a set of crustal blocks. The viscoelastic block model is a time-dependent variation of the block model which accounts for viscoelastic (lower crust and mantle) relaxation from past slip events. Here we construct viscoelastic block models for the Western US, focusing on the Pacific Northwest and the earthquake cycle on the Cascadia megathrust. The western US is divided into blocks selected from an initial set of 137 microplates using the method of Total Variation Regularization (Evans *et al.*, 2015), allowing potential tradeoffs between surface faulting and megathrust coupling to be determined algorithmically from GPS observations. Trial depth-dependent viscoelastic structures and major fault recurrence intervals are prescribed; a 500-year recurrence interval is assigned to the Cascadia megathrust. Fault geometry, slip rate, and locking fractions are estimated simultaneously within the Total Variation regularized block model. For a range of mantle asthenosphere viscosity ( $4.4 \times 10^{18}$  Pa s to  $3.6 \times 10^{20}$  Pa s) we find that fault locking on the megathrust is concentrated in the uppermost 20 km in depth, and a locking rate contour line of 30 mm/yr extends deepest beneath the Olympic Peninsula, characteristics similar to previous time-independent block model results. Both average and maximum locking fraction required to fit the GPS velocity field depend on mantle viscosity, both being higher the lower the viscosity. Moreover, for viscosity less than  $\sim 5 \times 10^{19}$  Pa s, the amount of inferred locking is higher than that obtained using a time-independent block model. This suggests that future time-dependent models for a range of admissible viscosity structures could refine our knowledge of the locking distribution and its epistemic uncertainty.

## Seismotectonics Beyond the Plate Boundary

Poster Session · Wednesday · 20 April · Tuscany F

#### Seismic Imaging of a Continental Intraplate: Long-Term Persistence of Fossil Rifts and Hot Spots in the Central and Eastern United States

POLLITZ, F. E., USGS, Menlo Park, CA, USA; MOONEY, W. D., USGS, Menlo Park, CA, USA

Seismic surface waves from the Transportable Array of Earthscope's USArray are used to estimate phase velocity structure of 18 to 125s Rayleigh waves, then corrected for lateral crustal thickness variations (with CRUST1.0) and inverted to obtain three-dimensional crust and upper mantle structure of the Central and Eastern United States (CEUS) down to  $\sim 200$  km. The obtained lithosphere structure confirms previously imaged features in the CEUS, *e.g.*, the low seismic velocity signature of Proterozoic to Cambrian fossil rifts, the very low velocity at  $>150$  km depth below an Eocene volcanic center in northwestern Virginia, and the very low velocity along a corridor stretching from eastern New York to New Hampshire. The model also reveals new features. The high-velocity Granite-Rhyolite Province sharply bounds the Grenville front at mid-lithosphere depth, suggesting that it acted as a backstop during the Grenville orogeny ca. 1.2–1.0 Ga. High-velocity mantle extending  $\sim 200$  km deep stretches from the Archean Superior Craton well into the Proterozoic terrains (Granite-Rhyolite, Mazatzal and Yavapai provinces). This is consistent with independent seismic velocity images and suggests that the thickness of Proterozoic lithosphere is generally  $\sim 150$ – $200$  km. A deep low-velocity zone in central Texas is associated with the late Cretaceous Travis and Uvalde volcanic fields, and a similar deep low-velocity zone is located beneath the South Georgia Rift, which contains Jurassic basalts associated with the Central Atlantic magmatic province. Hotspot tracks may be associated with several of the low-velocity zones, and the central Texas, New York-New Hampshire, and southern Georgia zones may also be associated with the former rifted Laurentia margin. This suggests a systematic pattern whereby transient mantle thermal perturbations are accentuated near former failed rifts or rift margins.

#### Using the Locations of $M \geq 4$ Earthquakes to Delineate the Extents of the Ruptures of Past Major Earthquakes

EBEL, J. E., Boston College, Weston Observatory, Weston, MA, USA, ebel@bc.edu; CHAMBERS, D. W., Boston College, Department of Mathematics, Chestnut Hill, MA, USA, chambers@bc.edu

Some modern seismicity in the magnitude range between  $M_4$  and  $M_6$  in California and eastern North America preferentially occurs near the edges of past large ruptures. Once a large earthquake rupture has occurred, stress is concentrated at the edges of the rupture, and apparently this stress concentration can trigger earthquakes at or near the rupture edges many decades or even longer after a mainshock. Furthermore, the modern  $M \geq 4$  earthquakes in the vicinity of a past mainshock usually have the same focal mechanism as the earlier mainshock. There are a number of examples of this in California and Nevada, where there is a statistically significant correlation of the locations of  $M \geq 4$  earthquakes and the edges of 19th and 20th century fault ruptures in  $M_w \geq 6.5$  earthquakes. In contrast, the  $M \geq 4$  earthquakes near the epicenters of future ruptures in California are randomly scattered around the fault with no concentration near the ends of the future fault rupture. The concentration of earthquakes near the ends of earlier large ruptures in California becomes progressively less pronounced as the smallest magnitude in the data set is reduced from  $M_{4.0}$  to  $M_{3.0}$ . These observations also appear to be true for intraplate regions where aftershock sequences can last millennia. The identification of modern rupture-edge  $M \geq 4$  aftershocks can be used to help discover where and when past strong earthquakes took place, even if there is no historical record of the mainshock. This is of great importance for seismic hazard studies.

#### A Hybrid-Empirical Ground-Motion Relation for Central and Eastern North America

SHAHJOUEI, A., Cat Management and Analytics Center of Excellence at AIG, Philadelphia, PA, USA, alireza.shahjouei@aig.com; PEZESHK, S., Department of Civil Engineering, University of Memphis, Memphis, TN, USA, spezeskh@memphis.edu

A new hybrid-empirical ground-motion (GMM) model for central and eastern North America has been recently developed as part of the NGA-East research project by the authors using a hybrid-broadband simulation technique. Hybrid empirical estimates are calculated using modification factors between host and target regions as well as empirical GMMs from the host region. The regional adjustment factors are ratios of the intensity measures including peak ground



acceleration (PGA), peak ground velocity (PGV), and pseudo-spectral accelerations (SAs) in two regions. We have implemented a recently published hybrid broadband simulation technique by Shahjoui and Pezeshk (2015) to generate earthquake synthetic seismograms. Multiple earthquake shaking scenarios, which characterize the magnitude in the range of M5.0–8.0 are defined in the simulation approach, and the average horizontal components (RotD50) of PGA, PGV, and SAs (at spectral periods of 0.01–10s) are derived for both target (central and eastern North America) and host (western north America).

In this study, the authors updated the previously proposed GMM using additional earthquake simulations and considering the updated seismological and geological parameters. A comprehensive residual analysis is performed using the earthquake records available in the NGA-East database. The results are compared with the existing relations in the region.

### Using Geophysics and Geochemistry to Trace Quaternary Faults in the El Paso, Texas–Ciudad Juárez, Chihuahua Region

DOSE, D. I., University of Texas at El Paso, El Paso, TX, USA, doser@utep.edu; AVILA, V. M., University of Texas at El Paso, El Paso, TX, USA, avilavictorm@gmail.com; DENA-ORNELAS, O. S., Universidad Autonoma de Ciudad Juarez, Ciudad Juarez, Chihuahua, Mexico, oornelas@uacj.mx; HIEBING, M., University of Texas at El Paso, El Paso, TX USA, mhiebing@miners.utep.edu; MA, L., University of Texas at El Paso, El Paso, TX, USA, lma@utep.edu

The El Paso-Ciudad Juárez region is located within the southern Rio Grande rift, characterized by recent (<750,000 years) faulting and low-level seismicity. We have been using a combination of microgravity, resistivity soundings, and water well logs and water geochemistry data to trace faults within this metropolitan region of over 2.5 million people. Our results suggest the East Franklin Mountains fault (with evidence for 4 events within the last 64,000 years) extends 30 km south of the end of its mapped surficial trace beneath one of the most heavily urbanized regions of the two cities where basin fill exceeds 1800 m. SASW analysis indicates the local soils in this region are highly susceptible to failure due to the high water table and presence of clay. In addition, we have evidence for a series of concealed intrabasin faults within the eastern and western basins of the metropolitan area. It is uncertain if these intrabasin faults are capable of moderate to large earthquakes, but a M~2.5 event in 2012 appears to be associated with one of these faults.

### Crust and Upper Mantle Structure Beneath Eastern Flank of the Rio Grande Rift Revealed by Receiver Function Velocity Analysis

AGRAWAL, J., Baylor University, Waco, TX, USA, mohit\_agrawal@baylor.edu; PULLIAM, Baylor University, Waco, TX, USA, jay\_pulliam@baylor.edu; SEN, M. K., University of Texas at Austin, Austin, TX, USA, mkrinal@utexas.edu; GRAND, S.P., University of Texas at Austin, Austin, TX, USA

Studies of the Rio Grande Rift (RGR) present several possible Earth models and interpretations, which may be due to the diversity of the methodologies implemented and the specific location of the study. But due to lack of sufficient amount of data and its resolution, no mechanism could be established its place fairly concretely. To better constrain the seismic structure of crust and mantle lithosphere, we depth-migrated Ps and Sp receiver functions using data from the SIEDCAR (Seismic Investigation of Edge Driven Convection Association with Rio Grande Rift) and USArray Transportable Array (TA) deployments. We performed Common Conversion Point (CCP) stacking to improve the S/N ratio of receiver functions.

One of the goal of this study is to find an adequate 3D starting model using the complementary datasets mentioned above. This starting model will help in migrating the CCP stacked Ps and Sp receiver functions for major discontinuities (Ps receiver functions for the Moho; Sp receiver functions for the Lithosphere-Asthenosphere Boundary (LAB)) to their appropriate depths because it makes use of waves that sample earth structure in different, but complementary, ways (Ps and Sp receiver functions for average Vs (in crust) and Vp (mantle lithosphere) velocities, respectively). This is an important feature because the Moho and seismically defined "LAB" can divert the raypaths (and wavetypes) dramatically from their trajectories in a smooth structure, thereby degrading the quality and fidelity of the resulting images. These boundaries can be revealed by receiver function modeling and then introduced as a starting model used while migrating the CCP stacked Ps and Sp receiver functions.

An application to data acquired in southeastern New Mexico and west Texas, at an average station spacing of 35 km, reveals an abrupt increase in lithospheric thickness from west to east, from the Rio Grande Rift to the Great Plains craton. Previous studies found an elongated high velocity anomaly that extends to depths approaching 500 km in southeastern New Mexico and west Texas that

is distinct from the thick Great Plains lithosphere. Our stacked 3-D image confirms the anomaly's existence and shows that it is more laterally extensive than was previously indicated.

### Seismicity Associated with Northwest Trending Basement Faults, Southwest Montana, USA

SZKODY, J. A., Western Michigan University, Kalamazoo, MI, USA, jessica.a.szody@wmich.edu; STICKNEY, M. C., Montana Bureau of Mines and Geology, Butte, MT, USA, mstickney@mtech.edu; SCHMIDT, C. J., Western Michigan University, Kalamazoo, MI, USA, schmidt@wmich.edu

The  $M_w$  7.3 Hebgen Lake earthquake on August 18, 1959 has inspired the study of intraplate earthquakes within and around southwestern Montana. The region contains several long lived northwest-striking, northeast-dipping faults that cut Precambrian basement rocks. Late Cretaceous left-oblique thrust movement on these faults is associated with wide zones of brittle deformation of basement rock. We selected four regions within and around the Tobacco Root Mountains to investigate the relationship between earthquake hypocenter distribution and the most likely corresponding faults. We chose earthquakes with well resolved fault plane solutions and accurate hypocenter locations. Focal mechanisms reveal mainly right-oblique normal movement. Although we can reasonably associate the largest magnitude earthquakes (M2.7–M4.1) with known faults, the majority of the smaller magnitude earthquakes fall within the hanging wall, above the primary faults. All earthquakes have consistent northeast trending, gently plunging T-axes, but the nodal planes of smaller earthquakes have a wide range of orientations and slip senses. The highly fractured hanging wall basement rocks are a product of the Late Cretaceous deformation associated with the formation of anticlines in the sedimentary cover. Folding of the cover is observed in ten northwest trending faults, and shortening was accommodated in the basement by fracturing and faulting over distances of as much as 3 km in the hanging walls. We suggest that the seismicity in the hanging walls of the right-oblique normal faults were caused by slip on these earlier faults and fractures. Two of the four areas selected are within one kilometer of a known hot spring. It is possible that recharge water from the adjacent mountain ranges is heated at depth, travels up through larger faults and into the fractures, reducing the normal stress and causing slip, which results in small earthquakes within the hanging wall of major faults.

### The 6 November 2011 M5.6 Prague, Oklahoma Aftershock Sequence Studied Using Subspace Detection

MCMAHON, N. D., Colorado State University, Fort Collins, CO, USA, Nicole.McMahon@colostate.edu; BENZ, H. M., U.S. Geological Survey, National Earthquake Information Center, Golden, CO, USA, benz@usgs.gov; JOHNSON, C. E., Introspective Systems LLC, Brunswick, ME, USA; ASTER, R. C., Colorado State University, Fort Collins, CO, USA, Rick.Aster@colostate.edu; MCNAMARA, D. E., U.S. Geological Survey, National Earthquake Information Center, Golden, CO, USA, mcnamara@usgs.gov

The 6 November 2011 M5.6 earthquake near Prague, Oklahoma is the largest earthquake instrumentally recorded in Oklahoma history. A M4.8 foreshock on 5 November 2011 and the M5.6 mainshock triggered tens of thousands of detectable aftershocks along a 20 km splay of the Pennsylvanian-aged Wilzetta Fault Zone (WFZ) known as the Meeker-Prague fault. In response to this unprecedented earthquake, we deployed 21 temporary seismic stations surrounding the seismic activity. This sequence, with its prolific number of events and dense station coverage, provides an ideal target for subspace detection and subsequent microseismic characterization. We utilized a catalog of 767 previously located aftershocks to construct subspace detectors on 31 seismic stations. In the month following the main shock, more than 8,000 events with hypocentral uncertainties less than 400 m were located. The event locations provide unique insight into the spatio-temporal evolution of the aftershock sequence along the WFZ and its associated structures. We find that the crystalline basement and overlying sedimentary Arbuckle formation accommodate the majority of aftershocks. While we observe aftershocks along the entire 20 km length of the Meeker-Prague fault, the vast majority of earthquakes were confined to a 9 km wide by 9 km deep surface striking N54°E and dipping 83° to the northwest. Contrary to previous studies, we find a large number of events in the sedimentary Arbuckle formation above the basement. Event locations reveal structures at depth congruent with published regional velocity models and finite slip models. Our study demonstrates subspace detectors running on multiple stations can significantly increase the number of locatable events, thereby lowering the catalog's magnitude of completeness and providing extraordinary detail on the kinematics of the aftershock process and potential hazards for another large induced event.

## Recent Slip History and Surface Deformation Along the Southern Arm of the New Madrid Seismic Zone, Central United States from High Resolution Seismic Reflection Data and River Sediments

MAGNANI, M. B., R. Huffington Department of Earth Sciences, SMU, Dallas, TX, USA, mmagnani@smu.edu; HOLBROOK, J. M., School of Geology, Energy and Environment, TCU, Fort Worth, TX, USA, john.holbrook@tcu.edu

Seismicity in the New Madrid seismic zone (NMSZ) in the central US is generally interpreted in the context of a right-lateral restraining bend, where the Reelfoot Thrust acts as a transfer zone between two right-lateral strike-slip faults. This simple fault pattern at depth is not preserved at the surface, where seismic reflection and mapping data show that deformation is accommodated along complex fault patterns. In this paper we present existing seismic reflection profiles and recently acquired high-resolution marine reflection data across the southern arm of the NMSZ at Caruthersville, Missouri, integrated with allostratigraphic mapping, OSL and radiocarbon dating of surficial Holocene strata of the Mississippi River floodplain.

The seismic data show the presence of two faults interpreted as the Axial Fault (AF), located directly above the current seismicity, and as the Cottonwood Grove Fault (CGF), located ~5 km to the east, both deforming the Quaternary alluvium by ~20 m with an up-to-the-east sense of motion. South of Caruthersville, mapping of the river Holocene meander belt shows two fluvial events recording the river response to deformation along the projected location of the CGF. The older event, a short-lived and localized anastomosed reach in the otherwise meandering Mississippi River, developed within the century straddling AD900, and ended within three centuries thereafter. Later, a large (>36 km<sup>2</sup>) splay system, dated at AD1810±70 yrs, developed in this same location, and covered the older anastomosed river deposits. Several lines of evidence show that the first of the four main New Madrid earthquakes (1811-1812) ruptured on the CGF. Whether primary rupture occurred in the mapped area is still unconstrained, as is the relationship among the AF, the CGF, and the seismicity at depth. Possible scenarios include 1) the two faults as part of one (active) crustal structure, or 2) as separate structures of which only the AF is currently seismogenic.

## Velocity Structure and Seismic Anisotropy beneath the Mississippi Embayment and New Madrid Seismic Zone

NYAMWANDHA, C. A., University of Memphis—CERI, Memphis, TN, USA, nyamwandha@gmail.com; cnyamwndh@memphis.edu; POWELL, C. A., University of Memphis—CERI, Memphis, TN, USA, capowell@memphis.edu

The availability of high-resolution data from the New Madrid Seismic Network, the Earthscope Transportable Array (TA), and the FlexArray Northern Embayment Lithospheric Experiment (NELE) has provided insight into the velocity structure and seismic anisotropy beneath the Mississippi Embayment (ME) and the New Madrid Seismic Zone (NMSZ). We image a prominent low velocity anomaly with comparable V<sub>p</sub> and V<sub>s</sub> anomaly amplitudes in the upper mantle beneath the northern ME. The low velocity region dips to the southwest and extends to a depth of at least 300 km. Low velocities extend to shallow depths (about 50 km) below the northern end of the Reelfoot Rift. A region of high velocity in the lower crust separates the low velocities from the seismogenic upper crust hosting the NMSZ. Regions of high velocity with comparable V<sub>p</sub> and V<sub>s</sub> anomalies are present above and to the sides of the low velocity region. We attribute the observed low velocity anomaly to the presence of hot fluids upwelling from a flat slab segment stalled in the transition zone below the central U.S.; the thinned and weakened ME lithosphere, still at slightly higher temperatures from the passage of a mid-Cretaceous hotspot, provides an optimal pathway for the ascent of the fluids. The observed high velocity anomalies are attributed to the presence of mafic rocks emplaced beneath the ME during initial rifting in the early Paleozoic and to remnants of the depleted, lower portion of the lithosphere. Shear wave splitting patterns to the northeast and east of the ME suggest that the splitting is due to active flow in the asthenosphere whereas inside the ME, splitting complexity is attributed to relic lithospheric fabrics formed during past tectonic events including passage of the hotspot. The anisotropy may also be linked to the presence of a southwest dipping region of low P- and S-wave velocities below the ME or to deeper flow in the asthenosphere.

## 3d Averaged and Gradient P- and S- Wave Velocity Models for the Unconsolidated Mississippi Embayment Sediments

MOSTAFANEJAD, A., IRIS PASSCAL, Socorro, NM, USA, akram@passcal.nmt.edu; LANGSTON, C. A., CERI, University of Memphis, Memphis, TN, USA, clangstn@memphis.edu; CHAI, C., Department of Geosciences, Pennsylvania State University, University Park, PA, USA, cchai@psu.edu; AMMON, C. J., Department of Geosciences, Pennsylvania State University,

University Park, PA, USA, charlesammon@psu.edu; HERRMANN, R. B., Department of Earth & Atmospheric Sciences, Saint Louis University, St. Louis, MO, USA, rhb@eas.slu.edu

Velocity structure of the unconsolidated sediments of the northern Mississippi embayment is investigated using data collected from the Northern Embayment Lithosphere Experiment and the USArray transportable array with two different approaches. First, average S- and P-wave velocities of the sediments are determined via spectral ratio analysis of the horizontal-to-vertical (H/V) and the vertical-to-horizontal (V/H) power spectral ratio of a time window around teleseismic P-wave arrivals. The resulting shear wave velocity model matches very well with a model obtained from an H/V ambient noise study. The S-wave velocity model shows low velocity near the edges of the embayment with average velocities increasing with increasing sediment thickness, consistent with increased sediment compaction. Secondly, a linear gradient velocity model is obtained through simultaneous inversion of radial and vertical teleseismic transfer functions. Transfer functions were calculated by deconvolving a vertical array beam from the radial and vertical displacement at each station inside the embayment. The vertical array beam was constructed by stacking all vertical components for stations on bedrock and outside the embayment to reduce the effect of sediment scattering, improving the estimate of the source time function and stabilizing the deconvolution. Bounded Variable Least Square inversion was applied to invert for velocity nodes on top and bottom of the sediment layer. The 3D model has been used to get a preliminary sub-sediment structure image using body wave downward continuation and will be refined in subsequent joint inversions of high-frequency surface wave dispersion and potential fields data.

## Re-Evaluation of Interpreted Paleoseismic Sites in the Eastern Tennessee Seismic Zone: Evaluating Origin and Uncertainty of Potential Paleoseismic Data for Seismic Source Characterizations (SSC) in the Central and Eastern US (CEUS)

CLAHAN, K. B., Lettisi Consultants International, Inc., Walnut Creek, CA, USA, clahan@lettisci.com; LINDVALL, S. C., Lettisi Consultants International, Inc., Valencia, CA, USA, lindvall@lettisci.com; DEE, S., University of Nevada, Reno, NV, USA, sdee@unr.edu; SOWERS, J., Fugro Consultants, Walnut Creek, CA, USA, j.sowers@fugro.com; LEWANDOWSKI, N., Lettisi Consultants International, Inc., Walnut Creek, CA, USA, lewandowski@lettisci.com; TORO, G., Lettisi Consultants International, Boulder, CO, USA, toro@lettisci.com

The Eastern Tennessee Seismic Zone (ETSZ) is as an area characterized by high rates of historical seismicity, but is not explicitly included as a distinct seismic source in the CEUS SSC model (NUREG 2115). The ETSZ was modeled as part of a larger seismotectonic zone characterized by large M<sub>max</sub> values and spatial smoothing of seismicity to retain locally high seismicity rates. Since publication of the CEUS SSC report, researchers have continued to look for paleoseismic evidence for repeated large-magnitude earthquakes (RLME) in the ETSZ. Characterization of this evidence, including assessing uncertainty and alternative, non-seismic origins is critical to the proper evaluation of, and site-specific applications of the CEUS SSC.

Our evaluation included field reconnaissance and re-excavation of some proposed paleoseismic features located in the ETSZ as described by Hatcher *et al.* (2012). This involved assessing the level of uncertainty in alternate interpretations, and considering how this information could be used in the development of a RLME for the ETSZ region or other modifications to the CEUS SSC model.

Our results indicate that there is significant uncertainty as to the tectonic origin of some of the features described in Hatcher *et al.* (2012). We consider multiple working hypotheses for the nontectonic origin of these features, including mass movement, pedogenic processes, and karst-related collapse or subsidence. Additionally, sensitivity testing of the CEUS hazard model indicates the proposed paleoseismic evidence for two magnitude 6.5 or larger ETSZ events in the past 73ka described in Hatcher *et al.* (2012) are accounted for in the existing M<sub>max</sub> and magnitude frequency distribution. The current level of uncertainty of the proposed paleoseismic features identified in the ETSZ does not yet support the development of an RLME or fault source for the ETSZ. Further paleoseismic investigations could help resolve uncertainties and test alternative interpretations.

## Recent Fault Activity in the 1886 Charleston, South Carolina Earthquake Epicentral Area and its Relation to Buried Structures

PRATT, T. L., U. S. Geological Survey, Reston, VA, USA, tpratt@usgs.gov; SHAH, A. K., U. S. Geological Survey, Denver, CO, USA, ashah@usgs.gov; HORTON, J. W., U. S. Geological Survey, Reston, VA, USA, whorton@usgs.gov



gov; CHAPMAN, M. C., Virginia Tech, Blacksburg, VA, USA, [mcc@vt.edu](mailto:mcc@vt.edu); BEALE, J. N., Virginia Tech, Blacksburg, VA, USA, [jnbeale@gmail.com](mailto:jnbeale@gmail.com)

The 1886 Charleston, SC earthquake (M<sub>6.8-7.3</sub>), the largest known in the U.S. east of the Appalachian Mountains, occurred within an area of extensive Mesozoic rifting and beneath the ~800-m thick, subhorizontal Atlantic Coastal Plain (ACP) strata. We examine reprocessed seismic reflection data in the epicentral area to discern faults deforming the Cretaceous and Cenozoic ACP strata, and relate them to deeper structures revealed by the seismic profiles and filtered aeromagnetic data. Faults on the seismic profiles have sharp vertical displacements of strata, abrupt but small changes in dip, or folding of the ACP strata. Some of these faults dip steeply and displace deeper reflectors within South Georgia rift basin; in places they bound uplifted blocks of ACP strata. A prominent magnetic anomaly high has a NE-trending west edge in the epicentral area, with Cenozoic deformation imaged by nearby seismic profiles (Chapman *et al.* (BSSA, 2016). Other short-wavelength magnetic anomalies show disruptions aligned along NE trends. These latter disruptions appear to be related to seismically imaged faults displacing ACP strata. The amount of vertical uplift on faults imaged by the seismic data is nearly equal through the ACP section, indicating Cenozoic motion. Another NE-trending fault, crossing beneath the Ashley River ~15 km NW of Charleston, is interpreted based on disruptions of magnetic anomalies to align with lateral offsets of railroad tracks and NE-trending surface fissures. In contrast to these interpreted NE-trending faults, Chapman *et al.* (BSSA, 2016) infer a south-striking, west-dipping rupture zone for the 1886 shock on the basis of new hypocenter locations and focal mechanism solutions. This rupture zone projects to the surface near the 1886 epicenters inferred from shaking intensity and railroad damage. Modeling of scenario fault ruptures, better seismic monitoring, and subsurface imaging are needed to definitively resolve the 1886 earthquake rupture.

#### **New Measurements of Shear-wave Splitting in Saudi Arabia**

CHEN, S. W., USGS, Menlo Park, CA, USA, [chensw1228@gmail.com](mailto:chensw1228@gmail.com); MOONEY, W. D., USGS, Menlo Park, CA, USA, [mooney@usgs.gov](mailto:mooney@usgs.gov); KLEMPERER, S. L., Stanford Univ., Stanford, CA, USA, [sklemp@stanford.edu](mailto:sklemp@stanford.edu); SUZUKI, J., Cornell Univ., Ithaca, NY, USA, [suzuki.judith@hotmail.com](mailto:suzuki.judith@hotmail.com); ZAHRAN, H. M., Saudi Geological Survey, Jeddah, Saudi Arabia, [zahran.hm@sgs.org.sa](mailto:zahran.hm@sgs.org.sa); EL-HADIDY, S. Y., Saudi Geological Survey, Jeddah, Saudi Arabia, [youssef.sh@sgs.org.sa](mailto:youssef.sh@sgs.org.sa)

The lack of local seismic network has limited our understanding of the structure of the lithosphere and upper mantle beneath Saudi Arabia. The recently expanded Saudi Geological Survey (SGS) broadband seismic network now consists of 180 stations and provides the densest coverage to date. We present an analysis of shear-wave splitting to infer seismic anisotropy within and beneath the Arabian plate. Seismic anisotropy, as measured by the splitting of teleseismic S-wave phases, is commonly related to lateral flow in the upper mantle. Thus, our results provide key evidence for the geodynamic processes operating in this area. We primarily analyzed SKS phases, but because the back-azimuth coverage is limited in some directions, we also include a few SKKS observations. We selected a total of 1025 records of SKS phases and 23 records of SKKS phases from 488 M ≥ 6.0 events with epicentral distances between 85° and 135°. We also used some M = 5.5 to 5.9 events where the azimuthal coverage was insufficient. Our new observations for Saudi Arabia suggest splitting is generally aligned N-S, consistent with previous studies. Although the measured N-S orientation is inconsistent with the N40°E plate motion of the Arabian plate, it is consistent with northward asthenospheric flow originating at the Afar hot spot. We observe a 0.5s decrease in the average delay time between the fast and slow S-waves from west to east. We also observe a south-to-north, counter-clockwise rotation of fast directions of the split shear waves in the eastern portion of the Arabian plate. We theorize that the subducting Arabian plate beneath Iran blocks northward asthenospheric flow, and thus, flow progresses toward Turkey, where there is a slab gap.

#### **Pn Wave Geometric Spreading and Attenuation Models in and around the Tibetan Plateau**

ZHAO, L. F., IGG, Chinese Academy of Science, Beijing, China, [zhaolf@mail.iggcas.ac.cn](mailto:zhaolf@mail.iggcas.ac.cn); XIE, X. B., IGPP, University of California at Santa Cruz, Santa Cruz, CA, USA; YAO, Z. X., IGG, Chinese Academy of Science, Beijing, China, [yaozx@mail.iggcas.ac.cn](mailto:yaozx@mail.iggcas.ac.cn)

Both the geometric spreading and attenuation of seismic Pn waves are investigated in and around the Tibetan plateau, based on 25,352 broadband vertical-component digital seismograms recorded at 644 stations from 653 regional earthquakes between January 1994 and September 2013. The Pn-waveforms are collected from crustal earthquakes with magnitudes ranging mb4.1-6.5 and epicentral distances 200-2000 km. We extract Pn signals using a 0.7 km/s

group-velocity window and measure the noise in an equal-length time window before the first arriving P wave. By correcting the raw spectra with the noise, we obtain the Pn spectra between 0.1 and 20.0 Hz to further constrain the parameters of a frequency-dependent log-quadratic geometric spreading function and an apparent power-law Pn Q model. Using the two-station amplitude ratios of the Pn spectra and correcting them with the known spreading function, we remove the contributions of the source and crust from the apparent Pn Q and retrieve the P wave attenuation information along the pure upper mantle path. We then use both Pn amplitudes and amplitude ratios to obtain the upper mantle P wave attenuation. The source radiation patterns are considered in our calculation. Beneath the central and north parts of the Tibetan plateau, the Pn waves are highly attenuated, while relatively lower attenuation can be observed in the perimeter of the plateau, *i.e.*, the Himalaya mountains in the south, Tarim and Qaidam basins and Eastern Kunlunshan terrain in the north, and Sichuan basin in the east. These weak attenuation regions are likely where the old crustal fragments deposited during the collision between Indian and Eurasian plates. The strong attenuation is mainly observed in central and north Tibetan plateau, indicating strong thermal activities may take place in the crust and uppermost mantle in the areas. This work was supported by the National Natural Science Foundation of China (grants 41374065 and 41174048).

#### **Western US and Tibetan Crust in 3-D: A Preliminary Report**

CHEN, W. P., Zhejiang University & University of Illinois (Urbana-Champaign), Hangzhou, Zhejiang, People's Rep. China, [wpchen@uiuc.edu](mailto:wpchen@uiuc.edu); YU, C. Q., Massachusetts Institute of Technology, Cambridge, MA, USA, [yucq@mit.edu](mailto:yucq@mit.edu); JIANG, Y., Zhejiang University, Hangzhou, Zhejiang, People's Rep. China, [jiangyang2467@zju.edu.cn](mailto:jiangyang2467@zju.edu.cn)

We report 3-D variations of crustal properties in two broad regions of high elevation. The key method used is virtual deep seismic sounding (VDSS), or wide-angle reflection generated by S-P conversion at the free surface (the virtual source) near a seismic station. VDSS relies mainly on the phase SsPmp at distances between about 30 and 55 degrees where SsPmp is a post-critical reflection of large amplitude. VDSS offers several distinct advantages: 1) It returns a robust signal from the crust-mantle boundary even if the Moho is complicated or transitional in nature. 2) The signal is not particularly susceptible to undesirable signal-generated noise such as scatterings from thick sediments or intra-crustal discontinuities. 3) VDSS provides tight constraints on crustal buoyancy in spite of an inherent trade-off between overall crustal thickness and P-wave speed.

Results from data recorded during Project Hi-CLIMB, supplemented by those from the INDEPTH-3 deployment, confirm the trend of northward thinning of crust in central Tibet. More important, a zone of strong lateral variations in crustal thickness near the Bangong-Nujiang suture zone roughly coincides with the Indian mantle front, or the northern, leading edge of underthrust Indian lithospheric mantle ("Greater India") as revealed by high-resolution travel-time tomography. Furthermore, this zone delineates the overall structural trend of Tibetan crust to be sub-normal to the current direction of plate convergence.

Using data collected from the USArray component of EarthScope and other deployments, our results provide high-resolution estimate of crustal buoyancy over the entire western US. Positive residual topography is particularly pronounced on the edges of the Colorado Plateau (including the northern and southern Rocky Mountains, and the Snake River Plains) and the Basin and Range Province, indicating strong mantle support, from either thermal buoyancy or dynamic processes, of high elevations there.

#### **Joint Inversion for Lithospheric Density Variations Beneath the Tarim Block, Western China, and their Geodynamic Implications**

DENG, Y., Guangzhou Institute of Geochemistry, Chinese Academy of Sciences, Guangzhou, China, [yangfandeng@gig.ac.cn](mailto:yangfandeng@gig.ac.cn); LEVANDOWSKI, W., USGS, Golden, CO, USA, [wlevandowski@usgs.gov](mailto:wlevandowski@usgs.gov)

Although Indo-Eurasian collision causes widespread deformation in central Asia, the Tarim block has experienced minimal Cenozoic shortening. This apparent stability may either arise because strain is shunted into the lithospheric-scale fault zones bounding Tarim—essentially discretizing Eurasia into microplates—or because the Tarim block is stronger than its surroundings. Here, we jointly invert seismic velocity, gravity, topography, and heat flow for a 3D density model of the crust and upper mantle in this region. The actively deforming western and southern margins of Tarim—the Tien Shan, Kunlun Shan, and Altyn Tagh fault—are underlain by buoyant upper mantle with low velocity, which we propose to reflect hydration by mantle-derived fluids that have preferentially migrated along continental sutures. Low-density but high-velocity lithospheric mantle in southern Tarim underlies a suite of Permian plume-related mafic intrusions sourced in previously depleted mantle lithosphere. We posit that this region was further depleted, dehydrated, and strengthened by Permian magmatism. The Tarim crust



has high density, vs, vp, and vp/vs, consistent with a dominantly mafic composition. A trapped oceanic plateau beneath Tarim would have hosted both refractory mantle lithosphere (even before Permian melt-depletion) and mafic crust, and the existence of such a plateau is consistent with geochronological and aeromagnetic data. We propose that the southern and western margins of Tarim are weak, and strain focuses there because of lithospheric-scale variations in rheology, not because continental interiors inherently discretize into stable microplates. By contrast, strong south Tarim transmits N-S compression toward the Tien Shan, leading to the subduction of north Tarim beneath the range. This world-class example highlights that the local relationship between stress and strength, rather than inherited structures alone, can lead to strain sequestration in discrete zones.

#### Repeated Event Detection in Eastern Asia using Historical Archives

SLINKARD, M., Sandia National Laboratories, Albuquerque, NM, USA, meslink@sandia.gov; SUNDERMIER, A., Sandia National Laboratories, Albuquerque, NM, USA, asunder@sandia.gov; HECK, S., Sandia National Laboratories, Albuquerque, NM, USA, sheck@sandia.gov; YOUNG, C., Sandia National Laboratories, Albuquerque, NM, USA, cjyoung@sandia.gov; SCHAFF, D., Lamont-Doherty Earth Observatory, Palisades, NY, USA, dbschaff@ldeo.columbia.edu; RICHARDS, P., Lamont-Doherty Earth Observatory, Palisades, NY, USA, richards@ldeo.columbia.edu

We are exploring practical aspects of the application of waveform cross-correlation methods to high-precision studies of regional seismicity across broad regions of East Asia, taking advantage of the growth in continuous waveform archives and looking to a future when traditional event catalogs will yield to vastly superior data products for the community. In this study we created template waveforms from the full available station history (up to 30 years), and then reprocessed 6 years of raw data to explore repeated seismicity in eastern Asia. We developed the computational infrastructure to process tens of thousands of templates at each station over the multi-year period, and combine and validate detection results. Correlation thresholds for each individual template are set to have a given false alarm rate using our reverse-template method. Detections at a given station are validated by using a network approach ensuring detections were also seen at other stations. We find that many of the detected events are not in traditional bulletins; hence the multi-station comparison is essential. With 6 stations processed, we have found thousands of new events. Currently processed stations are 3-C stations from the GSN, and station processing is ongoing. Detection results are presented along with discussion of the magnitude variation within families of events detected by the same template, and the temporal and spatial reach of templates.

#### Seismic Hazard Assessment for Kwajalein

MUELLER, C. S., US Geological Survey, Golden, CO, USA, cmueller@usgs.gov; MILBURN, T. W., US Army Corps of Engineers ERDC, Vicksburg, MS, USA, troy.w.milburn@usace.army.mil

We apply the U.S. Geological Survey probabilistic methodology to estimate the seismic hazard at Kwajalein Island, Republic of the Marshall Islands. The site is far away from any plate boundaries, and there are no obvious faults or other localizing seismogenic features nearby that we can model. We therefore assume that hazard is controlled by sparse intraplate seismicity in the region, which is modeled using an earthquake catalog. Due to the remote location and limited historical network coverage, construction of a catalog is challenging. Recognizing the problems with standard catalogs, Wyession and others (1991, Pageoph) carefully relocated earthquakes in the region, moving many from spurious intraplate locations to plate boundaries. Their catalog lists 19 true intraplate earthquakes from 1963 to 1985 within about 1,000 km of Kwajalein. Unfortunately, reliable magnitudes could not be determined for many of these earthquakes. To use their catalog, we assume that earthquakes smaller than about magnitude 5 might have been missed, and that earthquakes larger than about magnitude 6 are probably well represented in original catalogs. A gridded rate model is constructed by combining three alternative pre-1986 catalogs, each assuming that all the unknown magnitudes are either 5.0, 5.5, or 6.0, with a modern (post-1985) catalog; the modern catalog adds eight earthquakes ranging in magnitude from 4.0 to 5.3. Alternative b values of 0.8 and 1.0 and a large smoothing distance of 200 km are used. Lacking a specific ground motion model for ocean intraplate earthquakes, we use several equations for crustal earthquakes in active tectonic regions. Results based on these modeling assumptions will be presented at the meeting.

## Theoretical and Methodological Innovations for 3D/4D Seismic Imaging of Near-Surface, Crustal, and Global Scales

Poster Session · Wednesday · 20 April · Tuscany F

#### Monte Carlo Inversion for a 3D Local Earthquake Tomography

LANZA, F., Michigan Technological University, Houghton, MI, USA, flanza@mtu.edu; WAITE, G. P., Michigan Technological University, Houghton, MI, USA, gpwaite@mtu.edu

The non-linear inverse problem of 3D local earthquake tomography is often tackled via linear approximations. Thus, the linear inversion results and the reliability estimates strongly depend on the initial reference velocity model. In this study, in order to address the uncertainties and the non-uniqueness of the linear model estimation problem, we employ a Monte Carlo non-linear inversion in which we consider a suite of randomly chosen velocity models. We randomly vary the starting velocity at each node of the model grid to explore the solution space. Comparisons between solutions are carried out in multiple steps by evaluating total residual errors, model variance and by statistics at each node. We investigate the capabilities of this approach at Pacaya volcano, in Guatemala, a persistently active basaltic volcano characterized by strombolian style eruptions and occasional lava flows. We located about 300 events within the and just below the cone with a temporary seismic network of 19 stations in January 2015. The stations were deployed between 100 and 1600 m of the active vent for approximately 10 days. The non-linear inversion will allow a better understanding of the possible models, and thus will increase our confidence in the interpretation of the tomographic inversion results.

#### Ambient Noise Tomography in Shanxi Rift

SONG, M. Q., Earthquake Administration of Shanxi Province, Taiyuan, Shanxi, China, smq28@126.com; WANG, X., Earthquake Administration of Shanxi Province, Taiyuan, Shanxi, China, 365372858@qq.com; LI, H. W., Earthquake Administration of Shanxi Province, Taiyuan, Shanxi, China, 347719545@qq.com; WU, H. Y., Earthquake Administration of Shanxi Province, Taiyuan, Shanxi, China, 7153701@qq.com; LIANG, X. J., Earthquake Administration of Shanxi Province, Taiyuan, Shanxi, China, 277051050@qq.com; JIN, Y. Z., Earthquake administration of Shanxi province, Taiyuan, Shanxi, China, 675047518@qq.com

In this work, we collected one year continuous vertical component waveform data recorded at 62 permanent stations in Shanxi and adjacent region in 2012. We further processed the seismic waveforms by bandpass filtering, frequency-time normalization, doing cross-correlation and stacking the cross-correlation functions, more than 1891 empirical Green's functions are acquired. Then, we picked out 1691 Rayleigh wave fundamental mode dispersion curves with high signal-to-noise ratio by FTAN method with application of multiple filtering technique and built the group velocity structure at periods from 5s to 40s by genetic algorithm with a spatial resolution of  $0.25^\circ \times 0.25^\circ$ . The inversion results of group velocity maps exhibited the lateral velocity changes of shear wave velocity at different depths. Strong lateral shear wave heterogeneities can be observed in the crust and upper mantle. At short periods (e.g. 10 to 14s) the group velocity maps are in good consistent with the geology features at the ground surface, with high speed anomalies in the mountain ranges and low-speed anomalies in the major sedimentary basins. The effects of shallow structures decrease with depth, thus, at the intermediate periods (e.g. 15 to 22s), the features of the topography gradually disappear. At longer periods (e.g. periods longer than 30s), the distribution of group velocity is obviously correlated to the crustal thickness. One important features of the group velocity distribution in the Shanxi region is that the Datong volcanic zone is dominated with low velocity anomalies. From period 18s to 50s the low velocity zone shrink from a large area to Datong and its vicinity, which implies that the Datong volcanic zone is still hot, and its root may be originated from deep depth (at least from asthenosphere) and the scale of the volcanic zone expands with the hot material uplift. And all of the Datong volcanic clusters may be originated from same source in the deep depth.

#### Seismic Structure Beneath the Northern Mississippi Embayment: Inverting Receiver Functions, Surface-Wave Dispersion, and Gravity Observations

CHAI, C., Pennsylvania State University, University Park, PA, USA, cchai@psu.edu; AMMON, C. J., Pennsylvania State University, University Park, PA, USA, charlesammon@psu.edu; HERRMANN, R. B., Saint Louis University, St. Louis, MO, USA, rhb@eas.slu.edu; MOSTAFANEJAD, A., IRIS PASSCAL

Instrument Center, Socorro, NM, USA, akram@passcal.nmt.edu; LANGSTON, C. A., University of Memphis, Memphis, TN, USA, clangstn@memphis.edu

The Mississippi embayment has a long and complex geological history that includes three episodes of major plate disruption and an enigmatic thermal event in the Cretaceous. The Reelfoot Rift is situated in the northern part of the embayment and hosts the New Madrid seismic zone, which was struck by three M7 or greater earthquakes in 1811-1812. Previous studies using potential-field observations, local earthquake tomography, and active seismic sources suggest significant crustal heterogeneity in the region. Recent teleseismic P-wave and surface-wave tomography studies also suggest substantial velocity variations in the upper mantle. Our goal is to determine regional-scale upper crustal structure and to relate it with deep crustal and upper mantle structure that undoubtedly exerts significant control on the tectonic processes of lithospheric strain accumulation and release through earthquakes. Data from the EarthScope Transportable Array, the New Madrid Cooperative Seismic Network, and an EarthScope Flex Array experiment—the Northern Embayment Lithosphere Experiment—provide an opportunity to improve seismic images. Combining multiple complementary observations has produced promising subsurface seismic images. We invert receiver functions together with surface-wave dispersion and gravity observations to construct a robust estimate of seismic structure beneath the region. The low-speed sedimentary fill of the northern embayment causes large amplitude sedimentary responses on receiver-function waveforms that mask deeper signals. Wavefield continuation and decomposition techniques can be used to remove sediment effects on receiver functions, but an accurate shallow model is needed. Thus our initial focus in areas of thick sediment cover is mapping variations in the shallow seismic structure so that we can eventually downward continue the surface receiver functions to access information on deeper structures and to include it in a multi-objective geophysical inversion.

#### **Connecting the Dots: Location and Continuity of Shallow Structures within the Seattle Fault Zone Interpreted from Land Based High-Resolution Seismic-Reflection Profiles**

ODUM, J. K., U.S. Geological Survey, Golden, CO, USA, odum@usgs.gov; STEPHENSON, W. J., U.S. Geological Survey, Golden, CO, USA, wstephens@usgs.gov; PRATT, T. L., U.S. Geological Survey, Reston, VA, USA; BLAKELY, R. J., U.S. Geological Survey, Menlo Park, CA, USA

Over the last three decades the regional structure and subsurface geometry of the Seattle Fault Zone (SFZ) has been much debated. Little is known about the continuity of proposed shallow SFZ structures within the Seattle urban area. Sixteen land-based P-wave seismic-reflection profiles were acquired at Bainbridge Island (2), West Seattle (5), Beacon Hill (3), and Mercer Island (6). Combined with marine seismic-reflection profiles in Lake Washington and Puget Sound, these 25 km of land based seismic-reflection profiles provide a detailed image of shallow (1 km depth) structures and faulting within the 4-7 km wide SFZ uplift. Data show evidence of anticlinal warped and north dipping Tertiary bedrock, thrust and back thrust faulting, and deformed Quaternary deposits. We present evidence that locates an inter SFZ fault, here interpreted to be the southernmost of 3 suspected SFZ thrust faults. Interpreted groups of seismic profiles define the westward trace of the Vasa Park fault, which correlates with a distinct east-west trending regional aeromagnetic lineament, and traces its continuity for ~30 km from Lake Sammamish westward to Bainbridge Island. Beacon Hill profiles show thrust and back thrust faulting and north dipping Tertiary strata, similar in appearance to a structure associated with an aeromagnetic anomaly, in an area where the aeromagnetic data is complexly distorted. Additionally, anticlinal structure and faulting proposed by Liberty and Pratt (2008) in the Bellevue area east of Seattle and near the southern margin of the SFZ, are imaged on southern Mercer Island profiles. Seismic profiles on Bainbridge Island that cross the Toe Jam fault scarp show a zone of deformed Quaternary strata. Collectively, these land based seismic profiles provide the shallow locations of previously proposed faults and suggest a continuity of a single fault, or closely spaced fault strands, for a length of approximately 30 km beneath the Seattle urban area.

#### **Shallow Structure and Location of the Piedmont Thrust Splay of the Hayward Fault, Oakland, California**

GOLDMAN, M. R., U.S. Geological Survey, Menlo Park, CA, USA, goldman@usgs.gov; CATCHINGS, R. D., U.S. Geological Survey, Menlo Park, CA, USA, catching@usgs.gov; TRENCH, D., Fugro Consultants, Walnut Creek, CA, USA, d.trench@fugro.com; BUGA, M., Fugro Consultants, Walnut Creek, CA, USA, m.buga@fugro.com; CHAN, J. H., U.S. Geological Survey, Menlo Park,

CA, USA, jchan@usgs.gov; CRILEY, C., U.S. Geological Survey, Menlo Park, CA, USA, ccriley@usgs.gov

The Piedmont Fault (PF) is interpreted as a thrust or reverse fault that may be associated with the historically active Hayward Fault (HF). The PF may represent a seismic risk due to its location in a densely populated urban area. In February 2015, we acquired high-resolution P- and S-wave seismic data across the approximately mapped trace of the PF at Dimond Canyon Park in Oakland, California to constrain the near-surface location and dip of the fault. Our seismic profile extended 315 m along a southwest to northeast trend. P- and S-wave data were acquired separately using hammer sources. Each shot was co-located with and recorded by 106 40-Hz (P-wave) and 4.5 Hz (S-wave) geophones, spaced 3 m apart. Both the P- and S-wave data show large differences in velocities on the southwest side of the profile ( $V_p = 600\text{-}2100$  m/s;  $V_s = 260\text{-}520$  m/s) compared to the northeast side ( $V_p = 800\text{-}3200$  m/s;  $V_s = 500\text{-}800$  m/s), with a near-vertical dip of velocity contours between the two sides. We interpret the abrupt, near-vertical zone of velocity transition to coincide with the PF.  $V_p/V_s$  and Poisson's ratio models show pronounced lows associated with the apparent fault zone. Reflection images show diffractions and near-surface (~5 m) breaks in the continuity of reflectors at the location of our interpreted fault. We also evaluated the velocity structure along the profile using two different 2-D surface-wave techniques (MASW and MALW) that show velocities and structures similar to those determined by the tomographic method. Based on our interpreted location of the PF, drilling studies are planned to evaluate the recency of faulting along the PF.

#### **Seismic Evidence of a Widely Distributed West Napa Fault Zone, Hendry Winery, Napa, California**

CATCHINGS, R. D., U.S. Geological Survey, Menlo Park, CA, USA, catching@usgs.gov; GOLDMAN, M. R., U.S. Geological Survey, Menlo Park, CA, USA, goldman@usgs.gov; CHAN, J. H., U.S. Geological Survey, Menlo Park, CA, USA, jchan@usgs.gov; CRILEY, C. J., U.S. Geological Survey, Menlo Park, CA, USA, ccriley@usgs.gov

Following the 24 August 2014  $M_w$  6.0 South Napa earthquake, surface rupture was mapped along the West Napa Fault Zone (WNFZ) for a distance of ~14 km, locally within zones up to ~2 km wide. Near the northern end of the surface rupture, however, several strands coalesced to form a narrow, ~100-m-wide zone of surface rupture. To determine the location, width, and shallow (upper few hundred meters) geometry of the fault zone, we acquired an active-source seismic survey across the northern surface rupture in February 2015. We acquired both P- and S-wave data, from which we developed reflection images and tomographic images of  $V_p$ ,  $V_s$ ,  $V_p/V_s$ , and Poisson's ratio of the upper 100 m. We also used small explosive charges within surface ruptures located ~600 m north of our seismic array to record fault-zone guided waves. Our data indicate that at the latitude of the Hendry Winery, the WNFZ is characterized by at least five fault traces that are spaced 60 to 200 m apart. Zones of low- $V_s$ , low- $V_p/V_s$ , and disrupted reflectors highlight the fault traces on the tomography and reflection images. On peak-ground-velocity (PGV) plots, the most pronounced high-amplitude guided-wave seismic energy coincides precisely with the mapped surface ruptures, and the guided waves also show discrete high PGV zones associated with unmapped fault traces east of the surface ruptures. Although the surface ruptures of the WNFZ were observed only over a 100-m-wide zone at the Hendry Winery, our data indicate that the fault zone is at least 400 m wide, which is probably a minimum width given the 400-m length of our seismic profile. Slip on the WNFZ is generally considered to be low relative to most other Bay Area faults, but we suggest that the West Napa Fault is a zone of widely distributed shear, and to fully account for the total slip on the WNFZ, slip on all traces of this wide fault zone must be considered.

#### **Three Dimensional $V_p$ and $V_p/V_s$ Structural Models for The Geysers, California**

TYAGL, A., University of Miami, Miami, FL, USA, adt20@miami.edu; LIN, G., University of Miami, Miami, FL, USA, glin@rsmas.miami.edu; WU, B., Institute of Disaster Prevention/Earthquake Science Department, Beijing, China, bwx112@miami.edu

The Geysers, located in Northern California, is the world's largest geothermal field. It is also one of the most seismically active regions, producing numerous small-magnitude earthquakes everyday. We present a new three-dimensional (3D) velocity model for The Geysers using the seismic data for over 230,000 events between 1984 and 2015 archived at the Northern California Earthquake Data Center. The simul2000 tomography algorithm is used to invert for the three-dimensional  $V_p$ ,  $V_p/V_s$  models and earthquake locations simultaneously. We first solve for a coarse 3D  $V_p$  model with uniform 4 km horizontal node spacing and depth nodes positioned at -2, 0, 2, 4, 6, 9, 12, 16 and 20 km (relative to

mean sea level); and then invert for both  $V_p$  and  $V_p/V_s$  models with a horizontal gridding of 2 km and the same depth layers as the coarse model. The resulting anomalies in the final fine-scale  $V_p$  and  $V_p/V_s$  models can be attributed to certain geologic features such as rock composition, fracture density and pore fluid content. Low  $V_p$  values are associated with fluid filled fractured rocks or dry gas filled rocks. The changes in the  $V_p/V_s$  ratio may indicate that water depletion and exploitation are the dominant processes in the study area. The new velocity model improves the absolute location accuracy of the seismicity in the reservoir. This will eventually provide the basis for a highly precise earthquake location catalog based on waveform cross-correlation data. High-resolution velocity structure and precise seismic locations are essential for exploring tectonic and induced seismicity, the fluid flow and other seismological studies at The Geysers.

#### **Internal Structure of the San Jacinto Fault Zone in the Trifurcation Area Southeast of Anza, California, from Data of Spatially-Dense Linear Arrays**

QIN, L., USC, Los Angeles, CA, USA, qin@usc.edu; BEN-ZION, Y., USC, Los Angeles, CA, USA, benzion@usc.edu; QIU, H., USC, Los Angeles, CA, USA, hongruiq@usc.edu; SHARE, P., USC, Los Angeles, CA, USA, pshare@usc.edu; ROSS, Z. E., USC, Los Angeles, CA, USA, zross@usc.edu; VERNON, F., IGPP, La Jolla, CA, USA

We analyze two years of data from a linear array composed of six 3-component sensors separated by about 25 m, and one-month data from 1108 vertical geophones in about 650 m x 650 m box configuration with instrument spacing 10-30 m, straddling the Clark branch of the San Jacinto fault zone southeast of Anza, California. The examined data include recordings from >10000 local events, the ambient seismic noise, and various teleseismic events. Automatic picking algorithms are used to identify P and S body waves, along with fault zone head waves refracting along a velocity contrast interface and trapped waves propagating in a low velocity waveguide structure. Preliminary results suggest a velocity contrast across the fault with the NE being the side with higher velocity, and the existence of a low velocity zone around the fault. Updated results will be presented in the meeting.

#### **Retrieval of the Empirical Green's Tensor using Ambient Noise Cross-Correlation at The Geysers Geothermal Field**

NAYAK, A., Berkeley Seismological Laboratory, Berkeley, CA, USA, avinashguddu07@berkeley.edu; TAIRA, T., Berkeley Seismological Laboratory, Berkeley, CA, USA, taira@berkeley.edu; DREGER, D. S., Berkeley Seismological Laboratory, Berkeley, CA, USA, dreger@seismo.berkeley.edu; GRITTO, R., Array Information Technology, Berkeley, CA, USA, Roland.Gritto@arrayinfotech.com

The Geysers in the Mayacamas Mountains, Northern California is the world's largest geothermal field. It has witnessed significant increase in small magnitude ( $M_W \geq 4.8$ ) seismicity since the 1960s in response to steam production and water injection for reservoir recharge. We apply ambient noise cross-correlation to continuous multi-component seismic records collected at The Geysers from March 2012 to August 2015. The cross-correlations of ambient seismic noise obtained at pairs of seismic sensors have been shown to converge over a period of time to the empirical Green's functions (GFs) or the seismic medium's response at one receiver for a unit force applied at the other receiver. The recording instruments are a mixture of 4.5 Hz/8.0 Hz surface and borehole geophones, an accelerometer, 1.0 Hz vertical-component short-period sensors and a broadband sensor, operated by LBNL and USGS. We apply same temporal and spectral normalization factors to all 3 components of recorded data to preserve relative amplitudes between different components of the interstation Green's Tensor, and compute cross-coherence after removing spikes from the spectra. We were able to retrieve significant energy in RR, TT and ZZ components of GFs at interstation distances  $< \sim 7$  km in the frequency passband of 0.2-0.9 Hz. Comparing the empirical GFs obtained from noise cross-correlation with amplitude-normalized synthetic GFs computed using 1D velocity models used at The Geysers provides confidence in the GFs obtained from noise. Synthetic GFs computed with the 3D wave propagation code "SW4", using a 3D velocity model for The Geysers (derived from inversion of arrival times of earthquake body waves), provide similar levels of waveform fits as the GFs of the average 1D velocity models. We also study the temporal evolution of the main arrivals and the coda of the GFs to probe possible clock errors and temporal changes in the subsurface shear wave velocities in the geothermal field.

#### **Imaging the 3D Structure at the Source Physics Experiment using Seismic Interferometry**

MATZEL, E. M., Lawrence Livermore National Laboratory, Livermore, CA, USA, matzel1@llnl.gov; MELLORS, R. J., Lawrence Livermore National

Laboratory, Livermore, CA, USA, mellors1@llnl.gov; PITARKA, A., Lawrence Livermore National Laboratory, Livermore, CA, USA, pitarka1@llnl.gov

In this study, we use several methods of seismic interferometry to obtain highly detailed images at the site of the Source Physics Experiment (SPE). The objective of SPE is to obtain a physics-based understanding of how seismic waves are created at and scattered near the source. In order to separate source-specific effects from those due to geological heterogeneity, we need a precise 3D seismic model. We focus on three interferometric techniques: Shot interferometry (SI) uses the SPE shots as rich sources of high frequency, high signal energy. Coda interferometry (CI) isolates the energy from the scattered wavefield. Ambient noise correlation (ANC) uses the energy of the ambient background field. In each case, the data recorded at one seismometer are correlated with the data recorded at another to obtain an estimate of the Green's function (GF) between the two. These GFs are then inverted to obtain the final seismic image. The large network of mixed geophone and broadband instruments at the SPE allows us to calculate thousands of these GFs.

Each technique has its advantages. SI and CI are very fast, because they require only short data segments, while ANC requires much longer continuous records. SI results in the highest frequency, highest SNR waveforms, but is constrained to paths along directions radially outward from the shot. CI has lower SNR, but because it includes both backward and forward scattering arrivals, can be used to image paths across seismic lines. SI and CI are excellent at resolving the shallow low velocity features that dominate the near field scattering observed on the SPE records. Because the spectrum of ANC is determined by the Earth's background noise field, it has the lowest frequency content, but can be applied to any two seismometers at any offset. These are the best for recovering the deepest structures along the longest paths. Our end result is a fully 3D tomogram of the subsurface with lateral resolution as small as 100 m.

#### **Seismic Imaging of Open Subsurface Fractures**

MYERS, S. C., LLNL, Livermore, CA, USA, myers30@llnl.gov; PITARKA, A., LLNL, Livermore, CA, USA, pitarka1@llnl.gov; MATZEL, E., LLNL, Livermore, CA, USA, matzel1@llnl.gov; AGUIAR, A. C., LLNL, Livermore, CA, USA, aguiarmoya1@llnl.gov

Injection of high-pressure fluid into the subsurface is proven to stimulate geothermal, oil, and gas production by opening cracks that increase permeability. The effectiveness of increasing permeability by high-pressure injection has been revolutionized by the introduction of "proppants" into the injected fluid to keep cracks open after the pressure of the stimulation activity ends. The network of fractures produced during stimulation is most commonly inferred by the location of micro-earthquakes. However, existing (closed) fractures may open aseismically, so the whole fracture network may not be imaged by micro-seismic locations alone. Further, whether all new fractures remain open and for how long remains unclear.

Open cracks, even fluid-filled cracks, scatter seismic waves because traction forces are not transmitted across the gap. Numerical simulation confirms that an open crack with dimensions on the order of 10 meters can scatter enough seismic energy to change the coda of seismic signals. Our simulations show that changes in seismic coda due to newly opened fractures are only a few percent of peak seismogram amplitudes, making signals from open cracks difficult to identify. We are developing advanced signal processing methods to identify candidate signals that originate from open cracks. These methods are based on differencing seismograms that are recorded before and after high-pressure fluid injection events to identify changes in the coda. The origins of candidate signals are located using time-reversal techniques to determine if the signals are indeed associated with a coherent structure. The source of scattered energy is compared to micro-seismic event locations to determine whether cracks opened seismically or aseismically. This work performed under the auspices of the U.S. Department of Energy by Lawrence Livermore National Laboratory under Contract DE-AC52-07NA27344.

#### **Ambient Noise Correlations on a Floating Ice Shelf: Wave Guiding, Temporal Monitoring, and Structural Inversion for the Ross Ice Shelf, Antarctica**

CHAPUT, J. A., Colorado State University, Fort Collins, CO, USA; ASTER, R., Colorado State University, Fort Collins, CO, USA; CHENEY, M., Colorado State University, Fort Collins, CO, USA; BAKER, M., Colorado State University, Fort Collins, CO, USA; BRENGUIER, F., Universite Joseph Fourier, Grenoble, France; MOREAU, L., Universite Joseph Fourier, Grenoble, France; NYBLADE, A., Penn State University; WIENS, D., Washington University; HERNANDEZ, S.; GERSTOFT, P.; DIEZ, A.; ANTHONY, R.

Ambient noise correlations were computed on a multiscale aperture array of broadband and short period stations deployed on the Ross Ice Shelf in 2014 to study a variety of problems particular to this unusual medium. The presence of



the underlying water layer and the strong parameter contrasts at the ice/water and water/crust boundaries have drastic effects on the nature of the correlation functions, and this is primarily observable through the identification of resonances on the vertical component of the correlations. However, where vertical correlation functions may be contaminated by these resonances, transverse correlations are in theory unaffected, and are furthermore only sensitive to ice shelf structure given the inability of Love waves to propagate in water. Love waves therefore present a unique opportunity to characterize the variability of ice parameters over time. Analysis of dispersion curves complemented by H/V ratios also permit a better constraint of the shallow most structure underlying the water layer. The drastic muddling effect of the ice/water coupled system on any attempt to probe deeper crustal structures under the Ross Sea implies that accurate constraints of these shallow layers are a vital step to further such efforts.

Given the advent of passive temporal monitoring methods, we further compute small phase changes in the correlation functions associated with strain variations caused by the temporal response of the ice shelf to tidal forcing and ocean swells. The interest here lies in bettering our understanding of the dynamic behavior and vulnerability of these systems in light of global climate change, as well as establishing benchmark studies for their study in the future.

### **Velocity Change in the Zone of a Moderate Mw = 5.0 Earthquake Revealed by Autocorrelations of Ambient Noise and by Event Spectra**

YON SEGGERN, D. H., Nevada Seismological Laboratory, Reno, NV, USA, yonsegg@seismo.unr.edu; ANDERSON, J. G., Nevada Seismological Laboratory, Reno, NV, USA, jga@seismo.unr.edu

The  $M_w = 5.0$  Mogul, Nevada, earthquake occurred on 26 April 2008 at 06:40:10 UTC just west of Reno, Nevada. This mainshock followed a long sequence of smaller earthquakes starting in February of that year and was followed by a fairly normal aftershock sequence. Due to the prolonged nature of the swarm, it was well instrumented, with several sensors very near the abnormally shallow source zone. High-quality recordings exist both for before and after the mainshock, including from a station (MOGL) directly above the mainshock zone.

From analysis of averaged MOGL autocorrelations of day-long records before and after the earthquake, we observe a 1% decrease in velocity in the source zone at the time of the mainshock. A synthesis of autocorrelations from reflectivity records for a medium with an equally small change in velocity replicates the appearance of our ambient-noise correlations before and after the mainshock. We consider the Mogul earthquake to be the smallest in the class of tectonic earthquakes for which velocity changes are reported.

Due to the large number of events recorded before and after the mainshock, we were able to process their signals into average H/V ratios before and after. A clear shift in the H/V peaks to lower frequencies occurred at the time of the mainshock. Other averages were computed for times out to approximately 80 days after the mainshock; when compared to the foreshock spectra, these later post-seismic H/V ratios show a "healing" of the coseismic effect. These H/V observations are believed to pertain to the very shallow soils in the source zone. In contrast, the autocorrelation observations do not indicate this healing clearly and are probably associated with the medium at depths extending into the source zone itself. Thus the physical mechanisms associated with these two observed coseismic changes are somewhat different responses to the near-zone, non-linear disturbance by the mainshock.

### **3D Passive Source Reverse Time Migration: A New Imaging Method using Converted Wave**

LI, J., University of Rhode Island, Narragansett, RI, USA, jjahang\_li@my.uri.edu; SHEN, Y., University of Rhode Island, Narragansett, RI, USA, yshen@uri.edu; ZHANG, W., University of Science and Technology of China, Hefei, Anhui, China, zhangwei.zw@gmail.com

3D passive source reverse time migration method has been fully developed during the past few years. This is a new method to overcome the limitation of receiver functions in imaging dipping, discontinuous and scattering structures. The basic idea is to back propagate the full waveform seismogram using elastic wave equation with finite difference method and then correlate the P and S wave field to image the velocity anomaly structure. We tested our method with teleseismic sources and showed our method have advantages in imaging complex structure such as subducting slabs, upwelling mantle plumes and mantle wedges. We also tested it with seismic array deployed in Mendocino Triple Junction region. We use earthquakes located 30 to 90 degrees from the study region with different back azimuth angles to fully illuminate study region. To avoid the station aliasing problem, pseudo stations are constructed by interpolating the wavefield at the sparse and uneven seismic stations on to regular grids. We showed some preliminary images of Mendocino Triple Junction structure and compare it with previ-

ous receiver function result. The two different methods showed similar structure except for the mantle wedge region.

### **Application of Effective Medium Theory to the Three-Dimensional Heterogeneity of Mantle Anisotropy**

SONG, X., University of Southern California, Los Angeles, CA, USA, xinsong@usc.edu; JORDAN, T. H., University of Southern California, Los Angeles, CA, USA, tjordan@usc.edu

A self-consistent theory for the effective elastic parameters of stochastic media with small-scale 3D heterogeneities has been developed using a 2nd-order Born approximation to the scattered wavefield [*Jordan, GJI*, 2015]. Here we apply the theory to assess how small-scale variations in the local anisotropy of the upper mantle affect seismic wave propagation. We formulate and calculate explicit solutions for anisotropic models in which the local elastic properties are specified by a constant stiffness tensor with hexagonal symmetry and a stochastically variable orientation. In our models, this orientation is guided by a Gaussian random vector field with transversely isotropic (TI) statistics. If the outer scale of the stochastic variability is small compared to a wavelength, then the effective seismic velocities are TI and depend on two parameters, a horizontal-to-vertical orientation ratio  $\xi$  and a horizontal-to-vertical aspect ratio,  $\eta$ . Using stiffness tensors constrained by laboratory measurements of peridotite and eclogite xenoliths, we explore the dependence of the effective  $P$  and  $S$  velocities on  $\xi$  and  $\eta$ . For peridotite-dominated models, the Voigt averages are controlled by the local reference stiffness tensor and the orientation ratio  $\xi$ , whereas the 2nd-order terms related to the heterogeneity aspect ratio  $\eta$  are small. In particular, if the hexagonal symmetry axis of the local anisotropy corresponds to the fast direction of wave propagation, then  $V_{PH} > V_{PV}$  and  $V_{SH} > V_{SV}$  for  $\xi > 1$ . We conclude that the geometrical anisotropy due to compositional and anisotropy layering is small compared to the anisotropy associated with the horizontal bias in the lattice-preferred orientation.

### **Joint Inversion of Seismic and Gravity Data Beneath the Iberian Peninsula for Crustal and Upper Mantle Structure**

SYRACUSE, E. M., Los Alamos National Laboratory, Los Alamos, NM, USA, syracuse@lanl.gov; MACEIRA, M., Los Alamos National Laboratory, Los Alamos, NM, USA, mmaceira@lanl.gov; VILLASENOR, A., Institute of Earth Sciences Jaume Almera, Barcelona, Spain, antonio@ictja.csic.es; ZHANG, H., University of Science and Technology of China, Hefei, China, zhang11@ustc.edu.cn

We present preliminary 3D  $V_p$  and  $V_s$  models for the Iberian Peninsula and surrounding areas, derived from the simultaneous inversion of body wave first-arrival times, surface wave dispersion curves, and gravity data. This joint inversion plays upon the relative sensitivities of each dataset. Body wave travel times constrain  $V_p$  and  $V_s$ , with sampling dependent on the natural distribution of seismicity. Throughout most of the region, the predominance of crustal earthquakes limit body wave sampling to the crust and uppermost mantle, while seismicity deeper than 100 km beneath the Gibraltar arc increases resolution locally. Phase- and group-velocity dispersion curves for Rayleigh waves between 6 and 40 sec, derived by ambient noise tomography using mainly data recorded by the IberArray experiment, strongly constrain crustal  $V_s$  independently of seismicity. Gravity constrains shallow crustal  $V_p$  and  $V_s$  independently of both seismicity and seismic station distributions, although it cannot constrain changes in velocity structure with depth in areas without seismic sampling. Gravity and velocity are related through empirical relationships between seismic velocity and density, so that both seismic and gravity datasets can be used in the same inversion.

Preliminary results of joint surface wave and gravity inversions show the main structural elements of the region, including most elevated velocities within the Mediterranean upper mantle, moderately high velocities associated with the Iberian Massif, and low velocities beneath the Pyrenees. Very prominent low-velocity anomalies surround the Gibraltar arc, where eastward subduction occurred during the Early and Middle Miocene.

### **Eikonal Tomography of the Southern California Plate Boundary Region**

QIU, H., USC, Los Angeles, CA, USA, hongruiq@usc.edu; BEN-ZION, Y., USC, Los Angeles, CA, USA, benzion@usc.edu; ZIGONE, D., University of Vienna, Wien, Austria, dimitri.zigone@univie.ac.at; LIN, F. C., University of Utah, Salt Lake City, UT, USA, FanChi.Lin@utah.edu

We use eikonal tomography to derive directionally-dependent phase velocities of surface waves for the plate boundary region in southern CA sensitive to the approximate depth range 1-20 km. Seismic noise and earthquake data recorded by the relatively dense regional network provide good spatial coverage and wide frequency range. We first calculate all available components of noise cross-correlations for year 2014 between 346 stations in the area. Rayleigh wave phase travel

times between 2 and 13 sec period are derived for each station pair using frequency-time analysis. For each common station, all available travel time measurements with sufficient signal to noise ratio and envelope peak amplitude are used to construct a travel time map for a virtual source at the common station location. By solving the eikonal equation, we then evaluate both phase velocity and propagation direction at each location for each virtual source. To achieve better ray path azimuthal coverage near the edges of the study area, we also apply these steps on regional earthquake data. Isotropic phase velocities and 2-psi azimuthal anisotropy are determined statistically using measurements from different virtual and earthquake sources. The obtained dispersion results of Rayleigh waves on a 6 km x 6 km grid are inverted for local 1D shear wave velocity structures using the procedure of Herrmann (2013). The results agree well with previous observations of Zigone *et al.* (2015) in the overlapping area. Clear velocity contrasts and low velocity zones are seen for the San Andreas, San Jacinto, Elsinore and Garlock faults. We also find 2-psi azimuthal anisotropy with fast directions parallel to geometrically-simple fault sections. Updated results will be presented in the meeting.

### 3D Full Waveform Tomography in Central Mexico

JUAREZ, A., Institute of Engineering, UNAM, Mexico City, Mexico, zu.alan.zu@gmail.com; RAMIREZ-GUZMAN, L., Institute of Engineering, UNAM, Mexico City, Mexico, leoramirezg@gmail.com; RABADE-GARCIA, S., Institute of Engineering, UNAM, Mexico City, Mexico, san.rabade@gmail.com

Full Waveform Inversion has recently become a popular method for Earth structure imaging, from local to global scales. In this research, we had successfully applied the Adjoint-Wavefield formulation of Full Waveform Tomography to improve a 3D velocity model of South-Central Mexico. We constructed our initial model by gathering previous tomographic studies together with a recent earthquake cross-correlations and surface wave tomography. Fréchet kernels were computed using an octree-based finite element numerical solutions of the 3D elastodynamic wave equation (Tu *et al.*, 2006). Model updates are solved using the Conjugate Gradient Method (Tromp, 2005). More than 30,000 misfit observations were made using the Generalized Seismological Data Functional (Gee & Jordan, 1992) for different phases on records from more than 120 ( $4.5 < M_w < 5.5$ ) earthquakes, recorded from 2010 to 2015 in Southern Mexico, recorded at 54 three-component stations in South-Central Mexico. Additionally, we included observations from more than 130 Green's Functions constructed from earthquake-record cross-correlations between pairs of stations. Synthetic seismograms computed using our updated model showed better fits over observed seismograms on periods larger than 5 seconds. Furthermore, our latest model showed correlation with geological structures, such as the Mexican Volcanic Belt and also reveals other heterogeneities in the shallow crustal depths.

### The Lithospheric Structure of the Central Anatolian Plateau

CLOUD, J., University of Missouri, Columbia, MO, USA, jlcq68@mail.missouri.edu; RUSSELL, J., University of Missouri, Columbia, MO, USA, jbrussell93@gmail.com; KU, W., University of Missouri, Columbia, MO, USA, wkb57@mail.missouri.edu; KAVIANI, A., Goethe University of Frankfurt, Frankfurt, Germany, geophysik.uni-frankfurt.de; BECK, S., University of Arizona, Tucson, AZ, USA, slbeck@email.arizona.edu; SANDVOL, E., University of Missouri, Columbia, MO, USA, sandvole@missouri.edu

The Anatolian plateau is a region which has a complex tectonic history including most recently the initiation of continental escape in the last 5 Ma; thus, studies of the Anatolian plateau offer insight into how the continental escape is initiated. Within the central portion of the Anatolian plateau, the Central Anatolian Fault (CAFZ) is a key boundary relative to mantle structure, however its relation to the crustal structure is less clear. We have used data from the "Continental Dynamics: Central Anatolian Tectonics" (CD-CAT) seismic array that consisted of 71 broadband seismometers deployed as a grid covering nearly all of Central Anatolia. Data was collected from 2013 to 2015 and the reverse two station method was used to calculate the effective seismic quality factor  $Q$  based on amplitude data of high frequency  $S_n$  phases. Results showed patterns of higher seismic  $Q$  values in the south near the Arabian plate, lower  $Q$  near the Mediterranean coast, possibly resulting from rolling back of the Cyprian Arc and also lower  $Q$  in Central Anatolia. Our resulting shear wave attenuation model revealed mostly high attenuation across the fault zone showing a change in mantle attenuation consistent with mantle upwelling and partial melting. We have also examined the frequency dependence to determine the contribution of scattering attenuation with respect to our effective  $Q$  measurements.

The second part of this project focused on the three dimensional earthquake velocity structure across the fault zone. Based on our calculated earthquake locations we were able to calculate a 3D model of crustal tomography. We have constructed a preliminary data set from 22,350 events from the first nine months of the CDCAT project. We found events concentrated along the East Anatolian Fault, and evidence of seismically active centers throughout central Anatolian which is consistent with internal deformation of the Anatolian plate.

### Rayleigh wave phase velocity structure of South China block and its neighboring regions

LÜ, J., 1. Earthquake Administration of Jiangxi Province, Nanchang, Jiangxi, China, 1. Earthquake Administration of Jiangxi Province; XIE, Z. J.; ZHENG, Y.; ZHOU, L. Q., China Earthquake Networks Center, Beijing, China, lqzhou@seis.ac.cn; ZHANG, Z. W., Earthquake Administration of Sichuan Province, Chengdu, Sichuan, China, zzw1983107@163.com; HU, R.; ZENG, X. F.; ZHA, X. H.,

Based on the continuous records in the vertical component from 609 broadband seismic stations deployed in and around the South China block during the period between 2010 and 2012, we obtained the Rayleigh wave phase velocity maps at periods from 6s to 50s are further obtained by the frequency-time analysis (FTAN) and surface wave inversion. The phase velocity distribution at periods between 6~10s is in good consistent with the geological features in the middle to upper crust. The phase velocities in the basins and the small scale rifts in the South China block are in low anomalies, while in the orogens and fold belts the phase velocities are mainly exhibit high anomalies. At the periods between 20~30s, the phase velocity map is divided into two major parts by the Taihangshan-Wuyishan Gravity Lineament where crustal thickness changes dramatically. To the west side of the lineament, the phase velocity map is dominated with low velocity, while to the east side which mainly exhibits high velocity anomalies. Among them the phase velocity in the east part of the south China block that is south to the Qinling-Dabie Orogen is higher than that in the eastern part of the North China block, demonstrating that the middle and lower crust under the South China block is colder and stronger than that in the North China Craton. The possible reason for this phenomenon is that the crust in the North China Craton was thinned and extended by the tectonic force, so that the mechanic strength of the middle to lower crust in the North China Craton is relatively weaker. For the periods between 40s and 50s, the distribution of phase velocity is mainly controlled by the lateral variations of the shear wave velocities in the crust and the upper mantle. At these periods, phase velocity in the east Tibetan Plateau is significantly low because of the thick crust, in the southeast part of the North China plain and the coastal regions in the south China are interlaced with high and low phase.

### Teleseismic Earthquake Signals Observed on an Ice Shelf: Prospects for Earth Imaging Employing Floating-Platform Seismographs

BAKER, M. G., Colorado State University, Michael.G.Baker@colostate.edu; ASTER, R., Colorado State University; CHAPUT, J., Colorado State University; ANTHONY, R., Colorado State University; WIENS, D., Washington University in St. Louis; NYBLADE, A., Pennsylvania State University; BROMIRSKI, P., Scripps Institution of Oceanography; GERSTOFT, P., Scripps Institution of Oceanography; STEPHEN, R., Woods Hole Oceanographic Institute; DIEZ, A., Scripps Institution of Oceanography

A 34-station broadband array was installed spanning the approximately 1000 km wide Ross Ice Shelf (RIS) in late 2014 in a two-year deployment. The data will be utilized for studies of the dynamic state of the ice shelf and for passive imaging of crustal and upper mantle velocity structures of the portion of West Antarctic Rift System located beneath RIS. The floating ice shelf platform presents significant and unusual challenges to the use of teleseismic body wave arrivals for imaging: (1) the presence of interfering signals in the microseism through long-period bands arising from the direct and indirect influences of ocean gravity waves; (2) large amplitude reverberations caused by strong impedance contrasts at the ice-water and water-sediment interfaces on either side of the water layer; and (3) water layer decoupling of steeply incident direct S-waves or P-to-S conversions in the solid Earth below the water layer. We present a modeling and signal to noise analysis of teleseismic seismograms recorded for late 2014-late 2015, and discuss the use of teleseismic and ambient P reverberations to image structure, including crustal thickness.

## Complexities in Site Response

Poster Session · Wednesday · 20 April · Tuscany F

### Magnitude Dependent Site Proxies for Soft Sites.

LEYTON, F., Centro Sismologico Nacional, University of Chile, Santiago, Chile, leyton@csn.uchile.cl; MONTALVA, G. A., Civil Engineering Dept., University of Concepción, Concepción, Chile, gmontalva@udec.cl

It is well known that different site proxies are suitable for different frequency ranges. We examine the data from soft sites in Chile that have been subjected to both strong and moderate events, and find that megathrust events are capable of exciting low frequencies that are well characterized by the site's predominant period. However, small to moderate events have more energy on higher frequencies that are better characterized by proxies like  $V_{s30}$ . We speculate that this difference is not related to non linearity but to the fact that strong magnitude events, because of their high displacements, are able to excite lower frequencies that others cannot. This could be the reason for the poor behavior of high frequency proxies in the case of Concepción during the 2010 Maule event, and thus we propose magnitudes dependent site proxies at least for soft sites.

### Mapping of $V_{s30}$ Assimilating Uncertain Velocity Profile and Measurement Errors

ANCHETA, T. D., Risk Management Solutions, Newark, CA, USA, tim.ancheta@rms.com; LEE, S. J., Risk Management Solutions, Newark, CA, USA, sean.lee@rms.com; MITRA, D., Risk Management Solutions, Newark, CA, USA, Devjyoti.Mitra@rms.com; RANGASWAMY, A., Risk Management Solutions, Newark, CA, USA, Ajith.Rangaswamy@rms.com

Mapping methods for  $V_{s30}$  have either focused on creating maps for small areas with dense measurements or maps for large areas with sparse measurements without focusing on data uncertainties. We propose a new approach for mapping  $V_{s30}$  that can incorporate both scales of mapping but also incorporate uncertainties associated with incomplete data (*i.e.* profiles less than 30 m) and measurement error. Measurement data may be classified as hard data or soft data namely error free deterministic data or stochastic data with uncertainty. One example of soft data for mapping  $V_{s30}$  is an extrapolated  $V_{s30}$  value from a profile less than 30 meters in depth. We develop a framework to generate the soft data accounting for uncertainty from velocity profiles of all depth ranges, and process the soft data together with error-free measurements through Bayesian Maximum Entropy (BME) of modern geostatistics. Additionally, hard data collected from various measurement methods (*e.g.* downhole, crosshole, non-destructive methods) may have different measurement errors. The measurement error is considered as another type of data uncertainty entering the BME spatial prediction to increase prediction accuracy. The resulting prediction maps have an increased mapping accuracy over traditional prediction methods not accounting for the data uncertainty sources. A large database of  $V_{s30}$  measurements is used collected within the United States and the mapping approach is applied to the Southern California region.

### Methodology of Adjoint-tomography Inversion of the Small-scale Shallow Sedimentary Basins

KUBINA, F., Comenius University Bratislava, Bratislava, Slovakia, kubina4@uniba.sk; MOCZO, P., Comenius University Bratislava, Bratislava, Slovakia, moczo@fmph.uniba.sk; KRISTEK, J., Comenius University Bratislava, Bratislava, Slovakia, kristek@fmph.uniba.sk; MICHLIK, F., Comenius University Bratislava, Bratislava, Slovakia, filip.michlik@fmph.uniba.sk

Anomalous earthquake motions and corresponding damage in earthquakes are often due to site effects in local surface sedimentary basins. Because majority of world population is located atop surface sedimentary basins, it is important to predict earthquake ground motion (EGM) at these sites during future earthquakes.

A major lesson learned from dedicated international tests focused on numerical prediction of EGM in local surface sedimentary structures (LSSS) is that it is hard to reach better agreement between data and synthetics without an improved structural model.

If earthquake records are available for sites atop a LSSS it is natural to consider them for improving the structural model. Computationally efficient adjoint tomography might be a proper tool. Adjoint tomography has proven an irreplaceable useful tool in exploring Earth's structure in the regional and global scales. It has not been widely applied for improving models of LSSS in numerical predictions of EGM.

A seismic wavefield in LSSS is relatively very complex due to diffractions, conversions, interference and often also resonant phenomena. In shallow basins,

the first arrivals are not suitable for inversion due to almost vertical incidence and thus insufficient vertical resolution. Later wavefield consists mostly of local surface waves often without separated wave groups. Consequently, computed kernels are complicated and not suitable for inversion without pre-processing.

The spatial complexity of a kernel can be dramatic in a typical situation with relatively low number of sources (local earthquakes) and surface receivers. This complexity can be simplified by directionally-dependent smoothing and spatially-dependent normalization that condition reasonable convergence.

A multiscale approach seems necessary given the usual difference between the available and true models. Interestingly, only a successive inversion of  $\mu$  and  $\lambda$  elastic moduli, and different scale sequences lead to good results.

### Removing the Effect of an Ice Layer on the P-wave Response: An Application to Antarctic Studies

GRAW, J. H., The University of Alabama, Tuscaloosa, AL, USA, jhgraw@crimson.ua.edu; HANSEN, S. E., The University of Alabama, Tuscaloosa, AL, USA, shansen@ua.edu; LANGSTON, C. A., The University of Memphis, Memphis, TN, USA, clangstn@memphis.edu; YOUNG, B. A., The University of Memphis, Memphis, TN, USA, bayoung6@memphis.edu; MOSTAFANEJAD, A., The University of Memphis, Memphis, TN, USA, mstfnjad@memphis.edu

Most of the Antarctic continent is covered by thick ice sheets, which can mask integral waveform conversions from crustal and upper mantle discontinuities in teleseismic transfer functions. Reverberations in the near-surface can make standard P-wave receiver functions difficult, if not impossible, to interpret, and it is necessary to remove the effects of the ice sheet to adequately image deep structure beneath a given area. In this presentation, we present a new approach using downward continuation and decomposition of the free-surface displacements for this purpose. Teleseismic P-wave data are recorded by the Transantarctic Mountains Northern Network (TAMNNET) in northern Victoria Land, and reference station data are taken from stations FISH and DEVL, which are part of the Polar Earth Observing Network (POLENET). The downward continuation and decomposition method requires that the ice thickness be known beneath a given location; therefore, we also utilize ice thickness estimates from the BEDMAP2 model as well as results from a previous study using the TAMNNET array. The data are analyzed by deconvolving the reference-stations' array beam from a given TAMNNET station to create a radial component P-wave transfer function. The downward continued waveform is decomposed into both upgoing and downgoing P- and S-wave potentials. The upgoing S-wave potential contains the most information and can be inverted for shear-wave velocity akin to receiver functions at the free-surface. We invert the upgoing S-wave potential using a standard least squares inversion technique that directly solves for the model rather than for model perturbations. The inverted waveforms yield Moho depths that lie within error bounds of previous TAMNNET studies, but the Moho, and possibly crustal and deeper mantle structure, are imaged at a much higher resolution than were previously acquired. This approach provides a new method to study the structure beneath the Antarctic ice sheets.

### Evaluation of Ground Motions Recorded During the 2014 South Napa Earthquake at the Crocket-Carquinez Downhole Arrays

LI, G. L., University of Nevada, Reno, NV, USA, gli@unr.edu; MOTAMED, R. M., University of Nevada, Reno, NV, USA, motamed@unr.edu; DICKENSON, S. D., New Albion Geotechnical, Inc., Reno, NV, USA, sed@newalbiongeotechnical.com

The August 24, 2014  $M_w$  6.0 South Napa Earthquake caused the strongest shaking in much of the northern San Francisco Bay region since the 1989  $M_w$  6.9 Loma Prieta earthquake. During this event, the Crocket-Carquinez Bridge Geotechnical Array #1 with the nearest rupture distance (Rrup) of 20.0 km recorded a ground surface Peak Ground Acceleration (PGA) of approximately 1.0 g. This compares to 0.44g recorded at the ground surface at the Crocket-Carquinez Bridge Geotechnical Array #2, located roughly 200 m away. This significant difference in PGA is thought to be due to the combination of surface topography and 2D effects, and to the influence of dynamic response of the bridge foundations.

This study investigates the influence of site effects and possible 2D effects on the unusually high PGAs in Arrays #1 and #2 as well as the prominent differences of ground motion characteristics at these adjacent arrays. Based on the conventional assumption, two bi-directional one-dimensional (1D) site response analysis models were developed for Arrays #1 and #2 using LS-DYNA, an advanced Finite Element (FE) program. It is found that finite element models of arrays were capable to reproduce the ground motions recorded by the mid-depth accelerometers fairly well throughout a wide range of frequency. However, they failed to capture the large amplitude of the motions as recorded at the ground surface especially at high frequency range. These observations suggest that the



amplifications of the ground motions at these 2 arrays were significantly influenced by 2D effects (surface waves, basin edge) and possibly structural response with surface waves emanating from the foundations. On the basis of the analyses performed to date the practical limitations of 1D site response analysis for the location of Arrays #1 and #2 have been identified. In light of these limitations a series of 2D analyses have been performed and comparisons made to the recorded motions.

#### Revisiting Earthquake Site Response in Vancouver, Canada

MOLNAR, S., University of Western Ontario, London, ON, Canada, smolnar8@uwo.ca; CASSIDY, J. F., Natural Resources Canada, Sidney, BC, Canada, john.cassidy@canada.ca; JACKSON, F., University of Western Ontario, London, ON, Canada, fjacks02@uwo.ca; BRILLON, C., Natural Resources Canada, Sidney, BC, Canada, camille.brillon@canada.ca

On December 30, 2015 a M 4.7 earthquake occurred within the subducting Juan de Fuca plate about 40-80 km south of greater Vancouver, British Columbia, Canada. This produced the strongest shaking in the region since the 2001 M6.8 Nisqually, Washington State, earthquake, and the first to occur since a dense strong-motion network was deployed in southwestern British Columbia. In this study, we focus on the ground shaking variation in British Columbia on a wide variety of soil conditions, from bedrock, to firm soil, to the thick (up to 600 m) unconsolidated Holocene sediments of the Fraser River delta. On bedrock, peak ground acceleration values of about 0.4% g were recorded, whereas soil sites showed peak ground accelerations up to 5% g. In this study we document site response using: single-station HV spectral ratios at each of the strong-motion recording sites, spectral ratios using nearby bedrock reference recordings; and reported felt intensities and compare with the results of previous studies using recordings of moderate earthquakes. As in previous earthquakes, the strongest observed shaking was observed near the northern part of the Fraser River delta, suggesting that basin edge effects and/or resonance effects are important.

#### Sensitivity Tests of Effects of Detailed Shear-Wave Velocity Profiles to 100 m Depth on Response Spectra, Clark County, Nevada

WEST, L. T., Nevada Seismological Lab., Univ. of Nevada, Reno, NV, USA, travisw@optimds.com; LOUIE, J., Nevada Seismological Lab., Univ. of Nevada, Reno, NV, USA, louie@seismo.unr.edu; PULLAMMANAPPALLIL, S., Optim, Reno, NV, USA, satish@optimsoftware.com

Near-surface geology has a substantial effect on ground motions and is critical to overall earthquake hazard analysis. As a result, the time average shear wave velocity down to 30 m ( $V_{s30}$ ) has become a determinant in current provisions for seismic design; and can be an effective means for estimating potential ground motions at sites with relatively simple near-surface geology. Unfortunately, site response calculated using only the  $V_{s30}$  parameter may not fully capture the true nature of complex shallow geology, especially that which relates to sharp velocity contrasts and inversions. In order to illustrate the effects of complex velocity structure on site response we calculated the one-dimensional linear-elastic spectral response at several sites in Clark County, Nevada, making use of the available Clark County Parcel Map  $V_s$  database. This extensive database, collected over three years, covers approximately 1500 km<sup>2</sup> and incorporates more than 10,000 individual Refraction Microtremor (ReMi) shear wave velocity profiles (SWVP) down to an average depth of 100 m. A range of sites representing varied geologic and subsurface conditions were selected from this database. For each model, the response and Fourier spectra utilizing both the “full” profiles, including all velocity layers of the SWVP and depth-to-bedrock, and then for the corresponding  $V_{s30}$  “simple” profile down to bedrock were calculated. These results show very similar spectral amplitudes and shape at periods longer than  $T=1.0$  sec; however, at higher frequencies, the spectral responses differ greatly in amplitude and complexity, with some profiles depicting an increase of nearly 30% in spectral amplitude at some peak frequencies. These results are based on direct measurements of each site, highlighting the effects of complex velocity structure on response spectra, and how using only  $V_{s30}$  may underestimate earthquake hazard in site characterization.

#### Improving Our Understanding of 1D Site Response Model Behavior: Physical Insights for Statistical Deviations from 114 KiK-net Sites

KAKLAMANOS, J., Merrimack College, North Andover, MA; BRADLEY, B. A., University of Canterbury, Christchurch, New Zealand

Nonlinear soil behavior often exhibits a strong influence on surficial ground motions, and these effects have been incorporated into site response models in various ways. However, site response models are associated with large uncertainties and can on occasion poorly replicate observed ground motions. In this study, nonlinear site response model predictions for 5626 ground motions at 114

vertical seismometer arrays of Japan's Kiban-Kyoshin network (KiK-net) are calculated using DEEPSOIL and compared to observed ground motions and predictions from linear and equivalent-linear analyses in SHAKE. Using this large database of one-dimensional (1D) site response model predictions, a variety of statistical analyses are performed to quantify the models' bias and precision, and these statistical analyses are paired with physical insights into site and ground-motion behavior.

As expected, there are deviations between the linear, equivalent-linear, and nonlinear site response models at large shear strains, particularly when using cumulative Arias intensity as a basis for comparison. Another less intuitive result is the fact that all models—linear, equivalent-linear, and nonlinear—tend to underpredict high-frequency ground motions in the aggregate. A number of physical hypotheses are tested at a subset of sites to help explain this persistent bias: for example, modifying the shear-wave velocity profile to include a depth-dependent gradient, randomizing the shear-wave velocity profile, increasing the small-strain shear modulus, and decreasing the small-strain damping ratio. Some of these alterations (particularly the usage of a depth-dependent shear-wave velocity gradient) have a significant impact on the model bias, even more so than changing the constitutive model for dynamic soil behavior. Using an unprecedented number of sites and ground motions, the results of this study provide some insights for improvements to 1D site response model predictions moving forward.

#### Estimation of $K_0$ Implied by the High-Frequency Shape of the NGA-West2 Ground Motion Prediction Equations

ZANDIEH, A., Lettis Consultants International, Inc., Boulder, CO, USA, zandieh@lettisci.com; CAMPBELL, K. W., CoreLogic, Inc., Oakland, CA, USA, kcampbell@corelogic.com; PEZESHK, S., Department of Civil Engineering, The University of Memphis, Memphis, TN, USA, spezeshk@memphis.edu

The spectral-decay parameter  $K_0$  is often used to account for the reduction of the high-frequency amplitude of ground motion caused by attenuation within the site profile. In this study, we used the inverse random vibration theory approach described by Al Atik *et al.* (2014) to calculate Fourier amplitude spectra from predicted values of response-spectral acceleration for all five NGA-West2 ground-motion prediction equations (GMPEs). We used these spectra to estimate  $K_0$  using the spectral-decay method. Each GMPE was evaluated for a NEHRP B/C site condition and for default estimates of depth to the top of rupture, hypocentral depth, and sediment (basin) depth. We derived estimates of  $K_0$  for magnitudes ranging from 3.5 to 8.0 and distances ranging from 5 to 20 km and used a mixed-effects model to derive equations for these estimates as a function of magnitude. We also calculated  $K_0$  from the geometric mean of the response-spectral accelerations of the GMPEs to check the sensitivity of the results to the two approaches and found that the values of  $K_0$  derived in this study using a mixed-effects model are in good agreement with these estimates. The values of  $K_0$  obtained in this study do not necessarily represent the physical high-frequency damping within the site profiles used to develop the NGA-West2 GMPEs. Instead, they are intended to represent the high-frequency shape of the median predicted spectral accelerations from the GMPEs. The  $K_0$  model developed in this study can be used in inversions to develop stochastic models that are intended to mimic the predictions from the NGA-West2 GMPEs and thus avoid the tradeoff between  $K_0$  and other high-frequency seismological parameters in the model.

#### Improved Estimation of Site Response using Random Vibration Theory

SEIFRIED, A. E., Lettis Consultants International, Boulder, CO, USA, seifried@lettisci.com; TORO, G. R., Lettis Consultants International, Boulder, CO, USA, toro@lettisci.com

Site-specific seismic hazard analysis accounts for the effect of local geologic conditions on the expected ground motions at a site. This analysis typically involves the propagation of ground motions defined for underlying rock conditions through the soil at a site to the surface. In engineering practice this is commonly and efficiently accomplished using a random vibration theory (RVT)-based equivalent-linear approach. Recent research demonstrates that site-specific response spectrum amplification factors (AF) obtained using RVT methods can be conservative by as much as 50% relative to those obtained using time history methods for some frequencies. An alternative RVT-based approach to calculating AF is used here to reduce unnecessary conservatism while maintaining computational efficiency. Many current RVT approaches utilize empirical adjustments to input ground motion duration to compute response spectral amplitude. Such adjustments are necessary when single-degree-of-freedom (SDOF) responses outlast the duration of excitation, but do not account for the increase in duration of excitation observed as time histories propagate through the site. This leads to overestimation of surface response, particularly at the modal frequencies of the

site. The approach used here instead focuses on the response bandwidth of the combined soil-SDOF system. A theoretical nonstationarity factor is used instead of an empirical duration adjustment to account for the difference between the input ground motion duration and the time required to excite the combined system. This change results in estimates of AF that are in better agreement with time history methods, particularly at the modal frequencies of the site. The impact of this approach on AF is generalized to the analysis of a variety of scenarios and conditions that may be encountered in a typical seismic hazard analysis. The significance of the impact to hazard calculations is also investigated.

#### **Joint Deconvolution of Borehole and Building Strong Motion Recordings: an Application to Three Different Test Cases**

PETROVIC, B., GFZ German Research Centre for Geosciences, Potsdam, Germany, petrovic@gfz-potsdam.de; PAROLAI, S., GFZ German Research Centre for Geosciences, Potsdam, Germany, parolai@gfz-potsdam.de; DIKMEN, S. U., Bogazici University, Kandilli Observatory, Istanbul, Turkey, umit.dikmen@boun.edu.tr; SAFAK, E., Bogazici University, Kandilli Observatory, Istanbul, Turkey, safak.erdal@gmail.com; PIANESE, G., Polytechnic University of Milan, Milan, Italy, giovanna.pianese@polimi.it; PAOLUCCI, R., Polytechnic University of Milan, Milan, Italy, roberto.paolucci@polimi.it; ORUNBAEV, S., Central Asian Institute for Applied Geosciences (CAIAG), Bishkek, Kyrgyzstan, s.orunbaev@caiag.kg; MOLDOBEKOV, B., Central Asian Institute for Applied Geosciences (CAIAG), Bishkek, Kyrgyzstan, b.moldobekov@caiag.kg

Estimating the seismic wavefield that is radiated back by a structure to a free field has become recently an important issue for the Engineering and Seismological communities, aiming at non-destructive testing of the dynamic properties of soils and buildings and at quantifying the impact of dynamic soil-structure interaction effects. The influence of the soil on the building response and of building vibrations on the ground motion have been shown both by empirical and theoretical studies. Multiple interactions between soil layers and structures have been studied by 2D and 3D numerical simulations of ground motion, that have also contributed to emphasize the so called site-city interaction.

In the past, the deconvolution interferometry was applied separately to recordings of sensors installed in buildings (earthquakes, generated sources, ambient vibration) to study wave propagation through the building, and to earthquake recordings of borehole sensors to investigate the wave propagation in shallow geological layers. However, the joint application to systems including both, soil and structure has received limited attention so far. As a matter of fact, waves traveling from the soil to the building and the wavefield radiated back from the building to the soil can only be analyzed if recordings of sensors installed both in a borehole and in nearby buildings are available and jointly analyzed.

In this study, a combined deconvolution interferometry is applied to three data sets consisting of borehole and building recordings with different soil and building characteristics; 1) Bishkek (Kyrgyzstan):  $v_{structure} < v_{soil}$ , 2) Istanbul (Turkey):  $v_{structure} = v_{soil}$  and 3) Mexico City (Mexico):  $v_{structure} > v_{soil}$ . The real input ground motion and the wavefield radiated back from the building to the soil are separated by application of the constrained deconvolution, and finally the energy that is radiated back from the building to the soil is estimated at different depths.

#### **Improved Risk Management through a Novel Semi-empirical SSI Model Calibration for Vertical Ground Motions**

DI ALESSANDRO, C., GeoPentech, Inc., Santa Ana, CA, USA, carola\_dialessandro@geopentech.com; DINSICK, A., GeoPentech, Inc., Santa Ana, CA, USA, andrew\_dinsick@geopentech.com

This paper presents a case history where the risk management team identified a need to broaden the currently available approaches to account for kinematic Soil-Structure Interaction (SSI) effects in vertical ground motions for the design of a new hospital at the Loma Linda University Medical Center. Horizontal and vertical site-specific ground-motion response spectra (controlled by the nearby San Jacinto Fault) and eleven sets of three-component time histories were provided to the design team which represented free-field (FF) conditions. Preliminary analyses indicated that vertical ground motions have a significant impact on the response of sensitive, non-structural components which need strengthening to reduce the potential life safety risks during the Maximum Considered Earthquake (MCE) at the site. Furthermore, the key vertical period range for the structure and components coincides with the period range where kinematic SSI effects result in the largest reduction in ground-motion intensity, relative to the free-field conditions. Although it has long been suspected that kinematic SSI has an impact on the vertical ground motions, to-date no publications are available to support the use of a model to develop vertical Foundation Input Motions (FIMs). In response to this problem, we developed an empirical database and computed frequency-dependent transmissibility function amplitudes (aka transfer func-

tions) between FIM and FF ground motions following the work by Stewart and Stewart (1997) and Kim and Stewart (2003); these transfer functions were then used to calibrate kinematic SSI effects for vertical ground motions by modifying the existing approaches for horizontal kinematic SSI (NIST, 2012). Based on this analysis, new models and refined procedures were developed and validated in a peer-reviewed framework to provide appropriate ground-motion time histories for the nonlinear response history analysis.

---

### **Induced Seismicity Monitoring: What is Really Needed?**

Oral Session · Thursday · 8:30 AM · 21 April · Tuscany 1/2

Session Chairs: Iain Weir-Jones and Steven Taylor

---

#### **Challenges and Strategies for Monitoring Induced Seismicity**

BATURAN, D., Nanometrics Inc, Kanata, ON, Canada, dariobaturan@nanometrics.ca; KARIMI, S., Nanometrics Inc, Kanata, ON, Canada, sepidehkarimi@nanometrics.ca; YENIER, E., Nanometrics Inc, Kanata, ON, Canada, emrahyenier@nanometrics.ca

Between 2013 and 2015, a number of seismic events characterized as induced with magnitudes above M3.0 were recorded in British Columbia, Alberta, Ohio and Oklahoma. Following increased public awareness and media scrutiny, many jurisdictions have put in place protocols to mitigate risks associated with induced seismicity. Most of the regulations introduced to date mandate the deployment of real-time seismic monitoring networks as drivers of operational traffic light systems. Using some of the regulatory protocols now in place, we address the best practice strategies associated with monitoring for induced seismicity. How many stations are needed to meet the monitoring mandate and what should be their geographical distribution? How many stations could be inoperative before the network does not meet its monitoring mandate? With a number of sensing technologies to choose from, including seismometers, accelerometers and geophones, which one provides the best combination of self-noise, clip level and frequency response to cover the seismic event magnitude and epicentral distance range? As most current "traffic light" protocol thresholds are based on magnitudes, which magnitude scale should be used? The networks initially deployed to manage risk associated with induced seismicity can provide additional benefits. Generated data sets can be used to assist operators in optimizing completion operations, identify or refine knowledge of geological structures, estimate the direction of in-situ stress regimes, monitor critical infrastructures and develop regional attenuation relationships for more accurate ground motion and magnitude estimates.

#### **TexNet: A New, Integrated Seismic Monitoring Program in Texas**

SAVVAIDIS, A., Bureau of Economic Geology, University of Texas at Austin, Austin, TX, USA, alexandros.savvaidis@gmail.com; YOUNG, M., Bureau of Economic Geology, University of Texas at Austin, Austin, TX, USA, michael.young@beg.utexas.edu; TINKER, S., Bureau of Economic Geology, University of Texas at Austin, Austin, TX, USA, scott.tinker@beg.utexas.edu; RATHJE, E. M., Department of Civil, Architectural and Environmental Engineering, Austin, TX, USA, e.rathje@mail.utexas.edu; FROHLICH, C. A., U.T. Institute for Geophysics, University of Texas at Austin, Austin, TX, USA, cliff@ig.utexas.edu; WALTER, J., U.T. Institute for Geophysics, University of Texas at Austin, Austin, TX, USA, jwalter@ig.utexas.edu; DE SHON, H., Department of Geology and Geophysics, Southern Methodist Univ., Dallas, TX, USA, hdeshon@mail.smu.edu; GALE, J. F., Bureau of Economic Geology, University of Texas at Austin, Austin, TX, USA, julia.gale@beg.utexas.edu; Hennings, P., Bureau of Economic Geology, University of Texas, Austin, Texas, USA, jphennings@gmail.com; EICHHUBL, P., Bureau of Economic Geology, University of Texas, Austin, Texas, USA, peter.eichhUBL@beg.utexas.edu; OLSON, J., Department of Petroleum and Geosystems Engineering, University of Texas at Austin, jolson@austin.utexas.edu; OLSON, H. C., Department of Petroleum and Geosystems Engineering, University of Texas at Austin, hily.olson@beg.utexas.edu; MARKMAN, A., Department of Psychology, University of Texas at Austin, markman@utexas.edu; KAHLOR, L. A., Moody School of Communication, University of Texas at Austin, kahlor@austin.utexas.edu

Potentially induced seismicity events have been recorded recently in the southern mid-continent of the U.S., including Texas. These events have led to substantial public discussion regarding cause and potential risks of damage to infrastructure and to public safety. In an effort to better understand the causes of these events, and to monitor earthquake activity in general, the 84th Texas Legislature included funding to create a statewide, seismic monitoring program, known as TexNet. The goal of TexNet is to provide authenticated data needed to evaluate the location, frequency and likely causes of natural and induced earthquakes, the latter potentially associated with the development of hydrocarbons and asso-

ciated disposal of wastewater. A better understanding of these events will help stakeholders avoid operational procedures that increase the risk of induced earthquakes.

TexNet will consist of at least 22 new permanent seismic monitoring stations across Texas, augmenting the 17 existing stations. Locations (at the time of this writing) are being focused on former locations of USArray Transportable Array, though final decisions will be based on baseline noise analysis and other logistical issues. In addition, 36 temporary (rapid response) seismometers will be deployed to further examine seismic events, particularly in areas with denser population or critical infrastructure.

TexNet will also focus on research to understand causal mechanisms, where possible. Research topics, already ongoing, include fault mapping, geomechanics, reservoir modeling, earthquake engineering, and improved communication strategies for the public and other stakeholders. Schedule-wise, we anticipate TexNet to be fully deployed and operational in 2016. In this presentation, we will discuss relevant aspects of the TexNet program and our vision for the future of integrated seismic monitoring in Texas.

#### **Induced Seismicity Monitoring and the Traffic Light Protocol**

TAYLOR, S. R., GeoEnergy Monitoring Systems, Los Alamos, NM, USA, [srt@geoems.com](mailto:srt@geoems.com); JARPE, S. P., GeoEnergy Monitoring Systems, Los Alamos, NM, USA, [sjarpe@geoems.com](mailto:sjarpe@geoems.com); HARBEN, P. E., GeoEnergy Monitoring Systems, Los Alamos, NM, USA, [pharben@geoems.com](mailto:pharben@geoems.com); WEIR-JONES, I., Weir-Jones Group, Vancouver, BC, Canada, [iainw@weir-jones.com](mailto:iainw@weir-jones.com)

Most fluid injection activities rely on a “Traffic Light” protocol which ties fluid injection activities to the location and magnitude of seismicity within a specified distance from a well. Typically, seismicity is monitored by state or province geological surveys in collaboration with national networks. In many areas, government monitoring networks are sparse and epicentral errors can be as large as 10 km. An area of 100 km<sup>2</sup> can encompass many injection wells with different operators. Additionally, reported magnitudes from sparse networks can have significant random errors and can be biased high through a statistical phenomenon known as data censoring due to signal to noise variations. The consequences associated with a traffic light system can be severe to an operator and may be unfounded. If the operator has access to seismic data collected near the affected facility it is possible to avoid a costly shutdown and instead implement mitigation efforts (e.g. reducing well pressures and volumes for a short period of time).

What is needed for an operator to comply with regulations and to mount a defense against poorly reported seismic locations or magnitudes? The data from observatory-grade systems typical are excellent and are capable of recording negative seismic magnitudes at local distances. However, traffic light regulatory systems typically call for no action on the part of an operator unless magnitudes are above local magnitude (ML) 2 within 3 to 5 km of a well. This means that seismic deployments necessary to meet regulatory requirements do not have to be overly expensive or complex. In many cases, a single station at a facility may be all that is necessary by providing event origin times, magnitude and distance (from S minus P arrival times). If seismic location is required then 3 or more stations are necessary. Event location and fault plane solutions have the benefit of visualizing trends of seismicity and the possibility of locating fractures and faults.

#### **The Eastern Kentucky Microseismic Monitoring Project: A Public-Private Collaborative Project at the Onset of Unconventional Oil and Gas Production in the Rome Trough, Eastern Kentucky**

CARPENTER, N. S., University of Kentucky, Lexington, KY, USA, [carpenter@uky.edu](mailto:carpenter@uky.edu); WANG, Z., University of Kentucky, Lexington, KY, USA, [zhenming.wang@uky.edu](mailto:zhenming.wang@uky.edu); MOORES, A. O., Nanometrics Inc., Kanata, ON, Canada, [andrewmoores@nanometrics.ca](mailto:andrewmoores@nanometrics.ca); ROCHE, S. L., Cimarex Energy Co., Tulsa, OK, USA, [SRoche@cimarex.com](mailto:SRoche@cimarex.com); WOOLERY, E. W., University of Kentucky, Lexington, KY, USA, [ewoolery@uky.edu](mailto:ewoolery@uky.edu)

In the central and eastern United States, felt earthquakes likely triggered by fluid injection from oil and gas production or wastewater disposal have dramatically increased in frequency since the onset of the shale gas boom. In the Rome Trough (RT) of eastern Kentucky, fracture stimulations and wastewater injection are ongoing and occur near historically active areas, including the source region of the 1980 mb 5.2 Sharpsburg earthquake to the northwest and the eastern Tennessee Seismic Zone to the south. Unlike in states surrounding and near to Kentucky (e.g., Ohio, West Virginia, and Arkansas), no seismic events related to subsurface fluid injections have been reported felt or detected by regional seismic networks.

Interest is emerging in development of the deep Cambrian Rogersville Shale in the RT that would use horizontal drilling and high-volume hydraulic fracturing. To characterize natural seismicity rates and the conditions that might

lead to induced or triggered events, the Kentucky Geological Survey is conducting a collaborative study, the Eastern Kentucky Microseismic Monitoring Project (EK MMP), prior to the onset of large-scale oil and gas production and wastewater injection. A temporary network of broadband seismographs is being deployed in the vicinity of dense clusters of Class II wastewater injection wells and near the locations of new, deep oil and gas test wells in eastern Kentucky. Project collaborators thus far include Nanometrics Inc. (instrumentation and support), Cimarex Energy Co. (instrumentation), and the Department of Earth and Environmental Sciences (research) at the University of Kentucky. Installation began in mid-2015 and by November, 2015, 12 stations were operating; more stations are planned for 2016. Data are acquired in real-time and in tandem with regional network data; real-time event detections and locations are being determined. Several micro-earthquakes unreported by regional networks have been located using EK MMP stations.

#### **Hybrid Seismic Denoising Using Higher Order Statistics and Improved Wavelet Block Thresholding**

MOUSAVI, S. M., University of Memphis, Memphis, TN, USA, [smousavi05@gmail.com](mailto:smousavi05@gmail.com); LANGSTON, C. A., University of Memphis, Memphis, TN, USA, [clangstn@memphis.edu](mailto:clangstn@memphis.edu)

We introduce a non-diagonal seismic denoising method based on the continuous wavelet transform with hybrid block thresholding. Parameters for the block thresholding step are adaptively adjusted to the inferred signal property by minimizing Stein's (1980) unbiased risk estimate. The efficiency of the denoising for seismic data has been improved by adapting the wavelet thresholding and adding a pre-processing step based on a higher order statistical analysis and a post-processing step based on Weiner filtering. Application of the proposed method on synthetic and real seismic data shows the effectiveness of the method for denoising and improving the signal-to-noise ratio of local microseismic, regional, and ocean bottom seismic data.

---

#### **Marine Paleoseismology: Assessing Offshore Hazards**

Oral Session · Thursday · 10:45 AM · 21 April · Tuscany 1/2

Session Chair: Neal Driscoll

---

#### **Central and Northern Cascadia Revised Segment Boundaries and Probabilities from Onshore and Offshore Core Data**

GOLDFINGER, C., Oregon State University, Corvallis, OR, USA, [gold@oce.orst.edu](mailto:gold@oce.orst.edu); GALER, S., Oregon State University, Corvallis, OR, USA, [steve.galer82@gmail.com](mailto:steve.galer82@gmail.com); BLACK, B., Oregon State University, Corvallis, OR, USA, [bran.black3125@gmail.com](mailto:bran.black3125@gmail.com); HAUSMANN, R., Oregon State University, Corvallis, OR, USA, [rbhausmann@gmail.com](mailto:rbhausmann@gmail.com); MASON, B., Oregon State University, Corvallis, OR, USA, [Ben.Mason@oregonstate.edu](mailto:Ben.Mason@oregonstate.edu); PATTON, J., Humboldt State University, Arcata, CA, USA, [quakejay@gmail.com](mailto:quakejay@gmail.com)

New and archive core, bathymetric, backscatter and seismic reflection data from the Oregon and Washington continental margin and several onshore lakes reveal new insights into segment rupture limits and recurrence. Offshore Washington, analysis of ~ 130 additional cores fills out the turbidite record in major canyon systems including Barkley, Nitinat, Juan de Fuca, Quillayute, Grays, Guide, and Willapa Canyons. Each has different post-glacial mechanisms of loading and dispersal of sediment via turbidity currents during high stands of sea level. As previously reported, the primary fan systems, the Astoria and Nitinat Fans, are largely inactive in the Holocene, with turbidity current activity limited to the proximal parts of the main channels, and Holocene deposition fading rapidly toward the middle and distal fans. The active systems contain between 15 and 23 likely correlative Holocene turbidites best explained by triggering by a series of 23 earthquakes, consistent with coastal and inland lake paleoseismic data in Washington and Canada. The new analysis also revises the formerly data-limited northern boundaries for the segments proposed in Goldfinger *et al.* (2008; 2012). Several “Segment B” ruptures likely extended north to Quinault Canyon, one event was resolved into two, and one Washington only event was added in 2013, for a total of 23 Holocene events. “Segment C” ruptures were found to extend to ~ the latitude of Astoria Canyon, but may remain data limited. The mean recurrence times for given sections of the coast are therefore revised to 434 years for the Washington Coast, and 352 years for the central and northern Oregon coast. Conditional time-dependent probabilities in the next 50 years also are revised to 10-17% for the Washington coast, and 15-20% for the central and northern Oregon coast. Preliminary results for lake turbidite records for Washington, northern and southern Oregon yield consistent results for similar latitude ranges.



### Determining Slip Along the Queen Charlotte-Fairweather Fault Zone

GREENE, H. G., Moss Landing Marine Labs, Moss Landing, CA, USA, greene@mml.calstate.edu; BARRIE, J. V., Geological Survey of Canada, Sidney, BC, Canada, vaughn.barrie@canada.ca; NISHENKO, S., Pacific Gas & Electric Company, San Francisco, CA, USA, SPN3@pge.com; CONWAY, K., Geological Survey of Canada, Sidney, BC, Canada, kim.conway@canada.ca; ENKIN, R., Geological Survey of Canada, Sidney, BC, Canada, randy.erkin@canada.ca; CONRAD, J., United States Geological Survey, Santa Cruz, CA, USA, jconrad@usgs.gov; MAIER, K. L., United States Geological Survey, Santa Cruz, CA, USA, kcolbe@usgs.gov; STACEY, C., Geological Survey of Canada, Sidney, BC, USA, copper.stacey@canada.ca

The Queen Charlotte-Fairweather (QC-FW) transform fault system separates the Pacific Plate from the North American Plate in the Pacific Northwest. It extends offshore from near the northern end of Vancouver Island, Canada through the Alexander Archipelago and into SE Alaska near Yakutat Bay. A joint Sitka Sound Science Center/Geological Survey of Canada cruise in 2015 investigated the southern part of this fault system, along the southern end of the 1949  $M_w$  8.1 Queen Charlotte Island earthquake rupture and north of the 2012  $M_w$  7.8 Haida Gwaii earthquake epicenter, using multibeam echo sounder bathymetric data, Knudson low power, 12 element, 3.5 kHz high-resolution Chirp seismic-reflection profiles, Benthos piston cores, IKU grab samples, and bottom camera photographs.

The surface expression of the QC-FW fault zone is well imaged offshore, west of the central Haida Gwaii Islands. Here, one of the larger submarine canyons along the western margin of Haida Gwaii heads at the shelf break and is tentatively named the "Cartwright Canyon". An approximate 800 m right-lateral offset occurs in the lower part of Cartwright Canyon where it intersects the fault zone, an ideal piercing point for determining slip. Gullies on the slope east of the fault zone are all truncated along faults and appear to be offset along a smeared bajada, or talus fans. Four gravity cores, two in the lower part of the canyon east of the fault zone and two within the lower offset part of the canyon west of the fault zone were collected, logged using a Multi-Sensor Core Logger, described, and sub-sampled for radiocarbon dating. The oldest sediment collected in these cores appears to be late Pleistocene in age (to be confirmed when dating is complete) and deposited during MIS stage 2 (~20 ka). Using this age and the 800 m offset we infer an approximate minimum slip rate of 40 mm/yr.

### Segmentation along the Newport-Inglewood Rose Canyon Fault Zone: Mapping and Implications for Rupture Propagation

SAHAKIAN, V. J., Scripps Institution of Oceanography, La Jolla, CA, USA, vjsahaki@ucsd.edu; BORMANN, J. M., University of Nevada, Reno, NV, USA, jrbormann@gmail.com; DRISCOLL, N. W., Scripps Institution of Oceanography, La Jolla, CA, USA, ndriscoll@ucsd.edu; HARDING, A. J., Scripps Institution of Oceanography, La Jolla, CA, USA, aharding@ucsd.edu; KENT, G. M., University of Nevada, Reno, NV, USA, gkent@unr.edu; WESNOUSKY, S. G., University of Nevada, Reno, NV, USA, wesnousky@unr.edu

Immediately offshore San Diego, Orange, and Los Angeles counties lies the Newport-Inglewood/Rose Canyon fault zone (NIRC), an active component of the southern California strike-slip fault system. Despite its close proximity to the densely populated coast, the NIRC fault geometry, segmentation, and expected earthquake behavior are not well constrained. Resolving these uncertainties will provide critical information to hazard models regarding potential earthquake magnitudes and ground shaking caused by rupture on the offshore portion of the NIRC.

This study presents an improved characterization of the offshore NIRC architecture and segmentation with bathymetry and subsurface observations from nested marine seismic reflection data of varying vertical resolutions. These data, collected in 1979, 2006, 2008, 2009, and 2013, are employed to map the NIRC location, strike, dip, as well as stepover location and width (where width is measured as the minimum horizontal distance between fault strands or termini). The resulting map and observations are then considered in empirical and physical models of throughgoing rupture on the NIRC to estimate a maximum potential magnitude on this fault zone.

Four main geometrical fault segments were identified, separated by three stepovers between 0.5 and 2 km in width. Empirical studies of rupture propagation imply that these stepovers could allow for throughgoing rupture. As a quantitative approach, we model the static coulomb stress changes resulting from rupture initiation scenarios, and consider how dynamic stress changes may be different. As a result of the static stress models, we find that earthquakes initiating on the central fault strand by Carlsbad Canyon favor bilateral, throughgoing rupture across the entire NIRC fault zone; we also find that the southernmost stepover may impede northerly rupture. Finally, according to these models, we

estimate the maximum potential magnitude on all mapped offshore strands to be  $M_w$  7.3.

### New High-Resolution 3D Imagery of Fault Deformation and Segmentation of the Newport-Inglewood Rose Canyon Fault and San Onofre Trend

HOLMES, J. J., Scripps Institution of Oceanography, La Jolla, CA, USA, jjholmes@ucsd.edu; DRISCOLL, N. W., Scripps Institution of Oceanography, La Jolla, CA, USA, ndriscoll@ucsd.edu; KENT, G. M., University of Nevada, Reno, NV, USA, gkent@unr.edu

The Inner California Borderlands (ICB) is situated off the coast of southern California and northern Baja. The structural and geomorphic characteristics of the area record a middle Oligocene transition from subduction to microplate capture along the California coast. Marine stratigraphic evidence shows large-scale extension and rotation overprinted by modern strike-slip deformation. Geodetic and geologic observations indicate that approximately 6-8 mm/yr of Pacific-North American relative plate motion is accommodated by offshore strike-slip faulting in the ICB.

The closest offshore fault, the Newport-Inglewood Rose Canyon (NIRC) Fault is a dextral strike-slip system running approximately 120 km from San Diego to the San Joaquin Hills near Newport Beach, California. Based on trenching and well data, the NIRC Fault Holocene slip rate is 1.5-2.0 mm/yr to the south and 0.5-1.0 mm/yr along its northern extent. An earthquake rupturing the entire length of the system could produce an  $M_w$  7.0 earthquake or larger.

West of the main segments of the NIRC Fault is the San Onofre Trend (SOT) along the continental slope. Previous work concluded that this is part of a strike-slip system that eventually merges with the NIRC Fault. Others have interpreted this as deformation due to a blind thrust system.

In late 2013, we acquired the first high-resolution 3D Parallel Cable (P-Cable) seismic surveys of the NIRC and SOT faults as part of the Southern California Regional Fault Mapping project aboard the R/V New Horizon. Analysis of these data volume provides important new insights and constraints on the fault segmentation and transfer of deformation.

Based on this new data, westward stepping geometry of large segments of the NIRC fault as well as identified a large compressional structure are observed. We've also mapped several parallel fault segments of the SOT on the continental slope that appear linked to westward jogs in right-lateral fault strands of the NIRC on the shelf.

### Modeling 3D Earthquake Scenarios on the Newport-Inglewood/Rose Canyon Fault

BOUDJEMA, M., Nevada Seismological Laboratory, University of Nevada, Reno, NV, USA, mboudjema@unr.edu; LOUIE, J., Nevada Seismological Laboratory, University of Nevada, Reno, NV, USA, louie@seismo.unr.edu; KENT, G., Nevada Seismological Laboratory, University of Nevada, Reno, NV, USA, gkent@unr.edu; SAHAKIAN, V., Scripps Institution of Oceanography, UCSD, La Jolla, CA, USA, vjsahaki@ucsd.edu; DRISCOLL, N., Scripps Institution of Oceanography, UCSD, La Jolla, CA, USA, ndriscoll@ucsd.edu

The Inner California Borderland hosts a system of strike-slip faults hundreds of kilometers in length. A UNR-Scripps collaboration is detailing the Newport-Inglewood/Rose Canyon (NI/RC) fault system and the surrounding sedimentary basins with high-res marine seismic surveys; one of the objectives of this project is to compute shaking from scenario earthquakes and examine the hazards the NI/RC fault system poses to coastal communities and critical facilities such as SONGS. Ground motion modeling uses LLNL's SW4 wave-propagation framework. SCEC's CVM-H provides crustal structure, defining thicknesses of onshore and offshore basins, as well as geotechnical shear velocities, supplemented with Vs30 values from UNR databases. Initial modeling focuses on low-frequency results comparing rupture directions on simple planar representations of segments along the NI/RC fault system, representing magnitude 6.8-7.2+ events. Sensitivity tests on segment selection and rupture directivity result in comparisons of peak ground velocities and synthetic seismograms across communities and critical facilities along the Southern California coast. In these results, strong ground motions can exceed 1 m/s directly above the fault ruptures but vary in a complex interplay between fault geometry and basin-edge location. Further, maximum shaking amplitudes can vary by 50% over distances of less than 2 km, even in 0.15 Hz simulations. The impingement of rupturing segments into deep basins can inject high shaking levels. The sensitivity test on rupture directivity suggests shaking amplifications of a factor of four. Shaking predictions will benefit from the detailed fault characterization being carried out by the UNR-Scripps collaboration. Further modeling will employ detailed models of NI/RC fault system strands, and multiple alternative rupture models on each fault segment,

building a probabilistic framework for 3D shaking prediction at coastal communities and critical facilities.

## Multi-Phenomenology Approaches to Explosion Source Studies

Oral Session · Thursday · 1:30 PM · 21 April · Tuscany 1/2  
Session Chairs: Catherine Snelson, Christopher Bradley, and G. Eli Baker

### Evaluation of a Seismic Event, 12 May 2010, in North Korea

KIM, W. Y., Lamont-Doherty Earth Observatory of Columbia University, Palisades, NY, USA, wykim@LDE0.columbia.edu; RICHARDS, P. G., Lamont-Doherty Earth Observatory of Columbia University, Palisades, NY, USA, richards@LDE0.columbia.edu; SCHAFF, D. P., Lamont-Doherty Earth Observatory of Columbia University, Palisades, NY, USA, dschaff@LDE0.columbia.edu; KOCH, K., Federal Institute for Geosciences and Natural Resources, Hannover, Germany, karl.koch@bgr.de

We have assessed seismological evidence bearing on claims that North Korea conducted a small nuclear test on 12 May 2010 in the vicinity of known underground nuclear tests in 2006, 2009, 2013, and 2016. Our principal method has been to compare the relative sizes of regional P-waves and S-waves.

We have measured P/S ratios at different frequencies, most importantly in the range from about 5 to 10 Hz, at first using data from the open station MDJ in northeast China, for two training sets of earthquakes, the other of explosions. We developed a linear discriminant function (LDF), that, in application to P/S measured at MDJ, does the best job of separating the earthquake and explosion populations. MDJ lacks data from the event of interest, but we have obtained regional data from stations of the nearby Dongbei Broadband Seismographic Network (DBSN), for the event of 12 May 2010 and for nearby underground nuclear tests conducted in 2006 and 2009. When our LDF is applied to DBSN data, and to data from stations SMT and NE3C in China, the LDF values measured from P/S ratios from known explosions are explosion-like; but for the event of 12 May 2010 the LDF values are all earthquake-like.

Though focused on a particular event, our method for characterizing earthquakes and explosions on the basis of their regional signals can be applied widely. Measurements of P/S based upon three-component waveform data provide better discrimination power than do those based upon vertical-component data alone.

Our presentation will in part review basic features of the use of Mahalanobis methods for event classification.

### Three-Component High Frequency Amplitude Models for Discrimination and Yield Estimation

PHILLIPS, W. S., Los Alamos National Laboratory, Los Alamos, NM USA, wsp@lanl.gov; FISK, M. D., Orbital-ATK, Newington, VA, USA, mark.fisk@orbitalatk.com; STEAD, R. J., Los Alamos National Laboratory, Los Alamos, NM USA, stead@lanl.gov; BEGNAUD, M. L., Los Alamos National Laboratory, Los Alamos, NM USA, mbegnaud@lanl.gov; YANG, X., Los Alamos National Laboratory, Los Alamos, NM USA, xyang@lanl.gov; BALLARD, S., Sandia National Laboratory, Albuquerque, NM USA

Local and regional distance discrimination and yield estimation is traditionally performed using vertical component data. The main reason for this is simplicity, but it also reflects the preponderance of vertical component arrays relied on by monitoring agencies. However, seismologists have shown that the use of three component (3C) data leads to additional stability and improved discrimination performance (e.g. Kim *et al.*, BSSA, 1997). As we push to lower detection thresholds, the closest stations to a small event will likely be 3C rather than an array. Using 3C waveforms also increases coverage for shear phases. We have used 3C analysis with coda data for years, and now extend direct phase propagation models using similar methodologies. We collect vertical, radial and transverse RMS amplitudes for local and regional phases, and, in parallel with coda analysis, model differences between the components as simple site terms. Alternatively, we could allow for distance dependent corrections to reflect particle motion effects. Further, amplitudes could be measured along expected particle motion directions, avoiding some of the relative site calibration. We have created global, two-dimensional, 3C models using GeoTess tessellation software that allows a spatially variable grid. Amplitudes were drawn from the entire IRIS collection of permanent and temporary networks. We employ source constraints from well-studied event clusters. Including 3C data improves discrimination performance globally, and for broad-area studies surrounding the Korean Peninsula and the western US in particular. We note that the Pn phase is less well modeled than

other phases, including Sn, which may be due to deep mantle paths and variable spreading effects.

### On Multi-Phenomenological Explosion Screening: Combining Waveform Signatures to Screen Above-Ground from Buried-Ejection Explosions

CARMICHAEL, J. D., Los Alamos National Laboratory, Los Alamos, NM, USA, joshuac@lanl.gov; SENTZ, K., Los Alamos National Laboratory, Los Alamos, NM, USA, ksentsz@lanl.gov; ARROWSMITH, S. J., Sandia National Laboratory, Albuquerque, NM, USA, sjarrow@sandia.gov; NEMZEK, R., Los Alamos National Laboratory, Los Alamos, NM, USA, nemzek@lanl.gov

Explosion monitoring operations collect and process waveform signatures of energetic events from geophysical environments to test two competing hypotheses: either an event is (1) an explosion of interest, or (2) it is not. We quantify how fusion of several such signatures effects the performance of a height-of-burst discrimination test. We then apply our methodology to data collected from ~70, ~10 kg solid charges detonated in shallow-buried and above-ground configurations. Using discriminants that we derive from energy partitioning of the waveform, we construct receiver operating characteristic (ROC) curves for multiple combinations for seismic, acoustic and electromagnetic signals. We use these general curves to quantify how inclusion of certain physical measurements improves analysts' ability to screen surface from buried, ejection explosions. We then demonstrate that such explosions can be distinguished with high probability when properly combined. Finally, we show that the screening-power of axis-symmetric mechanical waves triggered by shallow sources is range dependent, and best suited for local observation.

### A New Spectrogram-based Method for Automated Rg Detection

O'ROURKE, C. T., National Academy of Sciences, Albuquerque, NM, USA, colin.orourke@colorado.edu; BAKER, G. E., Air Force Research Laboratory, Albuquerque, NM, USA, glenn.baker.3@us.af.mil

The detection of the fundamental-mode Rayleigh wave Rg is important for monitoring studies because it indicates a shallow source, which are more often man-made. We have developed an automated Rg detector that uses spectrograms of seismic waves to search for a telltale low-frequency pattern. We have tested this detector using a large network of seismometers in Wyoming, which has recorded dozens of small-magnitude local earthquakes and hundreds of nearby coal-mining blasts. Our method sums the spectral amplitudes over the 0.4 to 0.8 Hz range and plots them over time, which produces a peak at the expected Rg arrival time. By establishing a simple set of trigger criteria to identify this peak we achieve successful Rg detection for explosion sources recorded across the entire array of >200 seismometers.

We compare our method to an existing Rg detection method that uses cross-correlation to find retrograde motion along the correct source-receiver back-azimuth. This method works well for stations in our network near the blast source, but we observe a distinct point at which the method breaks down; the sediment-bedrock contact along the eastern edge of the Bighorn Mountains scatters the Rg wave, which causes the cross-correlation detector to fail. Our method relies only on the frequency content, which is unaffected by this boundary, and achieves success across the entire array. This shows that our new method is robust for a tectonically complex region and provides critical context on event depth for local-distance monitoring.

### Cavity Radius Scaling and Seismic Radiation from Explosions

STROUJKOVA, A., Weston Geophysical Corp., Lexington, MA, USA, ana\_s@juno.com; VOROBIEV, O., Lawrence Livermore National Laboratory, Livermore, CA, USA, Vorobiev1@llnl.gov; CARNEVALE, M., Hager GeoScience Inc., Woburn, MA, USA

Measurements of the sizes and shapes of the cavities left by small chemical explosions were conducted following the explosion experiments in New England. The cavities were surveyed using the borehole techniques. The main objective of this study was to determine the relationship between the sizes of the cavities produced by chemical explosions and the explosive yield.

Comparison of the cavity radii determined in this study with historical data from other chemical and nuclear explosions in hard rock (e.g. granite) shows that it is consistent with a cubic root scaling and appears to be largely depth independent. The experimental results suggest that the seismic amplitudes are not directly controlled by the cavity sizes. In this model the cavity size does not represent the total volume change in the source region; instead it is determined by the rock strength. The material dilatation in the damage zone is a likely contributor to the total volume change for the explosions in hard rock. The explosions produced open fractures extending from the cavity along the borehole. These frac-



tures likely contributed to the volume change in the source region and affected radiated seismic waves.

The experimental measurements of the cavity sizes agree with the numerical simulation results using hydrodynamic code GEODYN, which confirm approximately cubic root scaling with yield and very weak dependence on the depth assuming the quality of rock mass is close in all events.

### **The Challenges of Discriminating Explosions from Earthquakes at Local Distances with P/S Methods**

WALTER, W. R., Lawrence Livermore National Laboratory, Livermore, CA, USA, walter5@llnl.gov; PYLE, M., Lawrence Livermore National Laboratory, Livermore, CA, USA, pyle4@llnl.gov; FORD, S. R., Lawrence Livermore National Laboratory, Livermore, CA, USA, ford17@llnl.gov

Regional distance (200-1600 km), high-frequency seismic P/S wave amplitude ratios have proven empirically effective at identifying explosions among a background of natural earthquakes. However the physical basis for the generation of explosion S-waves, and therefore the predictability of this P/S technique as a function of path, frequency and event properties such as size, depth, and geology, remains incompletely understood. A goal of current research, such as the Source Physics Experiments (SPE), is to improve our physical understanding of the mechanisms of explosion S-wave generation and advance our ability to numerically model and predict them.

At regional distances the lithospheric waveguide usually allows P/S discriminants to be applied over broad areas using relatively simple 1- or 2-D path corrections. In addition to the necessary path corrections, the main caveats to P/S discriminant effectiveness are: 1) the signals need to be sufficiently high frequency (usually  $> \sim 2$  Hz, sometimes higher) and, 2) the path attenuation must allow source generated S-waves to still be visible at the frequencies and recording stations of interest.

As we push the identification of explosions to even smaller yields, such as events with magnitudes less than 3, we need to examine P/S behavior at closer, local distances and even higher frequencies. We are using the SPE data along with small historic nuclear tests and earthquakes in southern Nevada to investigate local P/S discrimination. Surprisingly we have found that local P/S discrimination performs poorly at some stations across a broad range of frequencies from 4-64 Hz, in contrast to the excellent performance at regional distances. We are investigating strong structural focusing as a potential complicating issue at local distances. The upcoming 5-ton chemical explosion SPE-5 will generate new local and regional distance data to explore S-wave generation with distance and local versus regional P/S discrimination performance.

### **Source Characterization and Prediction of SPE5 from Full Waveform Inversions of SPE2, SPE3, and SPE4prime**

PHILLIPS-ALONGE, K., Sandia National Laboratories, Albuquerque, NM, USA, kephill@sandia.gov; KNOX, H., Sandia National Laboratories, Albuquerque, NM, USA, haknox@sandia.gov; OBER, C., Sandia National Laboratories, Albuquerque, NM, USA, ccober@sandia.gov; ABBOTT, R. E., Sandia National Laboratories, Albuquerque, NM, USA, reabbot@sandia.gov

The Source Physics Experiment is designed to improve our understanding of explosion-source phenomenology and ability to characterize explosions occurring at a variety of yields, depths of burial, and in complex media through the use of new physics-based modeling techniques. This is accomplished through the analysis of data from a series of controlled chemical explosions at the Nevada National Security Site. We use an adjoint-based full waveform inversion code to characterize the source and subsequently predict waveforms for the fifth shot in the series (SPE5), which is planned for Spring 2016. The code is based on discontinuous Galerkin techniques and has the capability of incorporating realistic geophysical models by allowing for unstructured meshes that align with material interfaces, and local polynomial refinement. Our velocity model is based on 3D tomography and includes shallow velocity data from AWD (Accelerated Weight Drop) surveys, detailed topography, and further refinement from medium inversions. Constraints for the inversions are provided by data from five geophone arrays extending radially away from the source with 100 m spacing. We perform two- and three- dimensional source inversions using different physics, numerical fluxes, and time integration techniques. A comparison of results from shots SPE2, SPE3, and SPE4 taking into account their differing yields allows for estimation of the source time function for SPE5, which is then used to predict waveforms observed at each station location. Pre-shot predictions followed by post-shot analysis will allow us to iteratively improve our models and techniques. Sandia National Laboratories is a multi-program laboratory managed and operated by Sandia Corporation, a wholly owned subsidiary of Lockheed Martin

Corporation, for the U.S. Department of Energy's National Nuclear Security Administration under contract DE-AC04-94AL85000.

### **Near-Field Modeling of SPE Experiments using an Upscaled Model based on Geophysical Characterization**

VOROBIEV, O. Y., LLNL, Livermore, CA, USA, vorobiev1@llnl.gov; EZZEDINE, S., LLNL, Livermore, CA, USA; HURLEY, R., LLNL, Livermore, CA, USA; ANTOUN, T., LLNL, Livermore, CA, USA; GLENN, L., LLNL, Livermore, CA, USA

This work describes the near-field modeling of wave propagation from underground chemical explosions conducted at the Nevada National Security Site in fractured granitic rock. Lab tests performed on granite samples excavated from various locations at the SPE site have shown little variability in mechanical properties. Granite at this scale can be considered as an isotropic medium. We have shown, however, that on the scale of the pressure waves generated during chemical explosions (tens of meters), the effective mechanical properties may vary significantly and exhibit both elastic and plastic anisotropies due to local variations in joint properties such as spacing orientation, joint aperture, cohesion and saturation. Since including every joint in a discrete fashion in computational model is not feasible for 1 km domain, we have developed a computational technique to upscale mechanical properties for various scales (frequencies) using geophysical characterization conducted during recent SPE tests at the NNSS. Stochastic representation of these features based on the field characterizations has been implemented into LLNL's Geodyn-L hydrocode. Scale dependency in mechanical properties is important in order to understand how the ground motion scales with yield. We hope that such an approach will not only provide a better prediction of the ground motion observed in the SPE but also will allow us to extrapolate results of the SPE to sources with bigger yields. We have validated our computational results by comparing the measured and computed ground motion at various ranges for SPE experiments of various yields. Using the new model we performed several computational studies to identify the most important mechanical properties of the rock mass specific to the SPE site and to understand their roles in the observed ground motion in the near-field. This work performed under the auspices of the U.S. DOE by LLNL under Contract DE-AC52-07NA27344. LLNL-ABS-679820

### **Near-Field to Far-Field Uncertainty Propagation and Quantification of Ground Motions Generated by the Source Physics Experiments (SPE)**

EZZEDINE, S. M., LLNL, Livermore, CA, USA, ezzedine1@llnl.gov; VOROBIEV, O. Y., LLNL, Livermore, CA, USA, vorobiev1@llnl.gov; HURLEY, R. C., LLNL, Livermore, CA, USA, hurley10@llnl.gov; PITARKA, A., LLNL, Livermore, CA, USA, pitarka1@llnl.gov; ANTOUN, T. H., LLNL, Livermore, CA, USA, antoun1@llnl.gov; WALTER, W., LLNL, Livermore, CA, USA, walter5@llnl.gov; GLENN, L. A., LLNL, Livermore, CA, USA, glenn5@llnl.gov

LLNL has developed an uncertainty quantification framework using HPC numerical codes to simulate from source to receivers—the ground motions observed during the Source Physics Experiments (SPE). Six SPE chemical shots are being conducted in fractured granitic rock at the Nevada National Security Site. To date we have successfully applied this framework to explain the near-field shear motions observed in the vicinity of SPE3 and SPE4prime source shots. However, systematic uncertainty propagation to the far-field seismic receivers has not been addressed yet. We build upon the same methodology and by using a coupling between the non-linear inelastic hydrodynamic regime in the near-field and the seismic elastic regime in the far-field. Several realizations of the stochastic discrete fracture network were generated conditional to the observed sparse data. These realizations were then used to calculate the ground motions generated from the SPE shots up to the elastic radius. The latter serves as the handshake interface for the far-field simulations. Using several realizations of near-field responses we have sourced the far-field elastic wave code and propagate the uncertainty to the receivers. We have analyzed the effect of different conceptual geological models using a nested Monte Carlo scheme and show that the variance of the predicted wave forms increases with distance from the source. We compare the observed frequency content at several gages with the simulated ones. We have observed skewness between the near- and the far-field responses which tends to decrease as the travel time and distances grow. The latter observations let us conclude that both regions experience different sampling of frequencies. We finally rank the primary sensitive parameters for both regions to drive and refine the field characterization data collection. This work performed under the auspices of the U.S. DOE by LLNL under Contract DE-AC52-07NA27344.



## Yield and Depth Dependence of Joint Response to Explosive Loading

STEEDMAN, D. W., Los Alamos National Laboratory, Los Alamos, NM, USA, [dwsteed@lanl.gov](mailto:dwsteed@lanl.gov); BRADLEY, C. R., Los Alamos National Laboratory, Los Alamos, NM, USA, [cbradley@lanl.gov](mailto:cbradley@lanl.gov)

The Source Physics Experiments (SPE) is a series of explosive shots of various size detonated at varying depths in a borehole in jointed granite. Through a combination of in-depth analysis of the experimental data and high-fidelity finite element simulations we describe a mechanism to explain the non-radial response of natural joint sets to a spherical loading wave.

Extensive analysis of data from a dense array of triaxial accelerometer packages in the first three shallow tests in this series revealed a characteristic velocity response. Simulation of the events using a complex, explicitly jointed 3-D finite element model allowed us to develop a contact model that can lead to that characteristic response. We hypothesize a mechanism: shear strain energy is stored on the joints during compression shock loading and then is suddenly released during the unload phase causing this non-ideal slip. Moreover, we hypothesize that this effect is likely mitigated by high in situ stress conditions relative to the loading caused by the explosive source. We demonstrate using data from a fourth more deeply buried, low yield explosive source that this is indeed the case. Development of a rational mechanistic model for this response can help to explain the appearance of off-radial wave energy generated from a spherical source.

This abstract is approved for public release, LA-UR-16-20008.

---

## Machine Learning and its Application to Earthquake and Explosion Signal Analysis

Oral Session · Thursday · 8:30 AM · 21 April · Tuscany 3/4

Session Chair: Timothy Draelos

---

### Adaptive Self-Tuning of Seismic Sensors

DRAELOS, T. J., Sandia National Laboratories, Albuquerque, NM, USA, [tjdrael@sandia.gov](mailto:tjdrael@sandia.gov); KNOX, H. A., Sandia National Laboratories, Albuquerque, NM, USA, [haknox@sandia.gov](mailto:haknox@sandia.gov); PETERSON, M. G., Sandia National Laboratories, Albuquerque, NM, USA, [mgpeter@sandia.gov](mailto:mgpeter@sandia.gov); LAWRY, B. J., Sandia National Laboratories, Albuquerque, NM, USA, [bjlawry@sandia.gov](mailto:bjlawry@sandia.gov); CHAEL, E. P., Sandia National Laboratories, Albuquerque, NM, USA, [epchael@sandia.gov](mailto:epchael@sandia.gov); YOUNG, C. J., Sandia National Laboratories, Albuquerque, NM, USA, [cjyoung@sandia.gov](mailto:cjyoung@sandia.gov)

The quality of automatic detections from seismic sensor networks depends on a large number of data processing parameters that interact in complex ways. The largely manual process of identifying effective parameters is painstaking and does not guarantee that the resulting controls are the optimal configuration settings, yet achieving superior automatic detection of seismic events is closely related to these parameters. We present an automated sensor tuning (AST) system that learns near-optimal parameter settings for each sensor using neuro-dynamic programming (reinforcement learning). AST adapts the current parameter settings to the current state of the environment by leveraging cooperation within a neighborhood of similar sensors. After a stabilization period, the AST can adapt in near real-time to changing conditions and automatically self-tune a signal detector to identify (detect) only signals from events of interest. The overall goal is to reduce the number of missed legitimate event detections and the number of false event detections. Our current work focuses on reducing false signal detections early in the seismic pipeline processing, which leads to fewer false events and has a significant impact on reducing analyst time and effort. Applicable both for existing sensor performance boosting and new sensor deployment, this system provides an important new method to automatically tune complex remote sensing systems. Systems tuned in this way will achieve better performance than is currently possible by manual tuning, and with much less time and effort devoted to the tuning process. With ground truth on detections in simulated seismic waveforms from a network of stations, we show that AST increases the probability of detection while decreasing false alarms. We also show improved performance on actual data from a seismic sensor network monitoring the Mount Erebus Volcano in Antarctica.

### Empirical Seismic Phase Separation from Polarization Analysis

JONES, J. P., Portland, OR, USA, [thuban@uw.edu](mailto:thuban@uw.edu); EATON, D., University of Calgary, Calgary, AB, Canada, [eatond@ucalgary.ca](mailto:eatond@ucalgary.ca); CAFFAGNI, E., Universität Wien, Vienna, Austria, [enrico.caffagni@univie.ac.at](mailto:enrico.caffagni@univie.ac.at)

Robust similarity measures have many applications in seismology, from non-volcanic tremor detection to borehole sensor alignment. Similarity is typically defined using correlation-based measures. However, in a recent paper, we intro-

duced an adaptive method to quantify seismic phase similarity based on polarization analysis of short time windows with robust feature similarity metrics. Here we demonstrate that empirical separation of seismic phases follows directly from our method.

We begin by extending polarization similarity to the time-frequency domain using wavelet packet (WP) decomposition. Three cost functionals are proposed to isolate narrow band energy, detect transients, and isolate quasi-static phase content, respectively, with example applications of all decompositions. Because WP coefficients are band-limited, we can approximately separate seismic phases in both time and frequency by clustering with a dissimilarity matrix constructed from feature distances. However, time resolution is limited by the length and overlap fraction of the feature histograms.

We extend our method to data from three-component sensor arrays by adapting existing multidimensional clustering techniques. Compared with traditional seismic detectors, our algorithms are effective down to an empirical lower limit for feature distinguishability (-4 to -6 dB). Hence, changes in seismic phase content can be detected by our method when signals are so emergent that the ratios of their short- and long-term amplitudes don't appear to change. Because real-time application requires efficient parallelization, a seismic detector based solely on polarization similarity remains a work in progress.

### SpectRobot: Automated Time/Frequency Pattern Recognition in the Gabor Spectrogram

LEES, J. M., University of North Carolina, Chapel Hill, NC, USA, [jonathan.lees@unc.edu](mailto:jonathan.lees@unc.edu); BOWMAN, D. C., University of North Carolina, Chapel Hill, NC, USA, [haksaeng@live.unc.edu](mailto:haksaeng@live.unc.edu)

We report on new methods for automated extraction of continuous line segments on Gabor spectrograms. These represent time-varying, narrow band spectral signals that provide important constraints on the source physics of phenomena such as volcanic tremor and stratospheric gliding. Volcanic tremor occurs when conduits resonate, either associated with vent or crack resonance during gas emission following explosions. Infrasound recordings using free floating platforms in the middle stratosphere also exhibit extended periodic signals at a variety of frequencies, typically between 1-20 HZ. These signals, possibly contained within waveguides above the tropopause, undergo significant gliding and modulation. In both cases significant noise and occasional broad band bursts further complicate the process. Our approach is to augment previously developed image processing methods to estimate ridge continuity on spectrograms and to form the basis for pattern recognition on varying quasi-harmonic tremor. Standard routines such as pixel opening and closing, threshold estimation and edge detection will be illustrated. Characterization of the resonant frequencies of volcanic tremor shed light on conduit dimensions and fluid properties and can provide critical, time sensitive information used for hazard mitigation. Examination and comparison of waveguide phenomena in the stratosphere will provide a basis for interpretation of these strange signals.

### Data Mining for Earthquake Detection using Computationally Efficient Search for Similar Seismic Signals

BERGEN, K. J., Stanford University, Stanford, CA, USA, [kbergen@stanford.edu](mailto:kbergen@stanford.edu); YOON, C. E., Stanford University, Stanford, CA, USA, [ceyoon@stanford.edu](mailto:ceyoon@stanford.edu); BEROZA, G. C., Stanford University, Stanford, CA, USA, [beroza@stanford.edu](mailto:beroza@stanford.edu)

Seismic sensors collect massive quantities of data that contain a wealth of information about processes within the earth. Sophisticated signal processing tools are necessary to exploit these large data sets to identify previously unknown earthquakes. Seismologists are increasingly adopting data mining and machine learning techniques, developed in the computer science community, to process large seismic data sets. New earthquake detection methods, such as Fingerprint and Similarity Thresholding (FAST), enable waveform-similarity-based earthquake detection in long duration continuous seismic data (Yoon *et al.* 2015). FAST leverages locality sensitive hashing (LSH), a data mining technique for efficiently identifying similar items in large data sets, to detect similar waveforms without templates.

As algorithms make it possible to process larger data sets, full manual inspection of the detection results will become infeasible, and new tools will be required to process the output of similarity-based detection. We propose extensions to FAST for automating the removal of false alarms and improving the detection sensitivity. We use clustering methods to identify groups of similar waveforms for analysis, visualization, and removal of correlated noise or outliers. We use waveform classification as an additional means of false detection removal. We also explore data-driven approaches for feature extraction, the process that converts waveforms to binary "fingerprint" representations. We compare meth-

ods using both synthetic tests, for which ground-truth is available, and data from actual earthquake sequences.

#### **Automatic Detection and Classification of Seismic Events**

LI, Z., Georgia Tech, Atlanta, GA, USA, zli354@gatech.edu; PENG, Z., Georgia Tech, Atlanta, GA, USA, zpeng@gatech.edu

Currently most seismic networks record data in a continuous mode. The recorded data include signals generated by tectonic sources, anthropogenic sources, and ambient seismic noise. Tectonic sources consist of local/regional/global earthquakes, as well as tectonic tremors and slow earthquakes. Anthropogenic sources include daily traffic and industrial activities such as quarry blast. An automated detection technique of target seismic signals is fundamental to many research topics in modern seismology. However, the dramatic increase in seismic data volume, and the emergence of ultra dense networks raise significant challenges (and opportunities) for event detections. Here we present our on-going efforts in constructing an automated toolbox for detection and classification of seismic events. We apply network-based pattern recognition techniques for detection of local earthquakes and other types seismic events, as long as the signals are coherent across the network. Following detection, the identified events are discriminated by machine-learning classification tool according to their characteristic features, such as predominant frequency, frequency range, and event durations. Our package could potentially provide a powerful tool to accelerate research on various types of seismic events and improve our understanding of physical mechanisms.

---

### **Seismo-Acoustics and Infrasound**

Oral Session · Thursday · 10:45 AM · 21 April · Tuscany 3/4

Session Chairs: Stephen Arrowsmith and Omar Marcillo

---

#### **Assessment of Infrasound Signals Recorded on Seismic Stations and Infrasound Arrays in the Western US Using Ground Truth Sources**

PARK, J., Southern Methodist University, Dallas, TX, USA, pjh2521920@gmail.com; HAYWARD, C. T., Southern Methodist University, Dallas, TX, USA, hayward@smu.edu; STUMP, B. W., Southern Methodist University, Dallas, TX, USA, bstump@smu.edu

Infrasound propagation is affected by atmospheric conditions, varying in time and space. Ground truth for infrasonic sources provides a basis for documenting variations in infrasound observation as well as validating model predictions. We use data from a hybrid of single seismic stations (USArray Transportable Array) and infrasound arrays in a regional setting to assess these issues. Ground truth consists of 25 static rocket motor burn tests and 25 rocket body demolitions in Utah for the time period from 2003 to 2012. The rocket motor tests generate relatively long duration infrasound signals of up to 3 minutes with a frequency band of 5-15 Hz, while the rocket body demolitions produce more impulsive signals (<30 sec) with frequencies from 1 to 5 Hz. Based on a detector that relies on both STA/LTA ratio and spectral analyses, initial automatic infrasound detections were identified. These detections are then used in a signal association procedure using the closest three stations based on Delaunay triangulation. Phase velocity and azimuth estimates of the associated signals were used to identify signal detections that correlated with particular sources. The distributions of stations that detect particular signals vary as a function of range and azimuth illustrating seasonal patterns that depend on atmospheric conditions. The impulsive signals from the rocket body detonations are observed at greater distance (> 700 km) than the extended signals generated by the rocket burn test (up to 600 km). To quantify the infrasound energy attenuation from two different source types, infrasound amplitude measurements as a function range and azimuth are documented. Ray tracing models using the ground-to-space (G2S) atmospheric specifications are compared to these observations. This unique dataset provides the opportunity to assess the contribution of temporal atmospheric conditions to infrasound detection and document the predictive capabilities of this current atmospheric model.

#### **Explosive Yield Estimation from Acoustic Waveform Inversion Including Three-Dimensional Propagation Effects**

KIM, K., Lawrence Livermore National Laboratory, Livermore, CA, kim84@llnl.gov; RODGERS, A. J., Lawrence Livermore National Laboratory, Livermore, CA, USA, rodggers7@llnl.gov

Explosion forensics requires methods to estimate explosion size in terms of yield. Conventional methods determine the yield by scaling the observed blast waves according to a reference model. Near-surface explosions generate air-blast, which propagates as a non-linear shock wave near the source and transitions quickly into a linear acoustic wave. For most explosion forensics applications, acoustic wave

measurements may only be available since shock waves must be observed at close range. However, amplitudes of acoustic waves are greatly affected by variation of atmospheric conditions (*e.g.* temperature, sound speed, wind), and their impacts on the acoustic wave propagation are not included in conventional reference models that generally assume homogeneous atmosphere. In this study, we introduce a new technique for yield estimation based on acoustic waveform inversion and Green's functions computed in fully three-dimensional atmospheric models, including surface topography. The method can recover the time-history of an equivalent acoustic source to produce the observed acoustic wavefield. We define the reduced acoustic impulse as the indicator of the acoustic source magnitude, and show that as wave propagation effects are effectively modeled, the reduced acoustic impulse can be scaled appropriately to homogeneous reference models. We apply this acoustic-measurement-based technique to a wide range of surface chemical explosions and demonstrate its applicability. This method is extremely useful when shock data are not available and the acoustic propagation is significantly affected by atmospheric conditions and surface topography.

#### **Seismo-Acoustic Monitoring of Snowmelt Runoff in the Northern Colorado Rocky Mountains**

ANTHONY, R. E., Colorado State University, Fort Collins, CO, USA, robert.anthony@colostate.edu; ASTER, R. C., Colorado State University, Fort Collins, CO, USA, Rick.Aster@colostate.edu; RYAN, S. E., U.S. Forest Service, Fort Collins, CO, USA, sryanburkett@fs.fed.us; RATHBURN, S. L., Colorado State University, Fort Collins, CO, USA, Sara.Rathburn@colostate.edu

Flow and sediment transport in fluvial systems plays a critical role in shaping river morphology and aquatic ecosystems as well in the design of societal river infrastructure such as dams, bridges and water treatment facilities. Due to spatial-temporal variability of sediment flux and the hazards associated with in-channel measurements, traditional in-situ sampling techniques (*e.g.* portable samplers, sediment traps) are unable to provide a comprehensive record of sediment transport. They may also impact the very process they are measuring. Quantitative analysis of the relationships between river discharge, sediment transport, and excitation of the seismo-acoustic wavefield, has the potential to fundamentally augment physically-based sampling methods with a non-invasive and continuous monitoring methodology in some fluvial systems. For example, a recent seismo-acoustic study during a controlled flood event in the Grand Canyon identified distinct bedload transport signals in a high-energy river system. Extending this research to smaller, snowmelt-fed, mountain rivers with a high degree of seasonality to peak runoff, a short-period seismo-acoustic array was deployed adjacent to the South Fork of the Cache la Poudre River in the Northern Colorado Rocky Mountains during May-September of 2015 to capture pre-peak, peak, and post-peak runoff. Pressure transducers were also deployed to continuously measure river stage, and measurements of flow velocity, bedload, suspended sediment, and turbidity were taken throughout the study period. We examine the temporal variations in seismic and infrasonic spectra with discharge and sediment flux metrics to study their influences on the seismo-acoustic wavefield. Early analysis of the dataset shows strong and nonlinear associations between discharge and seismic energy, including a peak energy shift to lower frequencies with increasing discharge and periods associated with multimodal spectra containing gliding peak frequencies.

#### **Seismic Equivalents of Acoustic Multipoles and Volcanic Jet Scaling Laws**

HANEY, M. M., Alaska Volcano Observatory/USGS, Anchorage, AK, USA, mhaney@usgs.gov; MATOZA, R., University of California Santa Barbara, Dept. of Earth Science, Santa Barbara, CA, USA, matoza@geol.ucsb.edu; FEE, D., University of Alaska Fairbanks, Geophysical Institute/AVO, Fairbanks, AK, USA, dftee1@alaska.edu; ALDRIDGE, D. F., Sandia National Laboratories, Geophysics Department, Albuquerque, NM, USA, dfaldri@sandia.gov

Seismic and acoustic waves are manifestations of mechanical energy in the solid Earth and atmosphere, respectively. Here, we explore analogies between equivalent source theory in seismology (moment-tensor and single-force sources) and equivalent source theory in acoustics, *i.e.*, monopoles, dipoles, and quadrupoles [*e.g.*, Wouff and McGetchin, 1976]. Although infrasound from volcanic eruptions may be more complex than a simple monopole, dipole, or quadrupole assumption, these elementary sources are a logical place to begin to relate seismic and acoustic sources. Treating sources in such a unified way will be necessary in the application of seismo-acoustic waveform inversion at volcanoes, in which seismic and infrasound data are simultaneously reconciled for a common near-surface source (*i.e.*, volcanic explosion).

By considering the radiated power of a harmonic force source at the surface of an elastic halfspace, we show that a volcanic plume modeled as a seismic force has the same scaling as an acoustic dipole. This is surprising since, in seismology, the equivalent force system is a widely-used representation of moment ten-

sors. Here, we show from first principles that the seismic force source is dipolar in nature, since it can be equivalently represented as an explosion dipole and a pair of torque dipoles in a particular configuration. This forges a deep connection between the multipole expansion in acoustics and the use of forces and moments in seismology and suggests that an alternative description of seismic sources is possible.

### The Design of Free Flying Acoustic Stations

BOWMAN, D. C., University of North Carolina at Chapel Hill, Chapel Hill, NC, USA, danny.c.bowman@gmail.com; LEES, J. M., University of North Carolina at Chapel Hill, Chapel Hill, NC, USA, jonathan.lees@unc.edu; JONES, K. R., Sandia National Laboratories, Albuquerque, NM, USA, krjones@sandia.gov

Recent advances in sensor and digitizer miniaturization have permitted the deployment of free flying acoustic stations on balloons and unmanned aerial vehicles (UAVs). We describe the unique advantages and drawbacks of free flying acoustic sensors as well as the flight platforms used to deploy them. Balloon-borne stations can act as quasi-Lagrangian observation points, drastically reducing wind noise. They have over 50 km of vertical range and can capture signals that seldom reach the Earth's surface. However, buoyancy driven oscillation of the flight system, cable vibrations, vortex shedding, and interference from payload telemetry can complicate recordings made on balloons. UAVs permit precise placement of acoustic stations, but they can suffer from wind and propeller noise. They have limited flight time and cannot reach high altitudes. Balloon deployments more than several thousand meters above the Earth's surface must contend with changes in sensor corner frequency, exposure to extreme temperatures, and data recovery. We discuss results from infrasound sensor deployments on large ( $\sim 10^5$  m<sup>3</sup>) zero pressure and superpressure balloons, continuously ascending sounding balloons, solar powered hot air balloons, and an octocopter (UAV). Changes in frequency response due to decreased air density are also quantified. Finally, we describe the elements necessary for successful acoustic recording in the free atmosphere.

---

## Numerical Modeling of Earthquake Ground Motion, Rupture Dynamics and Seismic Wave Propagation

Oral Session · Thursday · 1:30 PM · 21 April · Tuscany 3/4  
Session Chairs: Peter Moczo, Steven Day, Emmanuel Chaljub, and Jozef Kristek

---

### Earthquake Ground Motion Simulations: SCEC Community Code Development and Validation Efforts

GOULET, C. A., SCEC, University of Southern California, Los Angeles, CA, USA, cgoulet@usc.edu; MAECHLING, P. J., SCEC, University of Southern California, Los Angeles, CA, USA, maechlin@usc.edu; JORDAN, T. H., SCEC, University of Southern California, Los Angeles, CA, USA, tjordan@usc.edu; LUCO, N., United States Geological Survey, Golden, CO, USA, nluco@usgs.gov; REZAEIAN, S., United States Geological Survey, Golden, CO, USA, srezaeian@usgs.gov

Over the last decade, the Southern California Earthquake Center (SCEC) research community has developed several software tools for the simulation of ground motions including the Broadband Platform (BBP), wave propagation codes used for high frequency deterministic ground motion simulation, and the CyberShake platform, a physics-based probabilistic seismic hazard analysis simulation tool. For simulated ground motions to be used in practical applications, it is essential to have them validated in a quantifiable fashion against existing observational data. Ground motions include complex features both in the time and frequency domains, which makes systematic and quantitative validation difficult to achieve. However, ground-motion properties controlling system response may be different for different types of structures or for different engineering design approaches. For example, elastic pseudo-spectral acceleration (PSA) is the main metric used in the general building code approach to design; however, for performance-based design, other ground-motion parameters, such as duration or inelastic PSA may be controlling factors. To support engineering use of ground motion simulations, our multi-disciplinary group of scientists and engineers has started to tackle the ground-motion simulation validation problem by developing application-specific validation "gauntlets", where a gauntlet is defined as one or more validation tests that support a specific use of ground-motion simulation data. By developing different validation gauntlets for different ground-motion simulation applications, we decouple part of the ground motion characterization complexity

and allow incremental progress on the validation front. In this presentation, we provide an overview of important past, current and future validation efforts of the various simulation codes led by several participants and collaborators under the SCEC umbrella.

### Taylor-expansion, Dispersion-relation Preserving, and Combined-approximation Finite-difference Schemes on the Staggered and Collocated Grids

ETEMADSAEED, L., University of Tehran, Tehran, Iran, letemad@ut.ac.ir; MOCZO, P., Comenius University Bratislava, Bratislava, Slovakia, moczo@fmph.uniba.sk; KRISTEK, J., Comenius University Bratislava, Bratislava, Slovakia, kristek@fmph.uniba.sk; ANSARI, A., International Institute of Earthquake Engineering and Seismology, Tehran, Iran, a.ansari@iiees.ac.ir; KRISTEKOVA, M., Slovak Academy of Sciences, Bratislava, Slovakia, kristekova@savba.sk

Numerical modelling of earthquake ground motion intensively uses finite-difference (FD) schemes on the staggered grid. The standard (2,4) or higher-order in space schemes have proven relatively efficient modelling tool if sufficiently accurate discrete representation of continuous material heterogeneity and material interfaces is implemented and efficient absorbing boundaries of a grid are used. At the same time it is obvious that the staggered grid is not efficient for including anisotropy, fault-boundary conditions, topography or recently also seismic noise. Naturally, a collocated grid offers possibilities to overcome inherent limitations of the staggered grid.

Another aspect of FD schemes is approximation of spatial and temporal derivatives. A standard way makes use of the Taylor expansion (TE). Alternative approaches have been developed in which coefficients are determined by minimizing an error defined so that grid-wave characteristics be close to true (physical) wave characteristics. One such approach was suggested by Tam and Webb (1994) who defined an error to minimize difference between the effective numerical wavenumber/frequency and true wavenumber/frequency in approximating spatial/temporal derivative. Tamm and Webb called their approach the dispersion-relation preserving (DRP). We investigate and compare accuracy of a family of FD schemes of various orders obtained with standard TE approach, DRP criterion and combined TE-DRP approach to approximate derivatives on the staggered and collocated grids.

### Modeling Nucleation and Propagation of Shear Rupture on Rough Faults with a Large Range in Wavelengths

TAL, Y., Massachusetts Institute of Technology, Cambridge, MA, USA, ytal@mit.edu; HAGER, B. H., Massachusetts Institute of Technology, Cambridge, MA, USA, bhager@mit.edu

Faults are rough at all scales and can be described as self-affine fractals. The deviation from planarity results in geometric asperities and a locally heterogeneous stress field, which affect the nucleation and propagation of shear rupture. To model faults with roughness extending over a large range in wavelengths, we refine the mesh near the fault using hanging nodes, thereby enabling accurate representation of the fault geometry. Moreover, to allow slip that is large relative to the size of the elements near the fault, we use the Mortar finite element method, in which non-matching meshes are allowed across the fault and the contacts are continuously updated. We introduce slip weakening and rate and state friction laws into the method and study both the nucleation and propagation of shear rupture, using variable time steps with a quasi-static scheme for the inter-seismic stage and a dynamic implicit Newmark scheme for the co-seismic stage.

For a static benchmark, we demonstrate that the method predicts accurately the stresses and displacements due to a uniform stress drop along a fault with a non-matching grid. We also design a benchmark problem to show that the method accurately models the behavior of the friction coefficient in response to a change in the slip rate on a fault governed by a rate and state friction law.

Simulations of a 10 meter long horizontal fault with different amplitude roughness and a simple slip-weakening friction law show the significant effect of roughness on: (1) Slip on the fault and consequently the seismic moment; (2) Stress drop; (3) Rupture properties, such as rupture velocity, breakdown zone, and the observed relation between shear stress and slip; and (4) Nucleation processes, in which the nucleation phases of the experimental nucleation model of Ohnaka (2000) are observed.

### Fault Zone Plasticity Effects Quantified by Spontaneous Rupture Simulations

ROTEN, D., San Diego State University, San Diego, CA, USA, droten@mail.sdsu.edu; OLSEN, K. B., San Diego State University, San Diego, CA, USA, kbolsen@mail.sdsu.edu; DAY, S. M., San Diego State University, San Diego, CA,



USA, sday@mail.sdsu.edu; CUI, Y., San Diego Supercomputer Center, La Jolla, CA, USA, yfcui@sdsu.edu

We explore the effects of fault zone nonlinearity on peak ground velocities (PGVs) by simulating a suite of surface rupturing earthquakes in a visco-plastic medium. Our simulations, performed with the AWP-ODC 3D finite difference code, cover magnitudes from 6.5 to 8.0, with several realizations of stochastic stress drop distributions for a given magnitude. We test three different models of rock strength, with friction angles and cohesions based on criteria which are frequently applied to fractured rock masses in civil engineering and mining. We use a minimum shear-wave velocity of 500 m/s and a maximum frequency of 1 Hz. In rupture scenarios with average stress drop (~3.5 MPa), plastic yielding reduces near-fault PGVs by 15 to 30% in pre-fractured, low-strength rock, but less than 1% in massive, high quality rock. These reductions are almost insensitive to the scenario earthquake magnitude. In the case of high stress drop (~7 MPa), however, plasticity reduces near-fault PGVs by 38 to 45% in rocks of low strength and by 5 to 15% in rocks of high strength. Because plasticity reduces slip rates and static slip near the surface, these effects can partially be captured by defining a shallow velocity-strengthening layer.

We also perform dynamic nonlinear simulations of a high stress drop M 7.8 earthquake rupturing a 250 km-long stretch of the southern San Andreas fault from Indio to Lake Hughes. With respect to the viscoelastic solution, nonlinearity in the fault damage zone and in near-surface deposits would reduce long-period (> 1 s) peak ground velocities in the Los Angeles basin by 15-50%, depending on the strength of crustal rocks and shallow sediments. These simulation results suggest that nonlinear effects may be relevant even at long periods, especially for earthquakes with high stress drop.

#### **A New Viscoelastic 3D 4th-order Staggered-grid Finite-difference Scheme for Media with Material Discontinuities**

KRISTEK, J., Comenius University Bratislava, Bratislava, Slovakia, kristek@fmph.uniba.sk; MOCZO, P., Comenius University Bratislava, Bratislava, Slovakia, moczo@fmph.uniba.sk; KRISTEKOVA, M., Slovak Academy of Sciences, Bratislava, Slovakia, kristekova@savba.sk; CHALJUB, E., ISTERre, Grenoble, France, Emmanuel.Chaljub@ujf-grenoble.fr

Sufficiently realistic models are necessary for numerical modeling of seismic wave propagation and prediction of earthquake motion. It is also obvious that the realistic physical model has to be sufficiently accurately represented by discrete grid models in the (spatial) domain numerical methods such as finite-difference (FD) methods.

Recently we have developed a new discrete representation of perfectly elastic heterogeneous medium with material discontinuities for the FD modeling of seismic wave propagation and earthquake motion. Numerous numerical tests against the discrete-wavenumber method and spectral-element method have proven very good accuracy of the representation.

Here we present a generalization for the case of the viscoelastic medium with rheology of the generalized Maxwell body in Emmerich-Korn definition, GMB-EK (equivalent to generalized Zener body, GZB) applied to the 3D staggered-grid 4-th order FD scheme. The generalization is based on the assumption that a contact of two viscoelastic media with the GMB-EK/GZB rheologies can be approximated by an averaged orthorhombic medium with the GMB-EK/GZB rheology. Anelastic coefficients (memory variables) of the averaged medium for a grid position are determined from quality factors for all 9 tensor components of the averaged orthorhombic medium. The proposed determination of anelastic coefficients ensures positivity of the coefficients.

The presented FD scheme uses computationally efficient coarse spatial distribution of the anelastic functions. Our definition of the anelastic functions and their spatial distribution account for all relaxation frequencies at any grid position of an anelastic function. This makes it possible to physically reasonably average medium at the contact.

Performance of the FD scheme with a new implementation of the anelastic behavior is demonstrated using numerical calculations.

#### **Ground Motion Simulation of Basin and Site Effects and the Resulting Structural Response of Representative Buildings**

RODGERS, A. J., LLNL, Livermore, CA, USA, rodgers7@llnl.gov; PITARKA, A., LLNL, Livermore, CA, USA, pitarka1@llnl.gov; MCCALLEN, D. B., Lawrence Berkeley National Lab & UCOP, Berkeley, CA, USA, David.McCallen@ucop.edu

Advances in numerical methods and computational power now make it possible to run simulations of earthquake ground motions and the resulting response of engineered structures including more frequencies relevant to building design. However, current engineering practice relies on very simple assumptions of a ver-

tically propagating, horizontally polarized plane-wave (SH1D) or a simple scale factor between horizontal and vertical components of motion (H-to-Z). These assumptions neglect rotational motions and greatly neglect surface wave particle motions, calling into question the realism of current practices. We report progress on three-dimensional (3D) anelastic simulations of earthquake motions from realistic sources and the response of simple basin and site conditions. We create simple, parameterized models of sedimentary basins and site conditions and show how earth structure impacts site response and basin-edge generated surface waves. Ground motions are then used to compute the response of representative multi-story steel moment frame buildings at a number of locations relative to the event and basin geometry. Initially we only use the translational components of motion applied to a rigid building foundation. But we will include rotational motions in further developments. Simulations allow us to compare the ground motion and building response under the common SH1D and H-to-Z assumptions to the fully 3D response. The building response functions, measured as inter-story drift, can inform hazard and site-specific performance-based design of engineered structures.

#### **Dynamic Modeling of Potential Earthquake Rupture Paths through Cajon Pass, Southern California**

LOZOS, J. C., California State University, Northridge, Northridge, CA, USA, julian.lozos@csun.edu; DOLAN, J. F., University of Southern California, Los Angeles, CA, USA, dolan@usc.edu; OGLESBY, D. D., University of California, Riverside, Riverside, CA, USA, david.oglesby@ucr.edu

Cajon Pass is the site of a complex junction of several active major faults. The right-lateral strike-slip San Jacinto fault splays off southeastward from the throughgoing, right-lateral strike-slip San Andreas fault. The Cucamonga thrust fault approaches both strike-slip faults, and likely penetrates and offsets them. Due to the number of active faults in the Cajon Pass area and their proximity to densely populated urban southern California, the seismic hazard and risk from ruptures in the pass is high. We use dynamic rupture modeling to determine possible rupture behaviors and lengths for Cajon Pass earthquakes, with particular focus on understanding interactions that may lead to or inhibit joint rupture of two or more faults in a single event. We incorporate realistic fault geometry, initial stresses, and surrounding geology into these models. Models incorporating only the San Andreas and San Jacinto faults tend to produce multi-fault rupture from a number of nucleation points. We also investigate how the cross-cutting Cucamonga thrust may affect rupture patterns on all three faults.

#### **Simulation of Strong Ground Motions for the 2011 Tohoku Earthquake with Considerations of Multiple Nonlinear Effects**

NOZU, A., Port and Airport Research Institute, Nagase, Yokosuka, Japan

To predict strong ground motions for future large earthquakes, it is important to take into account the effects of soil nonlinearity. The author has been developing a simple method to simulate strong ground motions taking into account the effects of soil nonlinearity (e.g., Nozu and Morikawa, 2003). The method, however, has been validated only for limited amount of strong motion data, partly because there was only a limited amount of strong motion data affected by soil nonlinearity. Therefore, in this article, making use of strong motion data for the 2011 Tohoku earthquake and the source model developed for the same earthquake by the author (Nozu, 2012), strong motion simulation with considerations of soil nonlinearity was conducted and its effectiveness was studied. Strong motion records with the evident effects of soil nonlinearity were selected and they were simulated using the source model and taking into account empirical site amplification and phase effects (Nozu *et al.*, 2009). Soil nonlinearity was considered using the method of Nozu and Morikawa (2003). The method uses two parameters to represent the effects of soil nonlinearity; one representing the reduction of averaged shear wave velocity within the sediment ( $\nu_1$ ) and the other representing the increase of averaged damping factor within the sediment ( $\nu_2$ ). In the simulation,  $\nu_1$  was basically determined based on Wakai and Nozu (2013) and  $\nu_2$  was determined so that the observed ground motion could be simulated as accurately as possible. As a result, it was found that, the duration of strong ground motions tended to be overestimated if the parameter  $\nu_2$  was not used for the sites with the effect of soil nonlinearity. In each of the target sites, the simulation result was improved by using these two parameters. Thus, the effectiveness of strong motion simulation with considerations of soil nonlinearity was confirmed. Based on the results, the application of the method for future earthquakes was also discussed.

#### **Scenario Earthquake and Ground Motion Simulations in the North China Basin: Effects of Heterogeneous Stress and 3D Basin Structure**

LIU, D., Geology&Geophysics Department, Texas A&M University, College Station, TX, USA, dunyuliu@tamu.edu; DUAN, B., Geology&Geophysics

Department, Texas A&M University, College Station, TX, USA, bduan@tamu.edu

A possible seismic gap along a 160-km-long fault segment running through Tianjin, a Chinese city of 11 million people and roughly 100 km southeast of Beijing, is inferred recently (Yin *et al.*, 2014). To examine consequences of a possible earthquake of magnitude 7.5 along the seismic gap, we perform scenario earthquake and ground motion simulations with spontaneous rupture source characterization and parallel computing. The dynamic source features depth-dependent normal stress and fractal stress drop distributions. 3D seismic velocity structure in the North China basin is constructed from deep seismic sounding profiles and data from oil industry. Basin transduced Rayleigh waves are used to determine the shear wave velocity of 1.0 to 1.5 km/s as the best predictor of basin structure. Three basins can be identified from the velocity structure in the study area. In heterogeneous stress cases, the ruptures show complex behaviors such as retardation and reinitiation, and the directivity effect collapses. However, given the same target magnitude, asperities in heterogeneous stress cases induce large slip-rate patches and stronger or at least similar level ground motion than the reference models with depth dependent while laterally uniform initial stresses, in which the directivity effect is clearly observed. The peak ground velocity at Tianjin Railway Station, which is located right on top of the fault, is about 3m/s, and the synthetic seismograms there feature short durations as it is outside the basins. In the basin between Tianjin and Beijing, which is of similar shape to the Los Angeles basin, the peak value of the amplitude spectrum occurs at the 10 seconds period. Moving to the basin edges, the peak value in the amplitude spectrum decreases and the period of the peak value departs from 10 seconds. Shaking inside the basin lasts as long as 150s. We find that the prolongation effect is more significant in closed basins than relatively open basins.

#### Soil-Topography Coupling Effects at Strong Motion Stations in California

MOHAMMADI, K., California Institute of Technology, Pasadena, CA, USA, kamimohamadi@caltech.edu; ASIMAKI, D., California Institute of Technology, Pasadena, CA, USA, domniki@caltech.edu

The material and geometric characteristics of near surface crustal layers, known as local site conditions, can significantly affect the seismic shaking relative to a homogeneous linear elastic half-space with flat ground surface. A complete site response analysis for strong ground motion should therefore account for the change in both geometry and material properties. Our recent studies have shown that the effects of topography coupled to site response can lead to ground motion aggravation larger than the superposition of site and geometry amplification. These *soil-topography coupling effects* arise from seismic waves trapped in the near surface soil layers, are amplified or deamplified as a consequence of stiffness contrast, and are further modified due to scattering caused by irregular interface and ground surface. In this study, we first investigate the coupling effects for 2D convex features through a systematic analysis. Two common scenarios of subsurface layering *i.e.* horizontal layering and surface layer of constant thickness have been added to the general form of dam-type topography. The resulting trends, which are presented in the form of dimensionless amplification factors, clearly demonstrate the nonlinear nature of coupling effects, which cannot be predicted by modifying simulations of topography effects on rock by 1D site amplification factors, *a posteriori*. We then quantify these coupling effects through 3D site-specific analyses at selected strong ground motion stations in California, which yield even larger amplification as result of out-of-plane scattering effects that interfere with the in-plane topography-soil coupling mechanisms.

---

### The Role of Shallow Slip on Faults

Oral Session · Thursday · 8:30 AM · 21 April · Tuscany 5/6  
Session Chairs: Sarah Minson, Benjamin Brooks, and Jessica Murray

---

#### Can We Predict Surface Deformation Patterns in Future Earthquakes with any Degree of Certainty? The Importance of Documenting Patterns of On- versus-off-fault Deformation in Large Earthquakes

DOLAN, J. E., Univ. of Southern California, Los Angeles, CA, USA, dolan@usc.edu

Accurate determination of patterns and proportions of on-fault versus off-fault surface deformation is of critical importance for a large number of problems in modern tectonics, including the proper interpretation of geomorphic data in fault slip rates studies, the use of such data for comparisons of geologic and geodetic rates in the search for strain transients and as a basic input to probabilistic seismic hazard assessments, the dynamics of near-surface rupture and the relationship

between rupture and fault structure, especially near structural complexities, the use of surface slip data as constraints in inversions for slip at depth in large earthquakes, with implications for the so-called “shallow slip deficit”, and the possibility of future micro-zonation based on a more thorough understanding of the relationship between fault maturity and near-surface structure and types of near-surface materials to better protect the built environment. The advent of new tools such as COSI-Corr sub-pixel image correlation, together with the proliferation of readily available high-resolution imagery, is allowing us the document patterns of surface deformation with ever-increasing detail. In this talk, I will describe the results of several studies in which we compared measurements of surface slip along “the fault” with overall patterns of total surface deformation revealed by image-correlation analyses. Such studies are beginning to reveal basic relationships between structural attributes of the fault (cumulative displacement, local structural details), the types of near-surface materials through which the rupture passes (*e.g.*, bedrock vs. thick sediments), and the degree to which co-seismic slip remains (or does not remain) localized along a fault all the way to the surface. These types of observations hold the promise of being able to predict, at least in a general sense, what to expect in terms of surface deformation patterns in advance of future large earthquakes.

#### Influence of Compliant Sediments on Shallow Slip and Rupture Dynamics

DUNHAM, E. M., Stanford University, Stanford, CA, USA, edunham@stanford.edu; LOTTO, G. C., Stanford University, Stanford, CA, USA, glotto@stanford.edu; ERICKSON, B. A., Portland State University, Portland, OR, USA, berickson@pdx.edu; ALLISON, K., Stanford University, Stanford, CA, USA, kallison@stanford.edu; JEPPESON, T. N., University of Wisconsin-Madison, Madison, WI, USA, trjpeppson@wisc.edu; TOBIN, H. J., University of Wisconsin-Madison, Madison, WI, USA, htobin@wisc.edu

Many faults are surrounded by sediments in the near-surface region. Our work uses dynamic rupture simulations to explore how these sediments influence the shallow rupture process, focusing on two settings: subduction zones with accretionary prisms and strike-slip faults passing through sedimentary basins. In subduction zones, the increased compliance and reduced wave speeds in frontal prisms have been suggested to enhance shallow slip and tsunami generation. We introduce compliant prisms, having properties constrained by core samples retrieved by the Japan Trench Fast Drilling Project and similar ocean drilling expeditions, in 2-D simulations of megathrust ruptures that capture the full seismic, ocean acoustic, and tsunami wavefields. In simulations of the 2011 Tohoku event, the compliant prism increases shallow slip by over 10 m, but because the horizontal extent of the prism is not much larger than the ocean depth, there is little effect on tsunami wave heights. In contrast, simulations employing relatively larger prisms and shallower oceans show enhancement of both shallow slip and tsunami heights, suggesting that assessment of the role of the prism must be done for specific subduction zone geometries. In a complementary study, we model earthquake sequences on strike-slip faults passing through sedimentary basins. Here the basin can either inhibit rupture (leading to sub-basin events) or facilitate large amounts of shallow slip in surface-rupturing events, depending on the past history of ruptures and the resulting stress field that develops. For certain combinations of basin depth and basin rigidity contrast with the surroundings, alternating sequences of sub-basin and surface-rupturing events occur. All of these examples reveal the important controls that near-surface sediments can have on the rupture process. Ongoing work extends the above studies by accounting for frictional properties of the sediments (typically velocity-strengthening) and inelastic yielding.

#### Large Shallow Slip on the Central Imperial Fault in the 1940 Earthquake: Evidence for a Shallow Asperity

ROCKWELL, T. K., San Diego State University, San Diego, CA, USA, trockwell@mail.sdsu.edu; KLINGER, Y., Institut de Physique du Globe de Paris, Paris, France, klinger@ipgp.fr

The Imperial fault in the Salton Trough of southern California ruptured from end to end on 18 May 1940. The mainshock nucleated along the northern third of the fault near its juncture with the Brawley fault and ruptured predominantly to the southeast in a series of 11 sub-events, the first four of which produced most of the seismic moment. Displacement at the surface averaged less than a meter along the northern third of the fault but ramped up to 5-7 m of surface offset in the region north of the international border, decreasing to 2-4 m of surface displacement for the southern half of the rupture south of the border. In contrast, the 15 October 1979 earthquake on the Imperial fault nucleated south of the zone of large 1940 displacement, rupturing in the sub-surface to the northwest beneath the zone of high 1940 slip, and only producing surface rupture along the northern third of the Imperial fault with offsets of similar magnitude as occurred in 1940. Strong ground motion recordings at El Centro suggest that as much as 75%



of the moment release occurred south of the border and not where large surface displacement was observed. Similarly, inversion of body waves places half of the moment release south of the border and only 27% in the region of large slip. These observations collectively argue for the presence of a shallow asperity along the central section of the Imperial fault, and that displacement at the surface was much greater than at depth. Paleoseismic observations in the border area support a longer return time for large displacements, with the penultimate large earthquake occurring around ca 1720 AD. The common assumption that deep slip is greater than surface slip fails for the 1940 Imperial Valley earthquake.

### Shallow Fault Slip and 'Off-Fault' Deformation From Some Recent Strike-Slip Earthquakes

**BROOKS, B. A.**, US Geological Survey, Menlo Park, CA, USA, [bbrooks@usgs.gov](mailto:bbrooks@usgs.gov); **BARNHART, W.**, University of Iowa, Iowa City, IA, USA, [william-barnhart-1@uiowa.edu](mailto:william-barnhart-1@uiowa.edu); **MINSON, S. E.**, US Geological Survey, Menlo Park, CA, USA, [sminson@usgs.gov](mailto:sminson@usgs.gov); **GLENNIE, C. L.**, University of Houston, Houston, TX, USA, [clglenni@central.uh.edu](mailto:clglenni@central.uh.edu); **MURRAY, J.**, US Geological Survey, Menlo Park, CA, USA, [jrmurray@usgs.gov](mailto:jrmurray@usgs.gov); **HUDNUT, K.**, US Geological Survey, Pasadena, CA, USA, [hudnut@usgs.gov](mailto:hudnut@usgs.gov); **ERICKSEN, T. L.**, US Geological Survey, Menlo Park, CA, USA, [tericksen@usgs.gov](mailto:tericksen@usgs.gov)

Quantifying the amount of 'on-' and 'off-' fault deformation for surface-rupturing earthquakes is critical to achieve a better understanding fault zone physics. Moreover, placing constraints on the relative amount of on- and off-fault deformation can help test for a proposed deficit in shallow slip observed in finite fault models from continental strike-slip earthquakes. The recent proliferation of high-resolution, near-field, optical and active-source (e.g. LiDAR) imaging techniques provides datasets that permit direct measurement of near- and farther-field deformation. We analyze the 2013  $M_w$  7.7 Balochistan and 2014  $M_w$  6.0 South Napa earthquakes. For both surface-rupturing events we compare near- (<100m) and medium- (100-250m) field deformation with far-field (> 1 km) deformation derived from either one data set (optical imagery, Baluchistan) or many datasets (LiDAR, InSAR, South Napa). For the Balochistan earthquake, 77% of surface deformation occurs within the near-field while nearly all deformation occurs within 250 m of the fault. Different studies of this earthquake, including geological surface mapping, show that both the definition of "off-fault" deformation and the availability of high-resolution, automated offset detection can bias the magnitude of inferred off-fault deformation by as much as 25-30%. For the South Napa Earthquake, the excellent reproduction of near-field deformation by a elastic dislocation model demonstrates that the rupture was not accompanied by significant off-fault deformation. This is contrary to the notion that 'immature' faults (those with less cumulative slip and less well-developed shear zones) are less likely to exhibit surface rupture and more likely to exhibit a shallow slip deficit and off-fault deformation. Our results highlight the need for rigorous techniques to measure "near-fault" deformation, and rapid, high-quality near-fault geodetic observations that cannot be achieved with traditional techniques.

### Shallow Slip Deficit and Low-angle Detachment Faulting in the 2010 El Mayor-Cucapah (Mexico) Earthquake Revealed with Differential Lidar

**NISSEN, E.**, Department of Geophysics, Colorado School of Mines, Golden, CO, USA, [enissen@mines.edu](mailto:enissen@mines.edu); **LAIJOIE, L.**, Department of Geophysics, Colorado School of Mines, Golden, CO, USA, [llajoie@mines.edu](mailto:llajoie@mines.edu); **ARROWSMITH, J. R.**, School of Earth and Space Exploration, Arizona State University, Tempe, AZ, USA, [ramon.arrowsmith@asu.edu](mailto:ramon.arrowsmith@asu.edu); **GLENNIE, C.**, Civil and Environmental Engineering, University of Houston, Houston, TX, USA, [clglennie@uh.edu](mailto:clglennie@uh.edu); **HINOJOSA CORONA, A.**, CICESE, Ensenada, Mexico, [alhinc@cicese.mx](mailto:alhinc@cicese.mx); **OSKIN, M. E.**, Earth and Planetary Sciences, University of California, Davis, CA, USA, [oskin@geology.ucdavis.edu](mailto:oskin@geology.ucdavis.edu)

In ground-rupturing earthquakes, slip estimated at depths of 100s of meters to a few kilometers typically exceeds offsets surveyed along the main fault trace. This so-called shallow slip deficit may reflect (1) the redistribution of near-surface slip onto subsidiary faults within a wider damage zone; (2) a genuine shortfall in shallow coseismic deformation that is recovered later in the earthquake cycle, such as by postseismic afterslip or long-term folding; or (3) artifacts that arise when InSAR data with poor correlation near the surface rupture are inverted for slip at depth. However, the degree of shallow slip deficit varies considerably between earthquakes, for reasons that may include differences in fault zone structural maturity, width, or geometry, variations in earthquake magnitude, contrasts in near-surface material properties, or combinations of these factors. We seek to clarify these relations by investigating the 2010 El Mayor-Cucapah (Mexico) earthquake, which involved slip along several discrete faults with differing structural characteristics rupturing through a variety of surface materials. We exploit dense field measurements (Fletcher *et al.*, 2014; Teran *et al.*, 2015) together with a unique three-dimensional surface deformation field established

by differencing pre- and post-event airborne lidar data (Glennie *et al.*, 2014). To establish the slip deficit on each rupture segment, we compare offsets surveyed at the principal fault scarp with lidar-derived surface displacements measured short distances (100s of meters) from the scarp, a proxy for slip at depth. A second goal is to resolve a discrepancy between field observations which implicate slip on low-angle detachments, and models based upon space geodetic and seismological data which support only sub-vertical structures. Extensional heave exceeds vertical throw only in the far northern rupture zone, where our results therefore confirm localized low-angle slip on parts of the Paso Superior fault.

### Characterization of Shallow Slip Variability in California UAVSAR Repeat-Pass Interferograms

**PARKER, J. W.**, Jet Propulsion Laboratory/California Institute of Technology, Pasadena, CA, USA, [Jay.W.Parker@jpl.nasa.gov](mailto:Jay.W.Parker@jpl.nasa.gov); **DONNELLAN, A.**, Jet Propulsion Laboratory/California Institute of Technology, Pasadena, CA, USA, [Andrea.Donnellan@jpl.nasa.gov](mailto:Andrea.Donnellan@jpl.nasa.gov); **GLASSCOE, M. T.**, Jet Propulsion Laboratory/California Institute of Technology, Pasadena, CA, USA, [Margaret.T.Glasscoe@jpl.nasa.gov](mailto:Margaret.T.Glasscoe@jpl.nasa.gov); **PIERCE, M.**, Indiana University, Bloomington, IN, USA, [marpierc@iu.edu](mailto:marpierc@iu.edu); **WANG, J.**, Indiana University, Bloomington, IN, USA, [wang208@iu.edu](mailto:wang208@iu.edu)

Of the UAVSAR repeat-pass differential interferograms in California, a growing collection capture surface rupture directly from earthquakes and also from triggered faulting. Characterization of shallow faulting is performed for part of the South Napa main rupture, where resolution is roughly 10 m and pixels are in certain places continuous across the fault with no holes or gaps. Profiles are consistent with reduced rupture in a surface layer a few tens of meters thick. Similar profile analysis applies to the secondary faulting which parallels the main rupture about 1 km to the east. Later interferograms enable characterization of the dislocation on the main fault afterslip after a few months. Additional favorable events revealing depth of slip are the triggered slip from the El Mayor-Cucapah earthquake on the Superstition Hills, Elmore, and Imperial faults, as well as the faulting associated with a M5.7 aftershock near the Elsinore fault, some of the surrounding small triggered faults, and triggered slip associated with the Brawley swarm. The latter can be assessed best with narrow strips of phase evaluated along roadways, avoiding the decorrelation prevalent in the agricultural landscape. The high resolution of UAVSAR enables improved characterization of shallow slip, and we show that free tools available through GeoGateway enable rapid assessment of many faulting events that are observed in a very sparse set out of hundreds of public interferograms.

### Constraining Models of Shallow Fault Slip with Remote Sensing Data

**GLASSCOE, M.**, Jet Propulsion Laboratory, California Institute of Technology, Pasadena, CA, USA, [Margaret.T.Glasscoe@jpl.nasa.gov](mailto:Margaret.T.Glasscoe@jpl.nasa.gov); **DONNELLAN, A.**, Jet Propulsion Laboratory, California Institute of Technology, Pasadena, CA, USA, [Andrea.Donnellan@jpl.nasa.gov](mailto:Andrea.Donnellan@jpl.nasa.gov); **LYZENGA, G.**, Jet Propulsion Laboratory, California Institute of Technology, Pasadena, CA, USA, [Gregory.A.Lyzenga@jpl.nasa.gov](mailto:Gregory.A.Lyzenga@jpl.nasa.gov); **PARKER, J.**, Jet Propulsion Laboratory California Institute of Technology, Pasadena, CA, USA, [Jay.W.Parker@jpl.nasa.gov](mailto:Jay.W.Parker@jpl.nasa.gov); **MILLINER, C.**, University of Southern California, Los Angeles, CA, USA, [milliner@usc.edu](mailto:milliner@usc.edu)

Determining the distribution of slip and behavior of fault interactions, particularly at shallow depths, is a complex problem. Field and remotely sensed data often lack the necessary coverage to resolve fault behavior, but realistic physical models may be used to more accurately characterize the complex behavior of faults constrained with observed data, such as UAVSAR. These results will improve the utility of using combined models and data to estimate earthquake potential. We model a fault embedded within a damage zone of reduced elastic rigidity that narrows with depth and forward model the shallow slip and resulting surface deformation. The fault segments and slip distributions will be modeled using the JPL GeoFEST software. GeoFEST (Geophysical Finite Element Simulation Tool) is a two- and three-dimensional finite element software package for modeling solid stress and strain in geophysical and other continuum domain applications [Lyzenga, *et al.*, 2000; Glasscoe, *et al.*, 2004; Parker, *et al.*, 2008, 2010]. New methods to advance geohazards research using computer simulations and remotely sensed observations for model validation are required to understand fault slip, the complex nature of fault interaction and plate boundary deformation. These models help enhance our understanding of underlying processes, such as transient deformation and fault creep, and can aid in developing observation strategies for sUAV, airborne, and upcoming satellite missions seeking to determine how faults behave and interact and assess their associated hazard. Models will also help to characterize this behavior, which will enable improvements in hazard estimation. Validating the model results against remotely sensed observations will allow us to better constrain fault zone rheology and physical properties,



having implications for the overall understanding of earthquake physics, fault interactions, and earthquake hazard, preparedness and risk reduction.

#### **Numerical Modeling of Surface Fault Rupture in Reverse Events**

BUELNA, M., Cal Poly, San Luis Obispo, CA, USA, mbuelna@calpoly.edu; MOSS, R. E. S., Cal Poly, San Luis Obispo, CA, USA, rmoss@calpoly.edu

A nonlinear Mohr-Coulomb constitutive model with a strain dependent yield surface and non-associated flow was employed to study the plastic soil properties which affect the rate of surface fault rupture propagation in reverse events. These numerical simulations show a trend for soils with higher stiffness to have a higher rate of rupture propagation. Additionally the study shows the effects of strain softening and hardening on the rate of rupture propagation. Soils which strain harden exhibiting ductile behavior typically require more basal offset to rupture to the surface than soils which strain soften exhibiting brittle behavior. These results agree with our previous fault box studies, which showed that soils with higher near surface shear wave velocity were more likely to propagate rupture to the surface for a given reverse event. The numerical modeling allowed for a more comprehensive evaluation of material types and fault angles than the fault box, and provided confidence in these findings.

#### **On Co- and Post-Seismic Slip of the 2014 South Napa Earthquake**

MINSON, S. E., U.S. Geological Survey, Menlo Park, CA, USA, sminson@usgs.gov; MURRAY, J. R., U.S. Geological Survey, Menlo Park, CA, USA, jrmurray@usgs.gov; BROOKS, B. A., U.S. Geological Survey, Menlo Park, CA, USA, bbrooks@usgs.gov; BECK, J. L., California Institute of Technology, Pasadena, CA, USA, jimbeck@caltech.edu; GLENNIE, C. L., NCALM, University of Houston, Houston, TX, USA, clglenni@central.uh.edu; ERICKSEN, T. L., U.S. Geological Survey, Menlo Park, CA, USA, tericksen@usgs.gov; HUDNUT, K. W., U.S. Geological Survey, Pasadena, CA, USA

The 2014  $M_w$  6.0 South Napa earthquake and its subsequent afterslip were recorded by an unprecedented variety of sensors including seismic, GPS, InSAR, UAVSAR, and Mobile Laser Scanning (MLS) instruments. This multitude of data sets holds the potential for providing better resolution of small-scale features of fault slip, especially shallow fault slip. However, there are several complications to jointly using these data. First, separating the co-seismic rupture from the post-seismic deformation is complicated by the fact that almost all of these data include signal from varying amounts of afterslip. Second, the full spatial resolution of the data can only be utilized if the modeling process does not enforce spatial smoothing. But, third, the need to remove spatial smoothing exacerbates the issue that, the higher the apparent spatial resolution of the data, the more important it is to consider the effects of errors in your model design. Such errors include those introduced by the assumed elastic structure of the Earth and fault geometry. We will explore the ways that information from these different data can be rigorously fused together in an inversion framework and present preliminary slip models resulting from such data integration.

#### **Bayesian Inversion for Fault Frictional Parameters and Afterslip Following the South Napa Earthquake**

MURRAY, J. R., U.S. Geological Survey, Menlo Park, CA, USA, jrmurray@usgs.gov; MINSON, S. E., U.S. Geological Survey, Menlo Park, CA, USA, sminson@usgs.gov

Early postseismic deformation due to the 24 August 2014  $M_w$  6 South Napa earthquake can be explained largely by afterslip, particularly on the southeast part of the rupture where the West Napa fault (WNF) borders a ~3 km deep sedimentary basin. The inference of sustained aseismic slip implies portions of the fault zone have velocity strengthening (VS) frictional properties. Characterizing spatially variable fault friction could shed light on the relationship between lithology (e.g., basin sediment) and fault slip modes (coseismic and aseismic), information that is relevant to forecasting coseismic slip and the likelihood of large afterslip.

We study WNF frictional properties via a model of stress-driven afterslip governed by steady-state VS friction parameterized by  $aV$ , the slip rate dependence of friction, and  $V$ , the initial velocity on the afterslip zone. Using Bayesian inversion of GPS position time series, we obtain the posterior probability distribution on  $aV$  and  $V$  with uniform priors from published results. Coseismic slip inferred from seismic data (Wei *et al.*, 2015) provides the initial stress step. We compare results using spatially uniform friction to those found when the two parameters are allowed different values inside and outside the basin-bordered area.

We find a mean uniform  $aV$  of 0.027 for the first month of afterslip. In the nonuniform model the mean  $aV$  inside and outside the basin is 0.025 and 0.06. While most GPS data are fit, even with nonuniform friction significant misfit

remains at some sites. This misfit and systematic residuals between observed and forward-modeled InSAR displacements suggest the geodetic data and coseismic source model are not compatible. Jointly estimating coseismic slip and friction parameters from multiple data types via Bayesian inversion would be a powerful tool to address this problem; we are exploring the computational feasibility of this approach.

---

## **Characterizing the Stress Field and Stress Drop for Earthquake Source Physics and Hazard Assessment**

Oral Session · Thursday · 1:30 AM · 21 April · Tuscany 5/6

Session Chairs: Patricia Martínez-Garzón, Jeanne Hardebeck, Marco Bohnhoff, and Karen Luttrell

---

### **Weak Fault Mechanisms Imply Creeping Faults**

SCHOLZ, C. H., Lamont Doherty Earth Observatory, Palisades, NY, USA, scholz@ldeo.columbia.edu

Since the widespread acceptance of the weak San Andreas hypothesis there has been extensive work done in the laboratory and field to find a physical mechanism for weak faults. Much laboratory work has been done on phyllosilicates, which have frictional strengths less than Byerlee's law. However, under all but a few conditions, the phyllosilicates are velocity strengthening and hence would promote aseismic rather than seismic slip. The presence of one of the weakest of these, saponite (Mg smectite) in the active strands of the SAF at SAFOD explains both the weakness ( $\mu \sim 0.2$ ) and the aseismic nature of the creeping section of the SAF. Saponite is a reaction product of serpentinite, which is found in the fault zone throughout the creeping section, but which is otherwise rare in continental faults. Friction with solution transfer creep can also result in weak faults but it is even more strongly velocity strengthening. At high slip velocity, that behavior can become cataclastic, with velocity weakening, so that a rupture could propagate in such a material if nucleated elsewhere. The net result would be a creeping fault that hosts earthquakes as a secondary contributor to moment release. The study of exhumed fault zones reveals little evidence for the presence of the weak clay minerals. Faults in phyllitic protoliths develop fault cores of phyllonite (mylonitized phyllosilicates) composed of the micas foliated with associated quartz and other minerals. Such faults are likely to be weak (though probably not as weak as the SAF hypothesis requires). They do not usually show the intense localization of shear associated with velocity weakening and seismic slip and so are probably mainly aseismic. In contrast to the creeping section of the SAF, most continental faults appear to be highly coupled, in which they are locked between large earthquakes. None of the mechanisms for weak faults are compatible with this behavior.

### **Stress Variations across the Central and Eastern United States and a 3-D Model of Stress in the New Madrid Seismic Zone**

LEVANDOWSKI, W., USGS, Golden, CO, USA, wlevandowski@usgs.gov; BOYD, O. S., USGS, Golden, CO, USA, olboyd@usgs.gov; RAMIREZ-GUZMÁN, L., UNAM, Mexico City, Mexico, LRamirezG@ingen.unam.mx

The stress field in the central and eastern United States is not uniform. Thus, it is imperative to consider local conditions, not only the regional stress field, in assessing the hazard posed by any given fault. Moment tensors reveal an average N73E horizontal maximal compression ( $\sigma_{Hmax}$ ) direction likely due to Mid-Atlantic ridge push, yet the style of faulting transitions from dominantly reverse in the east to strike-slip and to normal faulting in the western Great Plains. We derive an analytical solution for the deviatoric stress transmitted inward from the plate boundary as a function of viscosity, which we constrain geodetically to  $10^{22-23}$  Pa-s. This stress decreases from 10 MPa along the east coast to 5 MPa near the New Madrid seismic zone to less than 1 MPa in the western Great Plains. Superimposed on this broad pattern are reorientations of  $\sigma_{Hmax}$  in the New Madrid and Central Virginia seismic zones that we find are significant to >99% confidence. In each case, crustal density variations have previously been proposed to locally elevate and/or reorient deviatoric stress. At New Madrid, this reorientation is critical because known seismogenic faults are poorly aligned relative to far-field stress. To quantify the local stress perturbations due to lithospheric density variations, we jointly invert seismic velocity, gravity, and topography for a 3-D density model of the New Madrid region and use this estimate as input to a finite-element model of gravity-derived stress. The deviatoric component of the tensor sum of local, gravity-derived stress and far-field compression predicts not only the gross reorientation of  $\sigma_{Hmax}$  but also subtle variations across the region, substantiating our approach. Furthermore, dense lower crust beneath the seismic zone creates stress that interferes constructively with the far field, elevat-

ing deviatoric stress by some 5 MPa (to a regional maximum of ~10 MPa). Local, gravity-derived stress is an key factor in intraplate seismicity.

### **Inference of Stress from Faulting and Topographic Loading of Faults**

HETLAND, E. A., University of Michigan, Ann Arbor, MI, USA, eheland@umich.edu; MEDINA LUNA, L., University of Michigan, Ann Arbor, MI, USA, lmedina@umich.edu; STYRON, R. H., Earth Analysis, Seattle, WA, USA, richard.h.styron@gmail.com; HINES, T. T., University of Michigan, Ann Arbor, MI, USA, hines@umich.edu

Stress is a fundamental physical control on crustal deformation, particularly seismogenesis. Considerable effort has been devoted to the inference of stress from fault slip data (structural geologic measurements, focal mechanisms, coseismic slip models) over the last several decades. All of the methods used to infer stress follow from an assumption that when a fault slips, it does so in the direction in which it was loaded, which is attributed to work of R. Wallace and M. Bott in the 1950s. In the last few years, we have undertaken to estimate the stresses that led to several large earthquakes, using all available fault slip data within a Bayesian estimation framework. Using slip data alone, the orientations of principal stresses can be well constrained (the more disparity of slip directions and fault orientations results in tighter posterior constraints); however, the relative magnitudes of the principal stress are somewhat more weakly constrained and the absolute magnitude of stress can not be determined. Consideration of the stresses due to topographic loading along with the slip data can greatly increase the resolution of both the relative and absolute magnitudes of the principal stresses. Once stress is determined, it is possible to further constrain stress, fault friction, and fault pore-fluid pressures by assuming a Coulomb-Navier failure criterion. We have thus far focused our work on the 1999 Izmit, Turkey, 2008 Wenchuan, China, 2011 Tohoku-Oki, Japan, and 2015 Gorkha, Nepal earthquakes. In this presentation, we discuss how our methods addresses some of the challenges associated with the inference of stress from slip data (*e.g.*, ambiguities in resolving stress directions, complexity of stress model justified from data), show results from several of our focus earthquakes, and discuss interactions between topographic stresses and heterogeneities in fault slip during large earthquakes.

### **Stress Orientations along Megathrusts in Subduction Zones: Fault Strength and Seismic Coupling**

HARDEBECK, J. L., US Geological Survey, Menlo Park, CA, USA, jhardebeck@usgs.gov

Although the frictional properties of faults are difficult to observe directly, the frictional strengths of faults can be estimated indirectly by constraining the orientations of the stresses acting on the faults. A global investigation of stress orientations in subduction zones finds that the maximum compressive stress axis,  $\sigma_1$ , plunges systematically trenchward, making a 30°-60° angle to the subduction megathrust fault. These angles indicate that the megathrust faults are well-oriented for failure in the stress field, and therefore of similar strength to their surroundings. Several other lines of evidence (*e.g.* low heat flow, inferred high fluid pressures, coseismic stress rotations) imply that megathrusts are weak in an absolute sense. Together, these observations suggest that, in addition to the megathrust, the whole subduction zone is weak and can support only low deviatoric stress. There are significant differences in the angle of  $\sigma_1$  to the megathrust between different subduction zones, which are uncorrelated with either the age of the subducting plate or the thickness of sediments entering the trench. A weak correlation of stress orientation with seismic coupling is observed, with more strongly coupled subduction zones exhibiting angles to  $\sigma_1$  that are closer to 30°. In a low-stress environment, there is only a small difference in the coefficient of friction for faults with angles to  $\sigma_1$  in the range of 30°-60°, so this indicates only a small difference in strength between strongly- and weakly-coupled subduction zones. These results average over each subduction zone, possibly obscuring larger differences between locked and creeping patches. Comparisons between geodetically-derived coupling models and stress orientations for individual subduction zones will test whether the locked patches on a megathrust fault are of significantly different frictional strength than the creeping patches.

### **Revisiting Apparent Stress Drop as a Possible Tool for Distinguishing Swarm and Mainshock/Aftershock Sequences**

FISCHER, T., Charles University in Prague, Prague, Czech Republic, fischer@natur.cuni.cz

The static stress drop is a standard measure of decreasing the shear stress on a fault during an earthquake that is averaged along the whole rupture. It has been observed that stress drop does not vary significantly for different earthquakes and may be regarded as an invariant parameter of the rupture process at different scales. Stress drop scales with seismic moment, but is inversely proportional

to the third power of characteristic rupture dimension, which introduces large error in its estimates. The average stress drops of earthquakes range in units of MPa and systematic difference in stress drops of interplate and intraplate earthquakes was found. Much smaller stress drops in fractions of MPa are reported for slow earthquakes and in some cases also for earthquake swarms. To this purpose an alternative parameter, the effective stress drop was introduced, which makes use of the cumulative seismic moment and total activated area of seismic cluster. This way additional errors in seismic locations and simplifications of the adopted rupture model were introduced, which increase the uncertainty of the resulting stress drop.

In this paper we test how the effective stress drop is comparable to the static stress drop. To this purpose we compare the seismic moment released by a single rupture and by a seismic cluster and test the influence of synthetic errors in utilized parameters. We examine both approaches on seismic data from earthquake swarms in West Bohemia and areas with active volcanism.

### **Heat Flow Constraints on Fault-normal Stresses near the San Andreas Fault and Application to the Rupture Tip of Large Strike-slip Events and to Near-fault Deformation**

SLEEP, N. H., Stanford University, Stanford, CA, USA, norm@stanford.edu

The San Andreas Fault system near Parkfield is subparallel to the strike of compressional folds and thrust faults. The fault-normal traction on the main fault is on average a factor of  $\gamma = 1 + 2\mu(\sqrt{1+\mu^2}) + \mu$ , where  $\mu$  is the coefficient of friction for thrust faults, times the effective lithostatic pressure (lithostatic pressure minus hydrostatic pressure). A useful limit for thrust-fault  $\mu$  of 0.6 (where  $\gamma$  is 3.12) is obtained from heat flow by considering off-fault convergence at a rate of 1 mm/yr for 10 km across strike. That is, it is permissible to extrapolate the coefficient of friction in the Parkfield Pilot Hole from ~2 km to ~20 km depth. If the fault-normal traction is in fact this high, the well-known heat-flow constraint of average stresses of 10-20 MPa during slip on the main fault becomes more severe. Only a few percent of the total slip during earthquakes can occur at the peak stress before dynamic weakening mechanisms occur. The spatial dimension of the high-stress rupture-tip zone is ~10 m for  $\gamma = 3.12$  and ~100 m for  $\gamma = 1$ . High dynamic stresses during shaking occur within these distances of the fault plane. In terms of scalars, fine-scale tectonic stresses cannot build up beyond the difference between failure stress and dynamic stress. Plate scale slip causes local stresses to build up near geometrical irregularities of the fault plane. Strong dynamic stresses near the rupture tip facilitate anelastic deformation with the net effects of relaxing the local tectonic stress and accommodating local deformation around the irregularities. Conversely, movements along minor thrust faults should cause the normal traction on the main fault to be irregular. There also is a mild tendency for near-fault material to extrude upward, especially at shallow depths.

### **Regional Tectonic Stress Field and Earthquake Stress Drops in Southern California: Understanding Distributed Continental Plate Boundary Tectonics**

HAUKSSON, E., Caltech, Pasadena, CA, USA, hauksson@caltech.edu

More than 170,000 focal mechanisms were analyzed to constrain the tectonic stress field across southern California, including the maximum horizontal compressive stress ( $SH_{max}$ ) orientations and the style of faulting. The trend of  $SH_{max}$  exhibits significant regional and local spatial heterogeneities. It varies from west-northwest or north along the San Andreas system to north-northeast to the east in the Eastern California Shear Zone as well as to the west, within the Continental Borderland and the Western Transverse Ranges. The style of faulting exhibits similar complexity, ranging from predominantly normal faulting in the high Sierra Nevada, to strike-slip faulting along the San Andreas system, to three subparallel bands of thrust faulting in the western Transverse Ranges, including Wheeler Ridge area, Ventura basin, and Los Angeles basin.

We analyze the geographical distribution of stress drops and search for a possible dependency on state of stress and crustal geophysical parameters. We reanalyze the stress drop values of ~60,000 earthquakes which were originally determined by Shearer *et al.* (2006) and a new dataset from ~2000 to 2014 using the same spectral method. We use six crustal geophysics parameters to search for obvious correlations that may explain changes in the mean values of the stress drops: (1) crustal thickness, (2) isostatic gravity, (3) heat flow, (4) shear strain rate, (5) crustal stress regime, and (6)  $SH_{max}$  orientation and style of faulting. In particular, the crustal stress regime and style of faulting influence the stress drops as demonstrated by lower stress drops for north-northeast trending principal horizontal stress and in areas of dip-slip faulting. The mean variations in stress drops with heat flow, stress regime, crustal thickness, and density can be explained in the context of fault healing (grain boundary growth) and corresponding increase in fault zone strength on time scales modulated by the tectonic shear strain rate.

## Fluid Injection Impact on Fracture Reactivation Potential at The Geysers Geothermal Field

MARTÍNEZ-GARZÓN, P., GFZ German Research Centre for Geosciences, Potsdam, Brandenburg, Germany, [patricia@gfz-potsdam.de](mailto:patricia@gfz-potsdam.de); KWIAŁTEK, G., GFZ German Research Centre for Geosciences, Potsdam, Brandenburg, Germany, [kwiatek@gfz-potsdam.de](mailto:kwiatek@gfz-potsdam.de); BOHNHOFF, M., GFZ German Research Centre for Geosciences, Potsdam, Germany, [bohnhoff@gfz-potsdam.de](mailto:bohnhoff@gfz-potsdam.de); DRESEN, G., GFZ German Research Centre for Geosciences, Potsdam, Germany, [dre@gfz-potsdam.de](mailto:dre@gfz-potsdam.de)

We analyze the fault geometries and reactivation potential inferred from induced microseismicity recorded at The Geysers geothermal field with respect of spatio-temporal characteristics and seismological and geomechanical parameters such as moment magnitude, perturbation pressure needed for reactivation, hydraulic parameters and optimum friction coefficient. Reactivation potential is here quantified through the instability coefficient describing how close a particular fault geometry is to that of the optimally oriented fault. A statistical approach is here performed to calculate the statistically most likely fault instabilities from the stress field and focal mechanism uncertainties. We find that  $\approx 72\%$  of the analyzed seismicity reactivate favorably oriented faults and fractures. However, we also observe a number of severely misoriented fault planes with respect to the local stress field. Most of the observed severely misoriented faults occur at the depth of the open-hole section of the well injecting fluid nearby and during periods of increased injection rates, where the maximum pore pressure perturbation is expected. At the base of the reservoir, nearly all reactivated faults are optimally oriented. Reactivation of these fault planes can be generally well explained with a constant Byerlee friction coefficient of 0.6 and a perturbation pressure  $< 25$  MPa, in agreement with the expected combined effect of thermal stresses and pore pressure from fluid injection at The Geysers. Furthermore, a relation is observed between fault reactivation potential and moment magnitude, with the largest analyzed events occurring on the optimally oriented faults. These faults also host most of the seismicity and thus this observation could imply either larger probability of greater magnitudes on these faults following the Gutenberg-Richter relation or decreased fault complexity along these orientations.

## Regional-scale Models of Crustal Stress in Southern California, with Implications for Heterogeneous Tectonic Loading and In Situ Stress Magnitude

LUTTRELL, K., Louisiana State University, Baton Rouge, LA, USA, [kluttrell@lsu.edu](mailto:kluttrell@lsu.edu); SMITH-KONTER, B., University of Hawaii, Honolulu, HI, USA, [brkonter@hawaii.edu](mailto:brkonter@hawaii.edu)

The in situ crustal stress field fundamentally governs, and is affected by, the active tectonic processes in plate boundary regions, yet first order questions remain about the characteristics of that field and the implications for active faults. We investigate the nature of this stress field in southern California by combining previously developed models of stress orientation, stress from topography, and stress accumulation rate on major locked faults into two synthesis models. In the first, we estimate the magnitude of the in situ stress field by balancing in situ orientation indicated by earthquake focal mechanisms against the stress imposed by topography, which tends to resist the motion of strike-slip faults. Our results based on the most rugged topography along the San Andreas fault system indicate that differential stress at seismogenic depth must exceed 62 MPa, consistent with differential stress estimates from complementary methods. In the second, we develop a forward model of in situ stress based on topography, stress accumulation on locked faults, and a simple 2-D tectonic driving stress, in order to assess driving stress orientation and the relative importance of locked faults for the in situ stress state. We consider twelve independent segments of the San Andreas Fault System from Imperial Valley through Parkfield and find that observed heterogeneity in stress orientation cannot be accounted for by variations in fault geometry, earthquake cycle loading, or nearby topography. Instead we determine that the horizontal azimuth of driving stress varies by  $\sim 20^\circ$  along the San Andreas Fault and  $\sim 15^\circ$  along the San Jacinto fault. Our results suggest that in situ stress heterogeneity at the regional scale is more influenced by deep driving processes acting on a laterally heterogeneous crust than by perturbations to the stress field associated with major locked faults in the upper crust.

## Remote Triggering Inside Versus Outside Geothermal Fields in California

LIN, G., University of Miami, Miami, FL, USA, [glin@rsmas.miami.edu](mailto:glin@rsmas.miami.edu); ZHANG, Q., California Institute of Technology, Pasadena, CA, USA, [qizhang@caltech.edu](mailto:qizhang@caltech.edu)

Remote triggering in geothermal/volcanic regions by large earthquakes at regional distances has been globally observed and intensely studied since the 1992  $M_w$  7.3 Landers earthquake in California. However, most of the previous

studies were conducted at spatial scales of hundreds of kilometers and did not differentiate the actual operational geothermal fields with anthropogenic setting and their adjacent fault zones with natural setting. We present results from detailed analyses of the remotely triggered seismicity in three operational geothermal fields under active tectonic settings in California, including the Coso, the Salton Sea and the Long Valley caldera geothermal fields, corresponding to large distant earthquakes several hundreds of kilometers away. We compare the seismicity rate changes following the mainshocks and stress fields in each geothermal field and their adjacent fault zones based on the latest earthquake relocation and focal mechanism catalogs for the study areas. Our preliminary results show that geothermal fields respond differently to remote earthquakes from their vicinity that may be caused by the stress-state changes associated with the anthropogenic activity inside the geothermal field.

---

## Tsunami Resilience Strategies: Application of Tsunami Science and Mitigation Advancements to Protect Communities

Oral Session · Thursday · 8:30 AM · 21 April · Tuscan 7/8

Session Chairs: Rick Wilson, Kevin Miller, and Lori Dengler

---

## Evidence for Frequent Large Tsunamis in the Eastern Aleutians that Bridge the Boundary Between a Locked and Creeping Megathrust

WITTER, R. C., U.S. Geological Survey, Alaska Science Center, Anchorage, Alaska, USA, [rwitter@usgs.gov](mailto:rwitter@usgs.gov); BRIGGS, R., U.S. Geological Survey, Geological Hazards Science Center, Golden, Colorado, USA, [rbriggs@usgs.gov](mailto:rbriggs@usgs.gov); GELFENBAUM, G., U.S. Geological Survey, Pacific Coastal & Marine Science Center, Santa Cruz, California, USA, [ggelfenbaum@usgs.gov](mailto:ggelfenbaum@usgs.gov); ENGELHART, S. E., Department of Geosciences, University of Rhode Island, Kingston, Rhode Island, USA, [engelhart@uri.edu](mailto:engelhart@uri.edu); KOEHLER, R. D., Nevada Bureau of Mines and Geology, University of Nevada, Reno, Nevada, USA, [rkoehler@unr.edu](mailto:rkoehler@unr.edu); NELSON, A. R., U.S. Geological Survey, Geological Hazards Science Center, Golden, Colorado, USA, [anelson@usgs.gov](mailto:anelson@usgs.gov); LA SELLE, S., U.S. Geological Survey, Pacific Coastal & Marine Science Center, Santa Cruz, California, USA, [slaselle@usgs.gov](mailto:slaselle@usgs.gov); CORBETT, R., Department of Geological Sciences, East Carolina University, Greenville, North Carolina, USA, [CORBETTD@ecu.edu](mailto:CORBETTD@ecu.edu)

The 1957 Andreanof Islands earthquake ( $M$  8.6) generated a destructive, Pacific-wide tsunami and produced a 1200-km-long aftershock zone along the Aleutian megathrust. At the eastern end of the 1957 rupture, Driftwood Bay (Umnak Island) and Stardust Bay (Sedanka Island) lie along presently locked and creeping parts of the megathrust, respectively. Both bays face the Aleutian trench and were inundated by the 1957 tsunami. Here we compare geological evidence for frequent, large tsunamis since  $\sim 2.2$  ka at Driftwood Bay to published evidence for 6 tsunami deposits since  $\sim 1.6$  ka at Stardust Bay (Witter *et al.*, 2015), 200-km to the east.

Along the coast of Driftwood Bay, in a valley ringed by drift logs stranded up to 23 m above mean sea level (asl), we mapped 9 sand sheets up to 22.5 m asl that show features similar to modern tsunami deposits surveyed globally. Regional tide gages show that the sand sheets exceed the highest 100-yr storm surge heights.  $Cs-137$  activity measured in sediment above and below the youngest sand sheet indicates a time consistent with sand deposition by the 1957 tsunami. Drift logs lying stratigraphically above the youngest sand sheet match eyewitness reports of 23-m high tsunami runup nearby in 1957. The 9 sand sheets and C-14 ages indicate that large tsunamis have struck Driftwood Bay every 270–290 yr on average since  $\sim 2.2$  ka.

We use Bayesian age-depth models to compare tsunami deposit ages at Driftwood Bay and Stardust Bay. Among the youngest 6 sand sheets at both sites, different ages of two deposits suggest that at least twice in the past a tsunami inundated one site but not the other. However, statistically similar ages of 5 of the 6 tsunami deposits allow the interpretation that some deposits record the same tsunami generated by a rupture that spanned the presently locked and creeping parts of the Aleutian megathrust. If so, our results challenge the idea that modern interseismic coupling is a reliable proxy for long-term rupture potential.

## Earthquakes, Tsunamis, and Storms Recorded at Crescent City, California, USA

HEMPHILL-HALEY, E., Humboldt State University, Arcata, CA, USA, [emh21@humboldt.edu](mailto:emh21@humboldt.edu); KELSEY, H. M., Humboldt State University, Arcata, CA, USA, [hmk1@humboldt.edu](mailto:hmk1@humboldt.edu); LOOFBOURROW, C., Humboldt State University, Arcata, CA, USA, [cl100@humboldt.edu](mailto:cl100@humboldt.edu); CALDWELL, D., Stillwater Sciences, Arcata, CA, USA, [dlncldwll@gmail.com](mailto:dlncldwll@gmail.com); GRAEHL, N.,



Letts Consultants International, Boulder, CO, USA, nickgrahl@gmail.com; ROBINSON, M., Humboldt State University, Arcata, CA, USA

Stratigraphic evidence for coseismic land-level change, tsunamis, and storms is found beneath marshes in coastal northern California at Crescent City (CC). Previous studies at CC have focused on tsunamis, including the farfield tsunami from the 1964 Alaska earthquake, and nearfield tsunamis from earthquakes in the Cascadia subduction zone (CSZ). In addition to new data on tsunami inundation and coseismic land-level change, evidence for deposition by large storms shows another significant coastal hazard for the area.

Our results are from 3 wetland sites at CC: Marhoffer Creek, Elk Creek, and Sand Mine marsh. Marhoffer Creek marsh is adjacent to the coast 5 km north of CC, and at an elevation of > 3.4 m above NAVD88 (>1 m above highest tides). C-14 and diatom data show it has been a freshwater wetland for at least the past 1,800 yr. We identify tsunami deposits associated with two CSZ earthquakes (1700 C.E. and 1,650 yr BP) at Marhoffer Creek. Diatom data show that coseismic subsidence accompanied the 1700 C.E. earthquake; the tsunami deposit from that event extends 550 m inland from the beach. Cs-137 data show that thin sand layers about 70 m from the beach and 20 cm below the marsh surface were deposited by the farfield tsunami in 1964. Intercalated between the 1964 and 1700 tsunami deposits, and extending as far inland as the 1964 deposit, are storm deposits consisting of discontinuous layers of sand and detrital peat. The deposits are found in an interval about 0.5 m thick and at elevations above the highest winter tides. We surmise that at least some of these deposits record the ARKStorm of 1861-1862.

At Elk Creek, diatom data show coseismic subsidence in 1700 in addition to tsunami deposition. The 1964 tsunami deposit is thin and found only proximal to the Elk Creek channel. At Sand Mine marsh, association with coseismic subsidence is used to differentiate CSZ tsunamis in a complex ~100 m wide inundation zone shared by nearfield/farfield tsunamis and storms.

#### **Predicting Sediment Instability during Tsunami Loading: Hypothetical, Laboratory, and Field Case Studies**

MASON, H. B., Oregon State University, Corvallis, OR, USA, ben.mason@oregonstate.edu; FISCHER, R. M., Geosyntec Consultants, Oak Brook, IL, USA, Rfischer@geosyntec.com; ABDOLLAHI, A., Oregon State University, Corvallis, OR, USA, abdolla@oregonstate.edu; ADAMS, R. K., Oregon State University, Corvallis, OR, USA, adamsra@oregonstate.edu; EXTON, M. C., Oregon State University, Corvallis, OR, USA, extonm@oregonstate.edu

Subduction zone earthquakes create long-duration earthquake motions and tsunamis, which can significantly affect critical coastal infrastructure. Protecting critical coastal infrastructure, which is the overarching motivation for the presented work, is important for saving lives, ensuring economic rebound, and aiding the emergency response efforts following the disaster. This work focuses on sediment instability (*i.e.*, momentary liquefaction) caused by tsunami loading. A model for estimating the depth of momentary liquefaction and enhanced scour caused by tsunami loading is presented. The model is tested using a hypothetical tsunami, reduced-scale laboratory testing data, and field measurements from the 2011 Great East Japan Tsunami, and the model is used to predict potential sediment instability due to a potential Oregon coast tsunami. The results show that sediment instability may be significant or slight depending on the sediment's diffusion properties. The results imply that more work is needed to understand sediment diffusion properties, both for fully saturated and partially saturated sediments, at the shoreline. Finally, upcoming centrifuge tests, which will investigate the interaction of residual liquefaction caused by earthquake shaking and momentary liquefaction caused by ensuing tsunami loading, will be briefly discussed.

#### **The Global Tsunami Model (GTM) Network**

THIO, H. K., AECOM, Los Angeles, CA, USA, hong.kie.thio@aecom.com; LØVHOLT, F., NGI, Oslo, Norway, Finn.Lovholt@ngi.no; LORITO, S., INGV, Rome, Italy, stefano.lorito@ingv.it

The large tsunami disasters of the last decade and a half highlighted the need for a thorough understanding of the risk posed by relatively infrequent but disastrous tsunamis. Several parallel developments for probabilistic tsunami hazard analysis are ongoing and in an effort to coordinate and streamline these activities and towards implementing the Sendai Framework of Disaster Risk Reduction (SFDRR) we have established a Global Tsunami Model (GTM) with the aim of i) a better understanding of tsunami hazard and risk analysis on a global scale and ii) providing a portfolio of validated tools for tsunami hazard and risk assessment at different scales. This initiative has grown out of the tsunami component of the Global Assessment of Risk (GAR15) which resulted in a global model of fully probabilistic tsunami hazard and risk.

This complex assessment needs improvements based on the state-of-the-art research, *e.g.* in the treatment of uncertainty or inclusion of non-seismic tsunami sources, and in vulnerability and risk assessment. Currently, several dozens of researchers and practitioners worldwide are part of this network, and we will present the organizational structure and proposed technical framework that will allow researchers and practitioners to collaborate and exchange data and models among the network, help identify gaps in our current methodology and encourage further development of tsunami hazard and risk analysis.

#### **Local Tsunami Warnings: Perspectives from Recent Large Events**

MELGAR, D., University of California Berkeley, Berkeley, CA, USA, dmelgar@berkeley.edu; ALLEN, R. M., University of California Berkeley, Berkeley, CA, USA, rallen@berkeley.edu

Local tsunami warning requires rapid assessment and communication of the tsunami hazard for communities immediately adjacent to large earthquake. Here, the warning times are typically of minutes to tens of minutes. Local warning remains a challenging problem with very few systems worldwide capable of issuing such alerts. Here, we demonstrate a flexible strategy for local tsunami warning that relies on regional geodetic and seismic stations. Through retrospective analysis of four recent tsunamigenic events in Japan and Chile, we show that rapid earthquake source information, provided by methodologies developed for earthquake early warning, can be used to generate timely estimates of maximum expected tsunami amplitude with enough accuracy for tsunami warning. We validate the technique by comparing to detailed models of earthquake source and tsunami propagation as well as field surveys of tsunami inundation. Our approach does not require deployment of new geodetic and seismic instrumentation in many subduction zones, and could be implemented rapidly by national monitoring and warning agencies. We illustrate the potential impact of our method with a detailed comparison to the actual timeline of events during the recent 2015  $M_w$  8.3 Illapel, Chile earthquake and tsunami that prompted the evacuation of 1 million people.

#### **Drone Based Visual Tsunami Warning System**

HAYASHI MASA, M. H., Retired IBM Senior Engineer/Scientist, San Jose, CA, USA, mhaya0902@gmail.com; SCHIRLING PETER, Retired IBM Senior Engineer/Scientist, Burlington, VT, USA, vttrainman@ieee.org

The Really Big One could occur at the Cascadia Subduction Zone anytime, not if, but when, and casualties could be 13000. The existing tsunami warning systems are lacking in a way of convincing the public to heed the tsunami warnings. As the old sayings in English go "Seeing is believing". The Drone Based Visual Tsunami Warning System's drone stations/communication hubs would be placed at many West Coast cities/towns, and these hubs would connect all the regions as well as nationally. When an earthquake of a greater than set magnitude is detected, the drones would be deployed autonomously from the drone stations to search for a 1st tsunami wave. If a 1st wave is sighted, then a live 1st wave video with text warning messages would be transmitted to the public's cells, tablets, to warn all the public visually, aurally. In addition, the initial town/city's DESTRUCTION video warning messages would be transmitted to the other cities and provide a further urgency to evacuate. The fact is that even though the majority of the victims were aware of the tsunami warnings, the 2011 Japan Earthquake took almost 21000 lives. Over time, the human nature of underestimation, chronic tsunami warnings, etc. have resulted in this staggering apathy. The 1st wave arrived at Ofunato city (lost 446) and the Sendai region (lost approx. 10000), 33 minutes, and 65 minutes after the earthquake respectively. The 1st wave was sighted at the Ofunato seashore 8 minutes prior to the wave arrival, and if this live sighted tsunami warning had been transmitted to the Sendai region public, they would have had 41 minutes to evacuate. The 1st wave sighted video warning messages may not have provided enough urgency for some to evacuate, then, the live Ofunato city's DESTRUCTION video warning messages would have convinced the Sendai region public to evacuate immediately. Thus, this Drone Based Visual Tsunami Warning System would considerably mitigate the potential casualties in a future tsunami catastrophe.

#### **Investigation of Tsunami Generation due to Asteroid Water Impacts or Air Bursts and their Consequences on Coastline Cities**

EZZEDINE, S. M., LLNL, Livermore, CA, USA, ezzedine1@llnl.gov; DEARBORN, D. S. P., LLNL, Livermore, CA, USA, dearborn2@llnl.gov; MILLER, P. L., LLNL, Livermore, CA, USA, miller3@llnl.gov

Despite that the annual probability of an asteroid impact on earth is low, but over time, such catastrophic events are inevitable. Interest in assessing the tsunami generation and impact consequences has led us to develop a physics-based framework to seamlessly simulate the event from source (asteroid entry) to ocean

impact (splash) to long wave generation, propagation, and inundation of the shoreline. The non-linear effects of the asteroid impact on the ocean surface are simulated using the hydrocode GEODYN to create the impact source for the shallow water wave propagation code, SWWP. The GEODYN-SWWP coupling is based on the structured adaptive mesh refinement infrastructure; SAMRAI developed at LLNL and has been used in FEMA table-top exercises conducted in 2013 and 2014, and more recently, the 2015 Planetary Defense Conference exercise in Italy. We illustrate capabilities of this methodology by providing results of tsunami generation for different locations of asteroid impact off the East Coast of the United States, in the Gulf of Mexico, and near San Francisco. Often the size of the asteroid is not deterministically known; thus we explored the effect of asteroid size on the tsunami and landfall waves at several coastline cities of interest near the potential impact area. We construct the probability of wave height given the size of the asteroid and the location of the impact along the risk corridor. Such probability profiles can inform more sophisticated inundation models and advise emergency responses and disaster-mitigation efforts, and may be used for design of maritime protection (*e.g.* breakwaters walls) or assessment of risk to shoreline structures of interest (*e.g.* bridges, power plants).

This work was performed under the auspices of the U.S. Department of Energy by Lawrence Livermore National Laboratory under Contract DE-AC52-07NA27344.

### **Tsunami Debris Boat Forges Japan—California Connections and Promotes Tsunami Education Efforts**

DENGLER, L. A., Humboldt State University, Arcata, CA, USA

An estimated 1.5 million tons of debris were caught the Pacific-wide gyre system following the March 2011 tsunami. Debris began arriving on the West Coast of North America in spring 2012 and more than 2000 possible tsunami debris sightings have been reported to NOAA's tsunami debris web site since then. About sixty items have been verified as tsunami debris including a boat that beached near Crescent City in April 2013. Through the efforts of a group of California High School students, diplomatic efforts, and donations, the boat was returned to Japan in October 2014. The boat functions as a "social object", an item that sparks a common chord in people and make them want to interact with others and facilitate "milling", an essential first step in taking preparedness actions. The boat has become a celebrity in both the United States and Japan, featured in a Facebook film and as a display in Tokyo's National Museum. It has forged student exchanges and a sister school relationship between the high schools and communications between the two tsunami-vulnerable cities. A bilingual children's book "The Extraordinary Voyage of Kamome. A Tsunami Boat Comes Home" was published in November 2015. The book and an associated web site aimed for elementary grades, provides a window for discussing earthquakes, tsunamis, marine debris, preparedness and cultural awareness in the classroom and within families in a positive way. Over the next two years, we plan to develop further develop the web site to include interactive curriculum for use in the classroom and by families.

---

## **Advancements in Network Operations and Station Design**

Oral Session · Thursday · 1:30 PM · 21 April · Tuscany 7/8

Session Chairs: Kristine Pankow and David Wilson

---

### **Theoretical Limits on Detectability of Small Earthquakes**

KWIATEK, G., GFZ German Research Centre for Geosciences, Potsdam, Germany, [kwiatek@gfz-potsdam.de](mailto:kwiatek@gfz-potsdam.de); BEN-ZION, Y., University of Southern California, Department of Earth Sciences, Los Angeles, CA, USA

We investigate theoretical limits on detectability of small earthquakes ( $M_w$  -3.0 to 5.0) using synthetic seismograms for shear/tensile dislocations on kinematic circular ruptures, observed seismic noise and properties of several acquisition systems (instrument response, sampling rate). Simulated source time functions for shear/tensile dislocation events with different magnitudes, stress drops and rupture velocities provide estimates for the amplitude and frequency content of P and S phases at various observation angles. The source time functions are convolved with a Green's function for a homogeneous solid with given P, S attenuation coefficients and a given instrument response. The synthetic waveforms are superposed with average levels of the observed ambient seismic noise up to 1 kHz. The combined seismograms are used to calculate signal-to-noise ratios and expected frequency content of P and S phases at various locations. The results provide guidelines on designing local/regional seismic networks for detection of small events in various geological environments, and information relevant to analyses of earthquake source properties.

### **Detecting and Locating Seismic Events Without Phase Picks or Velocity Models**

ARROWSMITH, S. J., Sandia National Laboratories, Albuquerque, NM, USA, [sjarrow@sandia.gov](mailto:sjarrow@sandia.gov); YOUNG, C., Sandia National Laboratories, Albuquerque, NM, USA, [cjyoung@sandia.gov](mailto:cjyoung@sandia.gov); BALLARD, S., Sandia National Laboratories, Albuquerque, NM, USA, [sballar@sandia.gov](mailto:sballar@sandia.gov); SLINKARD, M., Sandia National Laboratories, Albuquerque, NM, USA, [meslink@sandia.gov](mailto:meslink@sandia.gov)

The standard paradigm for seismic event monitoring is to scan waveforms from a network of stations and identify the arrival time of various seismic phases. A signal association algorithm then groups the picks to form events, which are subsequently located by minimizing residuals between measured travel times and travel times predicted by an Earth model. Many of these steps are prone to significant errors which can lead to erroneous arrival associations and event locations. Here, we revisit a concept for event detection that does not require phase picks or travel time curves and fuses detection, association and location into a single algorithm. Our pickless event detector exploits existing catalog and waveform data to build an empirical stack of the full regional seismic wavefield, which is subsequently used to detect and locate events at a network level using correlation techniques. Because the technique uses more of the information content of the original waveforms, the concept is particularly powerful for detecting weak events that would be missed by conventional methods. We apply our detector to seismic data from the University of Utah Seismograph Stations network and compare our results with the earthquake catalog published by the University of Utah. We demonstrate that the pickless detector can detect and locate significant numbers of events previously missed by standard data processing techniques.

### **Semi-Auto Picking Using Array Seismogram Volume**

SHIMODA, N., Free University of Berlin, Berlin, Germany, [shimoda@geophysik.fu-berlin.de](mailto:shimoda@geophysik.fu-berlin.de); RESHETNIKOV, A., Free University of Berlin, Berlin, Germany, [anton@geophysik.fu-berlin.de](mailto:anton@geophysik.fu-berlin.de); SHAPIRO, S. A., Free University of Berlin, Berlin, Germany, [shapiro@geophysik.fu-berlin.de](mailto:shapiro@geophysik.fu-berlin.de)

Thousands of microseismic events are observed with arrays of geophones in a shale gas field. A number of arrays is limited because array layout is constrained by borehole geometries and monitoring costs. It is important to process details among geophones in the same array. Acquired seismograms are processed automatically to get hypocenter locations and magnitudes. To improve quality of the results, time-consuming manual processes, including P and S picking, are required.

PHASE consortium of Free University of Berlin has developed Common Receiver Gather (CRG) so far to achieve quick picking and pick validation. CRG consists of seismograms which are acquired at the same geophone during the same fracking stage. The event sequence is determined by Cross Correlation (CC) coefficients among the event seismograms. The time datum for each seismogram is based on CC lag times. Neighboring seismograms have a lot of similarity in CRG, therefore it is easier to identify P, S phases and other reflected waves.

Array Seismogram Volume (ASV) newly we proposed is combination of Shot Gather and CRG. In ASV, X-axis is Events, Y-axis is Receivers in the array, Z-axis is time. To get clear sight for phase identification, the events should be limited to which have enough similarity. We select one origin event and the 1st relative events which have more than 0.55 CC coefficient with the origin event. Additionally, events which have more than 0.60 CC coefficient with 1st relatives are selected as the 2nd relatives. The cutoff CC coefficient would be depended on data quality. Too high values provide very few events ASV, and too low values cause difficulties of phase interpretation. ASV outlook is similar to 3D reflection survey data in horizontal layered structure. Picking P and S on one trace, auto-pick process using CC can be applied to whole other events in ASV. In this presentation, we show the result of SAV application to real shale gas field dataset.

### **Near Real-time Discrimination of Quarry and Mining Related Seismicity in the Central and Eastern United States**

YECK, W. L., NEIC, Golden, CO, USA, [wyeck@usgs.gov](mailto:wyeck@usgs.gov); BENZ, H. M., NEIC, Golden, CO, USA, [benz@usgs.gov](mailto:benz@usgs.gov); EARLE, P. S., Golden, CO, USA, [pearle@usgs.gov](mailto:pearle@usgs.gov)

The recent increase in seismic station density in the Central and Eastern United States (CEUS) enables the United States Geological Survey's National Earthquake Information Center (NEIC) to significantly lower the earthquake detection threshold. Due to the abundance of small magnitude (< M2.5) quarry and mine related seismicity in the CEUS, lowering the earthquake detection threshold results in a large increase in number of detected seismic events, and therefore requires improved discrimination procedures. As an example, a recent detailed investigation of Pennsylvanian seismicity over a two-year period found that only 11 events out of 1355 detected events were unrelated to mining activity (Homman, 2015). As the primary mission of the NEIC is to characterize earth-



quake source parameters, we investigate techniques to discriminate mining seismicity in real-time as part of the routine cataloging process. We explore the use of correlation detectors to build mine-station specific detectors, therefore allowing for the real-time identification and location of mine related seismicity. We compare multiple correlation detection techniques, including match-filtering and subspace detection. Our results suggest that correlation detectors can effectively reduce the burden to NEIC analysts imposed by mining events. We discuss our efforts to incorporate these techniques into the framework of real-time operations at the NEIC.

#### References:

Homman, K. A. (2015), Seismicity in Pennsylvania, Masters Thesis, Pennsylvania State University.

### Small-aperture Seismic Array Data Processing using the Representation of Seismograms at Zero-amplitude Points

BROKESOVA, J., Faculty of Mathematics and Physics, Charles University, Prague, Czech Republic, Johana.Brokesova@mff.cuni.cz; MALEK, J., Institute of Rock Structure and Mechanics, AS CR, Prague, Czech Republic, malek@irms.cas.cz

We have developed a complex new algorithm for interpretation seismograms from small-aperture seismic arrays. It combines several well-known methods with new features. It is a robust, fast, efficient tool that can be applied easily to most of the existing arrays. The core of the algorithm is the approximation of the seismograms (expressed as ground-motion velocity) by a set of nearly monochromatic signals represented by precise times of zero-amplitude and/or extremal points and by the values of the ground-motion first derivative (acceleration) and/or the extremal values at those points. Extremal points of ground velocity coincide with zero-amplitude points of acceleration. Thus, we call our method the zero-amplitude representation. It enables identification of seismic waves propagating across the array and determination of wave properties, namely their true backazimuths and apparent velocities along the surface. The new technique is demonstrated both on synthetic and real examples. For real-data examples a strong and a major earthquake, recorded by the small-aperture array around the gas storage field at Haje-Pribram (Czech Republic) is taken into account: the Nepal earthquake of April 25, 2015,  $M_w$  7.8, about 6310 km from the array. We also derived rotational seismograms by the array-derived rotation method, and computed the apparent velocities and backazimuths via the zero-amplitude representation. These results all agree well with those obtained using both rotational and translational seismograms.

### New Research and Monitoring Opportunities with the Central and Eastern United States Seismic Network

SUMY, D. E., Incorporated Research Institutions for Seismology, Washington, DC, USA, danielle.sumy@iris.edu; BUSBY, R. W., Incorporated Research Institutions for Seismology, Washington, DC, USA, busby@iris.edu; WOODWARD, R. L., Incorporated Research Institutions for Seismology, Washington, DC, USA, woodward@iris.edu; BRUDZINSKI, M., Miami University of Ohio, Oxford, OH, USA, brudzimr@miamioh.edu

Recent earthquakes, such as the 2011 M5.8 Virginia earthquake, raised awareness of the comparative lack of knowledge (relative to the western US) about seismicity, site response to ground shaking, and the basic geologic underpinnings in this densely populated region. Several federal agencies, along with the IRIS Consortium, recognized the unique opportunity to retain EarthScope Transportable Array (TA) seismic stations beyond the standard two-year deployment as the Central and Eastern US Seismic Network (CEUSN; network code N4).

The CEUSN encompasses 159 broadband stations, nearly 40 with strong motion sensors. Former TA stations were selected for inclusion in the CEUSN based on location, with priority on regions of elevated seismic hazard that have not been traditionally heavily monitored and in regions proximal to nuclear power plants and other critical facilities. Stations were also selected to improve the overall spatial coverage of seismic stations in the CEUS, and transmit data in real time at 100 samples per second. The CEUSN, together with the existing backbone coverage of permanently operating seismometers in the CEUS, form a network of over 300 broadband stations.

The CEUSN stations all utilize the highly uniform TA station design, which facilitates efficient deployment, operation, and utilization of the data. Stations use simple vaults that provide low-noise performance in a wide range of terrains. Stations are autonomously powered and are never hardwired to communications links, which eliminates potential failures due to umbilical connections to the outside world. Automated analysis of station state-of-health channels contributes to the overall performance of the network, and the full 400 TA station

array routinely delivered over 99% data availability in real-time. Station calibration procedures validate station installation and performance, and over time, the design has been carefully evolved to enhance station performance.

### Field Studies of Non-double-couple and Mixed-source Proximal Earthquakes at The Geysers and Long Valley, California: Arrays and Experiments

EVANS, J. R., U.S. Geological Survey, Menlo Park, CA, USA, jrevans@usgs.gov; BROKESOVÁ, J. P., Charles University, Prague CZ, johana@karel.troja.mff.cuni.cz; MÁLEK, J., Czech Academy of Sciences, Prague CZ, malek@irms.cas.cz; HARTLINE, C., CalPine Corp, Healdsburg, CA, USA, Craig.Hartline@calpine.com; WILKINSON, S. K., U.S. Geological Survey, Mammoth Lakes, CA, USA, swilk@usgs.gov

We describe Rotaphone sensors and their abilities, locations in two field deployments, and experiments being performed with those data. Rotaphones are 6-degree-of-freedom (6DOF) sensors with 8 horizontal and 8 vertical 4.5-Hz geophones arranged in a 40-cm diameter ring; those we are using are of a mature 3rd design. By computation, these 16 channels yield 6DOF axes (3 translation and 3 rotation) with 4.5-Hz geophone responses. Brokešová and Málek developed the Rotaphone and method of computing 6DOF records from the raw signals; their technique uses precise relative calibrations, and summing or differencing signals across the ring. To date, we have used 2 of these Rotaphones at The Geysers in a huddle test (adjacent on a common foundation) to verify performance and perform 1-site studies. We have begun a deployment of 2 Rotaphones at Long Valley, shortly to be supplemented by a 3rd. In both cases, we anticipate that some of our target earthquakes will have large rotational components caused by non-double-couple or mixed sources. Both field locations have many such events and many of them within 1-2 km of the instruments at depths <3 km. We also anticipate studying events at ~20 km to evaluate single-site determinations of phase velocity (possible with one 6DOF site), and comparing these to array-determined velocities. If the methods are comparable, the single-station 6DOF method may simplify strong-motion site characterization. Last, we may test an hypothesis that larger-than-computed rotational motions seen at surface-emplaced strong-motion instruments may arise from very shallow material properties—unconsolidated, cracked, bioturbated materials, which often have extremely low wave speeds (<<1 km/s) and may have highly nonlinear elastic properties. This last experiment will be done by comparing records from a Rotaphone vaulted (~4-m deep) to another installed directly above it on a traditional grade-level concrete slab.

### Remote Determination of the In Situ Sensitivity of Galperin-Orientation Broadband Seismometers

HELLWEG, M., UC Berkeley Seismological Lab, Berkeley, CA, USA, peggy@seismo.berkeley.edu; UHRHAMMER, R. A. U., UC Berkeley Seismological Lab, Berkeley, CA, USA, bob@seismo.berkeley.edu; TAIRA, T., UC Berkeley Seismological Lab, Berkeley, CA, USA, taira@seismo.berkeley.edu

The sensitivity of a broadband seismometer with Galperin sensor orientation like an STS-2 can be determined remotely by two basic methods: 1) comparing its inferred ground motions with a reference seismometer, and 2) by exciting its calibration coil with a simultaneously recorded stimulus signal. The first method is limited by the accuracy of the reference seismometer and the second by the accuracy of the motor constant ( $G_c$ ) of the calibration coil. Both methods are also influenced by the signal-to-noise ratio (SNR) in the presence of background seismic noise and the degree of orthogonality of the tri-axial suspension in the seismometer.

For the STS-2, the manual gives the signal coil sensitivity (Gs) as  $1500 \pm 1.5\%$  V/(m/s) and  $G_c$  to only one decimal place (ie,  $G_c = 2$  g/A). The factory precision of  $G_c$  is not sufficient to determine the sensitivity of Gs to within 1.5%. Thus we need to determine  $G_c$  to enable allow calibration of the STS-2 via remote excitation of the  $G_c$  with a known stimulus.

The Berkeley Digital Seismic Network (BDSN) has 12 STS-2 seismometers with co-sited reference sensors (accelerometers) and they are all recorded by Q330HR data loggers with factory cabling. First we verify the sensitivity of the STS-2 signal coils (Gs) by comparing ground motions recorded by the STS-2 with those recorded by the co-sited strong motion accelerometer for an earthquake with high SNR in a common passband. Next we remotely (from Berkeley) excite the calibration coil with a 1 Hz sinusoid which is also recorded and, use the measured Gs values to solve for  $G_c$ . The resulting  $G_c$  values are typically 2.20-2.50 g/A (accurate to 3+ decimal places). Once the  $G_c$  values are found, the STS-2 absolute sensitivity can be determined remotely to better than 1% accuracy. The primary advantage of using strong motion accelerometers as the reference instrument is that their absolute calibration can be checked via tilt tests if the need arises.



### Detection and Characterization of Pulses in Broadband Seismometers

WILSON, D. C., USGS Albuquerque Seismological Laboratory, Albuquerque, NM, USA, [dwilson@usgs.gov](mailto:dwilson@usgs.gov); RINGLER, A. T., USGS Albuquerque Seismological Laboratory, Albuquerque, NM, USA, [aringler@usgs.gov](mailto:aringler@usgs.gov); HUTT, C. R., USGS Albuquerque Seismological Laboratory, Albuquerque, NM, USA, [bhutt@usgs.gov](mailto:bhutt@usgs.gov)

Pulsing, caused either by mechanical or electrical glitches, can significantly compromise the long period noise performance of broadband seismometers. High fidelity long period recordings are required for accurate calculation of quantities such as moment tensors,  $W$ -phase magnitudes, and normal mode measurements. Such pulses have long been recognized in accelerometers, and methods have been developed to correct these acceleration steps, but considerable work remains to be done to detect and correct similar pulses in broadband seismic data. We present a method for detecting and characterizing the pulses using data from a range of broadband sensor types installed in the Global Seismographic Network (GSN) and the Advanced National Seismic System (ANSS) backbone network. The technique relies on accurate instrument response removal and employs a moving window approach looking for acceleration baseline shifts. We find that pulses are present at varying levels in all sensor types studied. We compare mean long period noise values with pulse amplitude and frequency of occurrence. Our results delineate a maximum level of pulsing acceptable before long period recordings are significantly compromised.

### The Internet of Things: Geoscience-related Applications of Embedded Systems

SEPULVEDA, E., Baylor University, Waco, TX, USA, [frank\\_sepulveda@baylor.edu](mailto:frank_sepulveda@baylor.edu); PULLIAM, J., Baylor University, Waco, TX, USA, [jay\\_pulliam@baylor.edu](mailto:jay_pulliam@baylor.edu)

Consumers' awareness regarding the benefits of enhancing everyday objects with the ability to communicate, sense, and process information is rising due to the proliferation of commercial Internet of Things (IoT) devices. Easy-to-use, inexpensive, and relatively powerful Commercial-Off-The-Shelf (COTS) versions of the embedded technologies responsible for the rise of the IoT allow technological Do-It-Yourself enthusiasts (*i.e.*, IoT Makers) to create all manner of IoT devices. In this presentation we will discuss the emerging IoT technologies that would allow an IoT Maker, using skills common to geoscientists, to build their own IoT device; specifically, a geoscience-related IoT device capable of acquiring research-quality data. We begin with an overview of COTS embedded technologies. We continue with details regarding our integration of an embedded system (*i.e.*, Raspberry Pi 2 Model B) with a geoscience-related COTS data acquisition system (*i.e.*, REF TEK 130-01). Lastly, we highlight context-aware-computing and nodal processing applications that may benefit earthquake and engineering seismology.

---

### Active Tectonics, Faults and Large Earthquakes

Oral Session · Thursday · 8:30 AM · 21 April · Tuscany A  
Session Chairs: Sushil Kumar, Sudhir Rajaure, and Rama Sushil

---

### Geological Results and Archival Information on the Central Himalayan Earthquakes and Their Implications for Seismic Source Zones

RAJENDRAN, C. P., JN Centre for Advanced Scientific Research, Bangalore, Karnataka, India, [cprajendran@gmail.com](mailto:cprajendran@gmail.com); RAJENDRAN, K., Indian Institute of Science, Bangalore, Karnataka, India, [kusalaraj@gmail.com](mailto:kusalaraj@gmail.com); JOHN, B., National Institute of Rock Mechanics, Bangalore, Karnataka, India, [b\\_johnp@yahoo.co.in](mailto:b_johnp@yahoo.co.in); SANWAL, J., JN Centre for Advanced Scientific Research, Bangalore, Karnataka, India, [jaishrigeology@gmail.com](mailto:jaishrigeology@gmail.com); PARAMESWARAN, R., Indian Institute of Science, Bangalore, Karnataka, India, [revathy.parameswaranm@gmail.com](mailto:revathy.parameswaranm@gmail.com)

Combined historical and archeological information from India, Nepal and Tibet during last 1000 years suggests damaging earthquakes in the central Himalaya in AD 1255, 1344, 1505 1803 and 1833, although sources and magnitudes of some of these events remain less constrained. Evidence from trenches across the base of the Himalayan Frontal Thrust (HFT), suggests that the last great earthquake ( $M_w \geq 8.0$ ) in the Uttarakhand Himalaya (India) occurred between AD 1259 and 1433, and an earlier one between AD 1050 and 1250. The successive ruptures may have sourced on adjacent segments that overlapped at the trench site. The latter is also validated by the stalagmite data from the limestone cave situated on the duplex zone in the Kumaun Himalaya. Ruptures identified in the trench closely correlate with historical earthquakes of 1255 and 1344, and the former was reportedly more damaging in central Nepal. The trenches, however,

did not reveal any evidence of the 1803 ( $M_w \geq 7.5$ ) or 1505 ( $M \geq 7.5$ ) earthquakes. It is likely that the 1803 earthquake ruptured near the town of Uttarkashi, coinciding with a zone of rapid uplift, which has been linked to the emerging ramp-flat system of the Main Himalayan Thrust. Unlike the 1803 earthquake, the rupture extent of Tibet-Nepal border event of 1505 remains less constrained and other than the Tibetan sources, no contemporary damage reports on this earthquake have been obtained from the Indian side or Nepal. Our data suggest that while the frontal thrust in central Himalaya may have remained unruptured during the last ~700 years the hinterland structure (*e.g.* the duplex zone developing in the proximal part of the Main Himalayan Thrust) in the central Himalaya may have been relatively more active in generating major earthquakes ( $M_w \geq 7.5$ ). This distinction must be taken into consideration while evaluating the seismic hazard of the central Himalaya.

### Macroseismic Intensity Assignments in Kathmandu Valley for the 2015 M7.8 Gorkha, Nepal Earthquake Based on Structural Damage Statistics

MCGOWAN, S. M., USGS, Golden, CO, USA, [smcgowan@usgs.gov](mailto:smcgowan@usgs.gov); JAISWAL, K. S., USGS, Golden, CO, USA, [kjaiswal@usgs.gov](mailto:kjaiswal@usgs.gov); WALD, D. J., USGS, Golden, CO, USA, [wald@usgs.gov](mailto:wald@usgs.gov)

The April 25, 2015  $M_w$ 7.8 Gorkha, Nepal earthquake caused significant loss of life and property in Central Nepal. Several strong ground motion instruments were operational in the Kathmandu Valley at the time of the mainshock, yet the data from only one (USGS KATNP station, a soil site) has been publicly available. To supplement the paucity of recordings, we assigned engineering damage classifications based on geolocated photographs of damaged and undamaged buildings from six different areas of the Kathmandu Valley chosen to each fall within 1 km of known seismic stations. After investigating the extent of structural and non-structural damage to over 300 buildings, we assigned 1998 European Macroseismic Scale (EMS-98) damage grades on a building-by-building basis. We applied EMS-98 procedures to aggregate/average these damage grades for a given location. We focused on damage to three specific building categories: a) low/mid-rise reinforced concrete frames with infill brick walls, b) unreinforced brick masonry bearing walls with reinforced concrete slabs, and c) unreinforced brick masonry bearing walls with timber framing. Evaluating dozens of photos of each construction category and individually assigning damage grades to each building (damaged or undamaged) produced a statistically-derived estimate of macroseismic intensity for that location. This analysis concludes that EMS-98 macroseismic intensities for the six study areas resulting from the Gorkha mainshock typically peaked in the VII-VIII range. While not immune from introducing a degree of subjectivity, this assignment process is more rigorous and objective than the more common approach of assigning intensities based upon anecdotal media or first-person accounts of shaking and damage. When the additional strong motion data become available, we can compare our detailed damage observations associated with three archetypical building types in the Kathmandu Valley with specific recorded ground motion parameters.

### Seismic Structure Beneath the Great Valley, Central California: Implications for the Tectonic Origin of the Isabella Anomaly

DOUGHERTY, S. L., U.S. Geological Survey, Pasadena, CA, USA, [sdougherty@usgs.gov](mailto:sdougherty@usgs.gov); HOOTS, C. R., University of New Mexico, Albuquerque, NM, USA, [charleshoots@gmail.com](mailto:charleshoots@gmail.com); HANSEN, S., University of New Mexico, Albuquerque, NM, USA, [stevehansen@unm.edu](mailto:stevehansen@unm.edu); SCHMANDT, B., University of New Mexico, Albuquerque, NM, USA, [bschmandt@unm.edu](mailto:bschmandt@unm.edu); CLAYTON, R. W., California Institute of Technology, Pasadena, CA, USA, [clay@gps.caltech.edu](mailto:clay@gps.caltech.edu)

The tectonic origin of the Isabella high-velocity anomaly in the upper mantle beneath California's southern Great Valley is unclear. Previous low-resolution seismic imaging studies of the region have been unable to identify the structural connection between this anomaly and the overlying lithosphere. The two dominant hypotheses attribute the Isabella anomaly to a fossil slab or the foundered lithospheric root of the Sierra Nevada batholith. The Central California Seismic Experiment (CCSE) was designed to distinguish between these hypotheses. We present results from the CCSE, which consisted of 44 broadband seismometers deployed in a linear array spanning from the Pacific coast, across the Great Valley, to the Sierra Nevada foothills. Forward modeling of the 2D structure of the crust is performed using local earthquakes recorded by the CCSE to provide constraints on the geometry and seismic velocity of the Great Valley. This sedimentary basin is thought to be filled with very low velocity material at shallow depths and partially underlain by a high-velocity ophiolite body. Hence, a well-constrained basin structure will be important in migrating receiver function and future surface wave tomography images to depth. The impact of the Great Valley basin structure on body waves is evident by an observed delay in P-wave arrival times on the radial component for stations located within the basin, indi-

cating a P-to-S conversion. Surface waves along the CCSE array also show a distinct slowing by the valley at periods <10 sec. Teleseismic events recorded by the CCSE reveal scattered waves arriving tens of seconds after the S-wave, which can be mapped to scattering points outlining an East-dipping structure at depth. A potential East-dipping interface in the upper mantle beneath the Great Valley is also seen in initial Ps and Sp receiver function images. The location and orientation of this structure is consistent with a fossil slab origin for the Isabella anomaly.

### **UCERF3-ETAS: Including Spatiotemporal Clustering for a California Operational Earthquake Forecast**

FIELD, E. H., USGS, Golden, CO, USA, field@usgs.gov

The Working Group on California Earthquake Probabilities (WGCEP) has been developing the third Uniform California Earthquake Rupture Forecast (UCERF3). With the long-term, time-dependent model published, which relaxes segmentation, includes multi-fault ruptures, and incorporates elastic rebound, we have now turned our attention to including spatiotemporal clustering. Recognizing that triggered events can be large and damaging, the ultimate goal is to deploy an Operational Earthquake Forecast (OEF) for California, now listed as one of the USGS's strategic-action priorities (<http://pubs.usgs.gov/of/2012/1088>; page 32). This presentation will demonstrate progress thus far on building a prototype, wherein we have added an Epidemic Type Aftershock Sequence (ETAS) component to UCERF3 (UCERF3-ETAS). Notably, our model represents a merging of ETAS with finite-fault based forecasts, as well as the inclusion of elastic rebound (both firsts, as far as we are aware). In fact, inclusion of elastic-rebound turns out to be critical in terms of replicating spatiotemporal clustering statistics (otherwise ~85% of large triggered events re-rupture the same fault, which we don't see in nature). Likewise, faults also need to exhibit characteristic magnitude-frequency distributions in order to produce reasonable results. This presentation will also outline efficient loss calculations and additional steps needed for taking UCERF3-ETAS operational.

### **Understanding of Active Tectonics of Himalayan Frontal Fault System in Northern India using Micro and Paleo Seismic Studies**

KUMAR, S., Wadia Institute of Himalayan Geology, Dehradun, Uttarakhand, India, sushil\_rohella@yahoo.co.in

The Himalaya overrides the Indian plate along a decollement fault, referred as the Main Himalayan Thrust (MHT). The 2400 km long Himalayan mountain arc in the northern boundary of the Indian sub-continent is one of the most seismically active regions of the world. The Himalayan Frontal Thrust (HFT) is characterized by an abrupt physiographic and tectonic break between the Himalayan front and the Indo-Gangetic plain. The HFT represents the southern surface expression of the MHT on the Himalayan front. The tectonic zone between the Main Boundary Thrust (MBT) and the HFT encompasses the Himalayan Frontal Fault System (HFFS). The zone indicates late Quaternary-Holocene active deformation. Late Quaternary intramontane basin of Dehradun flanked to the south by the Mohand anticline lies between the MBT and the HFT in Garhwal Sub Himalaya. Slip rate 13-15 mm/yr has been estimated on the HFT based on uplifted strath terrace on the Himalayan front (Wesnousky *et al.* 2006). An out of sequence active fault, Bhauwala Thrust (BT), is observed between the HFT and the MBT. The Himalayan Frontal Fault System includes MBT, BT, HFT and PF active fault structures (Thakur, 2013). The HFFS structures were developed analogous to proto-thrusts in subduction zone, suggesting that the plate boundary is not a single structure, but series of structures across strike. Seismicity recorded by WIHG shows a concentrated belt of seismic events located in the Main Central Thrust Zone and the physiographic transition zone between the Higher and Lesser Himalaya. However, there is quiescence in the Himalayan frontal zone where surface rupture and active faults are reported. GPS measurements indicate the segment between the southern extent of microseismicity zone and the HFT is locked. The great earthquake originating in the locked segment rupture the plate boundary fault and propagate to the Himalaya front and are registered as surface rupture reactivating the fault in the HFFS.

### **Comprehensive Comparison of the Campbell-Bozorgnia NGA-West2 and Three Pan-European Ground Motion Models**

CAMPBELL, K. W., CoreLogic Inc., Oakland, CA, USA, kcampbell@corelogic.com.

In 2006 we compared our newly developed Next Generation Attenuation (NGA-West1) ground-motion prediction equation (GMPE) with a contemporary GMPE developed for active crustal regions of Europe and the Middle East (pan-Europe) and proposed that our NGA GMPE could be used to estimate ground motions in these regions. Later studies by a number of investigators confirmed

that the NGA GMPEs were generally consistent with both available pan-European GMPEs and European strong-motion data. As a follow-up of that study, we perform a detailed comparison of our 2014 NGA-West2 GMPE with three newly developed GMPEs for the pan-European region. The comparisons are performed in terms of median predictions, standard deviations, and residual analyses with respect to our NGA-West2 database. These comparisons indicate that the scaling characteristics of the GMPEs are generally comparable in terms of attenuation and linear site response, but differ in terms of magnitude scaling, source-depth scaling, style-of-faulting effects, and nonlinear site effects. These differences are minimal for global moderate-to-large-magnitude events and are not found to be statistically significant for the pan-European events of similar magnitude in our database. These results lead us to suggest that our NGA-West2 GMPE can be used to estimate ground motions from moderate-to-large-magnitude earthquakes in Europe and the Middle East as a means of more reliably extending these estimates to large magnitudes and short distances of greater engineering interest and to include ground-motion scaling features that are not currently included in pan-European GMPEs because of insufficient data.

### **Fragility of Precariously-Balanced Rocks at Double Rock Site, Diablo Canyon Power Plant**

STIRLING, M. W., Geology Department, University of Otago, Dunedin, New Zealand, mark.stirling@otago.ac.nz; DELLA PASQUA, F. N., GNS Science, Lower Hutt, New Zealand, f.dellapasqua@gns.cri.nz; MADUGO, C. M., Pacific Gas and Electric Company, San Francisco, CA, USA; ABRAHAMSON, N. A., Pacific Gas and Electric Company, San Francisco, CA, USA

We report on recent work undertaken to quantify the fragility of precariously-balanced rocks (PBRs) in the vicinity of Diablo Canyon Power Plant (DCPP), coastal central California. PBRs and other fragile geological features presently provide the only means of testing suites of probabilistic seismic hazard curves at the low probability levels important for critical facilities. If the PBRs are fragile enough and old enough, then the information from the PBRs can be used to reject some of the epistemic uncertainty branches, leading to updated hazard estimates.

Seven PBRs exist on the sides of paleo-seastacks at the Double Rock site (southeast of DCPP). The paleo-seastacks rest on uplifted marine terraces with an estimated 80-120,000 year age range. The fragilities of three PBRs are characterized by the threshold peak ground accelerations (PGAs) that cause toppling failure. The toppling PGAs are estimated using simple methods based on the PBR geometries, as well as finite-element models for one of the PBRs. Toppling PGAs in the range of 0.2-0.4g are obtained. These PGAs have relatively short return periods of approximately 200-700 years based on the DCPP hazard curve, indicating that they may provide valuable constraints on the hazard curve at DCPP, depending on their ages. In the coming year, our models of the fragilities will be further verified by field and finite-element methods, and the age of at least one of the PBRs will be obtained in order to ascertain whether the PBRs are old enough to provide meaningful constraints on the DCPP hazard estimates. As we move to fully non-ergodic ground motion models at DCPP, the epistemic uncertainty in hazard will initially increase and additional constraints, such as those provided by PBRs, will be key for reducing the epistemic uncertainty range.

### **Sensitivity of Rupture Propagation to Nucleation Location and Slip Partitioning on the Imperial and Southern San Andreas Faults.**

KYRIAKOPOULOS, C., University of California, Riverside, CA, USA, christos@ucr.edu; MELTZNER, A. J., Earth Observatory of Singapore, Singapore; ROCKWELL, T. K., San Diego State University, San Diego, CA, USA; OGLESBY, D. D., University of California, Riverside, CA, USA

The large stepover region between the Southern San Andreas fault (SAF) and the Imperial fault (IF) has a great deal of seismic activity, which may suggest that there may exist faulting cross structures that link the two main faults. Paleoseismological data have indicated that the two most recent events along the southern SAF are indistinguishable from rupture on IF. Thus, it is an important question whether rupture could propagate between these two faults. If linking fault structures exist, what is the role of complex fault structure in potential stepover rupture? The stepover region between the two faults includes Mesquite Basin, a pull-apart between the IF and the Brawley fault zone (BFZ). North of the surface traces of the IF and BFZ, but south of Bombay Beach, microseismicity defines an elongate region known as the Brawley Seismic Zone (BSZ), that stretches NNW to SSE, from Bombay Beach to Mesquite Basin. At depth, microseismicity suggests further structural complexity, with numerous cross faults. No through-going southeastward extension of the SAF or northward extension of the IF or BFZ has yet been identified, and ruptures are generally considered unlikely to propagate through stepovers wider than 4-8 km. Furthermore, dynamic earthquake models suggests that the detailed geometry of a stepover, determines whether the stepover will allow or obstruct rupture propagation.

Here we are using the 3D finite element code FaultMod (Barall, 2009) in order to run a series of experiments that will help us investigate the sensitivity of rupture propagation to nucleation location, and the partitioning of slip across the faults. Our preliminary results indicate that if there are through-going fault structures between the main faults, rupture may propagate between the SAF and IF, and even across cross-faults connecting the two structures. We will discuss implications for fault rupture, ground motion, and seismic hazard in the region.

#### **Imaging 2015 Mw 7.8 Gorkha Earthquake and Its Aftershocks using Multiple Global Seismic Arrays**

GHOSH, A., University of California, Riverside, CA, USA, aghosh.earth@gmail.com; LI, B., University of California, Riverside, CA, USA, bli017@ucr.edu

Gorkha earthquake is the most well recorded event so far in the Himalayas. We use multiple global seismic arrays at teleseismic distances to image rupture propagation of the mainshock, and aftershock activities that follows. We use a back-projection technique to track rupture propagation using 4 completely independent seismic arrays. The arrays are calibrated using an empirical self-consistent spatial correction method. Four arrays generally agree and show consistent results. They reveal unidirectional rupture propagating west to east at an average velocity of 2 km/sec. The Gorkha event ruptures about ~120 km alongstrike for ~60 sec. The high frequency sources as imaged by the arrays are shifted downdip of the major slip patches resolved by inversion of lower frequency seismic data [Avouac *et al.*, 2015]. This also means an increased distance between Kathmandu and the high frequency sources, a major cause of damage to the structures. It partly explains lower than expected ground motion in Kathmandu valley. Interestingly, the rupture shows two branches at the late stage. It appears that before the rupture is arrested at the eastern end, it swerves around a strong patch leaving the patch unbroken. This patch is eventually broken after about two weeks producing the largest aftershock following the mainshock. In addition, we are scanning continuous seismic data to detect and locate aftershocks using the same global arrays. So far, we have detected twice as many aftershocks compared to a comprehensive global catalog. Random visual checks confirm number of newly detected events using nearby seismic stations. Broadly, aftershock pattern obtained by arrays look similar to the global catalog. But the array catalog provides new details helpful to understand dynamics of stress redistribution via aftershock activity. Multiple global seismic arrays, when combined in a self-consistent way, can provide high-resolution image of rupture propagation and aftershock distribution.

#### **Imaging Coseismic Deformation from Large Thrust Earthquakes on the Edges of the Tibetan Plateau with Geodetic and Seismic Data**

FIELDING, E. J., Jet Propulsion Laboratory, California Institute of Technology, Pasadena, CA, USA, Eric.J.Fielding@jpl.nasa.gov; LIANG, C. R., Jet Propulsion Laboratory, California Institute of Technology, Pasadena, CA, USA; HUANG, M. H., Jet Propulsion Laboratory, California Institute of Technology, Pasadena, CA, USA; SANGHA, S., Jet Propulsion Laboratory, California Institute of Technology, Pasadena, CA, USA; YUE, H., Seismological Laboratory, California Institute of Technology, Pasadena, CA, USA; AGRAM, P. S., Jet Propulsion Laboratory, California Institute of Technology, Pasadena, CA, USA; YUN, S. H., Jet Propulsion Laboratory, California Institute of Technology, Pasadena, CA, USA; SAMSONOV, S. V., Natural Resources Canada, Ottawa, ON, Canada; SIMONS, M., Seismological Laboratory, California Institute of Technology, Pasadena, CA, USA; PELTZER, G., JPL, Caltech, Pasadena, CA, USA; OWEN, S., JPL, Caltech, Pasadena, CA, USA; MOORE, A., JPL, Caltech, Pasadena, CA, USA

Four large  $M > 7$  thrust earthquakes have struck the edges of the Tibetan Plateau in the last decade: the 2005  $M 7.6$  Kashmir, the 2008  $M 7.9$  Wenchuan, and the 2015  $M 7.8$  Gorkha Earthquakes along with the 2015  $M 7.3$  Kodari Earthquake that was an aftershock of Gorkha. Each of these events ruptured thrust faults that are parts of the shortening in the Himalayas and Longmen Shan. The Kashmir and Wenchuan Earthquakes both ruptured relatively steeply dipping faults with major surface ruptures, while the two Nepal earthquakes of 2015 both ruptured deeper faults with shallow dips and did not cause significant surface ruptures. The Wenchuan Earthquake likely included some deeper slip on a shallowly dipping fault in addition to the main rupture near the surface. These events show the variety of coseismic slip of major earthquakes in the region. We integrate geodetic measurements from Global Positioning System (GPS) data and synthetic aperture radar (SAR) satellite images to image the three-dimensional vector fields of coseismic surface deformation for these four large events. We analyzed SAR data from the ALOS, ALOS-2, Sentinel-1A, Envisat, and RADARSAT-2 satellites. We combine less precise analysis of large scale displacements from the SAR images of the three satellites by pixel offset tracking or sub-pixel correlation,

including the along-track component of surface motion, with the more precise SAR interferometry (InSAR) measurements in the radar line-of-sight direction and with seismic waveforms. The InSAR measurements show that there was no detectable slip on the shallower part of the Main Himalayan Thrust up-dip from the large coseismic slip or on other thrust faults in the Himalayas, except for one area of very shallow triggered slip of up to 5 cm on a thrust to the north of the Himalayan Frontal Thrust, during the two events. The early Nepal interferograms appear to rule out any shallow afterslip up-dip from the mainshock and aftershock ruptures at the time of this writing.

#### **Neotectonics of Java, Indonesia: Crustal Deformation in the Overriding Plate of an Orthogonal Subduction System**

MARLIYANI, G. I., Arizona State University, Tempe, AZ, USA, gayatri.marliyani@asu.edu; ARROWSMITH, J. R., Arizona State University, Tempe, AZ, USA, ramon.arrowsmith@asu.edu; HAQ, S. S. B., Purdue University, West Lafayette, IN, USA, shaq@purdue.edu

Shallow earthquakes in the overriding plate of subduction zones can be devastating due to their proximity to population centers despite their smaller source areas than the megathrust. Damaging effects are greater in the volcanic arc, as in Java, as ground shaking is amplified by surficial deposits of unconsolidated volcaniclastic sediments. Identifying the upper-plate structures and their potential hazards is key for minimizing the dangers they pose and is an important overall contribution to subduction zone research. Our field- and remotely-based mapping of active faults and folds in Java, supplemented by results from our paleoseismic study and physical models of the system, suggest that Java's deformation is distributed over broad areas along small-scale structures. Java is segmented into three main zones based on distinctive structural patterns. East Java is dominated by NW-SE normal faults, Central Java by E-W folds and thrust faults, while NE-SW strike-slip faults dominate West Java. We evaluate controls on strain partitioning and localization using sandbox modeling aided by digital image correlation. We track surface motions of the models to determine the deformation fields and interpret the style and distribution of expected earthquakes. The strain in response to collision is partitioned into thrusting and strike slip faulting. The thrust faults are approximately normal to the plate margin while the strike slip faults are parallel to it. The models enable us to evaluate parameters, identified by field observations, to assess their relative importance in governing Java's pattern of deformation. Our models test the effects of convergence obliquity, geometry, preexisting weaknesses, asperities and the lateral strength contrast and suggest that slight variations in convergence obliquity does not affect the deformation pattern significantly while the margin shape, lateral strength contrast and perturbation of deformation from asperities does.

#### **Crustal Response to Spatiotemporal Variations of Coseismic Slip along the Combined 1999 Izmit-Düzce Rupture**

BOHNHOFF, M., GFZ Potsdam, Potsdam, Germany, bohnhoff@gfz-potsdam.de; ICKRATH, M., GFZ Potsdam, Potsdam, Germany, michele.ickrath@gmx.de; DRESEN, G., GFZ Potsdam, Potsdam, Germany, dre@gfz-potsdam.de

The North Anatolian Fault Zone (NAFZ) in NW Turkey as one of the most active and best studied strike-slip faults provides a unique opportunity to study earthquake related relaxation processes through analyzing co- and postseismic deformation thereby providing key information for the understanding of rock rheology. We study the spatial and temporal distribution of seismicity related to the two consecutive 1999  $M > 7$  Izmit and Düzce earthquakes. A high-resolution aftershock catalogue including more than 10,000 hypocenters extending along the combined rupture zone and extending from prior to the Izmit event to after the Düzce event is studied. Spatial and temporal distribution of events allow to identify distinct seismically active and inactive fault patches. Their location is related to the co- and postseismic deformation within and below the seismogenic layer, respectively. Four seismically inactive patches extending 30-50 kilometers along the rupture zone and down to 10 kilometers depth are identified with a systematic spatial shift between them introduced by the Düzce mainshock. The cumulative distribution of sub-areas hosting coseismic slip, aftershock clusters and postseismic creep shows that the entire upper (seismogenic) and lower (ductile) portion of the crust along the combined Izmit and Düzce rupture zone is activated between rupture initiation and a two-year postseismic period. This observation was only achieved due to the subsequent occurrence of two adjacent  $M > 7$  strike-slip earthquakes in combination with a distinct local seismic and geodetic monitoring. Our findings suggest that a coseismically introduced lateral and vertical slip deficit is systematically compensated postseismically in both the brittle and ductile portion of the crust.



## Seismic Risk Management: From Earthquake Science, Seismic Risk Assessment, and Communication to Decision Making

WANG, Z., University of Kentucky, Lexington, KY, USA, zmwang@uky.edu

Risk management is one of the most frequently used terms in decision making in modern society. Society is facing all kinds of risk from natural and man-made hazards, such as hurricanes, earthquakes, tornadoes, floods, car crashes, chemical spills, train derailments, and terror attacks. It is essential for risk management to assess all risks based on the best science and communicate the risk clearly to stakeholders. Thus, seismic risk must be assessed based on the best earthquake science and communicated clearly in order to make more effective management decisions. Furthermore, seismic risk assessment is a complicated process and requires cooperative efforts between seismologists, engineers, and other professionals. Seismologists play an important role in seismic risk assessment. Certain methods can be used to better assess and communicate and manage seismic risk in the United States.

## An Open-Source Tool for Probabilistic Seismic Hazard Assessment Based on Monte Carlo and Random Fields Techniques

CHENG, Y., Bogazici University, Istanbul, Turkey, yin.cheng1983@gmail.com; AKKAR, S., Bogazici University, Istanbul, Turkey, sinan.akkar@boun.edu.tr

Monte Carlo (MC) simulation approach is an efficient and flexible alternative against conventional integral approach for seismic hazard and loss assessment when more complicated factors (e.g. spatial correlation of ground shaking, near-fault forward directivity, conditional hazard and loss assessment etc.) are involved in the analysis. Therefore, using Monte-Carlo simulation approach, we developed an open-source tool compiled within MATLABM for probabilistic seismic hazard assessment. Currently, the tool considers area and fault seismic sources with different magnitude recurrence models for hazard assessment. A wide range of ground motion prediction equations (GMPEs) that encompass local and global characteristics of ground motion is also incorporated within the tool. As indicated above, complex seismic hazard problems such as spatial correlation and near-fault directivity effects in multi-scale random ground-motion fields are implemented within the tool as well. Two sampling methods are available for the MC-based simulation of ground motion fields: sequential correlation-based approach and Cholesky decomposition approach. The integration of these two methods bring about more flexible and efficient seismic hazard and loss assessment for the geographically distributed portfolios. A visual interface is created for inputting necessary parameters and operating on the digital maps. Outputs of this software include simulated earthquake catalogues, simulated ground motions, seismic hazard curves, and seismic hazard maps at specified annual exceedance rates. We are currently improving this tool to include probabilistic loss assessment on top of already implemented probabilistic hazard features.

## Progress Toward a Uniform Magnitude Scale for Earthquake Hazard Assessment in Canada

BENT, A. L., Geological Survey of Canada, Ottawa, ON Canada

Canada is a large, tectonically diverse country where several different magnitude scales are in common use for quantifying earthquake size. For seismic hazard assessment purposes, however, it is important for magnitudes to be uniform across the country and through time. Currently, moment magnitude,  $M_w$ , is the preferred magnitude scale for hazard assessment. It is now routinely determined for moderate earthquakes nationwide but cannot be determined as rapidly as some other magnitude types, which are still used for rapid response.  $M_w$  is also difficult to determine reliably for the smallest earthquakes and directly from instrumental data for many historical earthquakes. Thus, reliable conversion equations are required. Previous work developed conversion relations for  $M_L$  in western Canada and for  $M_N$  in eastern Canada. The latter was found to be time dependent and the dependence largely attributed to the increasingly high frequencies at which magnitudes are calculated.  $M_{Lg}(f)$  is under consideration as an alternate magnitude scale in the east as it is better calibrated for high frequencies. An  $M_{Lg}(f)$ - $M_w$  conversion has been developed:  $M_w = M_{Lg}(f) - 0.08$ . The relation appears to be time independent. The best choice for attenuation model is under investigation. The eastern offshore region where  $M_L$  is used as the default magnitude was excluded from earlier studies because of a lack of  $M_w$  data. The routine use of regional moment tensors in this region in recent years has significantly increased the data set and a conversion relation indicating that  $M_L$  is 0.2 magnitude units greater than  $M_w$  on average has been established.

## The High Frequency Seismic Wave Field Generated from Breaking Ocean Waves and the Link to Time-variable Sea States

POPPELIERS, C., East Carolina University, Greenville, NC, USA, poppeliersc14@ecu.edu

Breaking waves in the near-shore are known to generate a significant amount of high frequency ( $f > 5$  Hz) seismic energy. We investigate the correlation between the spectrum of seismic energy and the local sea states. In two separate experiments, we deployed seismometer(s) within a few tens of meters of the high-tide line at a sand beach. For the first experiment, we deployed a single three-component broadband seismometer approximately 50 m from the sea shore and recorded continuously for approximately 10 days. Our observations show that during elevated sea states, and presumably larger breaking waves in the surf zone, the power spectral density of the wave-generated seismic energy shifts to lower frequencies and higher spectral amplitudes. The correlation of the seismic spectral power to the height and period of ocean waves suggests that seismic observations can be used as a proxy for local sea states, which may have implications for sea shore sediment transport. In the second experiment, we deployed an 8-element linear array along the dune crest adjacent to the beach. Power spectra show a similar response to large-wave/storm events. Also, we show results that suggest that we are able to estimate the direction of near-shore ocean swell; hence the direction of the breaking waves using slowness analysis. We suggest that conventional array seismology shows promise as a low-cost, robust new method for coastal wave climate monitoring.

## Rapid Late-Quaternary Slip in the Tersky Range, Central Kyrgyz Tien Shan.

CAMPBELL, G. E., University of Cambridge, Cambridge, England, gcbell3@gmail.com; WALKER, R. T., Oxford University, Oxford, England, richw@earth.ox.ac.uk; ABDRAKHMATOV, K., Kyrgyz Institute of Seismology, Bishkek, Kyrgyzstan, kanab53@yandex.com; MACKENZIE, D., Oxford University, Oxford, England, david.mackenzie@earth.ox.ac.uk; JACKSON, J. A., University of Cambridge, Cambridge, England, jaj2@cam.ac.uk; RIZZA, M., CEREGE, Aix-Marseille, France, rizza@cerge.fr; ELLIOTT, J. R., Oxford University, Oxford, England, john.elliott@earth.ox.ac.uk; RHODES, A., NERC Cosmogenic Isotope Analysis Facility, East Kilbride, Scotland, angelrodes@gmail.com

Modern GPS velocity measurements indicate that  $\sim 15$  mm/yr of N-S shortening, related to the Eocene-present India-Eurasia collision, is accommodated across the central Tien Shan of Kyrgyzstan, central Asia. The central Tien Shan region ( $\sim 76$ - $80^\circ$  E,  $\sim 40$ - $42^\circ$  N) is characterised by relatively high elevation (2,500-5,000 m) mountain terrain, and contains narrow (3-5 km), E-W elongate intramontane basins. However, little is known about the distribution of active faults, how shortening is accommodated, or the earthquake potential of this region. We present the first detailed field-based and satellite observations of the Karakudzhur reverse fault, and characterise the fault in its regional geological and tectonic setting, within the central and wider Tien Shan.

The Karakudzhur fault extends  $\sim 40$  km E-W along the northern margin of the Karakudzhur intramontane basin. Along the fault's length, 2.5-30 m vertical offsets preserved in alluvial deposits, in addition to landslide deposits, indicate that the fault is active and has generated at least several large, surface-rupturing earthquakes in the late Pleistocene. We use radiocarbon, luminescence (post-infrared IRSL of feldspar), and Uranium-series dating methods to estimate a preliminary uplift rate of  $\sim 0.17$ - $2.20$  mm/yr. Significantly, fresh surface ruptures, which offset a loess river-terrace cap dated with radiocarbon charcoal samples, indicate that a substantial surface-rupturing earthquake has occurred since at least  $\sim 350$  years BP.

Additionally, we present the first field observations and cosmogenic ( $^{10}\text{Be}$ ) age constraints of an impressive uphill-facing 2-5 m vertical scarp, preserved in alluvial deposits on the S slope of the high western Tersky mountains. The formation of this uphill-facing scarp, which is sub-parallel to the main E-W Karakudzhur basin-margin reverse fault, may be associated with stress changes related to reverse faulting along the Karakudzhur fault.

## A Note on the Scatter of Strong-motion Data in the Context of the Specific Barrier Model

HALLDORSSON, B., Earthquake Engineering Research Centre, University of Iceland, Selfoss, Iceland, skykkur@hi.is; PAPAGEORGIOU, A. S., University of Patras, Patras, Greece, papaga@upatras.gr; SONNEMANN, T., Earthquake Engineering Research Centre, University of Iceland, Selfoss, Iceland, tsonne@hi.is

Reliable simulations of high-frequency earthquake strong ground motion time histories are based on seismological models that have been calibrated on the basis of recorded data. As a result, peak ground motion parameters such as PGA, PSA,

etc. derived from suites of synthetic strong-motion time histories capture the median trend of data as a function of *e.g.* distance and frequency, respectively, for a given earthquake magnitude. However, the variability associated with peak parameters from earthquake strong-motion data is generally not captured in time history simulations from simple seismological models if their key parameters are not allowed to vary from their mean values. A feasible way of incorporating such variability into simulations is to use a simple, yet physically consistent seismological model. Therefore, we model the earthquake source using the specific barrier model (SBM) in the context of the stochastic modelling approach. The mean value of the key SBM parameter, the local stress drop, has been estimated for earthquakes in Greece. Variations of the corresponding theoretical earthquake source spectra are introduced quantifying the effects of various subevent populations on the earthquake source and empirical models accounting for directivity effects. The variations in site conditions are accounted for using actual borehole data. By varying other physical parameters of the model we show to what extent the seismological model can incorporate the variability of the earthquake source, path and site conditions to match the observed variability of strong-motion. Finally we discuss the corresponding implications on the level of source complexity (subevent populations) of earthquakes of different magnitudes. That in turn has important implications for using the specific barrier model in modelling the earthquake as an extended source for hybrid near-fault simulations.

#### **Tectonic Geomorphology and Paleoseismology of the Gatún Fault in Central Panamá**

GATH, E. M., Earth Consultants International, Santa Ana, CA, USA, gath@earthconsultants.com; GONZALEZ, T., Earth Consultants International, Santa Ana, CA, USA, gath@earthconsultants.com; ROCKWELL, T. K., Earth Consultants International, Santa Ana, CA, USA, gath@earthconsultants.com; FRANCESCHI, P., Autoridad del Canal de Panamá, Corozal, Panamá, pfranceschi@pancanal.com

The Gatún fault, a primary east-west structural feature in central Panamá, has a strong geomorphic signature that can be readily observed in aerial photographs and digital elevation models. The fault forms an abrupt southern margin to the Sierra Maestra Mountains, and all rivers and streams that cross the fault are affected at the fault crossing. Most large rivers are left-laterally deflected, and all streams that cross the fault have a 1- to 2-meter, and locally as high as 5-meter near-vertical nickpoint at or immediately upstream of the fault. Paleoseismic trenching of the Gatún fault east of Gatún Lake has shown that this fault has experienced at least two, and possibly three, surface-rupturing earthquakes since 1490 AD. Based on 3-D trenching of a 3 ka channel thalweg that is offset 19-20 m, the left-lateral slip rate on the Gatún fault is 6-9 mm/yr with a maximum of 20% north-side up normal slip, and the most recent earthquake in the mid-late 1800s generated at least 0.7+0.2 meters of left-lateral surface offset that apparently went unnoticed at the time. Our best estimate is that this 40 km segment of the Gatún fault has a recurrence interval of ~M6.8 earthquakes every 100-170 years based on the last three events, but if the fault is capable of multi-segment, less-frequent ruptures, the earthquakes could potentially be as large as M7.4 if the entire 120 km fault were to rupture. We suspect, but cannot prove, that triggered slip resulted in soil fracturing on the Gatún fault during the 1991 M7.6 earthquake on the North Panamá Deformed Belt off the Caribbean coast of eastern Costa Rica. These findings are important for the seismic stability analysis of the AD 1913 Gatún Dam across the Chagres River, one of the most critical structures in the Panamá Canal.

#### **Complicated Kinematics Of The Southern Cascadia Subduction Zone Near The Mendocino Triple Junction**

MCPHERSON, B. C., Humboldt State University, Arcata, CA, US

The southern Cascadia subduction zone, in the vicinity of Mendocino triple junction, has experienced almost daily intraplate earthquake activity since 1974, when monitoring first began. As a result of the interactions of the three plates within this region, high stresses result in a “cloud” of earthquakes developing north of the triple junction, with the earthquakes occurring within both the overriding North American and the subducting Gorda plates. The Pacific plate, the strongest of the three plates comprising the triple junction, is devoid of earthquake activity. We use this “cloud” of intraplate earthquakes, and selected focal mechanisms, to define the geometry of the locked portion of the subducted zone, as well as the location of the subducting Gorda plate. The coastal towns of Arcata, Eureka, Ferndale and Fortuna are directly above this hazard.

Also, we will show that the accumulation of strain recorded by the permanent GPS network for the last decade is not a linear process. Instead, we see localized strain rate increases/decreases before some offshore Gorda plate earthquakes and (coseismic) steps in strain in most offshore Gorda quakes. All of these observations are in contrast to the style of deformation seen farther north.

---

## Joyner Lecture

Oral Session · Thursday · 5:15 PM · 21 April · Naples Ballroom

---

### **Joyner Lecture: Site Response Uncertainty and its Implications for Seismic Risk Characterization**

STEWART, J. P., University of California, Los Angeles, CA USA, jstewart@seas.ucla.edu

Along with source and path effects, site response analysis is a vital component of earthquake ground motion characterization. Ground motion prediction equations (GMPEs) include terms for modeling site response that are based on simple metrics of site condition, such as the time-average shear wave velocity in the upper 30 m ( $V_{S30}$ ). Because site terms in GMPEs are derived from global databases, and are based on incomplete information on site conditions, their predictions represent average levels of site response conditional on  $V_{S30}$ . Such predictions are referred to as ergodic.

Actual site response at a given site is likely to differ from this global average. Viewed in this context, the actual site response for a particular site and intensity measure is the sum in log units of the ergodic estimate from a global model and a (generally unknown) site term (denoted  $\eta_S$ ). If the level of site-specific error ( $\eta_S$ ) can be identified and used to adjust the ergodic model, the ground motion analysis is more accurate (*i.e.*, bias is removed) and the dispersion of the predicted ground motions is reduced. Therefore, site-specific evaluations of site response are useful and will often reduce hazard levels at long return periods (due to uncertainty reduction). The questions are how should these evaluations be performed, how reliable are the resulting site response estimates, and how can the results be used in a probabilistically rigorous manner as required for hazard- or risk-based applications?

With this in mind, the lecture will cover:

1. The physical processes responsible for site effects;
2. The manner by which these processes are (or are not) reflected in relatively generic site factors used in GMPEs and in building codes;
3. Effectiveness of site-specific geotechnical ground response analyses to estimate site effects;
4. Recommended procedures for evaluating site-specific site response and its implementation in hazard/risk characterization for critical facilities.

---

## Active Tectonics, Faults and Large Earthquakes

Poster Session · Thursday · 21 April · Tuscany F

---

### **Improved Comparison of PBRs With Hazard Maps for Rocks Near the San Andreas Fault in the Mojave Desert**

BRUNE, J. N., University of Nevada, Reno, NV, USA, brune@seismo.unr.edu; BRUNE, R. J., Costa Mesa, CA, USA, richbrune@sbcglobal.net; ANDERSON, J. G., University of Nevada, Reno, NV, USA, jga@unr.edu; BIASI, G. P., University of Nevada, Reno, NV, USA, glenn@unr.edu

Brune (SRL 1999) concluded that the then-current USGS 2% in 50-yr hazard maps (NSHM) were too high compared to predicted fragilities of precariously balanced rocks (PBRs) near the San Andreas fault in the Mojave desert. Anderson and Brune (SRL, 1999) suggested that this could be caused in part by an inappropriate use of the ergodic assumption. Purvance *et al.* (2008), using refined methodologies, concluded that PBRs in the Mojave region remained inconsistent with 2002 USGS NSHMs. Hazard reductions particularly in 2008 due to NGA-2 and some in 2014 have successively improved comparisons. In this study we report on improvements to PBR constraints in this region from additional rocks and improved fragility estimates using photogrammetric methods. Ages of the added PBRs are well constrained from widespread rock varnish, indicating that rock shapes have experienced little change in the Holocene.

We compare new results with the 2014 NSHMs. Although there are some exceptions, nominal probabilities of PBR overturning at Lovejoy Buttes are not compellingly inconsistent. Remaining questions, however, are motivating new developments on many fronts. Comparison of rock fragilities versus distance to the SAF and other faults using the SCEC-hosted PBR archive indicates consistency with median ground motions, but not with GMPE uncertainties. New studies suggest lower ground motion uncertainties, *e.g.*, reduction of the aleatory sigma for hard rock sites and smaller source variability based on repeated strong ground motions (Yagoda—Biran and Anderson, SSA, 2015a and 2015b). Future studies should use actual waveforms to understand the effects of rupture directivity, source complexity and ground motion directionality at PBR sites. We are calculating PBR responses to broadband waveforms using the composite source model of earthquake ruptures (Anderson, SRL 2015). Important potential tools include SCEC CyberShake and Broadband Platform initiatives.



## The Location of Indian Lithosphere Beneath Tibet: Insights from Group and Shear Wave Velocity Structure

GILLIGAN, A., Imperial College London, London, UK, a.gilligan@imperial.ac.uk; PRIESTLEY, K., University of Cambridge, Cambridge, UK, kfp10@cam.ac.uk

Processes occurring in large, hot, orogenic settings are not yet well understood. From the seismic properties of the lithosphere in areas of active continental collision we can gain insights into deformation processes occurring in present-day orogenies and make inferences about ancient orogenies. Tibet is an excellent natural laboratory for investigating collisional processes: it is the largest and highest orogenic plateau on Earth today. We measure new group velocity dispersion curves using data from regional earthquakes received at stations in West Tibet, Pakistan and Southern India. Additionally, we measure group velocity dispersion curves from ambient noise cross-correlations for the West Tibet network. From these dispersion curves we obtain new fundamental mode Rayleigh Wave group velocity maps for periods from 5–70s for Tibet. The dense path coverage at the shortest periods due to the inclusion of ambient noise data allows features as small as ~100km scale to be resolved. The group velocity variations seen in these maps correspond well with known geological and tectonic features. In particular, there is a strong correlation between low velocity group velocity at short periods and areas of thick sediments. The Rayleigh wave group velocity maps are used to invert for shear wave velocity profiles to a depth of 120km. A mid crustal low velocity layer (~10% decrease in velocity) is observed throughout much of Tibet, with the exception of the northern part of West Tibet. We attribute this to radiogenic heating of the crust. The transition from the crust to the mantle occurs at lower shear velocities in the eastern part of the plateau than in the western part. This cautions against the use of a velocity proxy for mapping out crustal thickness in this region, and suggests that there may be important differences between East and West Tibet.

## Empirical Observations of the Influence of Steps on Rupture Propagation

BIASI, G. P., University of Nevada Reno, Nevada Seismological Laboratory, Reno, NV, USA, glenn@seismo.unr.edu; WESNOUSKY, S. G., University of Nevada Reno, Center for Neotectonic Studies, Reno, NV, USA, wesnousky@unr.edu

We analyze mapped surface ruptures for empirical relationships between steps in fault traces and earthquake rupture extent. New summary maps are developed for 39 ruptures and combined with 37 from Wesnousky (BSSA, 2008) for a total of 46 strike-slip, 16 normal, and 14 reverse mechanism events. We find that ~90% of ruptures have at least one end at a mappable discontinuity, either a fault end or a step of 1 km or greater. Dip-slip ruptures cross larger steps than strike-slip earthquakes, with maxima of ~12 vs. ~5 km, respectively. Large steps inside strike-slip ruptures are rare; only 8% (5 of 62) are  $\geq 4$  km. A geometric probability distribution model of steps as “challenges” to rupture propagation predicts that steps of 1 km or greater stop rupture about 46% of the time. The rate is similar for dip-slip earthquakes as a group, but among dip-slip ruptures, steps are relatively more effective in stopping reverse ruptures and less effective in stopping normal ruptures. Toward evaluating the importance of step size on rupture propagation, we compare the relative incidence of steps inside ruptures, which are jumped, to steps at ends, where they have stopped ruptures. For a given step size the fraction of steps broken divided by the corresponding fraction that stop rupture is a measure of step effectiveness in stopping rupture. We define this as the passing ratio. A linear model for steps in strike-slip ruptures from 1 to 6 km leads to the passing ratio  $\approx 1.89 - 0.31 \cdot \text{step width in km}$ . Steps of ~3 km are equally likely to be broken or to terminate rupture, and steps  $\geq 6$  km should almost always stop rupture. Using a similar approach and small samples, we find that extensional steps are somewhat more effective than compressional steps in stopping ruptures. We also compiled the incidence of gaps of 1 km and longer in surface ruptures. Gaps occur in ~43% of ruptures and occur more frequently in dip-slip than strike-slip ruptures.

## Magnitude Thresholds Associated with Instruments of the Seismographic Network Used by the U.S. Coast and Geodetic Survey from 1930-1960

DEWEY, J. W., U.S. Geological Survey, Denver, CO, USA, jdewey@usgs.gov

The U.S. Geological Survey (USGS) stores a collection of original seismograms from a seismographic network that was used for global earthquake monitoring by the U.S. Coast and Geodetic Survey (USCGS) prior to the installation of the World-Wide Standardized Seismograph Network in the early 1960's. The collection was assembled in the 1980's in the course of the Historical Seismogram Filming Project, a project initiated by IASPEI and UNESCO and conducted by the National Oceanic and Atmospheric Administration with funding from the USGS and the U.S. Nuclear Regulatory Commission. Some of the seismograms were microfilmed in the course of that project, but others were not. For most sta-

tions of the USCGS network, USGS holdings of original seismograms date from the 1930's and later; holdings for individual stations have gaps from some time periods for which observations from the stations are documented in seismological bulletins. A purpose of the present study is to document the magnitude ranges for which seismograms of this collection are suitable for reanalysis by modern waveform modeling techniques. This part of the study is based on a review of studies conducted by others. On the basis of the reviewed studies, it appears that earthquakes of magnitude 5.5 and greater occurring from 1930-1960 in the continental U.S. were commonly well-enough recorded to be suitable for waveform modeling. A second purpose is to estimate the magnitude threshold above which earthquakes can be characterized by an instrumental magnitude using data from the USCGS network. This threshold varies with time and geographical position within the continental U.S., but examination of seismograms makes clear that many magnitude 4.3 and larger shocks from the period 1930-1960, whose sizes are currently characterized only by magnitudes inferred from macroseismic observations, may also be characterized by magnitudes calculated from instrumental data of the USCGS network.

## Compilation and Analysis of a Database of Local Tsunami Bulletins issued by the Pacific Tsunami Warning Center (PTWC) to the Hawaii Emergency Management Agency (HI-EMA) between October 2002 and July, 2015

SARDINA, V., Pacific Tsunami Warning Center, Honolulu, HI, USA, victor.sardina@noaa.gov; BECKER, N., Pacific Tsunami Warning Center, Honolulu, HI, USA, nathan.becker@noaa.gov; KOYANAGI, K., Pacific Tsunami Warning Center, Honolulu, HI, USA, kanoa.koyanagi@noaa.gov; WALSH, D., Pacific Tsunami Warning Center, Honolulu, HI, USA, david.walsh@noaa.gov; MCCREERY, C., Pacific Tsunami Warning Center, Honolulu, HI, USA, charles.mccreery@noaa.gov

The PTWC functions not only as official international tsunami warning center (TWC) for nations with coasts around the Pacific rim, the Caribbean, and other regions of the world, but also as the local TWC for the State of Hawaii, American Samoa, and Guam. As part of its routine operations, the PTWC has strived to send a local tsunami message product for any Hawaii earthquake with a 4.0 or larger magnitude within five minutes of origin time since at least October, 2002. To evaluate PTWC's performance in that regard, however, we must first compile a suitable local tsunami bulletin's database. For that purpose, we scanned all the available logs for the Federal Aviation Administration (FAA) and Global Telecommunications System (GTS) communications' circuits between 2002 and 2015 and retrieved 138 local bulletins. We parsed these bulletins and extracted the parametric data needed to evaluate PTWC's performance in terms of essential statistics such as message delay time, epicenter offsets, and magnitude residuals as compared with more authoritative earthquake source parametrizations. To that end, we cross-validated 126 of these local bulletins for events with magnitudes between 2.6 and 6.5 with the corresponding source parameters obtained from the USGS Hawaiian Volcano Observatory (HVO), the National Earthquake Information Center (NEIC), and the Global Centroid Moment Tensor (GCMT) Project online catalogs. Analysis of events with magnitude 4.0 or larger gives a median message delay time of 3 minutes, a median epicentral distance offset of 4.5 km, and a median magnitude residual of 0.2 unit. Several message delay outliers exist due to the fact that PTWC has sent local tsunami information statements (TIS) for felt events with magnitudes as small as 2.8 located west of the Big Island. Routine use of a synthetic Wood-Anderson magnitude since the beginning of 2011 appears to have brought consistency to PTWC's local magnitude estimates and a reduction in the message delays.

## Multi-Component C3 to Improve Amplitude Reliability for Hazard Analysis Using the Ambient Seismic Field

SHENG, Y., Stanford University, Stanford, CA, USA, yixiao2@stanford.edu; BEROZA, G. C., Stanford University, Stanford, CA, USA, beroza@stanford.edu; DENOLLE, M., Harvard University, Cambridge, MA, USA, mdenolle@fas.harvard.edu

Predicting the strength of shaking due to path effects is central to seismic hazard analysis. The Virtual Earthquake Approach proposed by Denolle et al (2013) takes the surface response determined from the ambient seismic field and corrects it for source depths and source mechanisms of earthquakes of interest. The method has shown promise for characterizing the strength of earthquake shaking for  $f < 0.5$  Hz; however, the method depends on reliable relative amplitudes among the 5 components of the Green's tensor (1 for SH/Love and 4 for P-SV/Rayleigh) that are used to calculate the strength of wave excitation from a moment tensor source.

To develop more reliable amplitudes we combine the C3 (cross-correlation of the coda of the cross-correlation) method with the Virtual Earthquake Approach. The C3 method can mitigate the asymmetry due to a lack of equi-par-



tioning in the ambient wavefield that can bias the Green's function calculated directly by cross-correlation (C1). Moreover, instead of only using vertical-to-vertical components in C1, we utilize multi-components, such as east-to-vertical and north-to-vertical components. The resulting amplitudes are better calibrated across components. We find that the Green's functions calculated with multi-component C3 are comparable with the Green's functions directly calculated by C1, which serves as a validation for our approach, but they are more symmetric.

#### Earthquake-Protective Desks for Vulnerable Bhutanese Schools

TSCHERING, K. E., GeoHazards International, Thimphu, Bhutan, karma@geohaz.org; BRUNO, I., Bezalel Academy of Art and Design, Jerusalem, Israel, idbruno@gmail.com; O'DONNELL, A., AIR-Worldwide, Boston, MA, USA, aodonnell@air-worldwide.com; KIANIRAD, E., AIR-Worldwide, Boston, MA, USA, ekianirad@air-worldwide.com; SONAM, K., Ministry of Education, Thimphu, Bhutan, karsonpokto@gmail.com; TUCKER, B. E., GeoHazards International, Menlo Park, CA, USA, tucker@geohaz.org

Hundreds of millions of children around the world in low- and middle-income countries risk death and serious injury in seismically unsafe schools. These students learn to "drop, cover and hold on" under their desks during earthquake shaking, but heavy debris falling during earthquakes can crush many of these desks. Though staying inside is unsafe, running out of a collapsing school, through narrow corridors and few exits, is also.

The long-term solution is to replace or retrofit these vulnerable schools, but this is not possible in the short term. For example, the replacement cost of a typical Bhutan school is about \$1 million USD, while a retrofit, if feasible, is perhaps 30% of that, and there are approximately 500 schools in Bhutan, most of which appear seismically vulnerable. Even if the funding and the skilled workforce required were available, providing earthquake-resistant schools would take decades, while a major earthquake could strike any day.

Recently designed "earthquake-protective desks," strong enough to withstand exceptionally heavy loads, large-enough to shelter two students and light enough to be easily moved, might quickly and affordably protect children until safe buildings are available. Such desks could also provide an additional measure of safety from falling hazards in earthquake-resistant schools.

In January 2016, we initiated a project that will test whether Bhutanese furniture manufacturers, trained in our project, can produce these earthquake-protective desks with a quality and price acceptable to Bhutan's Ministry of Education (MoE).

This paper reports on progress achieving the expected outcomes: (1) six Bhutanese companies trained to manufacture earthquake-protective desks, (2) an estimate of the price of these desks, (3) the capacity of the MoE to provide quality assurance of the manufactured desks, and (4) a comparison of the cost/benefit of alternative means to reduce death and injury in Bhutan schools due to earthquakes.

#### Advancing the Presentation of Earthquake Hazard: The USGS NSHMP Unified Hazard Tool

POWERS, P. M., USGS, Golden, CO, USA, pmpowers@usgs.gov; MARTINEZ, E. M., USGS, Golden, CO, USA, emartinez@usgs.gov; FEE, J. M., USGS, Golden, CO, USA, jimfee@usgs.gov

The U.S. Geological Survey (USGS) national seismic hazard modeling project (NSHMP) creates and regularly updates seismic hazard models for the conterminous US, Alaska, Hawaii, and various U.S. territories. Model updates are accompanied by probabilistic hazard source models computed at regularly spaced points in latitude and longitude and for multiple spectral periods and site classes and are available for download on the USGS website.

More than a decade ago we started to provide these data, and related hazard products and analyses, such as deaggregations, conditional mean spectra, custom hazard maps, and earthquake probability maps, via dynamic web-applications. Over time, their popularity has risen along with the expectation that future hazard models would be readily available via web-applications upon release. However, given ever more complex source models, multiple codebases for calculating hazard, and more sophisticated ground motion models that support more periods, site classes, and source-to-site parameterizations, this is not the case.

To better support the deployment of past, present, and future models, we present a new Unified Hazard Tool. The tool brings together the rapid delivery of precomputed static data sets and dynamic hazard and related calculations. It permits deployment of new models rather than requiring model-specific applications and code. It also brings all spatial data related to hazard (*e.g.* hazard and earthquake probability maps, source models) together in a unified interface. The

tool relies on the Java-based nshmp-haz library and an XML-based generalized hazard source model description. nshmp-haz is a functional hazard calculation platform that we developed to leverage the benefits of the multiple, historic codebases (OpenSHA, USGS fortran codes) and to have a single codebase to calculate static data products while also supporting web-services across multiple models and regions.

#### Improved Estimation of Temporal Variation in Earthquake Detectability with Time-dependent Smoothness Constraint

IWATA, T., Tokiwa University, Mito, Ibaraki, Japan, tiwata@tokiwa.ac.jp

A key in the evaluation of earthquake detectability is to consider the temporal variation of the detectability. For this purpose, Ogata and Katsura (1993, GJI; hereafter OK1993) proposed a Bayesian smoothing to estimate the temporal variation in the detectability with a constant strength of smoothness constraint. As an extension of this, Iwata (2015, AOGS) has introduced the estimation with time-dependent strength of the smoothness constraint, because the estimate with the constant strength is biased for a sequence such as an aftershock activity where the seismicity rate is not constant.

The assumption of the time-dependency of the strength results in the introduction of a non-Gaussian state space model for the estimation, and thus the sequential Monte Carlo (SMC) is used as an algorithm in Iwata (2015). This algorithm works well if our goal is only for the estimation of the temporal variations in earthquake detectability and strength of the smoothness constraint. However, the model of OK1993 contains other parameters such as b-value, and the parameters should be optimized simultaneously. In an ordinary statistical approach, the optimization is done by the maximization of a (marginal) likelihood, but the precise calculation of the likelihood is difficult if we use SMC. This is because the numerical error arising from the random property of the Monte Carlo method contaminates the calculation of the likelihood.

Here, to overcome this difficulty, a non-Gaussian filter/smoothing algorithm suggested by Kitagawa (1987, JASA) is introduced for the estimation. In this algorithm, the probability density function of a non-Gaussian distribution is approximated by a set of step functions and the estimation is carried out without any random computational error; thus, an appropriate optimization of the other parameters is possible. Actually, through a numerical experiment, it is confirmed that the estimation error with this algorithm is lessened, compared to that with SMC.

#### Additional Period and Site Class Maps for the 2014 USGS National Seismic Hazard Model

SHUMWAY, A. M., USGS, Golden, CO, USA, ashumway@usgs.gov; PETERSEN, M. D., USGS, Golden, CO, USA, mpetersen@usgs.gov; POWERS, P. M., USGS, Golden, CO, USA, pmpowers@usgs.gov; REZAEIAN, S., USGS, Golden, CO, USA, srezaeian@usgs.gov

The 2014 update of the USGS National Seismic Hazard Model (NSHM) included maps of probabilistic ground motions for 2% and 10% probabilities of exceedance in 50 years, derived from hazard curves for peak ground acceleration (PGA), and 0.2 and 1.0 second spectral accelerations for NEHRP site class BC. We now include ground motions for additional spectral periods and site classes. For both the central and eastern US (CEUS) and western US (WUS), additional curves and maps for 0.1, 0.3, 0.5, and 2.0 second spectral accelerations are available. The WUS additionally includes curves and maps for 0.75, 3.0, 4.0, and 5.0 second spectral accelerations. The use of region-specific suites of weighted ground motion models (GMMs) precludes the calculation of ground motions for a uniform set of periods and additional site classes over the entire US. In the CEUS, because there is no consensus on an appropriate site-amplification model to use, we calculate additional curves for NEHRP site class A, for which most stable continental GMMs were originally developed. In the WUS, however, the active crustal NGA-West2 GMMs and the subduction GMMs allow the calculation of ground motion based on Vs30 or site class, so we provide curves and maps for NEHRP site classes B, C, CD, D, and DE. Sensitivity analyses in the form of GMM magnitude-distance scaling relations, uniform response spectra, and hazard curves show that select GMMs give unrealistic results at specific periods and site classes. In these rare instances, the GMM in question is removed from the hazard curve calculation and its weight is redistributed to the remaining GMMs. Ratio maps show the removal of these GMMs result in hazard changes of less than 10%, except in the Pacific Northwest, which will be discussed. The 2014 USGS NSHM additional period and site class maps will be submitted to the Building Seismic Safety Council (BSSC) for consideration in the development of the next-generation of seismic design value maps.

## The Effect of Uncertainty in Predictor Variables on the Estimation of Ground-Motion Prediction Equations

KUEHN, N. M., PEER Center, University of California, Berkeley, Berkeley, CA, USA, kuehn@berkeley.edu; ABRAHAMSON, N., University of California, Berkeley, Berkeley, CA, USA, abrahamson@berkeley.edu

Ground-motion prediction equations are typically estimated via regression of a ground-motion parameter of interest (such as peak ground acceleration or spectral acceleration) against source, path and site related parameters such as magnitude, distance or  $V_{s30}$ , with physical considerations taken into account. The estimated variance, a measure of aleatory variability, is an important parameter for seismic hazard studies as it controls the shape of the hazard curve. Generally, the predictor variables are treated as error free in the regression. However, often magnitudes are converted from one scale to another (such as local magnitude to moment magnitude), or  $V_{s30}$  is inferred from local geology instead of measured. This measurement error leads to uncertainty in the predictor variables, which affects the estimation of the ground-motion model, in particular the aleatory variability—the measurement error is mapped into aleatory variability.

Here, we investigate the effect of measurement uncertainty error in predictor variables on ground-motion models. A simple measurement error model is employed, which treats the value of the predictor variable as a parameter to be estimated, constrained by its observed value and (known) variance of the measurement error. The model is cast in a Bayesian fashion to allow the inclusion of informative prior information, as well as a probabilistic interpretation of the results. We find that the inclusion of the uncertainty in magnitudes and  $V_{s30}$  in the regression reduces the values of the associated aleatory variability by about 15%, though the exact values depend on the specifics of the model. The median predictions are similar for models estimated with and without measurement uncertainty, but there is a significant change in the correlations of residuals between different response spectral periods, which are used for conditional mean spectra.

## Unusual Characteristics of Seismicity Preceding and Following The 2010 Simeulue, Sumatra Earthquake Mw 7.8

SIANIPAR, D. S., State College of Meteorology Climatology and Geophysics (STMKG), South Tangerang, Banten, Indonesia, dimas.salomo@gmail.com; SUBAKTI, H., State College of Meteorology Climatology and Geophysics (STMKG), South Tangerang, Banten, Indonesia, hendri.subakti@bmgk.go.id

To improve the understanding of the foreshock and aftershock characteristics in rupture zone, a sufficient number of earthquakes 60 days before and after the  $M_w$  7.8 Simeulue, Sumatra earthquake was examined. The foreshocks and aftershocks were selected in the epicentral and rupture zone of the strong mainshock. Two patterns of unusual seismicity preceding and following the mainshock of the 2010 Simeulue, Sumatra earthquake  $M_w$  7.8 were found by high precision relocation using double difference algorithm. The first pattern was which one corresponding with the subduction slab and the second was seismicity pattern like a thrust structure within the subducted plate. This study was answered the USGS comment that this earthquake was a complex earthquake with at least two large events occurring about 12 s apart, observed on broadband displacement seismograms. The updated finite fault model from Gavin Hayes was used for further analysis. The scale of the seismic energy-to-moment ratio, an important macroscopic parameter which reflects the basic physical process of seismic slip was also investigated. Two patterns of these scales of seismic energy-to-moment ratio were also found. From the coulomb stress transfer analysis, both of the initial point of the foreshocks area and the mainshock hypocenter, and also the intraplate seismicity pattern were located in the positive coulomb stress change (0.3–0.4 MPa) as a cumulative implication of two previous giant earthquake  $M_w$  9.0 and  $M_w$  8.6.

## Seismic Activity Characteristics of the 2015 Nepal Ms8.1 and Ms7.5 Earthquake

XUE, Y., China Earthquake Networks Center, Beijing, China, xueyan5619@seis.ac.cn; REN, X., China Earthquake Networks Center, Beijing, China, renxiao@seis.ac.cn; LIU, S. Q., Earthquake Administration of Tianjin Municipality, Tianjing, China, goodmorningabc@163.com; LIU, J., China Earthquake Networks Center, Beijing, China, liujie@seis.ac.cn; WANG, Y. X., Earthquake Administration of Tianjing Municipality, Tianjing, China, wangyx123@163.com

The 2015 Ms8.1 Nepal earthquake occurred as the result of thrust faulting with low dip angle unilateral rupture along the Himalayan seismic belt. The aftershocks spread over a region with 170 km long and 60 km width, striking along the direction of WNW-ESE. The mainshock and the strong aftershocks are all located at the two ends of this seismic region, while only few earthquakes occur in

the middle, where the main rupture of the Ms8.1 earthquake occurs. The strongest aftershock of Ms7.5 is located at the east end and is significantly triggered by the main shock. The Ms8.1 and Ms7.5 event occurred in the seismic gap between the 1505  $M_w$  8.2 Lo Mustang earthquake and the 1934  $M_w$  8.1 Nepal-Bihar earthquake. Moreover no earthquakes with  $M \geq 6.0$  occurs in the seismic gap since 1870. In the last 13 years, there exists a seismogenic gap of 590km long without  $M \geq 5.0$  earthquakes. Nineteen months before the 2015 Ms8.1 Nepal event, the seismogenic gap was broken. Noticed that the Ms8.1 earthquake sequence is located in the middle of the existing seismogenic gap, whose east and west parts are still quiescent. The calculated static Coulomb stress changes show that the Ms8.1 earthquake has apparent stress triggering effect to both sides of the faults. Taking into account the historical earthquake activity and the recurrence period, the seismic potential in the rupture zone of the 1505  $M_w$  8.2 is higher, comparing to the rupture zone of the 1934  $M_w$  8.4. The occurrences of the 2005  $M_w$  7.6 Pakistan event and the 2015 Ms8.1 Nepal earthquake indicate that the Himalayan seismic belt has started a relatively active phase for  $M_w \geq 7.0$  earthquakes.

Key words: the 2015 Nepal earthquake, rupture zone, seismic gap, stress triggering, Himalayan seismic belt

## Extending Seismological Database through the Digitization of Analog Seismograms with DigitSeis: An Example from the Harvard-Adam Dziewonski Observatory Collection

BOGIATZIS, P., Department of Earth and Planetary Sciences, Harvard University, Cambridge, MA, USA, petrosbogiatzis@fas.harvard.edu; ALTOE, I. L., Institute of Geosciences, Universidade de Brasília, Brasília, Brazil, altoeisabella@email.arizona.edu; KARAMITROU, A., Department of Geophysics, Aristotle University of Thessaloniki, Thessaloniki, Greece, alexkara@geo.auth.gr; ISHII, M., Department of Earth and Planetary Sciences, Harvard University, Cambridge, MA, USA, ishii@eps.harvard.edu; ISHII, H., Department of Earth and Planetary Sciences, Harvard University, Cambridge, MA, USA, hiromiishii@fas.harvard.edu

Over recent years, digital image processing methods have found a variety of applications in a plethora of scientific fields, among them seismology. One of the problems that such techniques can solve is the extraction of information from the vast amount of data, concealed within millions of seismograms that has been recorded in some form of paper or film during the analog era of seismology. Many of these records have been scanned or photographed and stored as digital raster images. These images must be converted into digital time series in order for them to be useful for research and to expand the available seismic database into the 1st half of the 20th century. DigitSeis is an open-source, interactive digitization software, written in MATLAB that performs this task by utilizing image processing algorithms. It automatically identifies and corrects for various geometrical distortions of seismogram images that are acquired through the original recording, storage, and scanning procedures. It also categorizes important features such as traces and time marks, corrects time-mark offsets from the main trace, and digitizes analyzes the combined trace to assign as accurate timing as possible. Although a large effort has been made to minimize human input, DigitSeis provides interactive tools for correcting possible errors of the automatic results and for challenging situations such as trace crossings. The effectiveness of the software is demonstrated with the digitization of seismograms from late 1930's recorded at the Harvard-Adam Dziewonski observatory (the stations is still in operation and is part of the Global Seismographic Network, station code HRV, network code IU). The spectral analysis of the digitized time series shows no spurious features that may be related to the occurrence of time marks. They also display signals associated with significant earthquakes, and a comparison with modern recordings reveals similarities in the background noise.

## Development of Ground Motion Data Catalog for Iran and Regions with Similar Tectonic Activities

FARAJPOUR, Z., International Institute of Earthquake Engineering and Seismology, Tehran, Iran, z.farajpour@iiees.ac.ir; ZARE, M., International Institute of Earthquake Engineering and Seismology, Tehran, Iran, mzare@iiees.ac.ir; PEZESHK, S., The University of Memphis, Memphis, TN, USA, spezeshk@memphis.edu

The purpose of this study is to development of a comprehensive database of ground motion records as a principal resource for the development and update of Ground Motion Models (GMMs) or Ground Motion Prediction Equations (GMPEs) for Iranian plateau. This area typically experiences moderate to large earthquakes with moment magnitudes  $M \geq 4$  every year. Main Iranian plateau's faulting has a strike-slip or reverse mechanism.

The database that is being developed will include ground motion data catalog for Iran and regions with similar tectonic activities. This catalog is adhering to the New Generation Attenuation (NGA-West2) project criteria. Following the

NGA-West2 procedures is appropriate due to high seismicity and active tectonic regime of the Iranian plateau and the depth of the earthquake event, which is defined as the continental crust.

Since near source ground motions covers a significant portion of the required data for GMMs or GMPEs, this study focuses on gathering near source shallow earthquakes data from Iran, Europe, and Eurasia locations with  $M \geq 6$ ; and  $R_{EPI} \leq 80$  km. For this study, we processed 260 three-component strong motion data from 22 of large Iranian earthquake events and in addition, we will add data other regions with similar tectonic features and shallow earthquake with depth less than 35 km.

Data for Iran are obtained from the Iran Strong Motion Network (ISMN). This network is not available online; however, it has data available for researchers. The metadata information is a collection of recordings from local accelerometric data providers, previously published regional and global databanks, and seismological agencies. These are currently the most reliable sources. The computed parameters to be imported in the catalog are: earthquake source characteristics, the source-to-site path, and recording station.

### Ground-Truth on the CSUEB Campus: Results from Integrating Geophysical, Geological and Geospatial Methods and Fault Trench Studies.

ABIMBOLA, A. O., California State University, East Bay, Hayward, CA, USA, ayoola.abimbola@csueastbay.edu; STRAYER, L. M., California State University, East Bay, Hayward, CA, USA, luther.strayer@csueastbay.edu; MCEVILLY, A. T., California State University, East Bay, Hayward, CA, USA, adrian.mcevilly@csueastbay.edu; CHAN, J. H., U.S. Geological Survey, Menlo Park, CA, USA, jchan@usgs.gov

An earthquake of  $>M6$  along the Hayward fault would be catastrophic, resulting in the damage of infrastructure, homes and potential loss of human lives. California State University, East Bay (CSUEB) lies within the Hayward fault zone of Northern California and is home to student residents. The CSUEB campus is bounded by the Hayward (HF) & Chabor (CF) Faults in the west and the East respectively, and is pervasively cut by anastomosing secondary splay faults.

In June 2015, three exploratory trenches were opened on CSUEB campus to evaluate faulting within the proposed construction area of new student housing. Previous work by Dibblee found minor faulting in this area that we consider to be splays of the CF. We took the opportunity to conduct active-source P and S-wave seismic surveys, coincident with all the three trenches. The purpose of work was to compare the results of these two methods, to further assess seismic hazard on campus, and to contribute to the ongoing effort to create a 3D model of the campus area.

P-waves and S-waves were generated by a 3.5kg sledgehammer, and was recorded on a 48- 69 channel seismic system. Surface wave data were also collected for Multichannel analysis of surface waves was used to derive the near surface S-wave Velocity models. P-wave and S-wave velocity models were used to compute  $V_p/V_s$  for each profile.

Lines 1, 2 and 3 were 141m, 204m and 189m in length respectively, with 3m receiver stations and source spacing. Velocity models show P-wave velocity structures that range from 200m/s to  $>5000$ m/s and S-wave velocities ranging from  $\sim 200$ m/s to  $>1300$ m/s.  $V_p/V_s$  ratios ranged from 1.3 to  $>5$ . Our trench sections showed shear zones are indeed present, which generally coincides zones of relatively high  $V_p/V_s$  ratios.

These are updated final results of our previous preliminary analysis and will be integrated into an ongoing research to produce a detailed 3-Dimensional model of the geology and tectonic setting of the Hayward fault zone.

### Compatibility of a Greek Within-Slab Earthquake Dataset with Published Ground-Motion Prediction Models

SKARLATOUDIS, A. A., AECOM, Los Angeles, CA, USA, andreas.skarlatoudis@aecom.com

I investigate the compatibility of the Abrahamson *et al.* (2015) and Zhao *et al.* (2006) ground-motion prediction equations (GMPEs), with the magnitude, distance and site scaling suggested by a dataset of within-slab earthquakes that occurred in the Greek subduction zone. The motivation for this study comes from a) the relatively small number of recordings from large subduction events, which to a certain extent limits the applicability and accuracy of the regional subduction GMPEs and b) the necessity of capturing the epistemic uncertainty in the probabilistic seismic hazard studies for the broader Aegean area, which is currently underestimated due to the small number of available regional or properly adjusted worldwide ground-motion prediction models. I use only Greek data and a mixed effects procedure, to evaluate inter-event and intra-event residuals of the data relative to the two GMPEs. The residual analysis shows a negative trend of bias (overprediction of the data by the GMPE) for periods shorter than 1s for both GMPEs. I attribute the differences to a) region-dependent differences of the

data properties used to derive the models and the Greek dataset and b) Greek dataset characteristics such as the ratio of back-arc and fore-arc data and the average hypocentral depth of the earthquakes in the dataset. The analysis shows that the magnitude scaling implied by the Greek dataset is similar to that of the two GMPEs. The study of intra-event residuals with distance reveals strong positive trends for the back- and negative trends for the fore- arc data, especially for the Abrahamson *et al.* (2015) model at short periods. The scaling of both GMPEs with respect to  $V_{S30}$  needs to be adjusted since the models underestimate the scaling of the Greek data at low  $V_{S30}$ . Based on this analysis, the modified GMPEs for median ground motions can be used for hazard analysis in Greece considering all the possible limitations arising from this procedure.

### A Note on the Probabilistic Seismic Hazard Assessments of Húsavík, North Iceland

KOWSARI, M., University of Iceland, Reykjavik, Iceland, milad@hi.is; HALLDORSSON, B., University of Iceland, Reykjavik, Iceland, skykur@hi.is

It is of primary importance for any seismically active region via Probabilistic Seismic Hazard Analysis (PSHA) to estimate as accurately as possible the long term probabilities of occurrence of ground motions in a given time interval. Húsavík as the second largest city of northern Iceland is located right on top of the highly active Húsavík-Flatey Fault (HFF). Based on the current nationwide seismic hazard estimation of Iceland, Húsavík appears in the zone of high earthquake hazard with the 10% probability of exceedance of 0.4g peak ground acceleration (PGA) in 50 years, not taking into site effects. Previous seismic hazard estimates of this region have relied on a single ground motion model and incorporated uncertainties in a limited way. In the present study, the Cornell-McGuire (CM-PSHA) and Monte-Carlo (MC-PSHA) methods, which are two robust and acceptable approaches in PSHA, are applied in the estimation of exceedance levels of PGA and spectral acceleration (SA). The fundamental part of the analysis deals with the selection of ground-motion prediction equations (GMPEs) based on three data-driven methods. Moreover, both aleatory and epistemic uncertainties are taken into account. In the context of modeling, aleatory variability is handled by integrating over the distribution of ground motion amplitudes about the median and epistemic uncertainty is considered by both logic tree and defining a representative suite of models. Finally, the disaggregation of the seismic hazard which overcomes the disadvantage of PSHA in term of losing the concept of design earthquake is performed to identify hazard-dominating events. The results of this study combine in the most accurate estimation of the earthquake hazard for the area to date. In the context of heavy industry being planned less than 300 meters from the HFF, the new hazard estimate has great practical significance, both for the plans of infrastructure development and for urban planning of the Húsavík area.

### A Comprehensive Study on a Site-Specific Hazard Analysis for a Liquid Natural Gas Tank Station

HAJI-SOLTANI, A., The University of Memphis, Memphis, TN, USA, hjsltani@memphis.edu; PEZESHK, S., The University of Memphis, Memphis, TN, USA, hjsltani@memphis.edu

The main purpose of this study is to perform a complete site-specific hazard analysis for a Liquid Natural Gas (LNG) tank station located in New Orleans, LA. The considered site is located in the Gulf Coast region where the thick sediments exhibit significantly different ground-motion attenuation in the region. A pressing concern in the evaluation of seismic hazard in this region is using the appropriate attenuation relationships which are not only tuned to the unique site condition of the region, but are also valid for longer periods required in LNG tank station seismic design. A probabilistic seismic hazard analysis (PSHA) will be done using both the National Seismic Hazard Mapping Program codes and the EZ-FRISK software considering the recently updated USGS2014 seismic sources and attenuation relationships for the central and Eastern United States. The results from both software packages will be compared and the horizontal and vertical response spectra for Operating Basis Earthquake (OBE) and Safe Shutdown Earthquake (SSE) conditions will be investigated. The soil characterization has been carried out by performing Crosshole seismic survey in order to determine soil profile to be used in the analysis. The soil has been assigned a soil-type of E, based on NEHRP soil classification. The associated uncertainties in soil thickness, the shear-wave velocity, and soil dynamic properties will be taken into account. The earthquake database will consist of both available recorded earthquakes and simulated ground-motions at the reference bedrock. Various available procedures will be used to choose the appropriate scaled ground-motions. The ground-motions at the ground surface level will be computed using both equivalent linear and nonlinear approaches and final results will be used to calculate the design response spectra. Furthermore, a set of three-component time series at ground surface will be generated for structural time history analyses.



## Spatial Relation Between Source Properties and Aftershock Distribution of the 2015 Nepal Earthquake

LIU, B. Y., Institute of Crustal Dynamics, CEA, Beijing, China, liuboyan\_lby@msn.com; SHI, B. P., University of Chinese Academy of Sciences, Beijing, China, bshi@ucas.ac.cn

Using the 2015  $M_w$  7.9 Nepal earthquake catalog from, we examined where the aftershocks occurred relative to the spatial distribution of the stress change derived from two kinematic source inversions of the fault slip distribution along the main fault. The patterns of the source slip and stress change distributions were much more concentrated and isolated on the main fault plane. About 2/3 of aftershocks with  $M > 3.0$  occurred in the stress increasing area, while a few aftershocks occurred in the area where stress dropped but with high stress change gradient. To obtain a plausible source slip model to explain the aftershock triggering mechanism, we calculated the source spectrums of slip and stress change in the wave-number domain. The resultant spectrum patterns of slip and stress change on the main fault exhibited decay rates of approximately  $k^{-3}$  and  $k^{-2}$ , respectively. We calculate the equilibrium radius  $r_c$  which indicates where the stress drop changes sign, is approximately  $0.7a$  and the area with a positive stress drop is approximately 51% of the total area of the asperity patch. This result indicates that a circular quadratic stress drop model is appropriate for characterizing the rupture process of the Nepal earthquake. This model shows that a positive stress change can occur in regions where a slip displacement exists, which implies that the aftershock might occur in the main fault slip zone, partially explaining the spatially distributed aftershock pattern. Furthermore, the circular quadratic stress drop model more accurately represented the source rupture behavior of the 2015 Nepal earthquake than the circular constant stress drop model.

## Ground-Motion Prediction Equation for Vertical Component Derived from Subduction Slab Earthquake Records

ZHAO, J., Southwest Jiaotong University, Chengdu, Sichuan, China, j.zhao@gns.cri.nz

A ground-motion prediction equation (GMPE) for vertical ground motions will be presented and the GMPE was derived based on strong-motion records from the subduction slab events in Japan. The earthquake category and earthquake locations were determined by Zhao *et al.* (2015). All K-net and KiK-net recording stations used in this study have a measured shear-wave velocity profile down to engineering bedrock. Over 4390 records from 126 earthquakes were used and site classes were used as the site parameter. The site classes were defined by the author in a previous study and nonlinear site term was not necessary. The GMPE covers PGA and 36 spectral periods up to 5.0s and all parameters were smoothed with respect to the logarithm of spectral periods for practical use while the best statistical property of the GMPE was essentially maintained for most spectral periods.

The total standard deviations for the GMPE in this study are generally similar to those of the GMPE (Zhao *et al.* 2016) for the horizontal components at many spectral periods. At spectral periods up to 0.6s, the between-event standard deviations in this study are considerably larger than those of the Zhao *et al.* (2016) model. The within-event standard deviations at spectral periods over 0.1s are considerably less than those from the GMPE by Zhao *et al.* (2016). At short spectral periods up to 0.35s P-wave velocity appears to have both statistically and practically significant effect on the predicted vertical spectrum.

### References

1. Zhao *et al.* (2015) An earthquake classification scheme adapted for Japan determined by the goodness-of-fit for ground-motion prediction equations, *Bull. Seismol. Soc. Am.*, Vol. 105, No. 5, pp. 2750–2763, October 2015, doi: 10.1785/0120150013.

2. Zhao, *et al.* (2016), Ground-Motion Prediction Equations for Subduction Slab Earthquakes in Japan Using Site Class and Simple Geometric Attenuation Functions, submitted to *Bull. Seismol. Soc. Am.*

## Activation of Dead Thrust Faults and Formation of Stable Back Thrusts due to Back Limb Rotation after Thrust-front Propagation: An Example from the Western Transverse Ranges, Southern California

LEVY, Y., SDSU/UCSD, San Diego, CA, USA, uvlevy@gmail.com; ROCKWELL, T., SDSU, San Diego, CA, USA, trockwell@mail.sdsu.edu

Fold-and-thrust belts evolve over time, can produce large-scale faults and potentially accommodate large magnitude earthquakes. The thrust fronts of these structures typically form large fold structures in their hanging walls, and they tend to propagate forward over time to form new thrust fronts. In the Santa Barbara and Ventura region of the Western Transverse Ranges (WTR) of southern California, the Pitas Point Thrust is interpreted as the current thrust front structure, and spatially stable back thrusts accommodate deformation in the hanging wall block of the thrust sheet (More Ranch fault, Rincon Creek fault,

other faults). In our work, we suggest that as the formerly active thrust front is being translated onto the back limb of the new frontal fold, it will rotate and may continue to slip by flexural slip due to this rotation. In addition, re-activation of the older thrust front faults, may form new back thrusts in the previous hanging wall, as a result of local compression. As an example we suggest that the Red Mountain fault in the WTR is just such a former thrust front that now continues to accommodate some slip in the back limb of the Ventura Avenue anticline. We interpret the nearly continuous overturned Tertiary stratigraphy of the Santa Ynez Mountains as a large anticlinorium that formed as the first thrust front over the (mostly) blind San Cayetano thrust, and that the thrust front propagated south with time to the Red Mountain fault and eventually to the currently active thrust front, the southward-vergent Pitas Point-Ventura fault. We further suggest that the steep dip angle of the Red Mountain fault, as observed near the surface, is a result of northward rotation of the fault, which causes it to flexurally slip. The northward rotation is also responsible for continued folding to the north (Ayers Creek syncline) and back thrusting on the hanging wall of the Red Mountain fault (Arroyo Parida fault).

## The Short-term and Impending Trace of Frequency and P Wave Dispersion in Datong Seismic Sensitive Window

ZHOU, L., China Earthquake Networks Center, Beijing, China, lqzhou@seis.ac.cn; ZHANG, Y., Department of Monitoring and Prediction, CEA, Beijing, China, zhangy@cea.gov.cn; SONG, M., The Earthquake Administration of Shanxi Province, Taiyuan, Shanxi Province, P. R. China, smq28@126.com; WANG, X., The Earthquake Administration of Shanxi Province, Taiyuan, Shanxi Province, P. R. China, 365372858@qq.com

Aftershock area of the Datong-Yanggao earthquake (Datong seismic sensitive window) is located in Datong basin of Shanxi rift and the earthquake risk zone of the central-northern part of Shanxi to the border of Shanxi-Hebei-Inner Mongolia. Datong seismic sensitive window exists in the intersection area of three faults, and the sensitive part of northern North China in seismotectonics. Through the 16 years seismic situation tracing, the variation of daily and monthly series frequency of this window is accorded with medium-strong earthquakes in Shanxi seismic belt and Zhangjiakou-Bohai seismic belt. On this basis, we carried out the study on P wave dispersion characteristics of station near Datong window. Applying the method to the SZZ station record of the Datong window earthquake sequence from 2001 we obtained the following results: before 6 earthquakes near and far from the Datong window, the medium quality factor ( $Q_m$ ) were the high values over 1 times mean square error; but  $Q_m$  returned gradually the background after these earthquakes. The medium quality factor ( $Q_m$ ) of SZZ station in contrast with  $Q_m$  eliminating the influence of depth and epicentral distance, the earthquake corresponding rate decreased from 0.9 to 0.5 and the fail rate increased from 0.1 to 0.5, and the anomaly corresponding rate decreased from 0.71 to 0.66 and the false rate increased from 0.29 to 0.34. 17 frequency anomalies occurred in the Datong window since 2001, including 4 anomalies corresponding to earthquakes, 1 anomaly caused by its aftershock activity, and 12 false anomalies. The earthquake corresponding rate and fail rate are 0.6 and 0.4, respectively; the anomaly corresponding rate and false rate are 0.24 and 0.76, respectively. The medium quality factor ( $Q_m$ ) compared with the frequency of Datong window, the earthquake corresponding rate is similar, while the anomaly corresponding rate of  $Q_m$  is better.

## A Two-tiered Approach to Event Calibration across the Zagros Mountains of Iran

KARASOZEN, E., Colorado School of Mines, Department of Geophysics, Golden, CO, USA, ekarasoz@mines.edu; NISSEN, E., Colorado School of Mines, Department of Geophysics, Golden, CO, USA; BERGMAN, E., Global Seismological Services, Golden, CO, USA; GHODS, A., Institute for Advanced Studies in Basic Sciences, Zenjan, Iran, aghods@iasbs.ac.ir

The Zagros mountains of Iran have the highest density of recorded earthquakes of any continental mountain belt in the world and therefore offer rich potential for investigating the tectonics of fold-and-thrust belts. However, the causative faults are mostly buried beneath a thick sedimentary cover, leading to competing hypotheses about how shortening is accommodated. The kinematics of the range are further obscured by large uncertainties in catalog earthquake locations, which in some instances are known to exceed 50 km. To overcome this problem, we developed a new two-tiered multiple-event relocation approach that yields orogen-wide, calibrated hypocentral parameters (latitude, longitude, origin time and in some instances depth) with minimal location bias. In the first stage, small clusters of well-recorded earthquakes are relocated (100s of events over a ~100 km spatial scale). This stage employs either a “direct” calibration, which takes advantage of recent improvements in station coverage, or an “indirect” calibration, which exploits independent location constraints from local aftershock

studies or InSAR solutions, both of which are especially plentiful in the Zagros. In the second stage, these cluster results are incorporated into a Bayesian relocation (involving the Bayesloc algorithm of Myers *et al.*, 2011) that yields improved hypocenters across the entire range (incorporating 1000s of events on a ~1000 km spatial scale). Here, we present an outline of the workflow and some preliminary results which nevertheless provide new insights into regional faulting. This study is the initial step in developing a location bias-free seismicity catalog for the entire Iran region, which will in turn provide a greatly improved basis for research into seismic hazards in the area.

### Development of Ground Motion Prediction Equation for East Malaysia Considering Shallow Crustal Earthquakes

ADNAN, A. B., eSEER-IKG-University of Technology Malaysia, Johor Bahru, Johor, Malaysia, azlanadnan@utm.my; HARITH, N., University Malaysia Sabah, Kota Kinabalu, Sabah, Malaysia, harithsheena@gmail.com; SHOUSHARI, A. V., University of Technology Malaysia, Johor Bahru, Johor, Malaysia, vsabdollah@gmail.com

The Ground Motion Prediction Equation (GMPE) model is derived for East Malaysia, for the prediction of horizontal component of ground motions. The time history databases surrounding East Malaysia were collected from local seismological network stations managed by Malaysian Meteorological Department (MMD), with data spanning from 2004 until 2012. The network has been operating for nearly 11 years with 30 permanent seismic stations installed to entire Malaysia's strategic locations. They consist of broadband and short period accelerometric sensor on real-time monitoring. The site conditions in each accelerometric network are varies from one station to another. The shear-wave velocity in the top of 30 m or VS30 has been used. Thus, the site conditions on soil type A (EC8) has been considered in the analysis. A total of 111 earthquake time histories including local earthquake events from entire Malaysia and Sumatra strike slip shallow crustal earthquakes were selected. These records came from 42 earthquakes retrieved from 28 seismic stations. The new GMPE for rock site in East Malaysia region is developed for peak ground acceleration. The model is derived using a local dataset from strike slip earthquake consisted of corrected and processed accelerograms at distances between 10 and 1000 km with moment magnitude in a range of 2.8 and 7.7. The models of GMPE developed is based on Zare *et al.*, 1999. This equation is derived by least-square method for the estimation of peak ground acceleration (PGA) and spectral acceleration for 5% damping ratio and for periods between 0.0 second and 5.0 seconds. The new developed GMPE of East Malaysia region is expressed as  $\text{Log(PGA)} = 0.2196M_w + 0.0019\text{Rhypo} - 0.8914 \text{Log Rhypo} + 1.5205$  where  $M_w$  is moment magnitude, Rhypo is hypo central distance with standard deviation 0.394. The new GMPE model developed in this study seems to provide better estimates for East Malaysia in comparison with various other GMPEs considered.

### Seismic Waveform Spectrum Shift of Foreshocks in North Tibetan Plateau

YANG, L. M., Earthquake Administration of Gansu Province, Lanzhou, Gansu, China, yanglm@gdszj.gov.cn; MEI, X. P., Earthquake Administration of Gansu Province, Lanzhou, Gansu, China; JIANG, J. J., Earthquake Administration of Gansu Province, Lanzhou, Gansu, China

By detecting the earthquake catalog in northeastern margin of Tibetan Plateau, we found the seismicity became more active before mid-strong earthquakes. There are some foreshocks occurred before the strong earthquake. The spectrum of the foreshocks closed to the main shock became narrower and the peak of the spectrum shifted to low frequency. Here we presented the analyzing results of the spectrum of foreshocks before two strong earthquakes occurred in North Tibet. One is Yushu earthquake with Ms7.1 occurred in 2010 and another is Yutian earthquake with Ms7.3 occurred in 2014. The results indicated obvious spectrum shift of foreshocks.

In order to investigate the characteristic of the waveform spectrum of foreshocks, we firstly compared the spectrum of foreshocks and normal events. As general, the main energy of the frequency spectrum of normal events is roughly around 0~5Hz distributed in a wider range, which represented the spectrum of normal background seismic activity.

Two hours before the main shock of Yushu earthquake, a small event with Ms 4.7 occurred, which is a typical foreshock. The results of its spectrum show that the dominant frequency is about 1.5 Hz or lower. Compared with the normal event, the spectrum range of foreshock became narrower, and shifted to the low frequency.

One day before the main shock of Yutian earthquake, an event with Ms 5.3 occurred, which is also a foreshock. The results of its spectrum is consistent with the case of foreshock before Yushu earthquake. The dominant frequency is about 1.5 Hz or lower, and shifted to the low frequency.

The phenomenon of waveform spectrum shift of foreshocks is consistent with the results of some experiment of rock breaking, and it may be associated with the enhancement of stress field in source area of the main shock, which could result in the metastable extension, medium broken, crack extension and nucleation. This work is helpful to understand the mechanism of the strong earthquake.

### Bimaterial Interfaces at the Karadere Segment of the North Anatolian Fault, Northwestern Turkey

NAJDAHMAJLI, B., GFZ German Research Centre for Geosciences, Potsdam, Germany, bita@gfz-potsdam.de; BOHNHOFF, M., GFZ German Research Centre for Geosciences, Potsdam, Germany, bohnhoff@gfz-potsdam.de; BENZION, Y., University of Southern California, Department of Earth Sciences, Los Angeles, CA, USA, benzion@usc.edu

We image velocity contrast (bimaterial) interfaces along the Karadere fault of the North Anatolian Fault Zone (NAFZ), towards the eastern part of the 1999 Izmit  $M_w 7.4$  rupture in NW Turkey, using waveforms recorded by a local seismic network. Applying an automatic procedure for identification and picking of fault zone head waves (FZHW) and direct P arrivals, and manually revising the picks through particle motion analysis, we identify two different groups of FZHW as well as fault zone reflected waves (FZRW). The first group of FZHW has a moveout with respect to the direct P arrivals with distance traveled along the fault, indicating a deep bimaterial interface down to the base of the seismogenic crust with an average velocity contrast of ~3.4%. The second group of FZHW has a constant time difference from the direct P arrivals, and is associated with a shallow local interface bounding a low velocity damage zone or basin structure. This zone exists on both sides of the fault trace and extends to a depth of 4-5 km. While the first group of FZHW exist on the slower crustal block, the second group of FZHW and FZRW are present generally on both sides of the fault. This added to the richness and complexity of the early P waveforms observed at stations close to a large fault. The relatively low velocity contrast across the Karadere fault compared to values to the west may have helped stopping the Izmit rupture.

### Variations in the Crustal Shear Wave Velocity Structure above the Peruvian Flat Slab

KNEZEVIC ANTONIJEVIC, S., University of North Carolina, Chapel Hill, NC, USA, sknezevi@live.unc.edu; WAGNER, L. S., Carnegie Institution for Science, Washington, DC, USA, lwagner@carnegiescience.edu; BECK, S. L., University of Arizona, Tucson, AZ, USA, slbeck@email.arizona.edu; ZANDT, G., University of Arizona, Tucson, AZ, USA, gzandt@email.arizona.edu; LONG, M. D., Yale University, New Haven, CT, USA; TAVERA, H., Instituto Geofisico del Perú, Lima, Perú, hernando.tavera@igp.gob.pe

The subduction of the Nazca Plate under the South American plate has resulted in the formation of the Andean mountain belt. However, the structure of this exceptionally thick continental crust is still poorly understood. Even less clear is how the change in geometry of the subducting Nazca Plate from steep to flat affects the overriding lithosphere. Here we study the flat slab in southern Peru by combining ambient noise with earthquake-generated Rayleigh wave phase velocities to image the shear wave velocity structure of the crust and uppermost mantle between ~10° and 18°S. We use a dataset collected over three-year period from 2011 to 2013 from three regional temporary broadband deployments, PULSE, CAUGHT, PERUSE, together with global seismic network stations in the area. We find that variations in the crustal shear wave velocity structure spatially coincide with changes in lithology between the major geomorphological units. Our images reveal predominantly low crustal velocities under granitic intrusions of Western Cordillera and high velocities under the Precambrian basement of the Eastern Cordillera. However, lower velocities along the Western Cordillera progressively increase to the north in the uppermost ~30 km of the crust. This may relate to formation of the flat slab and accompanying thermal shielding and cessation in volcanism that first occurred in the north [Hampel *et al.*, 2002]. In contrast, below ~30 km depth we observe a gradual decrease in velocities from south to north, consistent with the recently imaged slab tear located north of the Nazca Ridge and shallowest portion of the flat slab [Antonijevic *et al.*, 2015]. In the Subandean Zone we observe a pronounced low velocity anomaly centered around ~71°W ~12.7°S. This anomaly may relate to fluids within the Andean detachment fault and/or thick Quaternary sediments within the Subandean synclinal basin bound by thrust faults to the east and west.

### Lithospheric Structure of an Incipient Rift Basin: Results from Receiver Function Analysis of Bransfield Rift Basin, NW Antarctic Peninsula

BIRYOL, C. B., University of North Carolina, Chapel Hill, NC, USA, biryol@live.unc.edu; LEE, S. J., U.S. ARMY RESEARCH LABORATORY, Durham, NC, USA, stephen.j.lee28.civ@mail.mil; LEES, J. M., University of North



Carolina, Chapel Hill, NC, USA, jonathan.lee@unc.edu; SHORE, M. J., University of North Carolina, Chapel Hill, NC, USA, mshore@email.unc.edu

Bransfield Basin (BB), located northwest of the Antarctic Peninsula (AP) and southeast of the South Shetland Islands (SSI), is the most active section of the Antarctic plate margin. The region has long been a convergent plate boundary where the Phoenix plate was subducting southeastward beneath the Antarctic Plate. This region is thus characterized by long-lived (50 Ma) arc magmatism and accretion, giving way to metamorphism and uplift of Mesozoic-Cenozoic accretionary wedge material that forms the AP and SSI. Upon collision of the Antarctic-Phoenix spreading center with the subduction front near SSI (ca. 4 Ma), spreading deactivated and the Phoenix plate became a part of the Antarctic Plate. The collision of the spreading center gave way to opening of slab windows where the subduction trench meets the spreading ridge. After the cessation of spreading along the Phoenix-Antarctic spreading ridge, subduction of the Phoenix plate beneath AP and SSI slowed down dramatically and the Phoenix slab began to roll-back slowly along the South Shetland Trench (SST) towards the Pacific. As a consequence of inter-plate coupling, the roll-back of the Phoenix slab gave way to slow extension in the back arc region and opening (rifting) of the BB. Although there is consensus on the origin of the BB, the current configuration of the basin is still unclear. Most of the controversy stems from uncertainties regarding the crustal thickness of the BB.

We use data from existing permanent and temporary deployments in the region to compute teleseismic and local receiver functions to constrain the lithospheric structure and crustal thickness of the BB, as well as the AP and SSI. Preliminary results suggest the crust is rapidly thinning from 35 km to 20-25 km from the AP towards the South Shetland trench. High  $V_p/V_s$  ratios (~1.9) beneath BB and SSI, agree well with the incipient crustal rift of BB and the presence of partial melts.

---

## Advancements in Network Operations and Station Design

Poster Session · Thursday · 21 April · Tuscany F

---

### The Design and Data Translation of the Rotaphone, with an Example of the Instrument

MÁLEK, J., Czech National Academy, Prague CZ, malek@irms.cas.cz; BROKEŠOVÁ, J. P., Charles Univ, Prague CZ, johana@karel.troja.mff.cuni.cz; EVANS, J. R., U.S. Geological Survey, Santa Cruz, CA, USA, jrevans@usgs.gov

Rotaphones are special geophone systems enabling measurement of 6 axes of ground motion, 3 translational and 3 rotational (6-degrees-of-freedom; 6DOF). In 2015 a new version of this sensor was designed, built, and tested at various sites. It has 16 geophones (8 vertical and 8 horizontal) around the periphery of a rigid disk-shaped frame. The key in converting these 16 axes measurements to 6DOF axes is precise relative calibration of the geophones. The first calibration (response estimate) is by the geophone manufacturer. However, to reach the accuracy required for rotational-components, measurements derived from differential signals between geophones (~1 to 100 Hz), a procedure of relative calibrations is required. The properties of the geophones also change with temperature, pressure, and from material aging. Therefore, the calibration has to be done repeatedly during the field measurements (in-situ calibration). For this version of Rotaphone, we developed two methods of in-situ calibration. The first uses a seismic shaker that produces repeatable seismic pulses. The Rotaphone detects these pulses repeatedly while the instrument is rotated around its vertical axis by constant angle increments between pulses. By comparing individual measurements with the sum of all measurements, we can reach very precise cross-calibration anchored to the mean response of the geophones. The 2nd technique is enabled by the instrument's over-determination - we have at our disposal 16 geophones while only six components are to be determined. The calibration is made simultaneously with field measurements. Finally, we will calibrate all the Rotaphones we use at the Albuquerque Seismological Laboratory of the USGS; we expect those tests will be valid between about 0.5 and 37 Hz; they are relative to laboratory standards. Examples of Rotaphone installations and calibration accuracy are discussed. An operating example of a Rotaphone will be at the poster session.

### Feasibility of Tilt Measurement Using Seismometer Mass Position Data

BAINBRIDGE, G., Nanometrics Inc., Ottawa, ON, Canada, geoffreybainbridge@nanometrics.ca; KARIMI, S., Nanometrics Inc., Ottawa, ON, Canada, sepidehkarimi@nanometrics.ca; YENIER, E., Nanometrics Inc., Ottawa, ON, Canada, emrahyenier@nanometrics.ca; MOORES, A., Nanometrics Inc., Ottawa, ON, Canada, andrewmoores@nanometrics.ca

Force feedback seismometers provide mass position outputs which represent the time-averaged feedback force applied to each inertial mass, in order to cancel

external forces and keep it balanced at its center point. These external forces are primarily due to tilt and temperature. In a symmetric triaxial seismometer, tilt and temperature effects can be distinguished because temperature affects all 3 axes equally whereas tilt causes a different force on each axis. This study analyzes the resolution of tilt and temperature signals that can be obtained from a force-feedback seismometer, and the potential applicability of this data to applications such as volcano monitoring and cap rock integrity monitoring. Also the synergy of a combined seismic, tilt, and temperature instrument is considered.

### Short-Period Sensors with Extended Frequency Response for Earthquake Monitoring

BESEDINA, A. N., Institute of Geosphere Dynamics, Russian Academy of Sciences, Moscow, Russian Federation, besedina.a@gmail.com

Seismological monitoring contains enormously wide range of measurements—from extremely low-frequency motions (tides) to kilohertz frequency range (mine seismicity). Short-period seismometers are usually used for records weak seismic events with unknown sources. Sensor bandwidth limitations can lead to underestimation of radiated seismic energy due to losses in high-frequency part of signal. Short-period sensors with enhanced amplitude-frequency response in high-frequency part of the spectrum allow avoiding this instrumental problems.

In the last decade the main tendency of the global seismological observations consisted in increase of the quantity of broadband seismic stations. We asked whether short-period seismometers with enhanced amplitude-frequency response in low-frequency part of the spectrum could replace broadband sensors to evaluate earthquake magnitudes properly and at a reasonable cost. We assessed magnitude uncertainties between magnitudes determined by data of broadband and modified short-period sensors for earthquakes with  $M > 6$  recorded in 2014 at the territory of the Mikhnevo geophysical observatory, Russia. Data analysis consisted in body wave magnitude and surface wave magnitude estimation by means of standard seismological methods in terms of peak ground velocity in a certain periods range for body P-wave and surface waves. P-wave magnitude correction by 0.19 and surface magnitude correction by -0.06 evaluate apparent magnitudes with the standard deviation 0.12. These statistically base usage of short-period sensors with enhanced amplitude-frequency response for earthquake monitoring in addition or as an alternative to broadband seismometers. So, short-period seismometers with enhanced amplitude-frequency response both in high-frequency and low-frequency parts of the spectrum can be used to monitor both small seismic events and strong distant earthquakes. This work was supported by the Russian Foundation for Basic Research (project no. 16-35-00508).

### Seismic Observations of Surface-Hole Installation Techniques

SWEET, J., IRIS, Washington, DC, USA, justin.sweet@iris.edu; BEAUDOIN, B., IRIS/PASSCAL Instrument Center, Socorro, NM, USA, bruce@passcal.nmt.edu; BARSLOW, N., IRIS/PASSCAL Instrument Center, Socorro, NM, USA, barslow@passcal.nmt.edu; PFEIFER, C., IRIS/PASSCAL Instrument Center, Socorro, NM, USA, cathy@passcal.nmt.edu; REUSCH, M., IRIS/PASSCAL Instrument Center, Socorro, NM, USA, mouse@passcal.nmt.edu; ANDERSON, K., IRIS, Washington, DC, USA, kent@iris.edu

Advances in seismometer design have diversified the range of instruments available for use in temporary field installations. IRIS programs have helped steer development of these new instruments to meet evolving needs. PASSCAL now has a small pool of posthole broadband sensors, purpose built for direct burial. Near-surface posthole installations are a new, cost effective, and logistically simple technique for broadband emplacement that is an alternative to the vault installations used in portable broadband seismic experiments for nearly 30 years. Direct burial installation is limited to the time and effort required to dig the borehole and emplace the sensor, thus reducing both material costs and time to install.

We select a range of PASSCAL portable networks and compare their performance. Because PASSCAL networks have been deployed in a wide variety of environments, our results allow us to compare the noise performance of different installation types as well as variations among installation types in many different environments. Our initial analyses indicate that direct burial installations generally have lower noise levels than vault installations on horizontal channels at periods greater than about 10 seconds and on vertical channels at periods greater than about 30 seconds. In addition, we summarize observations from a variety of experiments using newly designed sensors and installations including Poker Flat, AK, South Pole, Antarctica, Taku Glacier, AK, and Nenana Basin, AK.

### Review of Recent Improvements in Design and Performance of the Alaska Regional Seismic Network

MERZ, D. K., Alaska Earthquake Center, Fairbanks, AK, USA, dkmerz@alaska.edu; BRUTON, C. P., Alaska Earthquake Center, Fairbanks, AK, USA,



cpbruton@alaska.edu; BUURMAN, H., University of Alaska, Fairbanks, AK, USA, hmbuurman@alaska.edu; DALTON, S. M., Alaska Earthquake Center, Fairbanks, AK, USA, smdalton@alaska.edu; RUPPERT, N. A., Alaska Earthquake Center, Fairbanks, AK, USA, nruppert@alaska.edu; WEST, M. E., Alaska Earthquake Center, Fairbanks, AK, USA, mewest@alaska.edu

Alaska is the most seismically active state in the U.S. The Alaska Earthquake Center (AEC) maintains a network of about 150 seismic stations throughout the state to monitor regional seismicity. Due to a concerted effort put into the infrastructure upgrades in the past 15 years, the AEC network is now 100% digital and 99% broadband. Alaska's vastly remote nature, abundant wildlife, and dynamic climate provide a challenging environment to maintain real-time acquisition of seismic data. In the past three years, the AEC has significantly improved real-time data returns through standardizing station design, increasing solar charging capacity on site, and utilizing Internet-based station monitoring tools.

Aging power component replacements were selected with an emphasis on reliability and efficiency. Solar arrays were supplemented with panels oriented to maximize charging capacity in the shoulder seasons.

The ability to track and maintain station health remotely has been greatly improved through the implementation of the network management tool Nagios and the use of IRIS MUSTANG web services. In addition to providing real-time diagnostics, these tools allow us to note behavior cycles that may affect data recovery and data quality.

These combined efforts have increased our average yearly data return rates from 80% to over 90% between 2013 and 2015. By investing in station design and data quality monitoring, we ensure stronger network performance and higher overall return rates to provide more reliable real-time acquisition of seismic data and reporting of earthquakes. In 2014 and 2015 AEC reported record number of earthquakes in Alaska.

### Waveform Recovery Enhancements in the Utah Network

RUSHO, J., University of Utah Seismograph Stations, Salt Lake City, UT, USA, jon@seis.utah.edu; HATCH, C., University of Utah Seismograph Stations, Salt Lake City, UT, USA, hatch@seis.utah.edu; DROBECK, D., University of Utah Seismograph Stations, Salt Lake City, UT, USA, drobeck@seis.utah.edu; PANKOW, K., University of Utah Seismograph Stations, Salt Lake City, UT, USA, pankow@seis.utah.edu

The University of Utah Seismograph Stations (UUSS) runs a diverse network with various instruments and telemetry paths. Several instruments have minimal storage capability for capturing triggered events; some stations have no such capacity. With the advent of very small scale computers based around System-on-a-Chip architectures, adding such hardware to existing stations or telemetry aggregation points has become a cost effective solution. For a minimal investment per site, usability of legacy equipment can be extended. Over the past three years, UUSS has been testing and deploying systems to provide enhanced data collection and to facilitate recovery in the event of telemetry outages. Our focus has been on strong-motion sites near the Wasatch Fault in the Salt Lake Valley and distant strong-motion sites that require extended travel for maintenance. Here, we report on three projects using the Raspberry Pi computers in the Utah network. The projects include: (1) installation at 32 strong-motion sites that use Kinemetrics K2/Etna instruments, providing on-site storage of 100+ days of continuous waveform data and telemetry back-fill capability; (2) installation at four mountain-top telemetry aggregation sites, providing data storage for both digital instruments telemetered to the site as well as storage for analog data which is digitized at the mountain top; and (3) testing Raspberry Pi computers with Reftek dataloggers to enhance waveform collection and backfill capability. To date, UUSS has had several successful data-recovery or data-backfill events, allowing us to recover 3-7 days of data that might have otherwise been lost using traditional telemetry means.

### Microseismic Network Design in 3D Velocity Models

WUESTEFELD, A., NORSAR, andreas.wuestefeld@norsar.no; NAESHOLM, S. P., NORSAR, peter@norsar.no; LANG, D., NORSAR, dominik@norsar.no

The demand on the versatility of microseismic monitoring networks has increased rapidly. In early projects, being able to locate any triggers was considered a success. These early successes lead to a better understanding of how to extract value from microseismic results. Today, operators, regulators, and service providers work closely together to find the optimum network design to meet various requirements. In this article we discuss three aspects that are of concern in the design phase of modern microseismic monitoring networks: 1) Magnitude of completeness; 2) Location accuracy; 3) Ground-motion hazard.

Using the well-documented example region around the San Andreas Fault Observatory at Depth (SAFOD) located north of Parkfield, California, we pres-

ent several approaches to these sometimes competing requirements. Modelling these parameters prior to installation of a sensor network, helps to identify the potential challenges to meet the survey objectives and thus appropriate changes to the design can be implemented.

We are modelling the performance of an hypothetical network of 11 sensors in the area. To highlight the importance of using the correct velocity model, we then compare these performance predictions with those for a simplistic 1D velocity model, commonly the only available source of velocity for hydraulic fracturing projects.

Our results show that assuming a simple 1D velocity model neglects local ray bending effects that strongly affect location accuracy estimates and detection limit estimates. This is important in helping to design efficient monitoring networks.

### A Procedure for CISN Ground Motion Packet Association

HAGOS, L., California Geological Survey, Sacramento, CA, USA, Lijam.Hagos@conservation.ca.gov; HADDADI, H., California Geological Survey, Sacramento, CA, USA, Hamid.Haddadi@conservation.ca.gov; SHAKAL, T., California Geological Survey, Sacramento, CA, USA, Tony.Shakal@conservation.ca.gov

ShakeMaps produced by the California Integrated Seismic Network (CISN) make use of observed peak ground motion data that are exchanged between the networks in a form of packets. These ground motion packets contain amplitude parameters of PGA, PGV, PSA (at periods 0.3, 1 and 3 seconds) and their corresponding times. The majority of the exchanged packets come associated with an earthquake by the authoritative network. However, for those that come unassociated, the California Geological Survey (CGS) uses an event association scheme to associate them with an earthquake. In the absence of phase arrival times in the exchanged ground motion packets, a set of criteria is employed to associate packets, based on ground motion amplitudes and their times in the packets. These peak ground motion times depend on a number of factors including source-site distance, velocity structure, and duration of strong seismic shaking. Earthquake duration in turn is sensitive to the magnitude, frequency content of the seismic wave, site conditions and source complexity in the near field. Through analysis and evaluation of these factors, this study presents a scheme to associate ground motion packets with the corresponding earthquake based on estimates of travel times of seismic waves, hypocentral distances and amplitudes of peak ground motions. Low amplitude motions, generated by small magnitude earthquakes or due to very large source-site distances, may be contaminated by noise leading to an inaccurate report of earthquake ground motion amplitudes and their corresponding arrival times. In general, the event association scheme provides a distance dependent sliding time window where much of the ground motion energy falls. The scheme includes distance and magnitude constraints in order to filter out possible noisy data from getting associated. The results of this study will improve the quality of observed data entering into ShakeMap computation.

### Seismic Data Quality Control using DQA, Data Quality Analyzer

HOLLAND, A. A., U.S. Geological Survey, Albuquerque, NM, USA, aaholland@usgs.gov; BAKER, A. M., U.S. Geological Survey, Albuquerque, NM, USA, ambaker@usgs.gov; FALCO, N., Honeywell Technology Solutions Inc., Albuquerque, NM, USA, nfalco@usgs.gov; HOLLAND, J., U.S. Geological Survey, Albuquerque, NM, USA, jholland@usgs.gov; RINGLER, A. T., U.S. Geological Survey, Albuquerque, NM, USA, aringler@usgs.gov; WILSON, D., U.S. Geological Survey, Albuquerque, NM, USA, dwilson@usgs.gov

The U.S. Geological Survey's Albuquerque Seismological Laboratory (ASL) has several initiatives underway to enhance and track the quality of data produced from ASL-operated seismic networks (CU, NE, IC, IU, IW, and US), and to improve communication about data problems to the user community. The newly developed Data Quality Analyzer, DQA, is a tool developed to provide station quality data in a quantitative and automated manner.

The DQA consists of a metric calculator, a database, and a web interface: The metric calculator compares hashes of metadata and data to detect changes in either and performs subsequent recalculations as needed. This ensures that the metric values are up to date and accurate. Metric values and limited station descriptions are stored in the database. The Web interface dynamically loads station data from the database and allows the user to make requests for time periods of interest, review specific networks and stations, select specific metrics to visualize, and plot metrics as a function of time.

The quantification of data quality is based on the evaluation of various metrics (e.g., availability, gap count timing quality, daily noise levels relative to long-term noise models, and comparisons between broadband data and event synthetics). Users may select which metrics contribute to the assessment and those metrics are aggregated into a "grade" for each station. The DQA is being actively

used for station diagnostics and evaluation based on the completed metrics. Use of DQA at the ASL has helped identify instrument failures, problematic installations, as well as metadata issues and provides consistent and comparable measures of station performance. The ASL is in the process of making the metrics more flexible and is developing higher frequency metrics that may be more applicable to regional networks and as well as aftershock deployments.

### **The EarthScope USArray Array Network Facility (ANF): Metadata, Network and Data Monitoring for the Transportable Array in Alaska**

EAKINS, J., Univ. of California, San Diego, La Jolla, CA, USA, jeakins@ucsd.edu; VERNON, F., Univ. of California, San Diego, La Jolla, CA, USA, fvernon@ucsd.edu; COX, T., Univ. of California, San Diego, La Jolla, CA, USA, tacox@ucsd.edu; MARTYNOV, V., Univ. of California, San Diego, La Jolla, CA, USA, vmartynov@ucsd.edu; TYTELL, J., Univ. of California, San Diego, La Jolla, CA, USA, jtytell@ucsd.edu; REYES, J., Univ. of California, San Diego, La Jolla, CA, USA, reyes@ucsd.edu; DAVIS, G., Univ. of California, San Diego, La Jolla, CA, USA, gadavis@ucsd.edu; MEYER, J., Univ. of California, San Diego, La Jolla, CA, USA, jmeyer@ucsd.edu; BUSBY, R., IRIS, Washington, DC USA, busby@iris.edu

The Array Network Facility (ANF) at UC San Diego is responsible for: the delivery of all EarthScope USArray Transportable Array stations (74 remaining Lower48 and an eventual total of ~250 stations in Alaska/Canada) to the IRIS Data Management Center primarily via real-time data flow with additional transmission of baler archive data; station command and control; verification and distribution of metadata; providing useful interfaces for personnel at the TA Alaska Array Operations Facility (access to state of health information, immediate confirmation of successful installations while they are at remote locales, and coordinated equipment tracking interface); and quality control for all data. To meet these goals, we use the Antelope software package to facilitate data collection and transfer, generation and merging of the metadata, monitoring of data-loggers, and analyst review of individual events.

Our datacenter has evolved over the past twelve years of TA operations and uses a virtualized infrastructure. Additional web tools have been developed using MongoDB and JSON technologies.

Currently nine networks contribute data to enhance and add to the capabilities of the Transportable Array. As part of the quality control process, automatic processing and daily analyst review, associates arrivals against available regional network bulletins. Consistently high data return rates are a goal for USArray operations with a median daily return rate for seismic data of 97% maintained over 12 years of operations. In addition to 124 broadband seismic channels, 32 strong motion sensors, 115 setra microbarometers and infrasound sensors, and 8 full weather packages return multiple channels of data.

Visit <http://anf.ucsd.edu> for more information on the project and current status.

### **Array Network Facility Operations for the Central and Eastern United States Seismic Network**

COX, T., Univ. of California, San Diego, La Jolla, CA, USA, tacox@ucsd.edu; VERNON, F., U, La Jolla, CA, USA, fvernon@ucsd.edu; EAKINS, J., Univ. of California, San Diego, La Jolla, CA, USA, jeakins@ucsd.edu; DAVIS, G., Univ. of California, San Diego, La Jolla, CA, USA, gadavis@ucsd.edu; MEYER, J., Univ. of California, San Diego, La Jolla, CA, USA, jmeyer@ucsd.edu; REYES, J., Univ. of California, San Diego, La Jolla, CA, USA, reyes@ucsd.edu; TYTELL, J., Univ. of California, San Diego, La Jolla, CA, USA, jtytell@ucsd.edu; BUSBY, R., IRIS, Washington, DC, USA, busby@iris.edu

When the USArray Transportable Array (TA) entered and moved through the central and eastern United States, it serendipitously coincided with an increase in seismicity in the area. Recognizing the unique opportunity for more long-term monitoring in a region long underserved by seismic monitoring, several Federal agencies worked to create the Central and Eastern United States Network (CEUSN). Field operations conducted by IRIS established 159 stations as part of the N4 network by reinstalling equipment into existing TA vaults or permitting new sites. Thirteen other networks contribute additional stations to bring the CEUSN to a total of over 300 active stations.

Consisting of a variety of sensor types, the CEUSN is providing the eastern United States with first-of-its-kind comprehensive seismic network coverage. All N4 stations record broadband data at 100, 40, and 1 sps. 40 stations have strong motion sensors returning 100 sps in real-time, with the possibility of 200 sps in triggered mode. In addition, all N4 stations have a Setra microbarometer and Hyperion infrasound sensor, and 8 stations have a Vaisala weather package.

The Array Network Facility (ANF) at the University of California San Diego, conducts all real-time operations for the network. The CEUSN consistently performs with excellent data return rates of greater than 99%. During

2015, the automatic system detected nearly 3000 events with detection thresholds down to M2.7, with the possibility for tuning to pick up lower magnitude events. Beyond the current archiving of all waveform data and metadata at the DMC, the ANF will be implementing QuakeXML as an additional means of data sharing.

To see the current status of network deployment, realtime earthquake maps, special event information, and more, visit <http://ceusn.ucsd.edu>

### **Data Sets and Data Delivery Services from the Northern California Earthquake Data Center**

NEUHAUSER, D. S., UC Berkeley Seismological Laboratory, Berkeley, CA, USA, doug@seismo.berkeley.edu; ZUZLEWSKI, S., UC Berkeley Seismological Laboratory, Berkeley, CA, USA, stephane@seismo.berkeley.edu; ALLEN, R. M., UC Berkeley Seismological Laboratory, Berkeley, CA, USA, rallen@berkeley.edu

The Northern California Earthquake Data Center (NCEDC) provides a permanent archive and real-time data distribution services for a unique and comprehensive data set of seismological and geophysical data sets encompassing northern and central California. We provide access to over 85 terabytes of continuous and event-based time series data from broadband, short-period, strong motion, and strain sensors as well as continuous and campaign GPS data at both standard and high sample rates. The Northern California Seismic System (NCSS), operated by UC Berkeley and USGS Menlo Park, has recorded over 900,000 events from 1984 to the present, and the NCEDC serves catalog, parametric information, moment tensors and first motion mechanisms, and time series data for these events. We also serve event catalogs, parametric information, and event waveforms for DOE enhanced geothermal system monitoring in northern California and Nevada.

The NCEDC provides several ways for users to access these data. The most recent development are web services, which provide interactive, command-line, or program-based workflow access to data. Web services use well-established server and client protocols and RESTful software architecture that allow users to easily submit queries and receive the requested data in real-time rather than through batch or email-based requests. Data are returned to the user in the appropriate format such as XML, RESP, simple text, or MiniSEED depending on the service and selected output format. The NCEDC supports all FDSN-defined web services and a number of IRIS-defined and NCEDC-defined services, including a web service that delivers pre-assembled waveform sets for events. We also continue to support older email-based and browser-based access to data. NCEDC data and web services can be found at <http://www.ncedc.org> and <http://service.ncedc.org>.

---

## **Characterizing the Stress Field and Stress Drop for Earthquake Source Physics and Hazard Assessment**

Poster Session · Thursday · 21 April · Tuscany F

---

### **Using Finite Fault Inversions and Near-Field Data to Determine the Uncertainty Range of Co-Seismic Stress Drop of Large Earthquakes**

ADAMS, M. N., University of California, Santa Barbara, CA, USA, mareikeadams@uic.ucsb.edu; JI, C., University of California, Santa Barbara, CA, USA, ji@geol.ucsb.edu; TWARDZIK, C., University of California, Santa Barbara, CA, USA, cedric@ucsb.edu; ARCHULETA, R., University of California, Santa Barbara, CA, USA, archuleta@ucsb.edu

Rupture of a large earthquake leads to significant stress variation in the source region. Realistically, the static stress drop varies locally over the fault surface, and in most cases only its average value is properly constrained using seismic observations. Previous studies show that the median of the average stress drop is roughly constant (3–4 MPa) over a large range of the seismic moment (*e.g.* Kanamori and Anderson 1975), but the estimates of individual earthquakes can deviate from this median by a factor of 4 (*e.g.* Allmann & Shearer 2007). As stress drop is a key parameter in accurately estimating the strong ground motion, large uncertainties in stress estimation suggest a large uncertainty in predicting seismic hazard. We have developed a new procedure to see if we can robustly constrain the uncertainty range for the co-seismic stress drop of large earthquakes. For a given rupture event, our approach is to see whether we can simultaneously fit the observed waveforms and a target stress drop set a-priori. Then, we conduct a grid search across possible target stress drops. For each case, a series of modified finite fault inversions are conducted to find the solution matching the pre-assigned stress drop and seismic and geodetic data. Our recent analysis of the 2014 Rat Island  $M_w$  7.9 earthquake revealed that the lower bound of the energy based average stress drop could be well-constrained (~4MPa) using teleseismic waveforms. However, this dataset exhibits no sensitivity to an upper bound. The roughness

of the inverted slip distributions changed dramatically as the target stress drop increased, but the misfit remained nearly identical. Here we extend our analysis to a large shallow earthquake: the 2015  $M_w$  7.8 Nepal earthquake. We explore whether the good near source static observations (INSAR and GPS) can improve the estimation of the lower bound of the stress drop when compared to studies using teleseismic data, and increase the sensitivity to an upper bound.

### **Structural Context of the 2015 Pair of Nepal Earthquakes ( $M_w$ 7.8 And $M_w$ 7.3): An Analysis Based on Slip Distribution, Aftershock Growth and Static Stress Changes**

PARAMESWARAN, R. M., Indian Institute of Science, Bangalore, Karnataka, India, revathyparameswaran@ceas.iisc.ernet.in; RAJENDRAN, K., Indian Institute of Science, Bangalore, Karnataka, India, kusala@ceas.iisc.ernet.in; RAJENDRAN, C. P., Jawaharlal Nehru Centre for Advanced Scientific Reserach, Bangalore, Karnataka, India, rajendran@jncasr.ac.in

Large/great Himalayan earthquakes are believed to originate on the Main Himalayan Thrust (MHT), and their ruptures emerge along the Main Frontal Thrust (MFT). The rupture of the April 25, 2015 ( $M_w$  7.8) earthquake was east directed, with no part relayed to the MFT. Several papers have already been published on their source models, but questions remain on the potential role of structural control on the rupture and aftershock activity. We used teleseismic moment inversion of P- and SH-waves, and Coulomb static stress-changes to map the slip distribution, growth of aftershocks, and their relation to the thrust systems. Most aftershocks were sourced outside the stress-shadows of slip > 1.65 m, the largest of which occurred on May 12 ( $M_w$  7.3). Sourced on a contiguous patch of increased stress-change, this event is the first known example of a late, distant, and large aftershock associated with any large earthquake in the Himalaya. Eastward growth and the abrupt termination of aftershocks at around 86.5°E seem structurally controlled. Coseismic elevation change of ~1m inferred from the InSAR image overlaps with a previously mapped out-of-sequence thrust named PT2, which purportedly extends till 86.5°E. These spatial correlations along with the presence of some subtle, but co-linear surface deformation features raises the intriguing question whether the PT2 provided any structural control in the propagation and arrest of the rupture. The present study uses the pattern of co-seismic slip, static stress trigger models, and aftershock productivity to suggest that the role of out-of-sequence thrusting in the rupture process cannot be disregarded. Further, our analysis of the static stress-changes show that the up-dip portions of the frontal fault remain unbroken by the 2015 slip, and that the threats from large/great earthquakes remain.

### **Probabilistic Seismic Hazard Assessment for East Anatolian Fault Zone Using Planar Source Models**

GULERCE, Z., METU, Ankara, Turkey, zyilmaz@metu.edu.tr; MENEKSE, A., METU, Ankara, Turkey, akinmenekse@hotmail.com; OZACAR, A. A., METU, Ankara, Turkey, ozacar@metu.edu.tr; CETIN, K. O., METU, Ankara, Turkey, ocetin@metu.edu.tr; KAYMAKCI, N., METU, Ankara, Turkey, kaymakci@metu.edu.tr

The objective of this paper is to provide state-of-the-art probabilistic seismic hazard assessment (PSHA) maps for the East Anatolian Fault Zone (EAFZ) based on planar seismic source characterization models and up-to-date ground motion models. Development of planar seismic source models requires the definition of source geometry in terms of fault length, fault width, fault plane angles and segmentation points for each segment of EAFZ and associating the observed seismicity with defined fault systems. This complicated task was performed with the help of updated active fault maps of Turkey (Emre *et al.*, 2013), previously conducted geological site studies in the literature, and unified instrumental earthquake catalogue of Turkey (Kalafat *et al.*, 2011). Recently published global Next Generation Attenuation (NGA-West 2) ground motion prediction models (Bozorgnia *et al.*, 2014) and Turkey-Adjusted NGA-W1 models (Gülerce *et al.*, 2015) are used in the ground motion logic tree with equal weights. The results are presented in terms of the seismic hazard maps for accepted hazard levels in design codes for different spectral periods and for generic rock ( $V_{S30}=760$  m/s and  $V_{S30}=1100$  m/s) site conditions.

### **Study on Focal Mechanism Solutions and Stress Field of Lushan M7.0 Earthquake Sequence**

ZHANG, Z. W., Sichuan Earthquake Administration, Chengdu, Sichuan, China, zzw1983107@163.com; ZHOU, L. Q., China Earthquake Networks Center, Beijing, China, lqzhou@seis.ac.cn

Lushan, Sichuan M7.0 earthquake on 20 April 2013 occurred on the southern segment of the Longmen Shan fault zone which is collision and compressive boundary zone between Bayan Har block and South China block, it is another

destructive earthquake on Longmen Shan fault zone after the Wenchuan M8.0 earthquake in 2008. Focal mechanism presents pure thrust type, the spatial distribution of aftershocks show that the long axis is in accord with strike of Longmen Shan fault. The long axis is about 45 km and the short axis about 25km of the aftershock area. In order to investigate seismogenic structure and seismic mechanism of Lushan M7.0 earthquake on 20 April 2013, based on focal mechanism solutions of 114  $M \geq 3.0$  aftershocks from 20 April to 1 June 2013, we analyzed spatial and temporal distribution characteristic of focal mechanism and stress field. The results are as follows. The focal mechanism types of Lushan  $M \geq 3.0$  aftershocks show that thrust type is dominant faulting behavior, strike-slip type takes second place, normal type is least, the orientation of P-axis have a good consistency, the dominant direction is near NW-SE, dip angle is from 0° to 30°, it shows that aftershock activities are controlled by regional stress field. The change of S1 orientation with time is not obvious, it presents near NW direction, but its dip angle gradually becomes level, stress tensor variance gradually becomes big, and the focal mechanism is mainly thrust behavior all the time, but it becomes relatively untidy with time, it reflects that seismic source stress field continually adjusts with time. The depth profiles show that angle between S1 direction and causative fault strike is 80°~120° in most area, it is almost perpendicular to fault strike, the trend of focal fault plane is NW, it shows that Lushan earthquake sequence is controlled by near level compressive stress which is perpendicular to causative fault, it belongs to typical thrust fault.

---

## **Induced Seismicity Monitoring: What is Really Needed?**

Poster Session · Thursday · 21 April · Tuscany F

---

### **Performance Evaluation of the Regional Seismograph Network in Northeast British Columbia, Canada, for Monitoring of Induced Seismicity**

BABAIE MAHANI, A., Geoscience BC, Vancouver, BC, Canada, ali.mahani@mahangeo.com; KAO, H., Pacific Geoscience Center, Sidney, BC, Canada, honnkao@gmail.com; WALKER, D., BC Oil and Gas Commission, Victoria, BC, Canada, dan.walker@bcogc.ca; JOHNSON, J., BC Oil and Gas commission, Victoria, BC, Canada, jeff.johnson@bcogc.ca; SALAS, C., Geoscience BC, Vancouver, BC, Canada, salas@geosciencebc.com

An important factor in mitigation of seismic hazard from induced seismicity is properly established seismic networks suitable for consistent identification of small-to-moderate events (magnitudes less than 4). Here, we evaluate the performance of the newly established regional broadband seismic network in northeast British Columbia, Canada. The seismic network was designed for monitoring of induced seismicity due to oil and gas operations related to hydraulic fracturing and fluid injection in the region. We use regional and local earthquake catalogues for the period 1985-2015 in order to analyse magnitude of completeness and epicentral uncertainty. We also perform a theoretical assessment of minimum detectable magnitude across the study region based on analysis of ambient noise and simulated ground motions. From the frequency-magnitude distribution of the reported events in the regional earthquake catalogue, the magnitude of completeness has decreased ~1 magnitude unit from ~3 in the periods 1985-2013 to ~2 in the period 2013-2015 as a result of the establishment of new stations. The minimum detectable magnitude in the region is 1.6-2.6 based on the signal-to-noise ratio of 10 and higher at four or more stations. By comparing the regional and dense array catalogues we determine that the error in epicentral location in well-constrained areas by seismic stations, is below 3 km in both east-west and north-south directions. However, location uncertainties can be up to 10 km in the east-west direction in areas where the current regional network is sparse. The magnitude detection threshold in the Montney Play where most of the current oil and gas activities are taking place can be further reduced by up to 1 magnitude unit with the addition of 4 new stations.

### **Real-time Ground-motion Mapping based on an Automatic Response System (ARS), with Applications to Induced-seismicity Traffic Light Protocols**

ASSATOURIANS, K., Western University, London, ON, Canada, kassatou@uwo.ca; ATKINSON, G., Western University, London, ON, Canada, gatkins6@uwo.ca

We describe an Automatic Response System (ARS) that accesses and processes seismographic network data in real time. The program continuously checks an email account, which receives notifications concerning earthquake occurrence, allowing the ARS to respond to either an automated earthquake notification email, or a manual request concerning a specified time window. Upon earthquake occurrence, ARS uses ground-motion data to calculate the moment magnitude and stress drop of the event. The system tabulates response spectral ordinates at all recording stations (PSA, 5%-damped pseudo-acceleration), prepares and posts



ground-motion and intensity maps online, and emails a link to the information products to a list of recipients.

The ARS program can be configured to access a network database, or alternatively to draw data from a data center such as IRIS. After fetching the raw time series ARS applies routine signal processing procedures to obtain instrument-corrected ground motion time series and PSAs. The moment magnitude is obtained by fitting the low-frequency PSA amplitudes to the attenuation shape given by a regional ground-motion prediction equation (GMPE). Then the high-frequency PSA and moment are used to find the best-fitting stress drop. The derived magnitude and stress drop are used to generate an event-specific GMPE. In the final stage, ground motions are calculated for a grid of points using the event-specific GMPE, earthquake coordinates, and grid of site amplification factors. The information products are automatically posted to a website where they are displayed interactively within google maps that allow products to be zoomed, queried and downloaded. The information products are tailored to allow rapid decisions to be made for induced-seismicity applications. In particular, the ARS can be used to develop more effective traffic-light protocols that consider both the magnitude of events and the potential of the ground motions to reach damaging levels.

#### **Detecting Induced Micro-Seismic Events during Hydraulic Fracturing to build more Complete Event Catalogs**

SMITH, T., University of California, Santa Barbara, Santa Barbara, CA, USA, trevorsmith@umail.ucsb.edu; ARCE, A., University of California, Santa Barbara, Santa Barbara, CA, USA, arce@umail.ucsb.edu; JI, C., University of California, Santa Barbara, Santa Barbara, CA, USA, ji@geol.ucsb.edu

It has been reported that micro-seismic events induced by hydraulic fracture stimulations follows the Gutenberg-Richter (GR) relationship but often with b-values much larger than that of natural earthquakes. Here the borehole seismic observations of two hydraulic fracturing operations in different geological settings (Barnett Shale Fm. in Texas and Monterey Shale Fm. in Central California) are studied to build more complete event catalogs. Our initial analyses using original industry catalogs yield larger b-value estimations of 1.2 for Barnett Shale and 1.9 for Monterey Shale. We apply the template matched filter technique (MF, Shelly *et al.*, 2007) to detect small events and find up to 4 times more events than what were registered in the initial catalogs. The magnitude of completeness drops from -1.6 and -2.1 to -2.2 and -2.4, respectively in each new catalog. The corresponding b-value estimations become 1.3 and 1.1, respectively. These values are still larger than 1 but become consistent with relatively larger b-values for natural earthquakes in the shallow depth region (*e.g.*, 1.03-1.28 for earthquakes at 0-3 km, compared with 1.01-1.05 for 0-18 km, Mori and Abercrombie, 1997). We will further improve the catalogs with the Match and Locate algorithm (M&L, Zhang *et al.*, 2015). Our preliminary comparison of the MF and M&L methods using a small subset of data shows that the M&L algorithm is capable of detecting ~50% more events though the computational cost is much higher.

#### **Design and Realization of a Seismic Monitoring System for the Geothermal Production Site of Torre Alfina (Italy)**

BRAUN, T., INGV-Roma1, Arezzo (AR) Italy, thomas.braun@ingv.it; CARAPEZZA, M. L., INGV-Roma1, Roma (RM) Italy, marialuisa.carapezza@ingv.it; PAGLIUCA, N., INGV-Roma 1, Roma (RM) Italy, nicola.pagliuca@ingv.it; FAMIANI, D., INGV-Roma1, Roma (RM) Italy, daniela.famiani@ingv.it; FREPOLI, A., INGV-CNT, Roma (RM) Italy, alberto.frepoli@ingv.it; GATTUSO, A., INGV-Roma1, Roma (RM) Italy, alessandro.gattuso@ingv.it; LISI, A., INGV-CNT, Roma (RM) Italy, arianna.lisi@ingv.it; MARCHETTI, A., INGV-CNT, Roma (RM) Italy, alessandro.marchetti@ingv.it; BADIALI, L., INGV-CNT, Roma (RM) Italy; MELE, G., INGV-Roma1 (RM) Italy

The geothermal field of Torre Alfina is located in Central Italy, at the boundary between the regions Tuscany and Latium, at the northern extremity of the Vulcini quaternary volcanic complex. Geochemical and geophysical wells drilled in the 1970s and 1980s down to depths ranging from 563 to 2710 m revealed that Torre Alfina is a medium-enthalpy ( $T=140^{\circ}\text{C}$ ) geothermal field, hosted in buried fractured Mesozoic limestones.

Recently a multi-national industrial company received the license for the production of geothermal energy up to a maximum of 5 MW.

In 2013 the INGV was commissioned to realize a monitoring system that includes the observation of gas emissions, microseismicity and ground deformation.

National guidelines published recently by the Italian Ministry of Economic Development regulate in detail the governmental monitoring ordinances exclusively regarding the extraction of hydrocarbons and the fluid injection due to wastewater and  $\text{CO}_2$  storage but concerning geothermal energy production appropriate regulations are missing.

Following the recommendations, described in the Ministerial Decree that regulates the geothermal production activity, the seismic monitoring system should be capable to record (a) the local microseismicity during the phase of geothermal energy production and (b) the natural seismicity already 12 months before the beginning of the production operations.

In 2014 we started to install a seismic network consisting of 5 short period stations within a radius of 5 km (Inner Domain) and thereafter further 5 stations inside an area with a 10 km radius (Outer Domain). The seismic noise level recorded at the single stations is unfavorably high, due to an intensive colonization and numerous settlements of small and medium industries. Transients as well as persistent monochromatic disturbances are recorded very well especially at the southern stations, probably due to a low wave energy dissipation inside the layer of quaternary volcanic rocks.

#### **Using a Large-N Array to Probe Injection-induced Seismicity in Oklahoma**

DOUGHERTY, S. L., U.S. Geological Survey, Pasadena, CA, USA, sdougherty@usgs.gov; COCHRAN, E. S., U.S. Geological Survey, Pasadena, CA, USA, ecochran@usgs.gov; HARRINGTON, R. M., McGill University, Montreal, QC, Canada, rebecca.harrington@mcgill.ca

Injection-induced seismicity has an important impact on seismic hazard, particularly in regions with low rates of natural seismicity; however, further understanding of the predictability of these events based on injection practices and geological structure is necessary before hazard can be quantified reliably. In Oklahoma, wastewater disposal volumes have increased rapidly since 2008 and during this time a drastic increase in seismicity has resulted in a significant rise in seismic hazard in this region. To enhance monitoring of potential injection-induced seismicity (including microseismicity) and more definitively link seismic observations with operational injection parameters and geologic structure, a seismic dataset with denser station coverage than is commonly available is needed. A large-N array of 1,000-1,850 vertical-component nodal seismic sensors will be deployed over a 20-km-by-30-km region in Oklahoma for 2-4 weeks in spring 2016, targeting a sequence of likely-induced seismicity in a region of active injection. This dense array will be used to assess the locations, frequency, magnitudes, source properties, and spatiotemporal evolution of micro- and small earthquakes in an effort to improve our understanding of the relationship(s) between injection parameters and induced seismicity. Information on the locations and orientations of subsurface faults will also be obtained to improve our understanding of where future locations of injection-induced seismicity may occur and potentially the maximum expected magnitudes. Tomographic imaging of the shallow crust will provide additional details on the geologic structure and any potential preferential location of seismicity in or along a particular feature. The overall aim of this experiment is to enhance our understanding of injection-induced seismicity, potentially leading to more accurate seismic hazard assessments and improved hazard mitigation.

#### **Template Hunting For Small Events Using Frequency Domain Array Processing in Regions of Induced Seismicity**

LINVILLE, L. M., University of Utah, Geology and Geophysics, Salt Lake City, UT, USA, linville@seis.utah.edu; PANKOW, K. L., University of Utah, Geology and Geophysics, Salt Lake City, UT, USA, pankow@seis.utah.edu; KILB, D. L., Scripps Institute of Oceanography, La Jolla, CA, USA, dkilb@ucsd.edu; GARRETT, N., Scripps Institute of Oceanography, La Jolla, CA, USA, ngarrett777@cox.net

It is common practice to use waveform templates from seismicity catalogs in waveform matching techniques to increase the size and completeness of seismic catalogs. These improved catalogs are key in characterizing responses to changes in local conditions in areas subject to induced seismicity (*e.g.* where extraction and/or injection occurs). However, regional catalogs rarely contain a complete set of templates, especially for small events ( $< M2.5$ ), resulting in consistently omitted yet important event families from analysis. Here, we introduce an automated frequency domain coherence filter method developed for seismic arrays that successfully recognizes small magnitude events. The method is based on identifying low-level increases in band-limited energy sums in the frequency domain over multi-station distances, allowing us to assemble a more complete set of event templates. In this study, we tune the algorithm for data recorded by the EarthScope/USArray Transportable Array stations deployed in sedimentary basins in the Central United States. We find false positive rates remain low ( $< 10\%$ ) and, with very few exceptions, ComCat cataloged events are fully recovered by our method. Within the Forest City Basin, centered between Iowa and Missouri, we have identified over 250 auto-detected and analyst-reviewed events in the year 2011 that were not previously cataloged. Applying waveform matching to continuous data using these new event templates allows us to evaluate if these new templates belong to already known event families or if they identify new source zones. This

frequency domain detection method helps to clarify the diversity of templates and their characteristics within a region that ultimately can help establish priorities in induced seismicity monitoring.

### **Hydraulic Fracturing Operation Monitoring with Sparse Surface Networks; Duvernay Case Study**

BATURAN, D., Nanometrics Inc, Kanata, ON, Canada, dariobaturan@nanometrics.ca; KARIMI, S., Nanometrics Inc, Kanata, ON, Canada, sepidehkarimi@nanometrics.ca; LAW, A., Nanometrics Inc, Kanata, ON, Canada, andrewlaw@nanometrics.ca; YENIER, E., Nanometrics Inc, Kanata, ON, Canada, emrahyenier@nanometrics.ca

In certain shale reservoirs in North America, seismicity associated with hydraulic fracturing can be detected and characterized with the use of sparse surface networks of high-quality three-component instruments. Here we present the seismic processing results from a 20-stage single-well hydraulic fracturing operation in the Duvernay shale monitored by a local network of 9 broadband stations. We utilize three-component detection of compressional and shear waves along with waveform template matching to detect over 1500 events in the -1.0 to 2.6 ML magnitude range, with a final magnitude of completeness ( $M_c$ ) of  $\sim 0.5$ . Using grid-search and relative location methods with a 3D velocity model, the precision and clustering of solutions is optimized for first-pass evaluation of the hydraulic fracturing effectiveness, delineation of activated geological structures and induced seismic monitoring regulatory compliance. For larger magnitude events with sufficient signal to noise ratio, displacement spectral fitting is utilized to compute source parameters. Individual or composite fault plane solutions are derived for stronger events and used to perform principal stress axes inversion and determine fracture plane orientations. The spatial and temporal distribution of the recorded seismicity together with the catalog  $b$ -value of  $\sim 1.0$  appears to show the activation of pre-existing faults optimally oriented to the direction of the maximum horizontal stress. We therefore show that in environments with favorable surface noise levels, high in-situ stress regime and low anelastic attenuation, sparse surface networks can detect events down to magnitude -1.0 within the stimulated reservoir volume, along with induced seismicity on proximate faults. Consequently, sparse surface networks of high-quality seismic instruments can generate rich and informative data sets that make them a scalable, practical and cost-effective solution for hydraulic fracture imaging and induced seismic monitoring.

---

## **Machine Learning and Its Application to Earthquake and Explosion Signal Analysis**

Poster Session · Thursday · 21 April · Tuscany F

---

### **Unsupervised Classification of Microseismic Events**

LANGET, N., NORSAR, Kjeller, Norway, nadege@norsar.no; WUESTEFELD, A., NORSAR, Norway, andreas.wuestefeld@norsar.no; OYE, V., NORSAR, Norway, volker@norsar.no

During hydraulic fracturing, a large number of microseismic events is recorded. Characterizing this microseismicity will help to better understanding the processes involved in their generation, for example whether an event is caused by pore pressure changes or purely stress-triggered. An automated, near-real time classification will then enable the operator to identify potentially hazardous and non-hazardous events.

We show results on automated classification of a dataset with 78 stages and more than 20,000 events recorded on 48 three-component geophones. We base our classification on seismic "features", which are either seismic source parameters, or represent waveform characteristics (*e.g.* frequency content, signal shape, etc). We look at their evolution with time. The multi-stations data are also valuable as they show differences in function of their distance to the seismic swarms. Correlating all the information that is available is useful in order to determine which features are the most significant and which stations shall be used for a future classifier.

### **Improved Bulletin Generation using an Iterative Processing Framework**

BALLARD, S., Sandia National Laboratories, Albuquerque, NM, USA, sballar@sandia.gov; SLINKARD, M., Sandia National Laboratories, Albuquerque, NM, USA, meslink@sandia.gov; ENCARNACAO, A., Sandia National Laboratories, Albuquerque, NM, USA; DRAELOS, T., Sandia National Laboratories, Albuquerque, NM, USA; YOUNG, C., Sandia National

Laboratories, Albuquerque, NM, USA; BROGAN, R., EnSCO, Melbourne, FL, USA, brogan.ronald@ensco.com

Automatic seismic event bulletins are generally produced by performing two sequential processing steps: first station processing to find signal detections, then network processing to form events. This processing paradigm differs significantly from that applied by human analysts. Analysts bring to bear considerable human intuition acquired during the processing of past events and use that to iteratively reprocess data resulting in a significantly improved bulletin. Our Iterative Processing Framework (IPF) attempts to mimic analyst behavior during automatic bulletin generation. After a first pass through signal detection and signal association, the resulting events are compared to historical information with the goal of identifying expected signals which are missing from the set of signals currently available, or which are present but erroneous in some respect. Waveform data is reprocessed to improve the set of available signal detections and signal association is repeated when changes are made. The process is repeated until stability is achieved. IPF also introduces seismic events detected using waveform correlation into automatic processing prior to signal association, which can significantly reduce the number of signal detections available to confuse the automatic signal associator. We present results comparing IPF to traditional methods.

### **Explore Social Network Analysis using Seismic Array**

KONG, Q., UC Berkeley, Berkeley, CA, USA, kongqk@berkeley.edu; ALLEN, R., UC Berkeley, Berkeley, CA, USA, rallen@berkeley.edu

We are experimenting applying the techniques used in social network analysis back to seismic network. We try to characterize networked structures in terms of nodes (seismic station) and the ties or edges (relationships between the stations, *e.g.* similarities between the waveforms, characterized by the correlation coefficient) that connect them. We use several earthquakes recorded on the nodal seismic network (1) as the experimenting dataset. We first built a weighted graph model based on the similarities between the waveforms of the station pairs. Various metrics can be applied to quantify the character of the network. We also detected interesting communities using Louvain method (2), which may reflect some sub-structure in the Long Beach area. We are still in the process of exploring this idea, and will show more results at SSA meeting.

References:

(1) <http://www.nodalseismic.com/>

(2) Vincent D Blondel, Jean-Loup Guillaume, Renaud Lambiotte, Etienne Lefebvre, Fast unfolding of communities in large networks. Journal of Statistical Mechanics: Theory and Experiment 2008 (10), P10008 (12pp) doi: 10.1088/17425468/2008/10/P10008. ArXiv: <http://arxiv.org/abs/0803.0476>

### **Comparing Time and Frequency Domain ANN Methods for Rapidly Searching Large Seismic Signal Archives**

YOUNG, C., Sandia National Laboratories, Albuquerque, NM, USA, cyoung@sandia.gov; GONZALES, A., Sandia National Laboratories, Albuquerque, NM, USA, aigonza@sandia.gov; KWOK, J., Sandia National Laboratories, Albuquerque, NM, USA, jlkwok@sandia.gov

The use of waveform correlation to identify recurring similar events has become increasingly important as online archives of past signals continue to grow. Yet there is an inherent limitation in how widely the method can be applied due to the computational demands of searching large signal archives quickly. Recently, powerful new approaches have been developed to decrease the computational demands of searching for similar signals by exploiting approximate nearest neighbor (ANN) methods that interrogate the signal archive such that much of the archive is ignored when searching for closest matches, thereby dramatically reducing the number of correlations that need to be calculated. ANN methods have been applied by separate research groups to time and frequency domain representations of seismic signals, and both approaches have proven effective. In this study we perform a side-by-side comparison of both representations as applied to the problem of identifying signals from the IMS primary station MKAR. For each representation, we built a KLSH indexed archive using all associated signals from the IDC LEB catalog for 2002-2013 ( $\sim 308,000$  signals). We then tested the signal matching capability using the  $\sim 26,000$  IDC-detected signals from 2014, including a variety of regional and teleseismic phases (56% are teleseismic P). We used the LEB phase assignments as ground-truth to score the results.

### **Challenges for Adaptive Self-Tuning of Seismic Sensors: Detailed Case Study at Erebus Volcano, Antarctica**

KNOX, H. A., Sandia National Laboratories, Albuquerque, NM, USA, haknox@sandia.gov; DRAELOS, T. J., Sandia National Laboratories, Albuquerque, NM, USA, tjdrael@sandia.gov; YOUNG, C. J., Sandia National Laboratories, Albuquerque, NM, USA, cyoung@sandia.gov; CHAEL, E. P., Sandia National

Laboratories, Albuquerque, NM, USA, epchael@sandia.gov; PETERSON, M. G., Sandia National Laboratories, Albuquerque, NM, USA, mgpeter@sandia.gov; LAWRY, B. J., Sandia National Laboratories, Albuquerque, NM, USA, bjlawry@sandia.gov

Regardless of the scientific application (underground nuclear test monitoring vs. microseismic monitoring), the necessity for data-driven dynamic algorithms has become more apparent over the last decade of seismic and infrasound recording, especially given that continuous streams are assembling databases on the order of ~ 1TB per month. The detailed analysis of these large datasets requires more economic and personnel resources than are often available. Therefore, standard practice is to test the detection parameters on a subset of the data, which is frequently comprised of only a few stations in the network over a short time period (hours to days). These parameters are then applied across the network for a longer period of time, sometimes in perpetuity. It would seem straight forward enough to develop and/or apply existing dynamic algorithms that could address this shortfall, especially given the recent advances in pattern recognition fields (*e.g.*, facial recognition). However, the increased diversity of these somewhat sparse datasets provides additional challenges to making useful detections. The very dense network (~120 stations, 10 km radius) deployed during 2008 on Erebus Volcano, Antarctica, illustrates a subset of these challenges including: annual trends, diverse seismic sources, emergent onsets, and spatially isolated sources. Additionally, painstaking manual analysis of many controlled-source explosions and volcanic eruptions (identified through matched filtering) also demonstrates the need for spatial diversity in the detection parameters. Finally, we will show comparative results between the adaptive self-tuning algorithm developed at Sandia National Laboratories and the STA/LTA detection algorithm from the BRTT Antelope software package. Sandia Corporation, a wholly owned subsidiary of Lockheed Martin Corporation, for the U.S. Department of Energy's National Nuclear Security Administration under contract DE-AC04-94AL85000.

## Marine Paleoseismology: Assessing Offshore Hazards

Poster Session · Thursday · 21 April · Tuscany F

### Constraining the Paleoseismic History and Maximum Event Magnitude for the San Diego Trough Fault Zone, Offshore Southern California.

BORMANN, J. M., Nevada Seismological Laboratory, University of Nevada, Reno, NV, USA, jrbormann@unr.edu; KENT, G. M., Nevada Seismological Laboratory, University of Nevada, Reno, NV, USA, gkent@unr.edu; DRISCOLL, N. W., Scripps Institution of Oceanography, UCSD, La Jolla, CA, USA, ndriscoll@ucsd.edu; HARDING, A. J., Scripps Institution of Oceanography, UCSD, La Jolla, CA, USA

We use high-resolution multichannel seismic (MCS) reflection data acquired in 2013 to map the San Diego Trough fault (SDTF) as it offsets marine sediments for ~130 km between the US/Mexico border and the eastern margin of Avalon Knoll. Ryan *et al.* (2012) estimate a minimum Holocene right-lateral slip rate of  $1.5 \pm 0.3$  mm/yr for the SDTF, however the paleoseismic history of the fault is unconstrained. Including the SDTF in regional seismic hazard models requires assumptions about earthquake magnitude, rupture length, and recurrence interval that increase model uncertainty. Empirical scaling relationships indicate that a 200-km-long rupture of the SDTF and its southern extension, the Bahia Soledad fault, could produce a M7.7 earthquake. Our new data image the SDTF offsetting seafloor sediments in the southernmost San Pedro Basin, which suggests the potential for kinematic linkage between the SDTF and the San Pedro Basin fault (SPBF) mapped <5 km to the north. Linkage between these faults would increase the length of the system to >270 km and allow events on the SDTF to propagate closer to the LA Basin.

We use the new MCS data in combination with USGS and industry seismic profiles to evaluate the potential for end-to-end ruptures along the SDTF and SPBF systems. We identify three locations where thin lenses of submarine fan sediment mantle the SDTF, providing the ideal sedimentary record to characterize the paleoseismic history of the fault. Determining the timing of the most recent event at these locations will allow us to begin constraining the extent and variability of past earthquake ruptures and will improve estimates of the maximum magnitude for the SDTF. Due to the resolution of existing seismic data in the San Pedro Basin, a 30-km gap exists between observations of seafloor offset on the SDTF and SPBF systems. Until there is adequate high-resolution MCS coverage in the San Pedro Basin, these faults cannot conclusively be considered a continuous structure.

### Bradley Lake Revisited: Sedimentary Evidence for Shorter Return Periods

PATTON, J. R., Humboldt State University, Arcata, CA, USA, Jason.Patton@humboldt.edu; GOLDFINGER, C., Oregon State University, Corvallis, OR, USA, gold@ceos.oregonstate.edu

Recurrence of southern Cascadia subduction earthquakes is constrained by stratigraphic evidence onshore and offshore. The seismoturbidite record offshore has a higher frequency than the tsunami record in several locales. Bradley Lake contains the temporally longest and highest-frequency record of paleotsunamis along the Cascadia margin. Probably because tsunamis have a higher recording threshold in onshore lakes, the paleoseismologic record onshore most likely includes only a subset of the offshore paleoseismic record. Using additional geophysical methods, we are re-evaluating the stratigraphic record from Bradley Lake using sediment cores archived at the Oregon State University Core Facility. We are interested in whether additional analysis of these cores will yield a paleoseismic record equivalent to the offshore record at the same latitude.

Using new CT data, we use the published sedimentary facies to characterize and interpret the stratigraphic record from the lake. Using these facies interpretations and CT density-based well log correlation techniques, we correlate strata between each core and compare our results with those from the original 2005 published results and offshore cores.

In addition to published facies associations, we interpret an upward fining facies, commonly directly below the tsunami sand sheets, but also found between the tsunami deposits. Many of these units appear to be paired with an organic rich facies as are the tsunami deposits. This facies may result from hyperpycnal flow, storm flow, sublacustrine seismo-turbidites, or inundation from tsunamis of magnitude smaller than that required to transport sediment from the dunes to the west. The return period of the additional lake turbidites and sand sheets is combined is ~ 280 years, consistent with the offshore turbidite record and with tsunami models published in 2014 showing that some of the southern-most Cascadia earthquakes are unlikely to produce tsunami deposits in the lake.

### Upper Plate Structure and Forearc Deformation above the Kodiak Segment of the Alaska-Aleutian Megathrust

RAMOS, M. D., Boise State University, Boise, ID, USA, marlonramos@u.boisestate.edu; LIBERTY, L. M., Boise State University, Boise, ID, USA, lliberty@boisestate.edu; HAEUSSLER, P. J., USGS, Anchorage, AK, USA, pheustr@usgs.gov

The Kodiak Island segment of the Alaska-Aleutian megathrust ruptured with the Prince William Sound (PWS) segment during the 1964 Great Alaska Earthquake ( $M_w$  9.2). This devastating earthquake generated seismic uplift and subsidence as well as tectonic tsunamis that inundated multiple locations across the Gulf of Alaska and Pacific Ocean. The seismotectonic setting for Kodiak Island differs from PWS, and is evinced through differences in plate coupling and upper plate deformation between these two asperities. Current viscoelastic response models suggest the upper plate of the Kodiak segment undergoes a transition from completely locked at its southwest end to aseismic slip at its northeast end. Geologic interpretation and earthquake analyses of the Kodiak segment can reveal how it is releasing stress after 1964 and to what extent this segment ruptured coseismically. Legacy crustal-scale seismic reflection profiles were acquired and processed by the former Minerals Management Services, but never geologically interpreted. We interpret several of these profiles, oriented parallel and normal to the trench, that depict the structural evolution of the region from the forearc to the continental shelf offshore Kodiak Island. This work provides the basis for a detailed analysis of megathrust splay fault geometry to infer patterns of coseismic uplift due to the 1964 most recent event (MRE). Constraints from newly acquired sparker seismic data, along with compiled bathymetric data and tsunami modeling will be used to assess 1964 tsunamigenic fault source locations and spatial extent. In order to evaluate stress accumulation of the upper plate and to delineate faults at depth within our study region, we map earthquake b-values and perform hypocenter relocations along our interpreted seismic reflection profiles. Our results will enhance knowledge of the marine fault systems offshore Kodiak Island and their associated earthquake hazard by reconciling multiple geophysical datasets.

### Buenas no(t)ches: Geometry of Holocene Tidal Notches in Paleoseismic Studies, an Example from Perachora Peninsula, Greece

SCHNEIDERWIND, S., Inst. of Neotectonics and Natural Hazards, RWTH Aachen Univ., Aachen, Germany, s.schneiderwind@nug.rwth-aachen.de; KAZMER, M., Dept. of Paleontology, Eötvös Univ., Budapest, Hungary, mkazmer@gmail.com; BOULTON, S. J., Centre for Research Earth Sciences, Plymouth Univ., Plymouth, Devon, UK, sarah.boulton@plymouth.ac.uk; PAPANIKOLAOU, I. D., Lab. Mineralogy and Geology, Agricultural Univ. Athens, Athens, Greece, i.pap@aua.gr; STEWART, I. S., Centre for Research Earth Sciences, Plymouth Univ., Plymouth, Devon, UK, iain.stewart@plymouth.



Tidal notches are a generally accepted sea-level indicator that, when displaced from mean sea level, witness tectonic activity at or near coastlines. The formation of these paleoshoreline markers is generally discussed in terms of two current conflicting models. The first—the ‘tectonic model’—requires (active faulting induced) coastal uplift rates matching the rates of sea-level rise, with stable tectonic periods in between that are long enough for notch formation. The second—‘climatic model’—assumes notch formation is dominated by stable climatic conditions, implying that notches are regionally uplifted during unstable climate periods (no notch formation due to different conditions, *i.e.*, water temperature, water chemistry, absence/reduced of bio-erosion, wind, waves); this model requires uplift rates to be greater than the rate of sea-level rise. We have been testing both hypotheses in Gulf of Corinth area in the Eastern Mediterranean, where the tidal range is small and tectonic activity is high due to active faults and surface-rupturing earthquakes. Moderate to large ( $M > 6$ ) earthquakes on normal faults mean maximum coseismic vertical displacements of 1-1.5 m, where slip is partitioned c. 2/3 on the hanging wall and 1/3 on the foot wall. Discriminating associated coastal change information is problematic because tectonic uplift from a single seismic event is not likely to exceed several dm. High-resolution laser scanning, however, offers close-up views on notch exposures and has the potential to detect evidence for multiple sea-level markers in between major emergence. Statistically representative profiles along notch-cut along marine cliffs of the Perachora Peninsula were analyzed, firstly to corroborate previously described tidal notches, and then to identify similar morphologies in consistent geometries along the coast. The results, combined with precise dating of the notches, will help reconstruct the Holocene paleoseismic history of coastal faults.

#### **The Footprints of Typhoons on Seismic Records and their Implications on Small-scale Coupling Mechanisms in South China Sea**

XIAO, H., Tongji University, Shanghai, China, 15hanxiao@tongji.edu.cn; XUE, M., Tongji University, Shanghai, China, meixue@tongji.edu.cn; YANG, T., Tongji University, Shanghai, China, tyang@tongji.edu.cn; LIU, C. G., The First Institute of Oceanography, Qingdao, China; HUA, Q. F., The First Institute of Oceanography, Qingdao, China; XIA, S. H., South China Sea Institute of Oceanology, Guangzhou, China; HUANG, H. B., South China Sea Institute of Oceanology, Guangzhou, China; LE, B. M., Tongji University, Shanghai, China; HUO, D., Tongji University; PAN, M.H., Tongji University; LI, L., Tongji University

By investigating the footprints of typhoons on seismic records, we can understand their contributions to seismic noises as well as to small-scale coupling mechanisms of typhoon-land and typhoon-ocean-land. We analyze the signatures of typhoon KAI-TAK using seismic data from the ocean-bottom seismometers deployed in the central basin of South China Sea by Tongji University in 2012 as well as seismic stations on lands. Our preliminary results show that typhoons mainly enhance microseisms at the frequency band of ~0.1–0.5 Hz, including both long period double frequency and short period double frequency microseisms. A positive correlation observed between the amplitude of microseisms and the height of local ocean waves. Because OBSs are deployed at the bottom of ocean, single frequency microseisms are not prominent on them due to their fast attenuation with depth. During the typhoon KAI-TAK, the increase of LPDF energy is very small in OBSs while that is very high on land stations, indicating that LPDF microseisms are generated at nearby shorelines and can propagate towards the sea through the solid earth. However, the increase of SPDF energy is almost the same level for both OBSs and land stations indicating that the generation of SPDF is probably local. However, we also observe a small amount of energy arrives before the increases of the wave heights at the land station HK.HKPS. We derive that this energy may from a source that is not local: while LPDF can be generated at nearby shorelines and SPDF can be generated everywhere locally, they can both transmit through the solid part of the Earth to a station some distance away, *i.e.* HK.HKPS. In addition, we find that typhoons enhance not only the microseisms as expected but also the seismic energy from higher frequency bands. The spectrum amplitude during Typhoon periods, normalized by that of no-storm periods, shows that land stations produce stronger frequency seismic waves than OBSs.

## **Multi-Phenomenology Approaches to Explosion Source Studies**

Poster Session · Thursday · 21 April · Tuscany F

#### **Reflection Seismic Images from a Novel Seismic Source: Seeking Buried Targets at the Nevada National Security Site**

ROWE, C. A., Los Alamos National Laboratory, Los Alamos, NM, USA, char@lanl.gov; SNELSON-GERLICHER, C. M., Los Alamos National Laboratory, Los Alamos, NM, USA, snelsonc@lanl.gov; RALSTON, M. D., XRI Geophysics, matt.ralston@xrigeo.com

Through decades of underground nuclear testing, the subsurface at the Nevada National Security Site (NNSS), formerly named the Nevada Test Site, has been disturbed by numerous explosion events, collapse features, and emplacement infrastructure such as drifts, tunnels and underground chambers, needed to support the testing. In 2014, a new type of seismic controlled source, a large seismic hammer, was deployed to provide a line of seismic sources designed to aid in structural modeling of the subsurface in the vicinity of the Source Physics Experiment (SPE) site. The 2-D seismic reflection profile traversed over a series of known underground features. The seismic hammer is a 35-ton seismic source that is very repeatable. Although these data were acquired in a refraction sense to develop a velocity model, we have processed these data using reflection techniques to produce low-fold stacks.

Using the seismic data processing application, Ada, from XRI Geophysics,, we have produced a series of stacked record sections along the North-South refraction profile. Challenges in the data processing included irregular shot spacing, a lack of recorded seismic source time for any of the hammer drop events, as well as varying relative start times for the files for repeated, co-located hammer drops. As a result, this required some modifications within the software to process these data. Our goal is to identify diffractions that might delineate the location of these underground structures.

#### **Improved Seismic Characterization Using Joint Inversion of Disparate Data Types**

PRESTON, L., Sandia National Laboratories, Albuquerque, NM, USA, lpresto@sandia.gov; WATSON-ROSS, C., Sandia National Laboratories, Albuquerque, NM, USA, cwatso@sandia.gov

In support of the ongoing series of Source Physics Experiments (SPE), we have developed a 3-D local-to-regional scale seismic velocity model of the Nevada National Security Site (NNSS) using a joint inversion of body wave travel times, gravity measurements, and surface wave phase and group speed dispersion curves. The body wave data set includes absolute and differential P- and S-wave travel times from nearly 70,000 local earthquakes recorded from 2000 to 2014 on the University of Nevada Reno (UNR) southern Nevada network and active sources, including the SPE shots. This data set alone amounts to over 1.1 million absolute body wave picks and over 500,000 high-quality differential picks. To enhance near-surface velocity resolution we also augment this data set with 25,000 local measurements of gravity and are currently adding new constraints by expanding our surface wave database with more dispersion curves obtained via cross-correlation of ambient noise from UNR and SPE seismic stations throughout the region. We utilize a weighted, linearized, iterative inversion scheme to combine these disparate data types in order to solve for the optimal 3-D P- and S-wave velocity model and hypocentral locations given observed data subject to model smoothness constraints. We will discuss results of the inversion and how the addition of more double-difference and surface wave data alters and improves on previous results. We will also discuss some unique issues and advantages that arise with disparate data types and how combining different types of data can lead to improvements in overall model resolution.

Sandia National Laboratories is a multi-program laboratory managed and operated by Sandia Corporation, a wholly owned subsidiary of Lockheed Martin Corporation, for the U.S. Department of Energy's National Nuclear Security Administration under contract DE-AC04-94AL85000.

#### **High Resolution Regional Attenuation Modeling for the Source Physics Experiment**

PYLE, M. L., Lawrence Livermore National Laboratory, Livermore, CA, USA, pyle4@llnl.gov; WALTER, W. R., Lawrence Livermore National Laboratory, Livermore, CA, USA, walter5@llnl.gov; PASYANOS, M. E., Lawrence Livermore National Laboratory, Livermore, CA, USA, pasyanos1@llnl.gov

Seismic event amplitude measurement plays a critical role in the discrimination between earthquakes and explosions, and the estimation of their size. An accurate 2D model of attenuation is especially important for reasonable amplitude

estimation at small event-to-station distances. As part of the Source Physics Experiment (SPE), we develop a detailed attenuation model for the region around southern Nevada and test the model's usefulness in predicting amplitudes of local events. The SPE consists of a series of chemical explosions at the Nevada National Security Site (NNSS) designed to improve our understanding of explosion physics and enable better modeling of explosion sources. A high-resolution attenuation model will aid in the waveform modeling efforts of these experiments, and enable us to take a more detailed look at local event discrimination. To improve our understanding of the propagation of energy from sources in the area to local and regional stations in the western U.S., we invert regional phases to examine the crust and upper mantle attenuation structure of southern Nevada and the surrounding region. We consider observed amplitudes as the frequency-domain product of a source term, a site term, a geometrical spreading term, and an attenuation (Q) term (e.g. Walter and Taylor, 2001). Initially we take a staged approach to first determine the best 1D Q values; next we calculate source terms using the 1D model, and finally we solve for the best 2D Q parameters and site terms considering all frequencies simultaneously. Our preliminary results correlate well with the regional geology. With additional data we are working to develop a more detailed and higher frequency model of the region as well as move toward a fully non-linear inversion.

This work performed under the auspices of the U.S. Department of Energy by Lawrence Livermore National Laboratory under Contract DE-AC52-07NA27344. LLNL-ABS-680557

### **Observations of Explosion Seismic Energy Partitioning: Insights from the Source Physics Experiment**

FORD, S. R., LLNL, Livermore, CA, USA, sean@llnl.gov; PITARKA, A., LLNL, Livermore, CA, USA, pitarka1@llnl.gov; EZZEDINE, S. M., LLNL, Livermore, CA, USA, ezzedine1@llnl.gov; WALTER, W. R., LLNL, Livermore, CA, USA, walter5@llnl.gov; CHIANG, A., LLNL, Livermore, CA, USA, chiang4@llnl.gov; MELLORS, R. J., LLNL, Livermore, CA, USA, mellors1@llnl.gov

We evaluate the partitioning of seismic energy from explosions of the Source Physics Experiment using three-component measurement of ground motion in the near- and far-field. Methods for checking and correcting the data are presented so that observations of the partitioning can be made in absolute time and amplitude. We then evaluate several method for measuring seismic energy partitioning as a function of time and frequency. Using these methods we track the partitioning from near- to far-field for comparison with simulation. Prepared by LLNL under Contract DE-AC52-07NA27344.

### **Shear Motion Energy Budget for the SPE-4Prime Underground Explosion**

PITARKA, A., Lawrence Livermore National Laboratory, Livermore, CA, USA, pitarka1@llnl.gov; EZZEDINE, S., Lawrence Livermore National Laboratory, Livermore, CA, USA, ezzedine1@llnl.gov; VOROBIEV, O., Lawrence Livermore National Laboratory, Livermore, CA, USA, vorobiev1@llnl.gov; FORD, S., Lawrence Livermore National Laboratory, Livermore, CA, USA, ford17@llnl.gov; WALTER, W., Lawrence Livermore National Laboratory, Livermore, CA, USA, walter5@llnl.gov; ANTOUN, T., Lawrence Livermore National Laboratory, Livermore, CA, USA, antoun1@llnl.gov

Near- and far-field ground motion records of four underground chemical explosions performed in granite during the Source Physics Experiment (SPE) demonstrated that the explosions generated shear motion with significant energy and complex radiation pattern over a broad frequency range. Using numerical experiments performed with techniques that couple hydrodynamic modeling of shock waves with elastic modeling of seismic wave propagation, we have singled out the rock joint motion and near-source wave scattering as the main mechanisms of shear motion generation during SPE explosions. In this study we focus on quantification of the effects of wave propagation scattering on the energy budget of shear motion for the SPE-4Prime explosion. Measurements made on recorded and simulated far-field data for different frequency bands and several velocity models, representing different plausible structural complexities, are analyzed to investigate the azimuthal variation of shear motion energy, and characterize its behavior as a function of distance and underground structure. The results of these analyses can inform the development of new source discriminants based on local ground motion waveforms.

This work was performed under the auspices of the U.S. Department of Energy by Lawrence Livermore National Laboratory under Contract DE-AC52-07NA27344

### **Performance of High Frequency P/S Seismic Source Discriminant at Local Distances**

PITARKA, A., Lawrence Livermore National Laboratory, Livermore, CA, USA, pitarka1@llnl.gov; WALTER, W., Lawrence Livermore National Laboratory, Livermore, CA, USA, walter5@llnl.gov; CHIANG, A., Lawrence Livermore National Laboratory, Livermore, CA, USA, chiang4@llnl.gov; WAGONER, J., Lawrence Livermore National Laboratory, Livermore, CA, USA, wagoner1@llnl.gov; PYLE, M., Lawrence Livermore National Laboratory, Livermore, CA, USA, pyle4@llnl.gov; FORD, S., Lawrence Livermore National Laboratory, Livermore, CA, USA, ford17@llnl.gov

The regional high frequency P/S amplitude ratio has proven to be one of the most reliable discriminants between explosions and earthquakes. However recent applications of P/S ratio to local data show complications and poor performance. Part of the reason might be that due to the relatively large difference in source depth between seismogenic depth earthquakes and underground explosions at local distances, the underlying assumption of similar wave propagation effects between the two sources does not hold. The abundant high quality waveform data from underground chemical explosions and local shallow earthquakes, recorded during the Source Physics Experiment at the Nevada National Security Site, offer a unique opportunity for analyzing the applicability of P/S ratio discriminants to local distances. Using high-frequency simulations of ground motion from the SPE explosions and two local shallow earthquakes recorded on a dense array of stations covering a distance range of 1-10km, we have investigated the performance of P/S ratio at different frequency ranges. Ground motion simulations using a calibrated regional velocity model are used to investigate the correlation between structural complexities and P/S ratio performance at different azimuths and distances. In addition, synthetic seismograms are used to characterize local wave propagation effects and guide development of possible corrections to P/S ratio needed to account for wave path effects.

This work was performed under the auspices of the U.S. Department of Energy by Lawrence Livermore National Laboratory under Contract DE-AC52-07NA27344

### **Source Analysis of Underground Chemical Explosions from the Source Physics Experiment**

CHIANG, A., Lawrence Livermore National Laboratory, Livermore, CA, USA, chiang4@llnl.gov; FORD, S. R., Lawrence Livermore National Laboratory, Livermore, CA, USA, ford17@llnl.gov; PITARKA, A., Lawrence Livermore National Laboratory, Livermore, CA, USA, pitarka1@llnl.gov

Several physical mechanisms have been proposed to explain the generation of S-waves from underground explosions, such as asymmetries in the source, release of tectonic pre-stress, interactions with the free-surface, and heterogeneities in the Earth. An accurate description of the explosion source processes is an important step towards understanding which of these plausible mechanisms are actively contributing to the generation of S-waves and under what conditions. In this study we investigate the sensitivity of far-field waveforms to seismic source mechanisms by comparing simulated and recorded data from underground chemical explosions performed during the Source Physics Experiment. We use both forward and inverse waveform modeling approaches to estimate the source properties of the explosions, and compare solutions using different velocity models and at different frequency bands and distances. 1D and 3D velocity models are used to characterize wave propagation between the source and receiver. The 3D velocity models are constructed using available geological and geophysical data, and ambient noise seismic tomography, and the 3D Green's functions are computed using a numerical finite-difference approach. We will investigate the sensitivity of far-field ground motion to different levels of source complexities, such as a single isotropic source or complex sources with non-isotropic radiation (such as a double-couple) in the frequency range of 0.5 to 8 Hz. Prepared by LLNL under Contract DE-AC52-07NA27344.

### **Study of the Near-Source Effects on Local Seismic Signals: Case of SPE4prime.**

LARMAT, C. S., Los Alamos National Laboratory, Los Alamos, NM, USA, carene@lanl.gov; DELOREY, A. A., Los Alamos National Laboratory, Los Alamos, NM, USA, andrew.delorey@lanl.gov; STEEDMAN, D. W., Los Alamos National Laboratory, Los Alamos, NM, USA, dwsteed@lanl.gov; ROUGIER, E., Los Alamos National Laboratory, Los Alamos, NM, USA, erougier@lanl.gov; KNIGHT, E. E., Los Alamos National Laboratory, Los Alamos, NM, USA, knighte@lanl.gov; BRADLEY, C. R., Los Alamos National Laboratory, Los Alamos, NM, USA, cbradley@lanl.gov

There is a need to improve, in a quantitative way, the knowledge of how near-source explosion processes affect seismic signal at far-field distances. Seismic

signals remain important for locating and discriminating clandestine events in areas with no direct access but rely on models translating sources into seismic signatures. These models still have some issues such as explaining the level of shear-waves observed in some explosions. The Source Physics Experiment (SPE) that is currently underway at the Nevada National Security Site is focused on answering these questions by bringing in an unprecedented density of high-quality data near-source and far-field.

In the present paper, we report numerical modeling effort based on the coupling between hydrodynamic codes (Abaqus and CASH) and a seismic wave-propagation code SPECFEM3D. Abaqus and CASH are used to model the shocked, hydrodynamic region via equations of state for the explosive, borehole stemming and jointed/weathered granite. The Coupled Euler-Lagrange (CEL) method (recently advanced by developers at LANL) allow the modeling of the high deformation explosive regime coupling energy to a new phenomenological model for stored shear energy in jointed material. SPECFEM3D is based on the Spectral Element Method, a direct numerical method for full waveform modeling with mathematical accuracy (e.g. Komatitsch, 1998, 2002). The coupling interface is a series of grid points of the SEM mesh situated at the edge of the hydrodynamic code domain. Displacement time series at these points are computed from output of CASH or Abaqus and introduced to SPECFEM3D as histories. We will present validation tests and waveforms modeled for several SPE tests conducted so far, which present diverse geometries and scaled-depth-of-burials, with a focus on the last SPE4prime. Both the hydrodynamic and SEM models demonstrate wave energy scattering due to structure, weathering, local topography and 3D heterogeneities.

#### **Modeling Wave Propagation in Jointed Rock Masses at Variable Spatial Resolutions: Theory and Simulations for the Source Physics Experiments (SPE)**

HURLEY, R. C., LLNL, Livermore, CA, USA, hurley10@llnl.gov; VOROBIEV, O. Y., LLNL, Livermore, CA, USA, vorobiev1@llnl.gov; EZZEDINE, S. M., LLNL, Livermore, CA, USA, ezzedine1@llnl.gov; ANTOUN, T. H., LLNL, Livermore, CA, USA, antoun1@llnl.gov; WALTER, W., LLNL, Livermore, CA, USA, walter5@llnl.gov; GLENN, L. A., LLNL, Livermore, CA, USA, glenn5@llnl.gov

This work describes methods for modeling jointed rock masses at various spatial resolutions, with the primary goal of accurately and efficiently simulating wave propagation during the Source Physics Experiments (SPE) conducted at the Nevada National Security Site (NNSS). Our approach uses novel stress-updating schemes and anisotropic effective properties to model wave propagation and elastic deformation of jointed rocks at fine, moderate, and coarse spatial resolutions. At fine resolutions, computational cells use a special stress-update scheme to capture the effects of a single nonlinearly compliant joint on deformation and stress. At moderate resolutions, the stress-update scheme is extended to multiple, interacting, nonlinearly compliant joints, allowing for larger computational cells. At the coarsest resolution, nonlinearly elastic anisotropic effective properties are derived for a heavily jointed medium, enabling computational cells encompassing a large number of joints. Theories and methods at coarser resolutions are validated against those at finer resolutions by subjecting heavily-jointed representative volume elements (RVE) to various load paths. Elastic moduli and wave surfaces are compared at various resolutions to illustrate what information is retained and lost during the upscaling process. We use field characterization at NNSS to build models for the SPE that combine these methods in order to permit efficient wave propagation through jointed rock masses while retaining the important effects of joints and anisotropy on energy transport and wave conversion. We show that these methods enhance computational capabilities for SPE while providing new insights into joint interactions in rock masses, effective properties of jointed media, and anisotropic wave propagation.

This work performed under the auspices of the U.S. Department of Energy by Lawrence Livermore National Laboratory under Contract DE-AC52-07NA27344.

#### **Multi-Phenomenology Yield Estimation of Near-Surface Chemical and Nuclear Explosions**

RODGERS, A. J., LLNL, Livermore, CA, USA, roddgers7@llnl.gov; FORD, S. R., LLNL, Livermore, CA, USA, ford17@llnl.gov; RAMIREZ, A. R., LLNL, Livermore, CA USA, ramirez3@llnl.gov; KIM, K., LLNL, Livermore, CA USA, kim84@llnl.gov; DODGE, D. A., LLNL, Livermore, CA USA, dodge1@llnl.gov; KNAPP, D. R., LLNL, Livermore, CA USA, knapp22@llnl.gov; PITARKA, A., LLNL, Livermore, CA USA, pitarka1@llnl.gov; BULAEVSKAYA, V., LLNL, Livermore, CA USA, bulaevskaya1@llnl.gov

Near-surface explosions generate seismic ground motions and atmospheric overpressures, speed-of-sound (SOS) signals. However, SOS signal amplitudes

depend on both explosion yield ( $W$ ) and height-of-burst/depth-of-burial (HOB/DOB). Thus yield must be estimated simultaneously with HOB/DOB by combining seismic and overpressure data to counter strong trade-offs. Interpretation of SOS signal amplitudes for yield requires accurate models of excitation and propagation, which depend on the media: geologic material properties (wavespeeds, density and attenuation) for seismic and atmospheric properties for atmospheric (temperature, pressure, sound speed, wind). We show that seismic amplitudes behave differently for hard and soft rock emplacement conditions. We have developed algorithms to estimate yield and HOB/DOB for near-surface explosions by combining seismic and overpressure measurements at local distances ( $< 20$  km). The algorithms rely on a Bayesian approach for both the signal models and the W-HOB estimation process. For a collection of 32 chemical and nuclear explosions (CE, NE, respectively) ranging 100 kg to 18 kt we demonstrate that yields can be estimated with errors of 50% or less for three-quarters of the events and one half of the yields can be estimated within 25%. Yield estimation is currently better for larger explosions. We show that NE yields can be estimated with models based on CE assuming that nuclear explosions generate SOS signals with amplitudes equivalent to chemical explosions of one half the yield. To test our method we have computed synthetic signals using three-dimensional (3D) sub-surface seismic and atmospheric models and finite difference solvers. Advances in 3D acoustic propagation allow for waveform inversion to estimate the equivalent acoustic source strength and yield. We will describe recent improvements in methodologies and highlight needs for future research and development to improve yield estimation.

#### **The 12 August 2015 Tianjin, China Chemical Explosions**

ZHAO, L. E., Institute of Geology and Geophysics, Chinese Academy of Sciences, Beijing, China, zhaolf@mail.iggcas.ac.cn; XIE, X. B., IGPP, University of California at Santa Cruz, Santa Cruz, CA, USA, xxie@ucsc.edu; WANG, W. M., ITPR, Chinese Academy of Sciences, Beijing, China, wangwm@itpcas.ac.cn; HAO, J. L., IGG, Chinese Academy of Sciences, Beijing, China, haojl@mail.iggcas.ac.cn; YAO, Z. X., IGG, Chinese Academy of Sciences, Beijing, China, yaozx@mail.iggcas.ac.cn

On August 12, 2015, a series of explosions accidentally occurred at a container terminal in the east port city Tianjin, China. This accident caused big fire and mushroom clouds and resulted in enormous casualty and property loss. The local news reported that strong shakings were felt in a wide area, including part of the Hebei province. Seismograms generated by these chemical explosions are collected from 120 broadband stations of the China digital seismic network. By using the cross-correlation technique, we determine the time differences between the two major explosions at individual stations. These travel time differences are then used to determine the relative locations between the two major explosions,  $66.6 \pm 9.3$  m, using a high-precision relative location method. Both body- and surface-wave magnitudes are calculated for the largest explosion and the results are  $m_b(Lg) = 2.87 \pm 0.18$  and  $M_s = 2.14 \pm 0.28$ , respectively. By applying cross-correlation to the waveforms for the two major explosions, their amplitude ratio is 0.175, upon which the magnitudes of the second largest explosion can be estimated to be  $m_b(Lg) = 2.11$  and  $M_s = 1.42$ , respectively. Based on the sizes of craters generated by these explosions, the yield of the largest explosion is approximately 188.8 ton, and the yield of the second largest explosion is approximately 18.3 ton. The coefficient of energy conversion from explosion to radiated seismic waves is approximately 0.102. This work was supported by the National Natural Science Foundation of China (grants 41374065, 41174048).

---

### **Numerical Modeling of Earthquake Ground Motion, Rupture Dynamics and Seismic Wave Propagation**

Poster Session · Thursday · 21 April · Tuscany F

---

#### **Preliminary Numerical Validation of the Fault Mechanism of the 2007 Mw6.6 Niigata-Chuetsu-Oki Strong Ground Motion Earthquake by Spectral Element Method.**

GATTI, F., Lab. MSSMat—UMR CNRS 8579—CentraleSupélec, Chatenay Malabry, France, filippo.gatti@centralesupelec.fr; PAOLUCCI, R., DICA, Politecnico di Milano, Milano, Italy, roberto.paolucci@polimi.it; LOPEZ-CABALLERO, F., Lab. MSSMat—UMR CNRS 8579—CentraleSupélec, Chatenay Malabry, France, fernando.lopez-caballero@centralesupelec.fr; CLOUTEAU, D., Lab. MSSMat—UMR CNRS 8579—CentraleSupélec, Chatenay Malabry, France, didier.clouteau@centralesupelec.fr

In this paper, we present a validation study on the performance of the Spectral Element Method (SEM) in reproducing strong ground motion scenarios at the regional scale. The SEM is exploited to efficiently solve the elasto-dynamic equa-



tions in physical domains with complex geometries and in a wider range of frequency with the respect to other numerical schemes (*e.g.* finite differences). Those physics-based numerical models reproduce the kinematics of the fault mechanism, as well as topography-induced site effects. Moreover, wave propagation in heterogeneous viscous-elastic materials (such as crustal rocks and sedimentary basins) are performed too.

The aim of this paper is to reproduce the fault mechanism that originated the 2007 Niigata (west Japan) strong motion earthquake ( $M_w$  6.6) by means of a 3D numerical model of the region surrounding the hypocenter based on the SEM formulation. The model contains a kinematic description of the faulting mechanism, calibrated on seismological indications provided for the Niigata strong ground motion by the Japanese strong-motion seismograph networks. Moreover, the geological information available were exploited to create simplified homogeneous soil and rock deposits. Results were first validated on an independent solution for the case of a layered half-space and finite fault discretization, and subsequently, the verification of numerical simulations was performed on a wide strong motion record set, both from the Japanese KiKNet and KNET networks and from the local array installed at the Kashiwazaki-Kariwa nuclear power plant.

### **The SCEC Broadband Platform: Open-Source Software for Strong Ground Motion Simulation and Validation**

SILVA, F., Southern California Earthquake Center, Los Angeles, CA, USA, fsilva@usc.edu; GOULET, C., Southern California Earthquake Center, Los Angeles, CA, USA, cgoulet@usc.edu; MAECHLING, P., Southern California Earthquake Center, Los Angeles, CA, USA, maechlin@usc.edu; CALLAGHAN, S., Southern California Earthquake Center, Los Angeles, CA, USA, scottcal@usc.edu; JORDAN, T., Southern California Earthquake Center, Los Angeles, CA, USA, tjordan@usc.edu

The Southern California Earthquake Center (SCEC) Broadband Platform (BBP) is a carefully integrated collection of open-source scientific software programs that can simulate broadband (0-100Hz) ground motions for earthquakes at regional scales. The BBP scientific software modules implement kinematic rupture generation, low and high-frequency seismogram synthesis using wave propagation through 1D layered velocity structures, ground-motion intensity measurement calculations, and goodness of fit measurements for validation. These modules are integrated into a software system that provides transparent user-defined calculation of ground motion seismograms, using multiple alternative simulation methods, and software utilities that can generate plots, charts, and maps. The BBP has been developed over the last six years in a collaborative scientific, engineering, and software development project involving geoscientists, earthquake engineers, graduate students, and SCEC scientific software developers.

The BBP can run earthquake rupture and wave propagation modeling software to simulate ground motions for well-observed historical earthquakes and to quantify how well the simulated broadband seismograms match the observed seismograms. The BBP can also run simulations for hypothetical earthquakes. In this case, users input an earthquake location and magnitude description, a list of station locations, and a 1D velocity model for the region of interest, and the BBP software then calculates ground motions for the specified stations.

The current release of the SCEC BBP can be compiled and run on recent Linux systems with GNU compilers. It includes 5 updated simulation methods, 7 simulation regions covering California, Japan, and Eastern North America, the ability to compare simulation results against GMPs, and a simplified command line interface. The latest release also includes new ground-motion parameter computational tools to facilitate an engineering assessment of the results.

### **Source Depth and Azimuth Dependent Synthetic Lg Attenuation**

HUI, H., University of Missouri, Columbia, MO, USA, hhdhf@mail.missouri.edu; SANDVOL, E., University of Missouri, Columbia, MO, USA, sandvole@missouri.edu

The regional phase Lg has been the subject of many studies due to its ability to reliably estimate source yields and to characterize crustal attenuation, however, the relationship between effective Lg Q and the true intrinsic attenuation of the crust is not well understood. We are working to investigate this relationship by conducting a number of numerical experiments to better understand the nature of Lg scattering attenuation for different type of crustal models. We have partitioned our model by 8-nodes hexahedral meshes with SPECFEM3D-Cartesian which is based on Spectral Element Method. The time step is 0.02 s to make the simulation stable to generate high frequency enough for our study (about 0.8 Hz).

We have found that the thickness of crust affect the measurements of effective Lg Q. Using the same velocity and attenuation structure, thicker crust leads

to low Lg Q and thinner crust leads to high Lg Q. These numerical experiments are consistent with observations of low Lg effective Q (less than 200) in continental plateaus such as the Iranian and Tibetan plateau (TP). Our results would suggest that the crustal thickness itself can significantly lower effective Lg Q.

We have also studied effective Lg Q of models with different Moho structure (a flat Moho and with a step) and found that Moho step would lead to lower effective Lg Q than that of flat Moho. Furthermore, we calculated the effective Lg Q for different lines in our 2D TP model with two-station method and found an azimuthally dependent Lg Q. We found that for a flat Moho the value was approximately the same as the intrinsic attenuation and a much higher effective attenuation which is result from scattering along the wave path with a Moho step.

We have also modeled the group velocity delay of low frequency Lg, which is dependent on source depth. We found that the group velocity of long period Lg (below 0.6 Hz) is about 0.3 km/s slower for shallower events (2 km) than that of 20 km events.

### **High Frequency Regional Phase Modeling in Crustal Pinch and Bulge Structures Simulated with Radiative Transport**

SANBORN, C. J., University of Connecticut, Storrs, CT, USA, sanborn@phys.uconn.edu; WALSH, S., University of Connecticut, Storrs, CT, USA, stevenwalsh325@gmail.com; CORMIER, V. F., University of Connecticut, Storrs, CT, USA, vernon.cormier@uconn.edu

The differences between earthquakes and explosions are largest in the highest recordable frequency band. In this band, scattering of elastic energy by small-scale (less than a wavelength) heterogeneous structure can equilibrate energy on components of motion and stabilize behavior of the Lg wave trapped in Earth's crust. Larger-scale (greater than a wavelength) elastic and anelastic structure can still assume major control over the propagation efficiency or blockage of Lg and other regional phases. To investigate these effects, we model high-frequency (2-4 Hz) regional seismic wave codas with a radiative transport algorithm. The algorithm propagates packets of energy with ray theory through large-scale 3-D structure, and includes stochastic effects of multiple-scattering by small-scale heterogeneities described statistically within the large-scale structure. Source-radiation patterns are controllable and described by moment tensors. Seismograms of explosion and earthquake sources are synthesized in canonical models to predict effects on waveforms of paths crossing regions of crustal thickening (collisional mountain belts) and thinning (pull-apart basins and ocean/continent transitions). For paths crossing crustal thinning regions, Lg is amplified at receivers within the thinned region but strongly disrupted and attenuated at receivers beyond the thinned region. For paths crossing regions of crustal thickening, Lg amplitude is attenuated at receivers within the thickened region, but experiences little or no reduction in amplitude at receivers beyond the thickened region. Localized regions of intense scattering within laterally homogeneous models of the crust increase Lg attenuation but do not disrupt its coda shape. Computational experiments comparing coda waveforms of earthquakes and explosions predict that discriminants based on P/Lg amplitude ratios will best separate earthquake and explosion populations at 2 Hz and higher.

### **Source Geometry and Free Surface Influence on Earthquake Rupture Characteristics in the Subduction Zone of Mexico's Pacific Coast**

CARRILLO LUCIA, M. A., Institute of Engineering, UNAM, Mexico City, Mexico, mcarrillo@iingen.unam.mx; RAMÍREZ-GUZMÁN, L., Institute of Engineering, UNAM, Mexico City, Mexico, lramirezG@iingen.unam.mx

We present an analysis of corner frequency variations associated with changes in the geometry of the subduction slab along four regions of the Mexican Pacific coast and the free-surface feedback. We evaluated 74 earthquakes using velocity and acceleration records. The database includes earthquakes with magnitudes higher than 5.5 recorded between 1972 and 2015. The velocity records were instrumentally corrected, and accelerometric data was baseline corrected using Wang *et al.*'s (2011) proposal. We obtained source time functions through a least-square inversion method considering synthetic waveforms computed using a three-dimensional model in Central Mexico and the reciprocity theorem (*e.g.* Lee *et al.*, 2011). Once we obtained the slip functions, we analyzed them in the frequency domain and compared the values of corner frequencies in the four regions. We observed differences along the coast and depth, which suggests that the dipping angle of the subduction zone and the energy reflected from the free surface are important factors in the rupture process of earthquakes in these regions. Finally, to demonstrate the influence of the geometry and free surface, we used a 2D anti-plane dynamic rupture model for each region to explain the importance of the geometry and free-surface feedback given the appropriate initial conditions, friction laws, and crustal structure.

## Pointwise Functions for Flexible Implementation of Crustal Deformation Physics in PyLith

AGAARD, B. T., US Geological Survey, Menlo Park, CA, USA, [baagaard@usgs.gov](mailto:baagaard@usgs.gov); KNEPLEY, M. G., Rice University, Houston, TX, USA, [knepley@gmail.com](mailto:knepley@gmail.com); WILLIAMS, C. A., GNS Science, Lower Hutt, New Zealand.

The next stage of development for PyLith, a flexible, open-source finite-element code (<http://geodynamics.org/cig/software/pylith/>) for modeling quasi-static and dynamic crustal deformation with an emphasis earthquake faulting, focuses on refactoring the code to provide greater flexibility in support of a broader range of physics, discretizations, and optimizations for a variety of computer hardware. We separate the finite-element integration into a discretization-specific portion and discretization-independent pointwise functions associated with the governing equations. The discretization-specific portion is designed to accommodate arbitrary order finite elements and multiple implementations for optimization targeting specific hardware (e.g., CPU and GPU). The pointwise functions encapsulate the physics, including the governing equations and rheologies. Users can easily extend the code by adding new pointwise functions to implement different rheologies and/or governing equations. PyLith currently includes pointwise functions for quasi-static and dynamic elasticity for several elastic, viscoelastic, and elastoplastic rheologies. We plan to add pointwise functions for coupling of elasticity with fluid flow and incompressible elasticity. Tight integration with the Portable, Extensible Toolkit for Scientific Computation (PETSc) provides support for a wide range of linear and nonlinear solvers and time-stepping algorithms.

## Initiation of Dynamic Ruptures in Numerical Simulations and its Effects on Rupture Propagation and Ground Motion

GALIS, M., KAUST, Thuwal, Saudi Arabia, [martin.galis@kaust.edu.sa](mailto:martin.galis@kaust.edu.sa); AMPUERO, J. P., Caltech, Pasadena, CA, USA, [ampuero@gps.caltech.edu](mailto:ampuero@gps.caltech.edu); MAI, P. M., KAUST, Thuwal, Saudi Arabia, [martin.mai@kaust.edu.sa](mailto:martin.mai@kaust.edu.sa); KRISTEK, J., Comenius University Bratislava, Slovak Academy of Sciences, Bratislava, Slovakia, [kristek@fmph.uniba.sk](mailto:kristek@fmph.uniba.sk); MOCZO, P., Comenius University Bratislava, Slovak Academy of Sciences, Bratislava, Slovakia, [moczo@fmph.uniba.sk](mailto:moczo@fmph.uniba.sk)

We present guidelines for efficient initiation of dynamic ruptures in numerical simulations using an overstressed asperity. Our results indicate that the approach by Uenishi (2009)—predicting the minimum size of an overstressed asperity that allows initial rupture acceleration (regardless of the subsequent rupture evolution)—is applicable for estimating the critical size of the initiation zone in configurations with high background stress. For low background stress we developed a new estimate of critical area of the initiation zone based on fracture mechanics (Galis *et al.*, 2015). This estimate explicitly accounts for overstress. Additionally, we analyzed numerical artifacts caused by using an asperity with super-critical size and/or overstress. The analysis revealed that super-critical parameters lead to shorter duration of initiation, but can also lead to strong numerical artifacts (for example, artificial super-shear transition). Based on these results we also provide guidelines for choosing the optimal asperity parameters that lead to significantly shorter initiation time with minimized numerical artifacts. However, in Galis *et al.* (2015) we focused only on effects of initiation on the rupture propagation. Here, we also analyze effects of initiation on ground motion. For high background stress configurations, our analysis shows no observable hypocentral P- or S- waves—neither for slightly overcritical nor for super-critical parameters. On the other hand, for low background stress super-critical initiation produces strong hypocentral P- and S- waves whereas slightly overcritical initiation produces only marginal variations. For low as well as high background stress we find that the optimal parameters, as suggested by Galis *et al.* (2015), produces only negligible artifacts in the radiated wave field.

## Effects of the Wasatch Front, Utah, Sedimentary Basins on Earthquake Ground Motions from Observed and Simulated Waveforms

MOSCHETTI, M. P., US Geological Survey, Denver, CO, USA, [mmoschetti@usgs.gov](mailto:mmoschetti@usgs.gov); HARTZELL, S., US Geological Survey, Denver, CO, USA; RAMIREZ-GUZMAN, L., UNAM, Mexico City, Mexico; RENNOLET, S., US Geological Survey, Denver, CO, USA

We compare observed and simulated waveforms for earthquakes in the Wasatch Front, Utah, region to investigate the effect of the sedimentary basins abutting the Wasatch Range on earthquake ground motions. Waveform data are obtained from ANSS and the University of Utah regional network. The waveform comparisons comprise goodness-of-fit metrics and analyses of site response from seven earthquakes that occurred in the Wasatch Front region between 2010 and 2014. Long-period ( $T \geq 1$  s) time series from 3-D earthquake simulations are computed using the Hercules finite-element wave propagation code and the Wasatch Front

community velocity model (WFCVM). In support of the development of synthetic ground-motion-based seismic hazard maps for the Wasatch Front, we first investigated the ability of the WFCVM to reproduce long-period parameters of engineering interest (peak ground motions, response spectral accelerations, Fourier amplitudes, and durations) measured from the observed seismograms. Goodness-of-fit between the observed and simulated ground motions are computed with the Olsen and Mayhew (2010) algorithm, which assess the quality of agreement between the ground motion parameters. We find good agreement between the observed and simulated waveforms up to 0.25\*0.5 Hz. At higher frequencies goodness-of-fit is highly variable, especially within sedimentary basins, and there is a large discrepancy between the observed and simulated ground-motion durations. Using these time series records, we also computed spectral amplification factors for sites within and outside of the sedimentary basins. On average, we find large amplifications at soft-soil sites and an intriguing high variability within the basins, which may be caused by basin geometric features. Vertical cross sections of the displacement wave field are used to study the focusing of body waves and the excitation of basin-edge-induced surface waves.

## Ground Motion Simulations for Scenario Earthquakes in the Xianshuihe Seismic Zone of Southwestern China

ZHANG, L. F., Institute of Crustal Dynamics, Beijing, China, [lzh239@uky.edu](mailto:lzh239@uky.edu); WANG, Z. M., Kentucky Geological Survey, Lexington, KY, USA, [zmwang@uky.edu](mailto:zmwang@uky.edu)

The Xianshuihe Seismic Zone is located in southeast margin of Qinghai-Tibet Plateau and one of the most active zones in southwestern China. There are many strong earthquakes occurred in the zone, including Luhuo  $M_w$ 7.6, Daofu  $M_w$ 7.0, and Kangding  $M_w$ 7.6, etc. Stochastic finite-fault model was chosen to simulate ground motions for several scenario earthquakes that could be expected to occur in the Xianshuihe Seismic Zone by sufficiently considering the physical mechanism of earthquake. Stochastic finite-fault model is an important tool to simulate near-field earthquake ground motion and accounts for the source characteristics, attenuation, and site amplification. The simulated ground motions were compared with the observations. The simulated ground motions were also used to generate peak ground acceleration (PGA), peak ground velocity (PGV), and peak ground displacement (PGD) contour maps and compared with the historical intensity observations.

## Supershear Transition Analysis in 3D Rough Fault Dynamic Simulations

YAO, Q. Y., University of California, San Diego, La Jolla, CA, USA, [q1yao@ucsd.edu](mailto:q1yao@ucsd.edu); DAY, S. D., San Diego State University, San Diego, CA, USA, [sdday@mail.sdsu.edu](mailto:sdday@mail.sdsu.edu); SHI, S. Z. Q., San Diego State University, San Diego, CA, USA, [samzqshi@gmail.com](mailto:samzqshi@gmail.com)

Supershear rupture propagation has been documented from seismic observations for natural faults, like 2002 Denali earthquake (Dunham *et al.*, 2004) and observed in laboratory observations (Xia *et al.*, 2004). High resolution imaging has demonstrated that natural faults have complex geometries (Candela *et al.*, 2009). How could fault roughness affect the supershear transition on natural fault? Bruhat *et al.*, (2015) has analyzed supershear transition in 2D rough fault dynamic simulations, and shows that supershear transition is very sensitive to the background stress and local geometry. We have analyzed supershear transition in a database of more than 1000 3D rupture simulations. We have observed different triggering mechanisms of supershear transitions, including free surface S-P conversion (Kaneko *et al.*, 2010), high S-ratio (Liu *et al.*, 2008) on releasing bend at fault segments, stress focusing triggering (Dunham *et al.*, 2003) near restraining bend at fault segments. We also investigated the fault roughness generally weakens the supershear at free surface, however, in some rare cases, it would be influenced by the strong interaction of rupture front from free surface and from the nucleation center, which can strengthen the supershear rupture. With higher-amplitude fault roughness, it is more likely that the fault plane has more supershear phenomena, especially large supershear area, which can span more than 15% of the total fault area. Increasing the background stress leads more supershear phenomena generally.

## Extracting the Statistics of 3D Rough Fault Dynamic Rupture Simulations for Pseudo-Dynamic Source Generation

SAVRAN, W. H., San Diego State University, San Diego, CA, USA, [wsavran@ucsd.edu](mailto:wsavran@ucsd.edu); OLSEN, K. B., San Diego State University, San Diego, CA, USA, [kbolsen@mail.sdsu.edu](mailto:kbolsen@mail.sdsu.edu)

Spontaneous rupture modeling provides a physical framework to compute realistic broadband rupture models of earthquake faults. However, at this time, it is numerically unfeasible to use spontaneous rupture simulations directly for the large number of strong-ground motion simulations necessary for current state-of-

the-art seismic hazard projects (e.g., the Southern California Earthquake Center (SCEC) CyberShake and Broadband Platform Projects). Instead, we aim to capture the statistics of complex spontaneous rupture models in a method allowing for rapid and computationally inexpensive generation of physically realistic broadband kinematic source models. Recent studies (e.g., Dunham *et al.*, 2011; Shi and Day, 2013) have shown that fully dynamic rupture on geometrically complex (rough) faults is capable of capturing realistic spectral energy to frequencies of engineering interest (e.g.,  $\sim 10$  Hz+). Here, we analyze the statistics of the rupture fields computed from rough fault dynamic rupture simulations, namely total slip, peak slip velocity, and rupture velocity. We show preliminary results of the one-point and two-point statistical properties for an ensemble of dynamic rupture simulations, which consist of marginal probability density functions (PDFs) and correlations between the rough-fault profile and the three aforementioned source parameter fields. We model each source parameter field as a linear combination between a deterministic part, due to lithostatic stress and dynamic rupture effects, and its residuals, which we attribute to variations in the rupture process caused by the rough fault. Our preliminary findings show that the marginal PDFs of the source parameter residuals resemble Gaussian distributions, for all source parameter fields. Also, we find all source parameter fields to be positively correlated with the initial friction (ratio of shear traction to normal traction).

### Modeling Topographic Effects and Site Response on a Mesa near Los Alamos, New Mexico.

LARMAT, C. S., Los Alamos National Laboratory, Los Alamos, NM, USA, carene@lanl.gov; LEE, R. C., Los Alamos National Laboratory, Los Alamos, NM, USA, rcllee@lanl.gov

The goal of this study is to build physics-based models of topography and site effects for strong ground motions at Los Alamos National Laboratory, New Mexico. This work is part of an ongoing effort to characterize seismic hazard for this area that is controlled by a nearby normal fault system (Pajarito fault system). The area is characterized by a complex subsurface geology consisting of successive basalt, volcanic ash and sedimentary deposits cut by steep canyons as a result of erosion. The University of Texas collected passive and active seismic data in the summer of 2014 on and near a mesa near LANL thanks to the deployment of Ten Trillium Compact broadband seismometers. Seismic signals were recorded both before and during a refraction-type experiment using a large, truck-mounted vibrator generating P and SH motions in a bandwidth of  $\sim 2$ –20 Hz and at distances of 100 m to 2 km from the mesa. Sensors were deployed in two crossing profiles that spanned the top and three sides of the mesa. The mesa of  $\sim 25$  m height is representative of the local topography and geology with an elongated shape in the east-west direction ( $\sim 180$  m in width at the base).

Our model is constructed starting with a large geological and geophysical database collected to build a 3D structural model for geohydrology modeling. From that model, we build a mesh of hexahedra conforming to the major local geologic units. Our numerical model is based on the Spectral Element Method (SEM) that is a high-order finite element method with a remarkable low computational load. SEM is used to develop canyon and mesa responses from ground motions generated by the stationary surface vibrator, hypothetical earthquakes and background seismic noise.

The model is used to explain the response of the mesa to both ambient seismic noise and the active seismic experiment. In particular, the spectral ratio analysis of the ambient noise data showed amplifications above 5 on the horizontal components at frequencies  $\sim 1.5$  Hz.

---

## Seismo-Acoustics and Infrasond

Poster Session · Thursday · 21 April · Tuscany F

---

### Seismic and Ionospheric Signatures for the Study of Underwater Earthquakes: Modeling Developments

ROLLAND, L. M., Géoazur, Nice, France, lrolland@geoazur.unice.fr; LARMAT, C., Los Alamos National Laboratory, Los Alamos, NM, USA, carene@lanl.gov; RÉMILLIEUX, M., Los Alamos National Laboratory, Los Alamos, NM, USA, mcr1@lanl.gov; KHELFI, K., Institut de Physique du Globe de Paris, Paris, France; LOGNONNÉ, P., Institut de Physique du Globe de Paris, Paris, France

In the last decade, it has been established that major earthquakes, volcano eruptions and tsunamis create waves propagating in the ionosphere that are observable as Total Electron Content (TEC) perturbations. We report here theoretical investigations and numerical modeling of TEC signals induced by ground and

ocean motions aiming to a better quantitative understanding of these signals. Such development is needed to evaluate the benefit of incorporating TEC signals into tsunami early-warning systems. Recent studies show that current technology based on inland ground motions, geodetic measurement and tsunami gauges still needs improvement within 10 minutes after the earthquake/tsunami onset. In this study, we are using SPECSEM3D, a code based on the Spectral Element Method (SEM) to develop a numerical model of TEC perturbations. This model couples an elastic layer representing the Solid Earth to acoustic layers representing the ocean and atmosphere. Theoretical thermodynamics and physics considerations were used to develop an Earth atmosphere model parameterized for acoustic wave propagation. We will present results for different TEC events that show good fit with coseismic ionospheric observations; our model successfully predicts an acoustic pulse and fast-propagating ( $\sim 3.5$  km/s) Rayleigh-coupled waves as well as the acoustically resonant response of the atmosphere. This latter can be physically explained by multiple reflexions in the low atmospheric waveguide. Further quantitative examination aims to model attenuation effects, as well as finite fault effects (rupture history). We will also investigate how waves and TEC signal are affected by gravity (under the Cowling approximation), especially at low frequencies ( $\sim 4$  mHz). Finally, we will present results for the Planet Mars where a lander with a microbarometer is planned to be launched in the coming couple of years.

### Infrasound Scaling Characteristics from Small Earthquakes in the Utah Region

HALE, J. M., University of Utah Seismograph Stations, Salt Lake City, UT USA, jmhale@seis.utah.edu; PANKOW, K. L., University of Utah Seismograph Stations, Salt Lake City, UT USA, pankow@seis.utah.edu; ARROWSMITH, S. J., Sandia National Laboratory, Albuquerque, NM, USA, sjarrow@sandia.gov; STUMP, B., Southern Methodist University, Dallas, TX, USA, bstump@smu.edu; HAYWARD, C., Southern Methodist University, Dallas, TX, USA, hayward@smu.edu

Using a regional network of nine infrasound arrays located in Utah, we systematically search for epicentral infrasound from earthquakes in the seismically active Utah region between April 2007 and December 2014. This study expands on a previous study that analyzed data from 293 ( $M > 3.0$ ) earthquakes for the time period April 17, 2007–June 30, 2012. During the initial study, multiple infrasound detections for nine earthquakes with  $M$  3.6–5.9 were identified. These infrasound detections were recorded from normal, oblique normal, and strike-slip faulting earthquakes with depths between 5 and 12 km, recorded at epicentral distances of 156–695 km. This study analyzes an additional 157 earthquakes ( $M > 3.0$ ). For infrasound detections, we use ray-tracing through ground-to-space atmospheric models from the epicenters to each array to determine the atmospheric turning altitude regions and compare distance and wind corrected amplitudes with previously determined scaling relations. The infrasound observations in this study will contribute to the scaling relations for corrected amplitude versus magnitude and test our previous observation of slope differences in magnitude versus duration scaling relations for small and large earthquakes.

### Detection and Association of Seismoacoustic Data from a Series of Chemical Explosions in New Mexico

EULER, G. G., Los Alamos National Laboratory, Los Alamos, NM, USA, ggeuler@lanl.gov; BLOM, P. S., Los Alamos National Laboratory, Los Alamos, NM, USA, pblom@lanl.gov; ANDERSON, D. N., Los Alamos National Laboratory, Los Alamos, NM, USA, dand@lanl.gov

We present recent work on automated detection and association algorithms applied to seismoacoustic records from a series of 70 chemical explosions (COMP B) conducted at Los Alamos National Laboratory site Minie during May to June 2013. The seismoacoustic network consists of 14 seismic and infrasound sensors at distances within about 10 kilometers. The detections are found using an STA/LTA technique for single stations and an adaptive F-detector method for infrasound arrays. We then associated these detections by finding the association likelihood between every unique pair of detections to form detection sets with hierarchical cluster analysis. We find that our automated detection and association techniques successfully recovered the series of chemical explosions and the association linkages are informative about the relative limitations of the wave phenomenologies. We also discuss extending these techniques to regional distances to quickly create a seismoacoustic catalog of explosions such as mine blasts.

### Amplitude and Frequency Calibration on Infrasound Sensors

ZEILER, C. P., PSRF, Boulder, WY, USA, cleat.zeiler@us.af.mil; ALLISON, E., Chugach Information Technologies Inc., Boulder, WY, USA, fender.allison@



chugach.com; WUERTLEY, R., Chugach Information Technologies Inc., Boulder, WY, USA, ronald.wuertley@chugach.com

The Pinedale Seismic Research Facility (PSRF) has field-tested sensor packages for several decades. Over the last couple of years the PSRF has installed an infrasound test bed that uses equal-length manifolds to a piston driven source. In order to better understand the capability of the new test bed several experiments have been conducted. The first rounds of experiments have focused on the stability of amplitude and frequency measurements. The test bed uses an NB2000 as the reference sensor and Chapparral, Hyperion and IML sensors were used as the experimental sensors. The sensors and source are controlled by a Smart24 digitizer. One round of experiments was to test the sensors for deployment to ensure accurate data would be recorded and identify any malfunctioning units. The next round was to identify the IML sensor characteristics. In the final round of experiments we identify the stability of the test bed over several days and varying atmospheric conditions. Each experimental sensor was tested at least three times with varying frequency and amplitude levels. The test bed can run three instruments at a time and only the Hyperion instruments were unable to be tested together, due to configuration differences. The preliminary results show that there is a potential for differences in accuracy due to atmospheric changes. In general the amplitudes varied by less than 0.5% and the frequency was recovered with phase shifts on all functioning sensors. Overall we noted a 5-10% lower sensitivity from the manufactures reported calibration.

#### **A Global Infrasound Event Catalog**

ARROWSMITH, S. J., Sandia National Laboratories, Albuquerque, NM, USA, sjarrow@sandia.gov

The Comprehensive Nuclear Test Ban Treaty Organization is charged with generating automatic and manually reviewed global infrasound event catalogs for dissemination to national data centers. This is a challenging problem given the sparsity of International Monitoring System infrasound network, the time-varying atmospheric medium, and the large numbers of detections from local and coherent wave signals that can be falsely associated with detections at other arrays. By relying on a single algorithm, and without adequate ground-truth for assessment, it is difficult to estimate the missed detection rate. In this presentation, an independently generated global event catalog is presented that uses a completely different set of algorithms for infrasound event detection.

#### **Infrasound Waves in the Stratosphere: Sources and Implications for Atmospheric Dynamics**

BOWMAN, D. C., University of North Carolina at Chapel Hill, Chapel Hill, NC, USA, daniel.bowman@unc.edu; LEES, J. M., University of North Carolina at Chapel Hill, Chapel Hill, NC, USA, jonathan.lees@unc.edu

Infrasound arrays were lifted into the stratosphere over central New Mexico in August 2014 and September 2015. Stratospheric infrasound was very different than that recorded on the ground. The most distinct feature was numerous narrow band, frequency varying signals between 1 and 25 Hz. These appear and disappear over the course of hours, but overall activity seems to be related to the day night cycle. We speculate that these striking spectral features are a consequence of resonant scattering in narrow acoustic wave guides in the stratosphere. Other sources, such as a 17 Hz frequency invariant signal common to building ventilation systems, are considered as well. This signal was clearly seen in the stratosphere in 2014, but not in 2015. Pulses of broad band activity and background pressure fluctuations sometimes have Gaussian amplitude distributions. These we attribute to randomly oriented quadrupole radiators embedded in tropospheric turbulence. The ocean microbarom peak was present in the stratosphere but not on the ground, and we investigate whether this is due to atmospheric structure or low signal to noise ratios on surface sensors. A period of intense very low frequency infrasound (6 Pa peak to peak, ~250 second period) generated by thunderstorms was recorded during the 2015 flight. Such fluctuations have been observed in ionospheric soundings during intense convective activity, but rarely on the ground. We characterize this signal and discuss its implications for energy transfer to the upper atmosphere. The correspondence between thunder recorded on the ground and possible lightning-related signals in the stratosphere is discussed as well.

#### **Improving Infrasound Detection and Location Catalogs in the Western US Using Atmospheric Modeling**

DANNEMANN, F. K., Southern Methodist University, Dallas, TX, USA, fdannemann@smu.edu; PARK, J., Southern Methodist University, Dallas, TX, USA, junghyunp@mail.smu.edu; MARCILLO, O., Los Alamos National Laboratory, Los Alamos, NM, USA, omarcillo@lanl.gov; BLOM, P., Los Alamos National Laboratory, Los Alamos, NM, USA, pblom@lanl.gov; HAYWARD,

C., Southern Methodist University, Dallas, TX, USA, chayward@smu.edu; STUMP, B. W., Southern Methodist University, Dallas, TX, USA, bstump@smu.edu

Automated infrasound catalogs are useful for documenting repeated sources as well as evaluating detection performance across a given network under time-varying atmospheric conditions. An automated process for detection, association, and location is tested using data from three infrasound arrays (BRP, FSU, and HWU), which are cooperatively operated by the University of Utah and Southern Methodist University. The adaptive F-detector (Arrowsmith *et al.*, 2009) accounts for correlated and uncorrelated noise through modification of the conventional F-statistic to capture time-varying background noise and reduces false detections due to the presence of coherent noise. The Bayesian infrasound source location (BISL) method (Modrak *et al.* 2010) produces source location and time credibility contours from posterior probability density functions. The updated BISL methodology (Blom *et al.*, 2015) employs celerity and azimuth deviation distributions constructed from numerical propagation and historical atmosphere models (Marrillo *et al.*, 2013). Propagation-based models have been calculated from the Ground-to-Space (G2S) atmospheric database. We are testing a database-centric pipeline, InfraPyDB, to analyze large infrasound datasets. Infrasound array data is tested over a two-year time period (1 November 2010 to 31 October 2012) and compared to a previously constructed catalog of infrasonic events within the western US (Park *et al.*, 2014) to analyze changes in spatial and temporal confidence bounds of the source with the addition of propagation-based priors. The automatic detection estimates and source locations, especially for known repeated sources such as those at Dugway Testing Ground and Utah Test and Training Range, are compared to the previous infrasound catalog. This work demonstrates that both infrasound signal detection and source location can be improved by accounting for the effects of realistic atmospheric conditions in the source location processing.

---

### **The Role of Shallow Slip on Faults**

Poster Session · Thursday · 21 April · Tuscany F

---

#### **Paleoseismic Results from Two Sites on the Principal Strand of the August 24, 2014 South Napa Earthquake Rupture**

DAWSON, T. E., California Geological Survey, Menlo Park, CA, USA, timothy.dawson@conservation.ca.gov; RUBIN, R. S., California Geological Survey, Menlo Park, CA, USA, ron.rubin@conservation.ca.gov; MARESCHAL, M., California Geological Survey, Menlo Park, CA, USA, Maxime.Mareschal@conservation.ca.gov

The August 24, 2014 South Napa earthquake produced at least 12.5 km of clear surface rupture, extending from Cuttings Wharf in the south to north of Alston Park, located in the City of Napa, CA. Minor slip occurred on four additional strands east of the main trace. Our studies have focused on the western-most, principal fault strand, with two sites located ~4.7 km apart.

The South Avenue site is the southern-most site, and a trench was excavated spanning the rupture. Locally, the rupture produced ~10-20 cm of right lateral displacement. The fault has little geomorphic expression at the site; however, a ~1-km-long pre-existing scarp is coincident with the rupture ~0.5 km to the north. In the trench, the rupture can be traced up to the ground surface. Pleistocene alluvium is displaced an unknown amount across a fault zone that is ~2 m wide. Due to limited deposition since the late Pleistocene, the number of events and ages prior to the 2014 rupture are not constrained; however, the recognition of several faults, pervasively sheared deposits, and juxtaposition of units indicates repeated offsets have occurred prior to 2014.

The Buhman Ave trench site is located across a short, pre-existing 2-m-high scarp formed on colluvial deposits. Right-lateral slip measured on a fence adjacent to the trench is ~30-35 cm. The 2014 rupture is weakly expressed in the near surface. However, well-developed shear surfaces and juxtaposition of units is better expressed at depth, which we interpret as the result of an unresolved number of prior earthquakes. Charcoal samples were collected and radiocarbon results are pending; we infer the section is likely mid-late Holocene in age.

Based on these two trenches, our interpretation is the fault has ruptured multiple times in the Quaternary and likely the Holocene. This work illustrates the value of subsurface investigations for assessing activity of low slip-rate faults that are poorly-expressed geomorphically, or have distributed ruptures.

#### **Lidar Investigation of Scarp Degradation along the 1959 Hebgen Lake Earthquake Surface Rupture**

JOHNSON, K. L., Colorado School of Mines, Golden, CO, USA, kejohnso@mines.edu; NISSEN, E. K., Colorado School of Mines, Golden, CO, USA,

enissen@mines.edu; LAJOIE, L. J., Colorado School, Golden, CO, USA, lajoie@mines.edu

The 1959 MW 7.3 Hebgen Lake earthquake is the largest and most deadly earthquake to have occurred within the conterminous United States outside of California during the twentieth century. It predominantly ruptured the subparallel Hebgen and Red Canyon faults—the northeastern-most faults of the slowly extending Centennial Mountain Belt (~3 mm/yr)—and was carefully mapped shortly after the earthquake. Decades later, this early mapping coupled with modern topographic surveying provides a unique opportunity to learn how normal fault scarps degrade and evolve with time. Here, we use the first airborne lidar survey of the rupture, obtained through a seed grant from the National Center for Airborne Laser Mapping (NCALM), to build upon earlier efforts to monitor the scarp's degradation. We investigate scarp profiles at sites that were surveyed in 1980 and 2009, and, additionally, assess the degraded state of the scarp in areas that have not been revisited since the initial investigation. We identify topographic signals of composite scarps, aiming to resolve a disagreement over the number of Holocene ruptures (two to three from trenching, but five from chlorine-36 dating) on the Hebgen fault. The results, which we validate against forward modeling of single and multiple event scarps, improve constraints on regional sediment diffusion rates, and also provide a rare field example of a young, multi-event scarp. We also investigate whether all sites along the 1959 rupture record the same number of Holocene earthquakes, and whether the amount of slip at each site is consistent, helping reveal whether or not the Hebgen fault hosts characteristic earthquakes.

---

## Tsunami Resilience Strategies: Application of Tsunami Science and Mitigation Advancements to Protect Communities

Poster Session · Thursday · 21 April · Tuscany F

---

### USGS-National Tsunami Hazard Mitigation Program Workshop and Collaborations

ROSS, S. L., USGS, Menlo Park, CA, USA, sross@usgs.gov; WILSON, R. L., California Geological Survey, Sacramento, CA, USA, Rick.Wilson@conservation.ca.gov; WOOD, N. J., USGS, Portland, OR, USA, nwood@usgs.gov; GATELY, K., NOAA, Palmer, AK, USA, kara.gately@noaa.gov; GEIST, E. L., USGS, Menlo Park, CA, USA, egeist@usgs.gov; NICOLSKY, D. J., University of Alaska, Fairbanks, Fairbanks, AK, USA, djnicolsky@alaska.edu

A summary of outcomes from a workshop between the USGS and the National Tsunami Hazard Mitigation Program (NTHMP), being held on February 1-2, 2016, will be presented. The goal of the workshop is to improve collaboration between the NTHMP, its member states, and the USGS in order to provide better tsunami preparedness products for coastal communities. About 30 USGS scientists and 30 NTHMP members plan to participate in the workshop, which is scheduled just before the annual NTHMP meeting in Boulder, Colorado.

The NTHMP, funded by NOAA, is composed of two representatives (emergency manager and scientist) from each of the tsunami-vulnerable states, territories and regions in the U.S., plus representatives from NOAA, FEMA and the USGS. The NTHMP has three major subcommittees: the Warning Coordination Subcommittee (WCS), the Mitigation and Education Subcommittee (MES), and the Mapping and Modeling Subcommittee (MMS). The USGS is working with NOAA and the WCS to improve knowledge of subduction source geometries to help make tsunami forecast models more accurate. The USGS is also working with members of the MES on tsunami risk reduction efforts including tsunami evacuation modeling. The MMS has asked for input from the USGS on tsunami source characterization and standardization for scenario calculations and for tsunami vulnerability assessments; this tsunami source characterization effort will be a key focus of the workshop.

Outcomes and future collaborations defined during the workshop will be presented.

### NOAA National Tsunami Warning Center Operations during the 2015 Chile Earthquake and Tsunami

HUANG, P. Y., NOAA/NWS National Tsunami Warning Center, Palmer, AK, USA, paul.huang@noaa.gov; BAHNG, B., NOAA/NWS National Tsunami Warning Center, Palmer, AK, USA, bo.bahng@noaa.gov; GATELY, K., NOAA/NWS National Tsunami Warning Center, Palmer, AK, USA, kara.gately@noaa.gov; HALE, D. A., NOAA/NWS National Tsunami Warning Center, Palmer, AK, USA, David.hale@noaa.gov; KIM, Y. Y., NOAA/NWS

National Tsunami Warning Center, Palmer, AK, USA, yooyin.kim@noaa.gov; NYLAND, D., NOAA/NWS National Tsunami Warning Center, Palmer, AK, USA, david.nyland@noaa.gov; POPHAM, C., NOAA/NWS National Tsunami Warning Center, Palmer, AK, USA, christopher.popham@noaa.gov; WADDELL, J., NOAA/NWS National Tsunami Warning Center, Palmer, AK, USA, james.waddell@noaa.gov; WHITMORE, P. M., NOAA/NWS National Tsunami Warning Center, Palmer, AK, USA, paul.whitmore@noaa.gov

A major earthquake struck off the coast of central Chile on September 16, 2015 which triggered a Pacific-wide tsunami. The National Tsunami Warning Center (NTWC), in coordination with the Pacific Tsunami Warning Center (PTWC), issued an initial information statement with a magnitude of 7.9 to alert of the potential tsunami danger. On Bulletin 2, the earthquake magnitude was upgraded to 8.3 with information for the US west coast, Alaska, and Canada's Pacific coast to stay alert for more information as the tsunami threat was being evaluated for those regions. On Bulletin 4, the coastal areas from San Onofre State Beach to Ragged Point in southern California were put into a tsunami advisory and other NTWC areas were notified there was no tsunami danger. This notification occurred about 10 hours before impact in southern California.

A series of teleconferences were held with NWS Weather Forecast Offices, state warning points, the US Coast Guard, and Department of Defense throughout the event. The teleconferences allowed the NTWC to alert primary customers of any change in the tsunami alert status approximately 30 minutes prior to issuing any changes, and to provide a more detailed analysis of observations and forecasts than possible in official products.

A timeline of tsunami warning operations during the 2015 Chile earthquake is provided to illustrate NTWC operational activities. The timeline highlights the following:

- seismic and sea level data analysis,
- tsunami forecasting,
- interaction between agencies,
- hazard analysis and issuing of tsunami warning products, and
- communication with emergency management officials.

### Compilation and Analysis of a Database of Observatory Messages and Tsunami Bulletins issued by the Pacific Tsunami Warning Center (PTWC) for the Southwest Pacific Region between 2000 and 2015

SARDINA, Y., Pacific Tsunami Warning Center, Honolulu, HI, USA, victor.sardina@noaa.gov; WEINSTEIN, S., Pacific Tsunami Warning Center, Honolulu, HI, USA, stuart.weinstein@noaa.gov; BECKER, N., Pacific Tsunami Warning Center, Honolulu, HI, USA, nathan.becker@noaa.gov

The PTWC functions not only as the local tsunami warning center (TWC) for the State of Hawaii, American Samoa, and Guam, but also as the official international tsunami warning center (TWC) for nations with coasts in the Pacific, including those located in the Southwest Pacific (SWPA). Despite the challenges presented by round the clock monitoring of the seismic activity within this vast and remote region, PTWC scientists on duty strive to send a tsunami bulletin for any 6.5 or larger magnitude earthquake located in the SWPA region in less than the official requirement of 16 minutes from origin time. We characterized PTWC's performance for the SWPA region during the last 15 years relying on the compilation and cross-validation of 1660 observatory messages, and 257 official tsunami bulletins retrieved from the logs available for three different communication circuits. We parsed these messages and extracted the earthquake parameters reported by PTWC. We then calculated essential statistics such as message delay times, epicenter offsets, and magnitude residuals by comparing the message parameters with more authoritative source parametrizations reported by the National Earthquake Information Center (NEIC), and the moment magnitudes available from the Global Centroid Moment Tensor (GCMT) Project. Analysis of these statistics for the SWPA region reveals that PTWC has gradually reduced the time needed to send an observatory message from a median of 15 minutes in 2003 to 5 minutes and 49 seconds in 2015. Likewise, the PTWC has also reduced the time needed to send an official tsunami bulletin from a median of 43 minutes in the year 2000 to just 6 minutes in 2015. PTWC magnitude estimations have a median residual value of 0.2 magnitude unit, while epicenter locations within the SWPA region have median offsets of 13.1 km for observatory messages, and 11.1 km for official tsunami bulletins.

### "Beat the Wave" Cascadia Tsunami Evacuation Maps for Oregon Coastal Communities.

MADIN, I., Oregon Department of Geology and Mineral Industries, Portland, OR USA, ian.madin@state.or.us; GABEL, L. L., Oregon Department of Geology and Mineral Industries, Newport, OR, USA, laura.gabel@dogami.state.or.us; ALLAN, J. C., Oregon Department of Geology and Mineral

Industries, Newport, OR, USA; WATZIG, R. J., Oregon Department of Geology and Mineral Industries, Portland, OR, USA, [Rudie.Watzig@state.or.us](mailto:Rudie.Watzig@state.or.us)

A tsunami triggered by a future Cascadia subduction earthquake is one of the greatest natural hazards facing the Pacific Northwest and the Oregon coast. Few structures in Oregon communities are likely to survive the expected tsunami forces and damage within the inundation zone will be severe. However, the likely inundation zone can be modeled and mapped in advance, defining structures at risk and the area that must be evacuated. In 2013, the Oregon Department of Geology and Mineral Industries (DOGAMI) completed tsunami modeling and mapping for the entire Oregon coast and the information used to prepare evacuation maps that show residents where they need to go to reach safety. However, a limitation of these maps is the absence of information on the fastest and most direct routes to safety, as well as guidance on how quickly the public must travel in order to reach safety. Using least-cost-distance modeling in GIS, Wood and Schmidlein (2012) mapped the time required to evacuate communities, assuming a fixed walking speed, and accounting for land cover and slope. We have extended that approach by including information about wave arrival times derived from the Oregon tsunami inundation models. Using a grid of arrival times and least cost distance backlink rasters allows us to define "evacuation watersheds", so that for any point in a community, we know where the closest safe point is, and the wave arrival time at that location. This allows us to calculate, for any starting point, the speed an evacuee must maintain in order to reach safety ahead of the wave. The resulting "Beat the Wave" maps can help residents and city officials plan for improved evacuation. DOGAMI has completed a pilot project in Seaside Oregon, and is completing maps for Warrenton and Cannon Beach. It is our intention to prepare these maps for all Oregon coastal communities as funding allows.

#### The September 17, 2015, Chilean Tsunami in California: Response Activities and Field Observations

WILSON, R., California Geological Survey, Sacramento, CA USA, [Rick.Wilson@conservation.ca.gov](mailto:Rick.Wilson@conservation.ca.gov); LYNETT, P., University of Southern California, Los Angeles, CA USA, [plynett@usc.edu](mailto:plynett@usc.edu); SYNOLAKIS, C., University of Southern California, Los Angeles, CA USA, [costas@usc.edu](mailto:costas@usc.edu); MILLER, K., California Governors Office of Emergency Services, San Francisco, CA USA, [Kevin.Miller@caloes.ca.gov](mailto:Kevin.Miller@caloes.ca.gov)

On Wednesday, September 16, 2015, at 3:55 p.m. Pacific Time, a magnitude 8.3 earthquake occurred near the coast of central Chile. The National Tsunami Warning Center (NTWC) issued Tsunami Advisories for five Southern California counties: Orange, Los Angeles, Ventura, Santa Barbara and San Luis Obispo. Start of tsunami in California was forecasted at 0430 PDT on September 17.

The California Governor's Office of Emergency Services (CalOES) and California Geological Survey (CGS) participated in regularly-scheduled conference calls with the NTWC followed by calls with the county operational areas and state agencies. Web-cameras were monitored in San Diego, Marina Del Rey, and Cayucos but only minor currents were detected.

New tsunami planning documents provided by the state, called "Playbooks," were referenced for both potential coastal evacuations and harbor/port response activities. Because tides were relatively low and forecasted tsunami amplitudes were minimal (one foot or less), the least severe "Evacuation Playbook Plan" (Phase 1) and "Maritime Response Playbook Plan" (Plan A) were recommended.

After arrival, tsunami measurements were observed on tide gauges, which confirmed the Tsunami Advisory designation. In Ventura Harbor, where peak amplitudes of 1.2 feet were observed, field teams from the University of Southern California deployed video cameras and floating GPS units to monitor the tsunami. The field team provided near real-time video of the tsunami to CGS, CalOES, and the NTWC showing strong currents entering and leaving the harbor for a number of hours.

Post-event survey questionnaires were sent out by CGS to harbor and port officials. Results indicate that most of the harbor officials and county emergency managers referenced or used the tsunami Playbooks in their response. The event provided an opportunity for communities to practice their response and provided the impetus for them to update their plans. There were no reports of damage in California.

## The M7.1 Iniskin Earthquake, Alaska

Poster Session · Thursday · 21 April · Tuscany F

### M7.1 Iniskin, Alaska Earthquake of January 24, 2016: A Preliminary Review of Responses of Three Instrumented Buildings in Anchorage, Alaska

CELEBI, M. K., USGS, Menlo Park, CA USA, [celebi@usgs.gov](mailto:celebi@usgs.gov)

A preliminary review of the recorded responses of three prominent buildings in Anchorage, Alaska, to strong ground motions from the  $M_w$ 7.1 Iniskin, Alaska, earthquake is presented. The earthquake, located at a depth of 127 km within the subducting Pacific plate, occurred at 02:30:30 AM PST (epicentral coordinates: 59.66N, 153.45W, epicentral distance of approximately 260km from Anchorage) [[www.strongmotioncenter.org](http://www.strongmotioncenter.org), last accessed February 3, 2016]. The earthquake caused some of the strongest shaking in Anchorage since the well-known 1964 M9.2 earthquake (<http://earthquake.usgs.gov/earthquakes/events/alaska1964/>, last accessed February 3, 2016). Since that event, several structures (buildings, bridges) have been instrumented by the USGS.

In addition to an inventory of instrumented structures in Anchorage, we discuss three significant data sets acquired from accelerometer arrays deployed at each of three buildings. For this presentation, these buildings are identified by the number of stories (Table 1).

We identify essential dynamic characteristics of each building and summarize significant behavioral aspects such as beating and torsional motions. Table 1 shows the particulars of each building, including (H) height (m), recorded (A) ground level, (B) roof level peak accelerations (g), (C) roof level displacements (cm) and (DR) average drift ratios (%) computed using the peak displacements at the roof levels. These average drift ratios imply that the motions are at levels expected not to cause damage to the buildings.

Table 1: Three buildings, number of floors, heights, peak accelerations and displacements, average drift ratios [relevant data from [www.strongmotioncenter.org](http://www.strongmotioncenter.org), last accessed February 3, 2016].

Building	H	A	B	C	DR
14-story	51.5	.05	.09	4.6	.09
20-story	80.5	.07	.17	13.7	.17
22-story	74.0	.08	.19	29.1	.40

### Earthquake Ground Motions from the 2016 M7.1 Iniskin Earthquake in Anchorage, Alaska Related to Distribution of Sedimentary Deposits

CANNON, E. C., Golder Associates Inc., Anchorage, AK USA, [ecannon@golder.com](mailto:ecannon@golder.com); DUTTA, U., School of Engineering, University of Alaska, Anchorage, Anchorage, AK USA, [udutta2@uaa.alaska.edu](mailto:udutta2@uaa.alaska.edu); THORNLEY, J. D., Golder Associates Inc., Anchorage, AK USA, [John\\_Thornley@golder.com](mailto:John_Thornley@golder.com)

The January 24, 2016 M7.1 Iniskin earthquake was widely felt across the Cook Inlet region of southcentral Alaska. Located at the northeastern end of Cook Inlet, Anchorage experienced perceived shaking reaching moderate to strong levels across much of the community, with some areas reaching very strong levels, based on the United States Geological Survey ShakeMap for the earthquake and peak ground acceleration (pga) values from the Center for Engineering Strong Ground Motion Data (CESMD). The maximum pga recorded in Anchorage for this earthquake, based on CESMD data, was 0.211 g from a strong motion station located in southwest Anchorage. The distribution of ground shaking experienced is a function of the complex sedimentary deposits found in Anchorage, influenced by active tectonic and glacial processes. Utilizing published geologic literature, we subdivide Anchorage into regions based on surficial geology and subsurface data, and pga values (CESMD) for the earthquake, to examine the relationship between geologic setting and pga. The regions include the cohesive facies of the glaciomarine Bootlegger Cove Formation (BCF); cohesive BCF facies overlain by glacial outwash/alluvial deposits; glaciodeltaic deposits; and glacial and alluvial deposits that thin out to the east against bedrock of the Chugach Mountains. The region of the cohesive BCF facies located in southwest Anchorage had the largest recorded pga values, ranging from 0.078 g to 0.211 g, although one station recorded 0.034 g. The region of cohesive BCF facies overlain by glacial outwash/alluvial deposits along Cook Inlet had pga values ranging from 0.071 g to 0.171 g. These high pga values are consistent with previous studies of ground motion response for the cohesive BCF facies. The other regions had pga values ranging from 0.020 g to 0.168 g. This earthquake demonstrates the importance of continued efforts to understand the distribution of ground motion responses across the Anchorage area.

### Seismic Response of a Highway Bridge during the Iniskin Earthquake

YANG, Z., University of Alaska, Anchorage, AK, USA, [zyang2@uaa.alaska.edu](mailto:zyang2@uaa.alaska.edu); STILL, B., University of Alaska, Anchorage, AK, USA, [bastill@alaska.edu](mailto:bastill@alaska.edu); DUTTA, U., University of Alaska, Anchorage, AK, USA, [udutta2@uaa.edu](mailto:udutta2@uaa.edu)



alaska.edu; THORNLEY, J., Golder Associates, Inc, Anchorage, AK, USA, john\_thornley@golder.com

Frozen ground is significantly stiffer than unfrozen ground. For bridges supported on deep foundations, the bridge stiffness is also measurably increased higher in the winter months. Significant changes due to seasonal freezing in the bridge pier boundary conditions due to seasonal freezing require additional detailing in order to ensure a ductile performance of the bridge during the a design earthquake event. A bridge was instrumented with a network of accelerometers to monitor and study its seismic performance and assess the impact of seasonally frozen soil on the bridge performance. On January 24, 2016 the  $M_w$ 7.1 Iniskin earthquake shook the Cook Inlet region and provided a unique opportunity to evaluate the response of bridge with a fairly thick seasonally frozen ground. This paper reports the frost depth at the bridge site and the recorded bridge seismic response data from the Iniskin earthquake, and analyzed the impact of the seasonally frozen ground on the dynamic response of the bridge. Meanwhile a Finite Element (FE) model was created for this bridge by using the OpenSees simulation platform to analyze the results. It was found that when the frost depth reaches 1.2 m, the first transverse modal frequency increases about 200% when compared with the no frost case. The results show that seasonal frost has a significant impact on the overall dynamic behavior of bridges supported by pile foundations in cold regions, and that these effects should be accounted for in seismic design.

#### **Estimation of Site Response and its Correlation with Vs30 at Strong Motion Station Sites in Anchorage Basin from M7.1 Iniskin Earthquake, Alaska**

DUTTA, U., College of Engineering, University of Alaska, Anchorage, AK USA, udutta2@uaa.alaska.edu; THORNLEY, J., Golder Associates, Anchorage, AK USA, john\_thornley@golder.com; CANNON, E. C., Golder Associates, Anchorage, AK USA, ecannon@golder.com; YANG, Z. J., College of Engineering, University of Alaska, Anchorage, AK USA, zyang2@uaa.alaska.edu

The M 7.1 Iniskin earthquake of January 24, 2016 has caused well-felt shaking in the Cook Inlet region of southcentral Alaska particularly in the Anchorage basin, the highest population center of the State of Alaska. The Anchorage strong motion network (ASMN), operating in the Anchorage and its adjoining area since 1995 has registered the maximum peak ground acceleration (PGA) at the surface stations in the southwestern Anchorage and on the Chugach Mountains in the eastern part of the area (reference rock site) around 0.211g and 0.06g, respectively, as per the processed recorded data provided by the Center for Engineering Strong Ground Motion Data (CESMD) of the US Geological Survey. To understand the ground motions characteristics as a function of the complex sedimentary basin, the site response (SR) analysis of over 30 ASMN station sites have been carried out using standard spectral ratio technique. The technique uses computation of Fourier spectral ratio of a 10-sec time window following the S-wave arrival between any site and that of the reference in the frequency range 0.02-12.0 Hz from the recorded time series data. To study the spatial variability of the ground motions in the Anchorage basin, an average SR-map at 1 Hz (Low Frequency Band, LFB) and 5 Hz (High Frequency Band, HFB) has been prepared. The SR values at these two frequency bands are found to be consistent with the general trend of the previous SR studies carried out in the basin using fewer stations. A strong correlation between the SR and the uppermost 30m shear wave velocity data (Vs30) of the Anchorage basin has also been noticed. The availability of recorded data from the surface and downhole (9m) station sites at the reference rock site has been used to investigate the SR characteristic of the weathered rock layer that might be useful for correcting the SR response values at the various sites in the Anchorage basin

#### **USArray Transportable Array Observations of the 7.1 Mw Iniskin Earthquake in Cook Inlet, Alaska**

EAKINS, J., Univ. of California, San Diego, La Jolla, CA USA, jeakins@ucsd.edu; BUSBY, R. W., IRIS, Washington, DC USA, busby@iris.edu; VERNON, F., Univ. of California, San Diego, La Jolla, CA USA, fvernon@ucsd.edu; RUPPERT, N., Univ. of Alaska Fairbanks, Fairbanks, AK USA, naruppert@alaska.edu

The 7.1  $M_w$  Iniskin earthquake in Cook Inlet, Alaska was the largest earthquake recorded within the footprint of the USArray Transportable Array during the 12 year history of the rolling deployment, and was well recorded by the majority of the operational stations. There are around 136 stations contributing to the footprint in the region of the earthquake. At the Array Network Facility (ANF), six phase picks were found within ~100km and 72 within 1000km from a first pass by the automated grid search solution algorithm. Subsequent analyst review produced 9 P and S phase picks within ~100km and 133 within 1000km. Peak accelerations were recorded at AK\_BMR and TA\_N25K (4.5° and 4.7° from the

epicenter, respectively). A total of 25 stations clipped with the farthest station where clipping occurred, COLA, at a distance of 5.85°. The closest non-clipped broadband station was TA\_O18K (0.97°). Strong motion records are available from 34 stations. Reviewed picks for the aftershock sequence will be added by post-real-time analyst review. Due to communications issues, two stations took up to 13 hours to recover from mass positions offscale, which is unusual and 8 stations operating in the area have not yet returned data for the event. We would like to acknowledge the dedicated work of the Alaska TA field operations group and AEC staff for installation and service work at the Transportable Array sites that has contributed to the availability of this tremendous scientific data set.

#### **Aftershock Sequence of the 24 January, 2016 M7.1 Iniskin Earthquake, Southern Alaska**

RUPPERT, N. A., University of Alaska, Fairbanks, AK USA; HOLTkamp, S., University of Alaska, Fairbanks, AK USA; WEST, M., University of Alaska, Fairbanks, AK USA

The 24 January, 2016 M7.1 Iniskin earthquake in southern Alaska provided a rare opportunity to record aftershock sequence of a major intermediate depth earthquake. Due to cooperative nature of the Alaska regional seismic network the aftershock sequence was recorded by a combination of short period, broadband and strong motion sensors with comprehensive coverage in all azimuthal directions of the earthquake source region. The Alaska Earthquake Center located over 1,000 aftershocks through the end of January. Aftershock activity is expected to continue for weeks and potentially hundreds of additional aftershocks will be reported by the Earthquake Center. Completeness of the recorded aftershock catalog is estimated at M1.9. The aftershocks outline a steeply dipping 60 km long and 40 km wide plane aligned with the NE-striking focal plane of the moment tensor mechanism. This source is consistent with oblique reverse faulting caused by gravitational pull of the subducted slab. The aftershock depths range between 80 and 125 km. Location of the mainshock near the deepest southwest corner of the aftershock zone indicates unilateral rupture in up-dip and along-strike directions. Additionally, we utilize network matched filtering, using all analyst reviewed earthquakes as template events, to produce a robust catalog of aftershocks, including both near- or on-fault aftershocks and potentially triggered sequences. We will present enhanced aftershock catalog and discuss how this earthquake fits into tectonic framework of southern Alaska.

---

#### **Earthquake Source Parameters and Slip from Seismic, Geodetic and Laboratory Data: Theory, Observations and Interpretations**

Oral Session · Friday · 8:30 AM · 22 April · Tuscany 1/2  
Session Chairs: Vaclav Vavrycuk, Grzegorz Kwiatek, and German Prieto

---

#### **Accounting for 3D Earth Structure in Seismic Moment Tensor Inversion**

DREGER, D. S., UC Berkeley, Berkeley, CA, USA, ddreger@berkeley.edu; NAYAK, A., UC Berkeley, Berkeley, CA, USA, avinash@seismo.berkeley.edu; CHIANG, A., Lawrence Livermore National Laboratory, Livermore, CA, USA, chiang4@llnl.gov

Typically the seismic moment tensor is determined assuming 1D velocity models, or possibly multiple 1D velocity models to account for path variability. Often this assumption is adequate when determining the focal parameters of earthquakes, because as practice shows at the long-periods, when long-wavelengths are being modeled, the assumption of 1D path structure is reasonable. If the goal of the seismic moment tensor analysis is the recovery of non-double-couple and even isotropic source components then there is always concern that unaccounted path effects might bias the results of these more difficult to constrain components of the source. Using 3D finite-differences, and invoking source-receiver reciprocity, it is possible to generate Green's functions for 3D models to apply routinely for moment tensor applications. Examples will be presented for the regional distance nuclear discrimination problem in which it is hoped that accounting for 3D path effects could increase the short-period bandwidth of analysis and thereby improve monitoring of small magnitude, low-yield explosions. We will also present an application in which 3D Green's functions are applied in a continuous wavefield scanning scheme, GRiD MT (Kawakatsu, 1998), to study numerous micro-earthquakes occurring during an underground cavern collapse in a salt dome in Louisiana. The results show that while using two 1D velocity models is capable of recovering anomalous, volume increase components of the events, the consideration of 3D velocity model Green's functions improves waveform fits, reveals additional complexity of the sequence, and improves the study of events

occurring within the salt where the seismic wavefield is strongly refracted as it propagates into surrounding rock and sediments.

### Seismic Moment Tensors of Acoustic Emissions Recorded During Laboratory Rock Deformation Experiments: Sensitivity to Attenuation and Velocity Anisotropy

STIERLE, E., GFZ German Research Centre for Geosciences, Potsdam, Germany, stierle@gfz-potsdam.de; VAVRYCUK, V., Institute of Geophysics, The Czech Academy of Sciences, Prague, Czech Republic, vv@ig.cas.cz; KWIAATEK, G., GFZ German Research Centre for Geosciences, Potsdam, Germany, kwiatek@gfz-potsdam.de; CHARALAMPIDOU, E. M., Institute of Petroleum Engineering, Heriot-Watt University, Edinburgh, Scotland, UK, Elma.Charalampidou@pet.hw.ac.uk; BOHNHOFF, M., GFZ German Research Centre for Geosciences, Potsdam, Germany, bohnhoff@gfz-potsdam.de

The seismic moment tensors can provide information on the size and orientation of fractures producing acoustic emissions (AEs) and on the stress conditions in the sample. The moment tensor inversion of AEs is, however, a demanding procedure requiring carefully calibrated sensors and accurate knowledge of the velocity model. In the standard moment tensor inversion of field observations, the velocity model is usually isotropic and time independent. In laboratory experiments, the velocity model is often anisotropic and time dependent and attenuation might be significant due to opening or closure of micro-cracks in the sample during loading.

We study the sensitivity of the moment tensor inversion to anisotropy of P-wave velocities and attenuation of the rock sample. We show that retrieved moment tensors critically depend on anisotropy and attenuation and their negligence may lead to misinterpretations of the source mechanisms. The accuracy of the inversion also depends on the fracturing mode of AEs: tensile events are more sensitive to P-wave anisotropy and attenuation than shear events. We show that geometry of faulting in anisotropic rocks should be studied using the source tensors, since the P and T axes of the moment tensors are affected by velocity anisotropy and deviate from the true orientation of faulting. The stronger the anisotropy is, the larger the deviations are. Finally, we prove that the moment tensor inversion applied to a large dataset of AEs can be utilized to provide information on the attenuation parameters of the rock sample. The method is capable of measuring anisotropic attenuation in the sample and allows for detection of dilatant cracking according to the stress regime.

### Scaling of Finite-Source Parameters at Parkfield California

WOODDELL, K. E., UC Berkeley, Berkeley, CA, USA, wooddell@berkeley.edu; DREGER, D. S., UC Berkeley, Berkeley, CA, USA, dreger@seismo.berkeley.edu; TAIRA, T., UC Berkeley, Berkeley, CA, USA, taira@berkeley.edu; NADEAU, R., UC Berkeley, Berkeley, CA, USA, nadeau@seismo.berkeley.edu; MALAGNINI, L., Istituto Nazionale di Geofisica e Vulcanologia, Rome, Italy, luca.malagnini.ingv.it Istituto Nazionale di Geofisica e Vulcanologia

We determine finite-source slip models for Parkfield earthquakes ranging in magnitude from M1.8 to M4.1 by inverting relative moment rate functions (RMRF) obtained from empirical Green's function (eGF) deconvolution. The method is based on Mori and Hartzell (1990). We then use the derived slip models to estimate the stress change following the method of Ripperger and Mai (2004), and compare with published results for the 2004 Parkfield mainshock. Our results show that many microearthquakes display a level of complexity comparable to slip models of larger earthquakes. We will present the results in terms of the scaling of peak slip, average slip, and rupture area, as well as the peak and average stress drops inferred from the finite-source based stress change calculations. The preliminary results indicate that on average the events behave self-similarly, and the stress drops are consistent with corner frequency based estimates of Imanishi and Ellsworth (2006), Allmann and Shearer (2007), and Abercrombie (2014). On the other hand the peak slip and stress drops seem to follow the relationship proposed by Nadeau and Johnson (1998) in which the peak stress drop increases for decreasing scalar moment.

### Evidence for and Implications of Rupture Velocity Acceleration During Earthquake Rupture Onsets

MEIER, M. A., Caltech, Pasadena, CA, USA, mmeier@caltech.edu; HEATON, T. H., Caltech, Pasadena, CA, USA, heaton@caltech.edu; CLINTON, J. F., Swiss Seismological Service, ETH Zurich, Zurich, Switzerland, jclinton@sed.ethz.ch

In the study of earthquake source properties it is common practice to assume that rupture velocities  $v_r$  reach their steady-state value quasi-instantaneously after rup-

ture initiation. Here we show that this assumption is irreconcilable with the bulk of available seismic near-source observations. We use an extensive near-source record data set of shallow crustal earthquakes from a broad magnitude range (M2.0 – M7.6) to attain a maximally objective and parameter-free characterization of ground motion onsets. We find that shallow crustal earthquakes develop in two phases, each of which has distinct statistical properties: the events almost invariably start with an observable period of rapid potency rate growth,  $dP/dt \propto t^\eta$ , with  $\eta > 4$  independent of event magnitude. These growth rates strongly exceed predictions of standard rupture models ( $\eta_{\text{pred}} = 2$ ). Small earthquakes reach peak P-phase displacement amplitudes during this short initial period of 0.1-0.8 seconds. Large earthquakes subsequently transition to growing in the second phase with significantly lower growth rates,  $\eta \sim 1.5$ . We use scaling relations to demonstrate that the high growth rates in the first phase are likely caused by increasing rupture velocities  $v_r$ . Our observations suggest that small earthquake ruptures never reach their steady-state  $v_r$ . This implies that the common practice of assuming constant  $v_r$  in the study of small earthquakes source properties may introduce a strong bias and that some fundamental source characteristics, including spatial rupture dimensions and static stress-drops, have to be revised.

### Inversion for the Composite Moment Tensor

VAVRYCUK, V., Institute of Geophysics, Prague, Czech Republic, vv@ig.cas.cz

The composite moment tensor is defined in analogy to the composite focal mechanism as the averaged representative seismic moment tensor characteristic for a focal area under study. In contrast to the composite focal mechanism which provides information on shear faulting, the composite moment tensor can provide additional information on non-shear rupture mode and on physical conditions along the fault. The composite moment tensor is calculated by a joint inversion of multiple earthquakes which are associated with the same fault system and display a similar focal mechanism. The method utilizes amplitudes of P and/or S waves or full waveforms. Since the inversion is linear, it is fast and applicable to datasets of many earthquakes. The method is particularly suitable for the analysis of microseismicity, earthquake swarms or aftershock sequences, where observations of multiple earthquakes are available. The composite moment tensor can be retrieved even when the station configuration or data quality prevent from inverting for full moment tensors of individual earthquakes. The applicability of the method is demonstrated on micro-earthquakes that occurred during the 2008 West Bohemia earthquakes swarm, Czech Republic.

### Scaling and Uncertainty of PGA and PGV with Respect to Moment Magnitude 3.3-7.7: Implications for Stress Drop and the Moment Rate Function

ARCHULETA, R. J., Dept. of Earth Science, University of California, Santa Barbara, Santa Barbara, CA, USA, ralph.archuleta@ucsb.edu; JI, C., Dept. of Earth Science, University of California, Santa Barbara, Santa Barbara, CA, USA, ji@geol.ucsb.edu

We have used the NGAWest-2 database to compute the mean PGA and PGV as a function of moment magnitude M. We limit that data to stations within 50 km of the fault/hypocenter. All of the amplitudes are normalized to a distance of 10 km using simple 1/R scaling. The magnitude range of 3.0-7.8 is divided into 0.2 M bins for which we compute the mean PGA, PGV and their standard deviations assuming a log normal distribution. All but four of bins have more than 100 records with some having more than 500. For M 5.3-7.7 we find: log PGA  $\sim 0.18M$ , log PGV  $\sim 0.43M$ , with  $R^2$  coefficient of determination of 0.50 and 0.83, respectively. This proportionality has been found and explained before, e.g., Hanks and McGuire (1981), Boore (1983), Luco (1985). For M 3.3-5.3 we find: log PGA  $\sim 0.94M$ , log PGV  $\sim 1.04M$  with  $R^2$  of 0.99 and 0.995. These linear relationships were first observed by Boatwright *et al.* (2003) and are in some of the latest ground motion prediction equations, e.g., Abrahamson *et al.* (2014), with a slightly different break at M5.5. However, there is no explanation about this nearly perfect linear empirical relationship yet. The standard deviation (assuming log normal distributions for PGA and PGV) decreases with magnitude: -0.11M and -0.09M for PGA and PGV, respectively. This is consistent with more variability of the average stress drop as magnitude decreases.

We computed the ratio of PGA/PGV, which we call dominant frequency. Interestingly PGA/PGV  $\sim -1.12M$  with  $R^2$  of 0.92 over the full range of magnitudes. The nearly linear relationship between the magnitude and the log of PGA, PGV and PGA/PGV puts severe constraints on the shape of the moment rate function of small earthquakes with implications about the rupture process. This will be discussed at the meeting.

## M<sub>w</sub>(ML)—using ML to estimate M<sub>w</sub>—a continental approach

HERRMANN, R. B., Saint Louis University, St. Louis, MO USA, herrmarb@slu.edu; BENZ, H., US Geological Survey, NEIC, Golden, CO USA, benz@usgs.gov

$M_w$  is the definitive measure of earthquake size for the USGS, but is difficult to determine for small events ( $M_w < 3$ ) through regional moment tensor (RMT) inversions. Small events are often characterized by a local magnitude (ML) whose relation to  $M_w$  is poorly defined. ML has a simple definition, is not limited to a specific frequency, and has no inherent restriction on earthquake size other than signal-to-noise limitations. ML is therefore a candidate for estimating  $M_w$  for small events if an  $M_w$ (ML) relationship can be defined empirically or theoretically.

The IASPEI formula for ML, developed for Southern California, is

$$ML = \text{Log A}(\text{nm}) + 1.11 \text{ Log R} + 0.00189 R - 2.09$$

where R is the hypocentral distance in km and A is the one-half maximum peak-to-peak horizontal amplitude of the S-wave signal on a simulated Wood-Anderson instrument with unit gain. To determine an ML in other regions of North America, we use a plot of individual station ML estimates versus distance to adjust only the linear term in R. The linear term is indicative of anelastic attenuation, which is known to vary across the continent. We do not change the other terms, therefore requiring that observations of the same amplitude at short distances give the same magnitude irrespective of region. Regionally, we find that the linear coefficient is smaller in the Central and Eastern US and is larger in the Pacific Northwest as compared to that in the Southern California definition of ML.

Using data from over 800 events in our moment tensor catalog for North America, we investigate the  $M_w$ (ML) relationship. The relationship between  $M_w$  and ML is compatible with simple random vibration theory modeling that suggests that  $M_w \sim 2/3$  ML for small magnitudes ( $M_w < 4$ ) and  $M_w \sim 2$  ML for large events ( $M_w > 5$ ). Simple modeling shows that the standard error in the  $M_w$ (ML) is about 0.3. The scatter is interpreted in terms of the velocity model used for RMT inversion, source depth and mechanism.

## A Near-Field, Near-Instantaneous Earthquake Doublet ( $M_w$ 6.9, 6.7): Implications for Dynamic Triggering and Rupture Forecasting

NISSSEN, E., Colorado School of Mines, Golden, CO, USA, enissen@mines.edu; ELLIOTT, J. R., University of Oxford, Oxford, United Kingdom, john.elliott@earth.ox.ac.uk; SLOAN, R. A., University of Cape Town, Cape Town, South Africa, alastair.sloan@uct.ac.za; CRAIG, T. J., University of Leeds, Leeds, United Kingdom, T.J.Craig@leeds.ac.uk; FUNNING, G. J., University of California Riverside, Riverside, CA, USA, gareth@ucr.edu; HUTKO, A., Incorporated Research Institutions for Seismology (IRIS), Seattle, WA, USA, alex@iris.washington.edu; PARSONS, B. E., University of Oxford, Oxford, United Kingdom, barry.parsons@earth.ox.ac.uk; WRIGHT, T. J., University of Leeds, Leeds, United Kingdom, T.J.Wright@leeds.ac.uk

We document a large earthquake doublet that occurred in the Sulaiman mountains of Pakistan in 1997, which has important consequences for earthquake triggering and for rupture forecast modeling. Reported in all seismic catalogs as a single event, combined InSAR and seismological analyses reveal that initial rupture on a shallow, blind reverse fault ( $M_w$  6.9) was followed just 19 seconds later by a second rupture on another reverse fault 50 km away ( $M_w$  6.7). Slip on the second fault increased the total seismic moment by half and doubled both the combined event duration and the area of maximum ground shaking. Initiation of slip on the second fault occurs where Coulomb stress changes from the first event are probably negative, suggesting a dynamic triggering mechanism, though the responsible seismic phase is unclear. Our results have two major implications. (1) We confirm that large aftershocks can be triggered by transient stresses even at relatively short distances (10s of kilometers), before the largest surface waves have fully emerged. (2) Our results expose a flaw in contemporary earthquake rupture forecasts which, by disregarding such behavior, miss out on an important class of cascading, multiple-fault event.

## Observations and Physical Interpretations of Double-corner Frequency Source Spectra

DENOLLE, M. A., Harvard University, Cambridge, MA, USA, mdenolle@fas.harvard.edu; SHEARER, P. M., Scripps Institution of Oceanography UC—San Diego, La Jolla, CA, USA, pshearer@ucsd.edu

Understanding of earthquake source processes across multiple scales is fundamental to accurately assessing seismic hazard of great earthquakes. Can we distinguish physical processes of large ruptures from those of the more frequent smaller earthquakes? Earthquakes are self-similar if their fault geometry, source duration, and slip follow known scaling relations that preserve the shape of the

slip-rate (or moment-rate) function and its amplitude spectrum. Self-similar earthquakes have constant static stress drop and ratio of radiated energy  $E_R$  to moment  $M_0$  (scaled energy). The most common spectral shape has a single-corner frequency (or time scale) and a high-frequency falloff rate around 2 (Brune model). We estimate the moment-rate amplitude spectrum from all thrust earthquakes of magnitude 5.5 and above, shallower than 50 km, and recorded between 1990 and 2015 on the Global Seismic Network. We use a Green's function that captures the path effects (attenuation and geometrical spreading) estimated from a simplified Earth model and construct a transfer function that accounts for the destructive interference of the direct P wave with the depth phases pP and sP. A double-corner frequency amplitude spectrum, with an intermediate falloff rate of 1 and a high-frequency falloff rate of 2, better explains our P-wave spectra than the standard Brune model. The first corner frequency corresponds to the source duration and follows  $T_1 \sim M_0^{-3}$  for  $M < 7.5$  and  $T_1 \sim M_0^{-2}$  for larger earthquakes. We explore the physical processes that would induce a second time scale T2 or corner frequency in the system (pulse-like behavior, linear slip-weakening mechanism, different length scales in the system) and what would predict a scaling of T2 with moment. While both stress drop and scaled energy are constant with  $M_0$ , source geometry and spectral shape significantly change over earthquake size.

## Seismicity Statistics and Stress in Regions with High Tectonic Complexity: A Comparative Study of the Greater San Gorgonio and Ventura Regions in Southern California

GOEBEL, T. H. W., UCSC, tgoebel@ucsc.edu; HAUSSON, E., Caltech; PLESCH, A., Harvard; SHAW, J. H., Harvard,

The study of frequently occurring small-magnitude earthquakes provides rare insight into fault stress and heterogeneity at seismogenic depth. We analyze such earthquakes in two regions with high tectonic complexity, *i.e.* the Ventura basin (VB) and San Gorgonio pass (SGP) regions in southern California. VB is characterized by highly variable, deep seismic activity and contains a series of thrust faults. The rapid convergence rates across VB suggest that several of these faults slip at high rates and may be capable of producing large-magnitude earthquakes. SGP, on the other hand, marks the location of a structural knot in the San Andreas fault system, resulting in distributed deformation across a series of strike-slip and thrust faults which generally exhibit low geologic slip rates.

We perform a quantitative comparison between seismicity characteristics including focal mechanisms, stress drops, and principle stress orientations between SGP and VB. The direction of largest compressive stress in VB is oriented approximately N-S, in agreement with the larger scale compressional tectonics within the area. The principle stresses in SGP, on the other hand, exhibit a wide range of distributions leading to the observed variations in faulting mechanisms. Similarly, earthquake stress drops are heterogeneous in SGP, varying between 1 to 25 MPa whereas the VB region shows consistently low stress drops around 1 MPa. Earthquake hypocenter locations in VB are generally more aligned with the main mapped fault traces compared to SGP which shows a diffuse seismicity cloud with relatively higher fractal geometry. In both study areas, there is a close connection between the regional stress fields, earthquake stress drops and the spatial distribution of earthquake hypocenters. Thus, spatial variations in stress-drops are sensitive to the interplay between local variations in crustal characteristics and fault properties and can provide important insights into regional seismic hazard.

## Source Parameters in the Middle East Estimated by Accounting for Lateral Variations in Coda Amplitudes

PASYANOS, M. E., Lawrence Livermore National Laboratory, Livermore, CA USA, pasyanos1@llnl.gov; GOK, R., Lawrence Livermore National Laboratory, Livermore, CA USA, gok1@llnl.gov; WALTER, W. R., Lawrence Livermore National Laboratory, Livermore CA USA, bwalter@llnl.gov

We present a recently-developed method to account for observed lateral variations in coda amplitudes. Doing so lets us extend coda's well-known stability to higher frequencies, allowing us to perform source analysis of smaller earthquakes ( $M < 3.5$ ). A critical aspect of this effort is characterizing the propagation term to include scattering, which allows us to use observations out to longer distances and later in the coda. The recovered coda attenuation structure of the Middle East is both very similar to the attenuation structure derived from direct phases and also reflective of the tectonic structure of the region. We then apply the variations to hundreds of events in the region, and find a marked improvement in source spectra estimates, as measured by interstation scattering, particularly at higher frequencies ( $> 1$  Hz). The spectra we obtain are then used to estimate the scalar seismic moment (and hence  $M_w$ ), stress drop, and high-frequency spectral falloff of the events. We then look for variations in these parameters by magnitude, depth, and region.



### **Coseismic Slip Model of the Nov 17, 2015 $M=6.5$ South Lefkada Earthquake, Ionian Sea, Greece from Inversion of Geodetic Data**

GANAS, A., National Observatory of Athens, Greece, aganas@noa.gr; MELGAR, D., University of California, Berkeley, CA, USA, dmelgar@berkeley.edu; BRIOLE, P., Ecole Normale Supérieure, France, briole@ens.fr; PAPATHANASSIOU, G., Aristotle Univ of Thessaloniki, Greece, gpapatha@geo.auth.gr; GENG, J., Univ. of California, San Diego, CA, USA, jgeng@ucsd.edu; BOZIO NELOS, G., NKUA, Athens, Greece, georgebozionelos@gmail.com; ARGYRAKIS, P., NOA, Athens, Greece, pargyrak@noa.gr; VALKANIO TIS, S., NOA, Athens, Greece, valkaniotis@yahoo.com; MENDONIDIS, Evangelos NOA; MOSHO U, Alexandra NOA; ELIAS, Panagiotis NOA

On 17th November 2015, onshore Lefkada island, Ionian Sea, Greece, a  $M_w$ (NOA)=6.4 event occurred along a strike-slip fault with right-lateral sense of slip. Relocation of seismicity and inversion of geodetic data suggests that the seismic fault runs parallel to the west coast of Lefkada, along the Aegean–Apulia plate boundary. The earthquake measured  $M_w=6.5$  using the PGD relation of Melgar et al (2015, GRL). The fault plane strikes  $N20 \pm 5^\circ E$  and dips to east with an angle of about  $70 \pm 5$  degrees. The earthquake caused a lot of structural damage to south Lefkada and in particular to the villages of Agios Petros, Athani, Draganos and Komilio. Environmental effects include liquefaction, extensive rock falls and landslides. No surface ruptures were found in the field. Road cracks are interpreted as secondary phenomena of gravitational nature induced by ground shaking. The inversion of geodetic data suggests that the upper part of the fault is offshore very close to the coast, and at very shallow depth ( $0.5 \pm 0.5$  km), as constrained by the azimuth and amplitude of the ground motion at NOA GPS stations and InSAR Sentinel 1A observations (ascending orbit). The overall slip pattern was constrained with InSAR (see figure below) and high-rate GPS data were used to define the time dependent slip. We have not observed significant vertical motion of the shoreline and this is consistent with the predictions of the model.

### **Nucleation and Growth Process of the $M_w$ 6.2 Northern Nagano Prefecture, Japan, Earthquake of November 22, 2014**

NODA, S., USGS, Menlo Park, CA, USA, snoda@usgs.gov; ELLSWORTH, W. L., Stanford University, Stanford, CA, USA, wellsworth@stanford.edu

On November 22, 2014, a part of the Kamishiro fault in the northern Nagano prefecture, Japan, ruptured in a reverse faulting earthquake of  $M_w$  6.2. A foreshock sequence began 4 days before the event with locations concentrated in the immediate vicinity of the mainshock hypocenter. To investigate the nucleation and growth process of the earthquake, we model the slip history by solving a linear system defined by the representation theorem for seismic sources. We use empirical Green's functions derived from the foreshocks, non-negative least squares method for the matrix solver, and seismograms recorded on the nearby stations of NIED Hi-net and K-NET. To examine the detailed characteristic of the initial process, we use multiple short time windows in inversion, as it is difficult to explain the small initial phase using a longer time window with larger amplitude, as also indicated by Uchide and Ide (2007).

Our result demonstrates that the rupture initiates with a  $M_w$  3.5 sub-event in the first 0.15 s and then propagates away from the foreshocks, which were located using HypoDD, as a  $M_w$  4.5 sub-event at approximately 0.4 s. These 2 sub-events were nearly co-located to the south of the nucleation point. A large rupture began at 1.5 sec also to the south of the initiation point, which is consistent with an outcome from the identification of the P2 phases (e.g. Takenaka et al., 2009). The southerly rupture propagated to shallower depth, resulting in coseismic surface rupture (e.g. Okada et al., 2015). At about the same time, another large slip began to the north and propagated to deeper depths. Hence, we conclude that the nucleation and growth process of the event was cascade-like rather than the pre-slip model.

### **Stress Drop and Source Scaling of the 2011 Mineral, Virginia Mainshock and Aftershock Sequence**

WU, Q., Department of Geosciences, Virginia Tech, Blacksburg, VA, USA, wqimin86@vt.edu; CHAPMAN, M. C., Department of Geosciences, Virginia Tech, Blacksburg, VA, USA, mcc@vt.edu

Knowledge of source scaling and variation in stress drop are essential to a better understanding of source physics and strong ground-motion prediction. Due to the large measurement uncertainties in estimating the stress drop, many previous studies have found controversial results showing both self-similarity and non-self-similarity.

The aftershock sequence of the 2011 Mineral, Virginia earthquake was recorded by dozens of temporary stations deployed by several institutions. The well-located aftershocks are an important data set for investigation of the source scaling of small earthquakes in the eastern United States. We estimate corner

frequencies and stress drops for the aftershocks using the S-wave coda spectral ratio method. This method has been proven to produce more stable spectral ratios than the use of the direct S-waves. We carefully examine the decay of coda envelopes between selected event pairs, and the corner frequencies and stress drops are estimated by modeling the observed source spectral ratio with the omega-square source spectral model. Preliminary results from a data subset suggest that the scaling relation between the corner frequencies and the corresponding seismic moments for the whole earthquake sequence are non-self-similar. However, the smaller events are likely to follow self-similarity. On-going work using the entire dataset will confirm the reliability of this observation.

### **Earthquake Source Parameters for Earthquake Swarms Adjacent to Slow Slip, Tremor, and Large Earthquakes in the Oaxaca, Mexico Region**

BILEK, S. L., New Mexico Tech, Socorro, NM, USA, sbilek@nmt.edu; PHILLIPS, W. S., Los Alamos National Lab, Los Alamos, NM, USA, wsp@lanl.gov; BRUDZINSKI, M., Miami University, Oxford, OH, brudzimr@Miami0H.edu; CABRAL CANO, E., Instituto de Geofísica, UNAM, Cd Universitaria, Mexico, ecabral@geofisica.unam.mx; ARCINIEGA-CEBALLOS, A., Instituto de Geofísica, UNAM, Cd Universitaria, Mexico, maac@geofisica.unam.mx

Earthquake swarms, which are typically defined as seismicity clusters above the background rate, but without a clear mainshock, are commonly found in volcanic areas and increasingly along subduction margins. The mechanism for these swarms in subduction zones is still under debate, with possible links to nearby large earthquakes, slow slip, subducting topography, or fluid migration. Analysis of these earthquake clusters can provide useful information about the nature of the fault and earthquake interaction. Here we focus on earthquake swarms along the Oaxaca segment of Mexico. This portion of the Mexican subduction zone has experienced large megathrust earthquakes as well as non-volcanic tremor and slow slip, suggesting a complex fault system that allows a wide spectrum of slip. Seismic and geodetic instrumentation is also available above the megathrust to record these various slip episodes. We can use source characteristics of the swarm seismicity to probe the fault complexity. Along Oaxaca, the earthquake swarms ( $M$  1.5-5.5) span a wide spatial and temporal range. For our source parameter calculations, we form narrow-frequency band envelopes for pairs of earthquakes within the earthquake clusters, and use these envelopes to compute spectral ratios for each earthquake pair at each station. We determine seismic moment, corner frequency, and earthquake stress drop for each earthquake from these spectral ratios. We compare the source parameters for events within the clusters to examine temporal variations and compare between clusters to explore spatial variations that could be linked to other slip heterogeneity.

---

## **Research Efforts to Improve Regulatory Performance for Induced Seismicity**

Oral Session · Friday · 3:45 PM · 22 April · Tuscany 1/2

Session Chairs: David Eaton, Honn Kao, and Gail Atkinson

---

### **2016 USGS Seismic Hazard Model for Induced Seismicity**

PETERSEN, M., USGS, Denver, CO, USA, mpetersen@usgs.gov; MUELLER, C., USGS, Denver, CO, USA, cmueller@usgs.gov; MOSCHETTI, M., USGS, Denver, CO, USA, moschetti@usgs.gov; HOOVER, S., USGS, Denver, CO, USA, shoover@usgs.gov; RUBINSTEIN, J., USGS, Menlo Park, CA, USA, jrubin@usgs.gov; ELLSWORTH, W., Stanford University and USGS, Menlo Park, CA, USA, wellsworth@stanford.edu; LLENOS, A., USGS, Menlo Park, CA, USA, allenos@usgs.gov; MICHAEL, A., USGS, Menlo Park, CA, USA, michael@usgs.gov; MCGARR, A., USGS, Menlo Park, CA, USA, mcgarr@usgs.gov

Over the past several years, the seismicity rate has increased markedly in multiple areas of the central U.S. Studies have tied the majority of this increased activity to wastewater injection in deep wells and hydrocarbon production. Because these earthquakes are thought to be induced by human activities that change rapidly based on economic and policy decisions, their geographical distribution is difficult to forecast. Our 2014 USGS National Seismic Hazard Model and previous models are intended to provide the long-term hazard (2% probability of exceedance in 50 years) and are based on seismicity rates and patterns observed mostly from tectonic earthquakes. For this induced seismicity model we consider 1% probability of exceedance in 1 year as the basis of our discussion. Potentially induced earthquakes were identified in 21 areas across the Central U.S. Several factors are important in determining the hazard from induced seismicity: period of the catalog that optimally forecasts the next year's activity, earthquake magnitude-rate distribution, earthquake location statistics, maximum magnitude, ground motion models, and industrial factors such as injection rates. The indus-

trial data are not currently available in a form that we can implement in a 1-year model. Hazard model inputs have been evaluated by scientists and engineers to assess the range of acceptable models. Results will be presented at the meeting. Recent earthquakes in the Central U.S. have raised concern about the impacts of induced earthquakes on the built environment and have led to engineering and policy discussions about how to mitigate these effects for the more than 7 million people that live near areas of induced seismicity.

#### **A Predictive Statistical Model of Wastewater Injection-Induced Earthquakes in Oklahoma: Application of the Seismogenic Index**

LANGENBRUCH, C., Stanford University, Stanford, CA, USA, [langenbr@stanford.edu](mailto:langenbr@stanford.edu); ZOBACK, M. D., Stanford University, Stanford, CA, USA, [zoback@stanford.edu](mailto:zoback@stanford.edu)

Various studies suggest that the recent increase of earthquake activity in Oklahoma is caused by disposal of very large volumes of produced saltwater into formations overlying the crystalline basement. The triggering mechanism seems to be pressure diffusion in the fluid saturated pore and fracture space of rocks. The current activity of approximately one  $M > 4$  earthquake per week presents a significant seismic hazard especially in areas containing critical industrial facilities.

In case of fluid injection-induced earthquakes at geothermal and hydrocarbon reservoirs the quantitative predictive Seismogenic Index (SI) model exists. It is based on the triggering mechanism of pore pressure diffusion and utilizes the volume of injected fluid and deducible seismo-tectonic parameters to compute expected earthquakes. The SI assumes magnitude scaling according to the Gutenberg-Richter relation which originates from a fractal distribution of fault sizes.

We apply a modified form of the SI model to the seismicity in Oklahoma. The parameters of the fitted model can be used to forecast earthquake activity based on future wastewater disposal volumes. In agreement with the model of pressure diffusion and the Gutenberg-Richter law we observe proportionality between the cumulative number of earthquakes larger magnitude  $M$  and the cumulative volume of injected water. However, proportionality is only observed after a critical injection rate is exceeded. This threshold corresponds to the effective normal stress decrease necessary to overcome the frictional strength of faults located at a distance of 2-3 km from the injection sources. An observable time delay of approximately three month between the injection of fluid and the occurrence of earthquakes corresponds to a hydraulic diffusivity (permeability) of  $0.01\text{--}0.1 \text{ m}^2/\text{s}$  ( $0.1\text{--}1 \text{ mD}$ ).

If successful, our model would provide a basis for long term forecasting of how hypothetical reductions in saltwater disposal affect future seismicity.

#### **Geomechanical Modeling of Induced Seismicity from Multi-Stage Hydraulic Fracturing**

MAXWELL, S. C., IMaGE, Calgary, AB, Canada, [shawn.maxwell@itasca-image.com](mailto:shawn.maxwell@itasca-image.com); GROB, M., IMaGE, Calgary, AB, Canada, [melanie.grob@itasca-image.com](mailto:melanie.grob@itasca-image.com)

Over the last few years, Western Canada has seen an increase in the occurrence of induced seismicity from hydraulic fracturing, including a magnitude  $M=4.6$  event. The mechanism is attributed to increased pore pressure leading to fault activation and release of stored tectonic stress. Here we study the link between fluid injection and induced seismicity through geomechanical modeling of a multi-phase hydraulic fracturing treatment in the proximity of a fault. Several published examples illustrate how progressive hydraulic fracture stages can repeatedly activate a fault. Synthetic seismicity is used to quantify seismic energy released by the slippage on the fault for different injection scenarios. Moment release rate typically drops during the shut-in period, but depending on the distance between the fault and the injection point, a delay can be seen between the start of the injection and the increase of slip on the fault, thus acceleration of moment release rate can be observed during shut-in periods. Stress shadowing also has an influence on the moment release rate. This basic model could be used as a framework to examine the impact of other geomechanical characteristics or other operational factors to help mitigate seismicity when faults begin to be active. For example, to investigate if there are scenarios where flow-back the injection well can lead to further seismicity.

#### **Magnitudes Scale Discrepancies for Near-Event Receivers**

BUTCHER, A. C., University of Bristol, Bristol, [antony.butcher@bristol.ac.uk](mailto:antony.butcher@bristol.ac.uk); LUCKETT, R., British Geological Survey, Edinburgh, [rrl@bgs.ac.uk](mailto:rrl@bgs.ac.uk); KENDALL, J. M., University of Bristol, Bristol, [gljmk@bristol.ac.uk](mailto:gljmk@bristol.ac.uk); BAPTIE, B., British Geological Survey, Edinburgh, [bbap@bgs.ac.uk](mailto:bbap@bgs.ac.uk); VERDON, J.

P., University of Bristol, Bristol, [james.verdon@bristol.ac.uk](mailto:james.verdon@bristol.ac.uk); WOOKEY, J., University of Bristol, Bristol, [glxjw@bristol.ac.uk](mailto:glxjw@bristol.ac.uk)

As the UK is a country with low seismic activity, a  $M_L 2.4$  event triggered by hydraulic fracturing at Preese Hall, near Blackpool, caused wide spread public concern. This resulted in the British Geological Survey (BGS) installing seismic stations close to the epicentre. These recorded several subsequent, smaller events, which have been the subject of numerous studies. One of the interesting findings is a discrepancy between the magnitude calculated from waveforms on local stations and those calculated for more distant stations. The only earthquake to be recorded by both distant and local stations had a magnitude of  $M_L 1.2$ , as calculated on the national network, but local stations recorded amplitudes corresponding to a magnitude of  $M_L 2.3$ .

Like other countries, the regulatory approach adopted in the UK to manage the risk of induced seismicity is a 'traffic light' monitoring scheme, with a remedial action level, or 'red light', set at  $M_L 0.5$ . As the UK seismic network operates at a nominal detectability level of  $M_L > 2$ , the installation of local seismic stations is critical for the operation of this scheme. However, the suitability of the current UK local magnitude scale is questionable given that it was not calibrated using very near-receiver events. In fact, the evidence of magnitude discrepancies demonstrated at Preese Hall and elsewhere suggest that the scale is not suitable.

We test the viability of the UK local magnitude scale for near-event receivers using a catalogue of seismic events relating to coal mining near New Olleston, UK. This catalogue contains over 500 events recorded by a local network of 7 stations located between 0.5 and 5km from the epicentre. We calculate both  $M_L$  and  $M_W$ , and show the impact of distance on these two magnitude scales. Finally we suggest approaches to provide more robust magnitude assessment for near-event receivers.

#### **Discriminating Seismic Sources (Mining-induced Seismicity, Fluid Injection Induced Seismicity, and Tectonic Earthquakes) in Central Utah, USA**

STEIN, J. R., University of Utah, Salt Lake City, UT, USA, [J.Stein@utah.edu](mailto:J.Stein@utah.edu); PANKOW, K. L., University of Utah, Salt Lake City, UT, USA, [pankow@seis.utah.edu](mailto:pankow@seis.utah.edu); KOPER, K. D., University of Utah, Salt Lake City, UT, USA, [koper@seis.utah.edu](mailto:koper@seis.utah.edu); CHAMBERS, D., National Institute for Occupation Safety and Health, Spokane, WA, USA, [derrick.ja.chambers@gmail.com](mailto:derrick.ja.chambers@gmail.com)

An important goal of induced seismicity studies is to clearly discriminate induced earthquakes from naturally occurring earthquakes. In this study, we analyze seismic events recorded in central Utah along the Wasatch Plateau. Both mining-induced seismicity (MIS) associated with underground coal mines and tectonic earthquakes that are part of the intermountain seismic belt (ISB)—a continuous band of seismicity that extends from Montana to Arizona—have been the topic of many, well-documented studies in this region. Recently seismic events associated with wastewater injection wells have been suggested as a third potential source of seismicity in Central Utah. While there are injection wells in the area, it is not clear from an analysis of the University of Utah Seismograph Stations earthquake catalog that the injection wells induce a significant number of earthquakes. In this study, we use the following techniques to discriminate among seismic event types: (1) epicentral location relative to mine permit areas; (2) waveform matching techniques and a single-link clustering algorithm; (3) spectral ratio differences; and (4) differences in  $M_L$  and  $M_C$ . From this analysis, we conclude that at least 80% of the cataloged events located in the Wasatch Plateau between 1998 and 2011 are MIS. The remaining events consist of clear tectonic earthquake sequences, MIS most likely related to development work (as opposed to the more prolific production-related MIS), and in at least one case along the eastern edge of the Wasatch Plateau events related to fluid injection.

---

### **Deep Earthquakes and Surrounding Slab Structures**

Oral Session · Friday · 8:30 AM · 22 April · Tuscany 3/4  
Session Chairs: Zhongwen Zhan, Meghan S. Miller, and Germán Prieto

---

#### **Rupture Mechanism of the May 24, 2013 Mw8.3 Sea of Okhotsk Deep-Focus Earthquake**

ZHANG, H., EPS, Northwestern University, Evanston, IL, USA, [h Zhang@earth.northwestern.edu](mailto:h Zhang@earth.northwestern.edu); VAN DER LEE, S., EPS, Northwestern University, Evanston, IL, USA, [suzan@northwestern.edu](mailto:suzan@northwestern.edu); BINA, C., EPS, Northwestern University, Evanston, IL, USA, [craig@earth.northwestern.edu](mailto:craig@earth.northwestern.edu); GE, Z., SESS, Peking University, Beijing, Beijing, P.R. China, [zge@pku.edu.cn](mailto:zge@pku.edu.cn)

Deep-focus earthquakes occur at depths greater than 300 km. Candidate rupture mechanisms for deep-focus earthquakes include phase transformations (Green

and Burnley, 1989; Kirby *et al.*, 1991; Green *et al.*, 2016), thermal shear instabilities (Kanamori, 1998; Wiens, 2001), and dehydration embrittlement (Jung *et al.*, 2004).

The 2013  $M_w$  8.3 Sea of Okhotsk earthquake provides a new perspective in understanding the rupture mechanism of deep-focus earthquakes. Multi-array, multi-frequency back-projected teleseismic P wave trains from USArray (TA) and European networks (EU) and inverted teleseismic P waveforms from global seismic network stations (GSN) shows that the deep-focus earthquake's asymmetrical, bilateral rupture occurred on a sub-horizontal, curved fault plane and can be separated into three principal segments at rupture velocities of 3.6-4.6 km/s. The slab strike-perpendicular components of the mostly slab strike-parallel rupture for each of three segments are 23 km, 19 km, and 31 km wide, respectively. Each of the rupture distances is wider than the estimated thickness of the metastable olivine wedge.

The estimated widths of the ruptured segments outside of the metastable olivine wedge require an explanation beyond transformational faulting. Likewise, the large seismic efficiency of 0.6 determined by Ye *et al.* (2013) and fast rupture velocity preclude a thermal shear instability as the rupture mechanism. The simplest explanation of the earthquake would be that the dehydration embrittlement mechanism, which operated at intermediate depths, is still operating at these great depths. If the deep Okhotsk earthquake indeed represents dehydration, the entirety of the subducting Pacific lithosphere cannot be completely dry at these great depths. A more speculative possibility is that some other form of transformational faulting, perhaps involving transformation of metastable pyroxene to metastable akimotoite, may occur and accommodate the earthquake.

#### **Investigating the Effects of Plate Age and Tectonic Regime on the Rupture Dynamics of Intermediate-Depth Earthquakes using Dynamic Inversion**

TWARDZIK, C., UC Santa Barbara, Santa Barbara, CA, USA, cedric@ucsb.edu; JI, C., UC Santa Barbara, Santa Barbara, CA, USA, ji@geol.ucsb.edu

It has been suggested that the age of the subducting plate might have an impact on the rupture dynamics of intermediate-depth earthquakes because it affects the thermal structure of the cold core of the subducting slab. But, previous seismological studies have not detected any convincing evidence yet (*e.g.*, Piero and Prieto, 2015). However, in their analysis, the seismic data are used to constrain the kinematic parameters, *e.g.*, the seismic moment rate function. Meanwhile, the dynamic parameters (*e.g.*, stress drop and fracture energy) that might be sensitive to the thermal structure of the slab are inferred with additional assumptions. The rapid increase of computational power allows us now to directly constrain these dynamic parameters with inversions. We modify the dynamic inversion approach that was previously used to study shallow earthquakes (*e.g.*, Twardzik *et al.*, 2014) to directly search for stress conditions on the fault plane of intermediate-depth earthquakes such that the radiated waves fit the observed broadband teleseismic waveforms. We have applied this state-of-art algorithm to study the 2014  $M_w$  7.9 Rat Islands earthquake. Our preliminary results show that this earthquake has stress drop ranging from 2–7 MPa and fracture energy ranging from 1–12 MJ/m before we see a significant degradation of the waveform fit. These ranges are typical of large shallow earthquakes. This is consistent with previous studies (Vallee, 2013). To investigate the effect of plate age and tectonic regime, we have selected 3 additional large intermediate-depth earthquakes: The 1993  $M_w$  7.6 Kushiro-Oki, Japan; 2007  $M_w$  7.5 Northern Peru; and 2015  $M_w$  7.5 Hindu Kush. They span a large range of plate age (from ~20 to ~150 Myr), and different tectonic context (subduction zone and continental collision), allowing us to see whether the rupture dynamics are affected by these differences.

#### **Static and Dynamic Parameters of Intermediate-depth and Deep Earthquakes from Spectral Analysis and Source Inversions**

PRIETO, G. A., MIT; POLL, P., MIT; HERRERA, C., Universidad de Chile; RUIZ, S., Universidad de Chile; CRUZ-ATTENZA, V., UNAM,

We study the radiated energy and rupture duration for more than 500 deep and intermediate depth earthquakes (depth > 50 km and  $M > 5.5$ ). The average source time function is obtained by stacking broadband P-wave pulses recorded globally and used to measure the rupture durations, by comparing alternative versions of the same waveform. The radiated energy is obtained by integration of velocity spectrum observed at each station and corrected for radiation pattern and propagation effects.

Rupture duration shows that the depth reduction of the duration can principally be explained by incremental shear velocity with depth and that earthquakes are not self-similar. The existence of a different scaling law is further corroborated by the analysis of scaled energy, which is not constant as function of moment.

The radiated energy and rupture duration are combined to derive stress drop, apparent stress, efficiency and other source parameters of the rupture. The

global analysis of these parameters suggests how deep and intermediate depth events are systematically different from shallow earthquakes.

We further derive rupture velocity for some of the studied events, to get further information on the dynamic properties of the rupture process. For a small subset of the intermediate-depth and deep events we perform kinematic and dynamic source inversions using elliptical patches, where some dynamic source parameters can be derived and compared to our global estimates. In particular, the use of simple source models and elliptical patches allows for a consistent comparison of stress drop and efficiency estimates both at longer periods (source inversions) and higher frequencies (source spectral analysis).

We believe this may be a step towards improving our understanding of the earthquake's energy budgets for deep earthquakes using a combination of source inversions and source parameter estimates.

#### **Rupture Processes of $M > 7$ Hindu Kush Intermediate-depth Earthquakes**

ZHAN, Z., California Institute of Technology, Pasadena, CA, USA, zwzhan@gps.caltech.edu; YE, L., California Institute of Technology, Pasadena, CA, USA, lingling@gps.caltech.edu; LAY, T., University of California, Santa Cruz, CA, USA, tlay@ucsc.edu; KANAMORI, H., California Institute of Technology, Pasadena, CA, USA, hiroo@gps.caltech.edu

$M7$  intermediate-depth earthquakes struck the Hindu Kush region about every 10 years, a higher rate than in most other regions around the world. The latest one, the October 26, 2015  $M_w$  7.5 earthquake caused at least 399 casualties despite its large depth (212 km) and remoteness. Furthermore, these  $M7$  deep events often had weak but distinct initiation phases before the main slips, which complicate the imaging of their rupture processes. For example, the initiation phases for the 2002 and 2015 events are both about 10s long. Here we apply the sub-event method, back-projection, and finite-fault inversion to both teleseismic and regional data of these  $M7$  earthquakes to image their ruptures. We find that, although these events are located very close to each other, their rupture processes are very different, in terms of rupture direction, number of main slip patches, etc. Furthermore, we notice that these  $M7$  events probably overlap in significant parts of the main slips. Considering the frequent occurrence of these large earthquakes, we suggest that the subducting slab responsible may be undergoing substantial internal deformation.

#### **Source Models for Intermediate and Deep Focus Earthquakes: Parameterization and Non-uniqueness**

LAY, T., University of California Santa Cruz, Santa Cruz, CA, USA, tlay@ucsc.edu

Seismological methods are the primary means by which source processes of intermediate and deep focus earthquakes can be studied, although geodetic data occasionally have contributed constraints on relatively shallow intermediate depth events. With greatly expanded seismological observations being available for recent large earthquakes in subducting slabs, a variety of analysis procedures is commonly applied, and detailed characteristics of the space-time radiation of seismic energy are examined. Given the temporal separation of depth phases and the reduced levels of attenuation experienced for down-going direct seismic phases in the slab environment, teleseismic body wave observations provide better bandwidth information than typically viable for shallow events, and waveform features are potentially more directly interpretable in terms of source complexity. Methods that are commonly applied in the analysis of detailed rupture process of intermediate and deep focus earthquakes include short-period back-projection, subevent directivity analysis and waveform modeling, moment rate function directivity analysis, and finite-fault inversion of broadband waveforms. Overall source geometry and total seismic moment are commonly well-constrained by long-period point-source inversions of full ground motions (centroid-moment tensor inversions) or early ground motions (W-phase moment tensor inversions). Despite the relative simplicity of the wave propagation effects, there can be significant differences in source properties inferred for large intermediate and deep events, and there is often ambiguity even with respect to determining any dominant fault plane, even for predominantly double-couple moment tensor events. Inferences of stress drop, rupture velocity, rupture connectivity, and causal mechanism differ, in large part due to each investigator's choice of parameterization. The resulting trade-offs and limitations of models and inferred parameters are discussed here.

#### **Deformation of the Nazca Slab in the Deep Upper Mantle and Mantle Transition Zone beneath South America**

LONG, M. D., Yale University, New Haven, CT, USA, maureen.long@yale.edu; EAKIN, C. M., University of Southampton, Southampton, UK, caroline.eakin@gmail.com; SCIRE, A., University of Arizona, Tucson, AZ, USA, ascire@email.arizona.edu; BECK, S. L., University of Arizona, Tucson, AZ,



USA, slbeck@email.arizona.edu; WAGNER, L. S., Carnegie Institution for Science, Washington, DC, USA, lwagner@carnegiescience.edu; ZANDT, G., University of Arizona, Tucson, AZ, USA, gzandt@email.arizona.edu; TAVERA, H., Instituto Geofísico del Perú, Lima, Peru, hernando.tavera@igp.gob.pe

The origin of deep earthquakes and the processes that contribute to the deformation of subducting slabs remain enigmatic. Here we present constraints on the deformation of the Nazca slab beneath South America derived from seismic tomography and seismic anisotropy measurements. We rely mainly on data from the PULSE and CAUGHT experiments, recent deployments of broadband seismometers in Peru and Bolivia. The flat geometry of the Nazca slab beneath much of Peru yields an opportunity to directly measure shear wave splitting due to anisotropy within the slab itself. These measurements demonstrate that the fast direction of wave propagation aligns with the contours of the slab in the deep upper mantle. Numerical modeling for a suite of realistic olivine fabrics reveals that the measurements cannot be explained by fossilized fabric developed prior to subduction; instead, we favor a model that invokes along-strike extension induced by flattening of the slab during subduction. We infer that the fossil fabric has been overprinted during subduction and that the Nazca slab must therefore be sufficiently weak to undergo significant internal deformation. Models of the Nazca slab in the deep upper mantle and transition zone derived from finite frequency P and S wave tomography demonstrate that there is significant along-strike variation in the morphology of the Nazca slab. We see evidence for thickening of the slab in the mantle transition zone in some regions, while in other regions the slab appears to penetrate into the lower mantle with little evidence for slab stagnation. The considerable along-strike variability in the morphology and deformation of the Nazca slab in the deep mantle indicates that along-strike variations in the plate boundary may have a significant effect on the deformation and fate of the slab at depth.

#### **Detecting Slab Structure Beneath the Banda Arc from Waveform Analysis of Deep Focus Earthquakes**

MILLER, M. S., University of Southern California, Los Angeles, CA USA, msmiller@usc.edu; HOLT, A. F., University of Southern California, Los Angeles, CA USA, adamholt@usc.edu; SUN, D., USTC, Hefei, China, sdy2014@ustc.edu.cn

Utilizing 30 recently installed broadband seismometers in the Banda Arc region of the Indonesia archipelago we investigate the structure of subducting Australian slab. This region is of particular tectonic interest as it is the archetypal example of a young arc-continent collision along with known varied lithospheric structure of the incoming Australian plate. Previous tomographic images indicate a complicated subducted slab structure where gaps in fast velocity anomalies in the upper mantle are interpreted as slab tears and are linked to the variation in the incoming plate structures. The detailed shape and location of these tears are important for kinematic reconstructions and understanding the evolution of the entire subduction system. However, tomographic images are inherently smooth due to being produced with damped inversions and will then underestimate the sharpness of these structures. We investigate possible sharp-sided structures within and at the edges of the subducted plate from deep focus earthquakes occurring beneath the seismic stations. Preliminary results show that the energy associated with the P-wave first arrival indicates a large amount of variation between waveforms at different stations along the arc, both in terms of frequency content and maximum amplitudes. Two main features can be inferred from these initial results: (i) The high-f content of the seismic waves in the outer volcanic arc increases from east to west, (ii) In eastern Timor island, there is a region of very low high-f content. While point (ii) appears to align with previous inferences about the presence of a slab gap (as the gap lies between the source and the low high-f region), we have shown that this is likely a product of crustal structure. However the first point, regarding the along strike variation in the high-f content at the volcanic arc appears more robust, and may point to variations in subducting slab continuity, or thickness, below the active volcanic arc.

#### **The Role of Homologous Temperature in Global Earthquake Locations**

DAVIS, P. M., UCLA, Los Angeles, CA, USA, pdavis@epss.ucla.edu

Earthquakes occur in crust or mantle that is below a critical temperature for the tectonic strain-rate, such that stress builds up to the breaking point before it can relax due to creep. The limiting temperature depends on pressure, which is taken into account by finding a critical homologous temperature  $T_{\{Hc\}}=T/T_M$  above which earthquakes cease (where  $T, T_M$  are temperature and average melting temperature of constituent minerals). We propose that the G layer of ocean plates is an uppermost mantle layer of thickness  $\sim 50$  km that is thought to be composed of harzburgite and depleted peridotite from which basalt has been removed to form ocean crust. Thus it has a higher melting temperature than the

peridotite of the surrounding mantle, or the lower halves of plates. We find that  $T_{\{Hc\}}$  for ocean plates is  $\sim 0.55$ . For California earthquakes, it is also close to 0.55. Thicknesses of seismicity in deep subduction zones, determined from 2D polynomial fits to a relocated catalog, are  $\sim 50$  km, which suggests that the earthquake channel is confined to the G layer. We construct thermal models to find homologous temperatures that take into account the variation of thermal parameters as a function of temperature, pressure and mineral content, based on laboratory and equation of state estimates for pyrolyte and harzburgite, and latent heat from phase changes. We find that seismicity thicknesses in subducted slabs are also, on average, confined to  $T_{\{H\}} < 0.55$  pm 0.05. The cutoff for deep earthquakes is not sharp. However they appear unlikely to occur if homologous temperature is high  $T_{\{H\}} > 0.55$ . Exceptions to the rule are anomalously deep earthquakes such as those beneath Iceland and the Hawaiian hotspots where  $T_{\{Hc\}} > 0.65$ . These can be explained if volcanic strain-rates are 2 to 3 orders of magnitude higher than the strain-rates associated with tectonic earthquakes.

#### **Seismic Evidences for Dynamic Activity of the Japan Subduction Zone beneath Northeast China**

CHEN, Q. E., Institute of Geology and Geophysics, Chinese Academy of Sciences, Beijing, China, chenqf@mail.iggcas.ac.cn; LI, T. J., Institute of Geology and Geophysics, Chinese Academy of Sciences, Beijing, China

The Japan subduction zone is formed by the Pacific plate subducting beneath the Eurasian plate, and reaches  $\sim 600$ -km depth in Northeast China, where the deep earthquakes frequently occurred. The subducting Pacific Plate is one of key factors responsible for the lithosphere thinning and extension of Northeast China and adjacent regions whereas it lacks the directly seismic observations. On May 10, 2011, two months after the 2011  $M_w 9.0$  Tohoku-oki earthquake, a deep earthquake occurred in the Sino-Russian border region, perhaps a dynamic adjustment in response to the Tohoku-oki earthquake. Based on digital seismic waveform records of regional broadband stations in Northeast China and using the gCAP method (Zhu and Ben-Zion, 2013), we obtained full moment tensors of the deep earthquakes occurred on May 2011 and later. Our results for the 2011 deep earthquake are consistent with the gCMT results, *i.e.*, both indicating a significant non-double component. It may reflect the transient regional tectonic stress regime of the mantle transition zone in our study area caused by the occurrence of the 2011  $M_w 9.0$  Tohoku-oki earthquake. The stress regime of deep subduction zone beneath Northeast China has been inverted using 31 gCMT solutions of deep earthquakes between 1969 and 2013 by the Spatial and Temporal Stress Inversion program (Hardebeck and Michael, 2006). Our inversion results indicate that the study area is predominantly under a uniform compressional stress field tending to NWW. The orientation of maximum compressional stress axis is consistent with the direction and dip angle of the Japan subduction slab around Northeast China. The stress regime of deep subduction zone beneath Northeast China may be affected by the dynamic stress adjustment caused by shallow strong earthquakes in the subduction zone. This work was supported by the National Natural Science Foundation of China (grant 41130316).

#### **Early Aftershock Sequences of the 2015 Mw7.5 Hindu Kush Intermediate-Deep Earthquake by Waveform Matching Detection**

LI, C., School of Earth and Atmospheric Sciences, Georgia Tech, Atlanta, GA, USA, lchenyu@gatech.edu; PENG, Z., School of Earth and Atmospheric Sciences, Georgia Tech, Atlanta, GA, USA, zpeng@gatech.edu; YAO, D., School of Earth and Atmospheric Sciences, Georgia Tech, Atlanta, GA, USA, dyao30@gatech.edu

Earthquakes between 70 and 300 km depth are considered as intermediate-depth events, and typically have fewer aftershocks than shallow earthquakes. The physical mechanisms of intermediate-depth events and their aftershock generations are not well understood. The 2015  $M_w 7.5$  Hindu Kush earthquake occurred at a depth of 212.5 km beneath the Hindu Kush region of Afghanistan and caused up to 400 casualties. The mainshock and its aftershock sequence were well recorded by many stations within 500 km. A visual inspection of high-frequency waveforms revealed more than 10 aftershocks in the first hour after the mainshock, while only one was listed in the Advanced National Seismic System (ANSS) catalog. Here we apply a recently developed Waveform Matched-Filter Technique (WMFT) to detect the aftershocks of the 2015 Hindu Kush earthquake. Specifically, we use 58 catalog events between 08/26/2015 and 11/30/2015 as templates, and apply a 2-8 Hz filter to both the template and continuous waveforms. We then utilize a 6-s window around the P wave (1s before and 5s after) for all three components, and 12-s window around the S wave (1s before and 11s after) for three components to compute the cross-correlations (CC) for all possible channels. So far we have detected more than 200 aftershocks detected within 5 days after the mainshock. In comparison, only 13 template events were listed in the ANSS catalog. Most early aftershocks were located to the west of the main-

shock epicenter, consistent with the westward propagation of the mainshock rupture. The number of detected aftershocks decay with time following the Omori's law, with a decay constant  $p=0.8$ . Our next step is to apply the hypoDD method to relocate all detected events, and examine spatio-temporal evolutions of early aftershocks, as well as search for potential foreshocks in this region. A systematic analysis of intermediate-depth earthquake interaction could shed new lights on the deep slab geometry in the Hindu Kush region.

---

## Upper Crustal Passive Imaging for Hazards and Exploration

Oral Session · Friday · 1:30 PM · 22 April · Tuscany 3/4  
Session Chairs: John Louie and Ileana Tibuleac

---

### Mapping Love/Rayleigh Phase/Group Velocity Dispersion Between 2–100 Seconds in North America using Ambient Noise Cross-correlations and Earthquake Observations

HERRMANN, R. B., Saint Louis University, St. Louis, MO USA, herrmarb@slu.edu; BENZ, H., US Geological Survey, NEIC, Golden, CO USA, benz@usgs.gov; AMMON, C. J., Penn State University, State College, PA USA, cja12@psu.edu

For routine regional moment tensor inversion, we select pre-computed Green's functions based on their fit to inferred surface wave Love/Rayleigh phase/group velocity dispersion in the source region. To constrain depth of very shallow events, knowledge of shallow crustal structure is crucial. Short period surface-wave dispersion can provide this constraint. We report on the result of adding dispersion measurements based on ambient noise cross-correlation techniques to our earlier data set that just used group velocities from earthquake recordings. To focus on the shorter periods, we processed large data sets from the 40 Hz broadband channels of the Earthscope Transportable Array for the region east of 105W. After cross-correlation of ambient noise and subsequent stacking, group velocities are determined by multiple filter analysis (Herrmann, 1973) and phase velocities by application of the method of Snieder (2004) through an interactive procedure. Tomographic inversion results compare favorably to those of Ekstrom (2011) at long periods and Ekstrom (2013) at intermediate periods. The comparison of the independently determined dispersion highlights problems with individual determinations and suggests the need for period dependent weighting of each. We find that the ability to determine short period dispersion (2 sec) varies geographically and may depend on local structure and local noise sources. The major contribution of this effort is the focus on dispersion at periods less than 10 seconds.

### Joint Surface Wave and Earthquake Travel-Time Inversion for Western North Island, New Zealand, 3-D Velocity Model

EBERHART-PHILLIPS, D., GNS Science, Lower Hutt, New Zealand, eberhartphillips@ucdavis.edu; FRY, B., GNS Science, Lower Hutt, New Zealand

We have applied a joint inversion of surface wave group velocity (GV) and local earthquake (LEQ) data to the North Island, New Zealand, to improve the existing New-Zealand wide 3-D velocity model. This takes advantage of the differing sensitivities of surface and body waves. The data are complementary, particularly at shallow depths where the LEQ paths may show vertical smearing and the surface waves have horizontal smearing. The current New Zealand-wide model has 3-50 km grid spacing and sharply images the slab and forearc. The employed GV observations are 2-D models at discrete periods which were determined for Rayleigh wave dispersion curves measured from the 1744 interstation Green's Functions resulting from stacked cross-correlations of broadband ambient noise data. Quality is assigned based on the number of interstation paths that contribute to the GV observation. In the volume surrounding each GV observation, we distribute numerous points for relating the GV observation to the gridded 3D tomography model, analogous to points along a raypath. The partial derivatives at the points are computed using the GV sensitivity kernels for  $V_p$  and  $V_s$  (Herrmann, 2013), with  $V_s$  related to  $V_p$  and  $V_p/V_s$  perturbations. Thus, the GV observations are included along with the travel-time observations in a joint inversion to best fit the data and the existing tomography model. The result favors the GV where there is little travel-time resolution. The combined inversion used 3049 GV observations at 6-20 s period and 1509 LEQ that extend to 350 km depth, and reduced the GV data variance by 74% and the LEQ by 14%. The resulting model generally has better constrained depth of shallow anomalies, with decreased velocity in the upper 2 km in the western North Island, and slight focusing of crustal high velocity features at 8-km depth.

Herrmann, R. B. (2013). "Computer programs in seismology: An evolving tool for instruction and research." *Seis. Res. Lett.* 84: 1081-1088.

### Shear-wave Velocity model from Ambient Noise Tomography near the Sacramento/San Joaquin Delta, California

FLETCHER, J. B., U.S. Geological Survey, Menlo Park, CA USA, jfletcher@usgs.gov; ERDEM, J. E., U.S. Geological Survey, Menlo Park, CA USA, jerdem@usgs.gov

Shaking from earthquakes could rupture levees in the Sacramento/San Joaquin Delta and impact the quality of the fresh water delivered to about half the population of California. To improve estimates of seismic hazards for the levees, a shear-wave velocity model for the region is needed in order to simulate ground motion for sites in the Delta. Consequently, we use ambient noise tomography to determine first a model of Rayleigh wave velocities, which we then invert for a shear-wave velocity model for the region. We deployed portable recorders for several years (2011–2013) in and around the Delta, supplemented with data from the Berkeley Digital Seismic Network, and Transportable Array stations. Ground motion data from vertical components (Rayleigh waves) were processed for coherence, stacked and filtered to determine dispersion curves for every pair of stations. Block velocities were estimated using least-squares minimization and included a spatial smoothing constraint. Estimates of block velocity versus period at each grid point were inverted for shear-wave velocity using a least-squares algorithm. This algorithm produced very close fits to most dispersion curves. To assess the uncertainty, we also used a genetic code to invert the dispersion curves, which randomly picks a starting model. Further it is possible to invert a single dispersion curve many times using a different starting seed allowing a variance to be computed for each period or layer. Inversions from this method follow closely the inversion from the least-squares algorithm. In the model, the Central Valley is slow at depths less than 3 km compared to the mountain ranges on either side, but at 8 km depth is faster. The Pittsburgh/Kirby Hills and Midland faults bracket a low-velocity region associated with the RioVista Basin and there is a high velocity volume at mid-crustal depths that corresponds to a north-south trending high found in the gravity and magnetics in the Central Valley.

### Microtremor Array Measurements for Estimating S-wave Velocity Profiles in Sedimentary Basins in Pacific Northwest of The United States

HAYASHI, K., Geometrics, San Jose, CA, USA, khayashi@geometrics.com; CAKIR, R., Washington State Department of Natural Resources, Olympia, WA, USA, Recep.Cakir@dnr.wa.gov; WALSH, T. J., Washington State Department of Natural Resources, Olympia, WA, USA, tim.walsh@dnr.wa.gov

Resolving S-wave velocity ( $V_s$ ) structure in the top few kilometers is important to evaluate thick quaternary sediment effects on ground motions in sedimentary basins. Recently, passive surface wave methods, such as microtremor array measurements (MAM) and seismic interferometry have become popular methods to measure  $V_s$ . The MAM with spatial auto-correlation (SPAC) analysis is particularly attractive since the method works with relatively small number of sensors and short ambient noise data. To evaluate the applicability of the MAM to estimate  $V_s$  to a depth of few kilometers, we performed the MAM at 15 sites in several sedimentary basins from Seattle to Portland. We used 3-component accelerometers for data acquisition with variable station separations of 10 to 3000 meters per profile. We recorded 10 minutes to one hour ambient noise data, with a total of several hours of day- and night-time measurements. We then used the SPAC method to calculate phase velocities from the MAM data, and obtained clear dispersion curves between 0.2 and 30 Hz, with maximum phase velocity of about 1500 to 2800 m/s at 0.2 Hz. A Genetic Algorithm was used for the inversion and  $V_s$  profiles to a depth of several kilometers were estimated. The  $V_s$  profiles obtained have large differences depending on sites. A low  $V_s$  (less than 500 m/s) was determined at a depth of about 10 to 100 m, and a thick ( $V_s=700$  to 1000 m/s) layer was determined to a depth of 100 to 800 m. Bedrock with  $V_s$  higher than 2000 m/s was determined at a depth greater than 300 to 3000 m depending on the sites. These preliminary results have shown that using the MAM method is applicable to the rapid estimation of deep and shallow  $V_s$  profiles in the sedimentary basins. Examples from Seattle, Portland, and Olympia basins will be presented.

### Deep ReMi Imaging—Mapping Shear-Wave Velocities to 1 km Depth and Greater Using Refraction Microtremor

PULLAMMANAPPALLIL, S., Optim, Reno, NV, USA, satish@optimsoftware.com; PANCHA, A., Victoria University of Wellington, Wellington, New Zealand, Aasha.Pancha@vuw.ac.nz; LOUIE, J., Nevada Seismological Lab., University of Nevada, Reno, NV, USA, louie@seismo.unr.edu

The Refraction Microtremor (ReMi) technique, which came into use during 2002, has now become a standard tool for assessing shear-wave velocities for engineering applications. It is used for site-class studies as well as assessing ground conditions, including 1D and 2D velocity-depth profiling to shallow depths of



approximately 100 m. Over the last few years, we have successfully extended the application of the method to depths greater than 1 km. The use of deep ReMi, which relies primarily on ambient noise, for estimation of shear-wave velocities to kilometer depths, allows for mapping the thickness and velocity of deep basins. These data in turn can be used for accurate modeling and calibration of recorded earthquake ground motions in urban areas. Such models have the potential to be an essential part of seismic hazard evaluation. We present results from several deep ReMi studies conducted in Reno-Tahoe basins. In all cases data were acquired using wireless instruments coupled with low-frequency geophones deployed in 3 km long arrays across the densely populated urban environment. In addition to mapping basement as deep as 900 m, the lateral velocity variations reveal deep-seated fault structure. Characterization of previously unknown faults is vital towards quantifying earthquake ground motion and seismic hazard potential in densely populated urban areas. Modeling was constrained using gravity data and earthquake tomography models when available. We will also present uncertainty analyses that account for the trade-off between velocity and depth for the derived models and explore techniques that can constrain these ambiguities.

### Shear-wave Velocities to Depths Greater than 1 km Using the krSPAC Microtremor Array Method: Examples from Seattle, Washington and Charleston, South Carolina

STEPHENSON, W. J., U.S. Geological Survey, Golden, CO, USA, wstephens@usgs.gov; ODUM, J. K., U.S. Geological Survey, Golden, CO, USA, odum@usgs.gov; ASTEN, M. W., Monash University, Melbourne, VIC, Australia

Characterizing earthquake ground motions through 3-D simulations is becoming standard practice for seismic hazard assessment in urbanized regions. However accurate ground motion prediction requires shear-wave velocity ( $V_s$ ) data at depths that capture the extent of the sedimentary column (usually greater than 100 m), which can be difficult to obtain. We describe the application of the wavenumber-normalized spatial autocorrelation method (krSPAC) to obtain  $V_s$  at depths as great as 2500 m in two distinct geologic regions: Seattle, Washington, and Charleston, South Carolina. In a traditional SPAC approach, modeling high wavenumbers within the SPAC spectrum requires array symmetry. By contrast, in the krSPAC approach we transform observed coherency-versus-frequency spectra to coherency-versus-kr (where k and r are wavenumber and station separations, respectively) prior to  $V_s$ -versus-depth modeling. Through this transformation the requirement for array symmetry is eased. In the Seattle basin we acquired microtremor data at 11 sites to characterize  $V_s$  at depths of the Quaternary and upper Tertiary sedimentary deposits. We deployed seven-sensor nested asymmetrical triangular arrays, with interstation distances that varied from 170 m to 2000 m. From our microtremor data we interpret  $V_s$  to depths over 2200 m. Comparison of krSPAC  $V_s$  to previous interpretations from regional ambient noise tomography suggests a broadly comparable  $V_s$  structure in the 250 to 1000 m depth range. In the Charleston urban area, situated on Atlantic coastal plain sediments exposed to potential earthquake ground shaking, we acquired microtremor data at 10 sites using up to 10 nested but irregularly spaced sensors in each deployment, with interstation distances that varied from 60 m to 1000 m. Preliminary analysis of these data suggest that the base of the coastal plain sediments is resolved in the 500 m to 800 m depth range, and  $V_s$  of these sediments varies from ~200 m/s to ~750 m/s.

### Understanding the Behavior of Microtremor H/V Spectral Ratio using the Energy Partitions within a Diffuse Field Regime

SÁNCHEZ-SESMA, F. J., Instituto de Ingeniería, UNAM, Coyoacán, DF, Mexico, sesma@unam.mx; PIÑA-FLORES, J., Instituto de Ingeniería, UNAM, Coyoacán, DF, Mexico, ead2009@hotmail.com; PERTON, M., Instituto de Geofísica, UNAM, Morelia, Michoacán, Mexico, mathieu.perton@gmail.com; GARCÍA-JEREZ, A., Universidad de Almería, Almería, Spain, agj574@ual.es; LUZÓN, F., Universidad de Almería, Almería, Spain, fluzon@ual.es; KAWASE, H., DPRI, University of Kyoto, Uji, Kyoto, Japan, kawase@zeisei.dpri.kyoto-u.ac.jp; MATSUSHIMA, S., DPRI, University of Kyoto, Uji, Kyoto, Japan, matsushima@zeisei.dpri.kyoto-u.ac.jp; CAMPILLO, M., ISTERre, University J Fourier, Grenoble, France, Michel.Campillo@ujf-grenoble.fr

The microtremor H/V spectral ratio (MHVSR) is widely used in the assessment of soil conditions. Some interpretations link HVSR with either S wave amplification or Rayleigh wave ellipticity.

Here we assume microtremors, like coda of earthquakes are both diffuse fields resulting from multiple scattering within the Earth. Theory asserts that the average of the autocorrelation of motion components at a receiver measures the directional energy densities that are proportional to the imaginary parts of the Green's function for source and receiver at the same point.

We need the directional energy densities to compute the MHVSR. The experimental ratio  $H^2/V^2$  has a theoretical counterpart: the ratio  $2\text{Im}G_{11}/$

$\text{Im}G_{33}$ , where  $\text{Im}G_{11}$  and  $\text{Im}G_{33}$  are the imaginary parts of Green functions at the load point for horizontal and vertical components, respectively. This relationship has profound physical implications that are useful to understand the behavior of the MHVSR.

The partition of the radiated energy by surface loads shows that for a vertical load, about 67% of the radiated energy corresponds to Rayleigh waves, and for high frequency,  $\text{Im}G_{33}$  reflects only the properties of the uppermost layer. In contrast, for a horizontal load 77% of energy leaves the load point as SH and SV waves. These down-going shear waves produce a conspicuous stair like pattern in which the resonances appear naturally. Both  $\text{Im}G_{11}$  and  $\text{Im}G_{33}$  have a growing linear trend versus frequency that expresses the emission episode. The ensuing variation residuals correspond to pseudo-reflection events.

For horizontally layered medium, one can compute efficiently the imaginary part of the theoretical Green's functions using either DWN or Cauchy residue theorem to compute the pole contributions due to Rayleigh and Love normal modes in the complex k plane.

ACKNOWLEDGEMENTS. This research was partially supported by the AXA Research Fund and by DGAPA-UNAM under Project IN104712.

### Use of Ambient Noise Surface Wave Tomography for Weathering Corrections in Controlled-Source Seismic Reflection Exploration

HOLLIS, D. D., Consulting Geophysicist, San Gabriel, CA, USA, dan@telephysical.com; CLAYTON, R. W., Caltech, Pasadena, CA, USA, clay@gps.caltech.edu; LIN, F. C., University of Utah, Salt Lake City, UT, USA, gilllin2@gmail.com; BARKLAGE, M. E., NodalSeismic LLC, Signal Hill, CA, USA, mbarklage@nodalseismic.com

Recent developments in seismic instrumentation for petroleum and other resource exploration have enabled dense arrays of passive seismic data to be co-acquired along with controlled-source seismic reflection data. Data mining of these passive dense arrays has shown that passive seismic data provides data products that can be used to improve controlled-source imaging and provide subsurface information not available by the seismic reflection method. These developments have led to increased interest by the resource extraction industries in the use of passive seismic methods. One application of a passive seismic method is that is currently being used is the use of ambient noise surface wave tomography to determined weathering static corrections.

Ambient noise surface wave tomography creates velocity models that are used to correct for near-surface velocity changes that distort seismic reflection data, thereby improving the accuracy and S/N of reflection imaging. In the data acquisition phase, it has been shown that, generally, seismic stations are deployed a sufficient amount of time to allow surface-wave dispersion analyses of empirical Green's functions. The resulting shear wave velocity model from the dispersion analyses is converted to a P-wave velocity using a  $V_p/V_s$  ratio that is derived from well logs or other sources. Statics corrections are then computed using the P-wave velocity model and reference datum. Static corrections derived from passive seismic are then applied in the reflection data processing flow. Use of passively-derived statics does not preclude the use of refraction-based or other methods of determining static or residual weathering corrections.

### Shallow Crustal Imaging using Dense Geophone Arrays

LIN, F., University of Utah, Salt Lake City, UT, USA, FanChi.Lin@utah.edu; BOWDEN, D. C., Caltech, Pasadena, CA, USA, dbowden@caltech.edu; ALTHEYAB, A., King Abdullah University of Science & Technology, Thuwal, Saudi Arabia, abdullah.altheyab@kaust.edu.sa; TSAI, V. C., Caltech, Pasadena, CA, USA, dbowden@caltech.edu; SCHUSTER, G. T., King Abdullah University of Science & Technology, Thuwal, Saudi Arabia, gerard.schuster@kaust.edu.sa; CLAYTON, R. W., Caltech, Pasadena, CA, USA, clay@gps.caltech.edu; HOLLIS, D., NodalSeismic, Signal Hill, CA, USA, dan.hollis@nodalseismic.com

The application of ambient noise tomography to dense local arrays has now allowed detailed shallow crustal structure to be studied with unprecedented high resolution. In this presentation, I will summarize some of our recent work on deploying local dense geophone arrays, extracting useful seismic signals from ambient noise cross-correlations, and using noise cross-correlations to constrain shallow crustal structure. In particular, the recent methodological developments based on data from the Long Beach dense array will be discussed. These developments include (1) inverting isotropic and anisotropic velocity structure using eikonal tomography, (2) constraining site amplification factors based on wavefront tracking, and (3) using the surface wave backscattering migration technique to constrain fault zone structure. These new results show promise for high-resolution shallow crustal imaging for hazard assessment and exploration.



## Seismic Interferometry with Distributed Acoustic Sensing for Near-surface Monitoring of Critical Infrastructure

LINDSEY, N. J., UC Berkeley, Berkeley, CA, USA, natelindsey@berkeley.edu; AJO-FRANKLIN, J. B., Lawrence Berkeley National Laboratory, Berkeley, CA, USA, JBAjo-Franklin@lbl.gov; DOU, S., Lawrence Berkeley National Laboratory, Berkeley, CA, USA, SDou@lbl.gov; DREGER, D., UC Berkeley, Berkeley, CA, USA, ddreger@berkeley.edu; MARTIN, E. R., Stanford University, Stanford, CA, USA, emartin@stanford.edu; WAGNER, A., Cold Regions Research and Engineering Laboratory, Ft Wainwright, AK, USA, Anna.M.Wagner@erc.dren.mil; FREIFELD, B., Lawrence Berkeley National Laboratory, Berkeley, CA, USA, BMFreifeld@lbl.gov; DALEY, T., Lawrence Berkeley National Laboratory, Berkeley, CA, USA, tmdaley@lbl.gov

Ambient surface wave energy is used to study a broad range of geologic processes at the regional scale, but field-scale geotechnical applications largely still utilize an active source, despite available noise sources. Recent advancement of distributed acoustic sensing (DAS) technology—in which an inexpensive (~\$1/m) fiber optic cable, buried at the surface, is used to accurately sample surface wave energy in a near continuous fashion (>1 kHz) with high spatial resolution (>1 receiver/m) over potentially long ranges (10's of km)—represents a unique tool for shallow seismic property estimation (e.g., Vs30). Here we present data and results from two continuous-recording DAS experiments that seek to develop this technology for the purpose of high-latitude permafrost thaw detection and infrastructure monitoring through pre-failure detection of zones of decreased soil shear strength. We develop a data processing approach that utilizes adaptive stacking to analyze the large volume of data recorded on the 1000+ channel DAS array sampled at 1 kHz. We consider the spatial and temporal variability in the source field through beamforming and stability window analysis. Lastly, we utilize automated dispersion analysis with quasi-2D MC inversion to generate a shear wave velocity profile beneath a road in a region of discontinuous permafrost. Our results demonstrate the utility of using DAS for real-time shear-modulus monitoring in support of critical infrastructure.

---

## Secondary Earthquake Hazards and Losses

Oral Session · Friday · 8:30 AM · 22 April · Tuscan 5/6

Session Chairs: Eric Thompson and Kate Allstadt

---

### Searching for Correlations: Landslide Distribution from the 2015 M7.8 Gorkha, Nepal Earthquake

COLLINS, B. D., U.S. Geological Survey, Menlo Park, CA, USA, bcollins@usgs.gov; JIBSON, R. W., U.S. Geological Survey, Golden, CO, USA, jibson@usgs.gov; KARGEL, J. S., University of Arizona, Tucson, AZ, USA, kargel@hwr.arizona.edu; SHUGAR, D. H., University of Washington, Tacoma, Tacoma, WA, USA, dshugar@uw.edu; HARITASHYA, U. K., University of Dayton, Dayton, OH, USA, uharitashya1@udayton.edu

Identifying the causative factors behind the spatial distribution of earthquake-induced landsliding is paramount to estimating the expected impacts from future earthquakes. Case histories, including detailed post-event landslide inventories, provide baseline information required to build and test hazard models. As such, earthquakes occurring in steep areas of the world provide an opportunity for significantly refining earthquake-induced landslide hazard projections. The 25 April 2015 M7.8 Gorkha, Nepal earthquake and its aftershocks (including one M7.3) occurred in the central Himalaya mountain range and caused significant landsliding in a swath reaching from roughly Annapurna in the west to Mount Everest in the east. Shaking caused thousands of landslides throughout the affected region, distributed over an approximately 30,000 km<sup>2</sup> area in Nepal alone. In addition to causing hundreds of fatalities, landsliding led to river and road blockages throughout the mountainous Himalayan region. Here we present results from ground-, helicopter-, and satellite-based investigations of landslides caused by the earthquake. Our analyses of the spatial distribution of landsliding, combined with investigation of a suite of potential geologic, geographic, topographic, geomorphologic, and seismologic factors, confirms the use of conventional factors (i.e., modeled peak ground acceleration and topographic slope) for explaining the landslide distribution, but that novel correlations resulting from post-earthquake seismological investigations also provide additional insight.

### A New Method for Assessing Coseismic Landslide Hazard in Regions Without Historical Landslide Inventories

ROBINSON, T. R., Durham University, Durham, UK, tom.robinson@durham.ac.uk; KRITIKOS, T., University of Canterbury, Christchurch, New Zealand, theo.kritikos@gmail.com; DAVIES, T. R. H., University of Canterbury,

Christchurch, New Zealand, tim.davies@canterbury.ac.nz; ROSSER, N. J., Durham University, Durham, UK, n.j.rosser@durham.ac.uk

Coseismic landsliding presents a considerable hazard that is often overlooked in seismic hazard and risk analyses. This is particularly true for infrastructure networks such as roads and utilities, which historically have suffered greater losses from landslides and liquefaction than ground shaking. One of the reasons for coseismic landsliding being overlooked is the difficulty in modeling the spatial distribution of hazard resulting from a given earthquake. Currently, regional coseismic landslide hazard analyses require a comprehensive historic landslide inventory as well as a detailed understanding of the local geotechnical properties. However, very few locations globally have sufficient inventories. We present a new approach to assess coseismic landslide hazard specifically for areas without historical landslide inventories. The proposed model adapts previous methods and employs fuzzy logic and GIS to establish relationships between causative factors and slope failures in multiple regions with well-documented and substantially complete inventories. By comparing multiple factors across different environments, those factors that influence landslide occurrence similarly, irrespective of environment, can be identified. These relationships can then be applied in regions without historic inventories with the assumption they have the same influence. We compare inventories for the 1994 Northridge and 2008 Wenchuan earthquakes and find common influences on landslide occurrence from shaking intensity, topography, and distance from active faults and streams. We apply these relationships to the 1999 Chi-Chi earthquake, and successfully forecast the location of >90% of landslides, demonstrating the model can be meaningfully applied in regions where previous methods could not. We apply the model to scenario earthquakes in New Zealand and Nepal as an illustration of its potential uses beyond the regions used for modelling.

### Rapid Assessment of Liquefaction Movements for Use in Earthquake Loss Estimates

VAN BALLEGOOY, S., Tonkin and Taylor, Auckland, New Zealand, SvanBallegooy@tonkintaylor.co.nz; MARTIN, J. G., Golder Associates, Atlanta, GA, USA; DETERLING, O., University of Texas, Austin, TX, USA; SECARA, S., University of Texas, Austin, TX, USA; HU, J., University of Texas, Austin, TX, USA. (RATHJE, E., presenting).

Estimating financial earthquake losses due to liquefaction is challenging because of the difficulty in assessing the physical consequences of liquefaction (i.e., ground movements) and its effects on the physical infrastructure. However, rapid assessment of liquefaction-induced ground movements from satellite imagery can provide the needed information on liquefaction consequences to estimate financial losses.

The 2010-2011 Canterbury earthquake sequence is used to demonstrate this approach. A significant fraction of the financial losses from these earthquakes was due to liquefaction and lateral spreading along the Avon River that flows through Christchurch and its eastern suburbs. Detailed estimates of lateral movements due to liquefaction are generated using pairs of 0.5 m resolution satellite imagery and optical image correlation. These data show localized movements associated with lateral spreading with magnitudes between 0.5 and 3.0 m. This presentation will describe the data processing and satellite imagery requirements for generating the displacement estimates, and critically evaluate these estimates with respect to observations from field reconnaissance. The accompanying presentation will compare these displacements with the building-level financial losses from the earthquake sequence.

### Estimation of Liquefaction-Induced Land, Building and Infrastructure Damage from Measured Ground Surface Movements

VAN BALLEGOOY, S., Tonkin + Taylor Ltd, Auckland, New Zealand, SvanBallegooy@tonkintaylor.co.nz; RATHJE, E. M., University of Texas at Austin, Austin, TX, USA, e.rathje@mail.utexas.edu; O'ROURKE, T. D., Cornell University, Ithaca, NY, USA, tdo1@cornell.edu

Estimating earthquake damage due to liquefaction is challenging because of the difficulty in assessing the physical consequences of liquefaction (i.e., horizontal and vertical movements) and its effects on the built environment. However, rapid assessment of liquefaction-induced horizontal movements from satellite imagery and vertical movements from airborne LiDAR surveys can provide the needed information on liquefaction consequences to estimate the damage to land, buildings and infrastructure on a portfolio basis. This information is useful for estimating metrics such as financial losses, the loss of service from damaged infrastructure and the quantum of people that are likely to be displaced due to both building and infrastructure damage. The rapid assessment of these metrics after a disaster is essential to inform the planning for an effective post-disaster recovery phase.

The residential land and building damage and buried pipeline infrastructure damage from the 2010-2011 Canterbury earthquake sequence has been correlated with the horizontal and vertical liquefaction-induced movements. The results show that where the horizontal and vertical movements are small, the frequency of pipe breaks is low and occurrence of moderate-to-severe building foundation deformation is low. Conversely, where the horizontal and vertical liquefaction-induced movements are high, the frequency of pipe breaks increases and occurrence of moderate-to-severe building foundation deformation is high. The accompanying presentation discusses the methods used to estimate the liquefaction-induced movements from satellite imagery and airborne LiDAR surveys. This presentation will describe the land, buried pipeline and building damage datasets, the correlations with the liquefaction-induced horizontal and vertical movements and how these correlations can be applied to rapidly estimate the quantum of land, building and infrastructure damage in the aftermath earthquake disasters.

### Overview and Recent Progress on the Next-Generation of Liquefaction Assessment Project

STEWART, J. P., University of California, Los Angeles, CA, USA, [jstewart@seas.ucla.edu](mailto:jstewart@seas.ucla.edu); KRAMER, S. L., University of Washington, Seattle, WA, USA, [kramer@uw.edu](mailto:kramer@uw.edu); KWAK, D. Y., University of California, Los Angeles, CA, USA, [kwakdongyup@gmail.com](mailto:kwakdongyup@gmail.com); GREENFIELD, M. W., University of Washington, Seattle, WA, USA, [greenfie@uw.edu](mailto:greenfie@uw.edu); KAYEN, R. E., United States Geological Survey, Menlo Park, CA, USA, [rkayen@usgs.gov](mailto:rkayen@usgs.gov); TOKIMATSU, K., Tokyo Institute of Technology, Tokyo, Japan, [kohji@o.cc.titech.ac.jp](mailto:kohji@o.cc.titech.ac.jp); BRAY, J. D., University of California, Berkeley, CA, USA, [jonbray@berkeley.edu](mailto:jonbray@berkeley.edu); BEYZAEI, C. Z., University of California, Berkeley, CA, USA, [zbeyzaei@berkeley.edu](mailto:zbeyzaei@berkeley.edu); CUBRINOVSKI, M., University of Canterbury, Christchurch, New Zealand, [misko.cubrinovski@canterbury.ac.nz](mailto:misko.cubrinovski@canterbury.ac.nz); SEKIGUCHI, T., Chiba University, Chiba, Japan, [tsekiguc@faculty.chiba-u.jp](mailto:tsekiguc@faculty.chiba-u.jp); NAKAI, S., Chiba University, Chiba, Japan, [nakai@tu.chiba-u.ac.jp](mailto:nakai@tu.chiba-u.ac.jp); BOZORGNIA, Y., Pacific Earthquake Engineering Research Center, Berkeley, CA, [yousef@berkeley.edu](mailto:yousef@berkeley.edu)

The Next-Generation Liquefaction (NGL) project was launched to develop an open source global database for liquefaction case histories and liquefaction models. The purposes of NGL are to (1) substantially improve the quality, transparency, and accessibility of case history data related to ground failure; (2) provide a coordinated framework for supporting studies to augment case history data for conditions important for applications but poorly represented in empirical databases; and (3) provide an open, collaborative process for model development in which developer teams have access to common resources and share ideas and results during model development, so as to reduce the potential for mistakes and to mutually benefit from best practices. NGL at present is a concept developed from multiple international workshops; aside from concept development, work to date has focused on compiling high-value case histories. Herein, we describe the project motivation, explain and illustrate how data resources will be compiled and organized, summarize preliminary results from ongoing data collection, describe needed supporting studies, and review project status and next steps.

---

## Advances in Earthquake Science Using Digital Photogrammetry

Oral Session · Friday · 10:45 AM · 22 April · Tuscany 5/6  
Session Chairs: Nadine Reitman, Kendra Johnson, and Lia Lajoie

---

### Ultra-high Resolution Topographic Data for Earthquake Science: Laser Scanning Versus Photogrammetry

DELONG, S. B., U.S. Geological Survey, Menlo Park, CA, USA, [sdelong@usgs.gov](mailto:sdelong@usgs.gov); CROSBY, C. J., UNAVCO, Boulder, CO, USA, [crosby@unavco.org](mailto:crosby@unavco.org); PICKERING, A. J., U.S. Geological Survey, Menlo Park, CA, USA, [apickering@usgs.gov](mailto:apickering@usgs.gov); PRENTICE, C. S., U.S. Geological Survey, Menlo Park, CA, USA, [cprentice@usgs.gov](mailto:cprentice@usgs.gov); LIENKAEMPER, J. J., U.S. Geological Survey, Menlo Park, CA, USA, [jlienka@usgs.gov](mailto:jlienka@usgs.gov); RUBIN, R. S., California Geological Survey, Menlo Park, CA, USA, [Ron.Rubin@conservation.ca.gov](mailto:Ron.Rubin@conservation.ca.gov); DAWSON, T. E., California Geological Survey, U.S. Geological Survey, Timothy.Dawson@conservation.ca.gov; SCHARER, K. M., U.S. Geological Survey, Pasadena, CA, USA, [kscharer@usgs.gov](mailto:kscharer@usgs.gov); HECKER, S., U.S. Geological Survey Menlo Park, CA, USA, [shecker@usgs.gov](mailto:shecker@usgs.gov); CLAHAN, K. B., Lettis Consultants International, Inc. Walnut Creek CA, USA, [clahan@lettisci.com](mailto:clahan@lettisci.com); SICKLER, R. R. U.S.

Geological Survey Menlo Park, CA, USA, [sickler@usgs.gov](mailto:sickler@usgs.gov); SCHWARTZ, D. P. U.S. Geological Survey Menlo Park, CA, USA, [dschwartz@usgs.gov](mailto:dschwartz@usgs.gov);

Ultra-high resolution (cm-scale) topographic data (uHRT) have facilitated important advances in earthquake science. Two primary methods have emerged to collect field-site-scale uHRT: structure-from-motion (SfM) photogrammetry and terrestrial laser scanning (TLS). SfM is often regarded as a low-cost, faster alternative to TLS, requiring less rigorous procedures and equipment. TLS data are lauded for resolution, accuracy and the ability to measure 3D change at the sub-centimeter level. Here we report results from our recent applications of TLS, and to a lesser extent, SfM, to illustrate the relative merits of each method. We use TLS to 1) map ultra fine geomorphology; 2) to spatially relate subsurface stratigraphy and faults in trenches (captured with SfM) and surface geomorphic features at paleoseismic sites; 3) to map topographic features associated with active faults under canopy where airborne lidar resolution is insufficient; 4) to quantify coseismic and postseismic landscape change including solid modeling of features in TLS point clouds to quantify aseismic slip (*e.g.* 2014 South Napa Earthquake); 5) to locate and quantify offset of cultural features; and 6) to analyze fine-scale fault scarp and liquefaction features from prehistoric earthquakes. SfM excels at creating uHRT in low-vegetation sites particularly if aerial platforms are available. SfM is superior to TLS for generation of orthoimagery in trench and outcrop studies, and can rapidly quantify fine-scale earthquake deformation. As researchers consider collection of uHRT, project requirements and an understanding of the advantages and disadvantages of each method should drive technique selection. Inexpensive approaches to generating the best data for a given study may include 1) open-source SfM software and a wide range of SfM collection methods including airborne platforms, 2) community TLS resources such as the UNAVCO Geodetic Imaging program, or 3) collaboration with USGS and other TLS experts.

### The Landers Rupture Revisited: A Test Case in Computing Topography and Deformation From Legacy Aerial Photographs

LAJOIE, L. J., Colorado School of Mines, Golden, CO, USA, [llajoie@mines.edu](mailto:llajoie@mines.edu); JOHNSON, K. E., Colorado School of Mines, Golden, CO, USA, [kejohno@mymail.mines.edu](mailto:kejohno@mymail.mines.edu); NISSEN, E., Colorado School of Mines, Golden, CO, USA, [enissen@mines.edu](mailto:enissen@mines.edu); SCHARER, K. M., USGS, Pasadena, CA, USA, [kscharer@usgs.gov](mailto:kscharer@usgs.gov); HUDNUT, K. W., USGS, Pasadena, CA, USA, [hudnut@usgs.gov](mailto:hudnut@usgs.gov)

The 1992  $M_w$  7.3 Landers earthquake provided unparalleled observations of the surface deformation of a large, multi-segment rupture. The first earthquake rupture ever imaged with Interferometric Synthetic Aperture Radar (InSAR), Landers has also been the subject of extensive field mapping, paleoseismic, and seismological work. Despite these studies, important characteristics of the causative faults, including their shallow slip properties, past slip distributions, and long-term slip rates, remain poorly understood, in part because the majority of the rupture has never been scanned with airborne lidar and no high-resolution digital surface model for the rupture area exists. We are interested in quantifying the distribution of slip along the rupture and the degree of slip localization, for comparison with existing seismologic and satellite-based studies of the rupture. The development of Structure-from-Motion (SfM) technology enables reconstruction of high-resolution topography and surface texture from historical aerial photographs, provided there is sufficient overlap between adjacent scenes, and even in the absence of metadata such as photograph locations, elevations, and camera parameters. This study presents a workflow and preliminary results from generating and georectifying three-dimensional point clouds using negatives from a 1:6000 USGS aerial survey flown over the entire ~85 km rupture days after the earthquake. These results confirm that displacement measurements and patterns can be extracted and we check these against a wealth of field data in order to assess precision. Future work will attempt to capture the 3D deformation field by incorporating pre-event photographs and comparing the SfM approach with horizontal displacement measurements from pixel tracking recently published by Milliner *et al.* (2015).

### Quantifying Near-Field Deformation Patterns of Large Magnitude Strike-Slip Earthquakes Using High-Resolution Air Photos.

MILLINER, C., University of Southern California, Los Angeles, CA, USA, [milliner@usc.edu](mailto:milliner@usc.edu); DOLAN, J., University of Southern California, Los Angeles, CA, USA, [dolan@usc.edu](mailto:dolan@usc.edu); HOLLINGSWORTH, J., University of Grenoble, Grenoble, France, [hollingsworth.jc@gmail.com](mailto:hollingsworth.jc@gmail.com); SAMMIS, C., University of Southern California, Los Angeles, CA, USA, [sammis@usc.edu](mailto:sammis@usc.edu); ALLAM, A., University of Utah, Salt Lake City, Utah, USA, [aaallam@alaska.edu](mailto:aaallam@alaska.edu)



edu; LEPRINCE, S., Navdy, San Francisco, CA, USA, leprincs@caltech.edu; AYOUB, F., Caltech, Pasadena, CA, USA, fayoub@gps.caltech.edu

Measurements of near-field surface deformation from large magnitude earthquakes are an important source of information for faulting mechanics and kinematics. However, direct measurements of near-field, co-seismic surface deformation have proven difficult, traditional field surveys typically cannot observe the diffuse and subtle inelastic strain accommodated over wide fault-zones, while InSAR data typically decorrelates close to the surface rupture due to high phase gradients leaving 1-2km wide gaps of data. Using the program COSI-Corr we correlate pairs of high-resolution (1 m pixel size) pre and post-event optical air photos to quantify and directly compare the near-field, surface deformation properties of the 1992  $M_w = 7.3$  Landers and 1999  $M_w = 7.1$  Hector Mine earthquakes. This technique allows detailed measurement of the co-seismic slip distribution, as well as the magnitude and width of off-fault deformation with sub-pixel precision. From our analysis we find that the Landers event exhibited larger amounts of off-fault deformation over wider zones of faulting than Hector Mine, with 47% and 38% of displacement accommodated as diffuse, distributed shear over mean fault widths of 154 m and 133 m, for Landers and Hector Mine respectively. From the 2D, horizontal correlation results we also compute strain maps for both events revealing intricate faulting kinematics within structurally complex areas, such as step-overs and sites of fault branching, giving important insight into the behavior of fault interaction and rupture propagation. These results have key implications for better understanding how inelastic deformation fundamentally varies between different fault systems, improving the accuracy of estimated fault slip at shallow depths determined from finite-fault inversions that typically lack near-field data, and the apparent discrepancies between geodetic and geologically derived fault slip rates.

#### **Analysing Three-dimensional Surface Displacements from Pleiades Stereo Imagery for the 2013 Balochistan and 2010 El-Major Cucupah Earthquakes**

PARSONS, B., University of Oxford, Oxford, UK, barry.parsons@earth.ox.ac.uk; ZHOU, Y., University of Oxford, Oxford, UK, yu.zhou@earth.ox.ac.uk; ELLIOTT, J. R., University of Oxford, Oxford, UK, john.elliott@earth.ox.ac.uk; BARISIN, I., University of Oxford, Oxford, UK, Ivana.Barisin@earth.ox.ac.uk; WALKER, R. T., University of Oxford, Oxford, UK, Richard.Walker@earth.ox.ac.uk

We illustrate the potential of vertical and horizontal surface displacements determined with decimetric precision from very high-resolution (VHR) Pleiades satellite imagery for two recent earthquakes.

The 2013 Balochistan earthquake, a predominantly strike-slip event, occurred on the arcuate Hoshab fault in the eastern Makran linking an area of mainly left-lateral shear in the east to one of shortening in the west. The difficulty of reconciling predominantly strike-slip motion with this shortening has led to a wide range of unconventional kinematic and dynamic models. We determined the vertical component of slip on the fault using a 1-m resolution digital elevation model (DEM) derived for the 225 km long rupture from post-earthquake Pleiades imagery. We find a constant local ratio of vertical to horizontal slip through multiple past earthquakes, suggesting the kinematic style of the Hoshab fault has been constant throughout the late Quaternary. Geodetic and long-term records of strain accumulation may be reconciled by failure in large, distributed and rare earthquakes on a series of subparallel faults.

We acquired Pleiades tri-stereo imagery over a 40 km  $\times$  5 km area in Baja California, Mexico, part of the epicentral area of the 2010  $M_w$  7.2 El Mayor-Cucupah earthquake chosen to coincide with a post-seismic lidar DEM. Elevations from tri-stereo have slightly (~15%) smaller uncertainties than stereo as the tri-stereo DEM incorporates more observations. Elevation differences between the Pleiades and post-earthquake lidar DEMs show that the vertical accuracy of the Pleiades DEMs is ~0.3 m. By matching and differencing the Pleiades and pre-earthquake 5-m resolution lidar DEMs, we mapped metre and sub-metre offsets along the faults obtaining results comparable to a previous study that differenced the two lidar DEMs. By extension, we expect it to be possible to measure sub-metre vertical offsets occurring in earthquakes using pre- and post-earthquake VHR stereo imagery.

#### **Determining Source Characteristics of Historic and Prehistoric Earthquake Ruptures in Central Asia Using Multi-scale, Multi-platform Photogrammetry**

ELLIOTT, A. J., COMET, University of Oxford Department of Earth Sciences, Oxford, United Kingdom, austin.elliott@earth.ox.ac.uk; WALKER, R., COMET, University of Oxford Department of Earth Sciences, Oxford, United Kingdom, richw@earth.ox.ac.uk; PARSONS, B., COMET, University of Oxford Department of Earth Sciences, Oxford, United Kingdom, barry.parsons@earth.ox.ac.uk; GRUETZNER, C., COMET, University of Cambridge Department of Earth Sciences, Cambridge, United Kingdom, chg39@cam.

ac.uk; MACKENZIE, D., COMET, University of Oxford Department of Earth Sciences, Oxford, United Kingdom, david.mackenzie@seh.ox.ac.uk; AINSCOPE, E., COMET, University of Oxford Department of Earth Sciences, Oxford, United Kingdom, eleanor.ainscoe@oriel.ox.ac.uk; ABDRAKHMATOV, K., Kyrgyz Seismological Institute, Bishkek, Kyrgyzstan, kanab53@yandex.com

Large and devastating earthquakes struck the northern Tien Shan and Qilian Shan of Central Asia in the nascent days of instrumental seismology during the late 19th and early 20th centuries, including the 1889  $M_w \sim 8.3$  Chilik, Kazakhstan and 1932  $M_w$  7.6 Changma, China events. Their seismic sources are relatively poorly characterized by contemporary macroseismic and seismological data; however, modern high-resolution satellite imagery reveals their geomorphic traces preserved in the arid Central Asian landscape. To better understand the rupture processes of these complex events we derive high-resolution topographic models along the coseismic scarps through photogrammetry with ground-based, low-altitude, and satellite-based optical imagery. Measurement of the scarps on the combined imagery and topography reveals the extent and slip distribution of coseismic rupture in each of these events, showing that both earthquakes involved multiple faults with variable kinematics. We use a 1-m elevation model of the Changma fault derived from Pleiades satellite imagery to map the changing kinematics of rupture along strike, and measure long-term slip rates using OSL geochronology. Along the recently identified Saty fault, suspected to be the source of the 1889 earthquake in southern Kazakhstan, we construct high resolution (330 points per sq m) elevation models using quadcopter- and helikite-mounted cameras. From this topographic data we measure single-event oblique offsets of 6-10 m, consistent with the large inferred magnitude of the 1889 Chilik event. We use 1.5-m SPOT 6 satellite imagery to produce a regional elevation model of the fault ruptures, from which we identify three distinct, intersecting fault systems that each have >20 km of fresh scarps, which may all have resulted from the 1889 earthquake. High resolution, photogrammetric topography offers a low-cost, effective way to characterize rupture sources that are more complex than contemporary seismic recordings can detect.

---

### **Citizen Seismology: Citizens as an Information Source to Advance Earthquake Response and Science**

Oral Session · Friday · 1:30 PM · 22 April · Tuscany 5/6

Session Chairs: Michelle Guy and Remy Bossu

---

#### **Development of the Citizen Seismometer Network System Utilizing Smartphones and Applicability of these Data Estimating Seismic Damages**

NAITO, S., NIED, Tsukuba, Ibaraki, Japan, naito@bosai.go.jp; NAKAMURA, H., NIED, Tsukuba, Ibaraki, Japan, manta@bosai.go.jp; IKUO TAKAHASHI, NIED, Tsukuba, Ibaraki, Japan, ikuo@bosai.go.jp; AZUMA, H., NIED, Tsukuba, Ibaraki, Japan, azzie@bosai.go.jp; FUJIWARA, H., NIED, Tsukuba, Ibaraki, Japan, fujiwara@bosai.go.jp

There are more than 5,000 strong-motion seismic stations in Japan, and these observation points are managed by NIED, JMA and local governments. Furthermore, by utilizing these seismometers, NIED has been developing real-time earthquake information system named J-RISQ (http://www.j-risq.bosai.go.jp/report/en/). Once an earthquake occurs, J-RISQ immediately estimates distribution of seismic intensities in each 250m square mesh, then estimates population exposure and building damage of each prefecture and municipality.

Such densely seismic stations covering whole country cannot be seen in any other country, but it is not enough for recording regional earthquake responses. However, it is difficult to increase conventional strong-motion seismometers exponentially in terms of expenses. So, we developed the citizen seismometer network system by utilizing MEMS acceleration sensor inside mobile terminals such as iPhone, iPad, iPod touch. By installing Apps, these terminals can record waveform at sampling frequencies of 100Hz, then if Wi-Fi is available, the recorded data is automatically transmitted to the cloud server. Soon after that, users can access the distribution map of seismic intensities, and download and analysis data easily by use of a web browser through internet.

To verify this system, we have performed on-site experiments in many buildings. Also we have acquired a number of earthquake records larger than M5. These data show different seismic intensities and predominant frequencies according to the location or buildings.

By utilizing these multipoint seismic data generated by citizens, it is likely to be get more detail information about local seismic responses, furthermore, it is possible to improve the accuracy and rapidity of real-time damage estimation system like J-RISQ.

Acknowledgement:



This research was partially supported by SIP (Cross-ministerial Strategic Innovation Promotion Program) under the leadership of Cabinet Office, Government of Japan.

### **Validation and Calibration of Predictive Relationships between Earthquake Intensity and Tweets Rate for Improving Real-Time Estimation Intensity**

KROIYVITSKAYA, Y. Y., Western University, London, ON, Canada; TIAMPO, K. F., CIRES, University of Colorado, Boulder, CO, USA; QIN, J., SHARCNET, Western University, London, ON, Canada; BAUER, M. A., Western University, London, ON, Canada

Intensity is a common measure for evaluation of seismic impact designed to standardize those measurements and their subsequent evaluation and response. Modern intensity assessment procedures process a variety of information sources, which can be divided into two main groups. The first group of sources is conventional and represented by physical sensors, such as seismographs and accelerometers. The second group of data sources are social sensors, such as witness observations of the earthquake consequences. Bringing new data sources to the second group could help to speed up the existing calculation of the intensity and improve the accuracy of those assessments in a more timely fashion. One potentially important data source of this type of data is the widespread micro-blogging platform Twitter. In our previous studies, empirical relationships between tweets rate and observed Modified Mercalli Intensity (MMI) were developed using data from the M6.0 South Napa, CA earthquake that occurred on August 24, 2014. Use of this relationship allows for the analysis of streaming data sources from both physical and social sensors to produce real-time intensity maps. These same relationships could potentially decrease latency in intensity calculations for future earthquakes in California and in other places around the world. However, there is a strong need for their validation and calibration in regions other than California. In this study we validate empirical relationships between tweets rate and observed MMI using data from earthquakes that occurred in California, Japan and Chile during the March-April 2014 period. We compare the quality and evolution of intensity maps from social data sources over 10-minute time intervals immediately following the earthquakes with USGS instrumental intensity maps and calculate the associated error.

### **MyShake: Smartphone based Seismic Network**

KONG, Q., UC Berkeley, Berkeley, CA, USA, kongqk@berkeley.edu; ALLEN, R., UC Berkeley, Berkeley, CA, USA, rallen@berkeley.edu; SCHREIER, L., Deutsche Telekom Silicon Valley Innovation Laboratories, Mountain View, CA, USA, Louis.Schreier@telekom.com; KWON, Y. W., Utah State University, Logan, UT, USA, young.kwon@usu.edu

MyShake is a citizen science project that harnesses the accelerometers in personal smartphones to record earthquake shaking data for research, hazard information and warnings. Our goal is to build a seismic network that consists of daily used smartphones to monitor earthquakes. We developed an android application—MyShake, running on the phone that has the function to distinguish earthquake shakings from daily human activities based on the different patterns behind the movements. It can also be triggered by the traditional earthquake early warning (EEW) system to record for a certain amount of time to collect earthquake data. When MyShake is triggered by the earthquake-like movements, it sends the trigger information back to our server which contains time and location of the trigger, at the same time, it stores the waveform data on local phone first, and upload to our server later. Trigger information from multiple phones will be processed in real time on the server to find the coherent signal to confirm the earthquakes. Therefore, the app provides the basis to form a smartphone seismic network that can detect earthquake and even provide warnings. In this presentation, we will report our system design and the performance after we release our application to the public.

### **LastQuake: A Smartphone App for Rapid Public Information, Rapid Crowdsourcing and Seismic Risk Reduction**

BOSSU, R., EMSC, Paris, France; ROUSSEL, F., EMSC, Paris, France; MAZET-ROUX, G., EMSC, Paris, France; STEED, R., EMSC, Paris, France

LastQuake is a free smartphone application focusing on felt earthquakes, the only ones that matter for the public. It provides very rapid detections, typically within a couple of minutes based on flashsourcing (real time analysis of website traffic) and Twitter Earthquake detections (TED). It collects testimonies through thumbnail-based questionnaires, comments and geo-located pictures. There are currently 90 000 applications in operation worldwide for 120 000 downloads.

In conjunction with our websites, LastQuake proved efficient for rapidly collecting testimonies, even in remote regions, or after violent earthquakes. For example, 2 000 testimonies have been collected for the January 2016 M 6.7

Manipur (India) earthquake, 800 of them being collected within the first 30 minutes.

We will show that, in an approach similar to flashsourcing and TED, surges in the number of active applications can be used to rapidly detect felt earthquakes. Furthermore, we will show that when such a surge occurs the location of the application can be used to automatically map the felt area and perform magnitude estimates within a few minutes without using any seismic data.

Finally, the next evolutions of the application will be presented. It is based on the results of an online survey performed in June 2015 among the Nepal users who strongly requested the integration of safety instructions to know what to do after an earthquake. It will be offered by popping-up visual items providing safety advice on actions that should and should not be performed (*e.g.*, move away from buildings; do not call emergency service except if people are injured) on the smartphones of people who have just been through strong shaking. This may contribute at little cost to risk reduction by limiting potentially fatal mistakes, reducing societal impact, and easing rescue operations.

### **AcceleROB: Low-cost Accelerometric Stations in Belgium**

LECOCQ, T., Royal Observatory of Belgium, Brussels, Belgium, thomas.lecocq@oma.be; RAPAGNANI, G., Royal Observatory of Belgium, Brussels, Belgium, giovanni.rapagnani@oma.be; VLEMINCKX, B., Royal Observatory of Belgium, Brussels, Belgium, bart.vleminckx@oma.be; CAMELBECK, T., Royal Observatory of Belgium, Brussels, Belgium, thierry.camelbeck@oma.be

The AcceleROB project aims at covering Belgium with low-cost accelerometric stations in order to obtain true-ground motion measurements for any M3.5+ earthquake.

“AcceleROB” is an acronym for “Accelerometric station of the Royal Observatory of Belgium”. A complete AcceleROB includes a RaspberryPi micro-computer, a power supply, a network cable, a JoyWarrior Accelerometer and a tripod brick. This setup allows installing the sensor without the need to leave a computer permanently switched on. If a permanent internet connection is not available directly at the place, a pair of Devolo (secure Ethernet over powerline) is provided. No difficult installation is required: when connected to the internet the station automatically connects through SSH to a SeisComp3 server and provides a port routing back to its Seedlink server. The station consumes less than 3 watts (7 watts with the Devolo) and has a bandwidth of approximately 365 bytes per second (30 MB/day). The sensors are calibrated to be sensitive to accelerations from approximately 0.001 g, which should be met by any earthquake of local magnitude  $ML=3$  or larger.

Its small size and simple installation make that almost anyone can host an AcceleROB. The only requirements are a secure and quiet place provided with a permanent power supply and internet connection. Because of the low-consumption and low-bandwidth, also no compensation has to be given, being a host is therefore completely voluntary. Currently the first 90 stations are being deployed. The obtained ground motion data can be used to provide real-time information when an earthquake occurs, analyze Did-You-Feel-It data and calibrate or construct ground motion models in seismic hazard assessments.

---

## **Short- and Long-Term Deformation on Active Faults: Integrating Geodetic, Geologic and Seismic Constraints on Slip Rates and Off-fault Deformation in the Walker Lane and Beyond**

Oral Session · Friday · 3:45 PM · 22 April · Tuscany 5/6  
Session Chairs: William Hammond, Rich Briggs, Rich Koehler, and Corné Kreemer

---

### **Geodetic Slip Rates and Uncertainties in the Eastern California Shear Zone and Walker Lane**

EVANS, E. L., U.S. Geological Survey, Menlo Park, CA, USA, eevans@usgs.gov

Strain rates in the eastern California shear zone (ECSZ) and Walker Lane, measured by geodetic methods, are complicated by potentially overlapping strain signals of many closely spaced faults, making it difficult to constrain slip rates on any individual fault. Fault slip rates can be estimated by modeling fault systems, based on space geodetic measurements of surface ground displacement (GPS and InSAR). However, models (*e.g.*, block models) that include elastic deformation due to locked faults require fault geometries to be prescribed, and geodetic slip rate estimates may vary widely due to measurement and epistemic (model) uncertainties. We address this ambiguity in the ECSZ and Walker Lane in two ways. First, we combine published geodetic slip rate estimates and compare them on a georeferenced grid. Within each geographic grid cell, a number of metrics are

considered based on the suite of fault slip rates in the cell, including geometric moment, total slip rate, formal uncertainties, and variation among models. This approach assumes that all published geodetic slip rate estimates are equally valid, and therefore variability among models serves as a proxy for epistemic uncertainties in geodetic slip rates. Second, we address the potential role of fault system geometry in the ECSZ and Walker lane with total variation regularization (TVR), an L1 regularization method that allows for an algorithmic assessment of the best-fitting block model geometry based on geodetic observations. These two approaches independently assess geodetic constraints on fault slip, and systematically identify regions that may require more careful consideration in terms of modeling the complex set of faults in the ECSZ and Walker Lane.

### Seasonally Varying Strain Rate and Its Relationship with Seismicity in the California-Nevada Area

ZENG, Y., USGS Geological Hazard Science Center, Golden, CO, USA, zeng@usgs.gov

Traditional Global Positioning System (GPS) velocities are measures of the average linear trends in GPS time series after correcting for seasonal signals. This study explores the seasonally varying velocity by applying a least-square fitting to the daily GPS time series on a one-year moving time window with daily steps to develop smoothly varying linear trends and seasonal amplitudes from the original noisy data. I applied this approach to the California-Nevada continuous GPS network data from 2001-2014. In general, I found significant variations in both the GPS velocity amplitudes and phases with time, particularly in places where GPS velocities are small. I then computed the time dependent GPS strain rate maps from those velocity fields and compared them with regional seismicity distributions. Following the approach of Helmstetter *et al.* (2007) and Shen *et al.* (2007), I used the strain rate as a predictor of regional seismicity. I found that much of the regional seismicity collocates with the highest secular strain rates since strain is concentrated mostly along the San Andreas Fault system and other major California faults. Seasonal variation has little influence on them. However, along the Mohawk Valley Lineament to the central Walker Lane and continuing south to the Las Vegas shear system, seasonally varying strain rate appears to dominate the secular rate and leads to a substantial improvement on the predictive power of local seismicity by up to 80% in some months of the year prior to 2010. This phenomenon was interrupted by the occurrence of the 2010  $M_w$  7.2 El Mayor-Cuicapa earthquake, triggering seismicity in the California-Nevada region, and then by the following severe drought that continues throughout the area since 2011. It suggests that the interaction of the seasonally varying strain rate with the local hydrologic system may have led to the variation in seismicity along the region.

### Can Paleoseismic and Slip Rate Data be Replicated? Insights from the San Andreas Fault in the Carrizo Plain

GRANT LUDWIG, L., University of California Irvine, Irvine, CA USA, lgrant@uci.edu

An increasingly important question in the earth sciences and other non-laboratory sciences is whether or not the results of published studies can be independently verified through replication. This is especially important if the results are foundational for science or policy. Paleoseismic data and geologic slip rates provide insights to fault processes, and input to seismic hazard models and assessments. Geologic slip rates, geodetically-measured surface strain rates, and rates of moment release derived from paleoseismic data are often inconsistent, leading to questions about significance and interpretation of published results. Most paleoseismic data sets and geologic slip rates are derived from single studies conducted at specific sites. Repetition of studies and replication of results is rarely possible. The San Andreas fault (SAF) in the Carrizo Plain is one of the few faults which has been investigated multiple times at keystone paleoseismic sites. Three slip rate measurements at Wallace Creek agree within measurement uncertainty, and a slip rate measurement at Van Matre Ranch is consistent. Thus the slip rate studies of the SAF in the Carrizo Plain have been replicated. Similarly, average millennial-scale rupture intervals at the Bidart Fan paleoseismic site have been replicated within error of measurement and published 3 times. In contrast to slip rate and average repeat time, attempts to replicate or refine slip-per-event measurements have yielded significantly different results. The differences might be the result of different methods, or epistemic uncertainty in the data.

### Stringing Pearls Along the Wasatch Fault Zone: An Objective Look At Earthquake Rupture Length and Fault Segmentation

BIASI, G. P., University of Nevada Reno, Reno, NV, USA, glenn@unr.edu; DUROSS, C. B., Geologic Hazards Science Center, U.S. Geological Survey, Golden, CO, USA, cduross@usgs.gov; BENNETT, S. E. K., Seattle Field Office, U.S. Geological Survey, Seattle, WA, USA, sekbennett@usgs.gov

We adapt the Stringing Pearls methodology (Biasi and Weldon, BSSA, 2009) to the normal faulting regime of the Wasatch fault zone (WFZ) to develop viable fault-rupture histories and estimate the spatial extent and frequency of ruptures. We construct rupture scenarios using the timing and uncertainty of 50 individual post-5 ka earthquake observations from 13 paleoseismic trench sites along the central 250 km of the WFZ. The number of possible earthquake correlations is large enough to provide a variety of candidate multi-site ruptures. This approach makes no assumptions about fault segmentation and thus provides an independent assessment of WFZ segmentation models. We score rupture scenarios by (1) comparing along-strike cumulative predicted displacement to field observations of latest Pleistocene- and Holocene-to-present fault slip rates and (2) internal dating consistency of site-to-site earthquake correlations. Ensembles of the best ranking rupture scenarios are used to identify spatial and temporal patterns of surface rupture. Scenarios of 23 to 39 ruptures consistent with the paleoseismic event timing data are found with an average displacement misfit of <2 m, using length-displacement scaling adapted from Hanks and Bakun (BSSA, 2008). Scenarios having too many large or small ruptures tend to over- or under-predict cumulative displacement, respectively. Scenarios using scaling adapted from Wells and Coppersmith (BSSA, 1994) generally require more, smaller earthquakes. Best-fitting displacement scores come with scenarios of 26-32 ruptures. Mean rupture length is ~45 km, but depends on how far ruptures are modeled to continue beyond the final correlated paleoseismic site. Many scenarios reproduce slip-rate lows observed along the fault, such as near the Salt Lake City-Weber segment boundary. Best-fitting scenarios generally require several ruptures that are not restricted to a single segment of WFZ.

### Towards a Geodesy-based Picture of Strain Accumulation in the Los Angeles Basin

ROLLINS, J. C., California Institute of Technology, Pasadena, CA, USA, john.c.rollins@gmail.com; ARGUS, D. F., NASA Jet Propulsion Laboratory, Pasadena, CA, USA, argus@jpl.nasa.gov; LANDRY, W., California Institute of Technology, Pasadena, CA, USA, wlandry@caltech.edu; BARBOT, S. D., Earth Observatory of Singapore, Singapore, sylbar.vainbot@gmail.com; AVOUAC, J. P., California Institute of Technology, Pasadena, CA, USA, avouac@gps.caltech.edu

The Los Angeles region is contracting at >5 mm/yr in the north-south direction due to the misalignment of the Mojave section of the San Andreas with the direction of relative Pacific-North American plate motion. This contraction is accommodated by the accumulation of strain on thrust faults such as the Sierra Madre, Puente Hills and other systems and the release of that strain in damaging earthquakes such as the 1971 San Fernando, 1987 Whittier Narrows and 1994 Northridge shocks. A  $M > 7$  earthquake on one of these systems could constitute a worst-case-scenario event for the Los Angeles region, and so it is essential to use geodetic methods to constrain where, and how quickly, tectonic strain is accumulating on these faults. This problem is affected by the soft sediments of the Los Angeles basin, which amplify the elastostatic Green's functions that map slip rates at depth to velocities at the surface. Using a recently developed adaptive-meshing finite-difference method, we compute elastostatic Green's functions that incorporate the most up-to-date picture of lateral and vertical heterogeneities in elastic properties provided by the SCEC Community Velocity Model (CVM-H15.1), and use these Green's functions to invert long-term GPS velocities at the surface for the distributions of creep and locking on fault planes provided by the SCEC Community Fault Model and other sources. The possibility that these thrust faults root into a creeping decollement at depth has a strong effect on the solution; in fact much of the contractional gradient can be fit to creep at or near the long-term convergence rate on a decollement extending from the San Andreas to the base of the Compton thrust fault. Here we will present models that extend this approach to more complex fault configurations in order to tease out the rates of strain accumulation on individual faults within the basin and explore the trade-offs between different interpretations.



---

## NGA-East: Research Results and Ground-Motion Characterization Products for Central and Eastern North America

Oral Session · Friday · 8:30 AM · 22 April · Tuscany 7/8  
Session Chairs: Christine Goulet and Yousef Bozorgnia

---

### PEER NGA-East Overview: Development of a Ground Motion Characterization Model and Ground Motion Prediction Equations for Central and Eastern North America

GOULET, C. A., PEER Center, U. of California, Berkeley, CA, USA, [goulet@berkeley.edu](mailto:goulet@berkeley.edu); BOZORGNIA, Y., PEER Center, U. of California, Berkeley, CA, USA, [yousef@berkeley.edu](mailto:yousef@berkeley.edu); ABRAHAMSON, N. A., PEER Center, U. of California, Berkeley, CA, USA, [abrahamson@berkeley.edu](mailto:abrahamson@berkeley.edu)

The Next Generation Attenuation project for Central and Eastern North America (CENA), NGA-East, is a major multi-disciplinary project coordinated by the Pacific Earthquake Engineering Research Center (PEER). The project was co-sponsored by the U.S. Nuclear Regulatory Commission (NRC), the U.S. Department of Energy (DOE), the Electric Power Research Institute (EPRI) and the U.S. Geological Survey (USGS). NGA-East involved a large number of participating researchers from various organizations in academia, industry and government and was carried-out as a combination of 1) a scientific research project and 2) a model-building component following the NRC Seismic Senior Hazard Analysis Committee (SSHAC) Level 3 process. The science part of the project led to several data products and technical reports while the SSHAC component aggregated the various results into a ground motion characterization (GMC) model. The GMC model consists in a set of ground motion models (GMMs) for median and standard deviation of ground motions and their associated weights, combined into logic-trees for use in probabilistic seismic hazard analyses (PSHA).

NGA-East addressed many technical challenges, most of them related to the relatively small number of earthquake recordings available for CENA. To resolve this shortcoming, the project relied on ground motion simulations to supplement the available data. Other important scientific issues were addressed through research projects on topics such as the regionalization of seismic source, path and attenuation of motions, the treatment of variability and uncertainties and on the evaluation of site effects. Seven working groups were formed to cover the complexity and breadth of topics in the NGA-East project, each focused on a specific technical area. This presentation provides an overview of the NGA-East research program and its key products.

### NGA-East Database

KISHIDA, T., University of California, Berkeley, CA, USA, [tkishida@berkeley.edu](mailto:tkishida@berkeley.edu); GOULET, C. A., University of California, Berkeley, CA, USA, [goulet@berkeley.edu](mailto:goulet@berkeley.edu); ANCHETA, T. D., Risk Management Solutions, Newark, CA, USA, [tim.ancheta@rms.com](mailto:tim.ancheta@rms.com); CRAMER, C. H., University of Memphis, Memphis, TN, USA, [ccramer@memphis.edu](mailto:ccramer@memphis.edu); DARRAGH, R. B., Pacific Engineering and Analysis, El Cerrito, CA, USA, [bbalindavis@gmail.com](mailto:bbalindavis@gmail.com); SILVA, W. J., Pacific Engineering and Analysis, El Cerrito, CA, USA, [pacificengineering@juno.com](mailto:pacificengineering@juno.com); HASHASH, Y. M., University of Illinois at Urbana-Champaign, Champaign, IL, USA, [hashash@illinois.edu](mailto:hashash@illinois.edu); HARMON, J., University of Illinois at Urbana-Champaign, Champaign, IL, USA, [harmon4@illinois.edu](mailto:harmon4@illinois.edu); STEWART, J. P., University of California, Los Angeles, CA, USA, [jstewart@seas.ucla.edu](mailto:jstewart@seas.ucla.edu); WOODDELL, K. E., University of California, Berkeley, CA, USA, [katie.wooddell@gmail.com](mailto:katie.wooddell@gmail.com); YOUNGS, R. R., AMEC Environment and Infrastructure, Oakland, CA, USA, [bob.youngs@amecfw.com](mailto:bob.youngs@amecfw.com); MAZZONI, S., University of California, Berkeley, CA, USA, [silviamazzoni@yahoo.com](mailto:silviamazzoni@yahoo.com)

We summarize the attributes of a comprehensive ground motion database developed for the Central and Eastern North America (CENA) region. The database was developed as part of the Next Generation Attenuation Project for CENA (NGA-East), a large multi-disciplinary project coordinated by the Pacific Earthquake Engineering Research center (PEER). The NGA-East database includes the two- and three-component ground-motion recordings from numerous selected events ( $M \geq 2.5$ , distances up to 1500 km) recorded since 1988. The final database contains over 9,600 records from 81 earthquake events and 1379 recording stations. The NGA-East database constitutes the largest database of processed recorded ground motions from Stable Continental Regions (SRCs). The motivation behind the development of the empirical database is the same as for other NGA projects (NGA-West1 and NGA-West2), which is to be used, along with other information and data, for the development of ground motion models (GMMs). The NGA-East ground motion database, similar to those from the NGA-West projects, includes pseudo-spectral acceleration (PSA) for the 5%-damped elastic oscillators with periods ranging from 0.007 to 10 sec.

Additionally, the NGA-East database includes Fourier amplitude spectra (FAS) of the processed ground motions. The NGA-East database therefore consists of three groups of complementary products: the summary file referred to as the flat-file, which contains metadata, ground motion information and intensity measures on a record-per-record basis, the time series (acceleration, velocity, and displacement), and the corresponding Fourier spectra files. The NGA-East database products are also made available to the public through the PEER online ground motion tool. An overview of the NGA-East database attributes and development is presented.

### A Review of Seed Ground-Motion Models used in NGA-East

GRAVES, R. W., U. S. Geological Survey, Pasadena, CA, USA, [rwgraves@usgs.gov](mailto:rwgraves@usgs.gov); The NGA-East Ground-Motion Model Developer Working Group

The final NGA-East median ground-motion models (GMMs) were built on a set of 19 seed GMMs. Details of this development process are given in a related presentation by Kuehn et al (2016). Here, we describe how the 19 seed GMMs were selected from an initial set of 30 candidate models, as well as highlight some of the similarities and differences among the seed GMMs. To begin the process, the NGA-East Technical Integration (TI) team developed criteria to evaluate the vintage and redundancy of the candidate models, as well as their applicability to the range of magnitude ( $M=4-8.2$ ), distance ( $R=0-1200$  km) and frequency ( $f=0.1$  to 50 Hz, plus PGA) required in the final model. The initial screening found 10 of the candidate models (EPRI, 2013) had been updated and replaced by more recent versions. The 20 remaining GMMs come from a set created specifically for the NGA-East project by 11 developer groups using various combinations of empirical, hybrid-empirical, and simulation-based approaches. These GMMs are all applicable to footwall conditions in the mid-continent region (excludes Gulf Coast), and none includes an explicit source depth term. Adjustments for hanging-wall conditions, extension to Gulf Coast and depth scaling are addressed separately. After the initial screening, the TI team utilized visual comparison of response spectra for selected M and R combinations in order to investigate the scaling trends of the various GMMs. This process determined the range of frequencies over which a candidate model could be used as a seed model across the entire range of M and R values. To ensure a practical, efficient and consistent model-building process, the TI team excluded any model that could only be used over a subset of M and R ranges, ensuring a consistent number of seeds at each frequency. Ultimately, 19 GMMs were selected as seed models. Most are used over the entire target bandwidth (0.1–50 Hz, plus PGA), although a few are used only for limited frequency ranges.

### Treatment of Epistemic Uncertainties in Median Predictions for NGA East

KUEHN, N. M., PEER Center, University of California, Berkeley, CA, USA, [kuehn@berkeley.edu](mailto:kuehn@berkeley.edu); GOULET, C., PEER Center, University of California, Berkeley, CA, USA, [goulet@berkeley.edu](mailto:goulet@berkeley.edu); AL-ATIK, L., San Francisco, CA, USA, [linda.alatik@gmail.com](mailto:linda.alatik@gmail.com); ABRAHAMSON, N. A., University of California, Berkeley, CA, USA, [abrahamson@berkeley.edu](mailto:abrahamson@berkeley.edu); ATKINSON, G., Western University, London, ON, Canada, [gmattinson@aol.com](mailto:gmattinson@aol.com); GRAVES, R. W., U.S. Geological Survey, Pasadena, CA, USA, [rwgraves@usgs.gov](mailto:rwgraves@usgs.gov); YOUNGS, R. R., AMEC Foster Wheeler, Oakland, CA, USA; BOZORGNIA, Y., PEER Center, University of California, Berkeley, CA, USA, [yousef@berkeley.edu](mailto:yousef@berkeley.edu)

The proper quantification of epistemic uncertainty with respect to median ground motion predictions is a major focus for the NGA East project. Existing/newly developed Eastern ground-motion models (GMMs) are used to estimate a joint probability distribution for median predictions at different magnitude and distance scenarios. This is achieved by modeling the covariance between the median predictions of the existing GMMs at different magnitude/distance scenarios. This corresponds to putting a Gaussian process prior on the possible shape of GMMs, where the parameters of the GP are constrained by the existing GMMs. The joint ground-motion distribution is a continuous representation of the epistemic uncertainty associated with median ground-motion predictions, as implied by the underlying existing GMMs. A large number of samples is drawn from this distribution, which are approximately mutually exclusive and collective exhaustive. Each of these samples constitutes a viable GMM. To break the large number of sampled GMMs down to a reasonable number, high-dimensional visualization tools are used. The sampled GMMs are projected onto a two-dimensional map, which serves as an accessible representation of the high-dimensional joint ground-motion distribution. The center, body and range of the epistemic uncertainty is defined on the map, and a reasonable number of representative models is selected. Each of the sampled GMMs is compared to relevant data, and weights for the representative GMMs are calculated as expectations over their representative area on the map with respect to likelihood and residuals. The pro-



cess is repeated for different frequencies, and the resulting spectra are smoothed to assure a physical response spectral shape.

#### **Aleatory Variability Model for NGA-East**

ALATIK, L., Linda Alatik Consulting, San Francisco, CA, USA, linda.alatik@gmail.com; GOULET, C., PEER Center, Berkeley, CA, USA, goulet@berkeley.edu; ABRAHAMSON, N., PEER Center, Berkeley, CA, USA, abrahamson@berkeley.edu; YOUNGS, R., AMEC Foster Wheeler, Oakland, CA, USA, bob.youngs@amecfw.com; GRAVES, R., Southern California Earthquake Center, Los Angeles, CA, USA, rwgraves@usgs.gov; ATKINSON, G., The University of Western Ontario, London, ON, Canada, gmatkinson@aol.com

Recorded ground-motion data from Central and Eastern North America (CENA) were used to analyze the components of ground-motion variability in CENA. Trends of ground-motion variability with parameters such as magnitude, distance, and VS30 were analyzed and compared to trends of ground-motion variability in other regions, particularly the Western United States (WUS) using the NGA-West2 dataset.

The CENA dataset is limited in magnitude range to small-to-moderate magnitudes and in frequency content to frequencies between 1 and 10 Hz due to the bandwidth limitations of the recordings. Therefore, standard deviation models developed using the CENA ground-motion data could not be reliably extrapolated to large magnitudes and to frequencies outside of 1 to 10 Hz. As a result, standard deviation models from other regions such as WUS and Japan were used to inform the extrapolation of CENA standard deviations and overcome data limitations. Models were developed and evaluated in a logic tree framework for the between-event standard deviation ( $\tau$ ), single-station within-event standard deviation ( $\phi_{SS}$ ), and site-to-site variability ( $\phi_{S2S}$ ). In turn, these models were combined to develop single-station sigma ( $\sigma_{SS}$ ) and ergodic sigma models for CENA.

#### **Use of Seismic Hazard Calculations in the NGA East SSHAC Process**

YOUNGS, R. R., Amec Foster Wheeler, Oakland, CA, USA, bob.youngs@amecfw.com; GOULET, C. A., PEER Center, U. of California, Berkeley, CA, USA, goulet@berkeley.edu; ABRAHAMSON, N. A., PEER Center, U. of California, Berkeley, CA, USA, abrahamson@berkeley.edu; AL-ATIK, L., San Francisco, CA, USA, linda.alatik@gmail.com; ATKINSON, G. M., Western University, London, ON, Canada, gmatkinson@aol.com; GRAVES, R. W., U.S. Geological Survey, Pasadena, CA, USA, rwgraves@usgs.gov; KUEHN, N. M., PEER Center, U. of California, Berkeley, CA, USA, kuehn@berkeley.edu; BOZORGNI, Y., PEER Center, U. of California, Berkeley, CA, USA, yousef@berkeley.edu

An important component of the SSHAC Process is the use of seismic hazard feedback to inform the Technical Integration (TI) team on the identification of important issues and the implications of alternative assessments on the outcome of the model building. Because the focus of the NGA East project was on developing a ground motion model for the assessment of hazard at critical facilities in the central and eastern United States (CEUS), the natural choice for a seismic source model for providing hazard assessments is the CEUS SSC model developed by EPRI/DOE/NRC (2012). In order to use the CEUS SSC model efficiently for hazard feedback, it was condensed to produce mean hazard across the epistemic uncertainty in earthquake recurrence rates. The resulting condensed model was then used to provide feedback to the TI team on the effects of alternative representations of median ground motions, alternative representations of aleatory variability, and alternative representations of the epistemic uncertainty in the median models and aleatory variability. Additionally, the condensed model was used to provide a comparison of hazard produced by the NGA East model compared to that produced by the current model used for assessing hazards at nuclear facilities in the CEUS.

#### **Prediction Equation for Central and Eastern North America based on a Regionally-Adjustable Generic Ground Motion Model**

YENIER, E., Western University, London, ON, Canada, emrah.yenier@gmail.com; ATKINSON, G. M., Western University, London, ON, Canada, gmatkinson@aol.com

Limited ground-motion observations in central and eastern North America (CENA) create challenges in terms of developing a regional ground motion prediction equation (GMPE) for a wide range of magnitudes and distances using conventional empirical methods. We tackle this problem by adjusting a generic GMPE model based on the observed source and attenuation attributes in CENA.

The basis of the generic GMPE is an equivalent point-source simulation model whose parameters have been calibrated to empirical data in California. We use simulated motions to determine the decoupled effects of basic source

and attenuation parameters on ground motion amplitudes. The generic GMPE is defined as a function of magnitude, distance, stress parameter, geometrical spreading rate and anelastic attenuation, for a reference NEHRP B/C boundary site condition. We also include an empirical calibration factor to account for residual effects that are different or missing in simulations compared to observed motions in the target region. This provides a "plug-and-play" GMPE that can be adjusted for use in any region by modifying a few key model parameters based on the observed ground motions.

We calibrate the generic GMPE for CENA using the regional source and attenuation parameters as well as the empirical calibration factor determined from NGA-East ground-motion database. We infer a magnitude- and depth-dependent stress parameter model based on the values obtained from study events. The developed GMPE provides median predictions of ground motions in CENA for average horizontal-component peak ground motions and 5%-damped pseudo spectral acceleration ( $T \geq 10$  s), for wide ranges of magnitude (M3-M8) and distance ( $< 600$  km).

#### **Ground Motion Prediction Equations for the Central and Eastern United States**

GRAIZER, V., U.S. Nuclear Regulatory Commission, Washington, DC, USA, Vladimir.Graizer@nrc.gov

A new ground motion prediction equations (GMPE) G-15 model for the Central and Eastern North America (CENA) is presented. The G-15 model is based on a subset of the NGA-East database for the horizontal peak ground acceleration and 5%-damped pseudo spectral acceleration RotD50 component (Goulet *et al.*, 2014). This subset includes records from 48 earthquakes with 7116 data points from  $M \geq 3.75$ , and fault distances up to 1000 km. The CENA database is not sufficient for creating purely empirical GMPE with recordings covering mostly a range of moment magnitudes  $M < 6.0$  and a limited number of near-fault recordings. The functional forms of the G-15 model are derived from filters representing a particular physical phenomenon affecting the seismic wave radiation from the source, and follows the approach developed by Graizer and Kalkan (2007, 2009 and 2011) for active tectonic environment in the Western United States (WUS). Main changes in the functional forms for the CENA relative to the WUS model (Graizer and Kalkan, 2015) are a shift of maximum frequency of the acceleration response spectrum (RS) toward higher frequencies and an increase in RS amplitudes at high frequencies. The developed site correction is based on multiple runs of representative VS30 profiles through SHAKE-type equivalent-linear (EQL) codes combined with downhole earthquake observations. Site amplifications are calculated relative to the hard rock definition used in nuclear industry ( $VS=2800$  m/s). The number of model predictors is limited to a few measurable parameters: moment magnitude  $M$ , closest distance to fault rupture plane  $R$ , VS30, and anelastic attenuation factor  $Q_0$ . Incorporating  $Q_0$  as an input parameter allows adjustments based on the regional crustal properties. The model is applicable for the stable continental regions and covers the following range of magnitudes, fault distances, S-wave velocities and frequencies:  $4.0 \geq M \geq 8.5$ ;  $0 \geq R \geq 1000$  km;  $450 \geq VS30 \geq 2800$  m/s and frequencies of  $0.1 \geq f \geq 100$  Hz.

#### **A Simulation-Based Ground Response Model to Guide Development of a Generalized Site Amplification Model for Central and Eastern North America**

HARMON, J. A., University of Illinois, Urbana-Champaign, Urbana, IL, USA, harmon4@illinois.edu; HASHASH, Y. M. A., University of Illinois, Urbana-Champaign, Urbana, IL, USA, hashash@illinois.edu; STEWART, J. P., University of California, Los Angeles, CA, USA, jstewart@seas.ucla.edu; RATHJE, E. M., University of Texas, Austin, TX, USA, e.rathje@mail.utexas.edu; CAMPBELL, K. W., EQECat, Beaverton, OR, USA, kcampbell@eqecat.com; SILVA, W. J., Pacific Engineering and Analysis, El Cerrito, CA, USA, pacificengineering@juno.com; PARKER, G., University of California, Los Angeles, Los Angeles, CA, USA, parker@seas.ucla.edu; XU, B., University of Texas, Austin, TX, USA, xhq0924@gmail.com

As part of the NGA-East project, the geotechnical working group is conducting a number of parametric studies to develop new sets of amplification functions suitable for Central and Eastern North America (CENA) site conditions with a 3000 m/s shear-wave velocity (VS30) reference site that has been adopted by the NGA-East project as the hard-rock condition for CENA. Over 1 million total linear elastic, nonlinear, and equivalent-linear 1-D site response simulations have been conducted using the site-response program DEEPSOIL for a set of characteristic site profiles in CENA in order to capture the expected range of site amplification in the region. This simulation-based site amplification study will be merged with empirical observations (Parker *et al.*, 2016) to guide final NGA-East site amplification model development. Dependent variables in the study include site VS profiles of specified VS30, bedrock depth, strain-dependent soil properties, bedrock motion intensity, and their uncertainty. VS-dependent mod-

els for soil strength and small-strain damping consistent with estimated values of the Fourier amplitude spectral decay parameter  $\kappa$  were used to constrain nonlinear soil behavior and the value of  $\kappa$  observed at the ground surface. A parameterized nonlinear model of site amplification from simulation results is presented. The final NGA-East site amplification model, developed jointly by validating the simulation results with empirical data, is intended for broad application in characterizing site response with respect to the 3000 m/s reference rock site condition recommended by the NGA-East project in CENA.

### Empirical Seismic Site Amplification in Central and Eastern North America from NGA-East Ground Motion Database

PARKER, G. A., UCLA, Los Angeles, CA, USA, parker@seas.ucla.edu; STEWART, J. P., UCLA, Los Angeles, CA, USA, jstewart@seas.ucla.edu; HASHASH, Y. M. A., University of Illinois at Urbana-Champaign, Urbana, IL, USA, hashash@illinois.edu; RATHJE, E. M., University of Texas, Austin, TX, USA, e\_rathje@mail.utexas.edu; CAMPBELL, K. W., CoreLogic, Oakland, CA, USA, kcambell@corelogic.com; SILVA, W. J., Pacific Engineering and Analysis, El Cerrito, CA, USA, pacificengineering@juno.com; HARMON, J. A., University of Illinois at Urbana-Champaign, Urbana, IL, USA, harmon4@illinois.edu; XU, B., University of Texas, Austin, TX, USA

The Next Generation Attenuation East project (NGA-East), coordinated by the Pacific Earthquake Engineering Research Center (PEER), resulted in the development of 10 ground motion models (GMMs) applicable to very hard rock reference site conditions in central and eastern North America (CENA). Separate models for seismic site amplification are needed to predict ground motion intensity measures (IMs) for other site conditions, including weathered rock and soil. We present results relevant to the development of such models, which is the site amplification that can be inferred from NGA-East ground motion data using a non-reference site approach. Using three selected NGA-East GMMs, we calculate within-event rock residuals for peak ground acceleration (PGA), peak ground velocity (PGV), and 0.01–10 s pseudo-spectral accelerations (PSA). These rock residuals are computed relative to the GMMs conditioned at 760 meters per second (m/s), using a mixed-effects analysis to account for model bias and event terms. The residuals suggest that site amplification varies approximately linearly (in a log-log sense) with the average shear wave velocity in the upper thirty meters of the crust ( $V_{530}$ ), at least over a limited range of  $V_{530}$  values (approximately 200–1000 m/s). However, the slope of the relations using NGA-East data are generally flatter than those derived previously for active crustal regions, particularly for oscillator periods > 0.2 seconds. These results will be used with simulations (Harmon *et al.* 2016) to develop CENA site amplification models that consider nonlinearity and resonance due to seismic impedance of the site profiles, as well as other possible factors.

---

## Physical and Statistical Properties of Earthquake Swarms and Clustered Seismicity: Constraining Driving Mechanisms

Oral Session · Friday · 1:30 PM · 22 April · Tuscany 7/8  
Session Chairs: Christine Ruhl, Ilya Zaliapin, and Rachel Abercrombie

---

### Identification and Characterization of Earthquake Swarms in Southern California

SHEARER, P. M., U.C. San Diego, La Jolla, CA, USA, pshearer@ucsd.edu; ZHANG, Q., Caltech, Pasadena, CA, USA, qizhang@caltech.edu

Earthquake swarms are space-time clusters of seismicity that cannot easily be explained by typical aftershock behavior, and are likely triggered by external processes such as fluid migration and/or slow slip. However, swarm properties are not fully understood and how much swarm occurrence is related to the tectonic environment (*e.g.*, heat flow, stressing rate) or source characteristics (*e.g.*, focal mechanism, stress drop) is unclear. Systematic study of large numbers of swarms and their source properties should help to resolve these issues, but is hampered by the challenge of identifying swarms at a range of spatiotemporal scales from a large earthquake catalog. We have developed a new method to search for clusters by comparing the number of neighboring events to the background events in scalable space/time windows, similar to the idea of STA/LTA algorithms, and then discriminating swarms from aftershock clustering. We apply our method to search the entire southern California catalog from 1981 to 2014 and find 293 swarms in total. Besides two geothermal areas, the Salton Sea and Coso fields, abundant swarm events occur south of the Eastern California Shear Zone. Our results indicate that swarms are heterogeneously distributed in space and time,

but that higher swarm rates are generally found in regions of normal faulting. The major swarms in the Coso geothermal fields can be explained by fluid flow while large linear migration velocities are found near the Salton Sea.

### Earthquake Declustering via a Nearest-Neighbor Approach in Space-Time-Magnitude Domain

ZALIAPIN, I., University of Nevada, Reno, NV, USA; BEN-ZION, Y., University of Southern California, Los Angeles, CA, USA

We propose a new method for earthquake declustering based on nearest-neighbor analysis of earthquakes in space-time-magnitude domain. The nearest-neighbor approach was recently applied to a variety of seismological problems that validate the general utility of the technique and reveal the existence of several different robust types of earthquake clusters. Notably, it was demonstrated that clustering associated with the largest earthquakes is statistically different from that of small-to-medium events. In particular, the characteristic bimodality of the nearest-neighbor distances that helps separating clustered and background events is often violated for offspring of the largest earthquakes which include a mixture of various smaller clusters. This prevents using a simple threshold between the two modes of the nearest-neighbor distance distribution for declustering. The current study extends the nearest-neighbor approach to the problem of earthquake declustering. We re-emphasize that clusters of large regional events have space-time structure that is different from (and cannot be rescaled to) that of smaller events. To address this in the context of declustering, we combine (i) the bimodality of the nearest-neighbor distribution for small-magnitude clusters and (ii) intensity metrics that work well for large-magnitude clusters. The combined technique is applied to seismicity of different areas in California (San Jacinto, Coso, Salton Sea, Parkfield, Ventura, Mojave, etc.) to demonstrate its stability and efficiency in treating various clustering types. The results are compared with those of alternative declustering methods.

### Earthquake Swarms and Mainshock-aftershock Sequences Hosted by a Single Fault: The 2000-2014 Activity in West Bohemia/Vogtland

FISCHER, T., Charles University in Prague, Czech Republic, fischer@natur.cuni.cz; HAINZL, S., GFZ Potsdam, Potsdam, Germany, hainzl@gfz-potsdam.de; CERMAKOVA, H., Institute of Geophysics, Czech Academy of Sciences, Prague, Czech Rep.; BACHURA, M., Charles University in Prague, Czech Republic; VLCEK, J., Charles University in Prague, Czech Republic

The West Bohemia/Vogtland region, central Europe, is a place of repeating earthquake swarm activity and degassing of CO<sub>2</sub> of mantle origin. The previous seismicity was characterized by a swarm-type character with gradual onsets and decays, which were not related to mainshocks and the swarm seismicity was compliant with fluid triggering models. However, the latest activity in the year 2014 with hypocenters overlapping those of previous swarms consisted of three classical aftershock sequences triggered by three mainshocks with magnitudes from 3.5 to 4.4.

To decode the apparent system change from swarm-type to mainshock-aftershock characteristics, we have analyzed in detail the spatiotemporal characteristics of the aftershock sequences based on a relocated earthquake catalog. Our analysis shows that the three mainshocks occurred with unfavorably oriented mechanism in a step-over region of the fault plane with increased coulomb stress due to previous activity. Similar to the previous swarm activity most of the aftershocks occurred in-plane. In contrast to the swarms the aftershock decay is of Omori-Utsu type; the  $c$  and  $p$  parameters are however untypically large. By means of the epidemic type aftershock sequence (ETAS) model we show that an additional aseismic source with an exponentially decaying strength is needed to trigger a large fraction of the aftershocks. Corresponding pore pressure simulations with an exponentially decreasing flow rate show a good agreement with the observed spatial migration front of the aftershocks extending approximately with  $\log(t)$ . Thus we propose a scenario that the mainshock opened fluid pathways into the fault plane explaining the unusual high rate of aftershocks, the migration patterns, and the decrease of the aseismic signal due to a finite fluid source. This is in accordance with the observation of a sudden and steady increase of CO<sub>2</sub> flow rate in a nearby mofette that has initiated few days after the mainshock.

### Fluid-Faulting Evolution in High Definition: Connecting Fault Structure and Frequency-Magnitude Variations During the 2014 Long Valley Caldera, California Earthquake Swarm

SHELLY, D. R., U.S. Geological Survey, Menlo Park, CA, USA; ELLSWORTH, W. L., Stanford University, Stanford, CA, USA; HILL, D. P., U.S. Geological Survey, Menlo Park, CA, USA

An extended earthquake swarm occurred beneath southeastern Long Valley Caldera between May and November 2014, culminating in three magnitude

3.5 earthquakes and 1145 cataloged events on 26 September alone. The swarm produced the most prolific seismicity in the caldera since a major unrest episode in 1997-1998. To gain insight into the physics controlling swarm evolution, we used large-scale cross-correlation between waveforms of cataloged earthquakes and continuous data, producing precise locations for 8494 events, more than 2.5 times the routine catalog. We also estimated magnitudes for 18,634 events (~5.5 times the routine catalog), using a principal component fit to measure waveform amplitudes relative to cataloged events.

This expanded and relocated catalog reveals multiple episodes of pronounced hypocenter expansion and migration on a collection of neighboring faults. Given the rapid migration and alignment of hypocenters on narrow faults, we infer that activity was initiated and sustained by an evolving fluid pressure transient with a low-viscosity fluid, likely composed primarily of water and CO<sub>2</sub> exsolved from underlying magma. Although both updip and downdip migration were observed within the swarm, downdip activity ceased shortly after activation, while updip activity persisted for weeks at moderate levels. Strongly migrating, single-fault episodes within the larger swarm exhibited a higher proportion of larger earthquakes (lower Gutenberg-Richter *b* value), which may have been facilitated by fluid pressure confined in two dimensions within the fault zone. In contrast, the later swarm activity occurred on an increasingly diffuse collection of smaller faults, with a much higher *b* value.

#### **A Slow Rupture Episode Inferred from Seismic and Geodetic Data during the 2000 Miyakejima Dike Intrusion**

CATTANIA, C., Stanford University, Stanford, CA, USA, camcat@stanford.edu; RIVALTA, E., GFZ German Research Center for Geosciences, Potsdam, Germany, rivalta@gfz-potsdam.de; HAINZL, S., GFZ German Research Center for Geosciences, Potsdam, Germany, hainzl@gfz-potsdam.de; PASSARELLI, L., GFZ German Research Center for Geosciences, Potsdam, Germany, luigi.passarelli@gfz-potsdam.de; AOKI, Y., Earthquake Research Institute, University of Tokyo, Tokyo, Japan, yaoki@eri.u-tokyo.ac.jp

The 2000 Miyakejima dike intrusion triggered one of the largest seismic swarms ever recorded: this remarkable dataset, combined with surface deformation measured by GPS on the northern Izu islands, provides the opportunity to understand the physical mechanisms driving seismicity during diking.

After the initial propagation phase, the dike stopped and continued thickening for 3 months. We find that during this period earthquakes tend to cluster in short bursts, lasting few hours and migrating in both directions along the dike: we identify 6 of these sequences within 60 days. The largest burst comprised more than 500  $M_w \geq 1$  events in 13 hours and it propagated bidirectionally at a speed of ~1 km/h. Fault plane solutions for this sequence contain a mixture of normal, strike slip and oblique mechanisms: this indicates that the events are not located on a single fault, but on a complex fault network.

On the day of the burst, a baseline displacement of 6 cm was recorded between the islands of Kozushima and Nijima. We find that seismicity only accounts for a small fraction of the deformation, and we invert for aseismic dislocation sources representing dike opening and slow slip. Based on the variability of focal mechanisms, we do not model slow slip on a single fault, but instead we assume that it takes place on the same faults as the earthquakes. We find that this distributed aseismic slip, combined with dike opening, provides the best fit to the geodetic data. We conclude that dikes induced faulting occurs largely by intermittent, migrating slip episodes with a large aseismic component.

#### **Variability of Source Parameter Estimates for the 2008 Mogul Earthquake Swarm near Reno, NV using EGF-derived Spectral Ratios**

RUHL, C. J., Nevada Seismological Laboratory, University of Nevada, Reno, NV, USA, cruhl@unr.edu; ABERCROMBIE, R. E., Boston University, Boston, MA, USA, rea@bu.edu; SMITH, K. D., Nevada Seismological Laboratory, University of Nevada, Reno, NV, USA, ken@unr.edu

Shallow, low-magnitude earthquake activity began affecting the Mogul neighborhood of Reno, NV on 21 Feb 2008 and continued to build in intensity leading to a  $M_w$  4.9 mainshock on 26 Apr 2008. Relocations suggest that the earthquakes were triggered by a diffusive event (*e.g.*, aseismic slip) with distinct impulsive subclusters evolving on well-defined structures. Near-source, temporary broadband seismometers deployed before the mainshock provide high quality records of many events and an ideal opportunity to investigate any spatial, temporal, or magnitude dependence of stress drop throughout the swarm.

We use a spectral ratio method on both P- and S-waves to estimate source dimension and stress drop for 95  $M_L \geq 2.5$  earthquakes in the Mogul sequence. Empirical Green's functions (EGFs) are chosen by testing all earthquakes 0.5 magnitude units smaller than and within one estimated focal distance to the

event of interest and accepting only those which meet our strict objective criteria (*e.g.*, cross-correlation, bandwidth, and others suggested by Abercrombie 2013 & 2014). We fit individual EGF-derived spectral ratios using the original- and sharper-corner spectral source models (Brune, 1970; Boatwright, 1980) and estimate uncertainties using a grid-search around the best-fit corner frequency of the larger event. We then take both a weighted-mean and stacked-spectra approach to resolve the average corner frequency for each event. We compare corner frequencies estimated using (1) P-waves and S-waves, (2) various cross-correlation limits, (3) weighted-mean and stacked-spectra approaches, and (4) the two different source models. Visual inspection shows that some events have complex sources and/or signal limitations that are not well fit by any of our methods, while others are well resolved and remain consistent regardless of the technique used. We include only well constrained events in our interpretation of source parameters for this sequence.

#### **Exploring Statistical and Physical Properties of the 2015 San Ramon Earthquake Swarm, California**

TAIRA, T., Berkeley Seismological Laboratory, Berkeley, CA, USA, taira@berkeley.edu; XUE, L., University of California Santa Cruz, Santa Cruz, CA, USA; BURGMANN, R., University of California, Berkeley, CA, USA

The northernmost section of the Calaveras fault near San Ramon, California frequently experienced earthquake swarms. A notable swarm began on 13 October 2015 and lasted ~1 month. More than 500 events were recorded during this 2015 swarm by the Northern California Seismic System (NCSS). The real-time double-difference event locations [Waldhauser *et al.*, 2009, BSSA] suggest that the swarm activated two major segments (Segments A and B). The two segments are separated by ~500 m and form northeast striking structures at depth of 6-8 km based on planarity of seismicity. The largest, magnitude 3.6 event occurred on 19 October on Segment B. We used a matched filter approach [Shelly *et al.*, 2013, JGR] for identifying previously missed events to fully characterize the temporal evolution of the 2015 swarm. As template waveforms, we made use of the S-wave seismograms (duration is 5 seconds) in a frequency range of 5-10 Hz from 223 events ( $M \geq 1.5$ ) listed in the NCSS catalog. By analyzing continuous seismic data from 18 seismic stations, we were able to detect 1549 events with a median cross correlation of 0.35 (~15 times the median absolute deviation of the median correlation function). We estimated *b*-values for the two segments with a completeness magnitude of 1.0. The resultant *b*-value is ~0.85 for both Segments A and B, which may suggest that both segments are marked by high stressed patches [Tormann *et al.*, 2013, GJI]. To explore the underlying physical mechanism, we will apply the epidemic type aftershock sequence (ETAS) model to document the statistical properties of the swarm and to illuminate the roles of stress transfer and fluid diffusion [Hainzl and Ogata, 2005, JGR].

#### **Tidal Triggering of Earthquakes Near Parkfield, California**

DELOREY, A. A., Los Alamos National Laboratory, Los Alamos, NM USA, andrew.delorey@lanl.gov; JOHNSON, P. A., Los Alamos National Laboratory, Los Alamos, NM USA, paj@lanl.gov

Earthquakes are known to cluster in time and space due to correlated spatio-temporal variations in static and dynamic forcing and stress state. The pattern of clustering can reveal information about stress state, earthquake nucleation, and triggering mechanisms. Investigators have searched for evidence of tidal modulation or triggering of earthquakes for decades because tidal stresses are well characterized, periodic, global, and always present. Earth tides are caused by the gravitational pull of the sun and moon which induce periodic stresses with two important components related to the rotation of the Earth relative to the sun and moon (semi-diurnal, 12 and ~12.4 hours) and the orbit of the moon around the Earth (fortnightly, ~14.7 days).

Here we show that tidal stresses trigger earthquakes in the brittle upper crust, which is caused by and detectable due to interactions between the semi-diurnal and fortnightly stress cycles. The peak-to-peak amplitude of stress during a semi-diurnal cycle is >10x tectonic loading during the same period and critically stressed faults are rapidly destabilized during periods of highest semi-diurnal stress. Additionally, the overall seismicity rate increases when the maximum stress threshold is exceeded, a process correlated with the fortnightly period.

We find that earthquakes are correlated with tidal normal stresses indicating a moderate or high coefficient of friction in the shallow San Andreas Fault. That earthquakes are triggered during peak normal (extensional) tidal stresses suggests that pore pressures are below lithostatic pressure in the upper crust. These findings suggest tidal triggering can be applied to infer crustal stress state and pore pressure conditions, two properties of faults that are difficult to measure but are important for understanding earthquake physics and seismic hazards.



## The McAdam, New Brunswick Earthquake Swarm: Extremely Shallow, Natural Events

BENT, A. L., Geological Survey of Canada, Ottawa, ON, Canada, allison.bent@canada.ca; ADAMS, J., Geological Survey of Canada, Ottawa, ON, Canada, john.adams@canada.ca; BUTLER, K., University of New Brunswick, Fredericton, NB, Canada, kbutler@unb.ca; BURKE, K. B. S., University of New Brunswick, Fredericton, NB, Canada, kbsb@unb.ca; BROWN, J., University of New Brunswick, Fredericton, NB, Canada; HALCHUK, S., Geological Survey of Canada, Ottawa, ON, Canada, stephen.halcuk@canada.ca; PECI, V., Geological Survey of Canada, Ottawa, ON, Canada; HAYEK, S., Natural Resources Canada, Ottawa, ON, Canada, sylvia.hayek@canada.ca

In March 2012, hundreds of inhabitants of McAdam, New Brunswick reported feeling and/or hearing many earthquakes within a 1-2 km area of the village. The largest events ( $M_w < 2.0$ ) were recorded by regional seismographs, the closest being 65 km away. Because of the numbers of felt events, their localization, and public concern despite their small size, the Geological Survey of Canada (GSC) deployed weak and strong motion instruments at three sites about 1.5 km apart. The University of New Brunswick (UNB) later deployed a broadband seismograph at a fourth site. The GSC instruments were removed in August 2012 and the UNB instrument in January 2013. Activity largely died off by June 2012, but continued at a lower rate for a few months. There was a resurgence in activity late in 2015 with seven felt events occurring 7-9 December. The smallest felt event was  $M_w -1$ , and it is likely the 50+ events reported felt include many earthquakes of  $M_w < 0$ . In 2012, twenty-nine earthquakes, all reported felt and all with  $M_w < 1.8$ , were located, some by enough stations to allow precise depth determination. All the earthquakes were extremely shallow, 0.0-1.2 km. Epicenters lie in a WNW-ESE trending ellipse. A well-constrained composite focal mechanism indicated thrust faulting in response to regional NE-SW compression. A strong motion recorder recorded  $PGA=9\%g$  from a  $M_w \sim 1.0$  earthquake at about 0.8 km hypocentral distance. There was no human activity that could have induced or triggered the swarm. McAdam sits on Silurian metasediments intruded by the granitic Pokiok Batholith exposed just to the NW. No faults are mapped close to McAdam, but it might have occurred on a NW-SE splay of the Fredericton Fault. Further analysis to refine the depths, identify the rupture plane, and categorize events into families is underway. Swarms like this are probably common in eastern Canada, but are seldom this well reported or recorded.

## Communication Challenges Faced by Seismologists during Earthquake Swarm Periods

LAMONTAGNE, M., Geological Survey of Canada, Ottawa, ON, Canada, malamont@nrcan.gc.ca; FLYNN, B. W., Center for the Study of Traumatic Stress, Bethesda, MD, USA, brian.flynn@usuhs.edu; GOULET, C. A., SCEC, University of Southern California, Los Angeles, CA, USA, cgoulet@usc.edu

This session brings together a better understanding of earthquake swarms in terms of their physical and statistical properties. But when such swarm catches the public's attention, we, seismologists, face a difficult communications challenge. On the one hand, we don't want to create unnecessary anxiety, since most swarms eventually die off, but at the same time, we know that these events could be foreshocks of a larger, and possibly damaging, earthquake. What then is the seismologist to say that will remain within the scope of science while assisting the public and community leaders make appropriate choices related to unknown and potentially damaging future events? Probabilistic statements are scientifically verifiable but will provide little comfort to anxious people and will give no guidance about whether he/she should prepare or not to face an earthquake. We believe that the path out of these several dilemmas lies in the promotion of actions that allow individuals, families, and communities to acquire a sense of control and promote individual and collective efficacy, a key element of promoting resilience in a crisis. This way, seismologists can make use of a 'teachable moment', *i.e.* when people are ready to pay attention to, and take action based upon, useful and credible information. This course of action has the added benefit of enhancing positive response if an event does occur. We believe that the public is ready to accept the limitations of the Earth Sciences, especially if these limitations are paired with guidance that is reasonable, comforting, and makes logical sense. In addition, the public will respond well if science is delivered with a humane side. Based on these premises, we propose a typical message that should form the basis of press releases, web pages or tweets that we hope would be useful for seismologists who communicate during earthquake swarm periods.

## Seismicity and Seismic Hazards of the Walker Lane and Western Great Basin

Oral Session · Friday · 8:30 AM · 22 April · Tuscany A  
Session Chairs: John Anderson, John Louie, Richard Koehler, Corné Kreemer, and Wanda Taylor

### Fault Reactivation, Network Connectivity, and Strike-slip Deformation in the Transtensional Walker Lane

BRIGGS, R. W., Geologic Hazards Science Center, US Geological Survey, Golden, CO, USA, rbriggs@usgs.gov; STEPHENSON, W. J., Geologic Hazards Science Center, US Geological Survey, Golden, CO, USA, wstephens@usgs.gov; MCBRIDE, J. H., Department of Geological Sciences, Brigham Young University, Provo, UT, USA, john\_mcbride@byu.edu; GOLD, R. D., Geologic Hazards Science Center, US Geological Survey, Golden, CO, USA, rgold@usgs.gov; MCNAMARA, D. E., Geologic Hazards Science Center, US Geological Survey, Golden, CO, USA, mcnamara@usgs.gov

Detailed models of active fault networks are essential for generating the full range of plausible ruptures for probabilistic seismic hazard analysis (PSHA). The Walker Lane is a zone of distributed deformation east of the Sierra Nevada where normal faults are now reactivated in transtension. Despite 5-7 mm/year of dextral shear across the northern Walker Lane, throughgoing strike-slip faults have not been recognized at many latitudes and summed geologic slip rates underestimate geodetic slip rates. Historical Walker Lane ruptures, such as the 1932  $M 7.2$  Cedar Mountain earthquake, demonstrate the potential for highly distributed, multi-fault ruptures that link low-slip-rate faults in complex ways. We use legacy geophysical data, relocated seismicity, and fault surface trace mapping to assess the geometry and connectivity of the active northern Walker Lane fault network. Preliminary re-analysis of COCORP profile NV8 at  $\sim 40^\circ$  N shows previously unidentified coherent reflections within the Quaternary and Tertiary sedimentary basins along the transect. Closely-spaced, subparallel normal and strike-slip fault pairs imply that these faults intersect at shallow depths well within the seismogenic zone ( $< 12$  km), and we explore the potential for strike-slip deformation on moderately-dipping faults in the Walker Lane. We discuss examples where lateral or oblique slip on normal faults may give rise to basin-centered, distributed strike-slip deformation as a result of shallow strain partitioning. With the complexities of this reactivated fault network in mind, we outline central challenges to PSHA in the Walker Lane, including 1) considerable uncertainty in source-to-site distances for active faults in this zone of distributed deformation; 2) the ambiguous relationship of geodetically-measured surface strain to the complex fault network at depth; and 3) the potential for large ruptures to be distributed and involve multiple faults.

### Neotectonics Brings Interesting Challenges to the Assessment of Seismic Hazard in the Northern Walker Lane

WESNOUSKY, S. G., Center for Neotectonic Studies and Nevada Seismological Lab, Reno, NV, USA, wesnousky@unr.edu; PIERCE, I. K., Center for Neotectonic Studies and Nevada Seismological Lab, Reno, NV, USA, ian@nevada.unr.edu; MILAWSKY, E., Nevada Seismological Laboratory, Reno, NV, USA, elijahmlawsky@gmail.com; LOUIE, J., Nevada Seismological Laboratory, Reno, NV, USA, louie@seismo.unr.edu; KREEMER, C., Nevada Geodetic Lab and Nevada Bureau of Mines and Geology, Reno, NV, USA, kreemer@unr.edu; HAMMOND, W., Nevada Geodetic Lab and Nevada Bureau of Mines and Geology, Reno, NV, USA, whammond@unr.edu; FAULDS, J., Nevada Bureau of Mines and Geology, Reno, NV, USA, jfaulds@unr.edu; CARLSON, C., Nevada Bureau of Mines and Geology, Reno, NV, USA, ameanchad@hotmail.com; BRUNE, J.N., Nevada Seismological Laboratory, Reno, NV, USA; BORMANN, J. M., Nevada Seismological Laboratory, Reno, NV, USA

GPS defines the Walker Lane between Hawthorne and Reno as a northwestward oriented zone of about  $\sim 75$  km width that is accommodating  $\sim 5-7$  mm/yr of northwest directed right-lateral shear. The shear over time has resulted in cumulative right-lateral geologic offset of  $\sim 20-30$  km. There are though no major northwest striking strike-slip faults. The Walker Lane is instead characterized here by a generally en-echelon arrangement of the normal fault bounded Tahoe, Carson, Smith, Mason, Antelope, Bridgeport and Walker Lake basins. Reported geologic slip rates of the basin bounding faults are insufficient to account for the geodetically measured shear. These observations bring an interesting set of challenges to the assessment of seismic hazard in the area. The mismatch in geodetic versus geologic rates may be explained by inadequate geologic fault slip rate data, by the accommodation of slip by vertical-axis block rotations, or some measure of both. If vertical-axis rotations are important, the opening of basins will be asymmetric and slip rates may vary significantly along strike. It also remains problematic to

map geodetic strain rates into seismic hazard because the arrangement of mappable faults capable of producing large earthquakes is not continuous. Indeed, there are paths one may traverse across this latitude of the Walker Lane that do not intersect a significant mapped active fault. As a basis to illustrate these problems we present ongoing efforts and some initial findings resulting from collection and analysis of LIDAR for evidence of strike-slip along the major structures of the region, the application of cosmogenic, optically stimulated luminescence (OSL) and radiocarbon dating to identified offset surfaces to better quantify the rate at which faults are slipping in the region, and the collection of gravity and paleomagnetic observations to clarify both the current and long-term structural development of the basins and intervening fault blocks.

#### **Tectonic Evolution and Structural Framework of the Walker Lane: Implications for Seismic Hazards**

FAULDS, J. E., Nevada Bureau of Mines & Geology, University of Nevada, Reno, NV, USA, jfaulds@unr.edu; CARLSON, C. W., Nevada Bureau of Mines & Geology, University of Nevada, Reno, NV, USA, ameanhad@hotmail.com; HENRY, C. D., Nevada Bureau of Mines & Geology, University of Nevada, Reno, NV, USA, chenry@unr.edu; WESNOUSKY, S. G., Nevada Seismological Laboratory, University of Nevada, Reno, NV, USA, wesnousky@unr.edu

The Walker Lane (WL) and eastern California shear zone (ECSZ) accommodate ~20% (~10 mm/yr) of the Pacific-North America dextral motion. In contrast to the continuous 1100-km-long San Andreas fault, discontinuous ~5-250-km-long dextral and sinistral faults comprise the WL-ECSZ. Early-mid Miocene elimination of microplates along coastal southern California, S-ward steps in the Rivera triple junction, and an increase in plate motions induced deformation in the WL-ECSZ ~13 Ma along the N60°W Las Vegas shear zone (LVSZ). From ~13-6 Ma, the south part of the transform shifted east to the Gulf of California (GC), the Big Bend developed, and plate motions changed from N60°W to N37°W. The WL-ECSZ then shifted west ~11-6 Ma from LVSZ to a NNW belt in the western Great Basin. Here, dextral shear was favored as it paralleled plate motion, aligned with GC, and avoided the Big Bend bottleneck. By ~4 Ma, dextral shear propagated to the northern WL (NW Nevada) in concert with the N-ward migrating Mendocino triple junction.

The WL contains domains with contrasting structural styles. For example, the Pyramid Lake and Walker Lake domains consist of discrete NW dextral faults from ~50-100 km long. In contrast, the intervening Carson domain appears to lack major dextral faults but is instead dominated by a broad oroclinal flexure with fault blocks rotated up to 90° clockwise. The flexure accommodates >30 km of dextral shear, comparable to offset in the Pyramid Lake domain, and is accommodated by en echelon, closely-spaced E-W sinistral faults generally <20 km long. The shorter faults accommodating dextral shear suggest that larger earthquakes are less likely in the flexure than in areas with longer NW dextral faults. However, poorly understood boundaries of the Carson domain contain longer sinistral faults (e.g. Olinghouse fault), which may pose more significant hazards. Nonetheless, structural style and active fault lengths are critical in evaluating seismic hazards in the WL-ECSZ.

#### **Strong Ground Motions in Normal Faulting Earthquakes: Nevada, Japan, and Worldwide**

ANDERSON, J. G., Nevada Seismological Laboratory, University of Nevada, Reno, NV, USA, jga@unr.edu; KAWASE, H., Disaster Prevention Research Institute (DPRI), Kyoto University, Gokasho, Uji Kyoto, Japan, kawase.hiroshi.6x@kyoto-u.ac.jp; BIASI, G. P., Nevada Seismological Laboratory, University of Nevada, Reno, NV, USA, glenn@seismo.unr.edu

Hazard estimates in the eastern Great Basin and western Sierra Nevada region of Nevada and California have been developed by the USGS using the 2014 NGA West 2 models. Given the sensitivity of hazard to GMPEs, and considering the unique character of this region, it is worthwhile to consider whether the NGA models are optimal for this application. This paper will evaluate those models in the context primarily of recent data that postdates the cutoff date for the NGA West 2 database, with an emphasis on high frequencies.

First, the 2014 NGA models appear to be reasonably successful in a preliminary comparison to the Reno earthquake of Dec 23, 2015 (MW4.4). In contrast, the motions in the normal-faulting earthquakes in the Fukushima-Hamadori region of Japan are poorly predicted. Since the Fukushima Hamadori events are arguably the best-recorded normal faulting earthquakes, and there are 14 events over MW5 in the sequence, this discrepancy is a concern. Comparisons are complicated and multiple explanations for this discrepancy are possible: differences in stress drop, in crustal structure, in site response, or the potential that the average adjustments for normal-faulting mechanisms in the GMPEs have a regional dependence. We note that many of the normal-faulting data controlling the normal-faulting adjustments to the GMPEs come from European earthquakes,

so a global look at the data is required. This presentation will emphasize the use of wave-propagation models to reconcile the observations. Some preliminary observations are that the stress drop in normal-faulting events depends on depth, that the shape of the attenuation function with distance also depends on depth, and that wave propagation in a well-calibrated regional crustal model with an appropriate Q model is capable of modeling some systematic differences of the ground motion in different regions.

#### **Review of the Seismotectonics, Historical and Instrumental Seismicity of Nevada and Eastern California**

SMITH, K. D., Nevada Seismological Laboratory, University of Nevada, Reno, NV, USA, ken@unr.edu; RUHL, C. J., Nevada Seismological Laboratory, University of Nevada, Reno, NV, USA, cruhl@unr.edu; KENT, G. M., Nevada Seismological Laboratory, University of Nevada, Reno, NV, USA, gkent@unr.edu

Instrumental monitoring has seen revolutionary changes since the organization of regional networks under the USGS Advanced National Seismic System circa 2000. Nevada has a significant history of large earthquakes extending to the mid-late 1800s. From the early 1900s, through the mid-1950s, Nevada hosted no less than 7  $M \geq 6.5$  earthquakes since this period there has been a 60-year hiatus of  $M \geq 6.5$  earthquakes. Instrumental monitoring began at the Nevada Seismological Laboratory (NSL) in the 1960s with a handful of telemetered stations in the northern Nevada region. Digital processing began, along with other regional networks, in 1984 with NSL archiving waveform data through today. Digital seismograph station monitoring and the infrastructure to handle it was jump-started through NSL's participation in the DOE Yucca Mtn. project, which closed down in 2010. Recent growth in the number of high-quality broadband stations and a regional high-speed microwave has significantly improved response capabilities and the ability to closely monitor evolving earthquake swarms in Nevada that often evolve to include numerous  $M \geq 4$  earthquakes. Early analog monitoring systems would not have provided the data to closely monitor evolving earthquake sequences or illustrate the detail we now have in the magnitude completeness and spatial distribution of earthquake activity in the region. Since 1984, NSL has located 218,053 events within the region covered by our network, including 3  $M \geq 6.0$  (largest M6.3), 37 M5.0-5.9, and 354 M4.0-4.9. There have been 30,272  $M \geq 2.0$  earthquakes located since mid-1984. Significant earthquakes since 1984 include the 1986 Chalfant, 2008 M6.0 Wells, M5.7 Little Skull Mtn., and M5.6 Scotty's Junction events. NSL began routine regional surface wave moment tensor production in 2010 for all  $M \geq 3.5$  events, with 256 compiled to date. We summarize overall seismotectonics of the Nevada and eastern California region and highlight significant earthquakes.

---

#### **Risk Management Applications of Earthquake Seismology**

Oral Session · Friday · 10:45 AM · 22 April · Tuscany A  
Session Chairs: Delphine Fitzenz and Nico Luco

---

#### **Feedback from the 2015 ATC/USGS Seismic Hazard User-needs Workshop**

OLSEN, A. H., Applied Technology Council, Redwood City, CA, USA, aolsen@alumni.caltech.edu; LUCO, N., U.S. Geological Survey, Golden, CO, USA, nluco@usgs.gov; ROJAHN, C., Applied Technology Council, Redwood City, CA, USA, crojahn@atcouncil.org; POWERS, P. M., U.S. Geological Survey, Golden, CO, USA, pmpowers@usgs.gov

On September 21 and 22, 2015, the Applied Technology Council/U.S. Geological Survey (ATC/USGS) Seismic Hazard User-needs Workshop brought together over 100 geologists, engineers, and other professionals. The participants represented the broad and varied groups of professionals who use seismic hazard information developed by the USGS National Seismic Hazard Mapping Project. These users range from practitioners who do their own seismic hazard analyses to structural engineers to public-sector professionals who interpret seismic hazard in the context of public policy.

Several broad user needs emerged and were reiterated during the two-day workshop. There was no question of the need for the work that the National Seismic Hazard Mapping Project does, including the collection and assessment of geological studies, ground motion models, and hazard algorithms formalized as seismic hazard models as well as the user support provided by the Project personnel. The seismic hazard products available at the Project's website are essential to most user groups; the more technical users routinely use the Quaternary fault, hazard curve, deaggregation, and United States design maps tools. These users emphasized the importance of the timely update of the online hazard products and documentation for their work. Users also identified the need for earthquake



scenarios or deterministic ground motions, which the Project currently develops only for a limited number of uses. Earthquake scenarios would be used by technical and non-technical users, and the description of seismic hazard as a suite of deterministic ground motions could augment probabilistic hazard values, providing a parallel way to understand and communicate seismic hazard.

This presentation summarizes suggestions for improvements to the transfer of seismic-hazard knowledge and numerical values from the USGS National Seismic Hazard Mapping Project to the wider seismic hazard community.

**Project '17: Balancing Precision in Ground Motion Mapping with Uncertainty**  
HAMBURGER, R. O., Simpson Gumpertz & Heger, San Francisco, CA, USA, rohamburger@sgh.com; LUCO, N., U.S. Geological Survey, Golden, CO, USA, nluco@usgs.gov

In 1997, the U.S. Geological Survey (USGS) and Building Seismic Safety Council (BSSC) collaborated to develop seismic design maps for the 2000 International Building Code. The Project '97 spectral acceleration contour maps have since served, with periodic revisions (in 2003, 2009, and 2015), as the basis for seismic design procedures in the U.S. Earlier maps used broad zonation, with the zones relating to ground motion in an approximate manner. Zone 4 design effective peak ground acceleration was declared, over a broad region, to have a value of 0.4g. Values in other zones were taken as fractions of this. Engineers understood these design accelerations were approximate. Regardless, the values could be used for design of most structures and changed relatively infrequently. The Project '97 contour maps specified acceleration in 0.05g increments and, with interpolation, engineers derived design values with greater apparent precision. With continued research, the ground motion prediction equations used to produce the maps and the earthquake source characteristics changed. Mapped design acceleration values fluctuated, with  $\pm 20\%$  changes common, creating a lack of confidence among users. More troubling still was the yo-yo effect in which mapped values would first rise then fall. Most recently, an American Society of Civil Engineers committee initially rejected the 2014 edition of the maps based on a belief that the information portrayed was not substantially more valid than that contained in earlier editions. Dissatisfaction with the maps can be attributed to: lack of appreciation of the uncertainty underlying mapped values; 2) design procedures that treat the mapped values as highly certain; and 3) a mapping process that results in significant change in mapped values with each update. Project '17, a new joint USGS-BSSC project, is considering these and other issues and preparing recommendations for the next generation of maps to be incorporated into building codes.

#### Effects of Epistemic Uncertainty in Seismic Hazard Estimates on Building Portfolio Losses

KOTHA, S. R., GeoForschungsZentrum Potsdam, Potsdam, Germany, sreeram@gfz-potsdam.de; BAZZURRO, P., Istituto Universitario di Studi Superiori—IUSS, Pavia, Italy, paolo.bazzurro@iusspavia.it; PAGANI, M., GEM Foundation, Pavia, Italy, marco.pagani@globalquakemodel.org;

In catastrophe risk modeling, a defensible estimation of impact severity and its likelihood of occurrence can only be made through a rigorous treatment of uncertainty and the consideration of multiple alternative models. To limit the demand on computational time and resource, a frequent practice in the industry is to estimate the distribution of earthquake-induced losses using a simulated catalog of events from a representative mean ground motion hazard model for the region without epistemic uncertainties. This simplified approach is faster but may underestimate the likelihood of occurrence of the large losses that drive many decisions. Investigation through case studies on different portfolios of assets located in San Francisco Bay Region shows the potential for both a bias in the mean loss estimates and an underestimation of their central 70% inter-percentile ranges (between 15th and 85th empirical quantiles). An alternative simplified and computationally practical approach that removes or reduces such a bias in mean is proposed, which however did not show improvement in estimated inter-percentile range.

The original idea for this study was conceived several years ago during a discussion of one of the authors with Dr. Nesrin Basöz of GeoVera, Her contribution is gratefully acknowledged. This work also benefitted from the discussions with Dr. Nilesh Shome of RMS and Dr. Mario Ordaz of ERN. Most of the analytical work was done in 2013 at Understanding and Managing Extremes (UME) Graduate School, Pavia, Italy

#### Seismic Site Characterizations and Earthquake Loss Estimation Analyses for 25 Schools in Thurston County, Washington State

CAKIR, R., WADNR—Division of Geology and Earth Resources, Olympia, WA, USA, recep.cakir@dnr.wa.gov; WALSH, T. J., WADNR—Division of Geology and Earth Resources, Olympia, WA, USA, tim.walsh@dnr.wa.gov; HAYASHI, K., Geometrics Inc., San Jose, CA, USA, khayashi@geometrics.com;

NORMAN, D. K., WADNR—Division of Geology and Earth Resources, Olympia, WA, USA, dave.norman@dnr.wa.gov

The mission of The Washington Department of Natural Resources—Division of Geology and Earth Resources is to “reduce or eliminate risks to life and property from natural hazards.” We conducted active and passive seismic surveys, and estimated Shear-wave velocity ( $V_s$ ) profiles, then determined the NEHRP soil classifications using calculated  $V_{s30m}$  values at 25 public school sites in Thurston County, Washington. We conducted active and passive surveys: 1D and 2D MASW and MAM, P- and S-wave refraction, horizontal-to-vertical spectral ratio (H/V), and 2ST-SPAC to measure  $V_s$  and  $V_p$  at shallow (0-70m) and greater (10 to 500 or 10 -3000 meters) depths at the sites. We then ran Ground Penetrating Radar surveys along each seismic line to check possible horizontal subsurface variations between the survey line and the actual location of the school buildings. We estimated, 1D and 2D shear-wave velocities, 2D  $V_p$ ,  $V_p/V_s$  for top 30 to 70m depth range, and shear-wave velocities at depths (>30m) by using passive single-station (H/V) and array (MAM and/or 2ST-SPAC) measurements. These survey results were then used for calculations of  $V_{s30m}$  for determining the NEHRP site classifications; soil classes C and D were found at 12 and 13 school sites, respectively. These site classes were also used for determining soil amplification effects on the ground motions affecting structural damage estimations of the school buildings. The detailed  $V_s$  information can be used for further earthquake site response analyses. These seismic site characterization results associated with structural engineering evaluations were then used as inputs in FEMA Hazus-Advanced Engineering Building Module (AEBM) analysis to provide estimated casualties, nonstructural, and structural losses. Damage estimations from the Hazus-AEBM analysis can be used to prioritize future mitigation of the schools exposed to potential nearby and regional earthquakes.

#### Quantifying the Location, Width, and Style of Coseismic Surface-Fault Displacement at Gas Transmission Pipeline Fault Crossings in Northern California

GIVLER, R., Lettis Consultants International, Inc., Walnut Creek, CA, USA, givler@lettisci.com; HULL, A., Golder Associates, Redmond, WA, USA, ahull@golder.com; MADUGO, C., Pacific Gas & Electric Company, San Francisco, CA, USA, c7m0@pge.com; LIFTON, Z., Golder Associates, Redmond, WA, USA, Zachery\_Lifton@golder.com; LEWANDOWSKI, N., Lettis Consultants International, Inc., Walnut Creek, CA, USA, lewandowski@lettisci.com; THOMPSON, S., Lettis Consultants International, Inc., Walnut Creek, CA, USA, Thompson@lettisci.com; LOWRY, D., Golder Associates, Lakewood, CO, USA, Donald\_Lowry@golder.com

Pacific Gas and Electric Company maintains a program to evaluate the integrity of their gas transmission pipeline network where pipelines intersect mapped Holocene-active faults. In 2015, this program evaluated 63 pipeline fault crossings across 10 faults, a significant increase from previous years. These studies synthesized available geologic data to provide defensible assessments of the location of fault strands at the pipeline crossing and the probable width, style, and distribution of future coseismic deformation. A logic-tree-based deterministic fault displacement hazard analysis developed for this program (see companion abstract by Thompson *et al.*) used multiple fault parameters to estimate coseismic displacement. These displacement values were the basis for an analysis of post-earthquake gas pipeline pressure integrity using finite element pipe stress analysis. A challenge of the 2015 effort was that it included a wide range of fault activity rates, which varied from high slip rate faults (*e.g.*, Concord, Calaveras, Green Valley, and San Andreas faults) to low slip rate faults (<1 mm/yr) (*e.g.*, Clayton, Cordelia, and Pleasanton faults). The availability of site-specific data also varied considerably from very good (*e.g.*, nearby measurements of surface displacement from historic earthquakes) to little or no reliable information. These uncertainties were addressed through additional subsurface investigations, especially where reducing uncertainty had a clear impact on the engineering outcomes. In most cases the lack of site specific data (and/or the inability to collect more data) resulted in larger uncertainties and broader fault hazard zones. The keys to providing quality geologic information are to focus on (1) a transparent synthesis of geologic data (including a reasonable consideration of uncertainty) and (2) targeting field investigations to reduce uncertainty where new data may significantly impact the integrity assessments.

#### Risk Model for a System-Wide Dam Risk Reduction Program in Northern California

WOODDELL, K., Pacific Gas and Electric Company, San Francisco, CA, USA, KxWl@pge.com; DONAHUE, J., Geosyntec Consultants, San Francisco, CA, USA, jdonahue@geosyntec.com; WATSON-LAMPREY, J., Watson-Lamprey Consulting, Berkeley, CA, USA, jennie.watsonlamprey@gmail.com; ABRAHAMSON, N., Pacific Gas and Electric Company, San Francisco,



CA, USA, NAA2@pge.com; ABRAMSONWARD, H., Lettisi Consultants International, Walnut Creek, CA, USA, hans@lettisci.com; LEWANDOWSKI, N., Lettisi Consultants International, Walnut Creek, CA, USA, lewandowski@lettisci.com; MADUGO, C., Pacific Gas and Electric Company, San Francisco, CA, USA, C7M0@pge.com; THOMPSON, S., Lettisi Consultants International, Walnut Creek, CA, USA, thompson@lettisci.com

Pacific Gas and Electric (PG&E) has initiated a long-term program to quantify and manage the seismic risk to its hydroelectric system that includes 167 dams located in Northern California. A key issue for seismic risk studies is the large epistemic uncertainties in the estimated risk values. The first stage of this program is to perform a system-wide risk analysis including epistemic uncertainties in the risk estimates. The results will be used to rank PG&E's dams in terms of risk as well as quantify our confidence in our ability to resolve the differences in the risk between different dams. The goal is to use the risk ranking to prioritize risk mitigation efforts as part of a long-term risk reduction program. Most of PG&E's dams are in northeastern California and the national hazard maps do not have enough resolution of the faults in this region to meet PG&E's needs. Therefore, probabilistic seismic hazard analyses were performed for 167 dams using an updated seismic source model that captures the faults in the region and the epistemic uncertainties. (see companion abstract by Madugo *et al.*) Fragilities for dams are not usually developed in practice. In the initial risk evaluation, simplified fragilities based on proxies for the deformation of the dam are used. Rapid, simultaneous computation of seismic hazard for all dams is accomplished utilizing Amazon Web Services cloud computing and a system-wide fault description as the source input for each dam. "Tornado plots" showing the sensitivity of the risk and ground motion at the 10-3 and 10-4 hazard levels are used to identify the dam response, ground motion, and source characterization parameters that contribute the greatest uncertainty to the risk calculations. This list will be used to prioritize future seismic research that will lead to the greatest reduction in uncertainty in seismic risk at PG&E's dams.

#### **Modeling Community Disaster Resilience for Optimal Investment Strategies**

VAN DE LINDT, J. W., Colorado State University, Fort Collins, CO, USA, jvw@enr.colostate.edu; ELLINGWOOD, B. R., Colorado State University, Fort Collins, CO, USA, Bruce.Ellingwood@colostate.edu

Modeling the resilience of communities exposed to natural disasters depends on many disciplines including engineering, economics, sociology, and computer sciences. No one discipline has the ability to model resilience comprehensively; moreover, the measurement science necessary to support resilience assessments on a community scale does not exist. Thus in 2015 the U.S. National Institute of Standards and Technology (NIST) established the Center for Risk-Based Community Resilience Planning (CoE) headquartered at Colorado State University and including researchers from nine additional universities. The overarching goal is to establish the measurement science for community resilience assessment through three major research thrusts. Thrust 1 is developing a multidisciplinary computational environment with fully integrated supporting databases (NIST-CORE) which will enable the factors that determine community resilience to be fully understood. Nontechnical systems—financial, social and political institutions, healthcare, education, public administration—are being integrated, creating a nexus between social and technological infrastructure systems. Thrust 2 will produce a standardized data ontology, a robust data architecture, and effective data management tools to support this computational environment and permit databases from stakeholders to be integrated seamlessly. Thrust 3 will validate the data architecture through a series of testbeds. In this presentation, the science needed to model the resilience of a community will be introduced and explained in common terminology with the intent of making a business case for the sharing of risk-informed investment decisions between the private and public sectors. The CoE is beginning year 2 of 5 and therefore will be limited to damage, loss, and recovery trajectories based on the CoE's current state of progress as of April 2016.

#### **Case Studies of Financial Decision-Making using Near-Real-time Post-Earthquake Information**

WALD, D. J., U.S. Geological Survey, Golden, CO, USA, wald@usgs.gov; WORDEN, C. B., U.S. Geological Survey, Golden, CO, USA, cworden@usgs.gov; THOMPSON, E. M., U.S. Geological Survey, Golden, CO, USA, emthompson@usgs.gov; FRANCO, G., Guy Carpenter, London, UK, guillermo.e.franco@guycarp.com

Post-earthquake financial decision-making has evolved considerably over the past decade. In part, the advancement of post-earthquake financial instruments has been facilitated by the availability of rapid and accurate earthquake parameters and more quantitative geospatial hazard information. Insurers and reinsur-

ers, other private companies, governments, and aid organizations have shown increasing creativity in the utilization of near-real-time earthquake information for loss estimation, financial adjudication, and situational awareness. Such financial analyses can be of significant benefit to stakeholders, facilitating risk transfer, fostering sensible management of risk portfolios, and assisting disaster responders. Ultimately, these improvements can translate to benefits for the public at-risk. Three general categories of post-earthquake financial services and decision-making are described: 1) analysis of expected losses arising from an actual event against a portfolio of exposures, 2) triggering of payments for parametric insurance products, and 3) the use of quantitative loss estimates to manage disaster response and aid. Specific aspects of USGS earthquake information products are described that accommodate specific requirements of the financial sector and facilitate new and refined financial instruments. These developments include the generation of suites of standardized earthquake scenarios, both domestic and international; implementing directivity and spatial ground motion correlations; improved quantification of uncertainties; real-time product and data feeds; and a more explicit ShakeMap policy for version control and metadata. Financial decision-making case histories will be described, including examples for the Inter-American Development Bank, the California Earthquake Authority, and triggering strategies for several catastrophe bonds.

#### **Use of Seismic Data and Information in Validation of Natural Catastrophe Models and Other Applications in the Insurance Industry**

KARACA, E., AIG, New York, NY, USA, erdem.karaca@aig.com; ASLANI, H., AIG, New York, NY, USA, hesaam.aslani@aig.com

Natural catastrophe models have become essential tools for the insurance industry and are currently being used for various business applications including risk selection, pricing, management, and transfer. Robust quantification of risk, both at a specific location and across a portfolio of locations, is key to long-term profitability of insurance companies exposed to natural catastrophes such as earthquakes. As a result, many insurance companies heavily rely on internally or externally developed catastrophe models in their underwriting and risk management processes. Also, there is growing business interest and regulatory requirements for rigorous review and validation of both internal and external catastrophe models and quantification of associated uncertainties.

Development and validation of these models require detailed data (or component models where data is scarce) related to frequency and severity of underlying natural catastrophes, which is a unique challenge for earthquakes due to their infrequent nature relative to other catastrophes such as tropical cyclones. Data and information utilized range from historical earthquake catalogs to probabilistic rupture models for individual faults to ground motion prediction models for specific types of earthquakes. While some of this information is readily available and usable for some regions, there is significant variation in quality of seismic data, models and/or their documentation in other regions.

In this contribution, we present a number of case studies from the US and Japan illustrating use of seismic data and information in model validation studies. In case of the US, we highlight the importance of availability of alternative earthquake recurrence and ground motion models and present sensitivity of risk metrics used in insurance industry to these alternative models. In case of Japan, we focus on time-dependent modeling of major seismic sources and illustrate the impact of underlying assumptions on model outcome.

#### **Building an Earthquake Source Model for Hazard and Risk**

PORTO, N. M., Risk Management Solutions, Newark, CA, USA, natanya.porto@rms.com

Source models are used to calculate loss estimates from potential earthquake damage. This information helps set premiums and assess risk. When available, risk models are based on current hazard models, for example 2014 NSHM and UCERF3. However, hazard maps are often outdated, or simply unavailable for many regions globally. In these regions, we must build a source model from the ground up using the best available science. A typical source model consists of several components, which can include: background seismicity, crustal faults, and a subduction zone (if applicable). For background seismicity we need an earthquake catalog, magnitude length/area scaling relations, and preferential tectonic orientations. The earthquake catalog must be declustered, and completeness intervals known. For crustal faults we need geometry and rate. Fault traces can be obtained from geologic maps, or digital databases, but connectivity and depth needs to be inferred. Earthquake recurrence is typically determined from the slip/event rate of the fault. However, geologic slip rate is often poorly constrained or unknown, and can differ from geodetic rates. A subduction zone is also modeled using rate and geometry (often inferred from tomography and focal mechanisms). Rates are typically calculated from the earthquake catalog (a & b values) or using a characteristic model based on reoccurrence (paleoseismology). Presently, there

is no standard process for building a source model. Methods for: earthquake catalog declustering, simplifying fault geometry, and paleoseismology slip rates, are often different study by study. The quality and consistency of each of these pieces ultimately determines the accuracy of the final hazard and risk calculations. Therefore, a set of guidelines should be proposed for both reporting and implementing source model components, guidelines that would allow for a standardized modeling approach that could be updated in each iteration with the best available science.

### **A New Seismic Hazard Model for Loss Estimation in the Conterminous United States: Beyond the National Seismic Hazard Map**

THENHAUS, P. C., CoreLogic, Inc., Oakland, CA, USA, pthenhaus@corelogic.com; CAMPBELL, K. W., CoreLogic, Inc., Oakland, CA, USA, kcampbell@corelogic.com; GUPTA, N., CoreLogic, Inc., Oakland, CA, USA, ngupta@corelogic.com; SMITH, D. F., CoreLogic, Inc., Oakland, CA, USA, dfsmith@corelogic.com; KHATER, M. M., CoreLogic, Inc., Oakland, CA, USA, mkhater@corelogic.com

We developed a new seismic hazard model for loss estimation in the conterminous United States that is based primarily on hazard models developed by the 2014 USGS Seismic Hazard Mapping Project and the Working Group on California Earthquake Probabilities (WGCEP) Uniform California Earthquake Rupture Forecast, Version 3 (UCERF3) Project. Going beyond the USGS and WGCEP, these models are augmented with specific enhancements for purposes of economic loss estimation and risk management. For example, they are used to develop a stochastic event set that is based on a temporal simulation methodology that preserves event-clustering on the New Madrid fault zone. Both time-independent and time-dependent probability models are provided for the UCERF3 fault model and the Cascadia megathrust subduction faults to allow examination of the impact of time-dependency on expected losses in these regions. The latest ground-motion prediction equations (GMPEs) are used to estimate probability distributions of ground motion in each tectonic domain (*i.e.*, western U.S., subduction interface, subduction intraslab [Wadati-Benioff zone], and central and eastern U.S.). These include the 2014 NGA-West2 GMPEs that incorporate updated, enhanced ground-motion effects such as nonlinear soil behavior, hanging-wall effects, and basin response in addition to the standard seismic parameters of magnitude, distance, mechanism, and site response. Site amplification is included using the latest (2015) NEHRP site factors combined with a detailed national soil map and the latest soil data for California. In addition, sedimentary basin amplification is modeled in California and Puget Sound using available depths to the 1.0 and 2.5 km/sec shear-wave velocity horizons. Soil liquefaction and seismically-induced landslide hazards are incorporated as secondary perils using probabilistic global geospatial models that provide enhanced estimates of loss that go beyond consideration of earthquake shaking damage alone.

### **Understanding Science and Its Limitation in Catastrophe Modeling Through Robust Simulation**

LEE, Y., ImageCat, Inc., Long Beach, CA, USA, yjl@imagecatinc.com; WILLIAM, G., ImageCat, Inc., Long Beach, CA, USA, wpg@imagecatinc.com

Catastrophe modeling for natural disasters is widely used for risk mitigation and insurance pricing. Catastrophic events, however, inherently involve small probabilities but large socioeconomic consequences. The physical process of the natural hazards and system response are highly complex and never fully understood. Competing models or sub-models are common. To more completely account for the scientific uncertainty, a multiple-model approach is usually employed through one or more logic trees. Propagating uncertainties is complex, and closed-form solutions for the distributions of consequences are difficult or impossible to obtain. Conventionally, the emphasis is placed on reporting the consensus “mean” in hazard or risk assessment, and the uncertainty associated with alternative models is typically obscured. Although a single, merged representation is certainly desired, such an artificial “mean” hazard or risk assessment may significantly understate the potential for extreme consequences and leave decision makers with a false sense of security facing future catastrophe losses. Therefore, comprehensive characterization and communication of scientific uncertainty associated with multiple model approach is an essential step toward a more robust decision process.

Robust Simulation is a methodology and technology that develops estimates of catastrophic consequences through efficient sampling techniques and overcomes the weaknesses in conventional catastrophe modeling approaches, such as insufficient characterization of scientific uncertainty, lack of model transparency, overly complex but sometimes grossly inaccurate statistical treatment, computational inefficiencies, etc. In this study, we deploy a “Robust” version of the USGS 2014 NSHM models for hazard and risk analysis. Uncertainty arising through multiple scientifically credible models is preserved throughout the

modeling process and presented as an essential part of assessed seismic hazard and risk results.

### **Pinpointing the Cost of Natural Disasters: Local Devastation and Global Impact**

BOLTON, M. K., CoreLogic, Inc., Oakland, CA, USA, mbolton@corelogic.com; LARSEN, T., CoreLogic, Inc., Oakland, CA, USA, tlarsen@corelogic.com; DAVID, K. M., CoreLogic, Inc., Oakland, CA, USA, kdavid@corelogic.com

The 2011 Tohoku-oki earthquake caused in excess of \$200 billion in economic damages. For comparison, a single earthquake in California could cause over \$600 billion in economic damages. Insurance coverage of risk has not kept up with the increasing concentration of economic assets in natural-catastrophe-prone areas, leaving a void in coverage and the potential for extended disruption and delayed economic recovery. Business interruption risks from both the Tohoku-oki earthquake (Japan) and the Bangkok, Thailand floods of 2011 clearly demonstrate the linkage of regional events to the global economy and the systemic importance of ensuring rapid recovery.

A magnitude (M) 7.3 earthquake on the Puente Hills Fault underneath Los Angeles (LA), California is used as the basis of a case-study to examine a modeled view of the losses occurring from a large event. We identify and quantify economic impacts deriving from such an event that will impact a sector of the economy not traditionally discussed in this context. Recognition followed by quantification are key steps in mitigating long term negative impacts from earthquakes.

### **Systematic Generation of USGS Earthquake Scenarios**

THOMPSON, E. M., USGS, Golden, CO, USA, emthompson@usgs.gov; FIELD, N., USGS, Golden, CO, USA, field@usgs.gov; LUCO, N., USGS, Golden, CO, USA, nluco@usgs.gov; PETERSEN, M. D., USGS, Golden, CO, USA, mpetersen@usgs.gov; POWERS, P. M., USGS, Golden, CO, USA, pmpowers@usgs.gov; WALD, D. J., USGS, Golden, CO, USA, wald@usgs.gov; WORDEN, C. B., Synergetics, Inc., Ft Collins, CO, USA

The USGS often receives requests for scenario ShakeMaps. A ShakeMap scenario is a specific realization of the ground motion and impacts from a conceivable earthquake, such as those defined by the National Seismic Hazard Mapping Project, rendered as a ShakeMap and accompanied by standard ShakeMap products (*e.g.*, FEMA’s Hazus input files). We address two challenges for the routine production of ShakeMap scenarios: 1) There is currently no systematic framework for generating, delivering, or documenting the ShakeMap scenarios provided to users, and 2) there are differences in the shaking calculations in ShakeMap and the National Seismic Hazard Map. Our goal is to develop a framework for generating scenarios that address the needs of the vast majority of scenario users in terms of event selection, hazard calculation, documentation, metadata, and delivery. A challenging task is in defining an acceptable event set. Unlike in a probabilistic analysis, not all possible events can be included. For most scenario applications, it is not desirable to include all possible ruptures on the same fault from, for example, variations in the rupture extent, smaller magnitudes, or extremely rare multi-fault ruptures. However, the scenarios should include events that reflect recently relaxed fault segmentation rules, such as those in version 3 of the Uniform California Earthquake Rupture Forecast. In addition, multiple realizations of each specific fault rupture are required to represent reasonable variations in rupture directivity and the spatial distribution of shaking, which systematically affect loss calculations. As needed for some user applications, the event metadata must include information on the slip rate of the rupturing faults and the likelihood that the scenario could occur within a specified time span. This presentation provides an initial strategy for generating ShakeMap scenarios and seeks community input on how this framework can be modified to best suit users’ needs.

### **Potential Impacts of the Wasatch Fault on Salt Lake City, Utah: A Risk Analysis**

WILLIAMS, C. R., RMS, Newark, CA, USA, Chesley.Williams@rms.com; FITZENZ, D. D., RMS, Newark, CA, USA, Delphine.Fitzenz@rms.com

The Wasatch Fault is a key driver of seismic risk for Salt Lake City, Utah. We are developing an updated seismic risk model based on the most recent update to the National Seismic Hazard Maps. This model will include a stochastic event set of potentially damaging events, the latest ground motion prediction equations (*i.e.*, NGA-West2), detailed building exposure values, comprehensive information about primary construction characteristics (*i.e.*, construction, height, age) and spectral acceleration based building fragility curves. For the stochastic event set, the model produces losses at a detailed grid resolution. This allows for detailed spatial comparisons of key source modeling assumptions (*e.g.*, dip angle) on resulting losses.

A key component of the loss modeling is the estimation of exposure values and primary building characteristics. This loss analysis is focused on losses to property (*i.e.*, structures and contents) and includes a break down between residential, commercial and industrial exposure values and characteristics. The exposure values were developed based on a number of data sources including the U.S. census, Dun & Bradstreet and TomTom.

This presentation will include several risk results. We will summarize the characteristics of the events that cause damage in the Salt Lake City region. Key events on the Wasatch Fault will be examined in more detail showing the impacts of modeling assumptions such as magnitudes, dip angle, partial versus full versus floating rupture characterizations.

In addition to the source characterization for the Wasatch Fault from the National Seismic Hazard Maps, the model in development will include time dependent recurrence modeling assumptions. This presentation will include both the time dependent and time independent perspectives for recurrence. This impact on the risk results from these two perspectives will be presented as annualized and return period loss levels.

---

## Active Tectonics, Faults and Large Earthquakes

Poster Session · Friday · 22 April · Tuscany F

---

### Site Amplification Model Dependent on Site Natural Frequency and Sharpness of H/V peak using Ground Motions from Japanese NIED Network

KWAK, D. Y., UCLA, Los Angeles, CA, USA, [duckkwak@g.ucla.edu](mailto:duckkwak@g.ucla.edu); PARK, D., Hanyang University, Seoul, Korea, [dpark@hanyang.ac.kr](mailto:dpark@hanyang.ac.kr); STEWART, J. P., UCLA, Los Angeles, CA, USA, [jstewart@seas.ucla.edu](mailto:jstewart@seas.ucla.edu)

We present a site-specific site amplification model by adding a new term to an existing proxy-based site amplification model from NGA West2 project (called SS14; Seyhan and Stewart, 2014) using ground motions from Japanese NIED networks (K-NET and KiK-Net). The new term is proposed using the site natural frequency and the sharpness factor which are developed from the ratio of horizontal-to-vertical (H/V) components on surface motions. The sharpness factor reflects the sharpness of H/V peak, which is proposed in this study. It is known that the peak frequency of H/V is well correlated with the site natural frequency, whereas its amplitude is underestimated to the amplitude of the site amplification. As a result, the resulted peak frequency is widely used for the application of site characterization, but the sharpness of the peak or the presence of multiple peaks are rarely used or not well constrained for site amplification model in existing studies. In this study we consider both the peak frequency and sharpness of H/V as well as the presence of multiple peaks for the estimators of a site amplification model, which indeed have correlations to the site amplification. We parameterize the shape of H/V ratio by fitting one pulse for a single peak or two pulse functions for multiple peaks, and the sharpness factor is obtained from those parameters for each peak. The shapes of residuals (*i.e.*, data-based site amplification—SS14) are also parameterized by fitting the same format of pulse functions. The data-based site amplification is estimated using non-reference site approach (*i.e.*, the ratio of recorded surface intensity measures to inferred intensity measures for a reference rock condition). We fit a model to the parameters of the shapes of residuals as a function of site natural frequency and sharpness factor. The fitted model is added to SS14, which reduces the standard deviation of errors and better follows the trend of the data-based site amplification.

### Three Dimensional Earthquake Ground Motion Simulation for the Bengal Basin Region

HUDA, M. M., CERl, University of Memphis, Memphis, TN, USA, [mmhuda@memphis.edu](mailto:mmhuda@memphis.edu); TABORDA, R., CERl, University of Memphis, Memphis, TN, USA, [rtbrdros@memphis.edu](mailto:rtbrdros@memphis.edu)

This study presents the first-step results of a project with the goal of studying the ground motion characteristics of the Bengal Basin region in Bangladesh, south Asia, through physics-based, deterministic earthquake simulation. Given the scarcity of data in the region, simulation can help understand the expected response of the ground during earthquakes and its relationship with the deep sedimentary structure of the Bengal basin. Bangladesh is one of the most densely populated countries in the world, with more than one thousand people per square mile, and several cities exceeding a few millions inhabitants most of whom live in poorly constructed buildings. The country land is shaped by the Ganges delta—the largest delta system in the world, which rests over a sedimentary structure with thicknesses that can reach up to 20 km and is dominated by the different orogeny systems created by the collision between the Indian, Eurasian and Burmese tectonic plates. The region is bounded by the Dauki fault to the north

and north-east, the Bogra fault on the stable shelf region, boundary thrust faults in the Chitragong-Tripura fold belt region to the east, and the Madhupur fault and some other ambiguous faults inside the basin. For this study, we developed a first version of the three-dimensional velocity model based on available geological and geophysical information as an initial approximation. Using this initial model results and using a finite element parallel code, we produced a series of simulations based on past earthquakes. The simulations are done for low-frequency (<0.5Hz). The results are compared qualitatively with ground motion data from a few local earthquakes. Using these initial results we investigate the influence of basic features such as fault boundaries and basin depth on the end surface motion, and shed light over future steps necessary to better characterize earthquake ground motions in the region.

### Design and Efficacy of a Theory-based Intervention Intended to Motivate Seismic Risk Reduction in Nepal

SANQUINI, A. M., GeoHazards International, Menlo Park, CA, USA; THAPALIYA, S. M., Stanford University, Stanford, CA, USA; WOOD, M. M., California State University, Fullerton, Fullerton, CA, USA

Schools in Nepal bear extreme earthquake risk given the vulnerability of their structures and exposure to high seismic activity. A theory-based educational and motivational film in which Nepalese individuals described how and why they seismically retrofitted their local schools was developed, tested, and found to significantly increase: (1) knowledge of earthquake-resistant construction methods, (2) confidence in efficacy of such construction methods, (3) intention to financially support such construction, and (4) intention to recommend building earthquake resistant homes to others. This increase is statistically significant based on a matched-pair cluster randomized, controlled trial design with a test audience of 761 adults from 16 Kathmandu Valley schools in need of seismic work, using a 25-item survey instrument developed for this purpose. Our results support the theory of communicating actionable risk, which posits that people will take preparedness action when they know what to do, think it would work, and receive social cues such as knowing peers who took the affected action. Locals who had participated in making their own schools earthquake resistant were cast as peer role models in the film. We avoided using fear-based appeals, which may trigger maladaptive behavior when not accompanied by equally strong efficacy messages. Data collection was completed March 21, 2015, just five weeks before the magnitude 7.8 Gorkha earthquake struck central Nepal, collapsing thousands of vulnerable buildings, including school buildings. Schools depicted in the film had been strengthened before the disaster struck however, and survived the earthquake. To aid the reconstruction effort, the intervention film was updated with post-earthquake return visits to these schools, and released in Nepal. An English subtitled version may be viewed at <https://www.youtube.com/watch?v=KBxpAro1vU>.

### Geodetically-constrained Interseismic Deformation and Fault Activities in Southwestern Taiwan

HUANG, M., Jet Propulsion Laboratory, Pasadena, CA, USA, [mong@berkeley.edu](mailto:mong@berkeley.edu); EVANS, E., US Geological Survey, Menlo Park, CA, USA, [eevans@usgs.gov](mailto:eevans@usgs.gov); BURGMANN, R., UC Berkeley, Berkeley, CA, USA, [burgmann@seismo.berkeley.edu](mailto:burgmann@seismo.berkeley.edu)

Plate convergence at more than 80 mm/yr makes Taiwan one of the most active tectonic regions in the world. In this study, we use ascending and descending Interferometric Synthetic Aperture Radar (InSAR) data to reveal interseismic crustal deformation in western Taiwan. We combine GPS data from prior to the 1999  $M_w$  7.6 Chi-Chi earthquake with InSAR and GPS measurements from 2006-2010 to create a block model of interseismic crustal deformation. Geodetic observations show 20-40 mm/yr southwestward motion in the Pingtung plain relative to western Taiwan that indicates tectonic escape due to plate collision, and more than 10 mm/yr uplift in the southern part of the Western Foothills. We use a total variation regularization (TVR) algorithm to algorithmically assess the best-fitting block geometry based on the geodetic observations, simultaneously estimating block rotations and fault slip rates on block-bounding faults. The block model results imply that faults along the margins of the Western Foothills accommodate most of the interseismic deformation in southwestern Taiwan. In addition, both modern and Holocene river erosion rates show higher correlation with interseismic fault slip rates than with coseismic fault slips in southwestern Taiwan. Our results imply that, although large earthquakes could enhance sediment transport in a short period of time, higher interseismic slip rates lead to uplift and greater erosion rates on a longer time scale.

### Updating the Hawaii Source Model for Hazard and Risk

PORTO, N. M., Risk Management Solutions, Newark, CA, USA, [Porto@rms.com](mailto:Porto@rms.com); APEL, E. V., Risk Management Solutions, Newark, CA, USA,



Trey.Apel@rms.com; SEYHAN, E., Risk Management Solutions, Newark, CA, USA, Emel.Seyhan@rms.com

Seismic hazard in Hawaii can be modeled using three main components: background seismicity, crustal faults, and the appropriate ground motion prediction equations. The most recent USGS seismic hazard map for Hawaii, published in 1998, calculated hazard using background seismicity and area sources to model crustal faults. For our 2016 Hawaii model, we propose to update the background seismicity, crustal fault model, and GMPEs. In 1998 the crustal faults were mostly modeled as area sources at a constant depth. Since then, new data has become available showing more detailed fault geometry. There is the USGS Quaternary fault and fold database, and relocated earthquakes showing faults rooting into a potential decollement structure (Syracuse *et al.*, 2010). Using this information, we can now model the crustal fault with updated surface traces, and a dipping structure. We have extended the earthquake catalog to include earthquake since 1997, and updated the rates. In the 1998 model, rate was calculated using a varying b-value and summing a-values assigned to area polygons varying in size and shape (drawn based on areas of concentrated seismicity, and/or activity type). In our model we propose updating the background seismicity by using a uniform grid over the entire region, and propose using a constant regional b-value. The background seismicity will be modeled using a preferred tectonic orientation to generate a synthetic fault set, and assigned a minimum and maximum magnitude to these faults. Regarding the evaluation of ground motions in seismic hazard assessments, a well-selected suite of Hawaii-specific GMPEs is used. The updated GMPEs (Wong *et al.*, 2014 & Atkinson 2010) are valid for M3.5–7.5 over the RJB range of 10 to 400 km for PGA and PSA ( $T = 0.01 - 10.0$  sec). They account for both shallow (depth < 20km) and deep (> 20km) earthquakes including the 2006 M6.7 Kiholo Bay and M6.0 Hawi earthquakes.

### The Effect of True and Auxiliary Plane Solutions on Distance Definitions for Generating GMPEs

SANDIKKAYA, M. A., Hacettepe University, Department of Civil Engineering, Ankara, Turkey, abdullahsandikkaya@hacettepe.edu.tr

The automatic moment tensor solutions provide moment magnitude ( $M_w$ ) and fault plane solutions (generally two planes are given—one is true plane of faulting and the other is auxiliary). It is sometimes impossible to determine which plane is the true plane. Akkar *et al.* (2014; DOI: 10.1007/s10518-013-9506-8) proposed taking the arithmetic average of computed finite-fault distance metrics for two planes. Here, a part PEER NGA West-2 Database (Ancheta *et al.*, 2014; DOI: 10.1193/070913EQS197M) is used (data with  $M_w \geq 6$ , known strike and dip angles, measured VS30, rupture distance,  $Rrup < 200$ km and events with at least two records) to test the effect of true and auxiliary plane solutions on distance computation for generating GMPEs. The dataset which constitutes 975 recordings from 130 earthquakes. The same functional form with Akkar *et al.* (2014; DOI: 10.1007/s10518-013-9461-4) horizontal GMPE is used. However, the nonlinear site response term is not included. The main distance estimator is chosen as Joyner-Boore distance (RJB). But the analysis are also performed for Rrup. GMPE0 is generated with the given finite-fault distance metrics by PEER. GMPE1 and GMPE2 are produced with the distance metrics obtained from first and second nodal planes, respectively. Whereas, GMPE3 is the one that uses the arithmetic average of two planes. When the performances of the models (median estimates and standard deviations) are compared with GMPE0, at short distances (*i.e.*, RJB < 20km) the difference is small. For larger distances as expected the difference becomes negligible. Better results are obtained when Rrup is used as main distance metric. Thus, it is concluded that for small-moderate events ( $M_w \geq 6$ ) the average of Rrup can be considered as final distance metrics. These justifications are valid only for RJB and Rrup. For RX and Ry distances, more research is needed.

### Sources of Latency and Associated Design Trade-offs in Earthquake Early Warning Systems

CORDAHI, C., Nanometrics, Ottawa, ON, Canada; EASTON, D., Nanometrics, Ottawa, ON, Canada; HAYMAN, T., Nanometrics, Ottawa, ON, Canada; MACCHARLES, R., Nanometrics, Ottawa, ON, Canada

Low latency is a key contributor to the success of an Earthquake Early Warning (EEW) system. There are several points where latency is introduced between the instant in time that a digitizer produces a set of samples across its analog sensor channel inputs and the point at which the corresponding data reaches its destination for EEW analysis outside the instrumentation and networking domains. Typically long distances separate data sources from the location at which analysis is performed. These points of latency arise out of software, mathematical, and networking as well as physical constraints imposed upon the digitizer and associated communication systems. System designs must account for tradeoffs between

latency and resource (CPU) utilization, which has an effect on power consumption, and communication network bandwidth. Designers of seismological instrumentation used for EEW deployments must keep these trade-offs in mind and make clever implementation choices to minimize delay. System integrators and network operators must be fully aware of latency and its contributors in order to make the right configuration choices when commissioning EEW systems to ensure the lowest possible latency without compromising the accuracy of the early warning data product. We illustrate the tradeoffs being made at the identified latency points using an analysis of a typical deployment of a digitizer streaming live seismic data to a central site utilizing a Very Small Aperture Terminal (VSAT) communication system.

### The New Zealand Strong Motion Database and Performance of Response Spectral Models against New Zealand Data

VAN HOUTTE, C., GNS Science, Wellington, New Zealand, c.vanhoutte@gns.cri.nz

The New Zealand strong motion database contains 272 earthquakes recorded in New Zealand between 1968 and 2015, with moment magnitude,  $M_w$ , ranging from 3.5 to 7.8. Events have been classified as being in the shallow crust, on the subduction interface, or within the subducting slab. There are 3,979 recordings associated with these events, all of which have been manually processed according to an updated method for strong motion signal processing. 12 events have co-seismic slip distributions, derived using waveform data, geodetic data, or both. Site information includes the time-averaged shear-wave velocity in the first 30 m below ground surface, Vs30, the fundamental site period, Tsite, and the depth to 1 km/s, Z1. Two existing New Zealand ground-motion models for shallow crustal events, the McVerry *et al.* (2006) model and the Bradley (2013) model, are compared to the database, along with four NGA-West2 models. To evaluate the distance between the model and the dataset, the negative average sample log-likelihood is calculated, as a proxy for the Kullback-Leibler divergence. It is found that, in general, the NGA-West2 models are closer to the New Zealand data than New Zealand specific models. All models underpredict the data at long periods. This has important implications for developing a ground motion model logic tree for seismic hazard assessment.

### PG and LG Attenuation in Northeast China

RANASINGHE, N. R., New Mexico State University, Las Cruces, NM, USA, nrana001@nmsu.edu; GALLEGOS, A. C., New Mexico State University, Las Cruces, NM, USA, agall@nmsu.edu; HEARN, T. M., New Mexico State University, Las Cruces, NM, USA, thearn@nmsu.edu; NI, J., New Mexico State University, Las Cruces, NM, USA, jni@nmsu.edu; SANDVOL, E. A., University of Missouri, Columbia, MO, USA, sandvole@missouri.edu; PHILLIPS, S., Los Alamos National Laboratory, Los Alamos, NM, USA, wsp@lanl.gov

Using the reverse two-station and two-station methods we obtained frequency dependent Pg and Lg attenuation models of Northeast (NE) China. These models were based on seismograms collected from 423 and 452 crustal events (depths  $\geq 40$  km) for Pg and Lg, respectively. The events were recorded over a time period spanning from 1995 to 2013 using 195 seismic stations from the NorthEast China Extended Seismic Array (NECESSArray), several IRIS PASSCAL experiments, GSN permanent stations, and the Chinese and Korean national seismic networks. The attenuation models were generated at central frequencies ranging from 0.5 Hz to 3 Hz. A  $2^\circ \times 2^\circ$  resolution was achieved at all frequencies. We also solved for the geometric spreading terms of Lg and Pg by performing a least squares fit of the amplitude data. The best fit yields a spreading coefficient of 0.9 for Pg and 0.36 for Lg. Both Pg and Lg Q values increase rapidly in the Songliao Basin for higher frequencies ( $\geq 2$  Hz), while they stay relatively constant in the Great Xing'an Range. Pg shows higher Q values than Lg in the Songliao Basin. Low attenuation regions are found in the Great Xing'an Range, the Lesser Xing'an Range, and the Songen-Zhangguangcai Range. Overall, attenuation is high in the Songliao Basin, Sanjiang Basin, Bohai Basin, Erlian Basin, and Hailar Basin. The highest attenuation values are found in the vicinity of the Wudalianchi Volcanic Field, Changbaishan Volcano, several Quaternary volcanic regions, the southern Songliao Basin, west of Erlian Basin, Bohai Basin, and Sanjiang Basin. In general regions with low attenuation ( $Q > 800$ ) are characterized by a low heat flow value (< 70 mW/m<sup>2</sup>) and very thin (< 1 km) or no sediments. Regions with high attenuation are characterized by Holocene volcanoes, high heat flow and thick sediments.

### Source Parameters, Aftershocks, and the Abnormal Character of PmP Phases of the 11 May 2012 Mw4.8 Sunan Earthquake, Gansu, China

CHEN, J., Lanzhou institute of Seismology, Lanzhou, Gansu, China, chenjf163@163.com; CARPENTER, N. S., University of Kentucky, Lexington, Kentucky, USA, seth.carpenter@uky.edu; WANG, Z., University of Kentucky,

Lexington, Kentucky, USA, zmwang@uky.edu; YANG, L., Lanzhou Institute of Seismology, Lanzhou, Gansu, China, yanglm@163.com

On 11 May 2012 at 10:18 UTC, an  $M_w$  4.8 ( $M_s$  4.9) earthquake occurred in Sunan County of Gansu Province, China, along northeast margin of Qinghai-Tibetan Plateau. This earthquake caused moderate shaking in the surrounding area, which damaged residential houses (e.g., wall cracks) and caused landslides in the epicentral area (Chinese Intensity VI). We determined the main shock source parameters, relocated aftershocks, and modeled broadband waveforms from 14 stations within 300 km of the epicenter. The focal mechanism, determined by the CAP method, is predominantly strike-slip, with a component of thrust, and occurred at 5 km depth; the shallow focal depth might have contributed to stronger shaking in the epicentral area. The NW-striking, SW-dipping nodal plane is consistent with the strike and dip of the Huangcheng-Shuangta fault (HSF), which may have hosted the devastating 1927 Gulang  $M_s$  8.0 earthquake and is approximately 2 km NE of the epicenter. We used the double-difference location method to relocate aftershocks and found that they occurred at depths from 4 to 7 km on a well-defined plane striking W-SW and dipping at approximately  $65^\circ$  to the N-NW. This plane closely matches the second nodal plane of the mechanism, and is inconsistent with the HSF. Therefore, this earthquake likely occurred on an unmapped, ancillary fault associated with the HSF.

We also observed abnormally large PmP phases at particular stations with offsets from 100 to 170 km: PmP was as large as five times the amplitude of Pg. At other stations at similar offsets, however, no obvious PmP phase was observed. We tested the generation and development of the PmP phase using the F-K method and found that there is a strong influence of the source mechanism and focal depth on PmP-to-Pg amplitude ratios.

#### **Basin Edge and Depth Effects on Ground Motion Amplifications in the Kanto Basin, Japan**

SEYHAN, E., Risk Management Solutions, Newark, CA, USA, Emel.Seyhan@rms.com; KIM, B., Risk Management Solutions, Newark, CA, USA, Byungmin.Kim@rms.com

The Kanto basin, the largest basin in Japan, lies underneath metropolitan Tokyo and the greater Kanto area in Japan. It has a unique sedimentary basin geometry with the sediment thickness approaching up to 4 km (similar to Po Plain in Italy, Los Angeles basin) which corresponds to a site period of approximately 7 sec. It is acknowledged that deep, soft soil deposits within basins tend to amplify the long-period ground motions, causing damages specifically to high-rise buildings. Many ground motion prediction equations (GMPEs) [e.g., Next Generation Attenuation relationships for Western United States (NGA-West2)] have considered the basin depth effects. However, the basin edge effect, the phenomenon of ground motion amplifications due to the angle of incidence of the wave field and interference of reflected/refracted motions within the steeper dipping edges of deep basins, has not been studied well, and is not considered in the existing GMPEs. In this study, we aim to quantify the basin edge effects using the recordings in Japan. We collected strong ground motion recordings at stations located at the edge and center of the Kanto basin from NIED KiK-net network. We used a conventional approach to compute the amplification by taking the ratio of the pseudo-spectral acceleration at the surface to those within borehole. Using the database by Dawood (2015), we developed a simple ground motion amplification model to represent the ground motion amplification characteristics for non-basin sites. At the basin edge sites, the amplifications for short periods are larger than those at non-basin sites, while the amplification for long periods is similar for both basin edge sites and non-basin sites. The larger amplification at short periods in the basin edge sites is caused by the fact that the short period components are predominant in the basin edge where site period is relatively short. We observed large amplifications for long periods in the center of the basin, as expected.

#### **Ground-Motion Attenuation for the South Napa Earthquake in the Sacramento-San Joaquin Delta, California**

ERDEM, J. E., U.S. Geological Survey, Menlo Park, CA, USA, jerdem@usgs.gov; BOATWRIGHT, J., U.S. Geological Survey, Menlo Park, CA, USA, boat@usgs.gov; FLETCHER, J. B., U.S. Geological Survey, Menlo Park, CA, USA, jfletcher@usgs.gov

The  $M_6.0$  South Napa earthquake that occurred on August 24, 2014, was recorded by an extensive network of accelerographs. Baltay and Boatwright (2015) compiled and analyzed strong motion records obtained at 134 stations within 50 km and 292 stations within 100 km from the earthquake. They found that peak ground acceleration (PGA) and velocity (PGV) fall off significantly faster with distance than the NGA-West2 ground motion prediction equations published in Bozorgnia *et al.* (2014). This study focuses on ground motion attenuation within the Sacramento/San Joaquin Delta, situated approximately 50-75 km ESE of the

earthquake. We add 41 records from stations operated by the California State Department of Water Resources and by the USGS Tri-Valley Urban Array. We consider a subset of 79 stations located at azimuths from  $60^\circ$  to  $160^\circ$  and distances out to 170 km from the earthquake. We find that the Boore and Atkinson (2008) ground motion prediction equations fit PGA at 15 km and over-predict PGA by factors of 2 at 30 km and 4 at 70 km. These equations fit PGV at 20 km and over-predict PGV by factors of 1.4 at 30 km and 2.5 at 70 km. These results are consistent with the findings of Baltay and Boatwright (2015). This discrepancy could be caused by anelastic attenuation in the northern Bay Area that is stronger than the average for California. If these results are used to estimate the hazard in the Delta from large earthquakes on the Rodgers Creek and Green Valley faults, the risk of levee failure is substantially reduced, compared to estimations using the NGA-West2 ground motion prediction equations. We check these results using ground motion recordings from a set of smaller, less well-recorded earthquakes that have occurred in the northern Bay Area from 2009 to 2015.

#### **Study of Ground Motion Nonlinear Effects at CGS Geotechnical Arrays using Wave Propagation Analysis of Strong-Motion Data**

HADDADI, H., California Geological Survey, Sacramento, CA, USA, hhaddadi@conservation.ca.gov; SHAKAL, A., California Geological Survey, Sacramento, CA, USA, tshakal@conservation.ca.gov; HUANG, M., California Geological Survey, Sacramento, CA, USA, mhuang@conservation.ca.gov

The nonlinear effects of ground motions are studied by using the strong-motion records of the geotechnical arrays instrumented by the California Geological Survey's Strong Motion Instrumentation Program (CSMIP). The method of Normalized Input-Output Minimization Method (NIOM) is used to correlate ground motions recorded at different depths of the geotechnical arrays and study the nonlinearity effects.

California Geological Survey's CSMIP has instrumented and maintained over 30 geotechnical arrays. A subset of the arrays have recorded earthquakes with peak ground acceleration over 10%. For these stations, shear wave velocities determined from the weak ground motion records are compared with the velocities determined from the strong motion records to find out the cases that ground motion nonlinearity were occurred.

The peak ground acceleration, velocity and spectral acceleration ratios of the surface to depths at the geotechnical arrays are studied for weak and strong ground motions and the results are compared with the amplifications obtained from wave propagation analysis. Such amplification variations for weak and strong ground motions are also compared with the variations in shear wave velocities to see if there is any correlations that could be related to ground motion nonlinearity.

As the shear wave travel time in shallow ground layers for a typical geology type is short, the sampling rate of strong motion records should be high enough to capture shear wave velocity changes. In this study, wave propagation analysis are done using the strong motion records available with the highest sampling rate, and the determined shear wave velocities are compared with those from PS Suspension logging measurements.

#### **Increased Access to Observed Data and Synthetic Data using IRIS DMC Web Services**

TRABANT, C., IRIS Data Management Center, Seattle, WA, USA, chad@iris.washington.edu; HUTKO, A., IRIS Data Management Center, Seattle, WA, USA, alex@iris.washington.edu; VAN FOSSEN, M., IRIS Data Management Center, Seattle, WA, USA, mick@iris.washington.edu; WEEKLY, R. T., IRIS Data Management Center, Seattle, WA, USA, rtweekly@iris.washington.edu; BAHAVAR, M., IRIS Data Management Center, Seattle, WA, USA, manoch@iris.washington.edu; AHERN, T., IRIS Data Management Center, Seattle, WA, USA, tim@iris.washington.edu

Recently, significant developments at the IRIS Data Management Center (DMC) have increased access to observed data, through the IRIS Federator, and to synthetic data, through the Synthetics Engine.

Leveraging the implementation of standardized FDSN web services at many seismological data centers around the world, the IRIS Federator provides a mechanism to discover and easily request data from multiple centers. The main components of the IRIS Federator are a catalog of time series metadata holdings at each data center and a web service interface for searching the catalog. The service interface is designed to support client-side federated data access, a model in which the client (software run by the user) queries the catalog and then collects the data from each identified center. Support for the IRIS Federator has been added to some of the DMC's most popular data access clients. We anticipate adding more data centers to the Federator catalog system as they are implemented by FDSN partners.



The DMC's Synthetics Engine, or Syngine, presents a web service that provides on-demand synthetic seismograms. Syngine allows users to generate and access high-resolution, customizable traces generated within seconds. 3D axi-symmetric SEM synthetics are generated using TB scale databases of Green's Functions calculated for 1D Earth models using AxiSEM. Behind the scenes, the web service uses Instaseis, a system that rapidly calculates broadband synthetic seismograms from the pre-calculated databases. Currently, there are nine databases using four reference models with varying resolutions, up to 1 Hz. We will expand customization by adding support for variable source duration, source-time functions and finite-fault models. We will highlight enhancements to FetchSyn, including common post processing.

#### **Coseismic Deformation During the December 2015 Sarez Lake Earthquake Measured from Sentinel-1A, Alos-2, and Landsat-8 Data, with Insights into the Coseismic Fault Geometry**

SANGHA, S. S., University of California, Los Angeles, CA, USA, sssangha@ucla.edu; PELTZER, G., University of California, Los Angeles, CA, USA, peltzer@ucla.edu; FIELDING, E., Jet Propulsion Laboratory, California Institute of Technology, Pasadena, CA, USA; HUANG, M. H., Jet Propulsion Laboratory, California Institute of Technology, Pasadena, CA, USA; LIANG, C., Jet Propulsion Laboratory, California Institute of Technology, Pasadena, CA, USA

The 7 December 2015 Sarez Lake earthquake ( $M_w$  7.2) occurred ~100 km west of Murghob, Tajikistan and several hundred kilometers north of the India-Asia plate boundary. Its epicenter is close to Sarez Lake which was formed by a massive landslide triggered by a  $M$ 7.3 earthquake in 1911. The moment tensor solution indicates a strike-slip mechanism with a nodal plane striking 35°E, consistent with the direction of faulting bounding the Murghob Valley. We study the coseismic deformation of the 2015 Sarez Lake earthquake using radar interferometry data from the Sentinel-1 and ALOS-2 missions and optical data from Landsat-8. Sentinel-1A ascending and descending tracks centered over the Murghob Valley with 12 to 24 day repeat pass intervals provide well-resolved coseismic and initial post-seismic deformation signals, with a co-seismic signal across the fault of up to 80 cm in both ascending and descending lines of sight. Pre- and post-seismic Landsat-8 panchromatic images have been processed using an optical correlation technique to obtain horizontal displacements. Despite cloud coverage and snow conditions in the post-seismic image, the data indicates up to 5 m of horizontal shift produced by the event.

A preliminary inversion of the data indicates a shallow distribution of slip of up to 5 m on a NE striking fault north of the Sarez lake. A joint inversion of geodetic and seismological data for this event will be presented at the meeting.

#### **Establishing the Rupture Extent of A.D. 1255 Giant Medieval Earthquake through Paleoseismological Investigations and Bayesian Statistical Modeling**

MISHRA, R. L., Wadia Institute of Himalayan Geology, Dehradun, Uttarakhand, India, rajeebmishra88@gmail.com; SINGH, I., Wadia Institute of Himalayan Geology, Dehradun, Uttarakhand, India, gishug@gmail.com; RAO, P. S., Geological Survey of India, Hyderabad, Telangana, India; PANDEY, A., Wadia Institute of Himalayan Geology, Dehradun, Uttarakhand, India, rohitarij42@gmail.com; SAHOO, H. K., Department of Geology, Utkal University, Bhubaneswar, Odisha, India, hksaooogeol@gmail.com; JAYANGONDAPERUMAL, R., Wadia Institute of Himalayan Geology, Dehradun, Uttarakhand, India, ramperu.jayan@gmail.com

The results of a paleoseismological trench investigation carried across a ~10-m high fault scarp at the tea garden of Panijhora village, West Bengal in northeastern India, is presented here. Accelerator Mass Spectrometer (A.M.S.)  $^{14}\text{C}$  radiocarbon ages of six detrital charcoal samples widely scattered between 1688 B.C. and A.D. 1152 poorly constrain the date of the paleoearthquake that produced a minimum observed fault slip of ~5-m in the trench exposure. However, re-calibration of radiocarbon ages from previous trenches at Harmutty, Nameri, Chalsa and Marha Khola in the eastern Himalaya using Bayesian statistical analyses, confirms that the A.D. 1255 medieval earthquake was a giant surface-rupturing event of  $M_w \geq 9.0$  and had ruptured the Himalayan front over a length of ~800 kilometers between ~85.87° and 93.76° E longitudes.

## **Advances in Earthquake Science Using Digital Photogrammetry**

Poster Session · Friday · 22 April · Tuscany F

#### **Spatial Distribution of Displacement along the Northern Part of the 1983 M 6.9 Borah Peak Earthquake Rupture**

DUROSS, C. B., U.S. Geological Survey, Golden, CO, USA, cduros@usgs.gov; GOLD, R. D., U.S. Geological Survey, Golden, CO, USA, rgold@usgs.gov; PERSONIUS, S. F., U.S. Geological Survey, Golden, CO, USA, personius@usgs.gov; BRIGGS, R. W., U.S. Geological Survey, Golden, CO, USA, rbriggs@usgs.gov; REITMAN, N. G., U.S. Geological Survey, Golden, CO, USA, nreitman@usgs.gov; BUNDS, M. P., Utah Valley University, Orem, UT, USA, michael.bunds@uvu.edu; TOKÉ, N. A., Utah Valley University, Orem, UT, USA, nathan.toke@uvu.edu; JOHNSON, K., Colorado School of Mines, Golden, CO, USA, kejohnso@mymail.mines.edu; LAJOIE, L., Colorado School of Mines, Golden, CO, USA, llajoie@mymail.mines.edu; SCHWARTZ, D.P., U.S. Geological Survey, Menlo Park, CA, USA, dschwartz@usgs.gov

In 1983, about 36 km of the 130-km-long Lost River fault zone (LRFZ) in the Basin and Range Province ruptured in the M 6.9 Borah Peak earthquake. The greatest normal-faulting displacement (~2 m) occurred along the 24-km-long Thousand Springs section of the fault, but surface rupture extended north, across a prominent bedrock ridge that forms a structural boundary with the adjacent 16-km-long Warm Springs section. Understanding this rupture in the context of the structural complexity of the LRFZ is important to the characterization of multi-segment normal faults globally. Our investigation is focused on two issues: (1) what is the distribution of 1983 displacement on the Warm Springs and Thousand Springs sections and how does it compare to prehistoric slip on the LRFZ, and (2) what does the 1983 surface rupture imply about rupture boundaries along the LRFZ? To address these questions, we acquired low-altitude aerial photographs and used image-based (structure-from-motion) modeling to generate 5–10-cm digital surface models for the northern part of the 1983 rupture. We document at least 9 km of normal-fault rupture on the Warm Springs section, including a previously unrecognized, ~1-km-long fault splay. Using these surface models, we have remapped the northern end of the 1983 surface rupture and collected a new, high-density suite of along-strike displacement measurements. We compare these results to surface-offset measurements for prehistoric scarps along the LRFZ and Holocene earthquake displacements observed in unpublished paleoseismic trenches excavated shortly after the 1983 earthquake. We have also developed a protocol for measuring scarp offsets in complex normal-faulting environments and tools for partially automating displacement measurements. These data will allow us to evaluate the segmentation of the LRFZ, the significance of the 1983 multi-section rupture, and the value of displacement data in reconstructing the style and extent of prehistoric ruptures.

#### **Repeat Surface Analysis of the Phelan Creeks Reach of the San Andreas Fault, Carrizo Plain, CA**

SALISBURY, J. B., SESE, ASU, Tempe, AZ, USA, jbsalisb@asu.edu; ARROWSMITH, J. R., SESE, ASU, Tempe, AZ, USA, ramon.arrowsmith@asu.edu

The ability to rapidly acquire cost-effective high-resolution topographic data is revolutionizing our understanding of fault zone evolution. Immediately following co-seismic displacements and during the inter-seismic period, close temporal spacing of high-resolution surficial analyses is essential to understanding landscape response to active faulting. As the community moves toward determining slip and near field displacements by differencing pre- and post-earthquake point clouds, calibrating baseline results and understanding sensitivity of high-resolution topographic datasets to actual geomorphic change is increasingly important. We use low-altitude Structure from Motion (SfM) to conduct a repeat high-resolution surface analysis of the Phelan Creeks reach of the San Andreas fault (SAF) in the Carrizo Plain, CA at two-year spacing—eight and ten years after the original 2005 B4 lidar scanning. This reach of the SAF last ruptured in the 1857  $M_w$  7.9 Fort Tejon earthquake and consists of three downstream channel complexes on the southwest side of the SAF that have emanated from a pair of feeder channels ("Little" and "Big" Phelan Creeks) on the northeast side of the SAF. These channels have recorded progressive incision, offset, and abandonment along the SAF with offsets of ~16.5 m, ~130 m, and 230 m. We map the essential tectonic landforms at the Phelan Creeks site at significantly higher resolution than previously available from the B4 data and use the sequence of point clouds from our SfM studies to compare our high-resolution (sub-decimeter) point cloud results from different photo-acquisition methods (balloon vs. military-grade drone). Finally, where possible we quantify interseismic landscape changes from 2005 to 2015 using the B4 and SfM datasets.



### **Paleoseismology from Paleotopography: Combining Legacy and Modern Topographic Data for Earthquake Geology Studies**

**REITMAN, N. G.**, U.S. Geological Survey—Geologic Hazards Science Center, Golden, CO, USA, nreitman@usgs.gov; **BRIGGS, R. W.**, U.S. Geological Survey—Geologic Hazards Science Center, Golden, CO, USA, rbriggs@usgs.gov; **GOLD, R. D.**, U.S. Geological Survey—Geologic Hazards Science Center, Golden, CO, USA, rgold@usgs.gov; **DUROSS, C. B.**, U.S. Geological Survey—Geologic Hazards Science Center, Golden, CO, USA, cdross@usgs.gov

Recent earthquakes are routinely characterized by comparing pre- and post-event remote-sensing datasets, but many historical earthquakes lack baseline data and thus have not been the subject of detailed analyses. Here, we demonstrate that digital photogrammetric techniques like structure-from-motion (SfM) and satellite stereo photogrammetry can help overcome this challenge. These techniques make it possible to reconstruct 3D surface topography from most overlapping 2D photographs, and allow us to quantify deformation patterns for older historic surface-rupturing earthquakes with the same scrutiny that is routinely applied to modern events. We use three examples to demonstrate some of the uses of modern photogrammetric methods and document their utility in earthquake geology. First, we use SfM to reconstruct the pre-development tectonic surface of the heavily developed Mt. Rose Fan in Reno, Nevada. The resulting digital surface model (DSM) will be a critical element in investigations of the complex kinematics of Quaternary faulting in the region. Second, we use satellite stereo photogrammetry to make high-resolution (1.5-3 m) topographic models of large study areas to obtain regional topography at higher resolution than is currently available (e.g., 10 m NED data in U.S.) in support of post-earthquake and seismic hazard assessments. We illustrate this with an example from the 1954 Dixie Valley/Fairview Peak earthquake sequence. Finally, we combine the first two methods to construct pre- and post-earthquake DSMs of the surface rupture from the 1983 Borah Peak, Idaho, earthquake. We vertically difference these DSMs to quantify surface displacement along the rupture trace. These three examples illustrate how the combination of modern and legacy datasets can improve assessments of surface deformation from historic and prehistoric earthquakes and lead to more complete understanding of paleoseismic events.

### **Lidar and Luminescence Dating Analysis of Latest Pleistocene-Holocene Slip Rates on the Awatere Fault: Recent Updates to Fluvial Terrace Dating at Saxton River, South Island, New Zealand**

**ZINKE, R.**, University of Southern California, Los Angeles, CA, USA, rzinke@usc.edu; **DOLAN, J. F.**, University of Southern California, Los Angeles, CA, USA, dolan@usc.edu; **VAN DISSEN, R.**, GNS Science, Lower Hutt, New Zealand, R.VanDissen@gns.cri.nz; **MCGUIRE, C. P.**, University of California, Los Angeles, Los Angeles, CA, USA, mcguire.cp@gmail.com; **RHODES, E. J.**, University of Sheffield, Sheffield, UK, Ed.Rhodes@sheffield.ac.uk; **HATEM, A. E.**, University of Southern California, Los Angeles, CA, USA, ahatem@usc.edu; **GRENADE, J. R.**, University of Southern California, Los Angeles, CA, USA, grenader@usc.edu; **LANGRIDGE, R. M.**, GNS Science, Lower Hutt, New Zealand, R.Langridge@gns.cri.nz

We use high-resolution lidar imagery and luminescence dating to constrain incremental Holocene-late Pleistocene slip rates at the well-known Saxton River site on the Awatere fault, which is a primary fault in the Marlborough Fault System, South Island, New Zealand. Previous studies examining the ages and displacements of offset fluvial terraces and bedrock features at the Saxton River site suggest that slip rates along the Awatere fault have been highly variable since ~16 ka, exhibiting rates as low as ~3 mm/yr and as fast ~13 mm/yr, with an average of ~6 mm/yr (e.g., Mason *et al.*, 2006). Mapping on high-resolution lidar topographic data and additional field surveys yield revised measurements of the five fluvial terrace risers that have been offset by the Awatere fault at the Saxton River site. We present recent updates to the dating of those geomorphic features provided by post-IR50-IRSL225 luminescence ages. These new dates and more precisely constrained offset measurements allow us to more accurately constrain the incremental slip rates recorded at this site. Preliminary results suggest that the slip rate during latest Pleistocene-Holocene time has indeed varied considerably over millennial timescales. This study is part of a broader effort aimed at determining incremental slip rates and paleo-earthquake ages and displacements from all four main Marlborough faults. Collectively, these data will allow us to determine how the Marlborough system faults have worked together during the Holocene-late Pleistocene to accommodate plate-boundary deformation in time and space.

### **Incremental Holocene Slip Rates from the Hope Fault at Hossack Station, Marlborough Fault Zone, South Island, New Zealand**

**HATEM, A. E.**, University of Southern California, Los Angeles, CA, USA, ahatem@usc.edu; **DOLAN, J. F.**, University of Southern California, Los

Angeles, CA, USA; **LANGRIDGE, R. M.**, GNS Science, Lower Hutt, New Zealand; **ZINKE, R. W.**, University of Southern California, Los Angeles, CA, USA; **MCGUIRE, C. P.**, University of California Los Angeles, Los Angeles, CA, USA; **RHODES, E. J.**, University of Sheffield, Sheffield, South Yorkshire, UK; **VAN DISSEN, R. J.**, GNS Science, Lower Hutt, New Zealand

The Marlborough fault system, which links the Alpine fault with the Hikurangi subduction zone within the complex Australian-Pacific plate boundary zone, partitions strain between the Wairau, Awatere, Clarence and Hope faults. Previous best estimates of dextral strike-slip along the Hope fault are about  $\geq 23$  mm/yr  $\pm 4$  mm/year. Those rates, however, are poorly constrained and could be improved using better age determination in conjunction with high-resolution imagery. In this study, we use lidar- and field-based mapping and subsurface channel geometries at the Hossack site 12 km ESE of Hammer Springs to more precisely determine stream offsets that were previously identified by McMoran (1991). Specifically, we measured stream offsets across the fault of ~11 m, ~25 m, ~95 m and ~190m. Together with 65 radiocarbon ages on charcoal, peat, and wood and 25 pending post-IR<sub>50</sub>-IRSL<sub>225</sub> luminescence ages from the channel deposits, these offsets yield four different slip-rates spanning over the course of the Holocene. With a large spatial distribution of such numerous ages, we document the timing of initiation and abandonment of each channel, enhancing the geomorphic interpretation at the Hossack site as channels deform over many earthquake cycles. Our incremental slip rate results from the Hossack site may indicate temporally variable strain release along the Hope fault. This study is part of a broader effort aimed at determining incremental slip-rates and paleo-earthquake ages and displacements from all four main Marlborough faults. Collectively, these data will allow us to document Holocene-late Pleistocene patterns of linear and/or non-linear strain accumulation and accommodation within the Marlborough Fault system in four dimensions.

---

## **Behavior of Structures in Subduction Zones under Long Duration Earthquakes**

Poster Session · Friday · 22 April · Tuscany F

---

### **Quantifying Ground Motion Intensity to Estimate Collapse Vulnerability of Buildings and Application to 6-Story Steel Moment Frame Buildings in Los Angeles**

**BUYCO, J. K.**, California Institute of Technology, Pasadena, CA, USA, buyco@caltech.edu; **HEATON, T. H.**, California Institute of Technology, Pasadena, CA, USA, heaton@caltech.edu

We are developing a framework for determining the resilience of buildings to sidesway (P-Delta) collapse without the need for a large suite of nonlinear time history analyses. Current US seismic code and performance-based design recommendations both quantify ground motion intensity using acceleration response spectra. We have found that this works well for predicting inter-story drift due to moderate shaking, but other intensity measures such as peak filtered acceleration (PFA) are better indicators for predicting collapse.

PFA measures the peak of an acceleration record that is low-pass filtered at a cutoff period that depends on the fundamental period and ductility of the building in question. The PFA collapse prediction framework compares the PFA of a ground motion to the normalized (by building weight) ultimate base shear of a building and predicts sidesway collapse if the PFA exceeds the building's ultimate base shear.

We apply this framework to 6-story steel moment frame buildings designed by the authors to represent the state of engineering practice and building codes in Los Angeles over the course of the last few decades. We designed the buildings according to UBC 1994, UBC 1997, and IBC 2012 and computed each building's collapse characteristics (period, ductility, and ultimate base shear) from a finite element model. Using the PFA collapse prediction framework, we predict collapse (or no collapse) of these buildings to a set of strong ground motions, which vary from short to long duration. We then check the validity of these predictions by performing nonlinear time history analyses. Preliminary results indicate that steel moment frame buildings designed according to UBC 1997 and IBC 2012 are generally more resistant to collapse than the UBC 1994 buildings. This is especially true for buildings in near-fault regions, as near-source factors and more refined seismic maps are not included in UBC 1994.

### **Quantifying the Effect of Ground Motion Duration on Structural Collapse Risk**

**CHANDRAMOHAN, R.**, Stanford University, Stanford, CA, USA, reaganc@stanford.edu; **BAKER, J. W.**, Stanford University, Stanford, CA, USA, bakerjw@

stanford.edu; DEIERLEIN, G. G., Stanford University, Stanford, CA, USA, ggd@stanford.edu

The current practice of characterizing the seismic hazard at a site typically provides a description of only the response spectra of the anticipated ground motions, since a ground motion's response spectrum, which quantifies its amplitude and frequency content, has been shown to be well correlated to structural response. This study describes a procedure to compute source-specific conditional distributions of ground motion duration at a site, analogous to the method used to compute a conditional spectrum. Target distributions of ground motion duration are computed at three sites in Western USA: Seattle, Eugene, and San Francisco each with a different level of contribution to its seismic hazard from large magnitude interface earthquakes in the Cascadia subduction zone. The mean annual frequency of collapse of structures located near active subduction zones is shown to be underestimated if analyzed using typical short duration ground motions from the PEER NGA-West2 database, in place of hazard-consistent ground motions whose durations match the computed source-specific targets. The long duration ground motions used in the analysis were recorded from large magnitude interface earthquakes like the 2011 Tohoku (Japan), 2010 Maule (Chile), and 1985 Michoacan (Mexico) earthquakes. The effect of ground motion duration on structural response was successfully captured by using (i) structural models that accurately captured strength and stiffness deterioration and the destabilizing effect of gravity loads, and (ii) adequate controls for the effect of response spectral shape. These findings warrant including an explicit description of the durations of the anticipated ground motions, in addition to their response spectra, when characterizing the seismic hazard at a site and selecting hazard-consistent ground motions for structural performance assessment and design.

#### Effect of Long Duration Ground Motions on Bridge Columns

MOHAMMED, M. S., University of Nevada, Reno, NV, USA, mohammed@nevada.unr.edu; SANDERS, D. H., University of Nevada, Reno, NV, USA, sanders@unr.edu; BUCKLE, I. G., University of Nevada, Reno, NV, USA, igbuckle@unr.edu

The March 11, 2011 Tohoku Earthquake is a reminder of the possibility of a long duration large magnitude subduction earthquake along the Pacific northwest coast of the United States. Current seismic design codes do not consider ground motion duration effects on structures. There have been large differences in conclusions of previous research studies with regard to the effect of ground motion duration on structural performance. This presentation shows a comprehensive study that uses experimental and analytical methods to investigate the ground motion duration effects on bridge columns. The experimental program includes identical columns that were tested on a shake table using different motions including short duration and long duration motions. The purpose of the project is to propose new design provisions, if necessary, to include duration effects. Preliminary findings show that the duration of the ground motion significantly affects the collapse capacity of the bridge columns.

---

### Citizen Seismology: Citizens as an Information Source to Advance Earthquake Response and Science

Poster Session · Friday · 22 April · Tuscany F

---

#### Use of U. S. Geological Survey's "Did You Feel It?" Responses for Near Real-Time Earthquake Location

QUITORIANO, V., USGS, Golden, CO, USA, vinceq@usgs.gov; WALD, D. J., USGS, Golden, CO, USA, vinceq@usgs.gov

The U.S. Geological Survey has been collecting intensity questionnaire data from internet users with its "Did You Feel It?" (DYFI) system since 1999. DYFI relies on earthquake source parameters from the Advanced National Seismic System, the National Earthquake Information Center, and other seismic networks to associate user responses to particular events and initiate DYFI processing. In many cases, users who felt an earthquake submit their survey results several minutes before the source information is available, particularly for low-magnitude events not automatically associated by a network. We test a method to automatically locate the intensity centroid and estimate magnitude using DYFI responses alone. Our approach follows the Bakun and Wentworth strategy for evaluating historical events from macroseismic intensity data, while taking advantage of recently-developed intensity prediction equations specifically calibrated with DYFI data. We iterate over a grid of trial locations and magnitudes, compute the resulting intensity at each observation location, and select the location-

magnitude pair with the smallest computed versus observed intensity residuals. Evaluation was performed with six widely felt earthquakes (four US and two outside the US). For each event, we begin with a dataset comprised of the first three minutes of responses, and repeat the calculations every few minutes until we find a stable solution. We compare the DYFI solution with the instrumentally-derived magnitude, location, and origin time. Automated DYFI-based solutions, if deemed sufficiently robust, could be provided for initial awareness and comparison to network solutions for felt events.

#### Crowd-Sourcing Seismic Data for Research and Education Opportunities with the Quake-Catcher Network

COCHRAN, E. S., United States Geological Survey, Pasadena, CA, USA, ecochran@usgs.gov; SUMY, D. F., Incorporated Research Institutions for Seismology, Washington, DC, USA, sumy@iris.edu; DE GROOT, R. M., Southern California Earthquake Center, Los Angeles, CA, USA

The Quake Catcher Network (QCN; qcn.caltech.edu) uses low cost micro-electro-mechanical system (MEMS) sensors hosted by volunteers to collect seismic data. Volunteers use accelerometers internal to laptop computers, phones, tablets or small (the size of a matchbox) MEMS sensors plugged into desktop computers using a USB connector to collect scientifically useful data. Data are collected and sent to a central server with the Berkeley Open Infrastructure for Network Computing (BOINC) distributed computing software.

Since 2008, sensors installed in museums, schools, offices, and residences have collected thousands of earthquake records. We present and describe the rapid installations of very dense sensor networks that have been undertaken following several large earthquakes, including the 2010 M8.8 Maule, Chile and M7.1 Darfield, New Zealand earthquakes, and the 2015 M7.8 Gorkha, Nepal earthquake. These large data sets allow seismologists to develop new rapid earthquake detection capabilities and closely examine source, path, and site properties that impact ground shaking at a site. QCN data from New Zealand will soon be sent to the IRIS archives and near real-time data transfer to IRIS is scheduled in the near future. This will allow for easy access to QCN data through the typical IRIS data download tools. In addition, we are working on new developments that will include automatic output of data streams for potential use in ShakeMap and early warning.

In addition, we show how QCN has engaged a wide sector of the public in scientific data collection, particularly through the SCEC QCN-EPIcenter Network and NASA Mars InSight teacher programs. QCN provides the public with information and insight into how seismic data are collected and used for research purposes. Furthermore, we describe how students use data recorded by QCN sensors installed in their classrooms to explore and investigate earthquakes that they felt, as part of 'teachable moment' exercises.

#### A Web Interface for QCN Volunteers to Visualize Seismological Data

FROBERT, L., EMSC, Paris, France; BOSSU, R., EMSC, Paris, France; MAZET-ROUX, G., EMSC, Paris, France

The Euro-Med Seismological Centre (EMSC) has set up a Quake Catcher Network (QCN) server to promote this initiative in the Euro-Med region and among its members' institutes. There are currently 3 operating networks, those set-up by the local seismological institutes in Thessaloniki and Patrai cities (Greece) and one in the French West Indies; a fourth one is currently being deployed in Portugal. After this initial phase, an open call for participation will be launched on social networks to widen the participation to individuals within the Euro-Med region.

In order to improve participant retention and as a first step to develop seismological training of the volunteers, we have been developing within the H2020 project ENVRI+ a web interface to visualize stations and waveforms and offer basic filtering possibilities.

Users can map the locations of the sensors, the seismicity, visualize the period of activities of each sensor and filter them based on geography, type of sensors, or period of activity basis. Furthermore, when an earthquake is selected, the list of active sensors at the time of the seismic event appears as a function of epicentral distance. Waveforms can then be visualized on the interface and data can be downloaded in SAC format.

HTML5 Canvas is used for the figures and leaflet for the maps, while the underlying webservice relies on Mysql with data exchanged in the JSON format. All processing (filtering, Spectrogram, display) are done in the user's browser using Javascript.

We intend to make the interface available to QCN users and collect their feedback in order to evolve it further.

## Rapid Crowd-Sourced Earthquake Detections Integrated Into Traditional Seismic Processing

GUY, M., U.S. Geological Survey, Golden, CO, USA, mguy@usgs.gov; EARLE, P., U.S. Geological Survey, Golden, CO, USA, pearle@usgs.gov; TURNER, J., U.S. Geological Survey, Golden, CO, USA, jturner@usgs.gov

The USGS has been running a real-time system with crowd-sourced tweets as the only input to detect, locate, and assess the impact of felt earthquakes worldwide, since 2009. This system often finds small earthquakes that are undetected by traditional seismic algorithms in populated, yet sparsely instrumented, regions of the globe. In such regions the tweet-based detections often precede seismic detections, with 90% of them occurring in less than two minutes and some as fast as 20 seconds. The main drawbacks of the crowd-sourced system are false detections from tweets not associated with a felt earthquake, poor locations, and the lack of accurate magnitude estimates. This system has a false detection rate of about 10% and a median location accuracy of about 100 km for events with sufficient geolocated tweets. To overcome these limitations, we will integrate detections from expeditious, free, and ubiquitous crowd-sourced data with our existing real-time seismic data to produce more complete and rapid earthquake detections for awareness, response, and research purposes. To do this, we convert rapid tweet-based detections into an international standard seismic data exchange format and distribute them to existing seismic processing systems. The traditional seismic systems then use these rapid detections as a seed to associate seismic instrument data and compute more accurate locations, magnitudes, and other earthquake products. The advantage of this approach is that fewer seismic phase picks are required to make an association/detection if the general location and origin time of an earthquake is known. In turn the accuracy of the crowd-sourced detections will be improved by using seismic algorithms and reduce or eliminate the false tweet-based detections, when not supported by seismic data. This work will supplement a limitation of global seismic systems, namely rapidly detecting events in populated, sparsely instrumented areas, which today remains much of the globe.

---

## Deep Earthquakes and Surrounding Slab Structures

Poster Session · Friday · 22 April · Tuscany F

---

### Diverse Rupture Processes in the 2015 Peru Deep Earthquake Doublet

YE, L., California Institute of Technology, Pasadena, CA, USA, lingling@gps.caltech.edu; LAY, T., Univ. California Santa Cruz, Santa Cruz, CA, USA, tlay@ucsc.edu; KANAMORI, H., California Institute of Technology, Pasadena, CA, USA, hiroo@gps.caltech.edu; ZHAN, Z., California Institute of Technology, Pasadena, CA, USA, zwzhan@gps.caltech.edu; DUPUTEL, Z., Université de Strasbourg, Strasbourg cedex, France, zacharie.duputel@unistra.fr; TAVERA, H., Instituto Geofísico del Perú, Ate Vitarte, Peru, hernando.tavera@igp.gob.pe

Earthquakes in deeply subducted oceanic lithosphere can involve either brittle or dissipative ruptures. On 24 November 2015, a pair of deep (601 and 612 km) magnitude 7.5 and 7.6 earthquakes occurred 316 s apart, separated by about 55 km. We study the rupture processes of these events using two-event W-phase inversion, global and network based short-period P wave back-projection, finite-fault modeling, and subevent directivity analysis and inversion. The first event was a brittle rupture with a sequence of comparable size subevents extending unilaterally ~50 km southward with a rupture velocity of ~4.5 km/s. This earthquake triggered deep activity to the north including a second major event that had 40% larger seismic moment and the same duration, but smaller rupture area and lower rupture velocity, indicative of a more dissipative rupture. As for the nearby great 1994 Bolivia earthquake, dynamic stresses from brittle rupture may be essential to drive the onset of distinct dissipative failure processes in deep slabs.

### Slab2—Updated Subduction Zone Geometries and Modeling Tools

HAYES, G. P., USGS NEIC, Golden, CO, USA, ghayes@usgs.gov; MOORE, G., USGS NEIC, Golden, CO, USA, ginevramoore@usgs.gov; FLAMME, H., USGS NEIC, Golden, CO, USA, hflamme@usgs.gov; PORTNER, D. E., University of Arizona, Tucson, AZ, USA, portner@email.arizona.edu; HEARNE, M., USGS NEIC, Golden, CO, USA, mhearne@usgs.gov

The U.S. Geological Survey database of global subduction zone geometries (Slab1.0) combines a variety of geophysical data sets (earthquake hypocenters, moment tensors, active-source seismic survey images of the shallow subduction zone, bathymetry, trench locations, and sediment thickness information) to image the shape of subducting slabs in three dimensions, at approximately 85% of the world's convergent margins. The database is used extensively for a variety of purposes, from earthquake source imaging, to magnetotelluric modeling. Gaps in Slab1.0 exist where input data are sparse and/or where slabs are geometrically complex (and difficult to image with an automated approach). Slab1.0 also does

not include information on the uncertainty in the modeled geometrical parameters, or the input data used to image them, and provides no means for others to reproduce the models it describes.

Currently underway, Slab2 will update and replace Slab1.0 by: (1) extending modeled slab geometries to all global subduction zones; (2) incorporating regional data sets that may describe slab geometry in finer detail than do previously used teleseismic data, including regional tomography models; (3) providing information on the uncertainties in each modeled slab surface; (4) modifying our modeling approach to a fully-three dimensional data interpolation, rather than following the 2-D to 3-D steps of Slab1.0; (5) adding further layers to the base geometry dataset, such as historic moment release, earthquake tectonic providence, and interface coupling; (6) migrating the slab modeling code base to a more universally distributable language, Python; and (7) providing the code base and input data we use to create our models, such that the community can both reproduce the slab geometries, and add their own data sets to ours to further improve upon those models in the future. In this presentation we will describe our vision for Slab2, and present early results of this new modeling process.

## Focal Mechanisms of Intermediate-Depth Earthquakes Beneath the Northeast Caribbean

MEJIA, H. P., Baylor University, Waco, TX, USA, hannah\_mejia@baylor.edu; PULLIAM, R. J., Baylor University, Waco, TX, USA; POLANCO, E., University of Santo Domingo, Santo Domingo, Dominican Republic; PUJOLS, R., University of Santo Domingo, Santo Domingo, Dominican Republic; HUERFANO, V., University of Puerto Rico, Mayaguez, Puerto Rico

The Caribbean-North American plate boundary transitions from normal subduction beneath the Lesser Antilles to oblique subduction at Hispaniola before becoming almost exclusively transform in nature at Cuba. In the Greater Antilles, large earthquakes occur all along the plate boundary at shallow depths but intermediate-depth earthquakes (70-200 km focal depth) occur almost uniquely beneath the eastern Hispaniola. Previous studies have suggested that these earthquakes may be associated with, for example, opposing slabs subducting beneath the Muertos Trough (northward-dipping) and the plate boundary (southward-dipping), tearing of the subducting North American slab, or the westward drift of a subduction transform edge propagator (STEP) fault. A few of the larger-magnitude earthquakes have had centroid moment tensors computed for them but the great majority of events have uncertain mechanisms.

Seismic stations in the region have historically been sparse, so constraints on earthquake depths and focal mechanisms have been poor. In an effort to understand more about the tectonics of the region, fifteen broadband sensors were deployed in the Dominican Republic in 2014, increasing the number of stations to twenty-two. To determine the roles deep earthquakes play in regional tectonics, a catalog was created of events recorded jointly by our stations and by other broadband and short period stations in the region for which hypocentral depths are greater than 50 km and earthquake magnitudes greater than 3.5. All events have been relocated and focal mechanisms will be computed for as many events as possible. The earthquake's locations and mechanisms will help constrain a subducted slab edge and lithospheric tearing, if present.

---

## Earthquake Source Parameters and Slip from Seismic, Geodetic and Laboratory Data: Theory, Observations and Interpretations

Poster Session · Friday · 22 April · Tuscany F

---

### What Stress Drop Is Determined by the Far-field Spectrum When Stress on the Fault Is Heterogeneous?

CREMPIEN, J. G. F., University of California, Santa Barbara, Santa Barbara, CA, USA, jorge.crempien@ucsb.edu; ARCHULETA, R. J., University of California, Santa Barbara, Santa Barbara, CA, USA, ralph.archuleta@ucsb.edu; JI, C., University of California, Santa Barbara, Santa Barbara, CA, USA, ji@geol.ucsb.edu

Using the corner frequency measured from the displacement Fourier amplitude spectrum (FAS), à la Brune, is the most commonly used method to determine stress drop of an earthquake. For large-magnitude earthquakes, the stress drop on the fault is most likely spatially heterogeneous. This begs the question: how does the spectrally determined stress drop relate to the "average" stress drop that existed on the fault. There are different measures for "average" stress drop on the fault, e.g., simple spatial average, slip-weighted stress drop, etc. To address this question we have used the slip rate history on finite faults determined by dynamic rupture simulations (Schmedes *et al.*, 2010) to compute far-field S-waves. We use 16 stations, equidistant from the fault and spaced at 10° intervals. For the



16 stations we compute the FAS; we then log-average the spectrum at each frequency of the ensemble to determine an average spectrum used to determine a corner frequency. With the corner frequency, we determine a stress drop. For the dynamic rupture simulations, we know both the stress drop as well as the slip at each point on the fault. We compute both the simple spatial average stress drop, as well as the slip-weighted average stress drop for each rupture scenario. So far we have examined vertical strike slip faulting on fault that is  $\sim 30 \text{ km} \times 15 \text{ km}$ . The magnitudes of the simulated events range between  $M_w$  6.68-6.95. For the 21 different dynamic faulting scenarios, we find that the slip-weighted average stress drop has a range of  $\sim 1.6 \text{ MPa}$ , while the average spectral stress drop has a range of  $\sim 6.8 \text{ MPa}$ . The ratio of the standard deviations (based on natural log of the stress drops) is 4.8. This variation in both the range and ratio of standard deviations would explain why the standard deviation in seismological studies of stress drop is greater than that inferred for stress drop inferred from ground motion prediction equations (GMPE's), as shown by Cotton *et al.*, 2013.

#### Determination of Moment Tensors for the Earthquakes in the Central and Eastern US for Earthquakes below M4.0

DAHALL, N. R., Boston College, Chestnut Hill, MA, USA, dahall@bc.edu; EBEL, J. E., Boston College, Chestnut Hill, MA, USA, john.ebel@bc.edu

The routine computation of seismic moment tensors for earthquakes below M4.0 has not yet been achieved except in parts of California where the seismic station coverage is relatively dense. The standard frequency band of 0.05 Hz to 0.10 Hz used in regional moment-tensor inversions effectively includes only surface wave energy, and there typically is sufficient SNR only for events of M4.0 and higher. We test regional moment-tensor inversions that use higher frequency energy (up to 2.5 Hz), where we include also body waves in a cut-and-paste (CAP) inversion scheme to determine moment tensors for events as small as M3.0. We are testing our methods in the central and eastern U.S. (CEUS), where abundant TA data now exist for a number of earthquakes above M3.0. We are testing to find the appropriate frequency bands versus epicentral distances to be included in the inversion. The frequency band used to fit the data for the surface-wave windows can vary significantly from the one used for the body-wave windows. For the CEUS we are investigating data with epicentral distances in the range of 70 km to 400 km. The CEUS has rather significant lateral variations in crustal structure, which affects the computation of the Green's Functions necessary to produce appropriate synthetics. For this reason, for different source-receiver paths we are investigating using different crustal structures to produce Green's functions and perhaps using different frequency bands as well.

#### Implementation of Uncertainty of Green Functions in the Earthquake Source Inversion

HALLO, M., Charles University in Prague, Prague, Czech Republic, hallo@karel.troja.mff.cuni.cz; GALLOVIC, F., Charles University in Prague, Prague, Czech Republic, gallovic@karel.troja.mff.cuni.cz

Green functions (GFs) are an essential ingredient in waveform-based earthquake source inversions. Hence, their error due to imprecise knowledge of a crustal model is the major source of uncertainty of the inferred earthquake source parameters. Strategies how to incorporate the modeling error (uncertainty) of the GFs in waveform inversions have been recently introduced (Yagi and Fukahata, 2011; Duputel *et al.*, 2014). They rely on statistical description of the GFs uncertainty by means of the covariance matrix.

The proposed study is devoted to estimation of covariance matrix of full wavefield GFs (describing the effect of velocity model uncertainty) and application into the seismic source inversion. Since the covariance matrix estimation by Monte Carlo simulations is numerically very demanding and thus hardly applicable in practice, we propose simplified approaches. The simplification uses the "Approximate covariance function" based on GFs in the mean velocity model, which leads to a simple analytical formula for covariance function. The simplifications exhibit very good agreement with the Monte Carlo simulations, and may be easily implemented in currently existing inversion techniques. Furthermore, we will show the example of the application of the methodology on the case of the seismic source inversion on real dataset from Greece. The application demonstrates ability of this method to incorporate uncertainties of GFs in inversion and also advantages of such approach.

Duputel, Z., Agram, P.S., Simons, M., Minson, S.E. Beck, J.L., 2014. Accounting for prediction uncertainty when inferring subsurface fault slip, *Geophys. J. Int.*, 197 (1), 464-482.

Yagi, Y. Fukahata, Y., 2011. Introduction of uncertainty of Green's function into waveform inversion for seismic source processes, *Geophys. J. Int.*, 186 (2), 711-720.

#### Source Functions and Path Effects from Earthquakes in the Farallon Transform Fault Region, Gulf of California, Mexico that occurred during October 2013

CASTRO, R. R., CICESE, Departamento de Sismología, Ensenada, Baja California, Mexico, raul@cicese.mx; STOCK, J., California Institute of Technology, Pasadena, CA, USA, jstock@gps.caltech.edu; HAUKSSON, E., California Institute of Technology, Pasadena, CA, USA, ehauksson@gmail.com; CLAYTON, R., California Institute of Technology, Pasadena, CA, USA, rclayton@gmail.com

We determined source spectral functions, Q and site effects using regional records of body waves from the 19 October 2013 (M6.3) earthquake and eight aftershocks located in the Farallon transform fault region, 89 km east of Loreto, Baja California Sur, Mexico. We also analyzed records from a foreshock with M4.0 that occurred 37 hours before the main shock. The Farallon transform fault is one of the most active faults of the south-central Gulf of California (GoC) region, where most of the bigger earthquakes are strike-slip events. The distribution of the aftershocks indicates that the rupture generated by the main event propagated northwest with a length of approximately 30 km. We calculated 3-component S-wave spectra from ten events recorded by eleven stations of the Broadband Seismological Network of the GoC (RESBAN). The stations of this network are located around the GoC and provide a good azimuthal coverage. The spectral records were corrected for site effects, estimated calculating average spectral ratios between horizontal and vertical components (HVSR method). The site functions calculated with the HVSR method show small amplifications at most stations. However, stations NE74 and NE80, that are located on sandy sediments, have site amplifications that reach a factor of four at 1.6 and 0.7 Hz, respectively. The site corrected spectra were inverted to determine the source functions and to estimate the attenuation quality factor Q. The values of Q resulting from the spectral inversion can be approximated by the relations  $Q_p = 48 f^{0.9}$  and  $Q_s = 135 f^{0.6}$  for P and S waves, respectively. We used the source spectral functions obtained from the spectral inversion to calculate the corner frequencies that give the smallest residual between the  $\omega^2$  model and the observed source spectra and then we estimated stress drops with the Brune model. We estimated a stress drop of 1.7 MPa for the main event and smaller values for the rest of the events.

#### hybridMT—A MATLAB Software Package for Seismic Moment Tensor Inversion and Refinement

KWIATEK, G., GFZ German Research Centre for Geosciences, Potsdam, Germany; MARTÍNEZ-GARZÓN, P., GFZ German Research Centre for Geosciences, Potsdam, Germany; BOHNHOFF, B., GFZ German Research Centre for Geosciences, Potsdam, Germany

We present a software package hybridMT designed for MATLAB / command shell environments allowing to perform the seismic moment tensor inversion and refinement, optimized for earthquake data recorded by regional-to-local seismic networks as well as for acoustic emission activity. The package enables calculating unconstrained full, deviatoric and double-couple constrained moment tensors as well as to perform the moment tensor uncertainty assessment with bootstrap resampling. The moment tensor inversion may be performed directly in shell environment (by a dedicated command line tool) or conveniently through the MATLAB interface (m-functions). In addition to the moment tensor inversion routines we provide the MATLAB implementation of hybrid moment tensor technique. This methodology increase the quality of calculated seismic moment tensors from events forming a cluster by assessing and correcting for the poorly known path/site effects. The package has been tested on synthetic datasets, acoustic emission data recorded in laboratory experiments as well as on induced seismicity data from a geothermal site. The package is supplemented with extensive documentation, tutorials and dedicated website, and it is freely available and distributed under GPL license.

#### Triggering Processes in Fracture and Compaction Experiments: On the Importance of Large-scale Heterogeneities

DAVIDSEN, J., University of Calgary, Calgary, Canada; KWIATEK, G., GFZ German Research Centre for Geosciences, Potsdam, Germany; GOEBEL, T., University of California, Santa Cruz, CA, USA; STANCHITS, S., Terratek Schlumberger Co, Salt Lake City, UT, USA; DRESEN, G., GFZ German Research Centre for Geosciences, Potsdam, Germany; CHARALAMPIDOU, E. M., Heriot-Watt University, Edinburgh, United Kingdom; RUECK, M., GFZ German Research Centre for Geosciences, Potsdam, Germany

Natural seismicity is characterized by empirical laws such as the Gutenberg-Richter law and the Omori-Utsu law. The latter is a typical example for the spatio-temporal clustering of seismicity arising from triggering processes related to static and/or dynamic stress changes, yet the microscopic origin of the Omori-Utsu law is not well understood. Here, we study triggering processes in tri-axial compac-

tion and fracture experiments under constant displacement on sandstone and granite samples using spatially located acoustic emission events and their focal mechanisms. We present strong evidence that triggering of such events by other acoustic emission events plays an important role in the presence of large heterogeneities while such triggering is basically absent if no significant heterogeneities are present. In the former case, we recover all established empirical laws of seismicity including the Gutenberg-Richter law, a modified version of the Omori-Utsu law and the productivity law. For the Gutenberg-Richter law, we find that the  $b$ -value is smaller for triggered events compared to background events. Moreover, we show that triggered acoustic emission events have a focal mechanism much more similar to their associated trigger than expected by random chance.

#### **Estimating Directivity and Related Source Properties of Moderate Earthquakes in Southern California with Second Seismic Moments Utilizing Stacked Empirical Green's Functions**

MENG, H., University of Southern California, Los Angeles, CA, USA, haoranme@usc.edu; BEN-ZION, Y., University of Southern California, Los Angeles, CA, USA, benzion@usc.edu; MCGUIRE, J., Woods Hole Oceanographic Institution, Woods Hole, MA, USA, jmcguire@whoi.edu

We invert measurements of source-time-function duration for estimates of second degree seismic moments to estimate rupture area, duration, directivity, and centroid velocity of moderate earthquakes in southern California. The source time functions are derived using deconvolutions with stacked Empirical Green's Function (EGFs). These are obtained by selecting candidate EGFs based on locations, source mechanisms, signal to noise ratio (SNR) and magnitudes. After correcting for geometrical spreading, radiation pattern and moment magnitude, we align and stack P or S phases of the qualified candidates to eliminate possible directivity effects of a single EGF and increase the SNR. Results based on P and S waves with close take-off angles and azimuths are compared to establish the reliability of results. We also perform sensitivity analyses to test stability of the results to perturbations of focal depth ( $\pm 2.5$  km) and focal mechanism solution ( $\pm 20^\circ$ ) of the target events as well as measurement errors. The directivities estimated by our second moment analyses are consistent with independent results on spatial distributions of Peak Ground Accelerations. The results indicate that the procedure used to derive second moments provides a robust method for estimating directivity and related source properties of moderate earthquakes ( $3 < M < 5$ ) in Southern California. It also provides estimates of rupture area and hence stress drop that are free from model assumptions such as a circular crack or a spectral decay form.

#### **Estimating Rupture Directivity of moderate San Jacinto Fault Zone Earthquakes with Spectral Analysis**

ABOLFATHIAN, N., University of Southern California, nabolfat@usc.edu; BEN-ZION, Y., University of Southern California, benzion@usc.edu; ROSS, Z. E., University of Southern California, zross@usc.edu

We attempt to resolve directivity of moderate earthquakes in San Jacinto Fault Zone area by analyzing the azimuthal variations of corner frequencies of source spectra. The method uses spectral ratio of target events with  $M_w < 3.5$  to smaller Empirical Green's Function events (EGFs) to derive the source spectra of the target events. In addition to the usual selection criteria of EGFs, we examine the spatial distribution of amplitudes to ensure that the EGFs themselves have minimal directivity. We experiment with several procedures for deriving robust corner frequencies from the source spectra of the target events, and use the azimuthal distribution of the derived corner frequencies to infer on directivities. The average corner frequencies at the various stations provide estimates for the strain (and stress) drops of the events. Comparisons of derivations based on P and S waves help to establish robustness of the results.

#### **Enhancing Ground-motion Prediction with Near Real-time Rupture Directivity Assessment**

LUL, S. K. Y., California Institute of Technology, Pasadena, CA, USA, klui@caltech.edu; HELMBERGER, D. V., California Institute of Technology, Pasadena, CA, USA, helm@gps.caltech.edu

The current earthquake early warning system estimates the expected ground-motion intensity based on constrained earthquake location and seismic moment with 3 s of P waves at nearby stations. While those are valuable information to obtain, accurate estimation of focal mechanism, depth and rupture characteristics will also be crucial for the engineering community to further enhance building response prediction and the shake map. Here we propose a methodology that allows rapid and systematic assessment of the source characteristics and rupture properties of earthquakes. In an earlier study, we selected several intermediate sized ( $M_w$  4.4) earthquakes near Fontana as a test case and, using the Cut-and-

Paste waveform inversion method, successfully recovered moment magnitude and focal mechanism within 6 s after the first P-wave arrival. Focal depth can also be constrained within 10 s when the first S-wave arrival is included. In this presentation, a smaller earthquake that occurred in a similar location with  $M_w$  3.2 is selected to generate broadband empirical Green's functions. Applying a forward modeling approach, rupture directivity of the  $M_w$  4.4 earthquake can be estimated from the first 2 s of P waves. Once rupture properties are constrained, the ground-motion response for the stronger S waves that arrive later at farther distances can be accurately predicted using empirical Green's functions. We will also report on studies of other earthquakes with similar sizes within and outside of the Los Angeles Basin to assess how this methodology is accounting for the complicated path effects. This set of methodology can enhance the effectiveness of the earthquake early warning system, contributing to the mitigation of seismic hazard.

#### **Magnitude Scaling Relations for Small to Moderate Southern California Earthquakes from Body Wave Spectra of Over 13,000 Events**

ROSS, Z. E., University of Southern California, Los Angeles, CA, USA, zross@usc.edu; BEN-ZION, Y., University of Southern California, Los Angeles, CA, USA, benzion@usc.edu; VERNON, F. L., Scripps Institute of Oceanography, UCSD, San Diego, CA, USA, fvernon@ucsd.edu; WHITE, M. C., Scripps Institute of Oceanography, UCSD, San Diego, CA, USA, mcwhite@ucsd.edu

We develop a methodology for reliable estimation of the low-frequency asymptote of seismic body wave spectra of small local earthquakes. The procedure first identifies a set of constraints for the search range of source parameters from an average source spectrum recorded by a set of stations. These constraints are then used to tighten the search range for each individual station, while allowing for some variation due to source effects like directivity. The procedure avoids the assumption that a single source model is appropriate for all stations. A method for estimating the uncertainty in the derived moment/potency is also developed. The procedure is applied to >13,000 earthquakes with  $0 < ML < 5$  that occurred in the San Jacinto fault zone area in southern California during 2013. The derived  $M_w$  values follow a Gutenberg-Richter distribution with a larger  $b$ -value (1.22) than that associated with the ML values of the same earthquakes (0.94). The completeness magnitudes are  $M_w$  of 1.6 and ML of 1.0. The quantity ( $M_w - ML$ ) linearly increases in the analyzed magnitude range as ML decreases and an average earthquake with ML 0.0 in the area has an  $M_w$  of 1.0. The developed procedure and results have important implications for observational and theoretical earthquake studies.

#### **Source Parameters of the 25th April 2015 Nepal Earthquake and Its Aftershocks**

MITRA, S., Indian Institute of Science Education and Research, Kolkata, India, Supriyo Mitra <supriyomitra@gmail.com>; PAUL, H., Indian Institute of Science Education and Research, Kolkata, India; MANNA, S., Indian Institute of Science Education and Research, Kolkata, India; PRIESTLEY, K., University of Cambridge, Cambridge, United Kingdom, kfp10@cam.ac.uk; DAYAL, S., Bihar Disaster Management Authority, Bihar, India

The major  $M_w = 7.8$  earthquake which rocked the Nepal Himalaya on 25th April 2015 is the largest to have occurred in this region in the past 81 years. This event occurred by slip on a ~150 km long and 55 km wide, shallow dipping (~5°) segment of the Main Himalayan Thrust (MHT), causing the Himalaya to lurch southwestward by  $4.8 \pm 1.2$  m over the Indian plate. The mainshock ruptured the down-dip end of the frictionally locked segment of the MHT, initiating near the locking line and propagated up-dip. The rupture stopped ~8 km below the surface, loading the up-dip end of the MHT. The mainshock was followed by a large number of aftershocks among which four were larger than magnitude ( $M_w$ ) 6.5. These strong aftershocks occurred on fault(s) with similar orientation as the mainshock, contributing to strain release on the MHT. Moderate-to-light aftershocks originated close to the up-dip edge of the MHT, close to where the mainshock rupture stopped. We use regional and local waveform data to (a) relocate these aftershocks and (b) model the source mechanism of the moderate aftershocks ( $M_w > 5.0$ ). This will provide valuable constraints on the up-dip geometry of the MHT, presence of ramps and associated back thrust underneath the Himalayan foothills. Our study will also highlight the adjacent segments of the Himalaya where significant unrelieved elastic strain has accumulated and may rupture in similar or greater earthquakes in the future.

#### **Attenuation and Source Characteristics of the December 30, 2015 M4.7 Vancouver Island In-Slab Earthquake**

GHOFRANI, H. G., Western University, London, ON, Canada, hghofra@uwo.ca; ATKINSON, G. M. A., Western University, London, ON, Canada,



gmatkinson@aol.com; ASSATOURIANS, K. A., Western University, London, ON, Canada, kassatou@uwo.ca

The moment magnitude ( $M$ )4.7 Vancouver Island earthquake of December 30, 2015 (48.62°, -123.3°) was a normal-faulting in-slab event located approximately 21 km NNE of Victoria, B.C., at a depth of 60 km. The moderate earthquake was felt roughly 150 kilometers in all directions across much of B.C.'s South Coast and parts of Washington State. Ground motions from this event are retrieved and processed from all stations within 500 km from the epicenter. We compared the observed vertical-component 5% damped pseudo-acceleration (PSA) values from this earthquake to the in-slab ground-motion prediction equation (GMPE) suite used in the 2015 National Building Code of Canada (NBCC; Atkinson and Adams, 2013) for the reference site condition B/C ( $V_{s30} = 760$  m/s). The vertical components are expected to have minimal amplification, making them more suitable for comparison with GMPEs for B/C site conditions. Preliminary analysis suggests that the observed PSA values from this earthquake are dramatically lower than the expected values for a  $M_{4.7}$  in-slab event as predicted by the 2015 NBCC GMPE models. We develop an event-specific GMPE for this event to further characterize the source and attenuation parameters, and facilitate comparison of the source spectrum to seismological models. Our preliminary analyses suggest that the combination of anomalous site response at the nearest rock stations (e.g. PGC, as discussed by Atkinson and Cassidy, 2000), and factors such as the seismic radiation pattern need to be considered in understanding the observed ground motions from this earthquake.

### Impact of Uncertainty in Magnitude-Area Scaling Relations on SCEC Broadband Platform Simulations

BAYLESS, J. R., UC Davis / AECOM, Folsom, CA, USA, jeff.bayless@aecom.com; SKARLATOUDIS, A. A., AECOM, Los Angeles, CA, USA, andreas.skarlatooudis@aecom.com; SOMERVILLE, P. G., AECOM, Los Angeles, CA, USA, paul.somerville@aecom.com

There is an unresolved debate about the way in which the rupture areas of large crustal earthquakes scale with seismic moment. This debate has its origins in Hanks and Bakun (2002; 2008) who proposed bilinear source-scaling relations assuming constant stress-drop scaling for  $M \geq 6.7$  and a transition to non-self-similar scaling for  $M > 6.7$ . In self-similar models (e.g. Leonard, 2010), average fault displacement, fault length and fault width all increase uniformly together. The differences in magnitude estimates for a given fault rupture area from the different scaling models have a relatively minor impact on the estimation of ground motion amplitudes using GMPEs. However, for numerical waveform simulations in which the fault area is fixed, a change in 0.2 units in magnitude has been shown to have a significant impact on the produced synthetic waveforms.

The SCEC Broadband Platform (BBP) provides the opportunity to study in detail the impact of different Magnitude-Area scaling relations using the already-implemented simulation methods. We utilize the simulated waveforms computed from the BBP Phase 1 validation project (Dreger *et al.*, 2013.), the dimensions of which are loosely based on the Leonard (2010) scaling relations. To examine the sensitivity of the simulations to the scaling model, we fix the fault length and recalculate the events of interest using the fault width calculated from the Hanks and Bakun (2008) relation and compare the RotD50 spectra. We also study the relative behaviors of the simulations using an appropriate suite of event scenarios.

Both the EXSIM and UCSB simulation methods appear largely unaffected by the decrease in fault width associated with HB08 scaling. For the Graves & Pitarka (GP) method, at short periods (<1 sec) the change to smaller fault area results in a slight decrease in the level of simulated motions. For GP and SDSU, at long periods (>1 sec) the change to smaller fault area results in an increase in average RotD50 up to 30%.

---

## NGA-East: Research Results and Ground-Motion Characterization Products for Central and Eastern North America

Poster Session · Friday · 22 April · Tuscany F

---

### Improved CENA Regression Relationships between Modified Mercalli Intensities and Ground Motion Parameters

OGWENO, L. P., University of Memphis—CERI, Memphis, TN, USA, logweno@memphis.edu; CRAMER, C. H., University of Memphis—CERI, Memphis, TN, USA, ccramer@memphis.edu

Using the Next Generation Attenuation (NGA) East database, we have updated and extended the relations of Dangkua and Cramer (2011). We developed magni-

tude and distance independent linear regression relationships between Modified Mercalli Intensity (MMI) in the range of  $I \geq \text{MMI} \geq \text{VII}$  and PGA, peak ground velocity (PGV), and twenty-one pseudo spectral accelerations (PSAs) for Central and Eastern North America (CENA). We corrected for recently acknowledged differences between community internet intensities (CII) and MMI by adding to ENA CII the difference between Bakun and Hopper (2004) and Atkinson and Wald (2007) intensity prediction equations (IPEs) for MMI and CII respectively. We performed residual analysis to evaluate for any discrepancies and dependency with magnitude and distance. For the magnitude dependency analysis, we used the corner frequency and moment magnitude equations of Kramer 1996 with an average Brune stress drop of 140 bars (Atkinson and Boore, 2006) to obtain the corner magnitude for a bilinear fit. Below the transition magnitude we fit a linear magnitude dependence and above it a constant. This bilinear magnitude dependence is especially important for longer periods, which are different from the shorter ground motion periods (less than 1 s) that contribute most to intensity values. The residuals show homoscedasticity with zero mean and are serially correlated. The serial correlation was corrected using Cochran-Orcutt procedure. Our new ground-motion intensity correlation equations (GMICE) for CENA are invertible for obtaining both CII and MMI from peak ground motion (PGM) of interest and vice versa.

### Hybrid Empirical Ground-Motion Prediction Equations for the Gulf Coast Region

HAJISOLTANI, A., The University of Memphis, Memphis, TN, USA, hajtstani@memphis.edu; PEZESHK, S., The University of Memphis, Memphis, TN, USA, spezeshk@memphis.edu; ZANDIEH, A., Lettis Consultants International, Inc., Boulder, CO, USA, arash.zandieh@live.com

The main purpose of this study is to develop GMPEs for the Gulf Coast region using a hybrid empirical method (HEM). The HEM uses stochastically simulated ground motion intensity measures (GMIMs) in the host and target regions to develop adjustment factors that are applied to empirical GMIM predictions in the host region. The Gulf, the target region in this study, is a wide sedimentary region, which is centrally located between the eastern Rocky Mountains (western side) and the Appalachian Mountains (eastern side). Considering western North America as the host region, we will use five new NGA-WEST2 GMPEs developed by the Pacific Earthquake Engineering Research center (PEER). For the required seismological parameters in WNA, we will use Zandieh and Pezeshk (2015) results in which a set of point-source inversions have been performed to match the median NGA-West2 GMPEs for moment magnitudes less than 6.0 and rupture distances up to 200 km for a NEHRP site class B/C. For the Gulf coast region, we will use the most recent available seismological parameters in the literature. A moment magnitude range of 4.0 to 8.0 and rupture distances of up to 1000 km will be considered. The new GMPE will be derived for the 5%-damped pseudo-acceleration response spectra for a reference hard-rock site with  $V_{s30} = 3000$  m/s. The Pacific Earthquake Engineering Research (PEER) center recently published a set of new GMPEs developed for the Central and Eastern North America (CENA). All the models developed for CENA exclude the Gulf Coast region. This study will focus on the Gulf Coast region, which will supplement the other recently developed GMPEs, which exclude Gulf.

### Empirical Ground Motion Prediction Equations for Eastern North America with the Addition of Intensity Observations

ALNOMAN, M. N., University of Memphis, Memphis, TN, USA, malnoman@memphis.edu; CRAMER, C. H., University of Memphis, Memphis, TN, USA, ccramer@memphis.edu

The Next Generation Attenuation (NGA) East database of ground motions for eastern North America (ENA) contains 6048 records (GMRotd50 values) from 77 earthquakes in the magnitude range  $M_{2.2-6.8}$ . In this study we reevaluate our previous empirical GMPE's (Al Noman and Cramer, 2015) by adding modified ground motion estimates from intensity observations of large historical earthquakes to the NGA-East database to better constrain the predictions for  $M > 6$ . For a given historical earthquake, we use the new intensity vs. ground motion relations of Ogweno and Cramer (2016) to estimate ground motion values for a given observation of MMI. For historical earthquakes without instrumental magnitudes (the 1811-1812 New Madrid and 1886 Charleston earthquakes) we use the moment magnitudes from Cramer and Boyd (2014). The prediction equations are for peak ground acceleration (PGA), peak ground velocity (PGV), and 5% damped pseudo-absolute acceleration spectra (PSA) at 21 periods between 0.1 sec to 10 sec. Including historical intensity observations improves our observation-based understanding of ENA magnitude, distance and  $V_{s30}$  scaling and thus better constrains the empirical ground motion predictions above  $M_6$ . Our updated empirical GMPEs (2016 version) show improved predictions at longer periods (> 1 s) compared to the 2015 version.



## Improving Attenuation Models in the Central United States by Considering Source Radiation Pattern Effects

HOSSEINI, M., AECOM, Los Angeles, CA, USA, mehrdad.hosseini@aecom.com; SOMERVILLE, P. G., AECOM, Los Angeles, CA, USA, paul.somerville@aecom.com; THIO, H., AECOM, Los Angeles, CA, USA, hong.kie.thio@aecom.com

It is recently shown that radiation pattern and rupture directivity are important factors in determining the rate of decrease of Fourier amplitudes with distance (attenuation), and that low-frequency amplitudes can be contaminated by radiation pattern and directivity effects. The most common approach for developing GMPEs in the Central and Eastern United States is to use stochastic earthquake simulations which require separate characterization of intrinsic attenuation ( $Q$ ) and geometrical spreading. Hence, attenuation models cannot be reliably used to construct ground motion prediction equations unless radiation pattern and directivity are taken into account. We implemented a technique that improves the  $Q$  model by considering source radiation pattern effects. This technique uses source-receiver azimuth and fault plane orientation to model the theoretical source radiation pattern and corrects the amplitudes for it. We used seismogram synthesis technique to generate ground motion for a catalog of 23 recorded earthquakes at the location of 14 stations in the New Madrid Seismic Zone (NMSZ) where a 1-D velocity model with assumed  $Q$ -factors is used. It is observed the use of uncorrected synthetic Fourier amplitudes results in a biased inverted  $Q$  model. In addition, we inverted the corrected and uncorrected recorded amplitudes to estimate the quality factor in the NMSZ. Analysis indicates that obtained  $Q$  models are different between corrected and uncorrected amplitudes and that a correction for the source radiation pattern can improve the attenuation models in the Central Eastern United States.

## Comparison of Random Vibration Theory Peak Factor Formulations for the NGA-East Project

KOTTKE, A. R., Bechtel, San Francisco, CA, USA, akottke@bechtel.com

Random vibration theory (RVT) is used as part of Next Generation Attenuation project for Central and Eastern North America (NGA-East) to calculate a stable estimate of the response spectrum for a given Fourier amplitude spectrum. Part of this calculation relies on the peak factor formulation, which relates the root-mean-squared response to the peak response. As part of the NGA-East project, a review of the RVT methodology and peak factor formulations was prepared. This presentation reviews the recommendations on the use of RVT for the NGA-East project. The differences in the peak-factor formulations and modifications for the oscillator response are detailed. The Cartwright and Longuet-Higgins (1956) peak factor is commonly used in seismology, but only approximates the extreme value statistics. While the Vanmarcke (1975) peak factor more accurately defines the extreme statistics, but is not as commonly used. Regardless of peak factor formulation, the influence of the oscillator needs to be considered when computing the response spectrum.

## Investigation of the Path Effect Term in the New Madrid Seismic Zone

SEDAGHATI, F., The University of Memphis, Memphis, TN, USA, fsdghati@memphis.edu; PEZESHK, S., The University of Memphis, Memphis, TN, USA, spezeshk@memphis.edu

The single backscattering theory has been implemented to estimate coda quality factor functions for vertical and horizontal directions in the New Madrid seismic zone (NMSZ). In addition, horizontal geometrical spreading functions for distances up to 60 km have been computed in the NMSZ at different center frequencies, exploiting the coda normalization method. The initial database includes 284 three-component digital waveforms from 57 local earthquakes with moment magnitudes of 2.6 to 4.1 and hypocentral distances up to 200 km. These seismograms were recorded by 11 stations located in the NSMS and operated by the Center for Earthquake Research and Information (CERI) at the University of Memphis. Out of 284 total seismograms, 160 with hypocentral distances less than 60 km have been selected to evaluate the horizontal geometrical spreading functions.

$Q$ -factor values were evaluated for coda window lengths of 20, 30, 40, 50, and 60 sec at central frequencies of 1.5, 3, 6, 12, and 24 Hz. Then, a power law equation was used to calculate the frequency dependent coda quality factor functions. For a coda window length of 40 sec,  $Q_C^V = 598f^{0.54}$  and  $Q_C^H = 509f^{0.60}$  for vertical and horizontal directions, respectively. These amounts of  $Q_0$  and power

indicate that the NMSZ is a seismically moderate region with a moderate to relatively high level of heterogeneity. Similarly, the estimated geometrical spreading functions of geometric average of horizontal S-wave amplitudes are  $R^{-1.271}$ ,  $R^{-1.182}$ , and  $R^{-1.066}$  at central frequencies of 6, 12, and 24 Hz, respectively, at hypocentral distances up to 60 km.

## Applicability of Site Fundamental Frequency as a Descriptive Variable for Site Response in Central and Eastern North America

HASSANI, B., Western University, London, ON, Canada, bhassan7@uwo.ca; ATKINSON, G. M., Western University, London, ON, Canada, gmatkinson@aol.com

We use the NGA-East ground-motion database to show that site fundamental frequency ( $f_{peak}$ ), as measured from the horizontal-to-vertical spectral ratios ( $H/V$ ) obtained from 5%-damped pseudo spectral acceleration (PSA), is a good proxy measure for VS30 (time-averaged shear wave velocity in the upper 30 m) for sites in central and eastern North America (CENA). Measured VS30 values at recording stations are well-correlated with  $f_{peak}$ , allowing development of a predictive relationship for VS30. The uncertainty of the VS30 estimate using the  $f_{peak}$ -based model is significantly smaller (0.14 log10 units) than that for the proxy-based methods (e.g. topographic slope and surface geology proxies) used in the NGA-East database (0.25 log10 units).

We also examine the applicability of the Next Generation Attenuation-West2 (NGA-West2) site effects model (Seyhan and Stewart, 2014), which is an empirical VS30-based model, to sites in CENA. We determine residual site terms by comparing the observed CENA ground-motion amplitudes, adjusted to B/C site conditions using the western site-effects model, to the corresponding predicted amplitudes of a CENA ground-motion prediction equation for B/C site conditions (Yenier and Atkinson, 2015; YA15). Plotting the residual site terms versus their corresponding site fundamental frequencies ( $f_{peak}$ ) reveals significant  $f_{peak}$ -dependent trends at all frequencies. Average residual site terms for CENA sites, after the western site amplifications have been removed, can be as large as 0.45 in log10 units (a factor of 2.8) for frequencies  $f \approx f_{peak}$ . We find that at  $f < 1$  Hz, site terms in CENA scale with VS30, similar to the way they behave in the NGA-West2 database. However, at higher frequencies the correlation of site amplification with VS30 decreases markedly in CENA. By contrast,  $H/V$  is a good predictor of the observed  $f_{peak}$ -dependent site terms, suggesting that  $H/V$  is a more reliable predictor of site amplification for sites in CENA.

## Hard-rock Amplification for NGA-East Sites

KTENIDOU, O. J., GFZ German Research Centre for Geosciences, Potsdam, Germany, ktenidou@gfz-potsdam.de; ABRAHAMSON, N. A., PEER Center, U. of California, Berkeley, CA, USA, abrahamson@berkeley.edu

In Ktenidou *et al.* (2016), residuals of acceleration response spectra were studied for hard-rock stations in the NGA-East dataset, and it was found that they do not scale as expected with the site-specific high-frequency attenuation factor,  $\kappa_0$ . Site-specific high-frequency amplification effects not considered in  $\kappa_0$  estimation were suggested as one possible reason for this. The trade-off between site amplification (impedance contrast) and site attenuation (damping) is an issue that may affect the way  $\kappa_0$  is interpreted, and though hard-rock sites were once considered free of site effects, this is not necessarily the case. In this study we look into individual hard-rock stations from the NGA-East dataset to isolate the effects of site amplification from the effects of  $\kappa_0$ .

Most hard-rock NGA-East sites are not well characterized, and many were assigned a Vs30 value of 2000 m/s by expert assessment. Ktenidou *et al.* (2016) found that the measured  $\kappa_0$  values at the rock-rock site exhibit large variability, but could not determine how much of this variability in  $\kappa_0$  is due to different site amplification patterns between sites. Here, we use two empirical approaches to estimate the site amplification: horizontal-to-vertical spectral ratio (HVSR) and mean site term for spectral acceleration ( $\delta s_2$ ) When there is no reference site available to perform traditional empirical spectral ratios, site amplification can be estimated using HVSR. Recently, another approach was proposed (Ktenidou *et al.* 2015), using residuals from ground motion prediction equations (GMPEs), namely the systematic deviation ( $\delta s_2$ ) of a site's response with respect to the average GMPE prediction. HVSR is computed on Fourier spectra, while  $\delta s_2$  is computed on response spectra, and hence has the advantage of being more compatible with GMPEs. Using these amplification estimates, we investigate if site amplification patterns can affect  $\kappa_0$  measurements, and if a better site proxy can be proposed for these sites.

## Physical and Statistical Properties of Earthquake Swarms and Clustered Seismicity: Constraining Driving Mechanisms

Poster Session · Friday · 22 April · Tuscany F

### The 2015 San Ramon, CA Swarm: Operational Earthquake Forecasting and Background Rate Changes

ALLENOS, A. L., USGS, Menlo Park, CA, USA, allenos@usgs.gov; MICHAEL, A. J., USGS, Menlo Park, CA, USA, michael@usgs.gov

Earthquake swarms, typically modeled as time-varying background seismicity (*i.e.*, triggered by external driving forces rather than by other earthquakes), present a challenge for operational earthquake forecasting (OEF), which often uses earthquake clustering rather than background rate changes. One issue is that while the duration of earthquake clustering can be estimated with the modified-Omori law, it is difficult to forecast how long a change in background rate will last. To explore these issues, we apply the Epidemic-Type Aftershock Sequence (ETAS) model (Ogata, JASA, 1988), an earthquake rate model used for OEF, to the 2015 San Ramon swarm, which began in October and lasted several weeks, with almost  $100 \geq M \geq 3.6$  earthquakes. For the swarm, the best-fitting ETAS model's background rate has increased by almost two orders of magnitude over previous seismicity, and it has a decreased triggering productivity.

Previous swarms in the area include the 1970 and 1976 Danville swarms, 1990 Alamo swarm, and 2002 and 2003 San Ramon swarms. Compared to these swarms, the 2015 swarm involves a larger increase in background rate. A higher fraction of the 2015 swarm consists of background events, suggesting that there may have been a change in the driving mechanism for the 2015 swarm. However, an ETAS model fit to the earlier swarms forecasts the daily rates during the 2015 swarm well (with 90% of the observations in the 95% confidence limits of the forecast, despite a lower background rate), perhaps due to tradeoffs between background rate and aftershock productivity in the model. This suggests that in regions with swarms, an earthquake rate model based on previous swarm behavior can be developed to forecast rates specifically during swarms. However, it remains a challenge to determine when a swarm starts and such a model should be applied, and when a swarm ends and a model based on non-swarm seismic activity can be used.

### Optimized Physics-based Earthquake Forecasts for Inland Japan

SEGOU, M., British Geological Survey, Edinburgh, United Kingdom, msego@bgs.ac.uk; ZHUANG, J., Inst. of Statistical Mathematics, Tachikawa, Tokyo, Japan, zhuangjc@ism.ac.jp

We focus on the stress recovery processes after the  $M=9.0$  Tohoku mega-earthquake and how the above influences the earthquake probabilities in active faults of inland Japan. Recent studies present evidence about rapid stress recovery near the trench but as anticipated by rate-and-state friction law, returning to pre-Tohoku "normal" seismicity levels for the active faults in inland Japan is a slower process. We perform a retrospective forecast spanning 10 years (2004-2014) in the Niigata prefecture (mid-west Japan) using physics-based modeling, combining rate-and-state law and Coulomb stress changes, to study earthquake-triggering mechanisms. The key element of our innovation lies in the development of 429 forecast models, as a result of a stochastic optimization within short-time frames (10 days), in order to access the time and spatial variability of fault constitutive parameters. The aforementioned optimized forecast then competes with a benchmark statistical/empirical Epidemic-Type Aftershock Sequence (ETAS) model. The testing period starts with the  $M=6.8$  Chuetsu mainshock and ends on December 2014, approximately 9 months after the  $M=6.7$  post-Tohoku mid-Niigata on April 12th, 2011. The physics-based optimization goes hand in hand with uncertainty consideration related with the estimation of static stress changes (geometry of active faults, receiver depth, effective friction coefficient) following the  $M=6.8$  Chuetsu mainshock and important triggered events at the near source are, the 2007  $M=6.7$  Chuetsu-Oki and the  $M=6.2$  post-Tohoku event. The forecasts are evaluated for their predictability, spatial consistency and relative information gain by considering the statistical model as reference. We find that: (1) best-fit solutions correspond to stressing rates between 0.01 and 0.8 bar/yr immediately after the aforementioned mainshocks and (2)  $\Delta\sigma$  values vary between 0.1 and 2.0, for the few first days following the post-Tohoku and Chuetsu events.

### Capturing Fractal Fault Structure in Virtual Quake Simulations

WILSON, J. M., UC Davis, Department of Physics, Davis, CA, USA, jhwnilson@ucdavis.edu; RUNDLE, J. B., UC Davis, Departments of Physics and Geology, Davis, CA, USA, jbrundle@ucdavis.edu; SCHULTZ, K. W.,

UC Davis, Department of Physics, Davis, CA, USA, kwschultz@ucdavis.edu; TURCOTTE, D. L., UC Davis, Department of Geology, Davis, CA, USA, dlturcotte@ucdavis.edu; YIKILMAZ, M. B., UC Davis, Department of Geology, Davis, CA, USA, mbyikilmaz@ucdavis.edu

Virtual Quake is a computational simulation which attempts to mirror the physics of friction and elastic interactions between faults. Physically-based earthquake simulators can generate many thousands of years of simulated seismicity, allowing for a robust capture of the statistical properties of large, damaging earthquakes that have long recurrence time scales. Simulation parameters are adjusted so that natural earthquake sequences are matched in their scaling properties. Additionally, the topological complexity of fault systems on which earthquakes occur is captured. One strength of Virtual Quake is its modular design, allowing the fault model to be modified separately from the background physics simulation. Previous simulations of the California fault system treat fault segments as largely flat planes, while real faults demonstrate self-affine fractal structure. We present preliminary efforts to include this structure in Virtual Quake simulations, both for simplistic toy faults and realistic fault models of California.

### A Look at Slip and Dilation Tendencies on Preexisting Faults in Areas of Recent Earthquake Swarms in Western Nevada

MOLISEE, D. D., Nevada Seismological Laboratory, University of Nevada, Reno, NV, USA, dmolisee@unr.edu; RUHL, C. J., Nevada Seismological Laboratory, University of Nevada, Reno, NV, USA, cruhl@unr.edu

Fault kinematic studies, especially slip and dilation tendency calculations, have been widely used by the geothermal community to identify likely conduits for hydrothermal resources. Applying 3D stress orientations (*e.g.*, from geodetic strain fields) to mapped faults highlights those structures that are preferentially oriented to slip and/or dilate. Low magnitude earthquake swarms lack surface rupture; association with surface faults is not usually obvious. They are, however, commonly attributed to fluid movement in the crust, which would be facilitated near faults dilating in the current stress field. The slip and dilation method applied to areas of earthquake swarms may be useful in identifying potential host faults.

We apply slip and dilation calculations, completed using 3D Stress (3DStressV3.1A), to three earthquake swarms located within the western Basin and Range and Walker Lane regions: (1) the 2008 Mogul, NV  $M_w$  5.0 earthquake swarm, (2) the 2011 Hawthorne, NV swarm, and (3) the ongoing Sheldon swarm in NW Nevada near the Oregon border. Each of the sequences has a maximum magnitude between  $M_w$  4.7 and 4.9 and persisted several months or more. We have developed a set of relative relocations and compiled moment tensors from the Nevada Seismological Laboratory earthquake database for each sequence. We export both pre-existing faults (*e.g.*, USGS Quaternary Faults and Folds database) and visually identified fault traces in the areas of each swarm into 3D Stress and apply stress orientations derived from GPS strain fields processed by the Nevada Geodetics Laboratory. We compare the orientations of faults with high slip and dilation tendencies to moment tensor focal mechanisms and independently compute the slip and dilation tendencies from the moment tensor stress axes themselves. Using the results of these independent methods, we can identify potential host faults, both with and without direct association of faults with focal mechanisms.

### Moderate-to-Small Magnitude Seismicity Clusters Persist in Northwest Nevada for over 19 Months

RUHL, C. J., Nevada Seismological Laboratory, University of Nevada, Reno, NV, USA, cruhl@unr.edu; SMITH, K. D., Nevada Seismological Laboratory, University of Nevada, Reno, NV, USA, ken@unr.edu

Unusually long-duration, moderate magnitude swarm seismicity has persisted near the Sheldon National Wildlife Refuge in northwest Nevada for over 19 months as of Jan 2016. The Nevada Seismological Laboratory has located 7362 earthquakes since the first  $ML$  3.0 event on 12 Jul. 2014, with many more detections observed since deployment of temporary station COLR about 15 km from the source area on 17 Nov. 2014. The entire sequence to date includes 276 (30) earthquakes  $ML \geq 2.95$  ( $ML \geq 3.95$ ), occurring in distinct bursts of activity with no clear mainshock. We develop a set of double-difference relative relocations for earthquakes with 5 or more associated phases from both catalog- and cross-correlated-arrival time differences using only 5 seismic stations. While poor station coverage limits detailed analysis, relocated hypocenters do highlight a steeply east-dipping feature. The largest mapped surface faults in the vicinity of the Sheldon sequence are, however, west-dipping, range-bounding normal faults. Nonetheless, moment tensor solutions coupled with relocations suggest that the sequence has been evolving on one or more NNE-striking normal faults, consistent with strike orientations of splaying faults at the southern end of the Guano Valley fault zone. Waveforms well fit with double-couple solutions are inconsis-



tent with volcanic or magmatic injection processes often associated with swarm seismicity. Proposed mechanisms for nonvolcanic swarm sequences include geothermal fluid migration and local crustal spreading in step-overs of strike-slip systems. Another common observation in the Basin and Range and Walker Lane provinces is that seismicity tends to occur near the ends of faults on secondary planes oriented at high angles to major range-bounding normal faults. We suggest that this sequence is yet another example of swarm seismicity concentrated in the highly faulted transition zones between or at the ends of en echelon normal faults.

#### **Application of Template-Based Seismic Detection Methods to Recent Seismicity Near the M6.9 1983 Borah Peak, Idaho Earthquake**

PANG, G. N., University of Utah, Salt Lake City, UT, USA, yuupgn@gmail.com; KOPER, K. D., University of Utah, Salt Lake City, UT, USA, koper@seis.utah.edu; BURLACU, R., University of Utah, Salt Lake City, UT, USA, burlacu@seis.utah.edu

Beginning in March 2014, and continuing through the present, an energetic earthquake swarm has occurred near Challis, Idaho. The largest events in the earthquake swarm had moment magnitudes ( $M_w$ ) of 4.8 and 5.0, and occurred on April 13, 2014 and January 3, 2015, respectively. This swarm is significant because it is adjacent to the Lost River Fault, which produced the damaging M6.9 Borah Peak earthquake in 1983. In an earlier study, relocations of more than 100 events in 2014 outlined a NW-SE trend similar to the strike of the Lost River Fault. To better characterize the fault system in this relatively sparsely instrumented yet hazardous region, we are experimenting with template-based methods of event detection and location using continuous data from seismometers that have been deployed in the region throughout the recent swarm activity. The nearest of these stations is approximately 80 km southeast of the swarm and is part of the Idaho National Laboratory seismic network (IE), while approximately 15 other stations are sited at distances of 100–200 km as elements of the Montana Regional Seismic Network (MB), the Yellowstone Wyoming Seismic Network (WY), the Intermountain West Seismic Network (IW), and the US National Seismic Network (US). Initial results for calendar year 2014, using short-period vertical component data from two MB stations (MCMT and MOMT, at distances of 120 km and 150 km), indicate that about 4–5 times as many earthquakes are detectable with template-based seismic detection methods compared to conventional methods.

#### **Waveform Correlation Detection Methods as Applied to Utah Seismic Swarms**

BATCHELOR, C. E., University of Utah, Salt Lake City, UT, USA, chasebatch@gmail.com; KOPER, K. D., University of Utah, Salt Lake City, UT, USA, kkoper@gmail.com; PANKOW, K. L., University of Utah, Salt Lake City, UT, USA, pankow@seis.utah.edu; BURLACU, R., University of Utah, Salt Lake City, UT, USA, burlacu@seis.utah.edu

We define earthquake swarms as clusters of events that occur closely in space and time and do not exhibit a clear mainshock, in contrast to foreshock-mainshock-aftershock sequences. Swarms are especially common within the seismically active region of the Intermountain West. Of the ~1,500 earthquakes detected and located by the University of Utah Seismograph Stations (UUSS) each year, a fraction of these earthquakes occur in swarms. The source mechanism of swarms in Utah is not well understood, one hypothesis is that stress is induced by the propagation of either hydrothermal or magmatic fluids. To characterize this potential relationship, as well as the spatial and temporal characteristics of seismic swarms in Utah, waveform correlation methods were used to detect small events in a swarm sequence that were missed in routine UUSS earthquake cataloging. The analyzed swarm lasted from November 29 through December 4, 2003, and occurred near the Marysvale volcanic province in central Utah. Utilizing eight single component UUSS seismic stations at various distances from the swarm source, the event that correlated best with all other catalog events within the swarm was used as a template event and run against continuous seismic data for the entire duration of the year 2003. Events identified during this process that exceed a specified correlation value were identified as new detections within this swarm sequence. Templates were run in reverse over continuous data to determine correlation threshold values for each station in order to minimize false detections. This method has detected 47 to 147 new events (station dependent) in 2003 associated with the swarm. Future work will apply waveform correlation to three component stations for additional years to better understand the event propagation of these types of swarm sequences. We have also used a subspace method to detect events in this swarm and will document the differences between the detection methods considered here.

## **Research Efforts to Improve Regulatory Performance for Induced Seismicity**

Poster Session · Friday · 22 April · Tuscany F

#### **Characterization of Earthquake Site Amplification In Alberta, Canada for Induced-Seismicity ShakeMap Applications**

FARRUGIA, J. J., Western University, London, ON, Canada, jfarrugia@uwo.ca; ATKINSON, G. M., Western University, London, ON, Canada, gmatkinson@aol.com; MOLNAR, S., Western University, London, ON, Canada, smolnar8@uwo.ca

In Alberta, oil and gas operations, such as fluid injection and extraction wells and hydraulic fracturing, have led to a marked increase in seismic activity over the past decade. It has reached the point that ground motion amplification is a reality that has potentially devastating consequences, not only for the many pipelines that carry hydrocarbons across the province every day, but also other critical infrastructure. I therefore propose to develop and implement the first earthquake site characterization study of Alberta, Canada. The principal goal is to quantify earthquake ground shaking hazard through understanding the effects local geologic site conditions have on ground motion frequency content and amplitude. Loose unconsolidated materials generally increase or amplify earthquake ground shaking leading to observed damage. Thus, it is important that sites be characterized by their subsurface geologic conditions to evaluate their potential to amplify ground motions during earthquake shaking. I previously used earthquake data derived horizontal-to-vertical ratios of acceleration spectral response (H/V ratios) to perform a preliminary evaluation of earthquake site amplification in Alberta. I am now proposing a more robust site characterization for seismic stations in Alberta using in-situ geophysical data that will be acquired during a field campaign using ambient noise array and surface wave testing methods. Robust characterization of subsurface ground conditions at seismic stations is needed to improve the accuracy of future earthquake ground shaking estimates. Results from this study will provide insight into earthquake site response behaviour and variability in Alberta and define expected frequencies and amplitudes of earthquake shaking due to variable geology. This research is expected to deeply improve regulatory performance through the potential development of an intensity-based induced-seismicity traffic light response system for hydrocarbon extraction.

#### **Optimal Fault Orientations Determined from Focal Mechanisms for Oklahoma Earthquakes: 2010 to 2015**

DAROLD, A. P., USGS, Vancouver, WA, USA, adarold@usgs.gov; HOLLAND, A. A., USGS, Albuquerque, NM, USA

Focal mechanisms were calculated for 688 earthquakes that occurred within Oklahoma between 2010 and 2015. The greatest numbers of earthquakes are concentrated in central and north-central Oklahoma, and could create a sampling bias. The focal mechanisms are used to determine which fault orientations are optimal for failure within the contemporary stress field in Oklahoma. The focal mechanisms used in this compilation include Regional Moment Tensor solutions as well as first-motion focal mechanisms. From the orientations of the P- and T-axes of the 688 focal mechanisms used we estimated the contemporary maximum horizontal stress ( $s_1$ max) orientation to be N85°E, with a mean  $s_1$ max azimuth of 83.2° ± 21.3° and a median  $s_1$ max azimuth of 84.8°. Other groups have also estimated an  $s_1$ max of N85°E utilizing stress orientations obtained from wellbore image data and shear-velocity-anisotropy measurements from sonic dipole data. It is possible to define orientations of optimal, moderately optimal and sub-optimal distributions by constructing probability density functions of fault strike. The focal mechanism distribution is dominated by strike-slip motion on steeply dipping faults. Optimal orientations are 45°–60°, 105°–120° and 135°–150° and represent fault orientations most likely for failure. Moderately optimal orientations are 15°–45°, 60°–75°, 90°–105° and 120°–135° and represent fault orientations moderately likely for failure. All other orientations of fault strike are sub-optimal orientations and have a low likelihood of failure. These results do not indicate that failure will not occur on sub-optimal fault strikes, but rather that they are less likely. These results are applied to the most comprehensive Oklahoma fault map as a visual aid to identify significant fault orientations for determining the potential earthquake hazard of both naturally occurring and triggered seismicity.

#### **Monitoring Background Level of Seismicity in Regions with Shale Oil and Gas Potential in Eastern Canada**

LAMONTAGNE, M., Geological Survey of Canada, Ottawa, ON, Canada; LAVOIE, D., Geological Survey of Canada, Quebec City, QC, Canada, denis.



lavoie@canada.ca; KAO, H., Geological Survey of Canada, Sidney, BC, Canada, honn.kao@canada.ca

Two eastern Canadian areas have had some shale gas exploration activities in the last decade: southeastern New Brunswick (NB) and the St. Lawrence Lowlands (SLL) between Quebec City and Montreal (QC). In addition, starting in 2016 summer, some exploratory hydraulic fracturing (HF) for oil and gas will likely be done on the Island of Anticosti in the Gulf of St. Lawrence. Since 2012, the Department of Natural Resources Canada (NRCan) investigates possible relationships between HF and the changing pattern of local seismicity. One aspect is to define the pre-development seismicity reference line. Working retroactively in the SLL, earthquakes were compared in time and in space with the shale gas exploration work conducted between 2006 and 2010. Some shallow earthquakes were detected within 15 km of some HF wells but the hundreds of days between HF and earthquakes and the small injected volumes of fluids make any connection unlikely. In the Sussex area of NB, up to six real-time broadband seismograph stations have been in operation since 2012 to improve the monitoring of small local earthquakes. The region has a low level of natural seismicity and very few events have occurred in the hydraulic fracturing region. As in the SLL, the long period between their occurrences and HF (almost two years) makes a connection unlikely. In addition, when HF tests were done, it was found that no induced micro-earthquake occurred within the few hours during and following HF. Three new broadband seismograph stations have been deployed on Anticosti Island in the Fall of 2015. At the time of writing (Jan. 2016), no local earthquake has been recorded near the Island. For these three regions, the poster describes the results obtained up to now and gives examples of events that are either tectonic or induced in nature.

#### **Sensitivity Study for the 2016 USGS Seismic Hazard Model for Induced Seismicity**

HOOVER, S. M., USGS, Golden, CO, USA, shoover@usgs.gov; MOSCHETTI, M. P., USGS, Golden, CO, USA, mmoschetti@usgs.gov; PETERSEN, M. D., USGS, Golden, CO, USA, mpetersen@usgs.gov; MUELLER, C. S., USGS, Golden, CO, USA, cmueller@usgs.gov

The USGS National Seismic Hazard Model (NSHM) is updated about every 6 years for consideration in the seismic provisions of the International Building and Residential Codes. As the building code committee is one of the primary users of the NSHM and their needs are for a long-term seismic hazard model based on tectonic earthquakes, the 2014 update of the NSHM isolated and excluded potentially induced earthquakes from the model. However, the need to characterize the seismic hazard associated with induced earthquakes is clearly important. A preliminary set of induced seismicity hazard models and a sensitivity study was released by the USGS in 2015. After considering the 2015 preliminary models, an updated model will be released in spring 2016. This new model will assess the seismic hazard from tectonic and induced earthquakes.

This study presents a comparison of the probabilistic ground motions from the individual logic tree branches of the 2016 model. The branches studied include: rate models, declustering, b-value, catalog duration, smoothing distance, maximum magnitude (Mmax), ground motion models (GMMs), and hypocentral depth. We find that declustering and the GMMs have a large effect on seismic hazard. Also, Mmax has a significant effect on the 1-Hz spectral acceleration (SA) results, but little effect on the 5-Hz SA and peak ground acceleration (PGA) probabilistic ground motions. This is because of the greater sensitivity of 1-Hz SA ground motions to large-magnitude earthquakes compared to the 5-Hz SA and PGA ground motions. Hazard curves for the individual logic tree branches will be presented for Oklahoma City, Oklahoma and Dallas, Texas. Preliminary results indicate that ground motion values with one percent probability of exceedance in one year from the 2016 model are several times larger than the ground motion values for the 2014 NSHM.

#### **Seismic Real-time Monitoring of Induced Earthquakes at the Landau and Insheim Geothermal Reservoirs (SW Germany)**

BRÜSTLE, A., Geological Survey of Rhineland-Palatine, Mainz, Germany, andrea.bruestle@lgb-rlp.de; VASTERLING, M., Federal Institute for Geosciences and Natural Resources, Hannover, Germany, Margarete.Vasterling@bgr.de; SCHMIDT, B., Geological Survey of Rhineland-Palatine, Mainz, Germany, Bernd.schmidt@lgb-rlp.de; WEGLER, U., Federal Institute for Geosciences and Natural Resources, Hannover, Germany, ulrich.wegler@bgr.de

The Upper Rhine Graben is the region with the highest temperature gradient in Germany. Since 2007 at Landau and since 2012 at Insheim (5 km south of Landau) two geothermal power plants are running in the central Upper Rhine Graben. In 2009 at least two seismic events of ML 2.4 and 2.7 were felt at Landau and the surrounding area. The earthquakes were located in the region of the

power plant at depths of the geothermal reservoir. The hydraulic stimulation of the Insheim reservoir in April 2010 also caused two seismic events of ML 2.2 and 2.4, respectively, which were also felt. As a consequence the local seismic monitoring network of the company was densified by an additional scientific network within the research-project MAGS. Since October 2013 the follow-up research-project MAGS2 is focusing on the study of a potential interaction of the observed seismicity between the two geothermal systems. A seismic network of 14 surface stations is operated by the Federal Institute for Geosciences and Natural Resources (BGR, Germany). The network is completed by 4 borehole stations, operated by the local seismological survey of Rhineland-Palatine (LER, Germany) and industrial partner. The event detection is done by a real-time cross-correlation detector. Well-located observed events of each reservoir are defined as master events and the envelopes of these master events are cross-correlated with the ones of the real-time waveform data. The small network extension of less than 20 km makes a standard determination of the local magnitude impossible. Therefore a relative magnitude is determined from the amplitude of the master event and the detected event. Since the beginning of the project in October 2013 more than 350 events were automatically detected and classified as geothermal induced events. The seismic clouds of the Landau and Insheim reservoirs are clearly separated.

#### **Determining the Impact of Induced Seismicity—A Fully Integrated Modeling Approach**

BACHMANN, C. E., Lawrence Berkeley Laboratory, Berkeley, CA, USA, cebachmann@lbl.gov; FOXALL, W., Lawrence Berkeley Laboratory, Berkeley, CA, USA, wfoxall@lbl.gov; JEANNE, P., Lawrence Berkeley Laboratory, Berkeley, CA, USA, pjeanne@lbl.gov

While the concept of fluid-induced seismic activity has been studied over the last few decades, the increase in felt—and sometimes even damaging—events over the last few years has escalated the need to be able to model the ongoing processes and forecast possible induced seismicity. While the current seismic activity is often correlated with wastewater injection, the possibility of seismicity induced by the proposed long-term storage of carbon dioxide in the underground poses a potential risk for future projects.

In this study, we concentrate our efforts on Kimberlina, an area in the Southern San Joaquin Valley, identified by the DOE National Risk Assessment Partnership (NRAP) as a potential CO<sub>2</sub> injection demonstration site.

To obtain a complete estimate of the impact of a proposed fluid injection, it is important to include seismic hazard in the estimate of overall risk for an injection site. Here we describe combining the RSQSim earthquake simulator and the RiskCat code to estimate seismic hazard prior to injection. The physics-based earthquake simulator RSQSim is based on rate-state friction and was originally developed to model large-scale scenarios, such as, for example, those for the UCERF3 fault model in California. The code authors recently added the capability to account for increased overpressure resulting from fluid injection. We use seismicity catalogs generated by RSQSim simulations as input to RiskCat seismic hazard calculations. Ground motions are calculated within RiskCat by convolving the earthquake sources with pre-computed Green's functions.

In this study, we present the influence of the pore-pressure distribution due to injection at Kimberlina, calculated with the TOUGH2 flow code. By using pore-pressure distributions based on realistic input parameters, we are able to create realistic representations of expected seismicity and hazard. We propose that such physics-based methods can be used during the permitting stage of prospective projects.

#### **Science-based Decision Making in a High-risk Energy Production Environment**

WEISER, D. A., USGS and UCLA, Pasadena and Los Angeles, CA USA, dweiser@usgs.gov; JACKSON, D. D., UCLA, Los Angeles, CA USA, djackson@g.ucla.edu

When beginning energy production practices that may induce earthquakes, decisions must be made about acceptable risk. How much ground shaking is tolerable? We investigate strategies to help identify when geothermal production may lead to induced earthquakes. We review current and past mitigation strategies as well as existing protocol. A framework for making decisions about (potentially) risky earthquakes is presented. Timely and accurate scientific information can assist in determining the costs and benefits of changing production parameters. Helpful information includes a probability estimate of the "cost", the frequency of earthquakes of different sizes, and associate costs of different magnitude earthquakes.

Risk management decisions based on robust science, which are well communicated to stakeholders, are beneficial to mitigation efforts. Effective elements to communicate include risks and benefits of different actions (such as a traffic light system), factors considered when deciding what is acceptable risk, and the

probability of specific magnitude events. Clear visuals can aid the accessibility of information to multi-lingual communities and to those with low science-literacy. Social media may be helpful in disseminating information to a broad audience.

We present a case example for The Geysers geothermal field to discuss “acceptable” and “unacceptable” earthquakes in a probabilistic framework, and share the responses of geothermal field operators and nearby communities to smaller and larger magnitude earthquakes. What magnitude earthquake is tolerable (to both local residents and operators)? We use the USGS’s “Did You Feel It?” data archive to sample how often felt events occur and how many of those are above acceptable magnitudes.

#### **Detecting and Relocating Potentially Induced Earthquakes in Southern Kansas**

DOUGHERTY, S. L., U.S. Geological Survey, Pasadena, CA, USA, sdougherty@usgs.gov; COCHRAN, E. S., U.S. Geological Survey, Pasadena, CA, USA, ecochran@usgs.gov; HARRINGTON, R. M., McGill University, Montreal, QC, Canada, rebecca.harrington@mcgill.ca; RUBINSTEIN, J. L., U.S. Geological Survey, Menlo Park, CA, USA, jrubinstein@usgs.gov

The sudden appearance and dramatic increase in seismicity in southern Kansas beginning in early 2014 coincides with the expansion of oil and gas activities in this area, including wastewater injection, suggesting these events are being induced. A temporary, 14-station seismic network was deployed by the USGS across an 1,800 km<sup>2</sup> region in southern Kansas in spring 2014 to monitor the ongoing seismicity, with supplementation from regional and national networks. In the first 18 months of data collection, more than 4,000 events have been identified and located, forming clusters and lineations up to 10 km or more from high-rate injection wells. Higher-precision earthquake locations and a more complete event catalog are needed in order to more fully assess the potential spatiotemporal relationship between wastewater injection and seismicity and identify active fault planes. Catalog and waveform cross-correlation data for already identified events will be used to perform a double-difference relocation of their hypocenters. Additional and smaller magnitude earthquakes that were previously undetected will be searched for with a waveform-correlation-based event detection technique using catalog events as waveform templates. Newly detected events will be located and included in an updated double-difference hypocentral relocation of all events. Such event detection and relocation techniques have been successfully applied in recent studies to other induced sequences, such as in Ohio, Arkansas, and Italy. The detection and relocation of earthquakes in southern Kansas will enhance the event catalog in this region in terms of completeness and location precision, enabling us to more completely characterize the potentially induced seismicity in time and space, relative to active wastewater injection.

#### **The First Step Toward an Effective Traffic Light Protocol for Induced Seismicity: A Data-Sharing Framework for Earthquake Monitoring in Northeast British Columbia, Canada**

KAO, H., Geological Survey of Canada, Sidney, BC, Canada, honn.kao@canada.ca; MAHANI, A. B., Geoscience BC, Victoria, BC, Canada, ali.mahani@mahangeo.com; WALKER, D., BC Oil and Gas Commission, Victoria, BC, Canada, Dan.Walker@bcogc.ca; ATKINSON, G. M., University of Western Ontario, London, ON, Canada, Gmatkinson@aol.com; EATON, D. E., University of Calgary, Calgary, AB, Canada, eatond@ucalgary.ca

There is an increasing trend for regulatory agencies to establish “traffic light” protocols (TLP) as part of their decision-making process to reduce seismic risk associated with injection-induced seismicity (mainly due to hydraulic fracturing or wastewater disposal). The ultimate goal of a TLP is to achieve a balance between the economic benefit of industrial operations and the protection of public safety. Most existing TLPs define the threshold of different lights (“green”, “yellow”, or “red”) based on the magnitude of the induced earthquake, and sometimes, felt reports from local communities. Obvious deficiencies of this approach include uncertainties in the determination of magnitude, lack of link to the impact and consequences of reported event(s), and the neglect of other indicators that may be more relevant than magnitude. To make the TLP more effective, it is important to incorporate ground motion information in the process to better assess the actual risk and damage potential when a relatively large felt event occurs. Such a goal requires high station density and good calibration of a model characterizing source, attenuation and site effects. Using all stations funded by public funds in northeast BC as the backbone, we plan to establish a framework of data sharing that includes seismic data collected by the private sector for monitoring of regional earthquakes. This framework must satisfy important criteria in data quality, quantity and accessibility to enable the development of improved TLP protocols. It will provide necessary data for a reliable and consistent determination of earthquake source parameters, including origin time, epicenter, depth, and magnitude, and for the construction of real-time ground shaking maps. The

rapid and unambiguous determination of event and ground-motion parameters will benefit operators, regulators and the public. It will also benefit the research community by facilitating broad collaborations with improved databases.

---

## **Risk Management Applications of Earthquake Seismology**

Poster Session · Friday · 22 April · Tuscany F

---

#### **Seismic Source Model for a System-Wide Dam Risk Reduction Program in Northern California**

MADUGO, C., Pacific Gas and Electric Company, San Francisco, CA, USA, C7M0@pge.com; ABRAMSONWARD, H., Lettis Consultants International, Walnut Creek, CA, USA, hans@lettisci.com; HITCHCOCK, C., InfraTerra Consultants, Oakland, CA, USA, chitchcock@infraterra.com; LEWANDOWSKI, N., Lettis Consultants International, Walnut Creek, CA, USA, lewandowski@lettisci.com; PAGE, W., Pacific Gas and Electric Company, San Francisco, CA, USA, wdp7@pge.com; SAWYER, T., Piedmont Geosciences, Reno, NV, USA, Tom@piedmontgeosciences.com; THOMPSON, S., Lettis Consultants International, Walnut Creek, CA, USA, Thompson@lettisci.com; WOODDELL, K., Pacific Gas and Electric Company, San Francisco, CA, USA, KxWl@pge.com; DONAHUE, J., Geosyntec Consultants, San Francisco, CA, USA, jdonahue@geosyntec.com

Pacific Gas & Electric Company (PG&E) has initiated a long-term program to quantify seismic risk for its approximately 170 dams in California (see companion abstract by Wooddell *et al.*). The preliminary seismic source characterization (SSC) model for probabilistic seismic hazard analyses (PSHA) includes approximately 160 crustal fault sources, the Cascadia megathrust, and areal source zones to capture hazard from unmapped faults. SSC fault sources overlap with UCERF3-modeled faults along the boundaries of the Great Valley-Sierra Nevada microplate, but a majority of faults in the SSC model, particularly those located near PG&E dams within the Sierra Nevada and southern Cascade Ranges are not part of the statewide SSC models. These faults were characterized in part or in whole based on work performed by PG&E and other utilities for site-specific seismic hazard evaluation. All crustal faults in the SSC model are characterized using a simple logic tree approach that emphasizes uncertainty in source geometry, magnitude probability density functions, fault slip rate, and time-dependent recurrence. Some relevant findings of initial sensitivity analyses include: (1) uncertainty in time dependency is the largest contributor to total hazard uncertainty from the SSC model; (2) fault slip rate uncertainty is the second largest contributor, with a common pattern that geodetically-based slip rates differ significantly from geologic slip rates; (3) third-order contributors to hazard uncertainty include dip of nearby faults and the shape of and values anchoring the magnitude-frequency distribution; and (4) as expected, nearby faults frequently contribute most to high-frequency ground motions, and, although distant, the San Andreas and Cascadia megathrust sources contribute significantly to low-frequency ground motions at most dams. The system-wide risk reduction program will help prioritize future SSC model study efforts.

#### **Background Seismic Source Model Uncertainty Impacts on Hazard and Risk**

APEL, E., Risk Management Solutions, Newark, CA, USA, trey.apel@rms.com

In probabilistic seismic hazard and risk assessments seismic sources are typically divided into two groups: fault sources and background sources. Background sources can be modeled as areas, points or pseudo-faults. Rates for these sources are typically estimated using earthquake catalogs or paleoseismic data. When background sources are modeled as pseudo-faults, magnitude-length relationships, fault orientations, and maximum magnitudes are required to construct these pseudo-faults. In addition, rate estimations require completeness intervals, maximum magnitudes and parameters for smoothing. The uncertainties associated with these variables is often ignored or discarded in hazard and risk models, particularly when fault sources are the dominant contributor. Conversely, in areas like the Central and Eastern United States and Eastern Canada the hazard and risk is driven primarily by background sources and these uncertainties are much more significant. In this study we test the impact of using reasonable ranges of background parameters and compute the resulting epistemic uncertainties for the seismic hazard and risk in the Eastern United States and Canada. We use a suite of metrics to compare the various uncertainty models to assess 1) the impact on hazard and risk and 2) the epistemic uncertainty associated with choice of parameters. In areas where the seismic hazard is dominated by larger crustal faults (*e.g.* New Madrid) the choice of background parameters has little impact on the hazard or risk. However away from the New Madrid region the choice of param-



eters is more significant and may approach the size of the uncertainty associated with the ground motion prediction equation suite.

### **A Methodology for Quantifying the Hazard of Surface-Fault Displacement to Gas Pipelines in Northern California**

**THOMPSON, S.**, Lettis Consultants International, Inc., Walnut Creek, CA, USA, thompson@lettisci.com; **MADUGO, C.**, Pacific Gas & Electric Company, San Francisco, CA, USA, C7M0@pge.com; **LEWANDOWSKI, N.**, Lettis Consultants International, Inc., Walnut Creek, CA, USA, lewandowski@lettisci.com; **GIVLER, R.**, Lettis Consultants International, Inc., Walnut Creek, CA, USA, givler@lettisci.com; **INGEMANSSON, B.**, Pacific Gas & Electric Company, San Francisco, CA, USA, BXI1@pge.com

Pacific Gas and Electric's extensive network of gas transmission pipelines overlaps Northern California's extensive network of seismogenic faults. Understanding and mitigating the risk of pipeline failure from surface-fault rupture is a considerable engineering and seismological challenge to the utility. We developed a methodology to quantify displacement hazard at each pipeline-fault crossing, which represents an intermediate step in the evolution of risk-based engineering of lifelines. In keeping with current engineering practice focused on deterministic evaluation, our approach is to develop displacement hazard estimates for "Maximum Considered Earthquake (MCE)" scenarios that produce surface-fault displacement at the pipeline. Rather than the traditional deterministic approach of adopting a single MCE magnitude and a displacement from the MCE from a simple empirical scaling relation, our methodology considers epistemic uncertainty in the MCE through logic trees, and epistemic and aleatory uncertainties in the amount of displacement that may occur at the pipeline crossing site given the MCE. The scenario displacement hazard, therefore, is presented as an exceedance curve. Decision makers can then evaluate whether existing pipelines may be considered fit for service or in need of mitigation based on exceedance values that scale with pipeline importance or consequence of failure. The methodology can also incorporate information on fault slip rate or recurrence interval to convert deterministic exceedance curves into equivalent, simplified probabilistic hazard curves. The intended use of the simplified probabilistic hazard curves is as a ranking tool, whereby each pipeline-fault crossing can be "scored" or ordered by the annual probability of surface displacement exceeding the current pipeline capacity. We anticipate such information will be useful for prioritizing pipeline mitigation projects and will make the overall system more resilient to seismic hazards.

### **The Regularity of Very Large Complex Events, and its Impact on Risk**

**FITZENZ, D. D.**, RMS, Newark, CA, USA, delphine.fitzenz@rms.com; **NYST, M.**, RMS, Newark, CA, USA, marleen.nyst@rms.com

Complex ruptures happen and should definitely be incorporated into hazard and risk studies. Those ruptures typically jump across geometrical complexities, *e.g.*, from strike-slip to dipping faults, across step-overs. The two main challenges are: 1) quantify how often they might happen on average, and 2) estimate how regularly they might happen. While segment slip rate information and magnitude-frequency distribution on the fault system might help constrain the mean recurrence time (as in UCERF3), the aperiodicity needs other input. Recent studies have shown that the less mature the fault at a certain location, the less localized surface and near-surface slip is, and the larger the discrepancy between slip at depth and slip at the surface trace (Dolan and Haravitch, 2014). Also, step-overs are thought to be regions of increased fluid flow. So not only is the stress level there less likely to be homogeneous, but also healing mechanisms involving both friction and cohesion might be very spatially variable. Paleoseismological compilations in California (Biasi 2015) show larger aperiodicities near fault complexities. This can come from seeing different size events going through one point on a fault, so enough information to sort through event sizes are necessary. When not enough data is available to resolve an issue because of short observation window, it is customary to turn to earthquake simulators. In simulated faults that are defined as frictional interfaces only, UCERF3 compiled aperiodicities and found a trend with magnitude, with values as low as 0.1 or 0.2 for events larger than  $M_w=7.7$ . These low values have spectacular effects on both the average annual loss (basis for insurance premiums) and on the reserves needed to keep a company in business with a good rating. It is therefore important to further study the regularity of very large earthquakes in the context of complex geometries, localized vs broad deformation, and friction and cohesion healing.

### **Using MMI Shaking Probabilities to Assess the Exposure to Damaging Earthquakes in Canada**

**ALLEN, T.**, Natural Resources Canada, Sidney, BC, Canada, trevor.allen@canada.ca; **ONUR, T.**, Onur Seemann Consulting, Victoria, BC, Canada,

tuna@onurseemann.com; **SEEMANN, M.**, Onur Seemann Consulting, Victoria, BC, Canada, mark@onurseemann.com; **JOURNEY, M.**, Natural Resources Canada, Vancouver, BC, Canada, murray.journey@canada.ca; **HALCHUK, S.**, Natural Resources Canada, Ottawa, ON, Canada, stephen.halchuk@canada.ca

The Geological Survey of Canada has contributed seismic hazard information to underpin the seismic provisions of the National Building Code of Canada (NBCC) since 1953. Modern contributions are in the form of probabilistic seismic hazard analyses, which typically yield a ground-motion value with a chance of being exceeded at a given probability level. These ground motions are presented in terms of peak ground acceleration or response spectral metrics and are used to strengthen the seismic resilience of our built environment. Communicating hazard information to emergency managers, decision makers and the public quantitatively yet in an easy to understand format is often a challenging task. Onur *et al.* (2008) presented shaking probabilities for select communities across Canada for various levels of Modified Mercalli Intensity (MMI) using the 2005 NBCC hazard values as a basis. Macroseismic scales, such as MMI, fundamentally simplify communicating earthquake hazard and risk to those outside of engineering and seismological fields. We update the Onur *et al.* study using the fully probabilistic 2015 NBCC hazard values combined with recent ground-motion-to-intensity conversion equations to provide mean probabilities for Canadian communities to experience potentially damaging ground motions ( $MMI \geq VII$ ) for a range of planning horizons. The uncertainty associated with these probability levels is also considered. Generally, we find the standard deviation of MMI shaking probabilities to be in the order of 50 percent of the mean value. Finally, mean MMI shaking probabilities are superimposed with national-scale population data to assess the number of people and critical assets likely to experience damaging ground motions within a 50-year planning horizon. Results from this study are intended to better enable elected officials, community planners and emergency managers as well as the wider public to identify, understand and manage the earthquake threat in their communities.

---

## **Secondary Earthquake Hazards and Losses**

Poster Session · Friday · 22 April · Tuscany F

---

### **Towards Rapid Likelihood Estimation of Earthquake-Triggered Gravitational Mass Movements in Switzerland Based on Ground-Shaking Scenarios, Geomorphology and Geotechnical Information.**

**CAUZZI, C.**, Swiss Seismological Service (SED) at ETH Zurich, Zurich, Switzerland, carlo.cauzzi@sed.ethz.ch; **FÄH, D.**, Swiss Seismological Service (SED) at ETH Zurich, Zurich, Switzerland, donat.fah@sed.ethz.ch; **WIEMER, S.**, Swiss Seismological Service (SED) at ETH Zurich, Zurich, Switzerland, stefan.wiemer@sed.ethz.ch; **WALD, D. J.**, U.S. Geological Survey, Golden, CO, USA, wald@usgs.gov; **CLINTON, J.**, Swiss Seismological Service (SED) at ETH Zurich, Zurich, Switzerland, jclinton@sed.ethz.ch

Landslides, rockfalls and avalanches are a major hazard in mountain regions, and these events are frequently triggered by earthquake shaking. Even when the urban environment is not directly impacted by these phenomena, a high risk of deadly impacts still exists, as shown by the numerous climbers killed by avalanches and rockfalls triggered by the recent Nepal (April 2015) and Sabah, Malaysia (June 2015) earthquakes. In Switzerland, nearly all historical  $M > 6$  earthquakes have induced damaging rockslides, resulting in some cases in the destruction of settlements and loss of lives. Earthquake-triggered ocean and lake tsunamis generated by underwater landslides and rockfalls are also well documented. Notable is the case of the 1929 Grand Banks earthquake offshore Canada. In Switzerland, the earthquakes of Aigle 1581 and Unterwalden 1601 have been associated with lake tsunamis most likely induced by underwater mass movements. With this motivation, Cauzzi *et al.* (2015) investigated the potential use of geospatial proxies and earthquake shaking intensity in Switzerland for a near-real-time assessment of the likelihood of landslides/rockfalls by customising the global approaches of Nowicki *et al.* (2014) to Swiss conditions. In this contribution we update the results of Cauzzi *et al.* (2015) by investigating the possible use of: (a) frequency-dependent intensity measures (*e.g.*, PGA, PGV and response spectral ordinates); (b) different geomorphological proxies (*e.g.*, the topographic slope, its first derivative and their statistical distributions); (c) high-resolution (30 m and 90 m) elevation data and (d) the use of geotechnical information available at national/regional level. Our results show that adding (c) and (d) is key to improving our prediction of the different types of mass movements. Our calibration dataset comprises the damaging events ( $IEMS-98 \geq VII$ ) available in the Swiss earthquake catalogue ECOS-09. We discuss a prototype implementation in Swiss ShakeMap.



### Use of an Expanded Global Earthquake Data Set to Develop a Near Real-time Model for Predicting Seismically Induced Landslides

JESSEE (NOWICKI), M. A., Indiana University, Bloomington, IN USA, anowicki28@gmail.com; HAMBURGER, M. W., Indiana University, Bloomington, IN USA, hamburg@indiana.edu; WALD, D. J., U.S. Geological Survey, Golden, CO, USA, wald@usgs.gov; HEARNE, M., U.S. Geological Survey, Golden, CO, USA, mhearne@usgs.gov; ROBESON, S. M., Indiana University, Bloomington, IN, USA, srobeson@indiana.edu; THOMPSON, E. M., U.S. Geological Survey, Golden, CO, USA, emthompson@usgs.gov; TANYAS, H., University of Twente, Enschede, Netherlands, h.tanyas@utwente.nl; ALLSTADT, K., U.S. Geological Survey, Golden, CO, USA, kallstadt@usgs.gov

We present a globally applicable statistical model that can be used to rapidly estimate the probability and distribution of seismically induced landslides. This model utilizes ground-shaking estimates from the USGS ShakeMap tool, together with globally available proxies for landslide susceptibility factors. We can then automatically generate maps of landslide probabilities, with the ultimate goal of adding fatality and economic loss estimates due to secondary hazards into the USGS Prompt Assessment of Global Earthquakes for Response (PAGER) system. Our improved model includes observations from over 30 landslide-triggering earthquakes from a variety of tectonic and geomorphic settings for which we have obtained landslide inventories. This global database is combined with shaking estimates from the ShakeMap Atlas and globally available landslide susceptibility proxies as an input to a logistic regression to build a predictive landslide model. We test a large number of additional landslide proxies, including high-resolution (7.5 arc-second, roughly 250m) slope datasets, topographic position index, slope curvature and aspect, elevation, rock strength, lithology, land cover, mean monthly precipitation, and green vegetation cover. We also introduce a data-sampling scheme that addresses potential systematic errors associated with variability in landslide inventories. Our initial results indicate strong relationships between landslide occurrence, peak ground velocity, and slope, with weaker dependence on other properties. We apply this approach to scenario earthquakes to assess probabilities for future landslides in areas of known seismic risk. Ultimately, we hope to superimpose landslide probabilities on maps of population and infrastructure to estimate losses associated with landslides, and use this information along with a complete database of impact from historical landslide events to estimate the impact of landslides for any event for which a ShakeMap is produced.

### Updated Geospatial Liquefaction Model for Global Use

ZHU, J., Tufts University, Medford, MA, USA, jing.zhu@tufts.edu; BAISE, L. G., Tufts University, Medford, MA, USA, laurie.baise@tufts.edu

Liquefaction hazard and loss assessments can benefit from the geospatial approach (Zhu et al 2015), which predicts the probability of liquefaction from globally available layers as proxies for contributing factors to liquefaction and ShakeMap intensities. We have previously developed a liquefaction model using the geospatial approach and data from four earthquakes in Christchurch and Japan. This work updates the model to improve the performance and the generalization of the model. The updates include 1) expanding the liquefaction database, 2) addressing sampling for liquefaction point data, 3) testing interaction effects between explanatory variables, and 4) fine-tuning the model. First, we add 27 events to the database including four nonliquefaction events and one noncoastal event. To incorporate point data from the newly added events, we apply a sampling procedure. We test the sensitivity of the model coefficients to the sampling such as class imbalance and the spatial buffer width. Next, we assess the interaction effects between variables to account for the scenario when the coefficient of one predictor is dependent on the second predictor. Finally, we propose new models and evaluate the new models in different geographic regions. Given the broader database used in the model development and the cross-validation testing we have performed, we are confident that the proposed models can be applied accurately at the global scale. It must be noted that the meaning of the predicted probability from a liquefaction model is dependent on the nature of the observations used for developing the model. The lack of spatially complete liquefaction data limits the development of a probability estimator, and the proposed models are recommended to be used as classifiers.

### Combining Case History Observations with Different Completeness Levels in Empirical Ground-Failure Models

THOMPSON, E. M., USGS, Golden, CO, USA, emthompson@usgs.gov; WALD, D. J., USGS, Golden, CO, USA, wald@usgs.gov; ALLSTADT, K.,

USGS, Golden, CO, USA, kallstadt@usgs.gov; HEARNE, M., USGS, Golden, CO, USA, mhearne@usgs.gov

Empirical models of earthquake-induced liquefaction and landsliding fundamentally rely on case history observations for development, calibration, and assessment. In order to obtain reliable models, it is important to obtain observations that span a wide range of seismic (loading) and geologic and hydrologic (susceptibility) conditions. However, the availability of case histories is limited and their quality varies widely. Factors that affect the quality of a case history include the completeness, comprehensiveness, resolution, and type of attributes documented by the observations. Using liquefaction as an example, some case histories may include a comprehensive description of both the occurrence and non-occurrence of liquefaction, while other case histories may only include a handful of observations of occurrence. The use of incomplete data results in a ratio of occurrences-to-non-occurrences (*i.e.*, class balance) that is not representative of the actual frequency of occurrence. Prior work has shown that for logistic regression, a technique commonly used to develop statistical ground-failure models, if the class balance of the observations is not the same as the true class balance then the resulting probabilistic model will be severely biased. This problem is particularly important for ground failure case histories because there are only a handful of datasets that can be classified as complete, yet many of the incomplete case histories contain important and informative observations. Thus, the challenge is to combine these observations in a manner that avoids the class-balance bias. In this presentation, we present an algorithm that solves this problem by iteratively estimating the balance of incomplete data from complete data, and imposing this class on the incomplete data samples. We then apply this approach to real datasets to show the benefit of a systematic class-balance approach combining multiple datasets of variable completeness and quality.

### Spatiotemporal Modeling of Groundwater Elevation for Liquefaction Hazard and Loss Estimation

LEE, S. J., Risk Management Solutions, Newark, CA, USA, Sean.Lee@rms.com; AKITA, Y., Risk Management Solutions, Newark, CA, USA, Yasuyuki.Akita@rms.com; ANCHETA, T. D., Risk Management Solutions, Newark, CA, USA, Tim.Ancheta@rms.com

Quantifying liquefaction hazard and loss requires an accurate representation of spatial extent and severity of liquefaction as well as their uncertainties. Groundwater elevation is a vital input to liquefaction hazard estimation as it is strongly correlated with both the spatial extent and severity. The uncertainty of liquefaction extent and severity is also a vital input in estimating loss. Unfortunately, it is common to not include an accurate representation of groundwater elevation in liquefaction hazard or the effect of groundwater variation in loss estimation. The spatiotemporal dynamics of groundwater elevation could be a key driver to estimating accurate loss varied by region and season, but it is challenging to gain insight about the spatiotemporal variability due to lack of measurements of groundwater elevation over space and time. The objective of the study is to estimate spatiotemporal estimation of groundwater elevation while rigorously accounting for seasonal and regional variability as well as data uncertainty arising from incomplete measurements. We quantify spatiotemporal correlation structures over space and time and data uncertainty source, and process them through Bayesian Maximum Entropy of modern spatiotemporal geostatistics. The proposed methodology is showcased for a study area in the New Madrid seismic zone and demonstrates that it improves upon purely spatial geostatistics while newly representing spatiotemporal dynamics of groundwater elevation; a comparison of the liquefaction losses within HAZUS for select scenario events is also shown. The findings of the work are useful in understanding spatiotemporal changes of liquefaction hazard and eventually understanding the uncertainty of liquefaction hazard.

### Comparison of Liquefaction Triggering Methods on Borehole Data from Four Quadrangles in the Santa Clara Valley, California.

BRANUM, D. M., California Geological Survey, Sacramento, CA, USA, dbrantum@consrv.ca.gov; MOSKOVITZ, B., California Geological Survey, Sacramento, CA, USA, Bob.Moskovitz@conservation.ca.gov; REAL, C., California Geological Survey, Sacramento, CA, USA, Chuck.Real@conservation.ca.gov

Different methods to determine the hazard of possible liquefaction during a seismic event have been published in the last 20 years. Which methods should be used for creating a large-scale liquefaction map using geotechnical data collected from public borehole logs?

Several published methods of testing for liquefaction triggering (including Seed and others, 2003; Youd and others, 2001; Boulanger and Idriss, 2014; etc) are being performed on approximately 700 geotechnical boreholes from the

Santa Clara, California area. The boreholes are located in the San Jose East, San Jose West, Calaveras Reservoir and Milpitas 7.5-minute quadrangles and were collected as part of the Seismic Hazards Mapping Program. The dataset contains SPT-equivalent measurements along with other necessary geotechnical laboratory data. Comparisons are being made on Factor of Safety (FS) and Cyclic Stress Ratios (CSR) from the various calculated methods using a recently developed Python program. The program analyses each soil layer of a boring log and uses sample data to compile the best geotechnical description of the layer. Field blow counts are converted to SPT equivalent values and used in the equations to calculate CSR and FS.

The desired result of this study is to find which geotechnical conditions cause the largest variance in CSR and FS among the different methods. This will assist in data collection and processing for creation of large-scale liquefaction hazard maps.

---

## Seismicity and Seismic Hazards of the Walker Lane and Western Great Basin

Poster Session · Friday · 22 April · Tuscany F

---

### Geologic Model of the Development of Las Vegas Basin, Nevada

TAYLOR, W. J., University of Nevada Las Vegas, Geoscience, Applied Geophys Cntr, Las Vegas, NV, USA, wanda.taylor@unlv.edu; WAGONER, J., Lawrence Livermore National Laboratory, Earth Science Division, Livermore, CA, USA, wagoner1@llnl.gov; ABDELHALEEM, S. A., University of Nevada Las Vegas, Geoscience, Applied Geophys Cntr, Las Vegas, NV, USA, aliabdel@unlv.nevada.edu; LUKE, B., University of Nevada Las Vegas Civil & Environmental Eng., AGC., Las Vegas, NV, USA, barbara.luke@unlv.edu

We suggest that Las Vegas basin, southern Nevada, formed during two episodes of deformation: (1) Miocene right-lateral and normal faulting and (2) Pliocene-Quaternary normal and left-lateral faulting. In the basin, > 4.5 km of basin fill unconformably overlies Neoproterozoic to Mesozoic bedrock. Lithologic data from 6 deep wells and ~1150 wells that average 160 m in depth along with geologic map and geophysical data suggest the two episodes of deformation. Structural control on the Miocene basin-fill appears to be the ~N-striking Frenchman-River Mountains fault (FRMF) on the E side of the basin and the WNW-striking Las Vegas Valley shear zone (LVVSZ) on the N. Thickness of the Miocene sediments is largest near these faults suggesting significant Miocene offset. A Miocene basin is confirmed by the presence of Miocene Horse Spring Formation, Red Sandstone, and Muddy Creek Formations in wells and locally around the basin edges. In addition to ~50 km of right slip on the LVVSZ, basin-fill thickness requires at least 2.5 km of normal slip. The FRMF has ~5 km of normal slip based on basin-fill thickness, but some slip is Pliocene-Quaternary as evidenced by fault scarps. Changes in and the distribution of lithologies indicate a W shift in the basin depocenter between the Miocene and Pliocene-Quaternary. This shift represents a change in the particular faults that were active. Activity ceased or decreased on the LVVSZ and FRMF and increased on the Las Vegas Valley fault system (LVVFS), exposed near the central of the valley. The Pliocene-Quaternary depocenter shifted toward the LVVFS, suggesting that system was active then. The change in deformation through time is consistent with new map data along the NE edge of the basin suggesting that the Miocene LVVSZ is cut by post-4.5 Ma faults. The superimposed deformations and basins in the Las Vegas Valley exemplify changes in tectonism from Miocene to Pliocene-Quaternary seen elsewhere in the central Basin and Range province.

### Surface Slip during Large Owens Valley Earthquakes

HADDON, E. K., San Francisco State University, San Francisco, CA, USA, haddon@sfsu.edu; AMOS, C. B., Western Washington University, Bellingham, WA, USA, colin.amos@wwu.edu; ZIELKE, O., King Abdullah University of Science and Technology, Thuwal, Saudi Arabia, olaf.zielke@kaust.edu.sa; JAYKO, A. S., United States Geological Survey, Bishop, CA, USA, ajayko@usgs.gov; BURGMANN, R., Univ. of California, Berkeley, CA, USA, burgmann@seismo.berkeley.edu

The 1872 Owens Valley earthquake is the third largest known historical earthquake in California. Relatively sparse field data and a complex rupture trace, however, inhibited attempts to fully resolve the slip distribution and reconcile the total moment release. We present a new, comprehensive record of surface slip based on lidar and field investigation, documenting 162 new measurements of laterally and vertically displaced landforms for 1872 and prehistoric Owens Valley earthquakes. Our lidar analysis uses a newly developed analytical tool to measure fault slip based on cross-correlation of sub-linear topographic features and produce a uniquely shaped probability density function (PDF) for each

measurement. Stacking PDFs along strike to form cumulative offset probability distribution plots (COPDs) highlights common offset values corresponding to single- and multiple-event displacements. Dextral offsets for 1872 vary systematically from ~1.0-6.0 m and average  $3.3 \pm 1.2$  m ( $2\sigma$ ). Vertical offsets are predominantly east-side down from ~0.1 and 2.4 m, with a mean of  $0.8 \pm 0.5$  m ( $2\sigma$ ). The lateral-to-vertical ratio averaged at specific sites is ~6:1. Summing offset measurements across sub-parallel, overlapping ruptures implies net displacement averaging  $4.4 \pm 1.5$  m ( $2\sigma$ ) and a geologic  $M_w \sim 7.5$  estimate for the 1872 event. We attribute progressively higher-offset lateral COPD peaks at  $7.4 \pm 1.3$  m,  $12.4 \pm 1.2$  m, and  $16.6 \pm 1.4$  m ( $2\sigma$ ) to three earlier surface ruptures. Evaluating cumulative displacements in context with previously dated landforms in Owens Valley suggests relatively modest rates of fault slip, averaging between ~0.6-1.6 mm/yr ( $1\sigma$ ) over the late Quaternary.

### Holocene-Age Earthquakes and Surface Rupture Zoning of the West Tahoe Fault

SEITZ, G., California Geological Survey, Menlo Park, CA, USA, Gordon.Seitz@conservation.ca.gov; MARESCHAL, M., California Geological Survey, Menlo Park, CA, USA

The West Tahoe Fault is the primary range-bounding, east-dipping normal fault along the west margin of the Tahoe Basin. The most recent Lidar (Watershed Sciences, 2010) improved the identification of active fault traces. Our mapping shows a single strand extending north from the southern end, 2.5 km south of highway 50, splitting into two parallel strands at Fallen Leaf Lake, and extending offshore at Emerald Bay. The submerged portion of the fault is well expressed along the western base of Lake Tahoe, with scarps in lake-bottom sediments, and across the ~50 ka age McKinney Bay slide.

Lidar allowed the selection of a trench site with fine-grained surface sediments, near to Osgood Swamp. We observed a normal fault juxtaposing glacial deposits against datable peat-bearing and charcoal-rich alluvial sediments. Evidence for three earthquakes is based on scarp-derived colluvium, fissures, faulted scarp-related alluvium, liquefaction, and upward terminations of faults. Retrodeformation of the sediments results in vertical displacements of 1.4m, 0.8m and 1m from the most recent to oldest event, respectively. Results from multiple C-14 analyses place the most recent event at ~5.5 ka, the penultimate event at ~7.2 ka, and the oldest event at ~9 ka. These events are associated with offshore Lake Tahoe turbidites, and landslides in Fallen Leaf Lake. Vertical slip rate estimates from displaced on and offshore markers are 0.6-1.5 mm/yr.

If the number of on land events are representative of the faulting that created the offshore scarps then single event vertical displacements of 3-5 m can be expected for future earthquakes. This may have dire implications for earthquake generated lake tsunamis and permanent shoreline subsidence.

This research has contributed to seismic hazard assessments and specifically, surface rupture hazard zoning. A fault evaluation report (FER) and preliminary Alquist-Priolo (AP) maps for the Emerald Bay and Echo Lake 7.5 min maps have been released.

### Quaternary Faulting in the Pyramid Lake Basin, Northern Walker Lane, Nevada

DEE, S., Nevada Bureau of Mines and Geology, Reno, NV, USA, sdee@unr.edu; KELL, A., Nevada Seismological Laboratory, Reno, NV, USA, annie.kell@gmail.com; ANGSTER, S. J., University of Nevada Reno, Reno, NV, USA, angster41@gmail.com; KENT, G. M., Nevada Seismological Laboratory, Reno, NV, USA, gkent@unr.edu; DRISCOLL, N., Scripps Institution of Oceanography, San Diego, CA, USA, ndriscoll@ucsd.edu; FAULDS, J. E., Nevada Bureau of Mines and Geology, Reno, NV, USA, jfaulds@unr.edu; ANDERSON, R. P., University of Nevada Reno, Reno, NV, USA, ryan.b.anderson@wsu.edu

The Pyramid Lake basin is situated in a transition zone between the eastern margin of the northern Walker Lane and the western Basin and Range province. Recent multi-disciplinary studies have illuminated the style of Quaternary faulting, slip rates, and strain partitioning in the basin. These studies include geologic mapping, CHIRP and bathymetric surveys of Pyramid Lake, fault trenching, and slip rate estimates. Collectively these on and offshore studies demonstrate that faults in the basin can be divided into four strain-partitioned regions: 1) the well-developed northwest striking, right-lateral Pyramid Lake fault zone in the south, 2) the north striking, west dipping, Lake Range normal fault zone on the east, 3) a zone of discontinuous north and northwest striking, oblique-slip faults in the northwest, and 4) a zone of left-stepping, north striking, normal faults in the northeast.

New slip rate estimates for the northern Pyramid Lake fault zone using offset geomorphic features yield an average rate of 1.3 mm/yr. A vertical slip rate estimate on the Lake Range fault zone using offset horizons in CHIRP profiles is

1.0 mm/yr. Trenching of a Holocene fault scarp on the northwest side of the lake produced a vertical slip rate of 0.04 mm/yr.

The deformation rate along the Lake Range fault is 2-3 times faster than estimates from nearby faults in the western Basin and Range, indicating a kinematic link to the higher strain Walker Lane. The CHIRP data and bathymetry do not show a major through-going fault connecting the Pyramid Lake and Lake Range faults offshore, suggesting transfer of strain is either accommodated by onshore structures or a 1.5-2 km step. On and offshore fault mapping limits the northern termination of the Pyramid Lake fault zone to approximately the latitude of Anaho Island. The lower slip rate on the northwest side of the lake suggests that area may not be significantly influenced by Walker Lane deformation.

#### **Seismicity of the Southern Mina Deflection and the 2004-2005 Adobe Hill Earthquake Sequence, Nevada-California**

BACA, A., Nevada Seismological Laboratory, University of Nevada, Reno, NV, USA, [austinbaca1992@gmail.com](mailto:austinbaca1992@gmail.com); RUHL, C., Nevada Seismological Laboratory, University of Nevada, Reno, NV, USA, [cruhl@unr.edu](mailto:cruhl@unr.edu); HATCH, R., Nevada Seismological Laboratory, University of Nevada, Reno, NV, USA, [rachelhatch11@gmail.com](mailto:rachelhatch11@gmail.com); SMITH, K., Nevada Seismological Laboratory, University of Nevada, Reno, NV, USA, [ken@seismo.unr.edu](mailto:ken@seismo.unr.edu); KENT, G., Nevada Seismological Laboratory, University of Nevada, Reno, NV, USA, [gkent@seismo.unr.edu](mailto:gkent@seismo.unr.edu); LOUIE, J., Nevada Seismological Laboratory, University of Nevada, Reno, NV, USA, [louie@seismo.unr.edu](mailto:louie@seismo.unr.edu)

The Mina Deflection of western Nevada and eastern California is a persistent source of earthquake activity. Located within the Central Walker Lane, it is a distinct transition, transferring dextral slip from the southern Walker Lane in a series of sub-parallel left-lateral strike slip faults and normal faulted basins to the primary dextral faults of the central Walker Lane east of the Wassuk Range, near Hawthorne, Nevada. Dextral faulting ultimately extends into the Northern Walker Lane region, north of Lake Tahoe. The largest historical earthquake within the Mina Deflection was the 1934 M 6.5 Excelsior Mountain event, near Mina, Nevada. Since 2000 the Nevada Seismological Laboratory has located about 35,000 earthquakes within the Mina Deflection region. One of the more notable zones of seismicity extends ~40 km, in an arcuate geometry from Queens Valley, north of the White Mountains, into Mono Basin. The seismicity generally corresponds to an abrupt change in the orientation of closely spaced fault systems through the 2-4 Ma Adobe Hills volcanic field, from NW striking to the south to NE striking to the north into the Mina Deflection region. We would define the southern extent of the Mina Deflection, at this longitude, by this particular zone of seismicity that included the 2004-05 Adobe Hills sequence. The sequence included an  $M_w$  5.3 strike-slip event (9/18/2004; 23:02:17 UTC), followed 41 minutes later by another  $M_w$  5.3 strike-slip event, 3 km to the NE. Foreshocks in the near source area began at 07:02:44, 16 hours prior to the initial  $M_w$  5.3. Ninety-one earthquakes were located in the 16-hour foreshock period, including 6 Magnitude 3.0-3.9 events. The Nevada Seismological Laboratory located ~7000 earthquakes in the 2004-2005 sequence. Here we develop a set of high quality locations, short-period focal mechanisms and moment tensor solutions (for M 3.5+ events) to assess this unique zone of seismicity in the southern Mina Deflection region.

#### **The 2008 Wells, Nevada Earthquake Sequence: Application of Subspace Detection and Multiple Event Relocation Techniques**

NEALY, J. L., USGS NEIC, Golden, CO, USA, [jnealy@usgs.gov](mailto:jnealy@usgs.gov); HAYES, G. P., USGS NEIC, Golden, CO, USA, [ghayes@usgs.gov](mailto:ghayes@usgs.gov); BENZ, H. M., USGS NEIC, Golden, CO, USA, [benz@usgs.gov](mailto:benz@usgs.gov)

On February 21, 2008 at 14:16:02 (UTC), Wells, Nevada experienced a  $M_w$  6.0 earthquake, the largest earthquake in the state in the past 50 years. The event was felt throughout most of Nevada with shaking extending into Wyoming and Oregon. Here, we analyze in detail the spatiotemporal variations of the foreshock and aftershock sequence combining subspace detection and Bayesian multiple event relocation techniques using the 19 closest USArray Transportable Array stations and nearest permanent monitoring stations in Nevada and Utah. In order to provide a more complete catalog of the Wells sequence, we first apply a subspace detector over a seven-month study period (February 1, 2008 to August 31, 2008). By coupling this technique with a z-score based detection threshold, we are able to identify thousands of events in the months following the Wells mainshock as well as several foreshocks in the days leading up to the event. We apply Bayesian multiple event relocation to the 11,489 events associated over the seven-month period of the study and obtain accurate locations (to within ~2 km) for 4,662 earthquakes. The resulting catalog of earthquakes indicates that the aftershocks extend for about 20 km along the strike of the fault. Most aftershocks occur updip from the region of maximum slip (Dreger *et al.*, 2011) and along the

southern and northern edges of the zone of maximum slip, illuminating areas of post-mainshock strain increase.

#### **The Mw 4.3 December 22, 2015 Thomas Creek Earthquake, South Reno, Nevada**

HATCH, R., Nevada Seismological Lab., Univ. of Nevada, Reno, NV, USA, [rachelhatch11@gmail.com](mailto:rachelhatch11@gmail.com); BACA, A., Nevada Seismological Lab., Univ. of Nevada, Reno, NV, USA, [austinbaca1992@gmail.com](mailto:austinbaca1992@gmail.com); RUHL, C., Nevada Seismological Lab., Univ. of Nevada, Reno, NV, USA, [christineruhl@gmail.com](mailto:christineruhl@gmail.com); BRAILO, C., Nevada Seismological Lab., Univ. of Nevada, Reno, NV, USA, [kicrox@gmail.com](mailto:kicrox@gmail.com); SMITH, K. D., Nevada Seismological Lab., Univ. of Nevada, Reno, NV, USA, [ken@seismo.unr.edu](mailto:ken@seismo.unr.edu); LOUIE, J., Nevada Seismological Lab., Univ. of Nevada, Reno, NV, USA, [louie@seismo.unr.edu](mailto:louie@seismo.unr.edu); KENT, G., Nevada Seismological Lab., Univ. of Nevada, Reno, NV, USA, [gkent@unr.edu](mailto:gkent@unr.edu); RODGERS, A., Geophysical Monitoring Program, Lawrence Livermore National Lab., Livermore, CA, USA, [rodgers7@llnl.gov](mailto:rodgers7@llnl.gov)

The  $M_w$  4.3 Thomas Creek earthquake occurred on December 22, 2015 in the south Reno urban area (Origin Time: 22:46:07 PST; Lon: -119.7853; Lat: 39.4269; Depth: 9.6 km; ~8 km south of the venue for this meeting). The event was widely felt throughout the Reno-Tahoe area. An accelerometer 4.7 km S of the epicenter recorded a PGA of 8.3% g (see accompanying abstract, Rogers *et al.*; modeling basin ground motions). Approximately 150 events have been located to date in the sequence. The preliminary HYPODD relocations suggest the event occurred on a NNE-striking west-dipping structure, antithetic to a complex series of short, generally north-striking, east-dipping normal faults within the Carson Range frontal fault system and the Mt. Rose Pediment. Relocations give evidence for additional structures within the aftershock sequence. The primary west-dipping structure is interpreted to project to the surface on the west side of the Virginia Range along the eastern boundary of the Reno-area basin. This interpretation suggests active normal faulting bounds the eastern Reno basin, at this latitude. The regional surface wave moment tensor solution for the main event shows a well-constrained normal faulting mechanism striking N17E, accepting the west dipping structure as the operative fault plane. The aftershock sequence has included fifteen M 2.0-2.9 and four M 3.0-3.9 earthquakes, in addition to the  $M_w$  4.3 mainshock. Foreshock activity initiated abruptly twenty-eight minutes prior to the mainshock; the short foreshock period included twenty-two locatable events. Three of the sequence's four magnitude 3+ earthquakes occurred in the foreshock period and were also felt throughout the south Reno area. Within an approximately 15x15 km area centered on  $M_w$  4.3, 855 earthquakes have been located by the Nevada Seismological Laboratory prior to the Thomas Creek event. This has included twenty-three M  $\geq$  2.0 earthquakes, with the largest event an M 2.8 on November 11, 2010.

#### **Ground Motion Simulations of the December 22, 2015 Thomas Creek Earthquake, South Reno, Including 3D Basin Structure**

RODGERS, A. J., LLNL, Livermore, CA, USA, [rodgers7@llnl.gov](mailto:rodgers7@llnl.gov); HATCH, R., Nevada Seismological Laboratory, University of Nevada, Reno, NV, USA, [rachelhatch11@gmail.com](mailto:rachelhatch11@gmail.com); LOUIE, J., Nevada Seismological Laboratory, University of Nevada, Reno, NV, USA, [louie@seismo.unr.edu](mailto:louie@seismo.unr.edu); SMITH, K., Nevada Seismological Laboratory, University of Nevada, Reno, NV, USA, [ken@unr.edu](mailto:ken@unr.edu); RUHL, C., Nevada Seismological Laboratory, University of Nevada, Reno, NV, USA, [christineruhl@gmail.com](mailto:christineruhl@gmail.com); BRAILO, C., Nevada Seismological Laboratory, University of Nevada, Reno, NV, USA, [kicrox@gmail.com](mailto:kicrox@gmail.com); KENT, G., Nevada Seismological Laboratory, University of Nevada, Reno, NV, USA, [gkent@unr.edu](mailto:gkent@unr.edu); PULLAMMANAPPALLIL, S., Optim, Reno, NV, USA, [satish@optimsoftware.com](mailto:satish@optimsoftware.com)

The  $M_w$  4.3 Thomas Creek earthquake occurred within the southern part of Reno, NV on December 22, 2015 (22:46:07 local time), shortly before the abstract due date for this meeting. The event was widely felt throughout the Reno-Tahoe area. Such moderate earthquakes are crucial for validating 3D structural models and ground motion predictions for larger ( $M_w \geq 6$ ) scenario earthquakes in the Reno basin. Preliminary relocations suggest the event occurred on a west dipping structure, antithetic to the Mount Rose Fault Zone (MRFZ) in general. Regional waveform modeling reveals a normal focal mechanism. Details of the seismotectonics are reported in an accompanying abstract (Hatch *et al.*). We have modeled the recorded ground motions at stations within Reno-Tahoe area using the SW4 3D anelastic finite difference code. The basin structure is taken from the depth-to-basement model published by Abbott and Louie (2000) for the Reno-area basin. Material properties within the basin were established by seven deep refraction microtremor surveys of shear velocity to basement and varied to optimize fits to the observed waveforms and ground motion measurements. The event was recorded at several stations located within a focal depth. Consequently, the waveforms at these stations are strongly sensitive to the location, depth and focal



mechanism. We will investigate source parameters, including source finiteness. Preliminary modeling shows we can obtain reasonably good fits to peak ground velocity (PGV) measurements at the stations within the greater Reno area using a point source. The PGV fits with the 3D basin structure are better than those with an average plane-layered hard rock model. The basin structure is required to fit the long duration of shaking observed for the recorded ground motions in the basin. If possible, we will simulate large scenario earthquakes on the MRFZ informed by results from structure and source investigations of this event.

---

## Short- and Long-Term Deformation on Active Faults: Integrating Geodetic, Geologic and Seismic Constraints on Slip Rates and Off-fault Deformation in the Walker Lane and Beyond

Poster Session · Friday · 22 April · Tuscany F

---

### New Slip Rates and Characterization of Active Faults in Mason and Smith Valleys of the Northern Walker Lane using <sup>10</sup>Be Terrestrial Cosmogenic Nuclide (TCN) Surface Exposure Dating and Newly Acquired Lidar

PIERCE, I. K., Center for Neotectonic Studies, Nevada Seismological Lab, UNR, Reno, NV, USA, [ian@nevada.unr.edu](mailto:ian@nevada.unr.edu); WESNOUSKY, S. G., Center for Neotectonic Studies, Nevada Seismological Lab, UNR, Reno, NV, USA, [wesnousky@unr.edu](mailto:wesnousky@unr.edu); OWEN, L. A., Department of Geology, University of Cincinnati, Cincinnati, OH, USA, [lewis.owen@uc.edu](mailto:lewis.owen@uc.edu)

Mason and Smith Valleys are half-grabens within the Northern Walker Lane, east of Carson City and Reno, Nevada. We apply recently acquired 0.5-1 m/pixel lidar data and terrestrial cosmogenic nuclide (TCN) surface exposure ages to characterize the geometry, Quaternary expression, and slip rates of active faults in the two valleys. The majority of the range front fault in Mason Valley forms an alluvial-bedrock contact, and displays only one site where the active fault has cut and displaced older fan sediments. TCN ages of a ~10 m vertically faulted alluvial fan surface at this site are >100 ka, suggesting a <0.1 mm/yr vertical slip rate for the range bounding fault, significantly less than geodetic estimates. The new lidar data also reveal a previously unmapped northeast striking fault outboard of the range front at the northernmost part of Mason Valley that offsets Holocene sediments and shows morphology suggestive of left-lateral strike-slip. Analysis of lidar in Smith Valley shows a much more active range front fault than that of Mason Valley, with frequently offset late Quaternary fan surfaces along the northern half of the range, along with two additional previously unmapped northwest striking fault segments towards the center of the basin, that also offset Holocene sediments. The Artesia Fan along the Smith Valley range front is offset ~10 m, and TCN ages range from 10-30 ka, leading to a vertical slip rate of 0.33-1.0 mm/yr. The rate in this case appears to be in line with geodetic rates of deformation that have been reported by others.

### Characterizing the Quaternary Expression of Active Faulting along the Olinghouse, Carson and Wabuska Lineaments of the Northern Walker Lane using Lidar

LI, X., Institute of Geology, CEA, Beijing, China, [li\\_xinnan68@163.com](mailto:li_xinnan68@163.com); PIERCE, I. K. D., Center for Neotectonic Studies, Nevada Seismological Lab, UNR, Reno, NV, USA, [ian@nevada.unr.edu](mailto:ian@nevada.unr.edu); WESNOUSKY, S. G., Center for Neotectonic Studies, Nevada Seismological Lab, UNR, Reno, NV, USA, [wesnousky@unr.edu](mailto:wesnousky@unr.edu)

The Walker Lane accounts for a significant portion of the motion along the North American-Pacific transform plate boundary. It is a structurally complex zone that is composed of northwest-trending right-lateral, north-trending normal, and northeast-trending left-lateral faults and lineaments. The Northern Walker Lane in the vicinity of Reno to Walker Lake accommodates 5-7 mm/yr of dextral shear, in the absence of any through-going right-lateral strike-slip faults. This shear is primarily accommodated by block rotations. Previous studies have suggested that left-lateral strike-slip is accommodated by the Olinghouse, Carson, and Wabuska lineaments. Here, we will use newly acquired high resolution (0.5 m/pixel) lidar data combined with low sun-angle aerial photography and previous studies to describe the neotectonic characteristics of these lineaments. Initial reconnaissance of the imagery shows that the presence of Quaternary scarps in alluvium is limited and discontinuous along the length of the Carson and Wabuska lineaments, and is confined to only the northeastern extent of the Olinghouse fault. The morphology, geometry, and pattern of scarps along the Carson and Wabuska lineaments is consistent with strike-slip, but it is only along the Olinghouse that left-lateral offsets have thus far been unambiguously identified.

### Application of UAV Photography to Refining the Slip Rate on the Pyramid Lake Fault Zone, Nevada

ANGSTER, S., Center for Neotectonic Studies, Nevada Seismological Lab, UNR, Reno, NV, USA, [sangster@nevada.unr.edu](mailto:sangster@nevada.unr.edu); WESNOUSKY, S. G., Center for Neotectonic Studies, Nevada Seismological Lab, UNR, Reno, NV, USA, [wesnousky@unr.edu](mailto:wesnousky@unr.edu); HUANG, W., Institute of Geology, CEA, Beijing, China, [huangweiliang1987@gmail.com](mailto:huangweiliang1987@gmail.com); KENT, G., Nevada Seismological Lab, UNR, Reno, NV, USA, [gkent@unr.edu](mailto:gkent@unr.edu); NAKATA, T., Dept. of Geography, Hiroshima University, Hiroshima, Japan, [tnakata@hiroshima-u.ac.jp](mailto:tnakata@hiroshima-u.ac.jp); GOTO, H., Dept. of Geography, Hiroshima University, Hiroshima, Japan, [hgoto@hiroshima-u.ac.jp](mailto:hgoto@hiroshima-u.ac.jp)

The Pyramid Lake fault zone is a 50 km-long, active northwest trending right-lateral fault in the northern Walker Lane, located ~30 km east of Reno, NV. Previous paleoearthquake and slip rate studies report that the Pyramid Lake fault has produced four surface rupturing paleoearthquakes since  $15,475 \pm 720$  cal. yr B.P., three of which occurred after  $8,980 \pm 260$  cal yr B.P., and has an average minimum slip rate of  $2.6 \pm 0.3$  mm/yr since the late Pleistocene. These observations imply that coseismic offset for each paleoearthquake averaged 7–9 m, larger than expected from empirical scaling relationships for a strike-slip fault of its length. To reconcile this discrepancy, we used a small camera-mounted UAV to develop high-resolution digital elevation models and interpret previously unreported right-laterally offset geomorphic features along the northern section of the Pyramid Lake fault zone. Offset measurements at seven sites range from 8–21 meters. The ages of displaced features are interpreted from previous lake level and mapping studies of Lake Lahontan. From these observations, slip rate estimates at the sites range between 0.5–1.6 mm/yr. These lower values of slip rate require that coseismic displacements associated with previously reported paleoearthquakes average only 3–5 meters, within the range that would be predicted from empirical scaling relationships of rupture length and coseismic displacement.

### High-resolution Seismic Profiling Reveals Subsurface Faulting Associated with the 1934 M 6.6 Hansel Valley, Utah, Earthquake

BRUNO, P. P., The Petroleum Institute, Abu Dhabi, United Arab Emirates, [pbruno@pi.ac.ae](mailto:pbruno@pi.ac.ae); DUROSS, C. B., U.S. Geological Survey, Golden, CO, USA, [cdurross@usgs.gov](mailto:cdurross@usgs.gov); KOKKALAS, S., The Petroleum Institute, Abu Dhabi, United Arab Emirates, [skokkalas@pi.ac.ae](mailto:skokkalas@pi.ac.ae)

The 1934 ML 6.6 Hansel Valley, Utah, earthquake produced an 8-km-long by 3-km-wide zone of north-south trending faults and fractures at the southern end of Hansel Valley in the easternmost Basin and Range Province. Surface-rupture observations indicate less than 0.5-m of vertical displacement, possibly of secondary (shaking-related) origin. In contrast, seismicologic data indicate ~2 m of left-lateral strike-slip faulting. Resolving the origin and kinematics of faulting in the Hansel Valley earthquake is important to understanding how complex fault ruptures accommodate regions of continental extension. In this study we address three questions: (1) how does the 1934 surface rupture compare with faults in the subsurface, (2) are the 1934 fault scarps primary (fault-related) or secondary features, and (3) was the 1934 earthquake a strike-slip or normal-faulting earthquake? To address these questions we acquired a 6-km-long high-resolution seismic profile (6400 kg IIVI-MiniVib source; 5 m source and receiver spacing) across Hansel Valley, including the 1934 rupture. We interpret faulting as shallow as a few tens of meters and complex, east- and west-dipping normal faults to a depth of about 1 km. Spatial correspondence between the 1934 surface rupture and subsurface faults suggests that vertical faulting associated with the earthquake is of tectonic origin and that subsurface faulting is distributed across a ~5-km wide zone of deformation. These data clearly show complex basin faulting that is most consistent with extensional or transtensional tectonics. Although deeper seismic imaging is necessary to constrain the style of faulting at seismogenic depths, our study has important implications for understanding the link between surface and subsurface faults in regions of continental extension.

### A LiDAR and GPS Study of the Greater Truckee Meadows: Evidence for a Distinct Transition from Primarily East-west Dominated Extension to NW-trending Right-lateral Slip Centered in Reno, Nevada

BRAILLO, C. M., Nevada Seismological Laboratory, Reno, NV, USA, [cbraillo@nevada.unr.edu](mailto:cbraillo@nevada.unr.edu); KENT, G. M., Nevada Seismological Laboratory, Reno, NV, USA, [gkent@unr.edu](mailto:gkent@unr.edu); WESNOUSKY, S. G., Nevada Seismological Laboratory, Reno, NV, USA, [wesnousky@unr.edu](mailto:wesnousky@unr.edu); HAMMOND, W. C., Nevada Geodetic Laboratory, Reno, NV, USA, [whammond@unr.edu](mailto:whammond@unr.edu); KELL, A. M., Nevada Seismological Laboratory, Reno, NV, USA, [annie.kell@gmail.com](mailto:annie.kell@gmail.com); PIERCE, I. K., Nevada Seismological Laboratory, Reno, NV, USA, [ian@nevada.unr.edu](mailto:ian@nevada.unr.edu); RUHL, C. J., Nevada Seismological Laboratory, Reno, NV, USA, [christineruhl@unr.edu](mailto:christineruhl@unr.edu)

gmail.com; SMITH, K. D., Nevada Seismological Laboratory, Reno, NV, USA, ken@unr.edu

The Truckee Meadows (Reno, NV) sits in a tectonically complex region of western Nevada where Basin and Range extension transitions to Walker Lane-style right-lateral shear. Here MAGNET GPS data show that dextral trans-tension is active in the region. This study aims to better understand how trans-tension is partitioned along faults confirmed or newly identified in this urban setting, as strain accommodation in this area remains poorly understood. We use a new LiDAR survey of the Truckee Meadows (TM) and nearby basins to constrain fault geometry, length, distribution and slip rates. We compare these to slip rates estimated from a geodetic block model constrained by the GPS data. Faults with normal offset were measured using bare-earth LiDAR returns to determine the amount of vertical separation, and then converted to extension assuming a fault dip of  $60 \pm 10$  degrees. Since the primary geomorphic surfaces in this region are the result of Sierra Nevada glacial outwash deposits, we use previously published geologic maps to identify the ages of each surface the fault cuts. When integrated across several basin perpendicular transects near the Mt. Rose pediment, we calculate a total extension rate of  $0.87 (+0.40/-0.48)$  mm/yr for the southern TM basin. Slip rates from these fault scarps match the  $1.23 \pm 0.70$  mm/yr suggested by geodetic modeling within the uncertainty. We find that these NS striking faults primarily accommodate EW extension, and NW striking faults must accommodate the NW-directed shear seen in GPS velocities. This trend is bolstered by the discovery of a new NW-oriented fault on Peavine Mountain 6 km east of the Mogul seismicity trend. Our study provides further evidence that the TM sits at a critical transition from NS striking normal faults in the southern part of the basin to NW oriented strike-slip faults to the north, an observation that mimics regional tectonics and geomorphology of the adjacent Lake Tahoe and Truckee system to the west.

#### **Preliminary Tectonic Geomorphic Observations Along the East Reno Fault Zone, Nevada.**

KOEHLER, R., Nevada Bureau of Mines & Geology, University of Nevada, Reno, Reno, NV, USA, rkoehler@unr.edu

A discontinuous north-trending zone of un-named faults (herein the East Reno fault zone, ERFZ) extends for ~35 km from the northern end of Washoe Valley to Spanish Springs Valley east of Reno, Nevada. At this latitude, faults of the northern Walker Lane accommodate ~5-7 mm/yr of dextral transtension. The ERFZ overlaps and occurs in close proximity to other active faults including the Spanish Springs Valley, Spanish Springs Peak, and North Virginia Range faults. The kinematic role of the ERFZ in this complex zone of deformation is unknown and estimates on its slip rate and recurrence are non-existent. Previously published maps depict Holocene and late Pleistocene offsets along the zone, however detailed accounts of these observations are sparse.

Here we present preliminary observations on the Quaternary expression of the ERFZ based on analysis of historical aerial photographs, lidar hillshade models, and field reconnaissance with the primary goal of identifying promising sites for future paleoseismic study. Initial observations indicate that the fault zone is characterized by short 2-5-km-long traces that vary in orientation between N25°E to N30°W. In the eastern Truckee Meadows area, faults are characterized by sharp range-front escarpments bounding the Virginia and Pah Rah Ranges, however this area is highly urban and sites for detailed investigation are few. To the north, in Spanish Springs Valley, the zone transitions to intra-basin and piedmont faults that are well-expressed on lidar as grabens and large escarpments across late Pleistocene alluvial fan deposits. The scarps are consistent with normal displacement, and provide viable targets for future paleoseismic work. Aligned saddles, streams, and minor escarpments along several northwest-trending strands suggest that parts of the ERFZ may accommodate a component of dextral shear and possibly provide a tectonic linkage between other better-defined structures in the northern Walker Lane.

#### **Paleoearthquake Chronology from the Echo Playa Site on the Central Garlock Fault, California**

KEMP, C. D., Lettis Consultants International, Inc., Valencia, CA, USA, kemp@lettisci.com; HARTLEB, R. D., Lettis Consultants International, Inc., Valencia, CA, USA, hartleb@lettisci.com; LUTZ, A. T., Division of Safety of Dams, California Dept. of Water Resources, Sacramento, CA, USA, andrew.lutz@water.ca.gov; FROST, E. K., Lettis Consultants International, Inc., Valencia, CA, USA, frost@lettisci.com; LINDVALL, S. C., Lettis Consultants International, Inc., Valencia, CA, USA, frost@lettisci.com; ALM, S., Department of Geology, University of Kansas, Lawrence, KS, USA, s482a651@ku.edu; WALKER, J. D.,

Department of Geology, University of Kansas, Lawrence, KS, USA, jdwalker@ku.edu

Paleoseismic investigations at the Echo Playa site on the central Garlock fault south of Searles Valley reveal evidence of four well-resolved paleoearthquake events since about 1500 B.C. The Echo Playa site is the easternmost trench site on the Garlock fault and is situated within a roughly 150-m-wide and 1.5-km-long transtensional stepover that has formed a closed basin fringed by alluvial and colluvial deposits that grade into laterally continuous playa sediments. Two trenches were excavated across fault strands that have formed low, well-defined scarps along the playa margins exposed roughly 5 m of generally conformable stratigraphy.

Strong evidence for four surface-rupturing earthquakes is preserved within a roughly 30-m-wide zone of distributed deformation where correlative sets of faults and fissure fills terminate upward at the base of laterally continuous stratigraphic horizons. Calibrated radiocarbon dates of detrital charcoal were used to develop sedimentation rates from which our preferred event ages are interpolated. The most recent earthquake occurred between A.D. 1615 and 1820 preceded by the penultimate event between A.D. 470 and 730. The two earlier events occurred between A.D. 40 and 150, and 275 and 1950 B.C. The three most recent events are well-correlated in time with events recorded at sites to the west on the central and western Garlock fault, and correlation of the fourth event is also permissible. The continuous stratigraphy, lack of evidence for any hiatuses in sedimentation, and strong correlation with events at other sites suggest that all ruptures along this portion of the Garlock fault are recorded at the Echo Playa site. The strong inter-site event correlations imply that the previously hypothesized segment boundaries at Koehn Lake and the Quail Mountains do not appear to arrest large ruptures on Garlock fault, although the correlations do not preclude the possibility of smaller events that are closely spaced in time.

#### **New Lidar Topography Reveals Tectonic Geomorphology Along the 1958 Southern Fairweather Fault Surface Rupture, Southeast Alaska**

WITTER, R. C., U.S. Geological Survey, Alaska Science Center, Anchorage, AK, USA, rwitter@usgs.gov; BENDER, A., U.S. Geological Survey, Alaska Science Center, Anchorage, AK, USA, abender@usgs.gov; LEWINTER, A., Cold Regions Research and Engineering Laboratory, ACOE, Hanover, NH, USA, Adam.Lewinter@erc.dren.mil; HAEUSSLER, P., U.S. Geological Survey, Alaska Science Center, Anchorage, AK, USA, pheuslr@usgs.gov; BROTHERS, D., U.S. Geological Survey, Pacific Coastal & Marine Science Center, Santa Cruz, CA, USA, dbrothers@usgs.gov; DUROSS, C., U.S. Geological Survey, Geologic Hazards Science Center, Golden, CO, USA, cduross@usgs.gov; GLENNIE, C., National Center for Airborne Laser Mapping, Univ. of Houston, Houston, TX, USA, clglennie@uh.edu; KOEHLER, R. E., Nevada Bureau of Mines and Geology, University of Nevada, Reno, NV, USA, rkoehler@unr.edu; SCHARER, K., U.S. Geological Survey, Earthquake Science Center, Pasadena, CA, USA, kscharer@usgs.gov; PLAFKER, G., U.S. Geological Survey, Earthquake Science Center, Menlo Park, CA, USA, georgeplafker@sbcglobal.net

The 1958 Lituya Bay earthquake (M 7.7) ruptured >260 km of the Fairweather Fault in southeast Alaska, where the Yakutat block collides obliquely with North America. The fault, which accommodates ~46 mm/yr of dextral slip (>90% of the Pacific-North American Plate motion), ruptured in 1958 from Yakutat Bay to Cross Sound. Ice or water obscured ~80% of the 1958 surface deformation, but post-earthquake surveys along the southern ~30 km of the fault between Crillon Lake and Icy Point measured ~3–6.5 m of dextral offset, including >1 m of vertical offset at one site.

We use new airborne lidar data to map the geomorphic expression of the southern Fairweather Fault in densely vegetated, steep terrain, and to identify potential paleoseismic sites. Using a “HeliPod” helicopter-mounted lidar system, we surveyed three ice-free sections of the fault over areas 4–6.5 km long by 1–4 km wide. Bare-earth digital terrain models (DTMs) derived from last-return point clouds (~1 pt/m<sup>2</sup>) reveal 1–5 m-high mostly east-facing scarps, linear troughs, slopes, benches, shutter ridges, ponded alluvium, and dextrally offset landforms, including 12 stream channels offset 12–128 m, and 2 moraines offset 40–79 m.

Together the lidar DTMs and new offshore bathymetric data show a ~20° restraining bend and 3–4 km right step between the offshore and onshore fault traces at Icy Point. South of the restraining bend, the linear offshore fault trace expresses strike-slip morphology. Within the bend, an array of right-stepping en-echelon folds and faults appear to accommodate transpression. North of the restraining bend, fluvial and marine terraces that only occur west of the onshore fault trace indicate west-side-up transpressional deformation. The change in deformation style across the restraining bend coincides with the southernmost impingement of the Yakutat block in southeast Alaska. We identify promising field sites north of the bend to assess the paleoseismic record of the southern Fairweather Fault.



### **The 1990 Lee Vining, California, Earthquake and Implications for the Kinematics of the Central Walker Lane**

HUMPHREY, J. R., Lahontan GeoScience, Inc., Reno, NV, USA, jrhumphrey@lahontangeoscience.com

A M5.3 earthquake occurred on 24 October 1990, in the NW corner of the Mono Basin near Lee Vining, California. The Mono Basin is situated in the central Walker Lane (CWL) where a portion of slip accruing from NW-directed shearing between the Sierran microplate and North America steps east from the Sierra Nevada frontal fault system (SNFFS) to the central Nevada Seismic Belt via left-lateral faults. The proximity of the Lee Vining mainshock to the Mono Lake fault (MLF), part of the SNFFS, raises the question of whether this event was due to slip on the range front or represents transfer of strain east through the CWL. High-precision double-differenced relocations of events in the 1990 sequence were used to characterize the kinematics. The relocations show that the mainshock occurred 5 km east of the MLF at a depth of 12 km. Epicenters of the largest aftershocks exhibit a well-defined NE trend, in contrast to the N-NW strike of the MLF. A mapped N-NE-striking late Quaternary fault runs roughly parallel to the trend of the epicenters, although no surface rupture was observed. The focal mechanism for the mainshock and the NE epicentral alignment suggests left-lateral faulting striking N55E. Focal mechanisms from the largest aftershocks fall into two populations. Most of the seismic moment was released on planes striking ~N60E. The other group generally strikes N30E. This latter group approximately parallels the observed offset of the nearby mapped fault. Overall the style of deformation in the NW corner of the Mono Basin can be characterized as transtension, consistent with geodetic and geological strain indicators. The presumed faults of the largest events are roughly parallel to the NE strike of the North Mono Basin Escarpment and faults on the north shore of Mono Lake. The 1990 Lee Vining sequence appears to be part of a complex kinematic path for the transfer of slip from NW-striking dextral faults of the SNFFS to E-NE striking sinistral faults in the CWL.

### **Postseismic Deformation Following the 2010 M=7.2 El Mayor-Cucapah Earthquake: New Methods, Interpretations and Implications**

ROLLINS, J. C., California Institute of Technology, Pasadena, CA, USA, john.c.rollins@gmail.com; BARBOT, S. D., Earth Observatory of Singapore, Singapore, sylbar.vainbot@gmail.com; AVOUAC, J. P., California Institute of Technology, Pasadena, CA, USA, avouac@gps.caltech.edu

The 2010 M=7.2 El Mayor-Cucapah earthquake was followed by a complex post-seismic transient that included a rich sequence of aftershocks and off-fault surface creep, rapid early displacements in GPS timeseries suggesting localized afterslip and/or nonlinear viscoelastic relaxation, and a prolonged long-wavelength signal in GPS consistent with viscoelastic relaxation in the mantle and possibly the crust of the Salton Trough. Extending these observations and end-member models to a robust interpretation of the physics of deformation at depth requires a better understanding of uncertainties and trade-offs between relevant parameters such as the effective viscosity of ductile zones and the geometries of creeping faults. Three new developments are allowing us to proceed in this direction. First, we are applying the transient detection methods of Gualandi et al [2016] and Riel et al [2014] to formally extract the signals of postseismic deformation and their uncertainties from GPS timeseries with the minimum possible bias. Second, we are using a newly developed grid-search method that examines suites of physics-driven models and uses the Neighborhood Algorithm of Sambridge [1998] to efficiently find an ensemble of models that fits the extracted postseismic signals well, allowing us to explore trade-offs between model parameters in a high-dimensional space. Finally, we are using a new adaptive-meshing elastostatic solver [Landry and Barbot, in prep.] to assess the effect that the laterally heterogeneous elastic structure of the Salton Trough region has on models of coseismic and postseismic deformation. These methods pave the way towards robust, probabilistic interpretations of the physics of postseismic deformation following the El Mayor-Cucapah earthquake and will allow us to begin assessing aspects of the problem relevant to seismic hazard, such as the postseismic stress changes these processes may have imparted to nearby faults that extend towards the Los Angeles region.

### **A Reconnaissance Fault Activity and Fault Slip-Rate Analysis of Quaternary Faults in Central Nevada**

DEPOLO, C. M., NV Bur. Mines and Geology, Reno, NV, USA

A reconnaissance fault activity and fault slip-rate study was conducted in central Nevada as part of the DOE-sponsored Nevada Play Fairway Geothermal Project. Although many of the larger faults in central Nevada have been characterized through studies, many smaller faults have not. The larger faults with detailed study provided calibration of the potential geomorphic expression along faults

with different ages or different slip rates. Geomorphic observations of the faults in the study area were made on Google Earth to allow the review of hundreds of fault traces. Fault activity was based on the age of youngest offset units and/or apparent geomorphic expression of the most recent event. Latest fault rupture categories were historical, 15 ka, 130 ka, 750 ka, and Quaternary. The categories are inclusive of younger events to account for erosion and other factors. Fault slip rates were grouped in order of magnitude bins of 0.1, 0.01, 0.001, and 0.0001 m/ky. Faults were assigned to a slip-rate category unless other information was available. Vertical rates were estimated for normal faults using estimates of vertical offsets and approximated or constrained ages of offset units. These were used as a guide for assigning slip-rate categories. A few suspect strike-slip faults were identified in central and eastern Nevada, and several exist in the southwestern corner of the study area, in the Walker Lane. A similar relative geomorphic comparison with studied faults was used for strike-slip faults and a few lateral offsets were measured for rate estimates. Historical events were in the Central Nevada Seismic Belt. Faults in the rest of the activity categories are scattered throughout the study area, with exception of a few areas where events 15 ka and younger are not obvious. Considering fault slip rate, single-event offset correlated with fault length, and the age of the youngest event, many faults that are potentially beyond their seismic accumulation cycle were identified.

---

## **Upper Crustal Passive Imaging for Hazards and Exploration**

Poster Session · Friday · 22 April · Tuscany F

---

### **On the Relationship between Near-surface Attenuation and Scattering**

PILZ, M., Swiss Seismological Service—ETH Zurich, Zurich, Switzerland, marco.pilz@sed.ethz.ch; FAEH, D., Swiss Seismological Service—ETH Zurich, Zurich, Switzerland

At high frequencies, the acceleration spectral amplitude decreases rapidly; this has been modeled with the spectral decay factor  $\kappa$  ( $\kappa$ ). The path-corrected component of  $\kappa$ , often called  $\kappa_0$ , is typically thought to be local site characteristic, quantifying attenuation related to waves propagating vertically through the shallow layers beneath the study site. Despite the known importance of  $\kappa_0$  in a wide range of seismological applications, current approaches assume that all of the measured  $\kappa_0$  is due to attenuation, therefore neglecting the possibility that  $\kappa_0$  might also comprise a scattering component. This may cause overestimation of the actual attenuation effect on ground motion, and lead to possible overcorrections in GMPE adjustments.

To account for the scattering component, we will present a summary of statistical observations of the seismic wavefield. Its intrinsic properties show a clear dependency on the local shallow subsoil conditions. Differences in the structural heterogeneity of the shallow subsoil layers can produce different scattering regimes, therefore changing the character of motion from nearly ballistic to diffusive on frequency-dependent timescales for all materials. Such deviations from the ballistic behavior can be seen as indicative for the structural heterogeneities and the associated scatter. Quantifying the amount of scattering may allow computing a lower bound estimate for  $\kappa_0$  values. This means that, rather than simply being a modelling parameter,  $\kappa_0$  can be considered a real physical variable and should be treated as such.

### **Progress on the USGS National Crustal Model for Seismic Hazard Studies**

BOYD, O. S., USGS, Golden, CO, USA, olboyd@usgs.gov; SHAH, A. K., USGS, Denver, CO, USA, ashah@usgs.gov

Lateral and vertical variations of seismic wavespeed in the Earth's crust can have dramatic impacts on seismic wave propagation. Basins and thin layers of soft sediment, in particular, can substantially amplify ground motions. The frequency dependence of these motions can be very complex, impacting some man-made structures and not others. Urban Seismic Hazard Assessments, for example in Seattle, Washington, Los Angeles, California, and St. Louis, Missouri, characterize the near surface in great detail and show more precisely where, by how much, and at what shaking frequency earthquake ground motions will be amplified. Several ground motion prediction equations (GMPEs), which are a critical input to the USGS National Seismic Hazard Model, have recently included terms accounting for the effects of basins and low velocity shallow sediments. To exploit these more sophisticated GMPEs and produce Urban Seismic Hazard-like assessments on a national scale, the USGS has begun a project to compile information needed to produce a crustal model for the United States. Parameters within the model will include density, seismic velocity and attenuation, thickness of unconsolidated sediments, depth to crystalline basement or seismic equivalent, and depth to Moho constrained by, where available, seismic, gravity, magnetic, and



well data. Model values will be defined with 1-km spacing, with uncertainties dependent on the density and quality of input data sets. These may vary from 10s of meters in near-surface soil databases to many 10s of km in subsurface tomographic models. An interface to the model will be able to provide values needed for GMPEs, for example, the depths to 1.0 and 2.5 km/s shear wavespeeds, as well as interpolated 3d models for use with various Urban Hazard Mapping strategies. We review case studies in which the use of basin information has improved seismic hazard assessment and the datasets compiled thus far to produce the USGS National Crustal Model.

#### **Passive Seismic Body-Wave Interferometry using Noise Auto-correlations for Crustal and Upper Mantle Structure**

OREN, C., Purdue University, West Lafayette, IN, USA, [canoren87@gmail.com](mailto:canoren87@gmail.com); NOWACK, R. L., Purdue University, West Lafayette, IN, USA, [nowack@purdue.edu](mailto:nowack@purdue.edu)

In this study, we use ambient seismic noise recorded at selected broadband USArray Earthscope Transportable Array (TA) stations to obtain effective reflection seismograms using noise auto-correlations. Claerbout (1968) originally found that the positive lags of the auto-correlation for the seismic transmission response of a layered medium could be used to determine the reflection seismogram. In order to best retrieve the body-wave components of the Green's function beneath a station from ambient seismic noise, a number of processing steps are required. We first remove the instrument response and apply a temporal sign-bit normalization to remove the effects of the most energetic sources. We then investigate spectral whitening and test several operators for this, where undulations of the whitened power spectrum can be related to the pulse arrival times in the processed auto-correlation. A Butterworth filter is then applied to the auto-correlation functions to further remove the effects of surface waves, as well as high frequency noise. Hourly auto-correlations are then stacked for different time periods of one day, one month, and one year. On the final stack, different amplitude gain functions are applied, including automatic gain control (AGC), to equalize the correlation amplitudes. The robustness of the resulting ambient noise auto-correlations is first tested on selected TA stations in Nevada, where we are able to identify PmP and SmS arrivals similar to those found by Tibuleac and von Seggern (2012). We then investigated noise auto-correlations applied to selected USArray TA stations in the central U.S. and the results compare favorably with synthetic data derived from the crustal model, CRUST 1.0. We are now investigating what the shortest time interval would be, and under what conditions, in order to provide a good reflection stack without introducing bias.

#### **Retrieval of Green's functions in the Valley of Mexico using Historical Accelerations as Generalized Diffuse Fields**

BAENA-RIVERA, M., Instituto de Ingeniería, UNAM, Coyoacán, DF, Mexico, [mbaenar@gmail.com](mailto:mbaenar@gmail.com); PIÑA-FLORES, J., Instituto de Ingeniería, UNAM, Coyoacán, DF, Mexico, [ead2009@hotmail.com](mailto:ead2009@hotmail.com); PERTON, M., Catedra CONACYT—Geofísica UNAM, Morelia, Michoacán, Mexico, [mathieu.perton@gmail.com](mailto:mathieu.perton@gmail.com); PÉREZ-ROCHA, L. E., Inst Investigaciones Eléctricas,

Cuernavaca, Morelos, Mexico, [lepr@iie.org.mx](mailto:lepr@iie.org.mx); SÁNCHEZ-SESMA, F. J., Instituto de Ingeniería, UNAM, Coyoacán, DF, Mexico, [sesma@unam.mx](mailto:sesma@unam.mx)

In order to improve the characterization of Mexico City subsoil we construct tomographic maps of surface wave velocities associated to the recovered Green's functions for station pairs obtained from average cross-correlations between such pairs of locations.

We used the set of acceleration ballistic waveforms from historical strong earthquakes recorded by the Mexico City Accelerometric Network (MCAN), during the last 25 years. At each site, we assumed that this set of ballistic waveforms conforms a Generalized Diffuse Field (GDF). Each record in itself does not necessarily exhibit diffuse characteristics, except for the late coda. However, the averages of cross-correlations of the GDF allow retrieving the travel times of surface waves because of the scattering that seismic waves undergone from the origin in the subduction zone to the basin of Mexico.


We tested numerically a 2D model and found that the concept is correct for the special characteristics of illumination of the valley. We consider incidence of an equipartitioned cocktail of P, SV and Rayleigh plane waves, for both isotropic and partial illumination. In practice, this validates the use of these type of records to obtain the Green's function of synthetic models of alluvial valleys subjected to equipartitioned illumination.

On the other hand, the data required various processes to have a common reference time. This allows performing time-space (t-x) spectral analysis known as frequency-wavenumber (f-k) description, useful to infer the seismic response of the valley accounting for the effects of surface waves generated at the edges.

**ACKNOWLEDGEMENTS.** This research was partially supported by the AXA Research Fund and by DGAPA-UNAM under Project IN104712.

#### **Very Dense Ambient Noise Arrays for Subsurface Imaging**

RABADE, S., Instituto de Ingeniería, UNAM, [san.rabade@gmail.com](mailto:san.rabade@gmail.com); RAMIREZ-GUZMAN, L., Instituto de Ingeniería, UNAM; JUAREZ, A., Instituto de Ingeniería, UNAM; AGUIRRE, J., Instituto de Ingeniería, UNAM; AVILA CARRERA, R., Instituto Mexicano del Petroleo, IMP; SANCHEZ, J., Instituto de Ingeniería, UNAM,

Following the emergence of ambient noise correlation techniques and its successful application to global, regional, and local data sets, the deployment and processing of very large and dense arrays to map the shallow crust has become an important research topic in seismology. During 2014, two of these very dense arrays were deployed in Mexico to analyze the capabilities of the cross-correlation-based methods for mapping the subsurface to locate natural resources. The first experiment consisted of six moving sets of 5,000 three-component accelerometers, covering close to 250 km<sup>2</sup>. The second survey included ten moving sets of 1,000 three-component 10 Hz geophones, covering more than 100 km<sup>2</sup>. In this paper, we analyze the information with different techniques, including traditional ambient noise cross-correlations (Bensen *et al.*, 2007) and phase cross-correlations (PCC) (Schimmel *et al.*, 2011). We successfully extract surface and body waves and obtain preliminary images of the shallow crust. These experiments show the passive technique's potential to extract detailed velocity properties in densely populated areas where active source experiments are not feasible. 

# Index of Authors

- Aagaard, B. T. 534  
 Abakanov, T. 472  
 Abbott, R. E. 499  
 Abdelhaleem, S. A. 579  
 Abdollahi, A. 509  
 Abdrakhmatov, K. 515, 550  
 Abercrombie, R. E. 556  
 Abers, G. 470  
 Abimbola, A. O. 471, 520  
 Abolfathian, N. 570  
 Abrahamson, N. A. 475, 513, 519, 553, 554, 559, 572  
 Abramson Ward, H. 559, 576  
 Abuaiisha, M. 479  
 Adams, J. 557  
 Adams, M. N. 525  
 Adams, R. K. 509  
 Adnan, A. B. 522  
 Agram, P. S. 514  
 Agrawal, J. 485  
 Aguiar, A. C. 476, 490  
 Aguirre, J. 584  
 Ahdi, S. K. 476  
 Ahern, T. 564  
 Ainscoe, E. 550  
 Ajo-Franklin, J. B. 548  
 Akita, Y. 578  
 Akkar, D. S. 457, 464, 515  
 Al Noman, M. N. 455, 571  
 Al-Atik, L. 553, 554  
 Aldridge, D. F. 501  
 Aleqabi, G. 453  
 Allam, A. A. 460, 549  
 Allan, J. C. 537  
 Allen, R. M. 451, 452, 453, 474, 509, 525, 528, 551  
 Allen, T. 577  
 Allison, F. 535  
 Allison, K. 504  
 Allstadt, K. 578  
 Alm, S. 582  
 AlTheyab, A. 547  
 Altoé, I. L. 519  
 Amini, A. 479  
 Aminzadeh, F. 467, 469  
 Ammon, C. J. 486, 488, 546  
 Amos, C. B. 579  
 Ampuero, J. P. 464, 467, 534  
 Ancheta, T. D. 457, 476, 493, 553, 578  
 Anderson, D. N. 535  
 Anderson, J. G. 460, 491, 516, 558  
 Anderson, K. 523  
 Anderson, R. P. 579  
 Anderson, Z. 478  
 Angster, S. J. 579, 581  
 Ansari, A. 502  
 Anthony, R. E. 490, 492, 501  
 Antoun, T. H. 499, 531, 532  
 Aoi, S. 472  
 Aoki, Y. 556  
 Apel, E. V. 562, 576  
 Aranha, M. 451  
 Arce, A. 527  
 Archuleta, R. J. 525, 540, 568  
 Arciniega-Ceballos, A. 542  
 Argus, D. F. 552  
 Argyrakis, P. 542  
 Arrowsmith, J. R. 505, 514, 565  
 Arrowsmith, S. J. 498, 510, 535, 536  
 Asimaki, D. 464, 476, 504  
 Askan, A. 465  
 Aslani, H. 560  
 Assatourians, K. A. 526, 570  
 Asten, M. W. 547  
 Aster, R. C. 485, 490, 492, 501  
 Atkinson, G. M. 467, 468, 480, 526, 553, 554, 570, 572, 574, 576  
 Austin, K. 475  
 Avila Carrera, R. 584  
 Avila, V. M. 485  
 Avouac, J. P. 552, 583  
 Ayoub, F. 549  
 Azari Sisi, A. 465  
 Azzizadeh-Roodpish, S. 482  
 Azuma, H. 550  
 Babaie Mahani, A. 478, 526  
 Baca, A. 580  
 Bachmann, C. E. 575  
 Bachura, M. 555  
 Badiali, L. 527  
 Baena-Rivera, M. 584  
 Bahavar, M. 564  
 Bahng, B. 537  
 Bainbridge, G. 523  
 Baise, L. G. 578  
 Baker, A. M. 524  
 Baker, G. E. 498  
 Baker, J. W. 566  
 Baker, M. G. 490, 492  
 Ballard, S. 498, 510, 528  
 Baltay, A. 475  
 Bao, X. 478  
 Baptie, B. 480, 543  
 Barbot, S. D. 552, 583  
 Barisin, I. 550  
 Barklage, M. E. 547  
 Barnhart, W. 505  
 Baro, J. 479  
 Barrie, J. V. 497  
 Barstow, N. 523  
 Batchelor, C. E. 574  
 Baturan, D. 480, 495, 528  
 Bauer, M. A. 551  
 Bausch, D. 456  
 Bayless, J. R. 571  
 Bazzurro, P. 559  
 Beale, J. N. 486  
 Beaudoin, B. 523  
 Beck, J. L. 506  
 Beck, S. L. 492, 522, 544  
 Becker, N. 517, 537  
 Bédard, M. P. 455  
 Begnaud, M. L. 461, 498  
 Behr, Y. 452  
 Ben-Zion, Y. 460, 461, 482, 490, 491, 510, 522, 555, 570  
 Bender, A. 582  
 Bennett, S. E. K. 552  
 Bent, A. L. 454, 515, 557  
 Benz, H. M. 485, 510, 541, 546, 580  
 Bergen, K. J. 500  
 Berglund, H. 475  
 Bergman, E. 461, 521  
 Beroza, G. C. 469, 500, 517  
 Besedina, A. N. 523  
 Beyzaei, C. Z. 549  
 Bhat, H. S. 482  
 Biasi, G. P. 516, 517, 552, 558  
 Bilek, S. L. 462, 464, 480, 542  
 Bilham, 481  
 Bina, C. 543  
 Bindu, D. 456  
 Biryol, C. B. 522  
 Black, B. 496  
 Blakely, R. J. 489  
 Blewitt, G. 454  
 Blom, P. S. 535, 536  
 Blume, F. 475  
 Boatwright, J. 472, 564  
 Bodin, P. 451, 452, 475  
 Bogiatzis, P. 460, 519  
 Bohnhoff, M. 461, 477, 482, 508, 514, 522, 540, 569  
 Bolton, M. K. 561  
 Borgfeldt, T. 480  
 Bormann, J. M. 497, 529, 557  
 Boroschek, R. 449  
 Böse, M. 452  
 Bossu, R. 551, 567  
 Bott, J. 468  
 Boudjema, M. 497  
 Boulton, S. J. 529  
 Bouskova, A. 461  
 Bowden, D. C. 473, 547  
 Bowman, D. C. 500, 502, 536  
 Boyd, O. S. 506, 583  
 Bozionelos, G. 542  
 Bozorgnia, Y. 476, 549, 553, 554  
 Bradley, B. A. 494  
 Bradley, C. R. 500, 531  
 Brailo, C. M. 580, 581  
 Branum, D. M. 578  
 Braud, A. 474  
 Braun, T. 470, 527  
 Bray, J. D. 549  
 Brenguier, F. 490  
 Briggs, R. W. 508, 557, 565, 566  
 Brillon, C. 449, 494  
 Briole, P. 542  
 Brocher, T. M. 459  
 Brogan, R. 528  
 Brokešová, J. P. 511, 523  
 Bromirski, P. 492  
 Brooks, B. A. 505, 506  
 Brooks, E. M. 459  
 Brossy, C. C. 449  
 Brothers, D. 582  
 Brouillette, P. 455  
 Brown, E. 454  
 Brown, J. 557  
 Brudzinski, M. R. 466, 511, 542  
 Brune, J. N. 516, 557  
 Brune, R. J. 516  
 Bruno, I. 518  
 Bruno, P. P. 581  
 Brüstle, A. B. 471, 575  
 Bruton, C. P. 523  
 Buckle, I. G. 567  
 Buehler, J. S. 454  
 Buelna, M. 506  
 Buga, M. 489  
 Bulaevskaya, V. 532  
 Bunds, M. P. 565  
 Burgmann, R. 556, 562, 579  
 Burke, K. B. S. 557  
 Burlacu, R. 574  
 Busby, R. W. 511, 525, 539  
 Butcher, A. C. 543  
 Butler, K. 557  
 Buurman, H. 465, 476, 523  
 Buyco, J. K. 566  
 Cabral Cano, E. 542  
 Caffagni, E. 478, 500  
 Cakir, R. 546, 559  
 Caldwell, D. 508  
 Callaghan, S. 457, 533  
 Camelbeeck, T. 483, 551  
 Cameron, C. 465  
 Campbell, G. E. 515  
 Campbell, K. W. 494, 513, 554, 555, 561  
 Campillo, M. 547  
 Cannon, E. C. 538, 539  
 Cappa, F. 467  
 Carapezza, M. L. 527  
 Carlson, C. W. 557, 558  
 Carmichael, J. D. 498  
 Carnevale, M. 498  
 Carpenter, N. S. 496, 563  
 Carrillo Lucia, M. A. 533  
 Cassidy, J. F. 449, 494  
 Castro, R. R. 569  
 Catchings, R. D. 473, 489  
 Cattania, C. 556  
 Cauzzi, C. 577  
 Çelebi, M. K. 538  
 Cermakova, H. 555  
 Cetin, K. O. 526  
 Chael, E. P. 500, 528  
 Chai, C. 486, 488  
 Chaljub, E. 503  
 Chambers, D. W. 484, 543  
 Chan, J. H. 471, 473, 489, 520  
 Chandramohan, R. 566  
 Chang, J. 477  
 Chapman, M. C. 486, 542  
 Chaput, J. A. 490, 492  
 Charalampidou, E. M. 540, 569  
 Cheadle, B. 469  
 Chen, C. 477  
 Chen, J. 563  
 Chen, Q. F. 545  
 Chen, R. E. 456  
 Chen, S. W. 487  
 Chen, W. P. 487  
 Chen, X. 477  
 Cheney, M. 490  
 Cheng, Y. 457, 515  
 Chiang, A. 531, 539  
 Chiarabba, C. 466  
 Chung, A. I. 452, 474  
 Clahan, K. B. 486, 549  
 Clayton, R. W. 512, 547, 569  
 Clinton, J. F. 452, 540, 577  
 Cloud, J. 492  
 Clouteau, D. 456, 532  
 Cobb, S. E. 474  
 Cochran, E. S. 527, 567, 576  
 Collins, B. D. 548  
 Conrad, J. 497  
 Convertito, V. 468  
 Conway, K. 497  
 Corbett, R. 508  
 Cordahi, C. 563  
 Corlett, H. 466  
 Cormier, V. F. 533  
 Cottreau, R. 456  
 Cotton, F. 456  
 Cousins, J. 472  
 Cox, B. R. 449  
 Cox, T. 525  
 Craig, M. S. 473  
 Craig, T. J. 541  
 Cramer, C. H. 455, 468, 470, 482, 553, 571  
 Crempien, J. G. F. 568  
 Criley, C. J. 473, 489  
 Crosby, C. J. 549  
 Crow, H. 449  
 Crowell, B. W. 451  
 Cruz-Atienza, V. M. 482, 544  
 Cubrinovski, M. 549  
 Cui, Y. 457, 502  
 Currie, B. S. 466  
 D'Agostino, N. 458  
 Dahal, N. R. 569  
 Daley, T. 548  
 Dalton, S. M. 523  
 Damiao, L. G. 481  
 Daniels, R. 479  
 Dannemann, F. K. 536  
 Darbyshire, F. 454  
 Darold, A. P. 574  
 Darragh, R. B. 553  
 Daub, E. G. 458  
 David, K. M. 561  
 Davidsen, J. 479, 569  
 Davies, T. R. H. 548  
 Davis, G. 525  
 Davis, P. M. 545  
 Davis, T. A. 460  
 Dawson, T. E. 536, 549  
 Day, S. 455, 502, 534  
 Dayal, S. 570  
 de Groot, R. M. 567  
 De Gori, P. 466  
 De Shon, H. 495  
 Dearborn, D. S. P. 509  
 Dee, S. 486, 579  
 Deelman, E. 457  
 Deierlein, G. G. 566  
 Della Pasqua, F. N. 513  
 DeLong, S. B. 549  
 Delorey, A. A. 463, 531, 556

- Dena-Ornelas, O. S. 485  
Deng, Y. 487  
Dengler, L. A. 510  
Denlinger, R. P. 478  
Denolle, M. A. 517, 541  
dePolo, C. M. 583  
Deterling, O. 548  
Dewey, J. W. 517  
Dhakal, Y. P. 472  
Di Alessandro, C. 495  
Dickenson, S. D. 493  
Dieterich, J. H. 480  
Diez, A. 490, 492  
Dikmen, S. U. 495  
Diniakos, R. S. 464  
Dinsick, A. 495  
Dober, M. 468  
Dodge, D. A. 532  
Dolan, J. F. 503, 504, 549, 566  
Donahue, J. 559, 576  
Donnellan, A. 459, 463, 505  
Doser, D. I. 485  
Dosso, S. E. 449  
Dotray, P. J. 480  
Dou, S. 548  
Dougherty, S. L. 512, 527, 576  
Draeos, T. J. 500, 528  
Dragonov, D. 464  
Dreger, D. S. 465, 481, 490, 539, 540, 548  
Dresen, G. 477, 482, 508, 514, 569  
Driscoll, N. W. 451, 497, 529, 579  
Drobeck, D. 524  
Duan, B. 503  
Dunham, E. M. 504  
Duputel, Z. 568  
DuRoss, C. B. 552, 565, 566, 581, 582  
Dutta, U. 470, 538, 539
- Eakin, C. M. 544  
Eakins, J. 525, 539  
Earle, P. S. 510, 568  
Easton, D. E. 563  
Eaton, D. W. 469, 470, 478, 479, 480, 500, 576  
Ebel, J. E. 484, 569  
Eberhardt, E. 479  
Eberhart-Phillips, D. 546  
Edwards, B. 463  
Eichhubl, P. 468  
El-Hadidy, S. Y. 487  
Elias, P. 542  
Ellingwood, B. R. 560  
Elliott, A. J. 550  
Elliott, J. R. 515, 541, 550  
Ellsworth, W. L. 453, 467, 469, 542, 555  
Encarnacao, A. 528  
Engelhart, S. E. 508  
Enkin, R. 497  
Erberik, M. A. 465  
Erdem, J. E. 546, 564  
Erdik, M. 457  
Ericksen, T. L. 505, 506  
Erickson, B. A. 504
- Etemadsaeed, L. 502  
Euler, G. G. 535  
Evans, E. L. 484, 551, 562  
Evans, J. R. 511, 523  
Exton, M. C. 509  
Ezzedine, S. M. 499, 509, 531, 532
- Faeh, D. 583  
Fäh, D. 577  
Falco, N. 524  
Famiani, D. 527  
Fan, Z. 468  
Farajpour, Z. 519  
Farrell, J. 466  
Farrugia, J. J. 574  
Faulds, J. E. 557, 558, 579  
Fee, D. 501  
Fee, J. M. 518  
Felzer, K. R. 483  
Field, E. H. 513  
Field, N. 561  
Fielding, E. J. 514, 565  
Fischer, P. 462  
Fischer, R. M. 509  
Fischer, T. 507, 555  
Fisk, M. D. 498  
Fitzenz, D. D. 561, 577  
Flamme, H. 568  
Fletcher, J. B. 546, 564  
Flynn, B. W. 557  
Ford, S. R. 499, 531, 532  
Fox, A. 469  
Fox, O. 475  
Foxall, W. 575  
Franceschi, P. 516  
Franco, G. 560  
Fredricksen, A. 454  
Freifeld, B. 548  
Frepoli, A. 527  
Frey Mueller, J. T. 470, 471  
Frieberg, P. A. 466  
Frobert, L. 567  
Frohlich, C. A. 480, 495  
Frost, E. K. 582  
Fry, B. 463, 546  
Fujiwara, H. 550  
Fukuoka, Y. 460  
Funning, G. J. 541
- Gabel, L. L. 537  
Gale, J. F. 468, 480, 495  
Galer, S. 496  
Galis, M. 534  
Gallegos, A. C. 563  
Gallovic, F. 569  
Ganas, A. 542  
Ganesh, M. 456  
García-Jerez, A. 547  
Gardine, M. 470  
Garrett, N. 527  
Gately, K. 537  
Gath, E. M. 516  
Gatti, F. 532  
Gattuso, A. 527  
Ge, Z. 543  
Geist, E. L. 537  
Gelfenbaum, G. 508  
Geng, J. 542  
Gerstoft, P. 490, 492  
Gerzina, J. 480  
Ghods, A. 521
- Ghofrani, H. G. 570  
Ghosh, A. 462, 514  
Gill, D. 457  
Gilligan, A. 517  
Givler, R. 559, 577  
Glasscoe, M. T. 505  
Glenn, L. A. 499, 532  
Glennie, C. L. 505, 506, 582  
Goebel, T. H. W. 467, 541, 569  
Gok, R. 541  
Gold, R. D. 557, 565, 566  
Goldfinger, C. 496, 529  
Goldman, M. R. 473, 489  
Gonzales, A. 528  
Gonzalez, T. 516  
Gosselin, J. M. 449  
Goto, H. 581  
Gottlieb, M. 481  
Goulet, C. A. 502, 533, 553, 554, 557  
Graehl, N. 508  
Graizer, V. 554  
Grand, S. P. 485  
Grant Ludwig, L. 459, 552  
Grapenthin, R. 451, 471  
Graves, R. W. 457, 553, 554  
Graw, J. H. 493  
Greene, H. G. 497  
Greenfield, M. W. 549  
Gregory C. Beroza, G. C. 475  
Grenader, J. R. 566  
Gritto, R. 490  
Grob, M. 543  
Grützner, C. 462, 550  
Guilhem, A. 481  
Gulerce, Z. 526  
Gupta, N. 561  
Guy, M. 568
- Hachem, M. 464  
Haddadi, H. 524, 564  
Haddon, E. K. 579  
Haeussler, P. J. 529, 582  
Haffener, J. 477  
Hagen, M. H. 467  
Hager, B. H. 502  
Hagos, L. 524  
Hainzl, S. 555, 556  
Haji-Soltani, A. 520, 571  
HajNasser, Y. 469  
Halchuk, S. 557, 577  
Hale, D. A. 537  
Hale, J. M. 535  
Halldorsson, B. 456, 515, 520  
Hallo, M. 569  
Hamburger, M. W. 578  
Hamburger, R. O. 559  
Hammond, W. C. 454, 557, 581  
Han, L. B. 481  
Haney, M. M. 460, 476, 501  
Hansen, S. E. 493, 512  
Hao, J. L. 532  
Haq, S. S. B. 514  
Harben, P. E. 496  
Hardebeck, J. L. 483, 507
- Harding, A. J. 497, 529  
Haritashya, U. K. 548  
Harith, N. 522  
Harmon, J. A. 553, 554, 555  
Harrington, R. M. 527, 576  
Hartleb, R. D. 582  
Hartline, C. 477, 511  
Hartog, R. 475  
Hartzell, S. 534  
Hashash, Y. M. A. 553, 554, 555  
Hassani, B. 572  
Hatch, C. 524  
Hatch, R. 580  
Hatem, A. E. 566  
Haug, K. 466  
Hauksson, E. 467, 507, 541, 569  
Hausmann, R. 496  
Hawkins, A. 458  
Hayashi, K. 471, 473, 546, 559  
Hayashi Masa, M. H. 509  
Hayek, S. 557  
Hayes, G. P. 568, 580  
Hayman, T. 563  
Hayward, C. T. 501, 535, 536  
Hearn, T. M. 563  
Hearne, M. 456, 568, 578  
Heaton, T. H. 474, 540, 566  
Heck, S. 488  
Hecker, S. 549  
Heien, E. M. 484  
Hellweg, M. 452, 511  
Helmberger, D. V. 570  
Hemphill-Haley, E. 508  
Henderson, D. 481  
Henry, C. D. 558  
Henrys, S. 463  
Henson, I. 452  
Hernandez, S. 490  
Herrera, C. 544  
Herrmann, M. 477  
Herrmann, R. B. 486, 488, 541, 546  
Hetland, E. A. 507  
Hiebing, M. 485  
Hill, D. P. 465, 555  
Hines, T. T. 507  
Hinojosa Corona, A. 505  
Hitchcock, C. 576  
Hodgkinson, K. M. 475, 481  
Holbrook, J. M. 486  
Holland, A. A. 524, 574  
Holland, J. 524  
Hollingsworth, J. 549  
Hollis, D. D. 547  
Holmes, J. J. 497  
Holt, A. F. 545  
Holtkamp, S. 470, 539  
Hoots, C. R. 512  
Hoover, S. M. 542, 575  
Horspool, N. 456  
Horstmann, T. H. 471  
Horton, J. W. 486  
Horton, S. P. 478  
Hoshiba, M. 452
- Hosseini, M. 572  
Hosseini, S. M. 467, 469  
Hotovec-Ellis, A. J. 452, 466, 475  
Hough, S. E. 464, 469  
Hrafinkelsson, B. 456  
Hrubcova, P. 461  
Hu, J. 548  
Hu, R. 492  
Hua, Q. F. 530  
Huang, H. B. 530  
Huang, H. H. 466  
Huang, M. H. 514, 562, 564, 565  
Huang, P. Y. 537  
Huang, W. 581  
Huang, Y. H. 469  
Huda, M. M. 562  
Hudnut, K. W. 505, 506, 549  
Huerfano, V. 568  
Hui, H. 533  
Hull, A. 559  
Humphrey, J. R. 583  
Huo, D. 530  
Hurley, R. C. 499, 532  
Hutchison, A. 462  
Hutko, A. 541, 564  
Hutt, C. R. 512
- Ibs-von Seht, M. I. 471  
Ickrath, M. 514  
Ide, S. 462  
Ikuo Takahashi, 550  
Ingemansson, B. 577  
Ishii, H. 519  
Ishii, M. 460, 519  
Iwata, T. 518
- Jackson, D. D. 458, 483, 575  
Jackson, F. 494  
Jackson, J. A. 515  
Jaiswal, K. S. 456, 512  
Jarpe, S. P. 496  
Jaume, S. C. 474  
Jayangondaperumal, R. 565  
Jayko, A. S. 579  
Jeanne, P. 575  
Jeffries, C. 466  
Jeppson, T. N. 504  
Jessee (Nowicki), M. A. 578  
Ji, C. 525, 527, 540, 544, 568  
Jiang, J. J. 522  
Jiang, Y. 487  
Jibson, R. W. 548  
Jin, Y. Z. 488  
John, B. 512  
Johnson, C. E. 485  
Johnson, J. 478, 526  
Johnson, K. E. 549, 565  
Johnson, K. L. 536  
Johnson, P. A. 458, 463, 556  
Johnson, W. 481  
Jones, J. P. 500  
Jones, K. R. 502  
Jordan, T. H. 457, 459, 483, 491, 502, 533



- Journeay, M. 577  
 Juarez, A. 492, 584  
 Jurdy, D. 454  
 Juve, G. 457
- Kaiser, A. E. 472  
 Kaklamanos, J. 494  
 Kanamori, H. 544, 568  
 Kao, H. 454, 478, 526, 574, 576  
 Karaca, E. 560  
 Karakus, G. 474  
 Karamitrou, A. 519  
 Karasozen, E. 521  
 Kargel, J. S. 548  
 Karimi, S. 495, 523, 528  
 Kaviani, A. 492  
 Kawase, H. 450, 460, 547, 558  
 Kayen, R. E. 549  
 Kaymakci, N. 526  
 Kazmer, M. 529  
 Kell, A. M. 579, 581  
 Keller, G. R. 453  
 Kellogg, L. H. 458  
 Kelsey, H. M. 508  
 Kemp, C. D. 582  
 Kendall, J. M. 477, 543  
 Kent, G. M. 451, 497, 529, 558, 579, 580, 581  
 Khater, M. M. 561  
 Khelifi, K. 535  
 Khoshnevis, N. 482  
 Kianirad, E. 518  
 Kijko, A. 483  
 Kilb, D. L. 483, 527  
 Kim, B. 564  
 Kim, K. 501, 532  
 Kim, W. Y. 498  
 Kim, Y. Y. 537  
 Kishida, T. 476, 553  
 Klemperer, S. L. 487  
 Kley, J. 453  
 Klinger, Y. 504  
 Knapp, D. R. 532  
 Knepley, M. G. 534  
 Knezevic Antonijevic, S. 522  
 Knight, E. E. 531  
 Knox, H. A. 499, 500, 528  
 Kobayashi, T. 450  
 Koch, K. 498  
 Kocon, K. 466  
 Koehler, R. 508, 582  
 Kokkalas, S. 581  
 Kong, Q. 474, 528, 551  
 Koper, K. D. 543, 574  
 Kosaka, H. 450  
 Kotha, S. R. 456, 559  
 Kortke, A. R. 572  
 Kowsari, M. 520  
 Koyanagi, K. 517  
 Kraaijpoel, D. A. 467  
 Kraft, T. 477  
 Kramer, S. L. 549  
 Kravchenko, N. 472  
 Krebes, E. 480  
 Kreemer, C. 454, 458, 482, 557  
 Kristek, J. 493, 502, 503, 534  
 Kristekova, M. 502, 503
- Kritikos, T. 548  
 Kroll, K. A. 480  
 Kropivnitskaya, Y. Y. 551  
 Ktenidou, O. J. 572  
 Ku, W. 492  
 Kubina, F. 493  
 Kuehn, N. M. 457, 475, 519, 553, 554  
 Kulbayeva, U. 472  
 Kumar, S. 513  
 Kunugi, T. 472  
 Kwak, D. Y. 549, 562  
 Kwiatek, G. 477, 508, 510, 540, 569  
 Kwok, J. 528  
 Kwon, Y. W. 551  
 Kyriakopoulos, C. 513
- La Selle, S. 508  
 Lajoie, L. J. 505, 536, 549, 565  
 Lamontagne, M. 455, 557, 574  
 Landry, W. 552  
 Landwehr, N. 457  
 Lang, D. 524  
 Langenbruch, C. 543  
 Langet, N. 528  
 Langridge, R. M. 566  
 Langston, C. A. 450, 486, 488, 493, 496  
 Lanza, F. 488  
 Larmat, C. S. 531, 535  
 Larsen, T. 561  
 Lavoie, D. 574  
 Law, A. 480, 528  
 Lawry, B. J. 500, 528  
 Lay, T. 544, 568  
 Le, B. M. 530  
 Lebedev, S. 463  
 Lecocq, T. 551  
 Lee, R. C. 535  
 Lee, S. J. 493, 522, 578  
 Lee, Y. 476, 561  
 Lees, J. M. 462, 500, 502, 522, 536  
 Leprince, S. 549  
 Levandowski, W. 467, 487, 506  
 Levine, N. S. 474  
 Levy, Y. 521  
 Lew, M. 464  
 Lewandowski, N. 486, 559, 576, 577  
 LeWinter, A. 582  
 Leyton, F. 493  
 Li, B. 514  
 Li, C. 545  
 Li, G. L. 493  
 Li, H. W. 488  
 Li, J. 491  
 Li, L. 481, 530  
 Li, Q. 481  
 Li, T. J. 545  
 Li, X. 581  
 Li, Z. 501  
 Liang, C. 565  
 Liang, C. R. 514  
 Liang, X. J. 488  
 Liberty, L. M. 529  
 Lienkaemper, J. J. 549  
 Lifton, Z. 559
- Lin, F. 454, 547  
 Lin, F. C. 466, 473, 491, 547  
 Lin, G. 489, 508  
 Lindsey, N. J. 548  
 Lindvall, S. C. 486, 582  
 Linville, L. M. 527  
 Lisi, A. 527  
 Liu, B. Y. 521  
 Liu, C. G. 530  
 Liu, D. 503  
 Liu, J. 519  
 Liu, M. 453, 459  
 Liu, S. Q. 519  
 Liu, X. 461  
 Liukis, M. 483  
 Llenos, A. 542  
 Llenos, A. L. 573  
 Lognonné, P. 535  
 Long, F. 481  
 Long, M. D. 522, 544  
 Loofbourrow, C. 508  
 Lopez-Caballero, F. 532  
 Lorito, S. 509  
 Lotto, G. C. 504  
 Louie, J. 450, 494, 497, 546, 557, 580  
 Lovholt, F. 509  
 Lowry, A. R. 454  
 Lowry, D. 559  
 Loyd, T. W. 460  
 Lozos, J. C. 503  
 Lü, J. 492  
 Lucente, F. P. 466  
 Luckett, R. 543  
 Luco, N. 502, 558, 559, 561  
 Lui, S. K. Y. 570  
 Luke, B. 579  
 Luna, B. 481  
 Luttrell, K. 508  
 Lutz, A. T. 582  
 Luzùn, F. 547  
 Lynett, P. 538  
 Lyzenga, G. 505
- Ma, L. 485  
 MacCharles, R. 563  
 MacCormack, K. 466  
 Maceira, M. 461, 491  
 MacKay, M. 478  
 Mackenzie, D. 515, 550  
 Madin, I. 537  
 Madugo, C. M. 513, 559, 576, 577  
 Maechling, P. J. 457, 483, 502, 533  
 Maghsoudi, S. 479  
 Magnani, M. B. 486  
 Mahani, A. B. 576  
 Mai, P. M. 534  
 Maier, K. L. 497  
 Malagnini, L. 540  
 Málek, J. 511, 523  
 Manabe, S. M. 473  
 Mann, D. 475  
 Manna, S. 570  
 Marchetti, A. 527  
 Marcillo, O. 536  
 Mareschal, M. 536, 579  
 Marjiyono, M. 471  
 Marliyani, G. I. 514
- Martin, A. 472  
 Martin, E. R. 548  
 Martin, J. G. 548  
 Martin, S. S. 464  
 Martinez, E. M. 518  
 Martínez-Garzón, P. 477, 482, 508, 569  
 Martynov, V. 525  
 Marzocchi, W. 483  
 Mason, H. B. 496, 509  
 Matoza, R. 501  
 Matsushima, S. 450, 460, 547  
 Mattioli, G. S. 475, 481  
 Matzel, E. M. 461, 490  
 Maxwell, S. C. 543  
 Mazet-Roux, G. 551, 567  
 Mazzoni, S. 464, 553  
 McBride, J. H. 557  
 McCallen, D. B. 503  
 McCausland, W. A. 465  
 McCreery, C. 517  
 McEvelly, A. T. 471, 520  
 McGarr, A. 469, 542  
 McGowan, S. M. 512  
 McGuire, C. P. 566  
 McGuire, J. 570  
 McMahan, N. D. 485  
 McNamara, D. E. 467, 485, 557  
 McNutt, S. R. 476  
 McPherson, B. C. 516  
 McVerry, G. 472  
 Medina Luna, L. 507  
 Meertens, C. M. 475, 481  
 Mei, X. P. 522  
 Meier, M. A. 452, 540  
 Mejia, H. P. 568  
 Mele, G. 527  
 Melgar, D. 451, 509, 542  
 Mellors, R. J. 490, 531  
 Meltzner, A. J. 513  
 Mencin, D. J. 475, 481  
 Mendonidis, E. 542  
 Menekse, A. 526  
 Meng, H. 570  
 Meng, L. 464, 474  
 Meng, X. 463, 477  
 Merino, M. 453  
 Merz, D. K. 523  
 Meyer, J. 525  
 Michael, A. J. 483, 542, 573  
 Michlik, F. 493  
 Milawsky, E. 557  
 Milburn, T. W. 488  
 Miller, K. 538  
 Miller, M. S. 545  
 Miller, P. L. 509  
 Milliner, C. 505, 549  
 Milner, K. 457  
 Milner, K. R. 459  
 Minson, S. E. 505, 506  
 Mishra, R. L. 565  
 Mitra, D. 493  
 Mitra, S. 570  
 Mochizuki, K. 463  
 Moco, P. 493, 502, 503, 534  
 Moghimi, S. 464  
 Mohammadi, K. 504  
 Mohammed, M. S. 567
- Moldobekov, B. 472, 495  
 Molisee, D. D. 573  
 Molnar, S. 449, 494, 574  
 Montalva, G. A. 493  
 Mooney, W. D. 484, 487  
 Moore, A. 514  
 Moore, G. 568  
 Moores, A. O. 496, 523  
 Moreau, L. 490  
 Morency, C. E. 461  
 Mori, Y. 450  
 Morton, E. A. 462  
 Moschetti, M. P. 534, 542, 575  
 Moshou, A. 542  
 Moskovitz, B. 578  
 Moss, R. E. S. 472, 506  
 Mostafanejad, A. 486, 488, 493  
 Motamed, R. M. 493  
 Moucha, R. 454  
 Mousavi, S. M. 496  
 Mueller, C. S. 488, 542, 575  
 Murray, J. R. 505, 506  
 Myers, S. C. 476, 490
- Nadeau, L. 455  
 Nadeau, R. M. 481, 540  
 Naesholm, S. P. 524  
 Nagasaka, Y. N. 473  
 Nagashima, F. 450  
 Nagata, S. N. 473  
 Naito, S. 550  
 Najdahmadi, B. 522  
 Nakai, S. 549  
 Nakamura, H. 550  
 Nakata, T. 581  
 Nayak, A. 490, 539  
 Nealy, J. L. 580  
 Nelson, A. R. 508  
 Nemzek, R. 498  
 Neuhauser, D. S. 452, 525  
 Newman, A. V. 463  
 Ng, R. 473  
 The NGA-East Ground-Motion Model Developer Working Group 553
- Ni, J. 563  
 Nicolsky, D. J. 537  
 Nippres, S. 461  
 Nishenko, S. 461, 497  
 Nissen, E. K. 505, 521, 536, 541, 549  
 Nixon, C. 477  
 Noda, S. 453, 542  
 Nof, R. N. 453, 474  
 Nori Nakata, N. 475  
 Norman, D. K. 559  
 Nowack, R. L. 584  
 Nozu, A. N. 473, 503  
 Nyamwandha, C. A. 486  
 Nyblade, A. 490, 492  
 Nyland, D. 537  
 Nyst, M. 577
- Ober, C. 499  
 O'Connell, D. R. H. 449, 461  
 O'Donnell, A. 518  
 Odum, J. K. 474, 489, 547

- Ogiso, M. 452  
 Oglesby, D. D. 503, 513  
 Ogwari, P. O. 478  
 Ogweno, L. P. 571  
 Okubo, P. 452, 475  
 Olsen, A. H. 558  
 Olsen, K. B. 455, 457, 502, 534  
 Onur, T. 577  
 Oren, C. 584  
 O'Rourke, C. T. 498  
 O'Rourke, T. D. 548  
 Orunbaev, S. 472, 495  
 Oskin, M. E. 505  
 Owen, L. A. 581  
 Owen, S. 514  
 Oye, V. 528  
 Ozacar, A. A. 526
- Pagani, M. 559  
 Page, M. T. 469, 483  
 Page, W. 576  
 Pagliuca, N. 527  
 Pan, M. H. 530  
 Pancha, A. 546  
 Pandey, A. 565  
 Pang, G. N. 574  
 Pankow, K. L. 524, 527, 535, 543, 574  
 Paolucci, R. 495, 532  
 Papageorgiou, A. S. 515  
 Papanikolaou, I. D. 529  
 Papathanassiou, G. 542  
 Parameswaran, R. M. 512, 526  
 Park, D. 562  
 Park, J. W. 501, 536  
 Parker, G. A. 554, 555  
 Parker, J. W. 463, 505  
 Parolai, S. 472, 474, 495  
 Parsons, B. E. 541, 550  
 Passarelli, L. 556  
 Pasyanos, M. E. 530, 541  
 Patton, J. R. 496, 529  
 Paul, H. 570  
 Pechmann, J. C. 459  
 Peci, V. 557  
 Peltzer, G. 514, 565  
 Peng, Z. G. 463, 477, 481, 501, 545  
 Pérez-Rocha, L. E. 584  
 Perrin, N. 472  
 Personius, S. F. 565  
 Pertont, M. 547, 584  
 Pesicek, J. D. 465  
 Petersen, M. D. 459, 518, 542, 561, 575  
 Peterson, M. G. 500, 528  
 Petrovic, B. 495  
 Pezeshk, S. 484, 494, 519, 520, 571, 572  
 Pezzo, G. 466  
 Pfeifer, C. 523  
 Phillips, D. A. 475  
 Phillips, S. 563  
 Phillips, W. S. 461, 498, 542  
 Phillips-Alonge, K. 499  
 Pianese, G. 495  
 Pickering, A. J. 549  
 Pierce, I. K. 557, 581  
 Pierce, M. 505
- Pilz, M. 450, 472, 474, 583  
 Piña-Flores, J. 547, 584  
 Pitarka, A. 490, 499, 503, 531, 532  
 Plafker, G. 582  
 Plank, G. 451  
 Plesch, A. 541  
 Polanco, E. 568  
 Polet, J. 473  
 Poli, P. 544  
 Pollitz, F. F. 484  
 Popham, C. 537  
 Poppeliers, C. 515  
 Portner, D. E. 568  
 Porto, N. M. 560, 562  
 Powell, C. A. 453, 486  
 Powers, P. M. 518, 558, 561  
 Pratt, T. L. 486, 489  
 Prejean, S. G. 465  
 Prentice, C. S. 549  
 Preston, L. 530  
 Priest, J. 479  
 Priestley, K. 517, 570  
 Prieto, G. A. 544  
 Protti, M. 463  
 Pujols, R. 568  
 Pullammanappallil, S. 450, 494, 546, 580  
 Pulliam, J. 485, 512  
 Pulliam, R. J. 568  
 Pyle, M. L. 461, 499, 530, 531
- Qin, J. 551  
 Qin, L. 490  
 Qiu, H. 490, 491  
 Quitoriano, V. 567
- Rabade, S. 584  
 Rabade-Garcia, S. 492  
 Rahpeyma, S. 456  
 Rajendran, C. P. 512, 526  
 Rajendran, K. 512, 526  
 Ralston, M. D. 530  
 Ramirez, A. R. 532  
 Ramírez-Guzmán, L. 492, 506, 533, 534, 584  
 Ramos, M. D. 529  
 Ranasinghe, N. R. 563  
 Rangaswamy, A. 493  
 Rao, P. S. 565  
 Rapagnani, G. 551  
 Rathburn, S. L. 501  
 Rathje, E. M. 495, 548, 554, 555  
 Rayimbek, B. 472  
 Real, C. 578  
 Reicherter, K. R. 462, 529  
 Reitman, N. G. 565, 566  
 Rémillieux, M. 535  
 Ren, X. 519  
 Rennolet, S. 534  
 Reshetnikov, A. 510  
 Reusch, M. 523  
 Reyes, J. 525  
 Rezaeian, S. 502, 518  
 Rhoades, D. 483  
 Rhode, A. 461  
 Rhodes, A. 515  
 Rhodes, E. J. 566  
 Richards, P. G. 488, 498
- Richards-Dinger, K. B. 480  
 Ringler, A. T. 512, 524  
 Rivalta, E. 556  
 Rizza, M. 515  
 Robeson, S. M. 578  
 Robinson, M. 508  
 Robinson, T. R. 548  
 Roche, S. L. 496  
 Rockwell, T. K. 504, 513, 516, 521  
 Rodd, R. L. 462  
 Rodgers, A. J. 501, 503, 532, 580  
 Roeloffs, E. A. 478  
 Rojahn, C. 558  
 Rolland, L. M. 535  
 Rollins, J. C. 552, 583  
 Rong, M. 451  
 Rooney, T. 454  
 Rose, W. 454  
 Ross, S. L. 537  
 Ross, Z. E. 490, 570  
 Rosser, N. J. 548  
 Roten, D. 502  
 Roughley, C. 449  
 Rougier, E. 531  
 Roussel, F. 551  
 Rowe, C. A. 462, 464, 530  
 Rubin, R. S. 536, 549  
 Rubinstein, J. L. 467, 542, 576  
 Rueck, M. 569  
 Ruhl, C. J. 556, 558, 573, 580, 581  
 Ruiz, S. 544  
 Rundle, J. B. 458, 459, 484, 573  
 Ruppert, N. A. 470, 523, 539  
 Rusho, J. 524  
 Russell, J. 492  
 Ryan, S. E. 501
- Sachs, M. K. 484  
 Safak, E. 495  
 Sahakian, V. J. 497  
 Sahoo, H. K. 565  
 Salas, C. 478, 526  
 Saleeby, J. B. 467  
 Salisbury, J. B. 565  
 Sammis, C. 549  
 Samsonov, S. V. 514  
 Sanborn, C. J. 533  
 Sanchez, J. 584  
 Sánchez-Sesma, F. J. 547, 584  
 Sanders, D. H. 567  
 Sandikkaya, M. A. 563  
 Sandvol, E. A. 492, 533, 563  
 Sangha, S. S. 514, 565  
 Sanquini, A. M. 562  
 Sanwal, J. 512  
 Sardina, V. 517, 537  
 Sattari, A. 480  
 Savran, W. H. 534  
 Savvaidis, A. 495  
 Sawyer, T. 576  
 Schaff, D. P. 488, 498  
 Scharer, K. M. 549, 582  
 Schirling, P. 509  
 Schlittenhardt, J. S. 471
- Schmandt, B. 454, 466, 512  
 Schmidt, B. 575  
 Schmidt, B. S. 471  
 Schmidt, C. J. 485  
 Schmidt, D. A. 451  
 Schmitt, D. R. 477  
 Schneiderwind, S. 529  
 Scholz, C. H. 506  
 Schorlemmer, D. 483  
 Schreier, L. 551  
 Schultz, K. W. 484, 573  
 Schultz, R. 466, 478  
 Schuster, G. T. 547  
 Schutt, D. L. 454  
 Schwartz, D. P. 549, 565  
 Schwartz, S. Y. 463  
 Scire, A. 544  
 Secara, S. 548  
 Sedaghati, F. 572  
 Seemann, M. 577  
 Segou, M. 480, 573  
 Seifried, A. E. 494  
 Seitz, G. 579  
 Sekiguchi, T. 549  
 Seligson, H. 456  
 Sen, M. K. 485  
 Sentz, K. 498  
 Sepulveda, F. 512  
 Seyhan, E. 562, 564  
 Shah, A. K. 486, 583  
 Shahjoui, A. 450, 484  
 Shakal, T. 524, 564  
 Shapiro, S. A. 510  
 Share, P. 490  
 Sharma, N. 468  
 Shaw, J. H. 541  
 Shearer, P. M. 541, 555  
 Sheehan, A. 463  
 Shelly, D. R. 463, 465, 555  
 Shen, W. 453  
 Shen, Y. 491  
 Sheng, Y. 517  
 Shi, B. P. 521  
 Shi, J. 476  
 Shi, S. Z. Q. 534  
 Shi, Z. 455  
 Shimoda, N. 510  
 Shipman, T. 466  
 Shore, M. J. 522  
 Shoushtari, A. V. 522  
 Shugar, D. H. 548  
 Shuler, S. E. 473  
 Shumway, A. M. 518  
 Sianipar, D. S. 519  
 Sickler, R. R. 549  
 Silacheva, N. 472  
 Silva, F. 533  
 Silva, W. J. 553, 554, 555  
 Simons, M. 514  
 Singh, I. 565  
 Skarlatoudis, A. A. 520, 571  
 Skoumal, R. J. 466  
 Slater, D. 451  
 Sleep, N. H. 507  
 Slinkard, M. 488, 510, 528  
 Sloan, R. A. 541  
 Smit, A. 483  
 Smith, D. 452  
 Smith, D. F. 561
- Smith, K. D. 451, 556, 558, 573, 580, 581  
 Smith, R. B. 466  
 Smith, T. 527  
 Smith-Konter, B. 508  
 Snelson-Gerlicher, C. M. 530  
 Soehami, A. S. 471  
 Somerville, P. G. 571, 572  
 Sonam, K. 518  
 Sone, H. 477  
 Song, M. Q. 488, 521  
 Song, X. 491  
 Sonnemann, T. 515  
 Sowers, J. 486  
 Spencer, B. D. 459  
 Spies, T. S. 471  
 Spinelli, R. 470  
 Stacey, C. 497  
 Stanchits, S. 569  
 Stankovic, G. 461  
 Staudenmaier, N. 463  
 Stead, R. J. 498  
 Steed, R. 551  
 Steedman, D. W. 500, 531  
 Steenbergen, R. D. J. M. 467  
 Stein, C. 453  
 Stein, J. R. 543  
 Stein, S. 453, 459, 483  
 Stephen, R. 492  
 Stephenson, W. J. 474, 489, 547, 557  
 Stern, V. 466  
 Stewart, I. S. 529  
 Stewart, J. P. 457, 476, 516, 549, 553, 554, 555, 562  
 Stickney, M. C. 485  
 Stierle, E. 540  
 Still, B. 538  
 Stirling, M. W. 513  
 Stock, J. 569  
 Stork, A. L. 477  
 Strayer, L. M. 471, 520  
 Stroujkova, A. 498  
 Stump, B. W. 501, 535, 536  
 Styron, R. H. 507  
 Su, J. R. 481  
 Subakti, H. 519  
 Sumy, D. F. 467, 511, 567  
 Sun, D. 545  
 Sundermier, A. 488  
 Sianipar, D. S. 473  
 Suzuki, J. 487  
 Suzuki, W. 472  
 Sway, A. 456  
 Sweet, J. 523  
 Synolakis, C. 538  
 Syracuse, E. M. 461, 491  
 Szody, J. A. 485
- Taborda, R. 482, 562  
 Taira, T. 465, 481, 490, 511, 540, 556  
 Tal, Y. 502  
 Tanyas, H. 578  
 Tape, C. 460, 470  
 Tavera, H. 522, 544, 568  
 Taylor, S. R. 496  
 Taylor, W. J. 579

- Teague, D. P. 449  
 Templeton, D. C. 461  
 Thapaliya, S. M. 562  
 Thelen, W. A. 452, 475  
 Thenhaus, P. C. 561  
 Thio, H. K. 509, 572  
 Thomas, P. A. 459, 468  
 Thomas, W. A. 453  
 Thompson, E. M. 464, 560, 561, 578  
 Thompson, S. 559, 576, 577  
 Thornley, J. D. 470, 538, 539  
 Tiampo, K. F. 551  
 Tinker, S. 495  
 Tobin, H. J. 504  
 Toké, N. A. 565  
 Tokimatsu, K. 549  
 Tormann, T. 463  
 Toro, G. R. 486, 494  
 Trabant, C. 564  
 Trench, D. 489  
 Trugman, D. T. 458  
 Tsai, V. C. 460, 466, 473, 547  
 Tschering, K. E. 518  
 Tucker, B. E. 518  
 Turcotte, D. L. 458, 459, 484, 573  
 Turner, J. P. 449, 461, 568  
 Twardzik, C. 525, 544  
 Tyagi, A. 489  
 Tytell, J. 525
- Uhrhammer, R. A. 511
- Vahi, K. 457  
 Valkaniotis, S. 542  
 van Ballegooy, S. 548  
 van de Lindt, J. W. 560  
 van der Elst, N. J. 463, 483  
 van der Lee, S. 543  
 Van Boskirk, E. 481
- Van Dissen, R. J. 566  
 Van Fossen, M. 564  
 Van Houtte, C. 472, 563  
 Vanneste, K. 483  
 Vasterling, M. 575  
 Vavrycuk, V. 461, 540  
 Ventura, C. E. 449  
 Verdon, J. P. 543  
 Vernon, F. L. 451, 475, 490, 525, 539, 570  
 Verros, S. 456  
 Vidale, J. E. 451, 452, 475  
 Villafuerte, C. D. 482  
 Villasenor, A. 491  
 Vlcek, J. 555  
 Vlemminckx, B. 483, 551  
 Von Seggern, D. H. 491  
 Vorobiev, O. Y. 498, 499, 531, 532
- Waddell, J. 537  
 Wagner, A. 548  
 Wagner, L. S. 522, 544  
 Wagoner, J. 531, 579  
 Wagstaffe, D. 472  
 Waite, G. P. 454, 488  
 Wald, D. J. 456, 512, 560, 561, 567, 577, 578  
 Walker, D. 478, 526, 576  
 Walker, J. D. 582  
 Walker, R. L. 479  
 Walker, R. T. 515, 550  
 Wallace, L. 463  
 Walls, C. 475  
 Walsh, D. 517  
 Walsh, S. 533  
 Walsh, T. J. 546, 559  
 Walter, J. I. 463, 480, 495  
 Walter, W. R. 499, 530, 531, 532, 541  
 Wang, B. S. 481  
 Wang, F. 457  
 Wang, J. 505  
 Wang, W. M. 532
- Wang, X. 488, 521  
 Wang, Y. X. 519  
 Wang, Z. 451, 496, 515, 563  
 Wang, Z. M. 534  
 Ward, K. M. 460  
 Watson-Lamprey, J. 559  
 Watson-Ross, C. 530  
 Watzig, R. J. 537  
 Webb, S. 463  
 Weekly, R. T. 564  
 Wegler, U. 575  
 Weinstein, S. 537  
 Weir-Jones, I. 496  
 Weiser, D. A. 575  
 Wellik, J. 465  
 Wells, D. 464  
 Werner, M. 483  
 Wesnously, S. G. 497, 517, 557, 558, 581  
 West, L. T. 494  
 West, M. E. 470, 523, 539  
 White, D. J. 477  
 White, M. C. 570  
 White, R. A. 465  
 Whitmore, P. M. 537  
 Wiemer, S. 463, 477, 577  
 Wiens, D. 453, 490, 492  
 Wilkinson, S. K. 511  
 William, G. 476, 561  
 Williams, C. A. 534  
 Williams, C. R. 561  
 Williams, M. 451  
 Wills, C. J. 456  
 Wilson, D. C. 512, 524  
 Wilson, J. M. 484, 573  
 Wilson, R. I. 537, 538  
 Withers, K. B. 455  
 Witter, R. C. 508, 582  
 Wong, I. G. 455, 468  
 Wong, R. 479  
 Wood, M. M. 562  
 Wood, N. J. 537
- Wooddell, K. E. 540, 553, 559, 576  
 Woodward, R. L. 511  
 Wookey, J. 543  
 Woolery, E. W. 451, 496  
 Worden, C. B. 456, 560, 561  
 Worth, K. 477  
 Wotherspoon, L. 472  
 Wright, A. 464  
 Wright, T. J. 541  
 Wu, B. 489  
 Wu, H. Y. 488  
 Wu, J. 481  
 Wu, Q. 542  
 Wuertley, R. 535  
 Wuestefeld, A. 524, 528  
 Wysession, M. 453
- Xia, S. H. 530  
 Xiao, H. 530  
 Xie, X. B. 487, 532  
 Xie, Z. J. 492  
 Xu, B. 554, 555  
 Xue, L. 556  
 Xue, M. 530  
 Xue, Y. 519
- Yamada, T. Y. 473  
 Yang, J. 470  
 Yang, L. M. 522, 563  
 Yang, T. 530  
 Yang, X. 498  
 Yang, Z. J. 538, 539  
 Yao, D. D. 463, 481, 545  
 Yao, Q. Y. 534  
 Yao, Z. X. 487, 532  
 Ye, L. 544, 568  
 Yeck, W. L. 510  
 Yenier, E. 467, 468, 480, 495, 523, 528, 554  
 Yikilmaz, M. B. 458, 573  
 Yong, A. K. 472, 476  
 Yoon, C. E. 500
- Young, B. A. 493  
 Young, C. J. 488, 500, 510, 528  
 Young, M. 495  
 Youngs, R. R. 553, 554  
 Yu, C. Q. 487  
 Yu, J. 457, 483  
 Yue, H. 514  
 Yun, S. H. 514
- Zafir, Z. 464  
 Zahran, H. M. 487  
 Zaliapin, I. 458, 482, 555  
 Zandieh, A. 494, 571  
 Zandt, G. 522, 544  
 Zare, M. 519  
 Zechar, J. 483  
 Zeiler, C. P. 535  
 Zeng, X. F. 492  
 Zeng, Y. 459, 552  
 Zentner, I. 456  
 Zha, X. H. 492  
 Zhan, Z. 544, 568  
 Zhang, A. 464  
 Zhang, H. 461, 470, 481, 491, 543  
 Zhang, L. F. 534  
 Zhang, Q. 508, 555  
 Zhang, W. 491  
 Zhang, Y. 521  
 Zhang, Z. W. 492, 526  
 Zhan, J. X. 452, 521  
 Zhao, L. F. 487, 532  
 Zheng, Y. 492  
 Zhou, L. Q. 492, 521, 526  
 Zhou, Y. 550  
 Zhu, J. 578  
 Zhuang, J. 573  
 Zielke, O. 579  
 Zigone, D. 461, 491  
 Zinke, R. W. 566  
 Zoback, M. D. 543  
 Zuzlewski, S. 525